Qing-Hua Qin

Advanced Mechanics of Piezoelectricity

Qing-Hua Qin

Advanced Mechanics of Piezoelectricity

With 77 figures

高等教育出版社·北京
HIGHER EDUCATION PRESS BEIJING

Springer

Author
Prof. Qing-Hua Qin
Research School of Engineering
Australian National University
Canberra, Australia
E-mail: qinghua.qin@anu.edu.au

ISBN 978-7-04-034497-4
Higher Education Press, Beijing

ISBN 978-3-642-29766-3 ISBN 978-3-642-29767-0 (eBook)
Springer Heidelberg New York Dordrecht London

Library of Congress Control Number: 2012935855

© Higher Education Press, Beijing and Springer-Verlag Berlin Heidelberg 2013
This work is subject to copyright. All rights are reserved by the Publishers, whether the whole or part of the material is concerned, specifically the rights of translation, reprinting, reuse of illustrations, recitation, broadcasting, reproduction on microfilms or in any other physical way, and transmission or information storage and retrieval, electronic adaptation, computer software, or by similar or dissimilar methodology now known or hereafter developed. Exempted from this legal reservation are brief excerpts in connection with reviews or scholarly analysis or material supplied specifically for the purpose of being entered and executed on a computer system, for exclusive use by the purchaser of the work. Duplication of this publication or parts thereof is permitted only under the provisions of the Copyright Law of the Publishers' locations, in its current version, and permission for use must always be obtained from Springer. Permissions for use may be obtained through RightsLink at the Copyright Clearance Center. Violations are liable to prosecution under the respective Copyright Law.
The use of general descriptive names, registered names, trademarks, service marks, etc. in this publication does not imply, even in the absence of a specific statement, that such names are exempt from the relevant protective laws and regulations and therefore free for general use.
While the advice and information in this book are believed to be true and accurate at the date of publication, neither the authors nor the editors nor the publishers can accept any legal responsibility for any errors or omissions that may be made. The publishers make no warranty, express or implied, with respect to the material contained herein.

Printed on acid-free paper

Springer is part of Springer Science+Business Media (www.springer.com)

Preface

This book contains a comprehensive treatment of piezoelectric materials using linear electroelastic theory, the symplectic model, and various special solution methods. The volume summarizes the current state of practice and presents the most recent research outcomes in piezoelectricity. Our hope in preparing this book is to present a stimulating guide and then to attract interested readers and researchers to a new field that continues to provide fascinating and technologically important challenges. You will benefit from the authors' thorough coverage of general principles for each topic, followed by detailed mathematical derivations and worked examples as well as tables and figures in appropriate positions.

The study of piezoelectricity was initiated by Jacques Curie and Pierre Curie in 1880. They found that certain crystalline materials generate an electric charge proportional to a mechanical stress. Since then new theories and applications of the field have been constantly advanced. These advances have resulted in a great many publications including journal papers and monographs. Although many concepts and theories have been included in earlier monographs, numerous new developments in piezoelectricity over the last two decades have made it increasingly necessary to collect significant information and to present a unified treatment of these useful but scattered results. These results should be made available to professional engineers, research scientists, workers and postgraduate students in applied mechanics and material engineering.

The objective of this book is to fill this gap, so that readers can obtain a sound knowledge of the solution methods for piezoelectric materials. This volume details the development of solution methods for piezoelectric composites and is written for researchers, postgraduate students, and professional engineers in the areas of solid mechanics, physical science and engineering, applied mathematics, mechanical engineering, and materials science. Little mathematical knowledge besides the usual calculus is required, although conventional matrixes, vectors, and tensor presentations are used throughout the book.

Chapter 1 provides a brief description of piezocomposites and the linear theory of piezoelectric materials in order to establish notation and fundamental concepts for reference in later chapters. Chapter 2 presents various solution methods for piezoelectric composites which can be taken as a common source for subsequent chapters. It includes the potential function method, Lekhnitskii formalism, techniques of Fourier transformation, Trefftz finite element method, integral equation approach, shear-lag model, and symplectic method. Chapter 3 deals with problems of fibrous piezoelectric composites, beginning with a discussion of piezoelectric fiber push-out and pull-out, and ending with a brief description of the

solution for a piezoelectric composite with an elliptic fiber. Chapter 4 is concerned with applications of Trefftz method to piezoelectric materials. Trefftz finite element method, Trefftz boundary element method, and Trefftz boundary-collocation method are presented. Chapter 5 describes some solutions of piezoelectric problems using a symplectic approach. Chapter 6 presents Saint-Venant decay analysis of piezoelectric materials by way of symplectic formulation and the state space method. Chapter 7 reviews solutions for piezoelectric materials containing penny-shaped cracks. Chapter 8 describes solution methods for functionally graded piezoelectric materials.

I am indebted to a number of individuals in academic circles and organizations who have contributed in different, but important, ways to the preparation of this book. In particular, I wish to extend appreciation to my postgraduate students for their assistance in preparing this book. Special thanks go to Ms. Jianbo Liu of Higher Education Press for her commitment to the publication of this book. Finally, we wish to acknowledge the individuals and organizations cited in the book for permission to use their materials.

I would be grateful if readers would be so kind as to send reports of any typographical and other errors, as well as their more general comments.

Qing-Hua Qin
Canberra, Australia
May 2012

Contents

Notation

English symbols

a_{ij}, b_{ij}	reduced material constants defined in Eq. (1.26)
B_i	magnetic flux
$\mathbf{c}_i$	unknown coefficients in Eq. (4.9) and elastic stiffness constants in Chapter 3
c_{ijkl}, c_{ij}	elastic stiffness constants
d_{ij}	piezoelectric charge constants
D_i	electric displacements
e_{ijk}, e_{ij}	piezoelectric constants
$\tilde{e}_{ij}$	piezomagnetic coefficient
E_i	electric field
f_i	mechanical body forces
f_{ij}	elastic compliances
g_{ij}	piezoelectric voltage constants
H_i	magnetic field intensity
m_{ij}	reduced material constants defined in Eq. (6.5)
q_s	surface charge
Q	electric charge density
t_i	surface tractions
u, v, w	displacement in x, y, z directions, respectively
u_i	displacements

Greek symbols

α_{ij}	magnetoelectric coupling coefficient
Δ	$= c_{55}\kappa_{11} + e_{15}^2$
Δ_n	$= c_{55}^{(n)}\kappa_{11}^{(n)} + \left(e_{15}^{(n)}\right)^2$ for $n = 0,1,2,\cdots$, defined in Eq. (5.73)
Δ_*	$= \beta_{11}\nu_{11} - \lambda_{11}^2$ defined in Eq. (5.119)
ε_{ij}	elastic strains
θ	temperature change
κ_{ij}	dielectric constants
μ_{ij}	magnetic permeability
σ_{ij}	stresses
υ	Poisson's ratio
ϕ	electric potential
ψ	magnetic potential

Other symbols

$\partial/\partial x$	partial derivative of a variable with respect to x
[ ]	denotes a rectangular or a square matrix
{ }	denotes a column vector
$[\,]^{-1}$	denotes the inverse of a matrix
$[\,]^{T}$	denotes the transpose of a matrix
$(\bar{\ })$	a bar over a variable represents the variable being prescribed or complex conjugate
∇	$=\partial^2/\partial x^2+\partial^2/\partial y^2$

Chapter 1 Introduction to Piezoelectricity

This chapter provides a basic introduction to piezoelectricity. It begins with a discussion of background and applications of piezoelectric materials. We then present the linear theory of piezoelectricity, functionally graded piezoelectric materials(FGPM), and fundamental knowledge of fibrous piezoelectric composites(FPC).

1.1 Background

Piezoelectric material is such that when it is subjected to a mechanical load, it generates an electric charge (see Fig. 1.1(a)). This effect is usually called the "piezoelectric effect". Conversely, when piezoelectric material is stressed electrically by a voltage, its dimensions change (see Fig. 1.1(b)). This phenomenon is known as the "inverse piezoelectric effect". The direct piezoelectric effect was first discovered by the brothers Pierre Curie and Jacques Curie more than a century ago [1]. They found out that when a mechanical stress was applied to crystals such as tourmaline, topaz, quartz, Rochelle salt and cane sugar, electrical charges appeared, and this voltage was proportional to the stress.

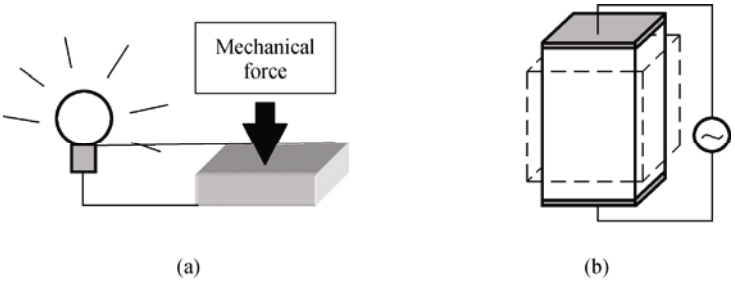

Fig. 1.1 Electroelastic coupling in piezoelectricity.(a) Piezoelectric effect: voltage induced by force. (b) Inverse piezoelectric effect: strain induced by voltage.

The Curies did not, however, predict that crystals exhibiting the direct piezoelectric effect (electricity from applied stress) would also exhibit the inverse piezoelectric effect (strain in response to applied electric field). One year later that property was theoretically predicted on the basis of thermodynamic consideration by Lippmann [2], who proposed that converse effects must exist for piezoelectricity, pyroelectricity (see Fig. 1.2), etc. Subsequently, the inverse piezoelectric effect was confirmed experimentally by Curies [3], who proceeded to obtain quantitative proof of the complete reversibility of electromechanical deformations in piezoelectric crystals. These events above can be viewed as the beginning of the history of piezo-

electricity. Based on them, Woldemar Voigt [4] developed the first complete and rigorous formulation of piezoelectricity in 1890. Since then several books on the phenomenon and theory of piezoelectricity have been published. Among them are the books by Cady [5], Tiersten [6], Parton and Kudryavtsev [7], Ikeda [8], Rogacheva [9], Qin [10,11], and Qin and Yang [12]. The first [5] treated the physical properties of piezoelectric crystals as well as their practical applications, the second [6] dealt with the linear equations of vibrations in piezoelectric materials, and the third and fourth [7,8] gave a more detailed description of the physical properties of piezoelectricity. Rogacheva [9] presented general theories of piezoelectric shells. Qin [10,11] discussed Green's functions and fracture mechanics of piezoelectric materials. Micromechanics of piezoelectricity were discussed in [12].

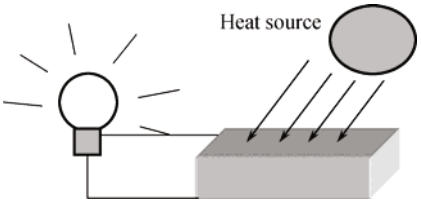

Fig. 1.2 Illustration of pyroelectricity.

In general, the piezoelectric effect occurs only in nonconductive materials. Piezoelectric materials can be divided into two main groups: crystals and ceramics. The best known piezoelectric material in the crystal group is quartz (SiO_2), the trigonal crystallized silica which is known as one of the most common crystals on the earth's surface. In the ceramics group, a typical piezoelectric material is barium titanate ($BaTiO_3$), an oxide of barium and titanium.

It should be mentioned that an asymmetric arrangement of positive and negative ions imparts permanent electric dipole behavior to crystals. In order to "activate" the piezo properties of ceramics, a poling treatment is required. In that treatment the piezo ceramic material is first heated and an intense electric field (> 2 000 V/mm) is applied to it in the poling direction, forcing the ions to realign along this "poling" axis. When the ceramic cools and the field is removed, the ions "remember" this poling and the material now has a remanent polarization (which can be degraded by exceeding the mechanical, thermal and electrical limits of the material). Subsequently, when a voltage is applied to the poled piezoelectric material, the ions in the unit cells are shifted and, additionally, the domains change their degree of alignment. The result is a corresponding change of the dimensions (expansion, contraction) of the lead zirconate titanate (PZT) material. In the poling treatment, the Curie temperature is the critical temperature at which the crystal structure changes from a nonsymmetrical (piezoelectric) to a symmetrical (non-piezoelectric) form. Particularly, when the temperature is above the Curie temperature, each perovskite crystal

(perovskite is a calcium titanium oxide mineral species composed of calcium titanate, with the chemical formula $CaTiO_3$) in the fired ceramic element exhibits a simple cubic symmetry with no dipole moment (Fig. 1.3(a)). At temperatures below the Curie point, however, each crystal has tetragonal or rhombohedral symmetry and a dipole moment (Fig. 1.3(b)).

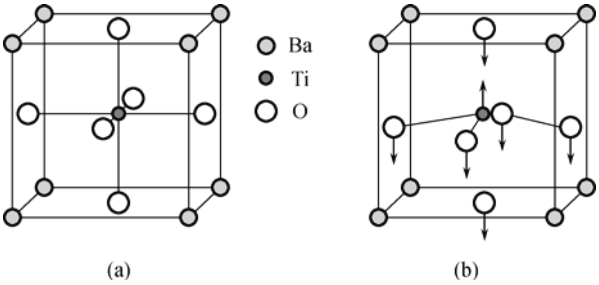

Fig. 1.3 Crystal structures with the Curie temperature.(a) Temperature above Curie temperature: symmetric. (b) Temperature below Curie temperature: non-symmetric.

Although piezoelectricity was discovered in 1880 it remained a mere curiosity until the 1940s. The property of certain crystals to exhibit electrical charges under mechanical loading was of no practical use until very high input impedance amplifiers enabled engineers to amplify their signals. In 1951, several Japanese companies and universities formed a "competitively cooperative" association, established as the Barium Titanate Application Research Committee. This association set an organizational precedent not only for successfully surmounting technical challenges and manufacturing hurdles, but also for defining new market areas. Persistent efforts in materials research created new piezoceramic families which were competitive with Vernitron's PZT. With these materials available, Japanese manufacturers quickly developed several types of piezoelectric signal filters, which addressed needs arising from television, radio, and communications equipment markets; and piezoelectric igniters for natural gas/butane appliances. As time progressed, the markets for these products continued to grow, and other similarly lucrative ones were found. Most notable were audio buzzers (smoke alarms), air ultrasonic transducers (television remote controls and intrusion alarms) and devices employing surface acoustic wave effects to achieve high frequency signal filtering.

The commercial success of the Japanese efforts attracted the attention of industry in many other countries and spurred new efforts to develop successful piezoelectric products. There has been a large increase in relevant publications in China, India, Russia and the USA. Since the piezoelectric effect provides the ability to use these materials as both sensors and actuators, it has found relevant applications requiring accurate measurement and recording of dynamic changes in mechanical variables such as pressure, force and acceleration. The list of applications continues

to grow and now includes [13] (a) aerospace: model testing, wind tunnel and shock tube instrumentation, landing gear hydraulics, rocketry, structures, ejection systems and cutting force research; (b) ballistics: combustion, explosion, detonation and sound pressure distribution; (c) biomechanics: multi-component force measurement for orthopedic gait and posturography, sports, ergonomics, neurology, cardiology and rehabilitation; (d) engine testing: combustion, gas exchange and injection, indicator diagrams and dynamic stressing; (e) engineering: materials evaluation, control systems, reactors, building structures, ship structures, auto chassis structural testing, shock and vibration isolation and dynamic response testing; (f) industrial/manufacturing: machining systems, metal cutting, press and crimp force, automation of force-based assembly operations and machine health monitoring; and (g) OEMs (original equipment manufacturer): transportation systems, plastic molding, rockets, machine tools, compressors, engines, flexible structures, oil/gas drilling and shock/vibration testers.

Judging by the increase in worldwide activity focused on using a large number of very precise piezoelectric sensors and actuators for active control in communications, navigation and packaging systems, and from the successes encountered in the last sixty years, it is expected that piezoelectricity will enjoy a continuing role in both fundamental and technical applications in the future.

In this chapter, the linearized piezoelectric formulations described in [10,11,14], the concept of FGPM and fiber piezocomposites, which will be needed in later chapters, are briefly summarized. The basic equations of linear electroelasticity are first reviewed, followed by a brief discussion of FGPM and FPC, which have important applications in practical engineering. Then some issues in interface and fracture mechanics in piezoelectricity are outlined.

1.2 Linear theory of piezoelectricity

1.2.1 Basic equations in rectangular coordinate system

This section recalls briefly the three-dimensional formulation of linear piezoelectricity that appeared in [11,14]. Here, a three-dimensional Cartesian coordinate system is adopted where the position vector is denoted by $\mathbf{x}$ (or x_i). In this book, both conventional indicial notation x_i and traditional Cartesian notation (x, y, z) are utilized. In the case of indicial notation we invoke the summation convention over repeated Latin indices, which can be of two types with different ranges: i, j, k=1,2,3 for lower-case letters and M, N=1,2,3,4 for upper-case letters. Moreover, vectors, tensors and their matrix representations are denoted by bold-face letters. The three-dimensional constitutive equations for linear piezoelectricity can be derived

by considering an electric enthalpy function H defined as [11]

$$H(\boldsymbol{\varepsilon}, \mathbf{E}) = \frac{1}{2} c_{ijkl}^{E} \varepsilon_{ij} \varepsilon_{kl} - \frac{1}{2} \kappa_{ij}^{\varepsilon} E_i E_j - e_{kij} \varepsilon_{ij} E_k \tag{1.1}$$

where the strain tensor $\boldsymbol{\varepsilon}$ (ε_{ij}) and the electric field vector $\mathbf{E}$ (E_i) are related to the displacement $\mathbf{u}$ and the electric potential ϕ by

$$\varepsilon_{ij} = \frac{1}{2}(u_{i,j} + u_{j,i}), \qquad E_i = -\phi_{,i} \tag{1.2}$$

in which a comma followed by arguments denotes partial differentiation with respect to the arguments, c_{ijkl}^{E}, e_{kij} and $\kappa_{ij}^{\varepsilon}$ are the elastic, piezoelectric, and dielectric constants, respectively. The superscript E in c_{ijkl}^{E} indicates that the elastic constants are measured at a constant electric field. The superscript ε in $\kappa_{ij}^{\varepsilon}$ indicates that the dielectric constants are measured at a constant strain. To simplify subsequent writing, we shall omit the superscripts E and ε in the remaining part of this book. The material constants in Eq. (1.1) can be reduced by the following consideration. According to the definition (1.2) we may write $\varepsilon_{ij}=\varepsilon_{ji}$. It follows that

$$c_{ijkm} = c_{ijmk} \tag{1.3}$$

Further, from $\sigma_{ij} = \sigma_{ji}$ we have

$$c_{ijkm} = c_{jikm}, \qquad e_{kij} = e_{kji} \tag{1.4}$$

In view of these properties, it is useful to introduce the so-called two-index notation or compressed matrix notation [10]. Two-index notation consists of replacing ij or km by p or q, i.e. $c_{ijkm}=c_{pq}$, $e_{ikm}=e_{iq}$, $\varepsilon_{ij}=\varepsilon_p$ when $i=j$, and $2\varepsilon_{ij}=\varepsilon_p$ when $i\neq j$, where i, j, k, m take the values 1-3, and p, q assume the values 1-6 according to the following replacements $11 \to 1$, $22 \to 2$, $33 \to 3$, 23 or $32 \to 4$, 13 or $31 \to 5$, 12 or $21 \to 6$.

Constitutive relations are obtained from the electric enthalpy function (1.1) as

$$\begin{aligned} \sigma_{ij} &= \frac{\partial H(\boldsymbol{\varepsilon}, \mathbf{E})}{\partial \varepsilon_{ij}} = c_{ijkl} \varepsilon_{kl} - e_{kij} E_k, \\ D_i &= -\frac{\partial H(\boldsymbol{\varepsilon}, \mathbf{E})}{\partial E_i} = e_{ikl} \varepsilon_{kl} + \kappa_{ik} E_k \end{aligned} \tag{1.5}$$

where σ_{ij} is the stress tensor and D_i the electric displacement vector. Making use of two-index notation mentioned above, Eqs. (1.5) are reduced to

$$\sigma_p = c_{pq} \varepsilon_q - \varepsilon_{kp} E_k, \qquad D_i = e_{iq} \varepsilon_q + \kappa_{ik} E_k \tag{1.6}$$

in which

$$\varepsilon_p = \begin{cases} \varepsilon_{ij} & (\text{when } i = j) \\ 2\varepsilon_{ij} & (\text{when } i \neq j) \end{cases} \tag{1.7}$$

In addition to the constitutive relation (1.5) above, three other forms of constitutive representation are commonly used in the linear theory of piezoelectricity to describe the coupled interaction between elastic and electric variables [11]. Each type has its own different set of independent variables and corresponds to a different electric enthalpy function, as listed in Table 1.1. It should be pointed out that an alternative derivation of formulae is merely a transformation from one type of relation to another. Some relationships between various constants occurring in the four types are as follows:

$$\begin{aligned} &\mathbf{c}^E = (\mathbf{f}^E)^{-1}, \quad \mathbf{e} = \mathbf{c}^E\mathbf{d}, \quad \boldsymbol{\kappa}^\varepsilon = \boldsymbol{\kappa}^\sigma - \mathbf{d}^{\mathrm{T}}\mathbf{c}^e\mathbf{d}, \quad \mathbf{f}^D = (\mathbf{c}^E)^{-1} - \mathbf{d}(\boldsymbol{\kappa}^\sigma)^{-1}\mathbf{d}^{\mathrm{T}}, \\ &\mathbf{g} = \mathbf{d}(\boldsymbol{\kappa}^\sigma)^{-1}, \quad \mathbf{c}^D = \mathbf{c}^E - \mathbf{c}^E\mathbf{d}(\boldsymbol{\kappa}^\varepsilon)^{-1}\mathbf{d}^{\mathrm{T}}\mathbf{c}^E, \quad \mathbf{h} = -\mathbf{c}^E\mathbf{d}(\boldsymbol{\kappa}^\varepsilon)^{-1}, \\ &\boldsymbol{\lambda}^\sigma = (\boldsymbol{\kappa}^\sigma)^{-1}, \quad \boldsymbol{\lambda}^\varepsilon = (\boldsymbol{\kappa}^\varepsilon)^{-1} \end{aligned} \tag{1.8}$$

Table 1.1 Four types of fundamental electroelastic relations.

Independent variables	Constitutive relations	Electric enthalpy functional
$\boldsymbol{\varepsilon}$, $\mathbf{E}$	$\begin{cases} \boldsymbol{\sigma} = \mathbf{c}^E\boldsymbol{\varepsilon} - \mathbf{e}^{\mathrm{T}}\mathbf{E} \\ \mathbf{D} = \mathbf{e}\boldsymbol{\varepsilon} + \boldsymbol{\kappa}^\varepsilon\mathbf{E} \end{cases}$	$H_0 = \frac{1}{2}\mathbf{c}^E\boldsymbol{\varepsilon}^2 - \frac{1}{2}\boldsymbol{\kappa}^\varepsilon\mathbf{E}^2 - \mathbf{e}\boldsymbol{\varepsilon}\mathbf{E}$
$\boldsymbol{\varepsilon}$, $\mathbf{D}$	$\begin{cases} \boldsymbol{\sigma} = \mathbf{c}^D\boldsymbol{\varepsilon} - \mathbf{h}^{\mathrm{T}}\mathbf{D} \\ \mathbf{E} = -\mathbf{h}\boldsymbol{\varepsilon} + \boldsymbol{\beta}^\varepsilon\mathbf{D} \end{cases}$	$H_1 = H_0 + \mathbf{E}\mathbf{D}$
$\boldsymbol{\sigma}$,$\mathbf{E}$	$\begin{cases} \boldsymbol{\varepsilon} = \mathbf{f}^E\boldsymbol{\sigma} + \mathbf{d}^{\mathrm{T}}\mathbf{E} \\ \mathbf{D} = \mathbf{d}\boldsymbol{\sigma} + \boldsymbol{\kappa}^\sigma\mathbf{E} \end{cases}$	$H_2 = H_0 - \boldsymbol{\sigma}\boldsymbol{\varepsilon}$
$\boldsymbol{\sigma}$, $\mathbf{D}$	$\begin{cases} \boldsymbol{\varepsilon} = \mathbf{f}^D\boldsymbol{\sigma} + \mathbf{g}^{\mathrm{T}}\mathbf{D} \\ \mathbf{E} = -\mathbf{g}\boldsymbol{\sigma} + \boldsymbol{\beta}^\sigma\mathbf{D} \end{cases}$	$H_3 = H_0 + \mathbf{E}\mathbf{D} - \boldsymbol{\sigma}\boldsymbol{\varepsilon}$

Having defined constitutive relations, the related divergence equations and boundary conditions can be derived by considering the generalized variational principle [10]:

$$\delta\iiint_\Omega [H(\boldsymbol{\varepsilon}, \mathbf{E}) - f_i u_i - Q\phi]\mathrm{d}\Omega + \int_{\Gamma_t} \overline{t}_i \delta u_i \mathrm{d}s + \int_{\Gamma_q} \overline{q}_s \delta\phi \mathrm{d}s = 0 \tag{1.9}$$

where δ is the variational symbol, f_i the body force vector, Q the electric charge density, and Ω is the solution domain. Γ_t and Γ_q are the boundaries on which the surface traction and surface charge are prescribed, respectively. $\overline{t}_i$ and $\overline{q}_s$ are the prescribed surface traction and surface charge, respectively.

The variational equation (1.9) provides the following results:

$$\sigma_{ij,j} + f_i = 0, \quad D_{i,i} + Q = 0 \qquad (\text{in } \Omega) \tag{1.10}$$

$$\sigma_{ij} n_j = \overline{t}_i \quad (\text{on } \Gamma_t), \quad D_i n_i = -\overline{q}_s \quad (\text{on } \Gamma_q) \tag{1.11}$$

and the constitutive equations (1.5), where n_i is the unit outward normal vector to Γ. Equations (1.10) are the elastic equilibrium equations and Gauss' law of electrostatics, respectively, Eqs. (1.11) are boundary conditions and Eqs. (1.5) the constitutive equations.

The boundary value problems defined by Eqs. (1.2), (1.5), (1.10), and (1.11) should be completed by the following essential boundary conditions:

$$u_i = \overline{u}_i \quad (\text{on } \Gamma_u), \quad \phi = \overline{\phi} \quad (\text{on } \Gamma_\phi) \tag{1.12}$$

where $\overline{u}_i$ and $\overline{\phi}$ are prescribed displacements and electrical potential, and Γ_u and Γ_ϕ are the parts of Γ $(= \Gamma_u \bigcup \Gamma_t = \Gamma_q \bigcup \Gamma_\phi)$ on which the displacement and electric potential are prescribed, respectively.

Substitution of Eq. (1.2) into Eq. (1.6), and later into Eq. (1.10), results in

$$\begin{aligned} c_{11}u_{1,11} + \frac{1}{2}(c_{11}+c_{12})u_{2,12} + (c_{13}+c_{44})u_{3,13} + \frac{1}{2}(c_{11}-c_{12})u_{1,22} \\ + c_{44}u_{1,33} + (e_{31}+e_{15})\phi_{,13} + f_1 = 0 \end{aligned} \tag{1.13}$$

$$\begin{aligned} c_{11}u_{2,22} + \frac{1}{2}(c_{11}+c_{12})u_{1,12} + (c_{13}+c_{44})u_{3,23} + \frac{1}{2}(c_{11}-c_{12})u_{2,11} \\ + c_{44}u_{2,33} + (e_{31}+e_{15})\phi_{,23} + f_2 = 0 \end{aligned} \tag{1.14}$$

$$\begin{aligned} c_{44}u_{3,11} + (c_{44}+c_{13})(u_{1,31}+u_{2,32}) + c_{44}u_{3,22} + c_{33}u_{3,33} \\ + e_{15}(\phi_{,11}+\phi_{,22}) + e_{33}\phi_{,33} + f_3 = 0 \end{aligned} \tag{1.15}$$

$$\begin{aligned} e_{15}(u_{3,11}+u_{3,22}) + (e_{15}+e_{31})(u_{1,31}+u_{2,32}) + e_{33}u_{3,33} \\ - \kappa_{11}(\phi_{,11}+\phi_{,22}) - \kappa_{33}\phi_{,33} + Q = 0 \end{aligned} \tag{1.16}$$

for transversely isotropic materials (class C_{6v}=6*mm*) with x_3 as the poling direction and the x_1-x_2 plane as the isotropic plane.

1.2.2 Boundary conditions

In electroelasticity theory, mechanical boundary conditions are formulated just as in classical elasticity theory. The electric boundary conditions are, however, still debated. The first attempt to define the electric boundary conditions over crack faces was by Parton [15]. He assumed that although the magnitude of the normal electri-

cal displacement component at the crack face is very small, the electrical displacement is continuous across the crack faces. He used the following electric boundary conditions:

$$\phi^+ = \phi^-, \qquad D_n^+ = D_n^- \tag{1.17}$$

Later, Hao and Shen [16] improved on the above assumption by considering the electric permeability of air in the crack gap. In addition to Eq. (1.17), they presented an equation for the boundary condition at crack faces:

$$D_n^+ = D_n^-, \qquad D_n^+(u_n^+ - u_n^-) = -\kappa_a(\phi^+ - \phi^-) \tag{1.18}$$

where κ_a is the permittivity of air. However, Eq. (1.18) has for a long time remained disregarded due to its complex mathematical treatment.

As pointed out by Suo et al. [17], the above assumption is not physically realistic as there will clearly be a potential drop across the lower capacitance crack. This is particularly true for those piezoelectric ceramics with permittivity 10^3 times higher than the environment (e.g. air or vacuum). For this reason, Deeg [18] proposed another set of electric boundary conditions over crack faces:

$$D_n^+ = D_n^- = 0 \tag{1.19}$$

Equation (1.19) are derived from the constitutive equation $D_n = \kappa_a E_n$. This is equivalent to having crack surfaces free of surface charge as the electrical boundary condition, and thus the electric displacement vanishes in the environment. We adopt Eq. (1.19) in most of the subsequent chapters because of its much simpler mathematical treatment and the fact that the dielectric constants of a piezoelectric material are much larger than those of the environment (generally between 1 000 and 3 500 times greater).

1.3 Functionally graded piezoelectric materials

Functionally graded materials (FGMs) are composite materials formed of two or more constituent phases with a continuously variable composition. This feature can eliminate the stress discontinuity that is often encountered in laminated composites and thus can avoid delamination-related problems. Traditionally, homogeneous laminas with different properties are bonded together to form laminated composite structures for engineering applications. The discontinuity of material properties across adjoining layers in a laminated composite can, however, result in crack initiation or delamination at the interfaces. To mitigate those disadvantages of laminated composite structures, a new class of piezoelectric materials called FGPMs has recently been developed. The FGPM is a kind of piezoelectric material intentionally designed to possess desirable properties for specific applications, and featuring ma-

terial composition and properties varying continuously in desired direction(s). Smart structures or elements made of FGPM are thus superior to conventional sensors, and actuators are often made of uni-morph, bi-morph and multimorph materials. This is because, for piezoelectric laminates with layered materials having homogeneous properties, large bending displacements, high stress concentrations, creep at high temperature and failure from interfacial bonding frequently occur at the layer interfaces under mechanical or electric loading. These effects can lead to reduced reliability and lifespan.

1.3.1 Types of gradation

The mechanical, electrical, magnetic, and thermal properties of FGMs are usually assumed to have the same functions of certain space coordinates. Three commonly-used graded forms are.

(1) Exponential material gradation.

All the material constants including elastic constants, piezoelectric parameters, dielectric constants, thermal expansion coefficients, and material density follow the exponential law:

$$M_{ij} = M_{ij}^{0} e^{\beta x} \tag{1.20}$$

where M_{ij} represents material constants such as c_{ij}, or f_{ij}, M_{ij}^{0} are the corresponding values at the plane x=0, and β denotes a material graded parameter.

(2) Quadratic material gradation.

All material constants are assumed to have the same power-law dependence on the coordinate x:

$$M_{ij} = M_{ij}^{0}(1+\beta x)^{n} \tag{1.21}$$

where n is the inhomogeneous constant determined empirically.

(3) Trigonometric material gradation.

For some special applications, the material constants of FGMs may follow a trigonometric law as [19]

$$M_{ij} = M_{ij}^{0}(a_1 \cos \beta X_2 + a_2 \sin \beta X_2)^{n} \tag{1.22}$$

where a_1, a_2, β and n are four material constants.

1.3.2 Basic equations for two-dimensional FGPMs

The field equations of electroelasticity reduce to two-dimensional form in two special cases which are of some interest.

(1) Plane strain.

Consider a transversely isotropic FGPM. In this case, according to Eq. (1.6), the *x*-*y* plane is the isotropic plane, and one can employ either the *x*-*z* or *y*-*z* plane for the study of plane electromechanical phenomena. Choosing the former, the plane strain conditions require that

$$\varepsilon_{yy} = \varepsilon_{zy} = \varepsilon_{xy} = E_y = 0 \tag{1.23}$$

By substitution of Eq. (1.23) into Eq. (1.6), we have

$$\begin{Bmatrix} \sigma_x \\ \sigma_z \\ \sigma_{xz} \\ D_x \\ D_z \end{Bmatrix} = \begin{bmatrix} c_{11} & c_{13} & 0 & 0 & e_{31} \\ c_{13} & c_{33} & 0 & 0 & e_{33} \\ 0 & 0 & c_{55} & e_{15} & 0 \\ 0 & 0 & e_{15} & -\kappa_{11} & 0 \\ e_{31} & e_{33} & 0 & 0 & -\kappa_{33} \end{bmatrix} \begin{Bmatrix} \varepsilon_x \\ \varepsilon_z \\ \gamma_{xz} \\ -E_x \\ -E_z \end{Bmatrix} \tag{1.24}$$

or inversely

$$\begin{Bmatrix} \varepsilon_x \\ \varepsilon_z \\ \gamma_{xz} \\ -E_x \\ -E_z \end{Bmatrix} = \begin{bmatrix} a_{11} & a_{13} & 0 & 0 & b_{31} \\ a_{13} & a_{33} & 0 & 0 & b_{33} \\ 0 & 0 & a_{55} & b_{15} & 0 \\ 0 & 0 & b_{15} & -\delta_{11} & 0 \\ b_{31} & b_{33} & 0 & 0 & -\delta_{33} \end{bmatrix} \begin{Bmatrix} \sigma_x \\ \sigma_z \\ \sigma_{xz} \\ D_x \\ D_z \end{Bmatrix} \tag{1.25}$$

where a_{ij}, b_{ij} and δ_{ij} are the reduced material constants. They are related to the elastic compliance tensor f_{ij}, the piezoelectric tensor g_{ij}, and the dielectric impermeability tensor β_{ij} by the following relations [20]:

$$\begin{aligned} &a_{11} = f_{11} - \frac{f_{12}^2}{f_{11}},\ a_{13} = f_{13} - \frac{f_{12}f_{13}}{f_{11}},\ a_{33} = f_{33} - \frac{f_{13}^2}{f_{11}},\ a_{55} = f_{55},\ b_{15} = g_{15}, \\ &b_{31} = g_{31} - \frac{g_{31}f_{12}}{f_{11}},\ b_{33} = g_{33} - \frac{g_{31}f_{13}}{f_{11}},\ \delta_{11} = \beta_{11},\ \delta_{33} = \beta_{33} - \frac{g_{31}^2}{f_{11}} \end{aligned} \tag{1.26}$$

with f_{ij}, g_{ij} and β_{ij} being defined in Table 1.1. In the constitutive equations (1.39) and (1.40), $-E_i$ is used instead of E_i because it will allow the construction of a symmetric generalized linear response matrix which will prove to be advantageous. When the constitutive equation (1.24) is substituted into Eq. (1.10) we obtain

$$\left(c_{11}u_{1,1} + c_{13}u_{3,3} + e_{31}\phi_{,3}\right)_{,1} + \left(c_{55}[u_{3,1} + u_{1,3}] + e_{15}\phi_{,1}\right)_{,3} + f_1 = 0 \tag{1.27}$$

$$\left(c_{55}[u_{3,1} + u_{1,3}] + e_{15}\phi_{,1}\right)_{,1} + \left(c_{13}u_{1,1} + c_{33}u_{3,3} + e_{33}\phi_{,3}\right)_{,3} + f_3 = 0 \tag{1.28}$$

$$\left(e_{15}[u_{3,1}+u_{1,3}]-\kappa_{11}\phi_{,1}\right)_{,1}+\left(e_{31}u_{1,1}+e_{33}u_{3,3}-\kappa_{33}\phi_{,3}\right)_{,3}+Q=0 \tag{1.29}$$

in which the material constants c_{ij}, e_{ij}, κ_{ij}, a_{ij}, b_{ij}, and δ_{ij} are functions of coordinates. When the Airy stress function approach is used to solve this equation [21], the solution can be divided into two major parts: a homogeneous solution part and a particular solution part. For the homogeneous solution part, the required strain compatibility equation and the Airy function U are, respectively, expressed by

$$\varepsilon_{1,33}+\varepsilon_{3,11}-\gamma_{13,13}=0 \tag{1.30}$$

$$\sigma_x=U_{,33},\quad \sigma_z=U_{,11},\quad \sigma_{xz}=-U_{,13} \tag{1.31}$$

For most applications of FGPMs, the material properties are designed to vary continuously in one direction only, say, the z-direction. Substituting Eqs. (1.2), (1.24), (1.25), and (1.31) into Eqs. (1.30) and (1.29), we have [21]

$$\left(b_{31}U_{,33}\right)_{,3}+\left(b_{33}U_{,11}\right)_{,3}-b_{15}U_{,113}=\left(\delta_{33}\phi_{,3}\right)_{,3}+\delta_{11}\phi_{,11} \tag{1.32}$$

$$\begin{aligned}&\left(a_{11}U_{,33}+a_{13}U_{,11}\right)_{,33}+\left(a_{55}U_{,113}\right)_{,3}+a_{13}U_{,1133}+a_{33}U_{,1111}\\&\quad=\left(b_{13}\phi_{,3}\right)_{,33}+b_{33}\phi_{,113}-\left(b_{15}\phi_{,11}\right)_{,3}\end{aligned} \tag{1.33}$$

(2) Anti-plane deformation.

In this case only the out-of-plane elastic displacement u_3 and the in-plane electric fields are non-zero, i.e.,

$$\begin{aligned}&u=v=0, \qquad w=w(x,y),\\&E_x=E_x(x,y),\quad E_y=E_y(x,y),\quad E_z=0\end{aligned} \tag{1.34}$$

Thus the constitutive equation (1.6) is simplified to

$$\begin{Bmatrix}\sigma_{xz}\\ \sigma_{yz}\\ D_x\\ D_y\end{Bmatrix}=\begin{bmatrix}c_{55}&0&0&e_{15}\\0&c_{55}&e_{15}&0\\0&e_{15}&-\kappa_{11}&0\\e_{15}&0&0&-\kappa_{11}\end{bmatrix}\begin{Bmatrix}\gamma_{xz}\\ \gamma_{yz}\\ -E_x\\ -E_y\end{Bmatrix} \tag{1.35}$$

The governing equations (1.10) become

$$\begin{aligned}&\left(c_{44}u_{3,1}+e_{15}\phi_{,1}\right)_{,1}+\left(c_{44}u_{3,2}+e_{15}\phi_{,2}\right)_{,2}+f_3=0\\&\left(e_{15}u_{3,1}-\kappa_{11}\phi_{,1}\right)_{,1}+\left(e_{15}u_{3,2}-\kappa_{11}\phi_{,2}\right)_{,2}+Q=0\end{aligned} \tag{1.36}$$

1.4 Fibrous piezoelectric composites

Due to the coupling effect between mechanical and electrical fields, piezoelectric

materials have been widely used in smart structures and other applications such as electromechanical sensors, ultrasonic transducers, hydrophones, micropositioning devices, buzzers, accelerometers, and structural actuators [10]. However, when serving as sensors and actuators, single-phase piezoelectric ceramic materials are often unable to meet the increased demands from modern industry for high mechanical performance and special structural functions, because of their intrinsic brittleness and the existence of microcracks and defects in most piezoelectric ceramic materials. To overcome these drawbacks, piezoelectric material is usually embedded in non-piezoelectric materials in the form of fiber-matrix composites [22]. A composite configuration for structural actuation with significant advantages over conventional piezoelectric actuators has been conceived, and the recent development of piezoelectric ceramic fibers <100 μm in diameter has enabled this concept to be realized. Nelson [22] has predicted that FPCs will find uses in contour control, non-destructive testing, vibration suppression, and noise control. The possibility of computer control using closed loop systems has led to FPC emerging as favored candidates for "smart" materials and structures. The first FPC were developed in the Active Materials and Structures Laboratory at the Massachusetts Institute of Technology and patented in 2000 [23]. Typically, an FPC comprises a monolayer of uniaxially aligned piezoelectric fibers embedded in a polymer matrix between two interdigitated surface electrodes through which the driving voltage is supplied. Since their initial development, significant advances have been made in many areas including fiber manufacture, matrix materials and design, electrode design, manufacturing techniques, and composite modeling.

At this time, various FPCs are used in practical engineering including:

(1) 1-3 piezo fiber composites.

The 1-3 piezoelectric composite is the classification given in Newnham's connectivity theory [24] for the identification of composites containing piezoelectric ceramic rods in a polymer matrix. In Newnham's connectivity theory there are ten important connectivity patterns in diphasic solids: 0-0, 1-0, 2-0, 3-0, 1-1, 2-1, 3-1, 2-2, 3-2, and 3-3. A 3-1 (or 1-3) connectivity pattern, for example, has one phase self-connected in three-dimensional layers, the other self-connected in one-dimensional chains. The 1-3 piezo fiber composites are produced with the aim of obtaining a combination of piezoelectric and mechanical properties which are useful in electromechanically transducing applications. In the 1-3 connectivity, parallel fibers are embedded in a matrix in the longitudinal (z) direction. Work on piezoelectric materials in transducers highlights the fact that piezoelectric composites have more desired properties than single phase piezoelectric materials. For example, a composite with PZT volume fraction of 40% can have a value of d_{33}, almost the same as the PZT ceramic itself.

Various fabrication processes exist for different configurations and connectivities of FPCs. In general, the fabrication processes include poling of the PZT fi-

bers/rods; the fibers are arranged in a mold, infiltrated with epoxy, cured, and diced to produce cube-shaped blocks; the composite can be poled at the very last stage or the fibers can be prepoled before embedding in the matrix. A typical method of fabricating composites presented in [25] is casting the polymer around the aligned PZT rods, the "lost wax" method, the "dice-and-fill" technique and a lamination process. PZT fibers may be produced by sol-gel processing, the relic process, or the viscous suspension spinning process [26]. Several processes using different organic solutions were prepared in terms of the stiffness of the fibers and compaction [27]. It was found that when a certain amount of specified solutions was added, the flexibility and compaction of the resulting fibers were optimized.

The material parameters for composites, such as compliance, stiffness, permittivity and piezoelectric constants, are obviously dependent on the arrangement of the matrix and fibers in the composite. Calculation of effective composite parameters as a function of volume fraction is based on the rules of mixture [28]. The calculation is based on the following assumptions: (a) Composite strain in the longitudinal direction (z) is equal to the fiber strain and also to the matrix in the same direction, and longitudinal composite stress is the weighted sum of the matrix stress and the fiber stress. (b) Lateral composite stress is equal to lateral fiber stress and also to the matrix stress, and lateral composite strain is the weighted sum of the corresponding matrix and fiber strains. (c) Longitudinal composite electric field is the same as that of matrix and also that of fiber. There is no lateral composite electric field. (d) Longitudinal composite electric displacement is the weighted sum of matrix and fiber electric displacement. It should be mentioned that most piezoelectric 1-3 fiber composite micromechanics models were initially developed for ultrasonic transducer applications, but their methods can be applied to applications of piezoelectric fiber composites in other smart structures. A review of the 1-3 piezoelectric composite in high-frequency (0.5 MHz) applications was given in [29].

(2) FPC with interdigitated electrodes (IDE).

The 1-3 piezo composites have already demonstrated substantial advantages over monolithic piezoelectric ceramics, but, as indicated in [30], one major drawback remains from the previous work in 1-3 piezo composites—low actuation performance. The high dielectric mismatch between fiber and matrix (approximately three orders of magnitude in size) seriously reduces the electric field available to the fiber material for actuation. Furthermore, high field concentrations in the polymer-based matrix often cause dielectric breakdown prior to poling. These problems can be addressed by introducing IDE technology into FPCs [31]. In 1993, Hagood et al. [32] developed something similar to a circuit layer with electrodes, called IDE, and placed them on the top and bottom surfaces of the piezoceramic layer. This allowed the electric field to be applied in the transverse direction of a piezoceramic, thus maximizing the transverse actuation. Later Bent and Hagood [31] introduced IDE to FPCs. As shown in Fig. 1.4 there are three main constituents of an FPC-IDE:

piezoelectric fibers, IDE and a polymer matrix. The fibers are typically circular in cross section and made by an extrusion process, but can also be fabricated using molding techniques or by slicing monolithic piezoelectric sheets to obtain fibers of rectangular cross section. The metallic electrodes are normally made using photolithography. The polymeric matrix material is perhaps the constituent with the widest range of acceptable materials. Ideally, the matrix will have outstanding mechanical, and dielectric properties and will bond to the fibers in a consistent manner.

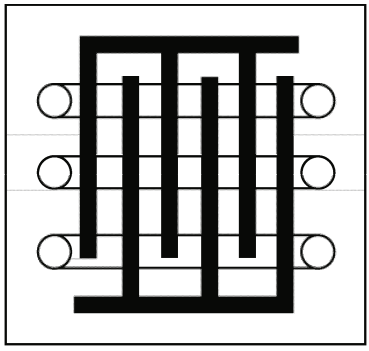

Fig. 1.4 FPC with IDE.

In the FPC-IDE shown in Fig. 1.4, fibers are aligned in plane, with orientation along the *z*-axis, while matrix material provides the load transfer and distribution along the fibers. The electrode patterns have fingers of alternating polarity, and exact mirror images on the top and bottom faces. Poling is predominantly along the *z*-axis direction. Application of an electric field produces primary actuation along the fibers and transverse actuation perpendicular to the fibers.

To model and investigate the improvement in the effective properties of FPC with IDE, Bent and Hagood [31] used an analytical model based on the uniform fields model (UFM) and a finite element model, both of which were formulated for a representative volume element (RVE). The UFM is a generalization of the well-known "rule of mixture" which uses parallel and series (Voight and Reuss) additions to model the effective properties of two-phase materials. The FPC consists of PZT fibers aligned within a graphite/epoxy lamina and is sandwiched between the IDE. As the name implies, the UFM assumes that the fields within the structure are uniform. The rest of the formulation is based on rules analogous to the rule of mixture for combining two different phases/materials in various configurations. This led to the development of combination models for more complex arrangements of the two phases. The UFM method, in fact, violates compatibility and equilibrium at some material interfaces. However, the large material mismatches make this method particularly well suited to modeling these types of composites [31].

(3) Hollow tube FPC.

Although FPC-IDE based on solid cross-section piezoelectric fibers are very useful for both longitudinal and transverse activation, they require high voltages and are constrained to nonconductive matrix materials. Particularly, they require the electric field to pass through the composite matrix. Due to the placement of the electrode on the matrix surface, electric field losses are significant, requiring high voltages for actuation. Moreover, the FPC-IDE limit the matrix to electrically nonconductive materials, which is particularly a problem in large structure and air vehicle applications where metals and carbon fiber composites are almost exclusively utilized in construction. To overcome these drawbacks, a new type of FPC has been fabricated using extruded hollow cross-section fibers [33]. Use of FPCs with hollow cross-section piezoelectric fibers can lower operating voltages and broaden the choice of possible matrix materials. In the hollow tube FPC, hollow fibers are individually electroded on both the inside and outside surfaces [27]. They are activated by an electric field applied directly across the walls of the fiber, generating longitudinal strain due to piezoelectric d_{31} mode. Even though the longitudinal strain is decreased by approximately half by using d_{31} versus the d_{33} mode used in solid fiber FPCs, the required voltage can be decreased by a factor of 10 or more since the electric field is applied only across the wall of the fiber instead of through the matrix, thereby eliminating field losses [34].

Several existing processes, based on molding or extrusion techniques, are available for fabricating hollow piezoelectric fibers [27]. Since the fibers have small diameters, on the order of 0.9 mm, a new manufacturing technique has been implemented called microfabrication by coextrusion (MFCX) [33]. MFCX is capable of inexpensively producing long ceramic forms (>100 mm long) with complex cross-section and small features. Manufacturing of fibers with MFCX consists of three major steps, formation of feed rod, extrusion, and burnout/sintering [35]. As described in [35], the feed rod formation process has two main steps. The first is to mix piezoelectric powder with thermoplastic polymers and to separately mix the same polymers with carbon black powder so that the two mixes have nearly the same viscosity. The piezoelectric mix is then formed into a round, thick-walled tube, while part of the carbon black mix is formed into a round cylinder with diameter exactly the same as the inside of the piezoelectric tube. The remainder of the carbon black mix is formed into a square cross-section block with the same dimension as the inlet to the extrusion die, while a circular hole is bored into the center of the square, with exactly the same diameter as the outside of the piezo tube. These three components are then assembled, with the carbon black cylinder inside the hollow piezo tube, which in turn is placed inside the square block. The extrusion process begins when the assembled feed rod is heated and inserted into the extrusion die, which turns to reducing the cross-section of the feeder rod by a factor of 25 or 40, depending on the desired final tube dimensions. The resulting “green” fibers are

then heated to and held at 1 300 ℃ for 48 hours during the burnout and sintering step. This causes the carbon to be burned off from the exterior and interior of the tube and causes the thermoplastics to be removed from the piezoceramic material, which produces a stronger, denser ceramic and is accompanied typically by a 30% reduction in the cross-section of the finished hollow tube.

To assess the strain response of a piezo tube FPC under an electric field, Zhang et al. [36] presented a simple model detailed as follows: For a tubular structure, the cylindrical polar coordinate system (r, θ, z) as shown in Fig. 1.5 is used. The problem is assumed to be axi-symmetric and all fields are independent of polar angle θ and the displacement u_θ=0. To simplify the analysis it is further assumed that the coupling terms containing both r and z in the displacements field can be neglected and u_r= $u_r(r)$, u_z=$u_z(z)$. Under these assumptions, the non-zero strain components are

$$\varepsilon_r = u_{r,r}, \qquad \varepsilon_\theta = u_r / r, \qquad \varepsilon_z = u_{z,z} \tag{1.37}$$

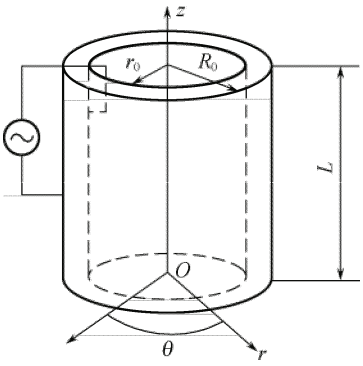

Fig. 1.5 Schematic drawing of a piezoelectric tube.

Making use of the constitutive equation (1.6), we have

$$\begin{aligned}
\sigma_r &= c_{11}\varepsilon_r + c_{12}\varepsilon_\theta + c_{12}\varepsilon_z - e_{33}E_r, \\
\sigma_\theta &= c_{12}\varepsilon_r + c_{11}\varepsilon_\theta + c_{12}\varepsilon_z - e_{31}E_r, \\
\sigma_z &= c_{12}\varepsilon_r + c_{12}\varepsilon_\theta + c_{11}\varepsilon_z - e_{31}E_r
\end{aligned} \tag{1.38}$$

where E_r is the applied electric field on the tube wall along the r direction. It is obvious that the electric field is not a constant inside the tube wall, and with a total voltage V applied on the tube, $E_r = V/[r\ln(R_0/r_0)]$ $(r_0 \leqslant r \leqslant R_0)$. In writing Eq. (1.38), Zhang et al. [36] also made the assumption that the tube is elastically isotropic to simplify the analysis. Making use of the equilibrium equation (1.10) and Eqs. (1.38), we can derive the basic elastic equations for this problem

$$\left(\frac{1}{r}\left[ru_r\right]_{,r}\right)_{,r} = -\left(\frac{1}{r}e_{31}E_r\right)\frac{a_{11}(1+\upsilon)(1-2\upsilon)}{1-\upsilon}, \qquad u_{z,z} = \text{constant} \tag{1.39}$$

where a_{11} is defined in Eq. (1.26), and υ is the Poisson's ratio. The solutions to Eq. (1.39) are then

$$u_r = ar + \frac{b}{r} + \left(\frac{e_{31}V}{\ln(R_0/r_0)}\right)\frac{a_{11}(1+\upsilon)(1-2\upsilon)}{1-\upsilon}, \qquad u_z = cz \tag{1.40}$$

in which a, b, and c are the integration constants which can be determined from the boundary conditions: $\varepsilon_z = d_{31}E_m$, where E_m is the average electric field in the tube and $E_m = 2V/[(R_0 + r_0)\ln(R_0/r_0)]$; at $r = R_0$ and r_0 there is no external stress on the tube wall, which implies $\sigma_r = 0$ at these two boundaries. Substituting Eq. (1.40) into Eq. (1.38) and using the boundary conditions, we obtain

$$a = E_m\frac{(1-2\upsilon)d_{33} - \upsilon d_{31}}{2(1-\upsilon)}, \qquad b = -R_0r_0E_m\frac{d_{33} + \upsilon d_{31}}{2(1-\upsilon)}, \qquad c = d_{31}E_m \tag{1.41}$$

All the strain components for the tube can be obtained from Eqs. (1.40) and (1.41). Making use of the solution, Zhang et al. [36] analyzed a typical hollow tube FPC and found that the effective piezoelectric constant in the radial direction of a tube could be changed from positive to negative by adjusting the ratio R_0/r_0 for piezoelectric materials. Therefore, it is possible to make a piezoelectric transducer with all the effective piezoelectric tensile constants having the same sign.

References

[1] Curie J, Curie P: Development par compression de l'eletricite polaire dans les cristaux hemiedres a faces inclines. Bulletin no. 4 de la Societe Mineralogique de France **3**, 90(1880) and Comptes Rendus Acad. Sci. Paris **91**, 294 (1880).

[2] Lippmann HG: Sur le principe de la conversation de l'eletricite ou second principe de la theorie des phenomenes electriques. Comptes Rendus Acad. Sci. Paris **92**, 1049 (1881).

[3] Curie J, Curie P: Contractions et dilations productes par des tensions electriques dans les cristaux hemiedres a faces inclines. Comptes Rendus Acad. Sci. Paris **93**, 1137 (1884).

[4] Voigt W: General theory of the piezo and pyroelectric properties of crystals. Abh. Gott. **36**, 1 (1890).

[5] Cady WG: Piezoelectricity, Vol. 1 & 2. Dover Publishers, New York (1964).

[6] Tiersten HF: Linear Piezoelectric Plate Vibrations. Plenum Press, New York (1969).

[7] Parton VZ, Kudryavtsev BA: Electromagnetoelasticity, Piezoelectrics and Electrically Conductive Solids. Gordon and Breach Science Publishers, New York (1988).

[8] Ikeda T: Fundamentals of Piezoelectricity. Oxford Science Publications, New York

(1990).
[9] Rogacheva NN: The Theory of Piezoelectric Shells and Plates. CRC Press, Boca Raton (1994).
[10] Qin QH: Fracture Mechanics of Piezoelectric Materials. WIT Press, Southampton (2001).
[11] Qin QH: Green's Function And Boundary Elements in Multifield Materials. Elsevier, Oxford (2007).
[12] Qin QH, Yang QS: Macro-Micro Theory on Multifield Behaviour of Heterogeneous Materials. Higher Education Press & Springer, Beijing (2008).
[13] Kistler: The Piezoelectric Effect, Theory, Design and Usage. http://www.designinfo.com/kistler/ref/tech_theory_text.htm (2010). Accessed 15 March 2011.
[14] Qin QH: Variational formulations for TFEM of piezoelectricity. International Journal of Solids and Structures **40**(23), 6335-6346 (2003).
[15] Parton VZ: Fracture mechanics of piezoelectric materials. Acta Astronautica **3**, 671-683 (1976).
[16] Hao TH, Shen ZY: A new electric boundary condition of electric fracture mechanics and its applications. Engineering Fracture Mechanics **47**(6), 793-802 (1994).
[17] Suo Z, Kuo CM, Barnett DM, Willis JR: Fracture mechanics for piezoelectric ceramics. Journal of the Mechanics and Physics of Solids **40**(4), 739-765 (1992).
[18] Deeg WF: The analysis of dislocation, crack, and inclusion problems in piezoelectric solids. PhD Thesis, Stanford University (1980).
[19] Sutradhar A, Paulino GH: The simple boundary element method for transient heat conduction in functionally graded materials. Computer Methods in Applied Mechanics and Engineering **193**(42-44), 4511-4539 (2004).
[20] Sosa H: On the fracture-mechanics of piezoelectric solids. International Journal of Solids and Structures **29**(21), 2613-2622 (1992).
[21] Zhong Z, Yu T: Electroelastic analysis of functionally graded piezoelectric material beams. Journal of Intelligent Material Systems and Structures **19**(6), 707-713 (2008).
[22] Nelson LJ: Smart piezoelectric fibre composites. Materials Science and Technology **18**(11), 1245-1256 (2002).
[23] Hagood N, Bent A: Composites for structural control. US Patent, 6048622 (2000).
[24] Newnham RE, Skinner DP, Cross LE: Connectivity and piezoelectric-pyroelectric composites. Materials Research Bulletin **13**(5), 525-536 (1978).
[25] Smith WA: The role of piezoelectric in ultrasonic transducers. IEEE 1989 Ultrasonic Symposium, 755-766 (1989).
[26] Safari A, Janas V, Jadidian B: Incorporation of piezoelectric $Pb(Zr,Ti)O_3$ fibre into ceramic/polymer composites. Proc. SPIE **2721**, 240-250 (1996).
[27] Brei D, Cannon BJ: Piezoceramic hollow fiber active composites. Composites Science and Technology **64**(2), 245-261 (2004).
[28] Chan HLW, Unsworth J: Simple model for piezoelectric ceramic polymer 1-3 composites used in ultrasonic transducer applications. IEEE Transactions on Ultrasonic, Ferroelectrics & Frequency Control **36**, 434-441 (1989).
[29] Chan HLW, Guy IL: Piezoelectric ceramic/polymer composites for high frequency applications. Key Engineering Materials **92-93**, 275-300 (1994).
[30] Bent AA, Hagood NW: Piezoelectric fiber composites with interdigitated electrodes.

Journal of Intelligent Material Systems and Structures **8**(11), 903-919 (1997).

[31] Bent AA, Hagood NW: Improved performance in piezoelectric fibre composites using interdigitated electrodes. Proc. SPIE **2441**, 196-212(1995).

[32] Hagood NW, Kindel R, Ghandi K, Gaudenzi P: Improving transverse actuation of piezoceramics using interdigitated surface electrodes. Proc. SPIE **1917**, 341-352 (1993).

[33] Cannon BJ, Brei D: Feasibility study of microfabrication by coextrusion (MFCX) hollow fibers for active composites. Journal of Intelligent Material Systems and Structures **11**(9), 659-670 (2000).

[34] Fernandez JF, Dogan A, Zhang QM, Tressler JF, Newnham RE: Hollow piezoelectric composites. Sensors and Actuators A: Physical **51**(2-3), 183-192 (1995).

[35] Williams RB, Park G, Inman DJ, Wilkie WK: An overview of composite actuators with piezoceramic fibers. Proc. SPIE **4753**, 421-427 (2002).

[36] Zhang QM, Wang H, Cross LE: Piezoelectric tubes and tubular composites for actuator and sensor applications. Journal of Materials Science **28**(14), 3962-3968 (1993).

Chapter 2 Solution Methods

In this chapter, the solution methods commonly used in analyzing the mechanical behavior of piezoelectric material are reviewed. The chapter begins with a summary of the potential function method in piezoelectricity, followed by a discussion of other methods including Lekhnitskii formalism, techniques of Fourier transformation, the Trefftz finite element method(FEM), the Fredholm integral equation and Abel equation, the shear-lag model, the symplectic method, and the state space approach.

2.1 Potential function method

Potential function formulation is well known for solving the system of equations in both the classical theory of elasticity and piezoelectricity. In this section, the potential function method for boundary value problems of three-dimensional (3D) piezoelectricity is briefly summarized [1,2]. For a 3D piezoelectric problem of hexagonal solids of class 6*mm*, the four unknowns u_1, u_2, u_3, ϕ are to be expressed in terms of four potential functions $\zeta(x_1, x_2, x_3)$, $\chi(x_1, x_2, x_3)$, $\varpi(x_1, x_2, x_3)$, and $\Theta(x_1, x_2, x_3)$ in such a way that [1]

$$u_1 = \zeta_{,1} + \chi_{,2}, \qquad u_2 = \zeta_{,2} - \chi_{,1}, \qquad u_3 = k\zeta_{,3} + \varpi_{,3}, \qquad \phi = \Theta_{,3} \tag{2.1}$$

where k is an unknown coefficient. Then, consider the problem of the piezoelectricity of a hexagonal body of class 6*mm* subjected to electroelastic loadings. The constitutive equations for the electroelastic field are expressed as

$$\boldsymbol{\sigma} = \mathbf{c}\boldsymbol{\varepsilon} - \mathbf{e}^{\mathrm{T}}\mathbf{E}, \qquad \mathbf{D} = \mathbf{e}\boldsymbol{\varepsilon} + \boldsymbol{\kappa}\mathbf{E} \tag{2.2}$$

where the superscript represents the transpose of a matrix, and

$$\boldsymbol{\sigma} = \begin{Bmatrix} \sigma_{11} \\ \sigma_{22} \\ \sigma_{33} \\ \sigma_{23} \\ \sigma_{31} \\ \sigma_{12} \end{Bmatrix}, \quad \mathbf{c} = \begin{bmatrix} c_{11} & c_{12} & c_{13} & 0 & 0 & 0 \\ c_{12} & c_{22} & c_{23} & 0 & 0 & 0 \\ c_{13} & c_{23} & c_{33} & 0 & 0 & 0 \\ 0 & 0 & 0 & c_{44} & 0 & 0 \\ 0 & 0 & 0 & 0 & c_{44} & 0 \\ 0 & 0 & 0 & 0 & 0 & (c_{11} - c_{12})/2 \end{bmatrix}, \quad \boldsymbol{\varepsilon} = \begin{Bmatrix} \varepsilon_{11} \\ \varepsilon_{22} \\ \varepsilon_{33} \\ \varepsilon_{23} \\ \varepsilon_{31} \\ \varepsilon_{12} \end{Bmatrix},$$

$$\mathbf{e} = \begin{bmatrix} 0 & 0 & 0 & 0 & e_{15} & 0 \\ 0 & 0 & 0 & e_{15} & 0 & 0 \\ e_{31} & e_{31} & e_{33} & 0 & 0 & 0 \end{bmatrix}, \quad \boldsymbol{\kappa} = \begin{bmatrix} \kappa_{11} & 0 & 0 \\ 0 & \kappa_{11} & 0 \\ 0 & 0 & \kappa_{33} \end{bmatrix},$$

$$\mathbf{D}=\begin{Bmatrix}D_1\\D_2\\D_3\end{Bmatrix},\qquad \mathbf{E}=\begin{Bmatrix}E_1\\E_2\\E_3\end{Bmatrix}$$

Making use of Eqs. (1.2) and (2.2) and then substituting Eq. (2.1) into the governing differential equations (1.10), in which all body forces and free charges are assumed to be zero, the following four equations result:

$$\begin{bmatrix} c_{11}\nabla+\alpha_1\dfrac{\partial^2}{\partial z^2} & (c_{13}+c_{44})\dfrac{\partial^2}{\partial z^2} & (e_{31}+e_{15})\dfrac{\partial^2}{\partial z^2}\\ (c_{13}+\alpha_2)\nabla+kc_{33}\dfrac{\partial^2}{\partial z^2} & c_{44}\nabla+c_{33}\dfrac{\partial^2}{\partial z^2} & e_{15}\nabla+e_{33}\dfrac{\partial^2}{\partial z^2}\\ (e_{31}+\alpha_3)\nabla+ke_{33}\dfrac{\partial^2}{\partial z^2} & e_{15}\nabla+e_{33}\dfrac{\partial^2}{\partial z^2} & -\kappa_{11}\nabla-\kappa_{33}\dfrac{\partial^2}{\partial z^2}\end{bmatrix}\begin{Bmatrix}\zeta\\ \varpi\\ \Theta\end{Bmatrix}=0 \tag{2.3}$$

$$\Delta\chi+\xi\frac{\partial^2\chi}{\partial z^2}=0 \tag{2.4}$$

where

$$\nabla=\frac{\partial^2}{\partial x^2}+\frac{\partial^2}{\partial y^2},\qquad \alpha_1=kc_{13}+(1+k)c_{44},\qquad \alpha_2=(1+k)c_{44},$$

$$\alpha_3=(1+k)e_{15},\qquad \xi=\frac{2c_{44}}{c_{11}-c_{12}}$$

This reduces to the formulation in [2] when k =0. In the following, we review briefly the results presented in [2]. To obtain the solution to Eq. (2.3), Wang and Agrawal [2] assumed that the solution of ζ, ϖ, and Θ had the following form:

$$\begin{Bmatrix}\zeta\\ \varpi\\ \Theta\end{Bmatrix}=\int_0^\infty\int_0^\infty\begin{Bmatrix}A\\B\\C\end{Bmatrix}\cos(\alpha x)\cos(\beta y)e^{mz}\,\mathrm{d}\alpha\,\mathrm{d}\beta \tag{2.5}$$

Substituting Eq. (2.5) into Eq. (2.3), we obtain

$$\begin{bmatrix} -c_{11}\gamma^2+\alpha_1m^2 & (c_{13}+c_{44})m^2 & (e_{31}+e_{15})m^2\\ -(c_{13}+\alpha_2)\gamma^2+kc_{33}m^2 & -c_{44}\gamma^2+c_{33}m^2 & -e_{15}\gamma^2+e_{33}m^2\\ -(e_{31}+\alpha_3)\gamma^2+ke_{33}m^2 & -e_{15}\gamma^2+e_{33}m^2 & \kappa_{11}\gamma^2-\kappa_{33}m^2\end{bmatrix}\begin{Bmatrix}A\\B\\C\end{Bmatrix}=0 \tag{2.6}$$

where $\gamma^2=\alpha^2+\beta^2$. For simplicity, define

$$m^2=\frac{\gamma^2}{\mu} \tag{2.7}$$

Substituting Eq. (2.7) into Eq. (2.6) and setting the determinant of the matrix to zero, we obtain

$$R_3\mu^3 + R_2\mu^2 + R_1\mu + R_0 = 0 \tag{2.8}$$

where

$$\begin{aligned}
R_0 &= -c_{44}(e_{33}^2 + c_{33}\kappa_{33}),\\
R_1 &= -2e_{15}e_{33}c_{13} + c_{33}c_{11}\kappa_{33} - 2e_{33}e_{31}(c_{13} + c_{44})\\
&\quad + c_{33}e_{15}^2 + c_{11}e_{33}^2 - 2c_{13}c_{44}\kappa_{33} + 2c_{33}e_{15}e_{31}\\
&\quad + c_{33}c_{44}\kappa_{11} - c_{13}^2\kappa_{33} + e_{31}^2c_{33},\\
R_2 &= -2e_{15}e_{33}c_{11} + c_{13}^2\kappa_{11} + 2c_{13}e_{15}^2 - c_{33}c_{11}\kappa_{11}\\
&\quad + 2e_{15}e_{31}c_{13} - c_{44}e_{15}^2 - c_{11}c_{44}\kappa_{33} + 2c_{13}c_{44}\kappa_{11},\\
R_3 &= c_{11}c_{44}\kappa_{11} + c_{11}e_{15}^2
\end{aligned} \tag{2.9}$$

The three roots of Eq. (2.8) are denoted by μ_j (j=1, 2, 3). Corresponding to the three roots, the roots of Eq. (2.6) can be written as

$$m = \pm\frac{\gamma}{\sqrt{\mu_1}}, \quad \pm\frac{\gamma}{\sqrt{\mu_2}}, \quad \pm\frac{\gamma}{\sqrt{\mu_3}} \tag{2.10}$$

It is obvious that the solution to Eq. (2.6) is not unique. To solve this equation, Wang and Agrawal took A=1 and solved the resulting equation. After a series of mathematical operations the solution of Eq. (2.5) is obtained as

$$\zeta = \int_0^\infty\int_0^\infty \cos(\alpha x)\cos(\beta y)\sum_{i=1}^{3}\begin{bmatrix} G_i\cosh\left(\gamma z/\sqrt{\mu_i}\right)\\ +H_i\sinh\left(\gamma z/\sqrt{\mu_i}\right)\end{bmatrix}\mathrm{d}\alpha\mathrm{d}\beta \tag{2.11}$$

$$\varpi = \int_0^\infty\int_0^\infty \cos(\alpha x)\cos(\beta y)\sum_{i=1}^{3} b_i\begin{bmatrix} G_i\cosh\left(\gamma z/\sqrt{\mu_i}\right)\\ +H_i\sinh\left(\gamma z/\sqrt{\mu_i}\right)\end{bmatrix}\mathrm{d}\alpha\mathrm{d}\beta \tag{2.12}$$

$$\Theta = \int_0^\infty\int_0^\infty \cos(\alpha x)\cos(\beta y)\sum_{i=1}^{3} c_i\begin{bmatrix} G_i\cosh\left(\gamma z/\sqrt{\mu_i}\right)\\ +H_i\sinh\left(\gamma z/\sqrt{\mu_i}\right)\end{bmatrix}\mathrm{d}\alpha\mathrm{d}\beta \tag{2.13}$$

where (b_1,c_1), (b_2,c_2), and (b_3,c_3) are the solutions of (B,C) of Eq. (2.6) corresponding to $m = \pm\gamma/\sqrt{\mu_1}$, $\pm\gamma/\sqrt{\mu_2}$ and $\pm\gamma/\sqrt{\mu_3}$ respectively, and G_i and H_i are arbitrary constants which are determined using the boundary conditions.

2.2 Solution with Lekhnitskii formalism

The mathematical method known as the Lekhnitskii formalism was developed

originally to solve two-dimensional problems in elastic anisotropic materials [3]. The evolution of the method and a number of extensions to electroelastic problems were described in Refs. [4-7]. In this section the Lekhnitskii formalism of generalized plane piezoelectricity presented in [7] is briefly summarized. For a complete derivation and discussion, the reader is referred to Refs. [3-6].

Consider a generalized plane problem of piezoelectric materials, in which all physical quantities, such as stresses, strains, displacements, electric fields, electric displacements and the electric potential, are functions of x and y only. The generalized plane strain constitutive equations are governed by Eq. (2.2) or equations located in the second column and fourth row of Table 1.1 as follows:

$$\begin{Bmatrix} \varepsilon_{11} \\ \varepsilon_{22} \\ 2\varepsilon_{23} \\ 2\varepsilon_{13} \\ 2\varepsilon_{12} \\ -E_1 \\ -E_2 \end{Bmatrix} = \begin{bmatrix} f_{11} & f_{12} & f_{14} & f_{15} & f_{16} & g_{11} & g_{21} \\ f_{12} & f_{22} & f_{24} & f_{25} & f_{26} & g_{12} & g_{22} \\ f_{14} & f_{24} & f_{44} & f_{45} & f_{46} & g_{14} & g_{24} \\ f_{15} & f_{25} & f_{45} & f_{55} & f_{56} & g_{15} & g_{25} \\ f_{16} & f_{26} & f_{46} & f_{56} & f_{66} & g_{16} & g_{26} \\ g_{11} & g_{12} & g_{14} & g_{15} & g_{16} & -\beta_{11} & -\beta_{12} \\ g_{21} & g_{22} & g_{24} & g_{25} & g_{26} & -\beta_{12} & -\beta_{22} \end{bmatrix} \begin{Bmatrix} \sigma_{11} \\ \sigma_{22} \\ \sigma_{23} \\ \sigma_{13} \\ \sigma_{12} \\ D_1 \\ D_2 \end{Bmatrix} \tag{2.14}$$

where the materials f_{ij}, g_{ij}, and β_{ij} are defined in Eq. (1.8) and Table 1.1. The derivation of these constants can be found in Ref. [7].

Equation (2.14) constitutes a system of seven equations in 14 unknowns. Additional equations are provided by elastic equilibrium and Gauss' law:

$$\sigma_{11,1} + \sigma_{12,2} = 0, \quad \sigma_{12,1} + \sigma_{22,2} = 0, \quad \sigma_{13,1} + \sigma_{23,2} = 0, \quad D_{1,1} + D_{2,2} = 0 \tag{2.15}$$

in which the absence of body forces and free electric volume charge has been assumed, and by two elastic conditions and one electric compatibility condition

$$\varepsilon_{11,22} + \varepsilon_{22,11} - 2\varepsilon_{12,12} = 0, \qquad \varepsilon_{13,2} - \varepsilon_{23,1} = 0, \qquad E_{1,2} - E_{2,1} = 0 \tag{2.16}$$

Having formulated the generalized plane problem, we seek a solution to Eqs. (2.14)-(2.16) subjected to a given loading and boundary condition. To this end, the well-known Lekhnitskii stress functions F, Ψ and induction function V satisfying the foregoing equilibrium equations are introduced as follows [7]:

$$\begin{aligned} &\sigma_{11} = F_{,22}, \quad \sigma_{22} = F_{,11}, \quad \sigma_{12} = -F_{,12}, \\ &\sigma_{13} = \Psi_{,2}, \quad \sigma_{23} = -\Psi_{,1}, \quad D_1 = V_{,2}, \quad D_2 = -V_{,1} \end{aligned} \tag{2.17}$$

Inserting Eq. (2.17) into Eq. (2.14), and later into Eq. (2.16) leads to

$$\begin{bmatrix} L_4 & L_3 & L_3^* \\ L_3 & L_2 & L_2^* \\ L_3^* & L_2^* & L_2^{**} \end{bmatrix} \begin{Bmatrix} F \\ \Psi \\ V \end{Bmatrix} = 0 \tag{2.18}$$

where

$$
\begin{aligned}
L_4 &= f_{22}\frac{\partial^4}{\partial x_1^4} - 2f_{26}\frac{\partial^4}{\partial x_1^3 \partial x_2} + (2f_{12} + f_{66})\frac{\partial^4}{\partial x_1^2 \partial x_2^2} \\
&\quad - 2f_{16}\frac{\partial^4}{\partial x_1 \partial x_2^3} + f_{11}\frac{\partial^4}{\partial x_2^4}, \\
L_3 &= -f_{24}\frac{\partial^3}{\partial x_1^3} + (f_{25} + f_{46})\frac{\partial^3}{\partial x_1^2 \partial x_2} - (f_{14} + f_{56})\frac{\partial^3}{\partial x_1 \partial x_2^2} + f_{15}\frac{\partial^3}{\partial x_2^3}, \\
L_3^* &= -g_{22}\frac{\partial^3}{\partial x_1^3} + (g_{12} + g_{26})\frac{\partial^3}{\partial x_1^2 \partial x_2} - (g_{21} + g_{16})\frac{\partial^3}{\partial x_1 \partial x_2^2} + g_{11}\frac{\partial^3}{\partial x_2^3}, \\
L_2 &= f_{44}\frac{\partial^2}{\partial x_1^2} - 2f_{45}\frac{\partial^2}{\partial x_1 \partial x_2} + f_{55}\frac{\partial^2}{\partial x_2^2}, \\
L_2^* &= f_{44}\frac{\partial^2}{\partial x_1^2} - (g_{14} + g_{25})\frac{\partial^2}{\partial x_1 \partial x_2} + g_{15}\frac{\partial^2}{\partial x_2^2}, \\
L_2^{**} &= -\beta_{22}\frac{\partial^2}{\partial x_1^2} + 2\beta_{12}\frac{\partial^2}{\partial x_1 \partial x_2} - \beta_{11}\frac{\partial^2}{\partial x_2^2}
\end{aligned}
\tag{2.19}
$$

Eliminating Ψ and V from Eq. (2.18) yields

$$
(L_4 L_2 L_2^{**} + 2L_3 L_3^* L_2^* - L_3^* L_3^* L_2 - L_4 L_2^* L_2^* - L_3 L_3 L_2^{**})F = 0 \tag{2.20}
$$

As discussed in [4] within the framework of anisotropic elasticity, Eq. (2.20) can be solved by assuming a solution of $F(z)$ such that

$$
F(z) = F(x_1 + \mu x_2), \qquad \mu = \alpha + i\beta \tag{2.21}
$$

where α and β are real numbers. By introducing Eq. (2.21) into Eq. (2.20), and using the chain rule of differentiation, an expression of the form $\{\cdot\}F^{(6)} = 0$ is obtained. A nontrivial solution follows by setting the characteristic equation equal to zero:

$$
(L_4 L_2 L_2^{**} + 2L_3 L_3^* L_2^* - L_3^* L_3^* L_2 - L_4 L_2^* L_2^* - L_3 L_3 L_2^{**})(\mu) = 0 \tag{2.22}
$$

Owing to the particular material symmetry of the piezoelectricity under investigation, the polynomial is expressed in terms of even powers of μ. This allows us to solve Eq. (2.22) analytically, rendering

$$
\mu_k = \alpha_k + i\beta_k \qquad (k = 1, 2, 3, 4) \tag{2.23}
$$

where $i = \sqrt{-1}$. Once the roots μ_k (k=1, 2, 3, 4) are known, the solution for the functions F, Ψ, and V is written as

$$
F(x_1, x_2) = 2\,\mathrm{Re}\sum_{j=1}^{4} F_j(z_j) \tag{2.24}
$$

$$\Psi(x_1,x_2)=2\,\mathrm{Re}\sum_{j=1}^{4}\Psi_j(z_j) \tag{2.25}$$

$$V(x_1,x_2)=2\,\mathrm{Re}\sum_{j=1}^{4}V_j(z_j) \tag{2.26}$$

where $z_j=x+p_jy$. By eliminating Ψ or V from Eq. (2.18), we can express the functions Ψ and V in terms of the function F as

$$\Psi_k=\begin{cases}\Lambda_k F_k' & (\text{for } k=1,2,4)\\ F'/\Lambda_k & (\text{for } k=3)\end{cases},\qquad V_k=\begin{cases}\Omega_k F_k' & (\text{for } k=1,2,3)\\ F'/\Omega_k & (\text{for } k=4)\end{cases} \tag{2.27}$$

where $F_k'=\mathrm{d}F_k/\mathrm{d}z_k$, and

$$\Lambda_k=\begin{cases}-\dfrac{l_3(\mu_k)l_2^{**}(\mu_k)-l_3^{*}(\mu_k)l_2^{*}(\mu_k)}{l_2(\mu_k)l_2^{**}(\mu_k)-l_2^{*}(\mu_k)l_2^{*}(\mu_k)} & (\text{for } k=1,2)\\ -\dfrac{l_3(\mu_k)l_2^{**}(\mu_k)-l_3^{*}(\mu_k)l_2^{*}(\mu_k)}{l_4(\mu_k)l_2^{**}(\mu_k)-l_3^{*}(\mu_k)l_3^{*}(\mu_k)} & (\text{for } k=3)\\ -\dfrac{l_4(\mu_k)l_2^{*}(\mu_k)-l_3(\mu_k)l_3^{*}(\mu_k)}{l_3(\mu_k)l_2^{**}(\mu_k)-l_2(\mu_k)l_3^{*}(\mu_k)} & (\text{for } k=4)\end{cases} \tag{2.28}$$

$$\Omega_k=\begin{cases}-\dfrac{l_2(\mu_k)l_3^{*}(\mu_k)-l_3(\mu_k)l_2^{*}(\mu_k)}{l_2(\mu_k)l_2^{**}(\mu_k)-l_2^{*}(\mu_k)l_2^{*}(\mu_k)} & (\text{for } k=1,2)\\ -\dfrac{l_4(\mu_k)l_2^{*}(\mu_k)-l_3^{*}(\mu_k)l_3(\mu_k)}{l_3^{*}(\mu_k)l_2^{*}(\mu_k)-l_3(\mu_k)l_2^{**}(\mu_k)} & (\text{for } k=3)\\ -\dfrac{l_2(\mu_k)l_3^{*}(\mu_k)-l_3(\mu_k)l_2^{*}(\mu_k)}{l_2(\mu_k)l_4(\mu_k)-l_3(\mu_k)l_3(\mu_k)} & (\text{for } k=4)\end{cases} \tag{2.29}$$

with

$$\begin{aligned}
&l_4(p)=f_{11}\mu^4-2f_{16}\mu^3+(2f_{12}+f_{66})\mu^2-2f_{26}\mu+f_{22},\\
&l_3(p)=f_{15}\mu^3-(f_{14}+f_{56})\mu^2+(f_{25}+f_{46})\mu-f_{24},\\
&l_3^{*}(p)=g_{11}\mu^3-(g_{21}+g_{16})\mu^2+(g_{12}+g_{26})\mu-g_{22},\\
&l_2(p)=f_{55}\mu^2-2f_{45}\mu+f_{44},\\
&l_2^{*}(p)=g_{15}\mu^2-(g_{14}+g_{25})\mu+g_{24},\\
&l_2^{**}(p)=-\beta_{11}\mu^2+2\beta_{12}\mu-\beta_{22}
\end{aligned} \tag{2.30}$$

Equations (2.24)-(2.26) can then be rewritten as

$$
\begin{aligned}
F &= 2\,\mathrm{Re}\left[F_1 + F_2 + F_3 + F_4\right],\\
\Psi &= 2\,\mathrm{Re}\left[\Lambda_1 F_1' + \Lambda_2 F_2' + F_3'/\Lambda_3 + \Lambda_4 F_4'\right],\\
V &= 2\,\mathrm{Re}\left[\Omega_1 F_1' + \Omega_2 F_2' + \Omega_3 F_3' + F'/\Omega_4\right]
\end{aligned}
\tag{2.31}
$$

With the aid of Eq. (2.31) we can obtain expressions for the stress and electric displacement components. Using Eqs. (2.17) and (2.31), we obtain

$$
\begin{Bmatrix}\sigma_{11}\\ \sigma_{22}\\ \sigma_{12}\end{Bmatrix} = 2\,\mathrm{Re}\sum_{k=1}^{4}\begin{Bmatrix}\mu_k^2\\ 1\\ -\mu_k\end{Bmatrix}F_k''(z_k)
\tag{2.32}
$$

$$
\begin{aligned}
\sigma_{23} &= -2\,\mathrm{Re}\left[\Lambda_1 F_1'' + \Lambda_2 F_2'' + F_3''/\Lambda_3 + \Lambda_4 F_4''\right],\\
\sigma_{13} &= 2\,\mathrm{Re}\left[p_1\Lambda_1 F_1'' + p_2\Lambda_2 F_2'' + p_3 F_3''/\Lambda_3 + p_4\Lambda_4 F_4''\right],\\
D_1 &= 2\,\mathrm{Re}\left[p_1\Omega_1 F_1'' + p_2\Omega_2 F_2'' + p_3\Omega_3 F_3'' + p_4 F''/\Omega_4\right],\\
D_2 &= -2\,\mathrm{Re}\left[\Omega_1 F_1'' + \Omega_2 F_2'' + \Omega_3 F_3'' + F''/\Omega_4\right]
\end{aligned}
\tag{2.33}
$$

Finally, using the constitutive equations (2.14) in conjunction with Eqs. (2.32) and (2.33) allows us to find expressions for the strain and electric field. They are

$$
\begin{aligned}
&\varepsilon_{11} = 2\,\mathrm{Re}\left[\sum_{k=1}^{4} u_k^* s_k'\right], \qquad \varepsilon_{22} = 2\,\mathrm{Re}\left[\sum_{k=1}^{4} v_k^* \mu_k s_k'\right],\\
&2\varepsilon_{12} = 2\,\mathrm{Re}\left[\sum_{k=1}^{4}(v_k^* + \mu_k u_k^*) s_k'\right],\\
&2\varepsilon_{13} = 2\,\mathrm{Re}\left[\sum_{k=1}^{4} w_k^* s_k'\right], \qquad 2\varepsilon_{23} = 2\,\mathrm{Re}\left[\sum_{k=1}^{4} w_k^* \mu_k s_k'\right],\\
&E_1 = -2\,\mathrm{Re}\left[\sum_{k=1}^{4} \Phi_k^* s_k'\right], \qquad E_2 = -2\,\mathrm{Re}\left[\sum_{k=1}^{4} \Phi_k^* \mu_k s_k'\right]
\end{aligned}
\tag{2.34}
$$

where

$$
s_1 = F_1', \quad s_2 = F_2', \quad s_3 = F_3'/\Lambda_3, \quad s_4 = F_4'/\Omega_4
\tag{2.35}
$$

$$
u_k^* = \begin{cases}
\mu_k^2 f_{11} + f_{12} - f_{14}\Lambda_k + f_{15}\mu_k\Lambda_k - f_{16}\mu_k + g_{11}\mu_k\Omega_k - g_{21}\Omega_k & (\text{for } k{=}1,2)\\
\Lambda_k(\mu_k^2 f_{11} + f_{12} - f_{16}\mu_k + g_{11}\mu_k\Omega_k - g_{21}\Omega_k) - f_{14} + f_{15}\mu_k & (\text{for } k{=}3)\\
\Omega_k(\mu_k^2 f_{11} + f_{12} - f_{14}\Lambda_k + f_{15}\mu_k\Lambda_k - f_{16}\mu_k) + g_{11}\mu_k - g_{21} & (\text{for } k{=}4)
\end{cases}
\tag{2.36}
$$

$$
v_k^* = \begin{cases}
\mu_k^2 f_{12} + (f_{22} - f_{24}\Lambda_k - g_{22}\Omega_k)/\mu_k + f_{25}\Lambda_k - f_{26} + g_{12}\Omega_k & (\text{for } k{=}1,2)\\
\Lambda_k(\mu_k f_{12} + f_{22}/\mu_k - f_{26} + g_{12}\Omega_k - g_{22}\Omega_k/\mu_k) - f_{24}/\mu_k + f_{25} & (\text{for } k{=}3)\\
\Omega_k(\mu_k f_{12} + f_{22}/\mu_k - f_{24}\Lambda_k/\mu_k + f_{25}\Lambda_k - f_{26}) + g_{12} - g_{22}/\mu_k & (\text{for } k{=}4)
\end{cases}
\tag{2.37}
$$

$$w_k^* = \begin{cases} \mu_k f_{14} + (f_{24} - f_{44}\Lambda_k - g_{24}\Omega_k)/\mu_k + f_{45}\Lambda_k - f_{46} + g_{14}\Omega_k & (\text{for } k=1,2) \\ \Lambda_k(\mu_k f_{14} + f_{24}/\mu_k - f_{46} + g_{14}\Omega_k - g_{24}\Omega_k/\mu_k) - f_{44}/\mu_k + f_{45} & (\text{for } k=3) \\ \Omega_k(\mu_k f_{14} + f_{24}/\mu_k - f_{44}\Lambda_k/\mu_k + f_{45}\Lambda_k - f_{46}) + g_{14} - g_{24}/\mu_k & (\text{for } k=4) \end{cases} \tag{2.38}$$

$$\Phi_k^* = \begin{cases} \mu_k^2 g_{14} + g_{12} - g_{14}\Lambda_k + g_{15}\Lambda_k\mu_k - g_{16}\mu_k - \beta_{11}\mu_k\Omega_k + \beta_{12}\Omega_k & (\text{for } k=1,2) \\ \Lambda_k(\mu_k^2 g_{14} + g_{12} - g_{16}\mu_k - \beta_{11}\mu_k\Omega_k + \beta_{12}\Omega_k) - g_{14} + g_{15}\mu_k & (\text{for } k=3) \\ \Omega_k(\mu_k^2 g_{14} + g_{12} - g_{14}\Lambda_k + g_{15}\Lambda_k\mu_k - g_{16}\mu_k) + g_{12} - \beta_{11}\mu_k & (\text{for } k=4) \end{cases} \tag{2.39}$$

Substitution of Eq. (1.2) into Eq. (2.34), and then integration of the normal strains and the electric field $E = -\text{grad}\,\phi$ produces

$$\begin{aligned} u_1 &= 2\,\text{Re}\left[\sum_{k=1}^{4} u_k^* s_k\right], \qquad u_2 = 2\,\text{Re}\left[\sum_{k=1}^{4} v_k^* s_k\right], \\ u_3 &= 2\,\text{Re}\left[\sum_{k=1}^{4} w_k^* s_k\right], \qquad E_1 = 2\,\text{Re}\left[\sum_{k=1}^{4} \Phi_k^* s_k\right] \end{aligned} \tag{2.40}$$

The integrating constants, which represent the rigid body motions, are ignored here[7].

Recapitulating, based on the procedure above the generalized plane strain piezoelectric problem is reduced to one of finding four complex potentials, s_i (i=1-4), in some region Ω of the material. Each potential is a function of a different generalized complex variable $z_k = x_1 + \mu_k x_2$.

2.3 Techniques of Fourier transformation

In this section we briefly examine the application of Fourier transform techniques to cracked piezoelectric materials. Yu and Qin [8,9] used Fourier transform techniques to study the crack-tip singularities and damage properties of thermopiezoelectric materials. They began with defining a Fourier transform pair

$$\hat{f}(\xi) = \frac{1}{\sqrt{2\pi}}\int_{-\infty}^{\infty} f(x)e^{i\xi x}\mathrm{d}x, \qquad f(x) = \frac{1}{\sqrt{2\pi}}\int_{-\infty}^{\infty} \hat{f}(\xi)e^{-i\xi x}\mathrm{d}\xi \tag{2.41}$$

and by introducing the shorthand notation given by Barnett and Lothe [10]. With this shorthand notation, the governing equation (1.10) and the constitutive relationship (1.6) can be rewritten as

$$\Pi_{iJ,i} = f_J \tag{2.42}$$

$$\Pi_{iJ} = E_{iJKm} U_{K,m} \tag{2.43}$$

where f_4=Q, and

$$\Pi_{iJ} = \begin{cases} \sigma_{ij} & (i, J = 1,\ 2,\ 3) \\ D_i & (J = 4;\ \ i = 1,\ 2,\ 3) \end{cases} \tag{2.44}$$

$$U_K = \begin{cases} u_k & (K = 1,\ 2,\ 3) \\ \phi & (K = 4) \end{cases} \tag{2.45}$$

$$E_{iJKm} = \begin{cases} c_{ijkm} & (i, J, K, m = 1,\ 2,\ 3) \\ e_{mij} & (K = 4;\ \ i, J, m = 1,\ 2,\ 3) \\ e_{ikm} & (J = 4;\ \ i, K, m = 1,\ 2,\ 3) \\ -\kappa_{im} & (J = K = 4;\ \ i, m = 1,\ 2,\ 3) \end{cases} \tag{2.46}$$

For generalized two-dimensional deformations in which $\mathbf{U}$ (=$\{u_1,\ u_2,\ u_3,\ \phi\}^{\mathrm{T}}$) depends on x_1 and x_2 only, where the superscript "T" denotes the transpose, a general solution can be obtained by applying the transform to Eq. (2.42) over x_1. This gives

$$\xi^2 \mathbf{Q}\hat{\mathbf{U}} + i\xi(\mathbf{R} + \mathbf{R}^{\mathrm{T}}) \frac{\partial \hat{\mathbf{U}}}{\partial x_2} - \mathbf{T} \frac{\partial^2 \hat{\mathbf{U}}}{\partial x_2^2} = 0 \tag{2.47}$$

in which we assume $f_J = 0$ in Eq. (2.42) for the sake of simplicity. The matrices $\mathbf{Q}$, $\mathbf{R}$, and $\mathbf{T}$ are 4×4 real matrices whose components are

$$Q_{IK} = E_{1IK1}, \qquad R_{IK} = E_{1IK2}, \qquad T_{IK} = E_{2IK2} \tag{2.48}$$

The solution of Eq. (2.47) can be obtained by considering an arbitrary eigenfunction of the form

$$\hat{\mathbf{U}} = \mathbf{a} e^{-i\eta x_2} \tag{2.49}$$

Substituting Eq. (2.49) into Eq. (2.47), it is found that

$$[\mathbf{Q}\xi^2 + \xi\eta(\mathbf{R} + \mathbf{R}^{\mathrm{T}}) + \eta^2 \mathbf{T}]\mathbf{a} = 0 \tag{2.50}$$

Letting p=η/ξ, we have eight eigenvalues p from Eq. (2.50), which consists of four pairs of complex conjugates [11]. Denote

$$\eta_M = \begin{cases} p_M \xi & (\xi > 0) \\ \overline{p}_M \xi & (\xi < 0) \end{cases} \tag{2.51}$$

where M=1, 2, 3, 4. It is obvious that Im(η_M)>0 for all ξ. Such a definition is expedient for development of the subsequent derivation. A general solution of Eq. (2.47) is obtained from a linear combination of the eight eigensolutions, say F_i and G_i

(i=1-4), which are obtained by replacing η in Eq. (2.49) with η_M (M=1-4), when the roots p_M are distinct. The result is

$$\hat{\mathbf{U}} = \sqrt{2\pi}(\mathbf{AFf} + \bar{\mathbf{A}}\mathbf{Gg})H(\xi) + \sqrt{2\pi}(\bar{\mathbf{A}}\mathbf{Ff} + \mathbf{AGg})H(-\xi) \tag{2.52}$$

where $H(\xi)$ is the Heaviside step function, and

$$\mathbf{F}(\xi, x_2) = \langle F_\alpha(\xi, x_2)\rangle = \langle e^{-i\eta_\alpha x_2}\rangle, \quad \mathbf{G}(\xi, x_2) = \langle G_\alpha(\xi, x_2)\rangle = \langle e^{-i\bar{\eta}_\alpha x_2}\rangle \tag{2.53}$$

Note that $\eta = p\xi$, **f** and **g** are two vector functions of ξ to be determined from the electroelastic boundary conditions of a given problem.

The transformed stress and electric displacements follow from the constitutive relation of Eq. (2.43):

$$\hat{\Pi}_1 = i\xi\sqrt{2\pi}(\mathbf{BPFf} + \bar{\mathbf{B}}\bar{\mathbf{P}}\mathbf{Gg})H(\xi) + i\xi\sqrt{2\pi}(\bar{\mathbf{B}}\bar{\mathbf{P}}\mathbf{Ff} + \mathbf{BPGg})H(-\xi) \tag{2.54}$$

$$\hat{\Pi}_2 = -i\xi\sqrt{2\pi}(\mathbf{BFf} + \bar{\mathbf{B}}\mathbf{Gg})H(\xi) - i\xi\sqrt{2\pi}(\bar{\mathbf{B}}\mathbf{Ff} + \mathbf{BGg})H(-\xi) \tag{2.55}$$

The traction-charge vector on a surface with normal $\mathbf{n}=(n_1, n_2, 0)$ can be found from Eqs. (2.54) and (2.55) as follows:

$$\begin{aligned}\hat{\mathbf{t}} = \hat{\Pi}_1 n_1 + \hat{\Pi}_2 n_2 &= i\xi\sqrt{2\pi}[\mathbf{B}(n_1\mathbf{P} - n_2\mathbf{I})\mathbf{Ff} + \bar{\mathbf{B}}(n_1\bar{\mathbf{P}} - n_2\mathbf{I})\mathbf{Gg}]H(\xi) \\ &+ i\xi\sqrt{2\pi}[\bar{\mathbf{B}}(n_1\bar{\mathbf{P}} - n_2\mathbf{I})\mathbf{Ff} + \mathbf{B}(n_1\mathbf{P} - n_2\mathbf{I})\mathbf{Gg}]H(-\xi)\end{aligned} \tag{2.56}$$

where **I** is the unit matrix.

Equations (2.52), (2.54), and (2.55) represent the solution for the elastic and electric fields in the Fourier transform space. The general solution for an electroelastic field in real space is obtained by applying the inverse Fourier transform to Eqs. (2.52), (2.54)-(2.56). The results are

$$\mathbf{U}(x_1, x_2) = \int_0^\infty [\mathbf{AFf} + \bar{\mathbf{A}}\mathbf{Gg}]e^{-i\xi x_1}\,\mathrm{d}\xi + \int_{-\infty}^0 [\bar{\mathbf{A}}\mathbf{Ff} + \mathbf{AGg}]e^{-i\xi x_1}\,\mathrm{d}\xi \tag{2.57}$$

$$\Pi_1(x_1, x_2) = i\int_0^\infty [\mathbf{BPFf} + \bar{\mathbf{B}}\bar{\mathbf{P}}\mathbf{Gg}]\xi e^{-i\xi x_1}\,\mathrm{d}\xi + i\int_{-\infty}^0 [\bar{\mathbf{B}}\bar{\mathbf{P}}\mathbf{Ff} + \mathbf{BPGg}]\xi e^{-i\xi x_1}\,\mathrm{d}\xi \tag{2.58}$$

$$\Pi_2(x_1, x_2) = i\int_0^\infty [\mathbf{BFf} + \bar{\mathbf{B}}\mathbf{Gg}]\xi e^{-i\xi x_1}\,\mathrm{d}\xi + i\int_{-\infty}^0 [\bar{\mathbf{B}}\mathbf{Ff} + \mathbf{BGg}]\xi e^{-i\xi x_1}\,\mathrm{d}\xi \tag{2.59}$$

$$\begin{aligned}\mathbf{t}(x_1, x_2) = i\int_0^\infty \xi[\mathbf{B}(n_1\mathbf{P} - n_2\mathbf{I})\mathbf{Ff} + \bar{\mathbf{B}}(n_1\bar{\mathbf{P}} - n_2\mathbf{I})\mathbf{Gg}]e^{-i\xi x_1}\,\mathrm{d}\xi \\ + i\int_0^\infty \xi[\bar{\mathbf{B}}(n_1\bar{\mathbf{P}} - n_2\mathbf{I})\mathbf{Ff} + \mathbf{B}(n_1\mathbf{P} - n_2\mathbf{I})\mathbf{Gg}]e^{-i\xi x_1}\,\mathrm{d}\xi\end{aligned} \tag{2.60}$$

For a given boundary value problem, the eight functions **f** and **g** are determined from the appropriate boundary conditions.

2.4 Trefftz finite element method

The solution methods discussed in the preceding sections are mostly based on analytical approaches. For a complex structure, however, a powerful numerical method is required to obtain a meaningful solution for electroelastic crack problems. Of all the numerical methods, the FEM and boundary element method (BEM) may be the most versatile computational tools to treat piezoelectric problems. Particularly, the Trefftz FEM has recently received attention from researchers in the field of solid mechanics. In the literature there are only a few papers addressing the application of Trefftz FEM to piezoelectric problems. Qin [12,13] introduced the Trefftz FEM for piezoelectric problems in 2003. Wang et al. [14] used Trefftz FEM and computed eigensolutions to determine singular electroelastic fields in piezoelectricity. In this section, the application of Trefftz FEM to piezoelectric problems is briefly examined.

2.4.1 Basic equations

Consider a linear piezoelectric material in which the constitutive relations, the differential governing equations and boundary conditions are given in Eqs. (1.5), (1.10)-(1.12), respectively. Moreover, in the Trefftz FE form, Eqs. (1.2), (1.5), (1.10)-(1.12) should be completed by the following inter-element continuity requirements:

$$u_{ie} = u_{if}, \quad \phi_e = \phi_f \qquad (\text{on } \Gamma_e \bigcap \Gamma_f, \text{ conformity}) \tag{2.61}$$

$$t_{ie} + t_{if} = 0, \quad D_{ne} + D_{nf} = 0 \qquad (\text{on } \Gamma_e \bigcap \Gamma_f, \text{ reciprocity}) \tag{2.62}$$

where "*e*" and "*f* " stand for any two neighboring elements. The equations mentioned above are taken as the basis to establish the modified variational principle for Trefftz FE analysis of piezoelectric materials [12].

2.4.2 Assumed fields

The main idea of the Trefftz FEM is to establish an FE formulation whereby intra-element continuity is enforced on a non-conforming internal displacement field chosen so as to *a priori* satisfy the governing differential equation of the problem under consideration [12]. With the Trefftz FEM the solution domain Ω is subdivided into elements, and over each element "*e*," the assumed intra-element fields are

$$\mathbf{U}=\begin{Bmatrix}u_1\\u_2\\u_3\\\phi\end{Bmatrix}=\begin{Bmatrix}\breve{u}_1\\\breve{u}_2\\\breve{u}_3\\\breve{\phi}\end{Bmatrix}+\begin{Bmatrix}\mathbf{N}_1\\\mathbf{N}_2\\\mathbf{N}_3\\\mathbf{N}_4\end{Bmatrix}\mathbf{c}=\breve{\mathbf{U}}+\sum_{j=1}\mathbf{N}_j\mathbf{c}_j=\breve{\mathbf{U}}+\mathbf{N}\mathbf{c} \tag{2.63}$$

where $\mathbf{c}_j$ stands for undetermined coefficient, and $\breve{\mathbf{U}}$ $(=\{\breve{u}_1,\breve{u}_2,\breve{u}_3,\breve{\phi}\}^{\mathrm{T}})$ and $\mathbf{N}$ are known functions. If the governing differential equation (2.42) is rewritten in a general form

$$\mathfrak{R}\mathbf{U}(\mathbf{x})+\mathbf{f}(\mathbf{x})=0 \qquad (\mathbf{x}\in\Omega_e) \tag{2.64}$$

where $\mathfrak{R}$ stands for the differential operator matrix for Eq. (2.42), $\mathbf{x}$ for the position vector, $\mathbf{f}$ $(=\{f_1,f_2,f_3,Q\}^{\mathrm{T}})$ for the known right-hand side term, the overhead bar indicates the imposed quantities, and Ω_e stands for the eth element sub-domain, then $\breve{\mathbf{U}}=\breve{\mathbf{U}}(\mathbf{x})$ and $\mathbf{N}=\mathbf{N}(\mathbf{x})$ in Eq. (2.63) must be chosen such that

$$\mathfrak{R}\breve{\mathbf{U}}+\mathbf{f}=0 \quad \text{and} \quad \mathfrak{R}\mathbf{N}=0 \tag{2.65}$$

everywhere in Ω_e. A complete system of homogeneous solutions $\mathbf{N}_j$ can be generated by way of the solution in Stroh formalism

$$\mathbf{U}=2\,\mathrm{Re}\{\mathbf{A}\langle f(z_\alpha)\rangle\mathbf{c}\} \tag{2.66}$$

where "Re" stands for the real part of a complex number, $\mathbf{A}$ is the material eigenvector matrix which has been well defined in the literature (see pp. 17-18 of [11]), $\langle f(z_\alpha)\rangle=\mathrm{diag}[f(z_1)\,f(z_2)\,f(z_3)\,f(z_4)]$ is a diagonal 4×4 matrix, and $f(z_i)$ is an arbitrary function with argument $z_i=x_1+\mu_i x_2$. μ_i (i=1-4) are the material eigenvalues[11].

The unknown coefficient $\mathbf{c}$ may be calculated from the conditions on the external boundary and/or the continuity conditions on the inter-element boundary. Thus various Trefftz element models can be obtained by using different approaches to enforce these conditions. In the majority of cases a hybrid technique is used, whereby the elements are linked through an auxiliary conforming displacement frame which has the same form as in the conventional FE method. This means that, in the Trefftz FE approach, a conforming electric potential and displacement (EPD) field should be independently defined on the element boundary to enforce the field continuity between elements and also to link the coefficient $\mathbf{c}$, appearing in Eq. (2.63), with nodal EPD $\mathbf{d}$ $(=\{d\})$. The frame is defined as

$$\tilde{\mathbf{U}}(\mathbf{x})=\begin{Bmatrix}\tilde{u}_1\\\tilde{u}_2\\\tilde{u}_3\\\tilde{\phi}\end{Bmatrix}=\begin{Bmatrix}\tilde{\mathbf{N}}_1\\\tilde{\mathbf{N}}_2\\\tilde{\mathbf{N}}_3\\\tilde{\mathbf{N}}_4\end{Bmatrix}\mathbf{d}=\tilde{\mathbf{N}}\mathbf{d} \qquad (\mathbf{x}\in\Gamma_e) \tag{2.67}$$

where the symbol "~" is used to specify that the field is defined on the element boundary only, **d**=**d**(**c**) stands for the vector of the nodal displacements which are the final unknowns of the problem, Γ_e represents the boundary of element e, and $\tilde{\mathbf{N}}$ is a matrix of the corresponding shape functions which are the same as those in conventional FE formulation.

Using the above definitions the generalized boundary forces and electric displacements can be derived from Eqs. (1.11) and (2.63), and denoted as

$$\mathbf{T}=\begin{Bmatrix} t_1 \\ t_2 \\ t_3 \\ D_n \end{Bmatrix}=\begin{Bmatrix} \sigma_{1j}n_j \\ \sigma_{2j}n_j \\ \sigma_{3j}n_j \\ D_j n_j \end{Bmatrix}=\begin{Bmatrix} \breve{t}_1 \\ \breve{t}_2 \\ \breve{t}_3 \\ \breve{D}_n \end{Bmatrix}+\begin{Bmatrix} \mathbf{Q}_1 \\ \mathbf{Q}_2 \\ \mathbf{Q}_3 \\ \mathbf{Q}_4 \end{Bmatrix}\mathbf{c}=\breve{\mathbf{T}}+\mathbf{Q}\mathbf{c} \tag{2.68}$$

where $\breve{t}_i$ and $\breve{D}_n$ are derived from $\breve{\mathbf{U}}$.

2.4.3 Element stiffness equation

Based on the two independent assumed fields, Eqs. (2.63) and (2.67), presented above, the element matrix equation can be generated by a variational approach [15]. For a three-dimensional piezoelectric problem, the variational functional can be constructed as [12]

$$\Psi_{me}=\frac{1}{2}\int_{\Omega_e}\mathbf{U}^{\mathrm{T}}\mathbf{f}\mathrm{d}\Omega-\int_{\Gamma_e}\mathbf{T}^{\mathrm{T}}(\tilde{\mathbf{U}}-\mathbf{U}/2)\mathrm{d}\Gamma+\int_{\Gamma_{te}}\tilde{\mathbf{U}}^{\mathrm{T}}\bar{\mathbf{T}}\mathrm{d}\Gamma \tag{2.69}$$

Substituting the expressions given in Eqs. (2.63), (2.67), and (2.68) into (2.69) produces

$$\Psi_{me}=\frac{1}{2}\mathbf{c}^{\mathrm{T}}\mathbf{H}_e\mathbf{c}-\mathbf{c}^{\mathrm{T}}\mathbf{G}_e\mathbf{d}+\mathbf{c}^{\mathrm{T}}\mathbf{h}_e+\mathbf{d}^{\mathrm{T}}\mathbf{g}_e+\text{terms without }\mathbf{c}\text{ or }\mathbf{d} \tag{2.70}$$

in which the matrices $\mathbf{H}_e$, $\mathbf{G}_e$ and the vectors $\mathbf{h}_e$, $\mathbf{g}_e$ are as follows:

$$\mathbf{H}_e=\int_{\Gamma_e}\mathbf{Q}^{\mathrm{T}}\mathbf{N}\mathrm{d}\Gamma=\int_{\Gamma_e}\mathbf{N}^{\mathrm{T}}\mathbf{Q}\mathrm{d}\Gamma \tag{2.71}$$

$$\mathbf{G}_e=\int_{\Gamma_e}\mathbf{Q}^{\mathrm{T}}\tilde{\mathbf{N}}\mathrm{d}\Gamma \tag{2.72}$$

$$\mathbf{h}_e=\frac{1}{2}\int_{\Omega_e}\mathbf{N}^{\mathrm{T}}\mathbf{f}\mathrm{d}\Omega+\int_{\Gamma_{\phi e}}(\mathbf{Q}^{\mathrm{T}}\breve{\mathbf{U}}+\mathbf{N}^{\mathrm{T}}\breve{\mathbf{T}})\mathrm{d}\Gamma \tag{2.73}$$

$$\mathbf{g}_e=\int_{\Gamma_{te}}\tilde{\mathbf{N}}^{\mathrm{T}}\bar{\mathbf{T}}\mathrm{d}\Gamma-\int_{\Gamma_e}\tilde{\mathbf{N}}^{\mathrm{T}}\breve{\mathbf{T}}\mathrm{d}\Gamma \tag{2.74}$$

To enforce inter-element continuity on the common element boundary, the unknown vector **c** should be expressed in terms of nodal DOF **d**. An optional relationship between **c** and **d** in the sense of variation can be obtained from

$$\frac{\partial \Psi_{me}}{\partial \mathbf{c}^{\mathrm{T}}} = \mathbf{H}_e\mathbf{c} - \mathbf{G}_e\mathbf{d} + \mathbf{h}_e = 0 \tag{2.75}$$

This leads to

$$\mathbf{c} = \mathbf{H}_e^{-1}(\mathbf{G}_e\mathbf{d} - \mathbf{h}_e) \tag{2.76}$$

and then straightforwardly yields the expression of Ψ_{me} only in terms of **d** and other known matrices:

$$\Psi_{me} = -\frac{1}{2}\mathbf{d}^{\mathrm{T}}\left(\mathbf{G}_e^{\mathrm{T}}\mathbf{H}_e^{-1}\mathbf{G}_e\right)\mathbf{d} + \mathbf{d}^{\mathrm{T}}(\mathbf{G}_e^{\mathrm{T}}\mathbf{H}_e^{-1}\mathbf{h}_e + \mathbf{g}_e) + \text{terms without } \mathbf{d} \tag{2.77}$$

Therefore, the element stiffness matrix equation can be obtained by taking the vanishing variation of the functional Ψ_{me} as

$$\frac{\partial \Psi_{me}}{\partial \mathbf{d}^{\mathrm{T}}} = 0 \Rightarrow \mathbf{K}_e\mathbf{d} = \mathbf{P}_e \tag{2.78}$$

where $\mathbf{K}_e = \mathbf{G}_e^{\mathrm{T}}\mathbf{H}_e^{-1}\mathbf{G}_e$ and $\mathbf{P}_e = \mathbf{G}_e^{\mathrm{T}}\mathbf{H}_e^{-1}\mathbf{h}_e + \mathbf{g}_e$ are, respectively, the element stiffness matrix and the equivalent nodal flow vector. The expression (2.78) is the elemental stiffness-matrix equation for Trefftz FE analysis.

2.5 Integral equations

An integral equation is, mathematically, an equation in which an unknown function appears under an integral sign. It is noted that most crack and stress singularity problems in piezoelectric structures and materials can be formulated in terms of a certain type of integral equation such as Fredholm, Volterra, and Abel integral equations. In order to provide fundamental knowledge and to enhance understanding of these integral equations which appear in coming chapters, a brief review of Fredholm, Volterra, and Abel integral equations is presented in this section.

2.5.1 Fredholm integral equations

A homogeneous Fredholm integral equation of the first kind is written as [16]

$$\int_a^b K(x,y)\phi(y)\mathrm{d}y = f(x) \qquad (a \leqslant x \leqslant b) \tag{2.79}$$

where the continuous kernel function $K(x,y)$ and the inhomogeneous term $f(x)$ are known functions. The equation is to be satisfied for x in the interval $a \leqslant x \leqslant b$, the same as the interval of integration. It is typical to find the unknown function $\phi(y)$. An inhomogeneous Fredholm equation of the second kind has the form

$$\phi(x) = \lambda \int_a^b K(x,y)\phi(y)\mathrm{d}y + f(x) \qquad (a \leqslant x \leqslant b) \tag{2.80}$$

where λ is a known constant. Given the kernel $K(x,y)$, and the function $f(x)$, the problem is to determine the function $\phi(y)$. A standard approach to solving Eq. (2.80) is called an integral equation Neumann series, which may be described as follows.

Take

$$\begin{aligned}
&\phi_0(x) \equiv f(x),\\
&\phi_1(x) = f(x) + \lambda \int_a^b K(x,y) f(y)\mathrm{d}y,\\
&\phi_2(x) = f(x) + \lambda \int_a^b K(x,y_1) f(y_1)\mathrm{d}y_1\\
&\qquad + \lambda^2 \int_a^b \int_a^b K(x,y_1)K(y_1,y_2) f(y_2)\mathrm{d}y_1\mathrm{d}y_2,\\
&\cdots\\
&\phi_i(x) = \sum_{i=0}^{n} \lambda^i u_i(x)
\end{aligned} \tag{2.81}$$

where

$$\begin{aligned}
&u_0(x) \equiv f(x),\\
&u_1(x) = \int_a^b K(x,y_1) f(y_1)\mathrm{d}y_1,\\
&u_2(x) = \int_a^b \int_a^b K(x,y_1)K(y_1,y_2) f(y_2)\mathrm{d}y_1\mathrm{d}y_2,\\
&\cdots
\end{aligned} \tag{2.82}$$

The Neumann series solution is then

$$\phi(x) = \lim_{n\to\infty} \phi_n(x) = \lim_{n\to\infty} \sum_{i=0}^{n} \lambda^i u_i(x) \tag{2.83}$$

Alternatively, if the kernel $K(x,y)$ is separable, i.e., it can be written in the form

$$K(x,y) = \sum_{i=1}^{n} M_i(x) N_i(y) \tag{2.84}$$

Equation (2.80) may be solved as follows. Let

$$\phi(x) = f(x) + \int_a^b K(x,t)\phi(t)\mathrm{d}t$$

$$= f(x) + \lambda \sum_{j=1}^{n} M_j(x) \int_a^b N_j(t)\phi(t)\mathrm{d}t = f(x) + \lambda \sum_{j=1}^{n} c_j M_j(x) \tag{2.85}$$

where

$$c_j = \int_a^b N_j(t)\phi(t)\mathrm{d}t \tag{2.86}$$

Now multiply both sides of Eq. (2.85) by $N_i(x)$ and integrate over dx, we have

$$\int_a^b \phi(x)N_i(x)\mathrm{d}x = \int_a^b f(x)N_i(x)\mathrm{d}x + \lambda \sum_{j=1}^{n} c_j \int_a^b M_j(x)N_i(x)\mathrm{d}x \tag{2.87}$$

By Eq. (2.86), the first term of Eq. (2.87) is just c_i. Now define

$$b_i = \int_a^b N_i(x)f(x)\mathrm{d}x, \qquad a_{ij} = \int_a^b N_i(x)M_j(x)\mathrm{d}x \tag{2.88}$$

So Eq. (2.87) becomes

$$c_i = b_i + \lambda \sum_{j=1}^{n} a_{ij}c_j \tag{2.89}$$

Equation (2.89) can be written in matrix form as

$$\mathbf{C} = \mathbf{B} + \lambda \mathbf{A}\mathbf{C} \tag{2.90}$$

So we have

$$(1 - \lambda \mathbf{A})\mathbf{C} = \mathbf{B}, \qquad \mathbf{C} = (1 - \lambda \mathbf{A})^{-1}\mathbf{B} \tag{2.91}$$

2.5.2 Volterra integral equations

It is noted from Eq. (2.79) that the integration limits of a Fredholm equation are constants. A Volterra integral equation of the first kind is obtained by replacing the upper integration limit b in Eq. (2.79) with the variable x:

$$\int_a^x K(x,y)\phi(y)\mathrm{d}y = f(x) \qquad (a \leqslant x) \tag{2.92}$$

Thus, for any fixed range of x, say $0 \leqslant x \leqslant h$, it is the same as a Fredholm equation with a kernel that vanishes for $y>x$. Consequently, all results for the Fredholm equation are still valid.

Like the definition of the Fredholm equation above, a Volterra integral equation of the second kind is an integral equation of the form

$$\phi(x) = \lambda \int_a^x K(x,y)\phi(y)\mathrm{d}y + f(x) \qquad (a \leqslant x) \tag{2.93}$$

where $K(x,y)$ is again a known integral kernel, $f(x)$ is a specified function, and $\phi(x)$ is the function to be determined.

As a special type of Volterra equation of the first kind, Volterra's singular equation

$$\int_a^x \frac{N(x,y)}{(x-y)^{\alpha}}\phi(y)\mathrm{d}y = f(x) \tag{2.94}$$

has received wide application in the field of fracture mechanics and computational engineering, where $N(x,y)$ is a specified bounded function and the exponent α is a positive number less than 1: $0<\alpha<1$.

Equation (2.94) can be solved by reducing it to an equation of the corresponding Volterra equation of the first kind with a bounded kernel. To this end, multiplying both sides of Eq. (2.94) by the function $1/(z-x)^{1-\alpha}$ and integrating with respect to x from a to z, we obtain

$$\int_a^z \frac{1}{(z-x)^{1-\alpha}}\left[\int_a^x \frac{N(x,y)}{(x-y)^{\alpha}}\phi(y)\mathrm{d}y\right]\mathrm{d}x = \int_a^z \frac{f(x)\mathrm{d}x}{(z-x)^{1-\alpha}} \tag{2.95}$$

or, upon application of the Dirichlet transformation the equation

$$\int_a^z \left[\int_y^z \frac{N(x,y)\mathrm{d}x}{(z-x)^{1-\alpha}(x-y)^{\alpha}}\right]\phi(y)\mathrm{d}y = f_1(z) \tag{2.96}$$

This is already a Volterra equation of the first kind with a bounded kernel

$$K(z,y) = \int_y^z \frac{N(x,y)\mathrm{d}x}{(z-x)^{1-\alpha}(x-y)^{\alpha}} \tag{2.97}$$

where the known function $f_1(z)$ is

$$f_1(z) = \int_a^z \frac{f(x)\mathrm{d}x}{(z-x)^{1-\alpha}} \tag{2.98}$$

The solution ϕ of Eq. (2.94) obviously satisfies the transformed equation (2.96).

2.5.3 Abel's integral equation

Abel's integral equation

$$\int_a^x \frac{\phi(y)}{(x-y)^\alpha}\mathrm{d}y = f(x) \qquad (0<\alpha<1) \tag{2.99}$$

is a particular case of the integral equation (2.94) when N=1. The integral equation may be solved explicitly in the following way: when N=1 the kernel of the transformed equation (2.96) has the constant value

$$\int_y^z \frac{\mathrm{d}x}{(z-x)^{1-\alpha}(x-y)^\alpha} = \int_0^1 \frac{\mathrm{d}t}{(1-t)^{1-\alpha}t^\alpha} = \frac{\pi}{\sin\alpha\pi} \tag{2.100}$$

in which $t=(x-y)/(z-y)$ has been used. Let $F(y)$ be any function which is continuous and has a continuous derivative throughout the solution domain I. Multiply Eq. (2.100) by $F'(y)\mathrm{d}y$ and integrate from a to z. That gives

$$\frac{\pi}{\sin\alpha\pi}[F(z)-F(a)] = \int_a^z\int_y^z \frac{F'(y)\mathrm{d}x\mathrm{d}y}{(z-x)^{1-\alpha}(x-y)^\alpha} \tag{2.101}$$

Applying Dirichlet's generalized formula to the second term of Eq. (2.101), we obtain

$$F(z)-F(a) = \frac{\sin\alpha\pi}{\pi}\int_a^z\left[\frac{1}{(z-x)^{1-\alpha}}\int_y^z \frac{F'(y)\mathrm{d}y}{(x-y)^\alpha}\right]\mathrm{d}x \tag{2.102}$$

Multiply Eq. (2.99) by $1/(z-x)^{1-\alpha}\,\mathrm{d}x$ and integrate and the equation takes the simple form a to z, thus obtaining

$$\int_a^z \frac{f(x)\mathrm{d}x}{(z-x)^{1-\alpha}} = \int_a^z \frac{1}{(z-x)^{1-\alpha}}\int_y^z \frac{\phi(y)\mathrm{d}y}{(x-y)^\alpha}\mathrm{d}x \tag{2.103}$$

If in Eq. (2.102) we let

$$F(x) = \int_a^x \phi(y)\mathrm{d}y \tag{2.104}$$

it will be seen that the preceding equation reduces to

$$\frac{\pi}{\sin\alpha\pi}\int_a^z \phi(y)\mathrm{d}y = f_1(z) \tag{2.105}$$

By differentiating Eq. (2.105), we obtain the value of this solution

$$\phi(z) = \frac{\sin\alpha\pi}{\pi}\frac{\mathrm{d}}{\mathrm{d}z}\int_a^z \frac{f(x)\mathrm{d}x}{(z-x)^{1-\alpha}} \tag{2.106}$$

Equation (2.106) can be further written in the form

$$\phi(z)=\frac{\sin\alpha\pi}{\pi}\left(\frac{f(a)}{z^{1-\alpha}}+\int_a^z\frac{[\mathrm{d}f(x)/\mathrm{d}x]\mathrm{d}x}{(z-x)^{1-\alpha}}\right) \tag{2.107}$$

2.6 Shear-lag model

The term shear-lag has been widely used to study strengthening mechanisms through the load transfer from matrix to reinforcement in composite materials. The shear-lag model was originally proposed by Cox [17] and subsequently modified by many researchers. It is assumed that the load transfer from matrix to fiber occurs via shear stresses on the surface between them. Cox's shear-lag model can be obtained by considering the free-body diagram of a differential element of the fiber, as shown in Fig. 2.1. For static equilibrium of the forces acting along the x direction, we have

$$(\sigma_\mathrm{f}+\mathrm{d}\sigma_\mathrm{f})\pi r^2-\sigma_\mathrm{f}\pi r^2+\tau_\mathrm{i}(2\pi r)\mathrm{d}x=0 \tag{2.108}$$

where $r = d/2$, σ_f is the fiber normal stress along the x direction at a distance from the end of fiber, τ_i is the interfacial shear stress at a distance from the end of fiber, and x is the coordinate along the fiber length.

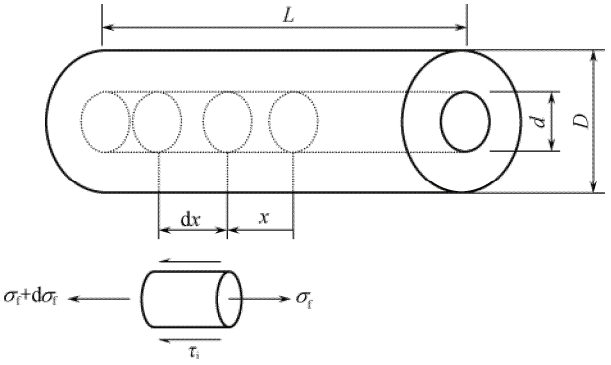

Fig. 2.1 Free-body diagram of a differential element of a fiber.

Equation (2.108) can be simplified to

$$\frac{\mathrm{d}\sigma_\mathrm{f}}{\mathrm{d}x}=-\frac{2\tau_\mathrm{i}}{r} \tag{2.109}$$

Equation (2.109) is referred to as the basic shear-lag equation.

Cox further assumed that the total shear forces on the neighboring annuli remain constant. That assumption leads to the following relationships:

$$2\pi r_k \tau_k \mathrm{d}x = \text{constant} \qquad (k = 1, 2, \cdots, n) \tag{2.110}$$

where r_k and τ_k are defined in Fig. 2.2. Equation (2.110) can be rewritten in the form

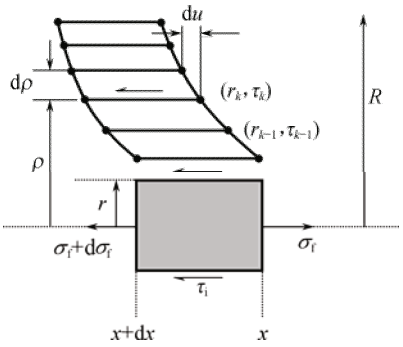

Fig. 2.2 Distribution of stresses and geometry of r_k and τ_k.

$$\frac{\tau_k}{\tau_l} = \frac{r_l}{r_k} \qquad (k, l = 1, 2, \cdots, n) \tag{2.111}$$

Thus, the shear stress τ in the matrix at any radius ρ is related to the interfacial shear stress, τ_i, of the fiber and fiber radius r by the following relation:

$$\tau = \tau_\mathrm{i} \frac{r}{\rho} \tag{2.112}$$

Using Eq. (2.112), the shear strain of the matrix near the fiber, which is a function of the displacement of the matrix, can be expressed as

$$\frac{\mathrm{d}u}{\mathrm{d}\rho} = \gamma = \frac{\tau}{G_\mathrm{m}} = \frac{\tau_\mathrm{i}}{G_\mathrm{m}} \left(\frac{r}{\rho} \right) \tag{2.113}$$

The difference between the displacement at R and that at r or the fiber surface at any point x can be obtained by integrating Eq. (2.113) with respect to ρ:

$$\left(u_R - u_r \right) = \int_{u_r}^{u_R} \mathrm{d}u = \frac{\tau_\mathrm{i} r}{G_\mathrm{m}} \int_r^R \frac{1}{\rho} \mathrm{d}\rho = \frac{\tau_\mathrm{i} r}{G_\mathrm{m}} \ln \left(\frac{R}{r} \right) \tag{2.114}$$

where $R=D/2$.

Substituting Eq. (2.114) into Eq. (2.109), we have

$$\frac{\mathrm{d}\sigma_{\mathrm{f}}}{\mathrm{d}x} = \frac{2G_{\mathrm{m}}(u_r - u_R)}{r^2 \ln(R/r)} \tag{2.115}$$

To determine the stress built up along the fiber, we need to establish the relationship of u_R and u_r with the fiber stress or strain. To simplify the following derivation, assume the fiber has no shear deformation, then $u_r = u_{\mathrm{f}}$ for any position r. Therefore

$$\frac{\mathrm{d}u_{\mathrm{f}}}{\mathrm{d}x} = \varepsilon_{\mathrm{f}} = \frac{\sigma_{\mathrm{f}}}{E_{\mathrm{f}}}, \qquad \frac{\mathrm{d}u_R}{\mathrm{d}x} \cong \varepsilon_{\mathrm{m}} \cong \varepsilon_{\mathrm{l}} \tag{2.116}$$

where ε_{m} and ε_{l} are respectively the longitudinal strains in the matrix and in the composite.

Differentiating Eq. (2.115) and using the relation in Eq. (2.116), we have

$$\frac{\mathrm{d}^2\sigma_{\mathrm{f}}}{\mathrm{d}x^2} = \beta^2(\sigma_{\mathrm{f}} - E_{\mathrm{f}}\varepsilon_{\mathrm{l}}) \tag{2.117}$$

where

$$\beta^2 = \frac{2G_{\mathrm{m}}}{r^2 E_{\mathrm{f}} \ln(D/d)} = \frac{2\pi G_{\mathrm{m}}}{A_{\mathrm{f}} E_{\mathrm{f}} \ln(D/d)} \tag{2.118}$$

with A_{f} being the area of fiber cross-secton, E_{f} the Young's modulus of the fiber, G_{m} the matrix shear modulus.

The solution of Eq. (2.117) is of the form

$$\sigma_{\mathrm{f}} = (\sigma_{\mathrm{f}})_{\mathrm{h}} + (\sigma_{\mathrm{f}})_{\mathrm{p}} \tag{2.119}$$

where $(\sigma_{\mathrm{f}})_{\mathrm{p}}$ is the particular solution and $(\sigma_{\mathrm{f}})_{\mathrm{h}}$ the homogeneous solution. They are

$$(\sigma_{\mathrm{f}})_{\mathrm{p}} = E_{\mathrm{f}}\varepsilon_{\mathrm{l}}, \quad (\sigma_{\mathrm{f}})_{\mathrm{h}} = A\sinh(\beta x) + B\cosh(\beta x) \tag{2.120}$$

The coefficients A and B can be determined from the boundary conditions:

$$\sigma_{\mathrm{f}} = 0 \qquad (\text{at } x = \pm L/2) \tag{2.121}$$

Substituting the boundary conditions (2.121) into Eq. (2.119) and after some mathematical manipulation, the resulting fiber and interfical shear stresses are

$$\begin{aligned} \sigma_{\mathrm{f}} &= E_{\mathrm{f}}\varepsilon_{\mathrm{m}}\left\{1 - \frac{\cosh(\beta x)}{\cosh(\beta L/2)}\right\}, \\ \tau_{\mathrm{i}} &= \frac{r}{2}E_{\mathrm{f}}\varepsilon_{\mathrm{m}}\beta\frac{\sinh\beta x}{\cosh(\beta L/2)} \end{aligned} \tag{2.122}$$

where L is the fiber length.

2.7 Hamiltonian method and symplectic mechanics

The strategy of simplifying a mechanical problem by exploiting symmetry so as to reduce the number of variables is one of classical mechanics' grand themes. It is theoretically deep, practically important, and recurrent in the history of the subject. The best-known general approach using the strategy is undoubtedly the symplectic Hamiltonian method [18], which uses displacements and associated general stresses as dual variables so that the boundary conditions are satisfied without any assumption of displacement or shape functions. Thus the complete solution space covering all kinds of boundary conditions along the edges can be obtained.

To illustrate the symplectic Hamiltonian method, we begin with considering the Principle of Virtual Work. It is one of the oldest principles in physics, which may find its origin in the work of Aristotle (384−322 B.C.) on the static equilibrium of levers. The principle of virtual work was written in its current form in 1717 by Jean Bernoulli (1667−1748) and states that a system composed of N particles is in static equilibrium if the virtual work

$$\delta W = \sum_{i=1}^{N} \mathbf{F}_i \cdot \delta \mathbf{x}_i = 0 \tag{2.123}$$

for all virtual displacements ($\delta\mathbf{x}_1, \cdots, \delta\mathbf{x}_N$) that satisfy physical constraints, where $\mathbf{F}_i$ is the force acting on the particle i. Given the commonness of systems of N particles with constraints, it is natural to seek a description of mechanics relevant only in the subset of 3D Euclidean space accessible to the system. The number of generalized coordinates required to specify completely the configuration of the system is called the number of degrees of freedom of the system. Typically, if a system of N particles, each having mass m_i and Cartesian coordinate $\mathbf{x}_i$ ($i = 1, \cdots, N$), is subjected to k holonomic constraints,

$$f_j(\mathbf{x}_1, \mathbf{x}_2, \cdots, \mathbf{x}_N, t) = 0 \qquad (j = 1, 2, \cdots, k) \tag{2.124}$$

we have $n = 3N - k$ generalized coordinates, q_i, which are *independent*.

It was Jean Le Rond d'Alembert (1717−1783) who generalized the principle of virtual work (in 1742) by including within it the accelerating force $-m_i \mathrm{d}^2\mathbf{x}_i / \mathrm{d}t^2$ (2.123):

$$\delta W = \sum_{i=1}^{N} (\mathbf{F}_i - m_i \frac{\mathrm{d}^2 \mathbf{x}_i}{\mathrm{d}t^2}) \cdot \delta \mathbf{x}_i = 0 \tag{2.125}$$

so that the equations of dynamics could be obtained.

To obtain the Lagrangian function of the system we need the *mapping* from the $n = 3N - k$ generalized coordinates to the usual Cartesian coordinates on R^3 for each

particle:

$$\begin{aligned}&\mathbf{x}_1 = \mathbf{x}_1(q^1, q^2, \cdots, q^n, t),\\ &\cdots\\ &\mathbf{x}_N = \mathbf{x}_N(q^1, q^2, \cdots, q^n, t)\end{aligned} \tag{2.126}$$

Note that this collection of mappings (2.126) is equivalent to a (single) time-parameterized mapping from the $3N$–k generalized coordinates $(q^1,\cdots,q^n)$ to the Euclidean hyperspace R^{3N} with $3N$ coordinates $(x_1, y_1, z_1,\cdots, x_N, y_N, z_N)$. Performing a Taylor expansion of the mapping, Eq. (2.126), about the point$(q^1,\cdots, q^n)$ (i.e., expanding $\mathbf{x}_i(q^1 + \delta q^1,\cdots, q^n + \delta q^n, t)$ about $(q^1,\cdots,q^n)$) at a fixed time t we obtain

$$\delta\mathbf{x}_i = \sum_{j=1}^{n} \frac{\partial \mathbf{x}_i}{\partial q^j}\delta q^j \tag{2.127}$$

The quantity $\partial\mathbf{x}_i/\partial q^j$ is analogous to the Jacobian of the transformation from $(q^1, \cdots, q^n) \Rightarrow (x_1, y_1, z_1,\cdots, x_N, y_N, z_N)$. Equation (2.127) can be used to cast D'Alembert's principle (2.125) in terms of the generalized coordinates

$$\delta W = \sum_{j=1}^{n}\left(\sum_{i=1}^{N}\left(\mathbf{F}_i - m_i\frac{\mathrm{d}^2\mathbf{x}_i}{\mathrm{d}t^2}\right)\cdot\frac{\partial\mathbf{x}_i}{\partial q^j}\right)\delta q^j = \sum_{j=1}^{n}\sum_{i=1}^{N}\left(\mathbf{Q}_i - m_i\frac{\mathrm{d}^2\mathbf{x}_i}{\mathrm{d}t^2}\cdot\frac{\partial\mathbf{x}_i}{\partial q^j}\right)\delta q^j = 0 \tag{2.128}$$

where $\mathbf{Q}_i$ is known as the generalized force acting on the particle i.

Making use of the relations

$$\begin{aligned}&r_i = \frac{\mathrm{d}\mathbf{x}_i}{\mathrm{d}t} = \frac{\partial\mathbf{x}_i}{\partial t} + \sum_{j=1}^{n}\frac{\partial\mathbf{x}_i}{\partial q^j}\dot{q}^j, \quad \frac{\partial r_i}{\partial\dot{q}^j} = \frac{\partial\mathbf{x}_i}{\partial q^j},\\ &m_i\frac{\mathrm{d}^2\mathbf{x}_i}{\mathrm{d}t^2}\cdot\frac{\partial\mathbf{x}_i}{\partial q^j} = \frac{\mathrm{d}}{\mathrm{d}t}\left(m_i r_i\cdot\frac{\partial\mathbf{x}_i}{\partial q^j}\right) - m_i r_i\cdot\frac{\partial r_i}{\partial q^j}\end{aligned} \tag{2.129}$$

and the definition of the kinetic energy of the system $K = \sum_{i=1}^{N} m_i r_i \cdot r_i / 2$, Eq. (2.128) leads to

$$\sum_{i=1}^{n}\left[\frac{\mathrm{d}}{\mathrm{d}t}\left(\frac{\partial K}{\partial\dot{q}^j}\right) - \frac{\partial K}{\partial q^j} - Q_j\right]\delta q^j = 0 \tag{2.130}$$

which is D'Alembert's principle in configuration space. Since the system is, by hypothesis, *holonomic*, the q^j form a set of independent coordinates. Any virtual displacement δq^j is independent of δq^k $(k \neq j)$ and, therefore, for Eq. (2.130) to

hold, each term in the sum must separately vanish. For non-trivial δq^j this can only happen if each coefficient vanishes, or, equivalently

$$\frac{\mathrm{d}}{\mathrm{d}t}\left(\frac{\partial K}{\partial \dot{q}^j}\right)-\frac{\partial K}{\partial q^j}-Q_j=0 \qquad (j=1,2,\cdots,n) \tag{2.131}$$

Equation (2.131) are frequently referred to as Lagrange's equations, in which we note that the generalized force Q_j is associated with any active (conservative or nonconservative) force $\mathbf{F}_j$. Hence, for a *conservative* active force derivable from a scalar potential function V (i.e., $\mathbf{F} = -\nabla U(q^1,\cdots, q^n,t)$), the ith component of the generalized force is $Q_i = -\partial U/\partial q^i$, and Lagrange's equation (2.131) becomes

$$\frac{\mathrm{d}}{\mathrm{d}t}\left(\frac{\partial L}{\partial \dot{q}^j}\right)-\frac{\partial L}{\partial q^j}=0 \qquad (j=1,2,\cdots,n) \tag{2.132}$$

where the Lagrangian is defined as: $L=K-V$.

The n second-order Euler-Lagrange equations (2.132) can be written as $2k$ first-order differential equations, known as Hamilton's equations (William Rowan Hamilton, 1805−1865), in a $2n$-dimensional *phase* space with coordinates $\mathbf{z} = (q^1, \cdots, q^k; p^1,\cdots, p^k)$, where the dual variable of p according to Legendre's transformation is

$$p_j(\mathbf{q},\dot{\mathbf{q}},t)=\frac{\partial L}{\partial q^j}(\mathbf{q},\dot{\mathbf{q}},t) \tag{2.133}$$

In terms of these new coordinates, the Euler-Lagrange equations (2.132) are transformed into Hamilton's canonical equations

$$\frac{\mathrm{d}q^j}{\mathrm{d}t}=\frac{\partial H}{\partial p^j}, \qquad \frac{\mathrm{d}p^j}{\mathrm{d}t}=-\frac{\partial H}{\partial q^j} \tag{2.134}$$

where the Hamiltonian function H is defined from the Lagrangian function L by the Legendre transformation (Adrien-Marie Legendre, 1752−1833):

$$H(\mathbf{q},\mathbf{p},t)=\mathbf{p}\cdot\dot{\mathbf{q}}(\mathbf{q},\mathbf{p},t)-L(\mathbf{q},\dot{\mathbf{q}}(\mathbf{q},\mathbf{p},t),t) \tag{2.135}$$

Using the definition of state vector $\boldsymbol{\nu} = \{\mathbf{q}, \mathbf{p}\}^{\mathrm{T}}$, Eq. (2.134) can be expressed as

$$\dot{\boldsymbol{\nu}}=\mathbf{H}\boldsymbol{\nu}+\mathbf{h} \tag{2.136}$$

where $\mathbf{H}$ is the Hamiltonian matrix and $\mathbf{h}$ is a $2n$-vector [18,19]. The Hamiltonian matrix $\mathbf{H}$ satisfies the matrix equation

$$\mathbf{JHJ}=\mathbf{H}^{\mathrm{T}} \tag{2.137}$$

where $\mathbf{J}$ is a symplectic matrix defined as

$$\mathbf{J}=\begin{bmatrix}0 & \mathbf{I}_n\\ -\mathbf{I}_n & 0\end{bmatrix},\quad \mathbf{J}^2=-\mathbf{I}_{2n},\quad \mathbf{J}^{\mathrm{T}}=-\mathbf{J} \tag{2.138}$$

With matrix **J**, a symplectic matrix **S** can be defined as

$$\mathbf{S}^{\mathrm{T}}\mathbf{J}\mathbf{S}=\mathbf{J} \tag{2.139}$$

As an application of symplectic mechanics we consider a plane stress problem with the strip domain V ($0\leqslant z\leqslant l,\ -h\leqslant x\leqslant h$) as shown in Fig. 2.3 [20]. The force equilibrium, constitutive, and boundary equations of the problem are respectively

$$\frac{\partial\sigma_x}{\partial x}+\frac{\partial\tau_{xy}}{\partial y}+f_x=0,\qquad \frac{\partial\tau_{xy}}{\partial x}+\frac{\partial\sigma_y}{\partial y}+f_y=0 \tag{2.140}$$

$$\begin{aligned}&\sigma_y=\bar{F}_{y1}(z),\quad \tau_{xy}=\bar{F}_{x1}(z)\qquad (y=-h)\\ &\sigma_y=\bar{F}_{y2}(z),\quad \tau_{xy}=\bar{F}_{x2}(z)\qquad (y=h)\end{aligned} \tag{2.141}$$

$$\sigma_x=\frac{E}{1-\upsilon^2}(\varepsilon_x+\upsilon\varepsilon_y),\quad \sigma_y=\frac{E}{1-\upsilon^2}(\varepsilon_y+\upsilon\varepsilon_x),\quad \tau_{xy}=\frac{E}{2(1+\upsilon)}\gamma_{xy} \tag{2.142}$$

where F_x and F_y are the body forces. The relationship between strain and displacement is expressed as

$$\varepsilon_x=\frac{\partial u}{\partial x},\qquad \varepsilon_y=\frac{\partial v}{\partial y},\qquad \gamma_{xy}=\frac{\partial v}{\partial x}+\frac{\partial u}{\partial y} \tag{2.143}$$

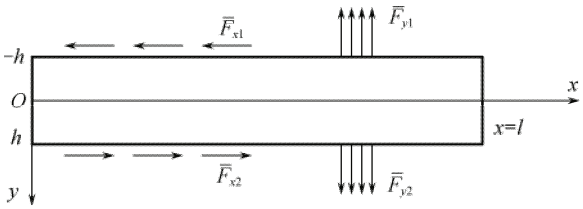

Fig. 2.3 Configuration of the strip domain and loading condition.

The corresponding potential variational functional and the strain energy density are then defined as

$$\delta U_{\mathrm{p}}=\delta\left\{(\mu_{\mathrm{e}}-uf_x-vf_y)\mathrm{d}x\mathrm{d}y-\int_0^l\left[(u\bar{F}_{x2}+v\bar{F}_{y2})_{y=h}-(u\bar{F}_{x1}+vF_{y1})_{x=-h}\right]\mathrm{d}x\right\}=0 \tag{2.144}$$

$$\mu_{\mathrm{e}}=\frac{E}{2(1-\upsilon^2)}\left[(\frac{\partial u}{\partial x})^2+(\frac{\partial v}{\partial y})^2+2\upsilon(\frac{\partial u}{\partial x})(\frac{\partial v}{\partial y})\right]+\frac{E}{4(1+\upsilon)}\left(\frac{\partial u}{\partial y}+\frac{\partial v}{\partial x}\right)^2 \tag{2.145}$$

To construct the corresponding Hamiltonian system, the x-coordinate is modeled as the time variable of the Hamiltonian system. If $\bar{F}_{xi} = \bar{F}_{yi} = 0$, the Lagrangian function of the problem is

$$L(w,u,\dot{w},\dot{u}) = \mu_e - uf_x - vf_y \tag{2.146}$$

The dual vectors **q** and **p** can then be defined as

$$\mathbf{q} = (w \quad u)^{\mathrm{T}}, \qquad \mathbf{p} = (\sigma \quad \tau)^{\mathrm{T}} \tag{2.147}$$

with

$$\sigma = \frac{\partial L}{\partial \dot{u}} = \frac{E}{1-\upsilon^2}(\dot{u} + \upsilon\frac{\partial v}{\partial y}), \qquad \tau = \frac{\partial L}{\partial \dot{v}} = \frac{E}{2(1+\upsilon)}(\dot{v} + \frac{\partial u}{\partial y}) \tag{2.148}$$

Equations (2.148) yields

$$\dot{u} = -\upsilon\frac{\partial v}{\partial y} + \frac{1-\upsilon^2}{E}\sigma, \quad \dot{v} = -\frac{\partial u}{\partial y} + \frac{2(1+\upsilon)}{E}\tau \tag{2.149}$$

Making use of Eqs. (2.140), (2.142), and (2.149), we have

$$\dot{\sigma} = -\frac{\partial \tau}{\partial y} - f_x, \quad \dot{\tau} = -E\frac{\partial^2 v}{\partial y^2} - \upsilon\frac{\partial \sigma}{\partial y} - f_y \tag{2.150}$$

Equations (2.149) and (2.150) can be written in matrix as

$$\dot{\mathbf{v}} = \begin{pmatrix} \dot{w} \\ \dot{u} \\ \dot{\sigma} \\ \dot{\tau} \end{pmatrix} = \begin{bmatrix} 0 & -\upsilon\frac{\partial}{\partial y} & \frac{1-\upsilon^2}{E} & 0 \\ -\frac{\partial}{\partial y} & 0 & 0 & \frac{2(1+\upsilon)}{E} \\ 0 & 0 & 0 & -\frac{\partial}{\partial y} \\ 0 & -E\frac{\partial^2}{\partial y^2} & -\upsilon\frac{\partial}{\partial y} & 0 \end{bmatrix} \begin{pmatrix} w \\ u \\ \sigma \\ \tau \end{pmatrix} + \begin{pmatrix} 0 \\ 0 \\ -f_x \\ -f_y \end{pmatrix} = \mathbf{H}\mathbf{v} + \mathbf{h} \tag{2.151}$$

The homogeneous solution of Eq. (2.151) can be obtained using the separation of the variable approach and the symplectic eigenfunction expansion. To this end, assume **v** in the form

$$\mathbf{v}(x,y) = \xi(x)\boldsymbol{\psi}(y) \tag{2.152}$$

Substituting Eq. (2.152) into Eq. (2.151) with **h**=0 yields the solution for $\xi(x)$:

$$\xi(x) = e^{\mu x} \tag{2.153}$$

and the eigenvalue equation:

$$\mathbf{H}\boldsymbol{\psi}(y) = \mu\boldsymbol{\psi}(y) \tag{2.154}$$

in which μ is an eigenvalue of the Hamiltonian operator matrix and $\boldsymbol{\psi}$ is given by

$$\boldsymbol{\psi}(y) = \begin{Bmatrix} \mathbf{q}(y) \\ \mathbf{p}(y) \end{Bmatrix} \tag{2.155}$$

Thus we have

$$\mathbf{v}(x, y) = e^{\mu x}\boldsymbol{\psi}(y) \tag{2.156}$$

It should be noted that the eigenvalue μ appears, in general, in n equal and opposite pairs, μ_i and $-\mu_i$ (i=1,2,$\cdots$,n) for a ($2n\times 2n$) Hamiltonian matrix $\mathbf{H}$, or else as μ_i and $1/\mu_i$ for a ($2n\times 2n$) symplectic matrix $\mathbf{S}$ [18,21]. Therefore, the $2n$ eigenvalues, when ordered appropriately, can be subdivided into the following two groups:

(a) $$\mu_i, \text{ with } \mathrm{Re}\,\mu_i < 0 \text{ , or } \mathrm{Re}\,\mu_i = 0 \bigcap \mathrm{Im}\,\mu_i < 0 \qquad (i = 1, 2, \cdots, n) \tag{2.157}$$

for a ($2n\times 2n$) Hamiltonian matrix $\mathbf{H}$, and

$$\mu_i, \quad \text{with } |\mu_i| \leqslant 1 \qquad (i = 1, 2, \cdots, n) \tag{2.158}$$

for a ($2n\times 2n$) symplectic matrix $\mathbf{S}$;

(b) $$\mu_{n+i} = -\mu_i \qquad (i = 1, 2, \cdots, n) \tag{2.159}$$

for a ($2n\times 2n$) Hamiltonian matrix $\mathbf{H}$, and

$$\mu_{n+i} = 1/\mu_i, \quad \text{with } |\mu_{n+i}| \geqslant 1 \qquad (i = 1, 2, \cdots, n) \tag{2.160}$$

for a ($2n\times 2n$) symplectic matrix $\mathbf{S}$.

Further, Zhong and Williams [18] pointed out that the eigenvectors of $\mathbf{H}$ (or $\mathbf{S}$) are related by the adjoint symplectic orthogonality relationship. Suppose that $\mathbf{y}_1$ and $\mathbf{y}_2$ are two eigenvectors of $\mathbf{H}$ (or $\mathbf{S}$), with corresponding eigenvalues μ_1 and μ_2 which are unequal, we have

$$\langle \boldsymbol{\psi}_i, \boldsymbol{\psi}_j \rangle = \int_{-h}^{h} \boldsymbol{\psi}_i^{\mathrm{T}} \mathbf{J} \boldsymbol{\psi}_j \mathrm{d}x = 0 \tag{2.161}$$

2.8 State space formulation

The idea of state space was used initially in system engineering and control theory. With state space representation, a system of linear differential equations for an engineering system can be described as

$$\begin{aligned}\dot{\mathbf{X}}(t) &= \mathbf{A}(t)\mathbf{X}(t) + \mathbf{B}(t)\mathbf{u}(t),\\ \mathbf{Y}(t) &= \mathbf{C}(t)\mathbf{X}(t) + \mathbf{D}(t)\mathbf{u}(t)\end{aligned} \tag{2.162}$$

where $\mathbf{X}(\cdot)$ is called the "state vector", $\mathbf{Y}(\cdot)$ is the "output vector", $\mathbf{u}(\cdot)$ is the "input (or control) vector", $\mathbf{A}(\cdot)$ is the "state matrix", $\mathbf{B}(\cdot)$ is the "input matrix", $\mathbf{C}(\cdot)$ is the "output matrix", and $\mathbf{D}(\cdot)$ is the "feedthrough (or feedforward) matrix" (see Fig. 2.4). For simplicity, $\mathbf{D}(\cdot)$ is often chosen to be the zero matrix, i.e. ,the system is designed to have no direct feed-through. Notice that in this general formulation all matrixes are assumed to be timevariant, i.e. ,some or all their elements can depend on time.

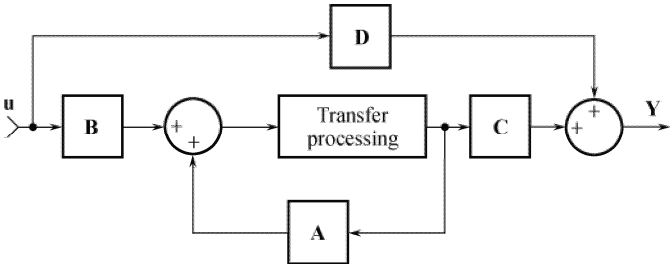

Fig. 2.4 A typical state space model.

This method was recently generalized to piezoelectric materials [22]. In the following, basic formulations of the state space method for piezoelectric materials presented in [22,23] are briefly described to provide a common source for reference in later chapters.

In [23], Sosa and Castro considered a two-dimensional piezoelectric material whose constitutive equation, strain-displacement and electric field-electric potential relations are, respectively, defined by Eqs. (1.24) and (1.2). The governing equation (1.10) reduces to

$$\sigma_{xx,x} + \sigma_{xz,z} = 0, \quad \sigma_{xz,x} + \sigma_{zz,z} = 0, \quad D_{x,x} + D_{z,z} = 0 \tag{2.163}$$

in which for simplicity all body forces and the electric charge density are assumed to be zero.

The basic idea behind the state space formulation is to describe a given physical system in terms of the minimum possible number of variables. Sosa and Castro achieved this by eliminating σ_{xx} and D_x from Eqs. (1.2), (1.24), and (2.163), presenting the following system of differential equations:

$$
\begin{aligned}
&u_{,z} = -w_{,x} + (\sigma_{zx} - e_{15}\phi_{,x})/c_{55},\\
&w_{,z} = (-\alpha u_{,x} + \kappa_{33}\sigma_{zz} + e_{33}D_z)/\gamma,\\
&\sigma_{zz,z} = -\sigma_{zx,x},\\
&\sigma_{zx,z} = \left(\frac{c_{13}^2}{c_{33}} - c_{11} - \frac{\beta^2}{\gamma c_{33}}\right)u_{,xx} + \left(\frac{\beta e_{33}}{\gamma c_{33}} - \frac{c_{13}}{c_{33}}\right)\sigma_{zz,x} - \frac{\beta}{\gamma}D_{z,x},\\
&\phi_{,z} = (-\beta u_{,x} + e_{33}\sigma_{zz} - c_{33}D_z)/\gamma,\\
&D_{z,z} = (-e_{15}\sigma_{zx,x} + \kappa\phi_{,xx})/c_{55}
\end{aligned}
\tag{2.164}
$$

where

$$
\begin{aligned}
&\alpha = c_{33}\kappa_{33} + e_{31}e_{33}, \quad \beta = c_{13}e_{33} - c_{33}e_{31},\\
&\gamma = c_{33}\kappa_{33} + e_{33}^2, \qquad \kappa = c_{55}\kappa_{11} + e_{15}^2
\end{aligned}
\tag{2.165}
$$

They then applied the Fourier transform (2.43) to Eq. (2.164), yielding

$$
\frac{\mathrm{d}}{\mathrm{d}z}\begin{Bmatrix} \hat{u}\\ \hat{w}\\ \hat{\sigma}_{zz}\\ \hat{\sigma}_{xz}\\ \hat{\phi}\\ \hat{D}_z \end{Bmatrix} = \begin{bmatrix} 0 & i\xi & 0 & c_{55}^{-1} & e_{15}c_{55}^{-1}i\xi & 0\\ \alpha i\xi/\gamma & 0 & \kappa_{33}/\gamma & 0 & 0 & e_{33}/\gamma\\ 0 & 0 & 0 & i\xi & 0 & 0\\ a_{41}\xi^2 & 0 & a_{43}i\xi & 0 & 0 & \beta i\xi/\gamma\\ \beta i\xi/\gamma & 0 & e_{33}/\gamma & 0 & 0 & -c_{33}/\gamma\\ 0 & 0 & 0 & e_{15}c_{55}^{-1}i\xi & -\kappa c_{55}^{-1}\xi^2 & 0 \end{bmatrix}\begin{Bmatrix} \hat{u}\\ \hat{w}\\ \hat{\sigma}_{zz}\\ \hat{\sigma}_{xz}\\ \hat{\phi}\\ \hat{D}_z \end{Bmatrix}
\tag{2.166}
$$

in which the assumptions are made that quantities u, $u_{,x}$, w, σ_{zz}, σ_{xz}, ϕ, $\phi_{,x}$, and D_z tend to zero as $|x| \to \infty$, and

$$
a_{41} = c_{11} + \frac{\beta^2}{\gamma c_{33}} - \frac{c_{13}^2}{c_{33}}, \qquad a_{43} = \frac{c_{13}}{c_{33}} - \frac{\beta e_{33}}{\gamma c_{33}}
\tag{2.167}
$$

Introducing the transformed state vector, $\hat{\mathbf{S}}(\xi, z) = \left\{\hat{u} \quad \hat{w} \quad \hat{\sigma}_{zz} \quad \hat{\sigma}_{xz} \quad \hat{\phi} \quad \hat{D}_z\right\}^{\mathrm{T}}$, Eq. (2.166) becomes

$$
\frac{\mathrm{d}\hat{\mathbf{S}}}{\mathrm{d}z}(\xi, z) = \mathbf{A}(\xi)\hat{\mathbf{S}}(\xi, z)
\tag{2.168}
$$

where $\mathbf{A}$ is a 6×6 matrix appearing in Eq. (2.166), whose only feature is having zeros in its main diagonal. The solution to Eq. (2.168) is given by [22]

$$
\hat{\mathbf{S}}(\xi, z) = \exp[z\mathbf{A}(\xi)]\hat{\mathbf{S}}(\xi, 0)
\tag{2.169}
$$

in which the exponential matrix is the transfer matrix that propagates the initial transformed state vector on the bounding surface into the field at depth z. Conse-

quently, the remaining task is to evaluate the transfer matrix $\exp[z\mathbf{A}]$, explicitly. Sosa obtained the solution by the following two steps:

(1) The eigenvalues λ of $\mathbf{A}$ are found from the associated characteristic equation:

$$\lambda^6 + p\xi^2\lambda^4 + q\xi^4\lambda^2 + r\xi^6 = 0 \tag{2.170}$$

where the coefficients p, q, and r, as functions of the material properties, are given by

$$\begin{aligned}
p &= \frac{1}{\gamma c_{55}}\left[\alpha c_{55} + \frac{\beta}{c_{33}}(2c_{33}e_{15} - e_{33}c_{55} - \beta) + \frac{\gamma}{c_{33}}(c_{13}c_{55} + c_{13}^2 - c_{11}c_{33}) - \kappa c_{33}\right], \\
q &= \frac{1}{\gamma c_{55}}\left[\frac{c_{33}c_{11} - c_{13}^2}{c_{33}}\left(c_{55}\kappa_{33} + 2e_{15}e_{33} + \frac{\kappa}{c_{55}} - \frac{e_{15}^2 c_{33}}{c_{55}}\right) - \kappa c_{13} + \frac{c_{13}}{c_{33}}(\alpha c_{55} + \beta e_{15})\right. \\
&\quad \left. - \frac{\kappa}{\gamma}(\alpha c_{33} + \beta e_{33}) + \frac{\alpha\beta}{\gamma}\left(e_{15} - \frac{e_{33}c_{55}}{c_{33}}\right) + \frac{\beta^2}{\gamma c_{33}}\left(c_{55}\kappa_{33} + e_{15}e_{33}\right)\right], \\
r &= \frac{\kappa}{\gamma^2 c_{55}}\left[\left(c_{13}^2 - c_{33}c_{11}\right)\left(\kappa_{33} + \frac{e_{33}^2}{c_{33}}\right) - \alpha c_{13} - \frac{\beta e_{33}c_{13}}{c_{33}}\right]
\end{aligned} \tag{2.171}$$

Sosa indicated that the roots of Eq. (2.170) can be found analytically. They can always be expressed in the following form:

$$\lambda_{1,4} = \pm a|\xi|, \qquad \lambda_{2,5} = \pm(b + ic)|\xi|, \qquad \lambda_{3,6} = \pm(b - ic)|\xi| \tag{2.172}$$

where a, b, and c are real numbers depending on the material properties.

(2) The matrix exponential is expanded into a matrix polynomial as

$$\exp[z\mathbf{A}] = a_0\mathbf{I} + a_1\mathbf{A} + a_2\mathbf{A}^2 + a_3\mathbf{A}^3 + a_4\mathbf{A}^4 + a_5\mathbf{A}^5 \tag{2.173}$$

where no higher powers of $\mathbf{A}$ are needed on account of the Cayley-Hamilton theorem, namely,

$$\mathbf{A}^6 + p\xi^2\mathbf{A}^4 + q\xi^4\mathbf{A}^2 + r\xi^6\mathbf{I} = 0 \tag{2.174}$$

The coefficients $a_0, \cdots, a_5$ in Eq. (2.173) are determined in terms of the eigenvalues of $\mathbf{A}$ by noting that each λ satisfies

$$\exp[z\lambda] = a_0 + a_1\lambda + a_2\lambda^2 + a_3\lambda^3 + a_4\lambda^4 + a_5\lambda^5 \tag{2.175}$$

Using Eq. (2.175) six times, each for each eigenvalue, generates an algebraic system of six equations with unknowns $a_0, \cdots, a_5$, whose solution is written as

$$a_i = \frac{1}{2}\sum_{j=1}^{3} \Lambda_{ij}\left[e^{\lambda_j z} + (-1)^i e^{-\lambda_j z}\right] \qquad (i = 1\text{-}5) \tag{2.176}$$

where

$$\Lambda_{0k}=\prod_{j=k+1}^{k+2}\frac{\lambda_j^2}{d_k},\qquad \Lambda_{1k}=\prod_{j=k+1}^{k+2}\frac{\lambda_j^2}{\lambda_k d_k},\qquad \Lambda_{2k}=\sum_{j=k+1}^{k+2}\frac{\lambda_j}{d_k},\qquad \Lambda_{3k}=\sum_{j=k+1}^{k+2}\frac{\lambda_j}{\lambda_k d_k},$$
$$\Lambda_{4k}=\frac{1}{d_k},\qquad \Lambda_{5k}=\frac{1}{\lambda_k d_k},\qquad d_k=(\lambda_{k+1}^2-\lambda_k^2)(\lambda_{k+2}^2-\lambda_k^2)\qquad (k=1,2,3) \tag{2.177}$$

Knowledge of the eigenvalues and, therefore, a_i from Eq. (2.176), together with the various powers of **A** provides the complete determination of the exponential matrix exp[z**A**]. Letting the exponential matrix be denoted by **B**(M, ξ, z), where the argument M emphasizes the dependence on the various material constants, one can write Eq. (2.169) as

$$\hat{\mathbf{S}}(\xi,z)=\mathbf{B}(M,\xi,z)\hat{\mathbf{S}}(\xi,0) \tag{2.178}$$

Thus, Eq. (2.178) gives the state vector consisting of the transformed stresses, displacements, electric potential, and electric displacement at an arbitrary depth z in the solution domain. Finally, solution (2.178) must be inverted to find the physical variables. Finding the inverse Fourier transform of Eq. (2.43) depends heavily on the problem under consideration. Sosa and Castro in [23] presented a detailed illustration of how to conduct the inverse Fourier transform of Eq. (2.178).

In this chapter, we have briefly introduced techniques of potential function, solution with Lekhnitskii formalism, techniques of Fourier transformation, Trefftz FEM, integral equations, shear-lag model, symplectic mechanics, and state space method, which are all used in later chapters.

References

[1] Ashida F, Tauchert TR, Noda N: A general-solution technique for piezothermoelasticity of hexagonal solids of class 6*mm* in Cartesian coordinates. Zeitschrift Fur Angewandte Mathematik Und Mechanik **74**(2), 87-95 (1994).

[2] Wang XQ, Agrawal OP: A new method for piezothermoelastic problems of solids of crystal class 6 *mm* in Cartesian coordinates. Computers & Structures **79**(20-21), 1831-1838 (2001).

[3] Lekhnitskii SG: Theory of Elasticity of An Anisotropic Elastic Body. Holden-Day, Inc., San Francisco (1963).

[4] Sosa H: Plane problems in piezoelectric media with defects. International Journal of Solids and Structures **28**(4), 491-505 (1991).

[5] Qin QH: A new solution for thermopiezoelectric solid with an insulated elliptic hole. Acta Mechanica Sinica **14**(2), 157-170 (1998).

[6] Qin QH, Mai YW: A new thermoelectroelastic solution for piezoelectric materials with

various opening. Acta Mechanica **138**(1-2), 97-111 (1999).
[7] Chue CH, Chen CD: Decoupled formulation of piezoelectric elasticity under generalized plane deformation and its application to wedge problems. International Journal of Solids and Structures **39**(12), 3131-3158 (2002).
[8] Yu SW, Qin QH: Damage analysis of thermopiezoelectric properties .1. Crack tip singularities. Theoretical and Applied Fracture Mechanics **25**(3), 263-277 (1996).
[9] Yu SW, Qin QH: Damage analysis of thermopiezoelectric properties .2. Effective crack model. Theoretical and Applied Fracture Mechanics **25**(3), 279-288 (1996).
[10] Barnett DM, Lothe J: Dislocations and line charges in anisotropic piezoelectric insulators. Physica Status Solidi B: Basic Research **67**(1), 105-111 (1975).
[11] Qin QH: Fracture Mechanics of Piezoelectric Materials. WIT Press, Southampton (2001).
[12] Qin QH: Variational formulations for TFEM of piezoelectricity. International Journal of Solids and Structures **40**(23), 6335-6346 (2003).
[13] Qin QH: Solving anti-plane problems of piezoelectric materials by the Trefftz finite element approach. Computational Mechanics **31**(6), 461-468 (2003).
[14] Wang HT, Sze KY, Yang XM: Analysis of electromechanical stress singularity in piezoelectrics by computed eigensolutions and hybrid-Trefftz finite element models. Computational Mechanics **38**(6), 551-564 (2006).
[15] Qin QH, Wang HT: Matlab and C Programming for Trefftz Finite Element Methods. CRC Press, Boca Raton (2009).
[16] Pipkin AC: A Course on Integral Equations. Springer-Verlag, New York (1991).
[17] Cox HL: The elasticity and strength of paper and other fibrous materials. British Journal of Applied Physics **3**(Mar.), 72-79 (1952).
[18] Zhong WX, Williams FW: Physical interpretation of the symplectic orthogonality of the eigensolutions of a Hamiltonian or symplectic matrix. Computers and Structures **49**, 749-750 (1993).
[19] Lim CW, Xu XS: Symplectic elasticity: theory and applications. Applied Mechanics Reviews **63**, 050802 (2010).
[20] Wang JS: Study on interface mechanics and local effects of multi-field coupled materials. PhD Thesis, Tianjin University (2007).
[21] Zhong WX, Williams FW: On the direct solution of wave-propagation for repetitive structures. Journal of Sound and Vibration **181**(3), 485-501 (1995).
[22] Sosa HA: On the modelling of piezoelectric laminated structures. Mechanics Research Communications **19**(6), 541-546 (1992).
[23] Sosa HA, Castro MA: On concentrated loads at the boundary of a piezoelectric half-plane. Journal of the Mechanics and Physics of Solids **42**(7), 1105-1122 (1994).

Chapter 3 Fibrous Piezoelectric Composites

In the previous two chapters we presented some fundamental ideas about piezoelectric composites and their mathematical treatment, including the linear theory of piezoelectricity and the corresponding solution techniques. We now try to generalize these ideas to a range of fibrous composite problems such as piezoelectric fiber push-out and pull-out, stress and electric field transfer between fiber and matrix, debonding criteria for the fiber push-out test, effective material properties of composites, and solutions of piezoelectric composites with an elliptic fiber. All these topics are analyzed within the framework of linear theory of piezoelectric materials.

3.1 Introduction

Piezoelectric fiber composites (PFCs), which comprise uniaxially aligned piezoelectric fibers embedded in a polymer matrix, have been widely used in recent years as transducers in applications such as sensors and actuators, sonar projectors, underwater use, medical ultrasonic imaging applications, and health monitoring systems [1]. There are currently four leading industrial types of actuators that hold promise for intelligent structure applications. The first type is referred to as 1-3 composites, manufactured by Smart Material Corp. [2], and is typically used for ultrasonic and acoustic control applications. Active fiber composite (AFC) actuators were developed at MIT and were the first composite actuators to focus primarily on structural actuation [3-5]. Third, macrofiber composites (MFC) were developed at NASA Langley Research Center, also for structural actuation purposes [6]. Lastly, the idea of active composites fabricated with hollow cross-section fibers has been proposed [7] as a means of lowering the typically high voltages required to actuate AFCs and MFCs.

It is noted that in the application of these smart composites, fracture induced by crack and interlaminar delimination is a major concern in many applications of PFCs, especially in aerospace where high structural reliability is required. Among various mechanisms contributing to the fracture resistance of composite materials, bridging by reinforcing fibers is considered to be of high interest because it provides direct closure traction to the bridged crack [8]. To correlate the interfacial mechanical properties and experimental results and to study the mechanical behavior of the interface of PFCs, it is necessary to develop theoretical models (or empirical formulation) for analyzing stress and electric fields in piezoelectric fiber tests such as the push-out test and/or the pull-out test. Based on shear-lag assumptions, the energy criterion and the Lamé solution for a 2D-axisymmetric problem,

many micromechanics models have been established over the past decades to provide a theoretical basis for single fiber pull-out tests. The Gao-Mai-Cotterell model [9] and its modifications [10-12] have provided a theoretical basis for the analysis of stress distribution, interface debonding and friction for the pull-out test, using a fracture mechanics approach. Zhou et al. [13] reported a theoretical model for evaluation of the interfacial properties of ceramic matrix composites (with no piezoelectric effect) in push-out tests, based on the fracture mechanics approach. For PFC, Liu et al. [8] presented a theoretical model of fiber pull-out for simulation of the relationship between crack-opening and bridging stress using a shear stress criterion. Gu et al. [14] extended the model in [8] to include electric field input. Recently, Qin et al. [15] developed a theoretical model for analyzing piezoelectric behavior in piezoelectric fiber push-out tests. Wang and Qin [16] presented a debonding criterion for determining interlaminar delimination during piezoelectric fiber push-out tests. Based on the model in [15] and some assumptions, Wang et al. [17] studied stress and electric field transfer in push-out tests under both electrical loading and mechanical loading.

On the other hand, increasing applications of fibrous piezoelectric composites have naturally increased interest in the micromechanics modeling for such materials. Early reports of the effective material properties of isotropic reinforced solids are due to Hill [18], and a companion work in 1964 [19] on mechanical properties of fiber-strengthened materials. Hill's report indicated that the overall elastic moduli of fibrous composites are connected by simple universal relations at given concentrations. Exact values of the effective properties can be determined when the phases have equal transverse shear modulus. In piezoelectric problems, Grekov et al. [20] studied the composite cylinder effective model for piezocomposites, Dunn and Taya [21] simplified the piezoelectric Eshelby's tensors of the elliptic fiber problem and put them in explicit form instead of elliptic integrals, and then they extended the dilute, self-consistent, Mori-Tanaka and differential micromechanics methods to cover piezoelectric composites. Schulgasser [22] found that the effective constants of a two-phase fibrous piezoelectric composite are connected by simple relations. Benveniste and Dvorak [23] showed that in such composites, uniform fields can be generated by certain loading conditions. The concept of uniform fields was further elaborated by Benveniste [24,25] in two-, three-, and four-phase composites with cylindrical microstructures. Chen [26] presented a number of exact results for overall moduli of a piezoelectric composite consisting of many perfectly-bonded phases of cylindrical shape. Mallik and Ray [27] reported improvement of the effective material coefficient of piezoelectric fiber reinforced composites by assuming the same electric field in both matrix and fiber phases. Huang and Kuo [28] directly extended the Eshelby type equivalent inclusion method to piezomagnetic composites and proposed an analogous simplification of Eshelby's tensors [29]. Jiang et al. [30,31] presented a three-phase confocal elliptical model, in which the generalized self-consistent method

for piezocomposites was developed as for thermo-electro-magneto-elastic composites. Recently, Tong et al. [32] presented a three-phase model under in-plane mechanical load coupling with thermo-electro- magnetical loads. Kumar and Chakraborty [33] developed an effective coupled thermo-electro-mechanical model of piezoelectric fiber reinforced composite using an approach based on strength of materials . This chapter, however, only includes most of the results appearing in [8,14-17,24-26,34,35].

3.2 Basic formulations for fiber push-out and pull-out tests

The geometric configuration of the micromechanical model used in the single piezoelectric fiber pull-out test and push-out test is shown in Fig. 3.1 [8,16], with an interfacial debonding crack of length l. A piezoelectric fiber polarized in the axial direction with radius a and length L is embedded at the centre of a coaxial cylindrical shell of epoxy matrix with external radius b. A uniform stress σ_a (tension in pull-out test and pressure in push-out test) and an electrical loading ϕ_a are applied at the end of the fiber ($z = 0$). The piezoelectric fiber is considered transversely isotropic and the epoxy is isotropic. In the following, basic formulations for the model shown in Fig. 3.1 are presented in order to establish notation and to provide a common source for reference in later sections of this chapter.

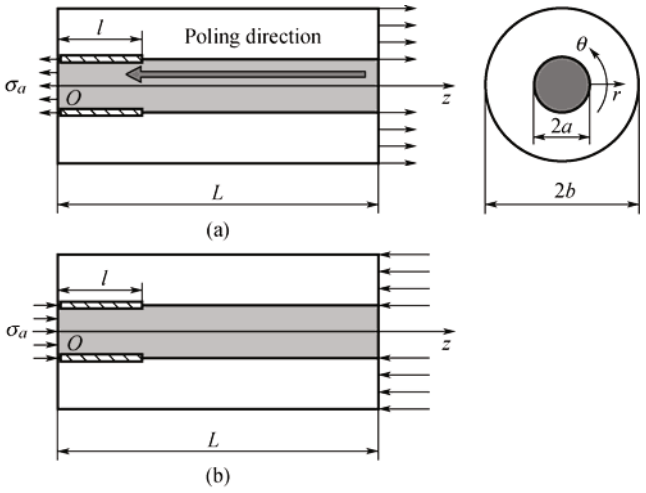

Fig. 3.1 Mechanics model of PFCs in (a) fiber pull-out test, (b) fiber push-out test.

Based on linear piezoelectric theory, the relationship between strains and stresses is expressed as [36]

$$\begin{bmatrix} \varepsilon_{rr}^{\mathrm{f}} \\ \varepsilon_{\theta\theta}^{\mathrm{f}} \\ \varepsilon_{zz}^{\mathrm{f}} \\ 2\varepsilon_{rz}^{\mathrm{f}} \end{bmatrix} = \begin{bmatrix} f_{11} & f_{12} & f_{13} & 0 \\ f_{12} & f_{11} & f_{13} & 0 \\ f_{13} & f_{13} & f_{33} & 0 \\ 0 & 0 & 0 & f_{55} \end{bmatrix} \begin{bmatrix} \sigma_{rr}^{\mathrm{f}} \\ \sigma_{\theta\theta}^{\mathrm{f}} \\ \sigma_{zz}^{\mathrm{f}} \\ \sigma_{rz}^{\mathrm{f}} \end{bmatrix} + \begin{bmatrix} 0 & g_{13} \\ 0 & g_{13} \\ 0 & g_{33} \\ g_{15} & 0 \end{bmatrix} \begin{bmatrix} D_r \\ D_z \end{bmatrix} \tag{3.1}$$

$$\begin{bmatrix} E_r \\ E_z \end{bmatrix} = -\begin{bmatrix} 0 & 0 & 0 & g_{15} \\ g_{13} & g_{13} & g_{33} & 0 \end{bmatrix} \begin{bmatrix} \sigma_{rr}^{\mathrm{f}} \\ \sigma_{\theta\theta}^{\mathrm{f}} \\ \sigma_{zz}^{\mathrm{f}} \\ \sigma_{rz}^{\mathrm{f}} \end{bmatrix} + \begin{bmatrix} \beta_{11} & 0 \\ 0 & \beta_{33} \end{bmatrix} \begin{bmatrix} D_r \\ D_z \end{bmatrix} \tag{3.2}$$

for pure mechanical loading, and

$$\begin{bmatrix} \varepsilon_{rr}^{\mathrm{f}} \\ \varepsilon_{\theta\theta}^{\mathrm{f}} \\ \varepsilon_{zz}^{\mathrm{f}} \\ 2\varepsilon_{rz}^{\mathrm{f}} \end{bmatrix} = \begin{bmatrix} f_{11} & f_{12} & f_{13} & 0 \\ f_{12} & f_{11} & f_{13} & 0 \\ f_{13} & f_{13} & f_{33} & 0 \\ 0 & 0 & 0 & f_{55} \end{bmatrix} \begin{bmatrix} \sigma_{rr}^{\mathrm{f}} \\ \sigma_{\theta\theta}^{\mathrm{f}} \\ \sigma_{zz}^{\mathrm{f}} \\ \tau_{rz}^{\mathrm{f}} \end{bmatrix} + \begin{bmatrix} 0 & d_{13} \\ 0 & d_{13} \\ 0 & d_{33} \\ d_{15} & 0 \end{bmatrix} \begin{bmatrix} E_r \\ E_z \end{bmatrix} \tag{3.3}$$

$$\begin{bmatrix} D_r \\ D_z \end{bmatrix} = \begin{bmatrix} 0 & 0 & 0 & d_{15} \\ d_{13} & d_{13} & d_{33} & 0 \end{bmatrix} \begin{bmatrix} \sigma_{rr}^{\mathrm{f}} \\ \sigma_{\theta\theta}^{\mathrm{f}} \\ \sigma_{zz}^{\mathrm{f}} \\ \tau_{rz}^{\mathrm{f}} \end{bmatrix} + \begin{bmatrix} \kappa_{11} & 0 \\ 0 & \kappa_{33} \end{bmatrix} \begin{bmatrix} E_r \\ E_z \end{bmatrix} \tag{3.4}$$

for electromechanical loading [17], where the superscripts "m" (in Eq. (3.5) below) and "f " refer to the variable associated with "matrix" and "fiber" respectively. In the above formula, (d_{ij}, g_{ij}) and (β_{ij}, κ_{ij}) are piezoelectric coefficient and dielectric constants, f_{ij} are components of elastic compliance. The constitutive relations of the elastic matrix are given by

$$\begin{Bmatrix} \varepsilon_r^{\mathrm{m}} \\ \varepsilon_\theta^{\mathrm{m}} \\ \varepsilon_z^{\mathrm{m}} \\ 2\varepsilon_{rz}^{\mathrm{m}} \end{Bmatrix} = \frac{1}{E} \begin{bmatrix} 1 & -\upsilon & -\upsilon & 0 \\ -\upsilon & 1 & -\upsilon & 0 \\ -\upsilon & -\upsilon & 1 & 0 \\ 0 & 0 & 0 & 2(1+\upsilon) \end{bmatrix} \begin{Bmatrix} \sigma_{rr}^{\mathrm{m}} \\ \sigma_{\theta\theta}^{\mathrm{m}} \\ \sigma_{zz}^{\mathrm{m}} \\ \sigma_{rz}^{\mathrm{m}} \end{Bmatrix} \tag{3.5}$$

The general equilibrium equations for the fiber-matrix system are given by

$$\frac{\partial \sigma_{zz}^j}{\partial z} + \frac{\partial \sigma_{rz}^j}{\partial r} + \frac{\sigma_{rz}^j}{r} = 0 \tag{3.6}$$

$$\frac{\partial \sigma_{rr}^j}{\partial r} + \frac{\partial \sigma_{rz}^j}{\partial z} + \frac{\sigma_{rr}^j - \sigma_{\theta\theta}^j}{r} = 0 \tag{3.7}$$

$$\frac{\partial D_r}{\partial r}+\frac{D_r}{r}+\frac{\partial D_z}{\partial z}=0 \tag{3.8}$$

where j=m, f. Making use of Eqs. (3.6) and (3.7), the equilibrium between the axial stress and the interfacial stress can be expressed as

$$\sigma_a=\sigma_{zz}^{\mathrm{f}}+\frac{1}{\gamma}\sigma_{zz}^{\mathrm{m}} \tag{3.9}$$

$$\frac{\mathrm{d}\sigma_{zz}^{\mathrm{m}}}{\mathrm{d}z}=\frac{2\gamma}{a}\tau_i(z) \tag{3.10}$$

$$\frac{\mathrm{d}\sigma_{zz}^{\mathrm{f}}}{\mathrm{d}z}=-\frac{2}{a}\tau_i(z) \tag{3.11}$$

where

$$\gamma=a^2/(b^2-a^2) \tag{3.12}$$

and all stresses appearing in Eqs. (3.9)-(3.11) are taken to be the corresponding average values with respect to the cross section. Substituting Eqs. (3.10) and (3.11) into Eq. (3.6) yields the shear stresses in the fiber and the matrix as follows:

$$\sigma_{rz}^{\mathrm{f}}=\frac{r}{a}\tau_i(z) \tag{3.13}$$

$$\sigma_{rz}^{\mathrm{m}}=\gamma\frac{(b^2-r^2)}{ar}\tau_i(z) \tag{3.14}$$

The electric field, E_i, is defined in Eq. (1.2), i.e.,

$$E_r=-\frac{\partial\phi}{\partial r},\qquad E_z=-\frac{\partial\phi}{\partial z} \tag{3.15}$$

To simplify the derivation of the theoretical model and without loss of generality, the axial stresses σ_{zz}^{f} and σ_{zz}^{m} are assumed to be functions of z only, and the electric potential which is caused by elastic deformation of the fiber is also independent of r [15], i.e.,

$$\sigma_{zz}^{\mathrm{f}}=\sigma_{zz}^{\mathrm{f}}(z),\qquad \sigma_{zz}^{\mathrm{m}}=\sigma_{zz}^{\mathrm{m}}(z),\qquad \phi=\phi(z) \tag{3.16}$$

For a long fiber ($L>>a$) polarized in the z-direction embedded in a relatively large matrix, this assumption is appropriate, and because of the transversely isotropic property of the piezoelectric fiber the following assumption is still acceptable:

$$\sigma_{rr}^{\mathrm{f}}(z)=\sigma_{\theta\theta}^{\mathrm{f}}(z)=q_i(z) \tag{3.17}$$

where $q_i(z)$ is the interfacial radial stress induced by Poisson contraction between the fiber and the matrix or/and applied electric field. Using Eqs. (3.2), (3.8), (3.15), and (3.16), the electric displacements in the fiber can be expressed in terms of fiber stresses as

$$D_z^{\mathrm{f}} = d_{15}\sigma_{zz}^{\mathrm{f}}, \qquad D_r^{\mathrm{f}} = d_{15}\sigma_{rz}^{\mathrm{f}} \tag{3.18}$$

Substituting Eq. (3.17) into Eq. (3.3), we obtain

$$\varepsilon_{rr}^{\mathrm{f}} = \varepsilon_{\theta\theta}^{\mathrm{f}} \tag{3.19}$$

Using the strain-displacement relationships in the axi-symmetric problem

$$\varepsilon_{rr} = \frac{\partial u_r}{\partial r} \quad \text{and} \quad \varepsilon_{\theta\theta} = \frac{u_r}{r} \tag{3.20}$$

we have

$$\frac{\partial u_r}{\partial r} = \frac{u_r}{r} \tag{3.21}$$

where u_r is the radial displacement. The solution of Eq. (3.21) shows that ε_r and ε_θ are independent of the coordinate r. Thus, it can be concluded that the axial electric field E_z is also independent of the variable r [14]. Integrating Eq. $(3.15)_2$ with respect to z, we obtain

$$\phi(r,z) = f_1(r) + f_2(z) \tag{3.22}$$

Substituting Eq. (3.22) into Eqs. (3.4) and (3.8), we have

$$f_1(r) = A\ln r + B \tag{3.23}$$

$$f_2(z) = \int \frac{1}{\kappa_{33}}[2d_{13}q_i(z) + (d_{33} - d_{15})\sigma_{zz}^{\mathrm{f}}(z)]\mathrm{d}z + Cz + D \tag{3.24}$$

in which A, B, C, and D are integral constants and, in general, it is assumed that B=D=0 because there is no effect on E_i and D_i after the differential operation [14]. Note that $f_1(r)$ approaches infinity when r tends to 0, which implies A=0. C can be determined by using the electric boundary condition, say,

$$D_z\big|_{z=0} = D_0 \tag{3.25}$$

where D_0 is the electric displacement applied at the end of the fiber. Making use of Eqs. (3.4) and (3.24), C can be determined as

$$C = d_{15}\sigma_a - D_0 \tag{3.26}$$

It can be seen from Eq. (3.24) that the electric potential is also independent of

the variable r.

In the frictional sliding interface, $0 \leqslant z \leqslant l$, the interfacial shear stress τ_i is governed by Coulomb's friction law [36]. That is,

$$\tau_i(z) = -\mu\left[q_0 - q_i(z)\right] \tag{3.27}$$

in which μ is a constant coefficient of friction and q_0 is the residual fiber clamping (compressive) stress in the radial direction caused by matrix shrinkage and differential thermal contraction of the constituents upon cooling from the processing temperature.

The outer boundary conditions of the matrix are given by

$$\sigma_r^{\mathrm{m}}\Big|_{r=b} = 0, \qquad \sigma_{rz}^{\mathrm{m}}\Big|_{r=b} = 0 \tag{3.28}$$

At the interface, the radial stresses and displacements of the fiber and matrix satisfy

$$\sigma_{rr}^{\mathrm{m}}\Big|_{r=a} = \sigma_{rr}^{\mathrm{f}}\Big|_{r=a} = q_i, \qquad u_r^{\mathrm{m}}\Big|_{r=a} = u_r^{\mathrm{f}}\Big|_{r=a} \tag{3.29}$$

At the bonded interface, $l \leqslant z \leqslant L$, the continuity of axial deformations requires that

$$u_z^{\mathrm{m}}\Big|_{r=a} = u_z^{\mathrm{f}}\Big|_{r=a} \tag{3.30}$$

The remaining task is to derive the differential equation for σ_{zz}^{f} and radial stress $q_i(z)$ due to elastic deformation in composites with a perfectly bonded interface or in the frictional sliding process after the interface is completely debonded. The detailed derivations for these two processes are provided in the following three sections.

3.3 Piezoelectric fiber pull-out

In this section a theoretical model presented in [8,14] is introduced for investigating the interaction between fiber deformation, pull-out stress and electric fields. The model can be used to examine stress distributions in the fiber under both mechanical and electric loads. In the following, the solutions for elastic and electric fields in both bonded region and frictional sliding region are presented.

3.3.1 Relationships between matrix stresses and interfacial shear stress

The radial and hoop stresses in the matrix can be expressed in terms of

$\tau_i(z)$ and $q_i(z)$ by way of the strain compatibility and equilibrium equations. Noting that by assumption, the axial stress is dependent on z only, the strain compatibility equation can be written as [14]

$$\sigma_{rr}^{\mathrm{m}} - \sigma_{\theta\theta}^{\mathrm{m}} = \frac{r}{1+\upsilon}\left(\frac{\partial \sigma_{\theta\theta}^{\mathrm{m}}}{\partial r} - \upsilon \frac{\partial \sigma_{rr}^{\mathrm{m}}}{\partial r}\right) \tag{3.31}$$

Substituting Eq. (3.31) into Eq. (3.7) we obtain

$$\sigma_{rr}^{\mathrm{m}} + \sigma_{\theta\theta}^{\mathrm{m}} = -\frac{r^2}{2a(1+\upsilon)}\frac{\partial \tau_i(z)}{\partial z} + F(z) \tag{3.32}$$

where the function $F(z)$ is to be determined by the boundary conditions. In the pull-out test, the boundary conditions for radial and hoop stresses can be assumed to be

$$\sigma_{rr}^{\mathrm{m}}\big|_{r=a} = q_i(z) \quad \text{and} \quad \sigma_{rr}^{\mathrm{m}}\big|_{r=b} = 0 \tag{3.33}$$

Thus, the solutions for radial and hoop stresses can be written as

$$\begin{aligned} \sigma_{rr}^{\mathrm{m}}(r,z) &= p_1(r)q_i(z) + p_2(r)\frac{\mathrm{d}\tau_i(z)}{\mathrm{d}z}, \\ \sigma_{rr}^{\mathrm{m}}(r,z) &= p_3(r)q_i(z) + p_4(r)\frac{\mathrm{d}\tau_i(z)}{\mathrm{d}z} \end{aligned} \tag{3.34}$$

where

$$p_1(r) = \gamma\left(\frac{b^2}{r^2} - 1\right),$$

$$p_2(r) = \frac{\gamma}{4a}\left\{2\eta_1 b^2\left[\ln\frac{b}{r} + \gamma \ln\frac{b}{a}\left(1 - \frac{b^2}{r^2}\right)\right] + \eta_2\left(1 - \frac{b^2}{r^2}\right)(r^2 - a^2)\right\},$$

$$p_3(r) = -\gamma\left(\frac{b^2}{r^2} + 1\right),$$

$$p_4(r) = \frac{\gamma\eta_1}{4a}\left\{2b^2\left[\ln\frac{b}{r} + \gamma\ln\frac{b}{a}\left(1 + \frac{b^2}{r^2}\right)\right] + 2(r^2 - b^2)\right\}$$
$$+ \frac{\gamma\eta_2}{4a}\left(-1 - \frac{b^2}{r^2}\right)(r^2 + a^2) + 4b^2$$

with

$$\eta_1 = 1 + \upsilon, \qquad \eta_2 = (3+\upsilon)/2$$

3.3.2 Solution for bonded region

In the solution for the bonded region, the following continuity conditions at $r=a$ can be used:

$$u_r^{\mathrm{f}} = u_r^{\mathrm{m}}, \qquad u_z^{\mathrm{f}} = u_z^{\mathrm{m}} \tag{3.35}$$

Making use of Eqs. (3.9) and (3.17) and the continuity condition (3.35), we have

$$q_i(z) = \frac{g_2 \dfrac{\mathrm{d}\tau_i(z)}{\mathrm{d}z} + g_3\beta(\sigma_a - \sigma_z^{\mathrm{f}}) - a_2\sigma_z^{\mathrm{f}} - a_3}{a_1 - g_1} \tag{3.36}$$

where

$$a_1 = f_{11} + f_{12} - \frac{2d_{13}^2}{\kappa_{33}}, \qquad a_2 = f_{33} - \frac{d_{13}(d_{33} - d_{15})}{\kappa_{33}}, \qquad a_3 = \frac{d_{13}(D_0 - d_{15}\sigma_a)}{\kappa_{33}}$$

$$g_1 = \frac{p_3(a) - \upsilon}{E}, \qquad g_2 = \frac{p_4(a)}{E}, \qquad g_3 = -\frac{\upsilon}{E}$$

Combining Eqs. (3.9), (3.11), (3.35) and (3.36) with axial displacements and stresses, a second-order differential equation of the axial stress in the fiber is obtained:

$$\frac{\mathrm{d}^2\sigma_{zz}^{\mathrm{f}}}{\mathrm{d}z^2} + A_1\sigma_{zz}^{\mathrm{f}} + A_2 = 0 \tag{3.37}$$

where

$$A_1 = M_1 / M, \qquad A_2 = M_2 / M$$

$$M = -\frac{a}{2}\left[(b_1 - h_1)g_2 - (a_1 - g_1)h_2\right],$$

$$M_1 = -(b_1 - h_1)(a_2 + \gamma g_3) + (a_1 - g_1)(b_2 + \gamma h_3),$$

$$M_2 = (b_1 - h_1)(-a_3 + \gamma g_3\sigma_a) + (a_1 - g_1)(b_3 - \gamma h_3\sigma_a)$$

$$b_1 = 2f_{13} - \frac{2d_{13}d_{33}}{\kappa_{33}}, \qquad b_2 = f_{33} - \frac{d_{33}(d_{33} - d_{15})}{\kappa_{33}}, \qquad b_3 = \frac{d_{33}(D_0 - d_{15}\sigma_a)}{\kappa_{33}}$$

$$h_1 = -\frac{\upsilon[p_3(a) + 1]}{E}, \qquad h_2 = -\frac{\upsilon p_4(a)}{E}, \qquad h_3 = \frac{1}{E}$$

For the case of the pull-out test shown in Fig. 3.1(a), the boundary conditions are

$$\sigma_{zz}^{\mathrm{f}}(0) = \sigma_a, \qquad \sigma_{zz}^{\mathrm{f}}(L) = 0 \tag{3.38}$$

The solution to Eq. (3.37) is then obtained as

$$\sigma_{zz}^{\mathrm{f}}(z) = k_1 e^{\lambda z} + k_2 e^{-\lambda z} - A_2 / A_1 \tag{3.39}$$

where

$$\lambda = \sqrt{-A_1}, \qquad k_1 = \frac{e^{-\lambda L}}{1 - e^{-2\lambda L}} \left[(1 - e^{-\lambda L}) \frac{A_2}{A_1} - e^{-\lambda L} \sigma_a \right],$$

$$k_2 = \frac{1}{1 - e^{-2\lambda L}} \left[(1 - e^{-\lambda L}) \frac{A_2}{A_1} + \sigma_a \right]$$

As mentioned in [14], based on Eq. (3.39), the interfacial shear stress $\tau_i(z)$ can be evaluated from Eq. (3.11). Then the interfacial normal stress $q_i(z)$ can be determined from Eq. (3.36). Meanwhile the electric potential can be calculated from Eqs. (3.22)-(3.24) with the proper boundary conditions, such as $\phi(L) = 0$.

In this chapter, the yielding shear stress, τ_y, is taken as the maximum shear stress at which debonding starts along the interface between fiber and matrix, if the shear stress at the interface reaches τ_y.

3.3.3 Solution for debonded region

In the case of friction sliding, the interfacial shear stress is determined from Coulomb's friction law (3.27). Making use of Eqs. (3.9), (3.11), (3.27), and (3.36), we obtain

$$\frac{\mathrm{d}^2 \sigma_{zz}^{\mathrm{f}}}{\mathrm{d}z^2} + B_1 \frac{\mathrm{d}\sigma_{zz}^{\mathrm{f}}}{\mathrm{d}z} B_2 \sigma_{zz}^{\mathrm{f}} + B_3 = 0 \tag{3.40}$$

where

$$B_i = N_i / N \qquad (i = 1, 2, 3)$$

$$N = -a\mu g_2 / 2, \qquad N_1 = a(a_1 - g_1)/2,$$
$$N_2 = -\mu(a_2 + \gamma g_3), \qquad N_3 = \mu[(-a_3 + \gamma g_3 \sigma_a) + (a_1 - g_1) D_0]$$

Equation (3.40) can be solved for fiber stress using the following boundary conditions [14]:

$$\sigma_{zz}^{\mathrm{f}}(0) = \sigma_a, \qquad \sigma_{zz}^{\mathrm{f}}(L - l) = 0 \tag{3.41}$$

The solution to Eqs. (3.40) and (3.41) can, then, be written as

$$\sigma_{zz}^{\mathrm{f}}(z) = k_3 e^{\lambda_1 z} + k_4 e^{\lambda_2 z} - B_3 / B_2 \tag{3.42}$$

where

$$\lambda_{1,2}=\frac{-B_1\pm\sqrt{B_1^2-4B_2}}{2},$$

$$k_3=\frac{e^{-\lambda_1(L-l)}}{1-e^{(\lambda_1-\lambda_2)(L-l)}}\left[(1-e^{\lambda_2(L-l)})\frac{B_3}{B_2}-e^{\lambda_2(L-l)}\sigma_a\right],$$

$$k_4=\frac{1}{1-e^{(\lambda_1-\lambda_2)(L-l)}}\left[(1-e^{-\lambda_1(L-l)})\frac{B_3}{B_2}+\sigma_a\right]$$

3.3.4 Numerical results

To illustrate applications of the theoretical model described above, numerical results are presented for a piezoelectric/epoxy system, of which the material properties are [8]: E=3 GPa, υ=0.4, f_{11}= 0.019 GPa^{-1}, f_{33}= 0.015 GPa^{-1}, f_{12} =–0.005 7 GPa^{-1}, f_{13} =–0.004 5 GPa^{-1}, f_{55}= 0.039 GPa^{-1}. The radii of the matrix and fiber are 3 mm and 0.065 mm, respectively. The piezoelectric parameters of the fiber are given by: d_{33}=390×10^{-12} m/V, d_{13} =–d_{15}=–190×10^{-12} m/V, κ_{11}=40×10^{-9} N/V^2, κ_{33}=16.25×10^{-9} N/V^2. The interfacial properties are approximately evaluated as τ_s=0.04 GPa and μ=0.8. The initial thermal stress q_0 is taken to be 0.

Figure 3.2 shows the stress and electric fields in the piezoelectric fiber, where the debonding length is 0.4 mm. In the debonded region ($0\leqslant z\leqslant 0.4$), both the fiber axial stress and the electric field are nearly constant. In the bonded area, their values reduce rapidly. In the boundary between the bonded and debonded regions, E_z has a significant increment.

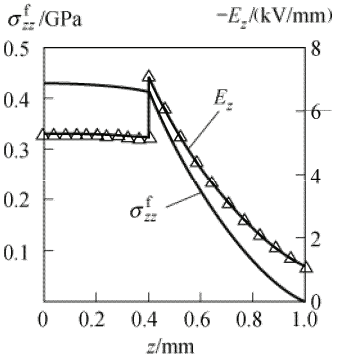

Fig. 3.2 Stress and electric fields in the piezoelectric fiber.

3.4 Piezoelectric fiber push-out

In the previous section we presented a theoretical model for simulating the me-

chanical behavior of PFCs in a pull-out test. Extension to the case of PFCs in the push-out test is described in this section. The mechanics model to be employed is shown in Fig. 3.1(b). Using the piezoelectric fiber push-out model presented in this section, the effect of piezoelectric constant and embedded fiber length on the mechanical behavior of fiber composites is investigated. The results show that there is a significant effect of the piezoelectric parameter and embedded fiber length on stress transfer, electric field distribution and load-displacement curve of the frictional sliding process.

3.4.1 Stress transfer in the bonded region

Stress transfer is of fundamental importance in determining the mechanical properties of fiber-reinforced composite materials. For the interface in PFCs, stress transfer is affected by the piezoelectric coefficient in addition to the micromechanical properties. In the following, the derivation of a second-order differential equation of σ_{zz}^{f} presented in [15,17] is briefly reviewed.

Consider the mechanics model shown in Fig. 3.1(b). The inner and outer boundary conditions of the matrix are given by

$$\sigma_{rr}^{\mathrm{m}}(a,z)=q_i(z),\qquad \sigma_{rz}^{\mathrm{m}}(a,z)=\tau_i(z),\qquad \sigma_{rr}^{\mathrm{m}}(b,z)=0,\qquad \tau_{rz}^{\mathrm{m}}(b,z)=0 \tag{3.43}$$

Then from Eqs. (3.14) and (3.43), we obtain [37]

$$\begin{aligned}\sigma_{rr}^{\mathrm{m}}(r,z)=&\gamma q_i(z)(b^2/r^2-1)+\frac{\gamma}{4a}\frac{\mathrm{d}\tau_i}{\mathrm{d}z}\\&\times\left\{2\eta_1 b^2\left[\ln(r/b)+\gamma(b^2/r^2-1)\ln(b/a)\right]+\eta_2(b^2-r^2)(1-a^2/r^2)\right\}\end{aligned} \tag{3.44}$$

$$\begin{aligned}\sigma_{\theta\theta}^{\mathrm{m}}(r,z)=&-\gamma q_i(z)(1+r^2/b^2)+\frac{\gamma}{4a}\frac{\mathrm{d}\tau_i}{\mathrm{d}z}\left\{2\eta_1 b^2\left[\ln(r/b)\right.\right.\\&\left.\left.-\gamma(b^2/r^2+1)\ln(b/a)\right]+4b^2+2\eta_1(b^2-r^2)+\eta_2(b^2+r^2)(1+a^2/r^2)\right\}\end{aligned} \tag{3.45}$$

Substituting Eqs. (3.44) and (3.45) into Eq. (3.5) yields

$$\begin{aligned}\frac{Eu_r^{\mathrm{m}}}{r}=&\gamma q_i(z)\left[(-\upsilon-1)b^2/r^2-1+\upsilon\right]-\upsilon\sigma_z^{\mathrm{m}}+\frac{\gamma}{4a}\frac{\mathrm{d}\tau_i}{\mathrm{d}z}\left\{2\eta_1 b^2(1-\upsilon)\left[\ln(r/b)\right.\right.\\&\left.-\gamma\ln(b/a)\right]+2\eta_1 b^2\gamma\ln(b/a)(-\upsilon-1)b^2/r^2+\eta_2\left(b^2+r^2\right)\left(1+a^2/r^2\right)\\&\left.-\upsilon\eta_2\left(b^2-r^2\right)\left(1-a^2/r^2\right)+4b^2+2\eta_1\left(b^2-r^2\right)\right\}\end{aligned} \tag{3.46}$$

$$\frac{E\partial u_z^{\mathrm{m}}}{\partial z} = 2\upsilon\gamma q_i(z) - \upsilon\sigma_z^{\mathrm{m}} - 2\upsilon\frac{\gamma}{4a}\frac{\mathrm{d}\tau_i}{\mathrm{d}z}\left\{2\eta_1 b^2\left[\ln(r/b) - \gamma\ln(b/a)\right]\right.$$
$$\left.+\eta_1\left(b^2 - r^2\right) + 2b^2 + \eta_2\left(a^2 + b^2\right)\right\} \tag{3.47}$$

For a fully bonded interface, the continuity conditions of axial and radial deformation between fiber and matrix are given in Eqs. (3.29) and (3.30). From Eqs. (3.1), (3.30) and (3.47), the radial stress of the fiber is obtained as

$$q_i(z) = \frac{1}{2(f_{13} - \gamma\upsilon/E)}\left\{\gamma\sigma_a/E - \left(\gamma/E + f_{33} + g_{33}d_{15}\right)\sigma_z^{\mathrm{f}} - 2\upsilon\frac{\gamma}{4Ea}\frac{\mathrm{d}\tau_i}{\mathrm{d}z}\right.$$
$$\left.\times\left[2\eta_1 b^2(1+\gamma)\ln(a/b) + \eta_1(b^2 - a^2) + 2b^2 + \eta_2(a^2 + b^2)\right]\right\} \tag{3.48}$$

Then, combining Eqs. (3.1), (3.29), (3.46), and (3.48) yields the differential equation of σ_z^{f} in the form

$$\frac{\mathrm{d}^2\sigma_z^{\mathrm{f}}(z)}{\mathrm{d}z^2} - A_1\sigma_z^{\mathrm{f}}(z) = A_2\sigma_a \tag{3.49}$$

where A_1 and A_2 are two constants:

$$A_1 = -\frac{-\gamma\upsilon/E + f_{13} + g_{31}d_{15} - B_1(\gamma/E + f_{33} + g_{33}d_{15})}{\frac{\gamma}{8}(C_1 + 2B_1\upsilon C_2/E)} \tag{3.50}$$

$$A_2 = \frac{-\gamma\upsilon/E - B_1\gamma/E}{\frac{\gamma}{8}(C_1 + 2B_1\upsilon C_2/E)} \tag{3.51}$$

with

$$B_1 = \frac{f_{12} + f_{11} - \gamma(-\upsilon - 1)b^2/(Ea^2) + \gamma(1-\upsilon)/E}{2(f_{13} - \gamma\upsilon/E)} \tag{3.52}$$

$$C_1 = 2\eta_1 b^2(1-\tau)(1+\gamma)\ln(a/b)/E + 2\eta_1 b^2\gamma\ln(b/a)(-\upsilon - 1)b^2/(Ea^2)$$
$$+ 2\eta_2(a^2 + b^2)/E + 4b^2/E + 2s_{11}\eta_1(b^2 - a^2) \tag{3.53}$$

$$C_2 = 2\eta_1 b^2(1+\gamma)\ln(a/b) + \eta_1(b^2 - a^2) + 2b^2 + \eta_2(a^2 + b^2) \tag{3.54}$$

$$\eta_1 = -2(1+\upsilon)/\upsilon \tag{3.55}$$

$$\eta_2 = -(1+\upsilon)/\upsilon - 1 \tag{3.56}$$

Using the stress boundary conditions

$$\sigma_z^{\mathrm{f}}(0)=\sigma_a,\qquad \sigma_z^{\mathrm{f}}(L)=0 \tag{3.57}$$

The axial stress in the piezoelectric fiber is given by

$$\sigma_z^{\mathrm{f}}(z)=K_1\sinh(\sqrt{A_1}z)+K_2\cosh(\sqrt{A_1}z)-\frac{A_2}{A_1}\sigma_a \tag{3.58}$$

where K_1 and K_2 are defined by

$$K_1=\frac{\dfrac{A_2}{A_1}-\left(1+\dfrac{A_2}{A_1}\right)\cosh(\sqrt{A_1}L)}{\sinh(\sqrt{A_1}L)}\sigma_a \tag{3.59}$$

$$K_2=\left(1+\frac{A_2}{A_1}\right)\sigma_a \tag{3.60}$$

In addition, using Eqs. (3.6), (3.7), and (3.17), $q_i(z)$ can be expressed as

$$q_i(z)=N_1\sigma_a-N_2\sigma_z^{\mathrm{f}}+N_3\frac{\mathrm{d}^2\sigma_z^{\mathrm{f}}}{\mathrm{d}z^2} \tag{3.61}$$

where N_i (i=1,2,3) are given by

$$N_1=\frac{\gamma}{2(Ef_{13}-\gamma\upsilon)},\qquad N_2=\frac{\gamma/E+f_{33}+g_{33}d_{15}}{2(f_{13}-\gamma\upsilon/E)},\qquad N_3=\frac{\gamma C_2\upsilon}{4E} \tag{3.62}$$

From Eqs. (3.2), (3.18), (3.58), and (3.61), the electric field E_z can be calculated by

$$E_z(z)=-2g_{31}q_i(z)+\left(\frac{d_{15}}{\kappa_{33}}-g_{33}\right)\sigma_{zz}^{\mathrm{f}}(z) \tag{3.63}$$

3.4.2 Frictional sliding

Once the interface debonds completely, the frictional sliding of the fiber out of the surrounding matrix will begin, which is the last stage of the push-out process. To better characterize this stage, theoretical analysis was conducted with the micromechanical model shown in Fig. 3.3.

For the sake of simplicity, we assume a small elastic deformation and a large displacement at the fiber-loaded end during sliding. Therefore, the elastic deformation of the fiber can be neglected, and the fiber axial displacement δ approximately equals the fiber sliding distance s, that is, $\delta\approx s$.

The governing equation for σ_z^{f} in this case can be derived in a manner similar

to the mathematical operation for Eq. (3.49). In fact, from the continuity condition of radial displacement (3.29) and Eqs. (3.6), (3.14), and (3.17), we have

$$q_i(z) = \frac{\gamma f_{13}}{D_1}\sigma_a - \frac{\gamma f_{13} - \upsilon / E + g_{31}d_{15}}{D_1}\sigma_z^{\mathrm{f}} + \frac{\gamma}{4a}\frac{C_1}{D_1}\frac{\mathrm{d}\tau_i}{\mathrm{d}z} \tag{3.64}$$

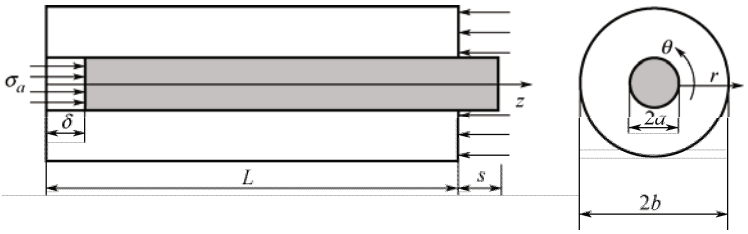

Fig. 3.3 A fiber-matrix cylinder model for frictional sliding in the push-out test.

Substituting Eq. (3.64) into Eq. (3.27) yields

$$\frac{\mathrm{d}^2\sigma_z^{\mathrm{f}}(z)}{\mathrm{d}z^2} + Q_1\frac{\mathrm{d}\sigma_z^{\mathrm{f}}(z)}{\mathrm{d}z} + Q_2\sigma_z^{\mathrm{f}}(z) = Q_3 \tag{3.65}$$

where Q_i (i=1,2,3) are given by

$$Q_1 = -\frac{4aD_1}{\mu\gamma C_1} \tag{3.66}$$

$$Q_2 = \frac{8(-\gamma\upsilon / E + f_{13} + g_{31}d_{15})}{\gamma C_1} \tag{3.67}$$

$$Q_3 = \frac{8D_1}{\gamma C_1}\left(\frac{-\gamma\upsilon}{D_1 E}\sigma_a - q_0\right) \tag{3.68}$$

with

$$D_1 = f_{12} + f_{11} - \gamma(-\upsilon - 1)b^2/(Ea^2) + \gamma(1-\upsilon)/E \tag{3.69}$$

Using the stress boundary conditions

$$\sigma_z^{\mathrm{f}}(s) = \sigma_a, \qquad \sigma_z^{\mathrm{f}}(L) = 0 \tag{3.70}$$

The solution to Eq. (3.65) is obtained as

$$\sigma_z^{\mathrm{f}}(z) = K_3 e^{\lambda_1 z} + K_4 e^{\lambda_2 z} + \frac{Q_3}{Q_2} \tag{3.71}$$

where s is the fiber sliding distance (see Fig. 3.3) and K_3, K_4, λ_1, λ_2 are given by

$$K_3 = Q_3 m_3 + n_3 \sigma_a , \qquad K_4 = Q_3 m_4 + n_4 \sigma_a \tag{3.72}$$

$$\lambda_1 = -\frac{1}{2} Q_1 + \frac{1}{2}\sqrt{Q_1^2 - 4Q_2} , \qquad \lambda_2 = -\frac{1}{2} Q_1 - \frac{1}{2}\sqrt{Q_1^2 - 4Q_2} \tag{3.73}$$

with

$$m_3 = \frac{e^{\lambda_2 L} - e^{\lambda_2 s}}{Q_2 (e^{\lambda_1 L + \lambda_2 s} - e^{\lambda_1 s + \lambda_2 L})} , \qquad m_4 = \frac{e^{\lambda_1 s} - e^{\lambda_1 L}}{Q_2 (e^{\lambda_1 L + \lambda_2 s} - e^{\lambda_1 s + \lambda_2 L})} \tag{3.74}$$

$$n_3 = -\frac{e^{\lambda_2 L}}{e^{\lambda_1 L + \lambda_2 s} - e^{\lambda_1 s + \lambda_2 L}} , \qquad n_4 = \frac{e^{\lambda_1 L}}{e^{\lambda_1 L + \lambda_2 s} - e^{\lambda_1 s + \lambda_2 L}} \tag{3.75}$$

In the process, the interfacial shear stress is governed by Coulomb's frictional law given in Eq. (3.27). Noting that fiber and matrix maintain contact in the radial direction, we have

$$u_r^{\mathrm{f}}(a, z) = u_r^{\mathrm{m}}(a, z) \tag{3.76}$$

Then, the radial normal stress can be expressed as

$$q_i(z) = M_1 - M_2 \sigma_a + M_3 \frac{\mathrm{d}^2 \sigma_z^{\mathrm{f}}}{\mathrm{d}z^2} \tag{3.77}$$

where M_i (i=1,2,3) are given by

$$M_1 = -\frac{\gamma \upsilon}{E D_1}, \qquad M_2 = \frac{-\gamma \upsilon / E + f_{13} + g_{31} d_{15}}{D_1} , \qquad M_3 = -\frac{\gamma C_1}{8 D_1} \tag{3.78}$$

Using Eqs. (3.2), (3.18), (3.71), and (3.77), the electric field can be obtained as

$$E_z(z) = -2 g_{31} q_i(z) + \left(\frac{d_{15}}{\kappa_{33}} - g_{33} \right) \sigma_z^{\mathrm{f}}(z) \tag{3.79}$$

Noting that the sum of the radial normal stress of the fiber should be negative, and the fiber and matrix can contact each other during the fiber sliding process, the radial stress must satisfy the expression

$$q_0 - q_i(z) \leqslant 0 \tag{3.80}$$

According to the distribution of the fiber stress fields in the push-out test, the axial stress reaches its maximum value at the fiber-loaded end $z = s$ ($s \geqslant 0$, and s is defined in Fig. 3.3), while the interfacial shear stress reaches its minimum value at the same location. Then Eq. (3.80) yields

$$q_0 - q_i(s) = 0 \tag{3.81}$$

Therefore the relationship between the applied stress σ_a and the axial dis-

placement δ ($\delta \approx s$) at the fiber-loaded end can be given as

$$\sigma_a = \frac{q_0(1 - m_3\lambda_1^2 e^{\lambda_1 s} - m_4\lambda_2 e^{\lambda_2 s})}{\frac{f_{13} + g_{31}d_{15}}{D_1} - \frac{\gamma\upsilon}{ED_1}(m_3\lambda_1^2 e^{\lambda_1 s} + m_4\lambda_2^2 e^{\lambda_2 s}) + \frac{\gamma C_1}{8D_1}(n_3\lambda_1^2 e^{\lambda_1 s} + n_4\lambda_2^2 e^{\lambda_2 s})} \tag{3.82}$$

3.4.3 PFC push-out driven by electrical and mechanical loading

The formulation presented above can handle push-out problems under mechanical loading only. In the following, discussion of PFC push-out testing subjected to both mechanical and electric loading is presented.

Consider now the electrical boundary conditions at the ends of the piezoelectric fiber:

$$\phi(0) = V, \qquad \phi(L) = 0 \tag{3.83}$$

From Eq. (3.24), we have

$$C = -\frac{V}{L} - \frac{1}{\kappa_{33}L}\int_0^L \left[2d_{13}q_i(z) + (d_{33} - d_{15})\sigma_z^{\mathrm{f}}(z)\right]\mathrm{d}z \qquad (D = V) \tag{3.84}$$

Following the procedure in Subsections 3.4.1 and 3.4.2, solutions of the stress fields in the bonded region ($l \leqslant z \leqslant L$) can be written as

$$\sigma_z^{\mathrm{m}}(z) = \gamma\omega\left(\sigma^* + \sigma_a\right)\left[1 - \exp(-\lambda z)\right] \tag{3.85}$$

$$\sigma_z^{\mathrm{f}}(z) = \sigma_a - \omega\left(\sigma^* + \sigma_a\right)\left[1 - \exp(-\lambda z)\right] \tag{3.86}$$

$$\tau_i(z) = \frac{a\lambda\omega}{2}(\sigma^* + \sigma_a)\exp(-\lambda z) \tag{3.87}$$

$$q_i(z) = -\frac{E\left[f_{13} - d_{13}(d_{33} - d_{15})/\kappa_{33}\right]\sigma_{zz}^{\mathrm{f}}(z) + \upsilon\sigma_z^{\mathrm{m}}(z) - Ed_{13}C}{E(f_{11} + f_{12} - 2d_{13}^2/\kappa_{33}) + 1 + 2\gamma + \upsilon} \tag{3.88}$$

in which

$$\omega = \frac{E\left[f_{13} - d_{13}(d_{33} - d_{15})/\kappa_{33}\right]}{E\left[f_{13} - d_{13}(d_{33} - d_{15})/\kappa_{33}\right] - \gamma\upsilon} \tag{3.89}$$

$$\sigma^* = -\frac{q_0 - q^*}{\rho\omega} \tag{3.90}$$

$$\lambda = \frac{2\mu\rho}{a} \tag{3.91}$$

$$\rho = -\frac{E\left[f_{13} - d_{13}(d_{33} - d_{15})/\kappa_{33}\right] - \gamma\upsilon}{E(f_{11} + f_{12} - 2{d_{13}}^2/\kappa_{33}) + 1 + 2\gamma + \upsilon} \tag{3.92}$$

$$q^* = \frac{Ed_{13}C}{E(f_{11} + f_{12} - 2{d_{13}}^2/\kappa_{33}) + 1 + 2\gamma + \upsilon} \tag{3.93}$$

The solutions of the stress fields in the bonded region ($l \leqslant z \leqslant L$) are obtained as

$$\sigma_z^{\mathrm{f}}(z) = \frac{\left(\frac{A_2}{A_1}\sigma_a + \sigma_l\right)\sinh\sqrt{A_1}(L-z) - \frac{A_2}{A_1}\sigma_a \sinh\sqrt{A_1}(l-z)}{\sinh\sqrt{A_1}(L-l)} - \frac{A_2}{A_1}\sigma_a \tag{3.94}$$

$$\sigma_z^{\mathrm{m}}(z) = \gamma\left(1 + \frac{A_2}{A_1}\right)\sigma_a - \gamma\frac{\left(\frac{A_2}{A_1}\sigma_a + \sigma_l\right)\sinh\sqrt{A_1}(L-z) - \frac{A_2}{A_1}\sigma_a \sinh\sqrt{A_1}(l-z)}{\sinh\sqrt{A_1}(L-l)} \tag{3.95}$$

$$\tau_i(z) = \frac{\lambda a\left[\left(\frac{A_2}{A_1}\sigma_a + \sigma_l\right)\cosh\sqrt{A_1}(L-z) - \frac{A_2}{A_1}\sigma_a \cosh\sqrt{A_1}(l-z)\right]}{2\sinh\sqrt{A_1}(L-l)} \tag{3.96}$$

where

$$\sigma_l = \sigma_{zz}^{\mathrm{f}}(l) = \sigma_a - \omega\left(\sigma^* + \sigma_a\right)\left[1 - \exp(-\lambda l)\right] \tag{3.97}$$

$$A_1 = \frac{2\left\{\gamma + E\left[f_{33} - d_{33}(d_{33} - d_{15})/\kappa_{33}\right] - 2\rho(\gamma\upsilon - Ef_{13} + Ed_{13}d_{33}/\kappa_{33})\right\}}{(1+\upsilon)\left[2\gamma b^2 \ln(b/a) - a^2\right]} \tag{3.98}$$

$$A_2 = -\frac{2\left\{\begin{array}{l}\left[\gamma + 2(\gamma\upsilon - Ef_{13} + Ed_{13}d_{33}/\kappa_{33})(\omega - 1)\rho\right] \\ +2\left[\gamma\upsilon - E\left(f_{13} - d_{13}d_{33}/\kappa_{33}\right)\right]q^*/\sigma_a + Ed_{33}C/\sigma_a\end{array}\right\}}{(1+\upsilon)\left[2\gamma b^2 \ln(b/a) - a^2\right]} \tag{3.99}$$

The electrical field E_z in both the debonded and bonded regions is given as

$$E_z = -\frac{1}{\kappa_{33}}\left[2d_{13}q_i(z) + (d_{33} - d_{15})\sigma_z^{\mathrm{f}}(z)\right] - C \tag{3.100}$$

3.4.4 Numerical assessment

To illustrate applications of the proposed theoretical model and to reveal the effects

of the electromechanical coupling on stress transfer behavior, numerical results are presented for a piezoceramic fiber/epoxy matrix system subjected to a push-out load. The material parameters are assumed to be the same as those used in Subsection 3.3.4. The radii of fiber and matrix are: $a = 0.065$ mm, $b = 3$ mm, $l = 0.6$ mm ($l = 0$ for fully bonded fiber), and $L = 2$ mm. The residual fiber clamping stress in radial direction q_0 is assumed to be –0.01 GPa and $\mu = 0.8$ [15,17].

Figures 3.4(a)-(d) shows the distribution of stresses and electric field as functions of the dimensionless axial distance z/L for a partially debonded piezoelectric composite system subject to a constant external stress $\sigma_a = 1.5$ GPa in the fiber push-out test. For comparison and illustration of the effect of electromechanical coupling on stress transfer behavior, the corresponding distribution of stresses for a non-piezoelectric fiber composite (NPFC) is also plotted in Fig. 3.4. It is found that the curves for PFC and NPFC have similar shapes. When subjected to applied stress of same value, the axial stress σ_z^{f} in PFC is smaller than that in NPFC (Fig. 3.4(a)). It can also be seen from Figs. 3.4(a) and 3.4(c) that both axial and radial stresses in the fiber gradually decrease as z/L increases. Figure. 3.4(c) demonstrates that there is a larger radial stress in the PFC and it decays more rapidly than that in NPFC, which leads to a larger interface shear stress in the debonded region

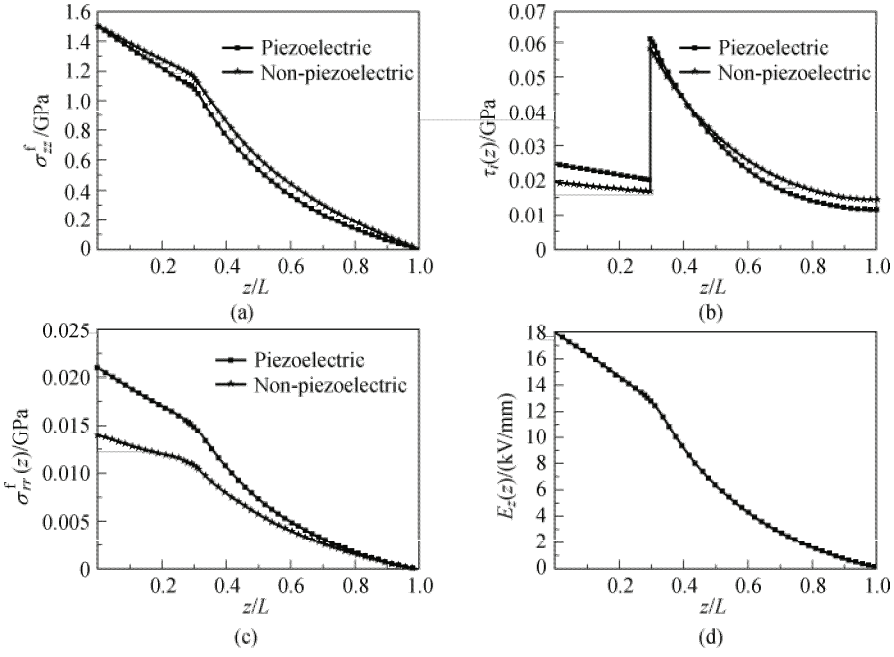

Fig. 3.4 Plot of (a) fiber axial stress, (b) interface shear stress, (c) fiber radial stress, (d) electric field for the piezoelectric fiber push-out under mechanical loading.

of PFC in Fig. 3.4(b) due to the Coulomb friction law (3.27). This phenomenon can be attributed to the piezoelectric effect in piezoelectric fiber; a larger applied stress is required in PFC to produce the same axial stress as in NPFC. The difference in the stress fields between these two composite systems is controlled by piezoelectric coefficients, which were investigated in [15] for fully bonded composites. When the piezoelectric coefficients and dielectric constants are set as zero, piezoelectric fiber degenerates to non-piezoelectric fiber. Figure 3.4(d) shows the variation of electrical field as a function of axial distance z/L. The variation of E_z with z/L is very similar to that of the fiber axial stress.

Figures 3.5(a)-(d) shows the distribution of stresses and electric field as functions of dimensionless axial distance z/L for a partially debonded piezoelectric composite system subject to electrical loading and a constant external stress $\sigma_a = 1.5$ GPa in the fiber push-out test. In order to study the effect of positive and negative electric loading on stress transfer, electric potentials of 5 000 V, 0 V, and –5 000 V are applied at the end of piezoelectric fiber ($z = 0$). Figure 3.5(a) shows that the fiber axial stress decays more rapidly under negative electric potential than under positive electric potential. It can also be seen from Fig. 3.5(c) that negative electric potential leads to a larger radial stress in the piezoelectric fiber than applied positive electric potential, whose positive electric potential accordingly causes a

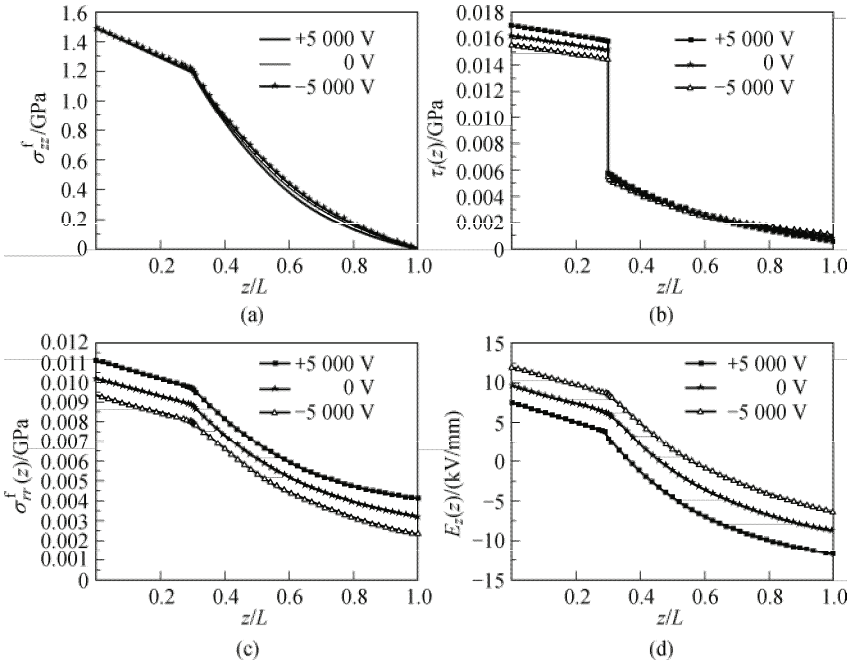

Fig. 3.5 Plot of (a) fiber axial stress, (b) interface shear stress, (c) fiber radial stress, (d) electric field for the piezoelectric fiber push-out under electrical and mechanical loading.

larger interface frictional shear stress in debonded region in Fig. 3.5(b). This is because when piezoelectric fiber is subjected to an electric potential applied parallel to the polarization direction, expansion occurs in the same direction and shrinkage occurs in the transverse direction [38]. For a positive applied electric potential, the hoop stress developed is in compression, while for a negative applied electric potential, the hoop stress developed is in tension. In Fig. 3.5(d), the distribution of electric field in the piezoelectric fiber is plotted via *z/L*, and it depends heavily on the applied electric field.

Figures 3.6-3.11 apply to problems with fully bonded fiber. Figures 3.6 and 3.7 present the distribution of fiber axial stress and interfacial shear stress at the first stage of push-out for different embedded fiber lengths. At the fiber end ($z/L=0$), the applied stress is given by $\sigma_a = -0.05$ GPa. It is evident that the stress distribution in the piezoelectric fiber is similar to that in conventional material fiber such as carbon fiber. The fiber axial stress decays rapidly near the fiber-loaded end and the rate of decay varies with the embedded fiber length. The curves in Fig. 3.7 show clearly that the maximum interfacial stress is not very sensitive to variation of fiber length when $L \geqslant 2$ mm , and the interfacial stress remains almost constant when $z/L \geqslant 0.6$, which is quite similar to the finding in [37].

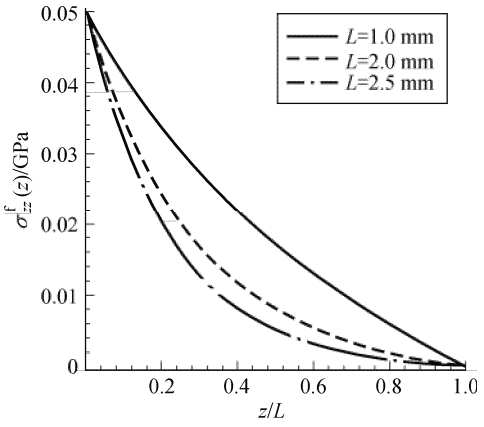

Fig. 3.6 The distribution of fiber axial stress $\sigma_{zz}^{f}(z)$ in fully bonded interfaces of different lengths (applied load stress σ_a is –0.05 GPa).

To study the effect of the piezoelectric parameter and electro-mechanical coupling on stress transfer, stress distribution is plotted in Figs. 3.8 and 3.9 for both non-piezolectric fiber and piezoelectric fiber with different d_{15} where the fiber length $L = 2.0$ mm. Figure 3.8 shows that axial stress decreases along with increase in the piezoelectric constant d_{15}, i.e., axial stress will be smaller at any given position *z/L* for a larger value of d_{15}. Axial stresses decay more rapidly in piezoelectric fiber than in non-piezoelectric fiber. The situation in Fig. 3.9 is

slightly different. There is a critical location $z_c / L \approx 0.24$ at which d_{15} has no effect on interfacial shear stress. It is evident from Fig. 3.9 that shear stress will increase when $z<z_c$ and decrease when $z>z_c$, along with an increase in the value of d_{15}. This phenomenon indicates that the higher the value of d_{15}, the higher the rate of decrease in both axial and shear stress. A comparison of the shear stress distributions in piezoelectric and non-piezoelectric fiber is also made and plotted in Fig. 3.9, and their significant difference is observed.

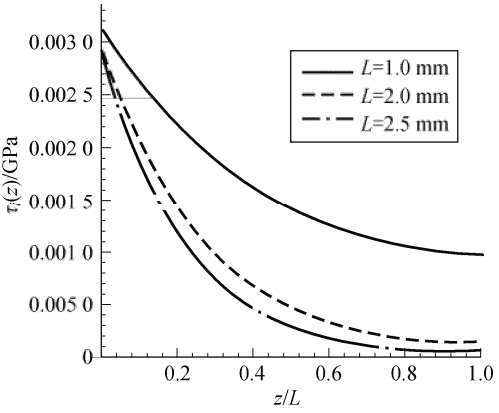

Fig. 3.7 The distribution of interfacial shear stress $\tau_i(z)$ in fully bonded interfaces of different lengths (applied load stress σ_a is –0.05 GPa).

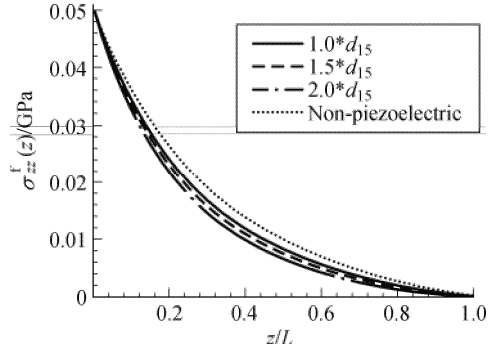

Fig. 3.8 The distribution of fiber axial stress $\sigma_{zz}^{f}(z)$ in a fully bonded region (applied load stress σ_a is –0.05 GPa and $d_{15} = 190 \times 10^{-12}$ m/V).

Because of the piezoelectric effect, an electric field exists in the fiber. The distribution of the electric field in axial direction E_z is shown Figs. 3.10 and 3.11. It can be seen from these two figures that the distribution of the electric field and the effect of the fiber length and the parameter d_{15} are quite similar to those of the

stress field (Figs. 3.6-3.9).

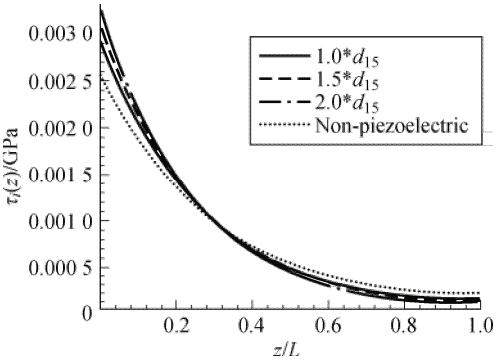

Fig. 3.9 The distribution of interfacial shear stress $\tau_i(z)$ in a fully bonded region (applied load stress σ_a is –0.05 GPa and $d_{15} = 190 \times 10^{-12}$ m/V).

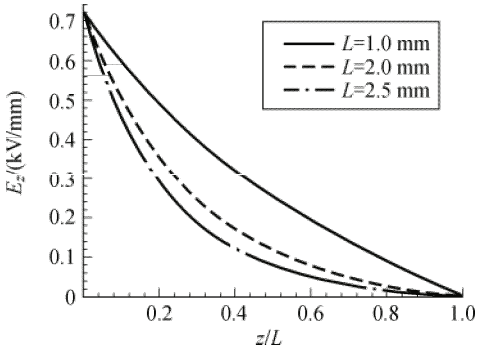

Fig. 3.10 The distribution of electric fields in piezoelectric fiber for different embedded lengths (applied load stress σ_a is –0.05 GPa and $d_{15} = 190 \times 10^{-12}$ m/V).

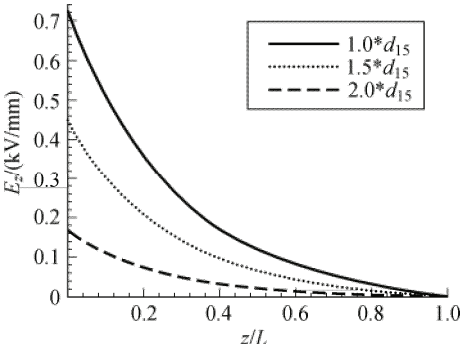

Fig. 3.11 The distribution of electric field in a piezoelectric fiber for different values of d_{15} (applied load stress σ_a is –0.05 GPa and $d_{15} = 190 \times 10^{-12}$ m/V).

3.5 Interfacial debonding criterion

In the previous two sections theoretical models were described for simulating fiber pull-out and push-out processes. A debonding criterion for identifying interfacial delimination during fiber push-out testing of PFC is introduced in this section. The debonding criterion can be used for investigating the debonding process of piezoelectric fiber in the push-out test under combined electrical and mechanical loading. The description in this section is based on the results presented in [16].

Unlike in NPFCs, there are electrical fields induced by the piezoelectric effect or inverse-piezoelectric effect of PFCs. Owing to this phenomenon, the debonding criterion for NPFCs is not directly applicable. To incorporate the piezoelectric effect in the debonding criterion we consider a cracked piezoelectric elastic body of volume V in which traction P, frictional stress t, and the surface electrical charge ω are applied. S_P, S_t and S_ω are the corresponding surfaces respectively, as shown in Fig. 3.12. For the sake of simplicity, the matrix is assumed to be a piezoelectric material whose piezoelectric coefficients and dielectric constants equal zero. In our analysis, the debonding region is taken to be a crack (see Fig. 3.12).

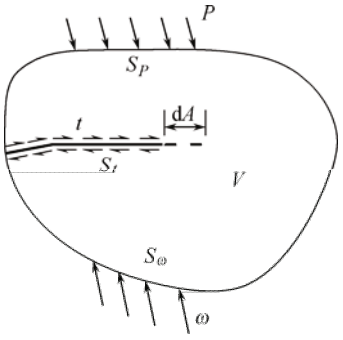

Fig. 3.12 A piezoelectric elastic body with a frictional crack under electromechanical loading.

Based on the principle of energy balance, the variation of energy in the piezoelectric system for crack growth dA along the friction surface under electromechanical loading is

$$\mathrm{d}\Pi = -G_c \mathrm{d}A - \mathrm{d}W_\mathrm{f} \tag{3.101}$$

where G_c is fracture energy, W_f is the work done by friction stress during crack growth,

$$W_\mathrm{f} = \int_{S_T} (t + t_0) v \mathrm{d}S \tag{3.102}$$

and Π is the generalized mechanical and electrical energy stored inside the pie-

zoelectric body:

$$\Pi = \frac{1}{2}\int_{\Omega}(e+e_0):(s+s_0)\mathrm{d}\Omega$$
$$-\frac{1}{2}\int_{\Omega}(D+D_0):(E+E_0)\mathrm{d}\Omega-\int_{S_P}Pu\mathrm{d}S+\int_{S_\omega}\omega\Phi\mathrm{d}S \tag{3.103}$$

in which v is the relative slip of crack surfaces and t_0 is the tangential component of pre-stress (or initial stress) on the crack surfaces. s_0, D_0, e_0, and E_0 are selfequilibrium initial stress, electrical displacement, strain, and electrical field respectively, and $s+s_0$ and $D+D_0$ balance the applied loads.

Using the basic theory of piezoelectricity (3.1)-(3.8), one can easily prove the corresponding reciprocal principle of work and the principle of virtual work for piezoelectric material:

$$\int_{\Gamma}t_i^1u_i^2\mathrm{d}\Gamma-\int_{\Gamma}\omega^1\Phi^2\mathrm{d}\Gamma+\int_{\Omega}f_i^1u_i^2\mathrm{d}\Omega=\int_{\Gamma}t_i^2u_i^1\mathrm{d}\Gamma-\int_{\Gamma}\omega^2\Phi^1\mathrm{d}\Gamma+\int_{\Omega}f_i^2u_i^1\mathrm{d}\Omega \tag{3.104}$$

$$\int_{\Gamma_t}\overline{t}_i\delta u_i\mathrm{d}\Gamma+\int_{\Omega}t_i\delta u_i\mathrm{d}\Omega-\int_{\Gamma_\omega}\overline{\omega}\delta\Phi\mathrm{d}\Gamma-\int_{\Omega}q\delta\Phi\mathrm{d}\Omega=\int_{\Omega}(\sigma_{ij}\delta\varepsilon_{ij}-D_i\delta E_i)\mathrm{d}\Omega \tag{3.105}$$

Using the two principles (3.104) and (3.105) and following a method similar to that employed for fiber pull-out analysis [39], it can be proved that U_t against the incremental debonding length, l, is equal to the energy release rate G_i for the debonded crack, that is

$$2\pi aG_i=\frac{\partial U_t}{\partial l} \tag{3.106}$$

in which U_t is the total elastic energy and electrical energy stored in the fiber and matrix, which can be expressed in the following form:

$$\begin{aligned}U_t=&\int_0^l\int_0^a\left[\sigma_z^{\mathrm{f}}\varepsilon_z^{\mathrm{f}}-D_zE_z\right]\pi r\mathrm{d}r\mathrm{d}z+\int_l^L\int_0^a\left[\sigma_z^{\mathrm{f}}\varepsilon_z^{\mathrm{f}}-D_zE_z\right]\pi r\mathrm{d}r\mathrm{d}z\\&+\int_0^l\int_a^b\left[\frac{(\sigma_z^{\mathrm{m}})^2}{E^{\mathrm{m}}}+\frac{2(1+\upsilon^{\mathrm{m}})}{E^{\mathrm{m}}}(\sigma_{rz}^{\mathrm{m}})^2\right]\pi r\mathrm{d}r\mathrm{d}z\\&+\int_l^L\int_a^b\left[\frac{(\sigma_z^{\mathrm{m}})^2}{E^{\mathrm{m}}}+\frac{2(1+\upsilon^{\mathrm{m}})}{E^{\mathrm{m}}}(\sigma_{rz}^{\mathrm{m}})^2\right]\pi r\mathrm{d}r\mathrm{d}z\end{aligned} \tag{3.107}$$

Then the following energy criterion is introduced:

$$G_i\geqslant G_{ic} \tag{3.108}$$

in which G_{ic} is the critical interface debonding energy release rate.

In Eq. (3.107), U_t is a complex function of the material properties of the constituents and geometric factors. Performing the mathematical operation over the debonded and bonded regions for a piezoelectric-epoxy composite system by utilizing a numerical quadrature approach, G_i derived in this study can be obtained as a second-order function of the applied stress σ_a for a fiber/matrix system with given debonding length *l*.

To illustrate the effect of electromechanical coupling on the debonding behavior of PFCs and to verify the proposed debonding criterion for the piezoelectric fiber push-out problem, a numerical example is considered for two composite systems, namely piezoelectric fiber/epoxy and non-piezoelectric fiber/epoxy. The parameters of the piezoelectric fiber and matrix are given as [8]:

$$f_{11} = 0.019\ \text{GPa}^{-1},\ f_{33} = 0.015\ \text{GPa}^{-1},\ f_{12} = -0.005\ 7\ \text{GPa}^{-1},$$
$$f_{13} = -0.004\ 5\ \text{GPa}^{-1},\ f_{55} = 0.039\ \text{GPa}^{-1},\ d_{33} = 390\times10^{-12}\ \text{m/V},$$
$$d_{31} = -d_{15} = -190\times10^{-12}\ \text{m/V},\ g_{33} = 24\times10^{-3}\ \text{V}\cdot\text{m/N},$$
$$g_{31} = -11.6\times10^{-3}\ \text{V}\cdot\text{m/N},\ e_{33} = 16.25\times10^{-9}\ \text{N/V}^2,\ E_{\text{m}} = 3\ \text{GPa},\ \upsilon_{\text{m}} = 0.4$$

The radii of fiber and matrix are given by: $a = 0.065$ mm, $b = 3$ mm, $l = 0.6$ mm, and $L = 2$ mm. The residual fiber clamping stress in the radial direction q_0 is –0.1 MPa and $\mu = 0.8$ [8]. It should be pointed out that real piezoelectric fibers have a wide variety of shapes and sizes. In general, the radius *a* of a piezoelectric fiber is about $5/400$ μm, and the fiber length $L < 200$ mm (More details as to the shape and size of a piezoelectric fiber can be found elsewhere [15,40-42]). In a real single fiber push-out test, in general, the ideal single fiber composite is the one with the value of the matrix radius *b* being variable, *b*>>*a*, and *L* between 1/2 mm (see[43] for details).

The geometric configuration and properties of non-piezoelectric fiber matrix and interfaces are the same as those of its counterpart, the piezoelectric fiber, except that the piezoelectric coefficients and dielectric constants are set as zero.

To illustrate the effect of electrical loading on stress transfer behavior, Fig. 3.13 presents the distributions of interfacial shear stress as functions of dimensionless axial distance *z*/*L* for partially debonded PFCs in the fiber push-out test. In the calculation, the debonding length is set to be $l = 0.6$ mm. The distribution of interfacial shear stress in PFC is similar to that in NPFC [13], in that both show a jump at the point l/L (i.e., the interface between the debonded and bonded regions). It is evident from Fig. 3.13 that there is a larger interface shear stress in the debonded region under an applied negative electrical potential. This is because, for piezoelectric fiber, expansion occurs in the same direction and shrinkage occurs in the transverse direction when the fiber is subjected to an electrical field applied parallel to the po-

larization direction. For an applied positive electrical potential, the hoop stress induced is in compression while for a negative applied electrical potential, the hoop stress developed is in tension [38]. Therefore, an applied negative electrical loading leads to a larger shear stress in the debonded region than that induced by a positive electrical loading, according to the Coulomb friction law(3.27).

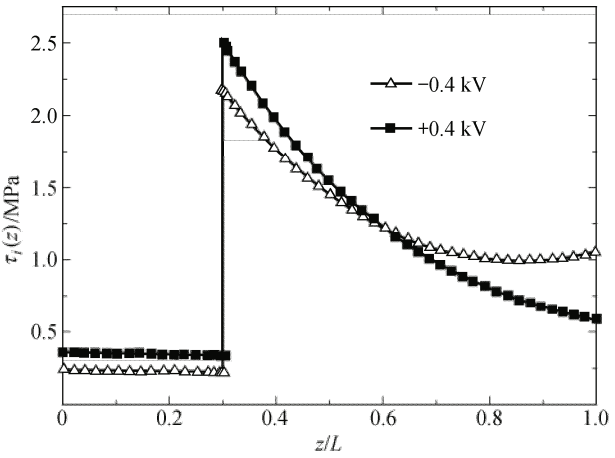

Fig. 3.13 Distribution of interfacial shear stress $\tau_i(z)$ under different electrical loadings for a constant mechanical loading $\sigma_a = 0.06$ GPa.

The effect of interfacial properties on PFC performance is shown in Fig. 3.14, showing the variation of electrical field as a function of axial distance *z*/*L* for several values of the parameters of interfacial properties. It can be seen that the electrical field decreases along with either an increase in the residual compressive stress q_0 or an increase in the Coulomb frictional coefficient μ. These results indicate that for piezoelectric composites, the interfacial properties not only control the stress transfer between fiber and matrix but also have an important influence on the distribution of the electrical field. It should be mentioned that at the transition point from the debonded region to the bonded one there is no jump in electrical field, unlike in the case of interfacial shear stress. This phenomenon is very different from the result obtained in [8], and this difference is mainly attributed to the fact that in our model the expressions for σ_{rr}^{m} and $\sigma_{\theta\theta}^{\mathrm{m}}$ do not include the term $\tau_{i,z}$ owing to the use of Lamè's solution [37]. It is also evident from Fig. 3.15 that the results depend largely upon the piezoelectric constant d_{15}.

To study effect of piezoelectric coefficient on the debonding process, the results of energy release rate are plotted in Fig. 3.15 as a function of debonding length l for different piezoelectric coefficients d_{15}. From this figure we can see that the normalized energy release rate G_i / G_m increases along with an increase in the

value of d_{15}. In addition, the energy release rate increases distinctly along with an increase in the value of l/L until it reaches a maximum. This finding implies that the piezoelectric effect has an important influence on the fiber debonding process during fiber push-out.

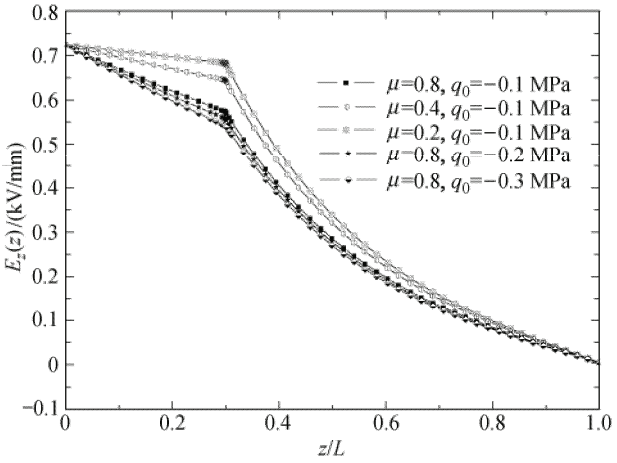

Fig. 3.14 Distribution of electric field in piezoelectric fiber under mechanical loading $\sigma_a = 0.06$ GPa for different interface property parameters.

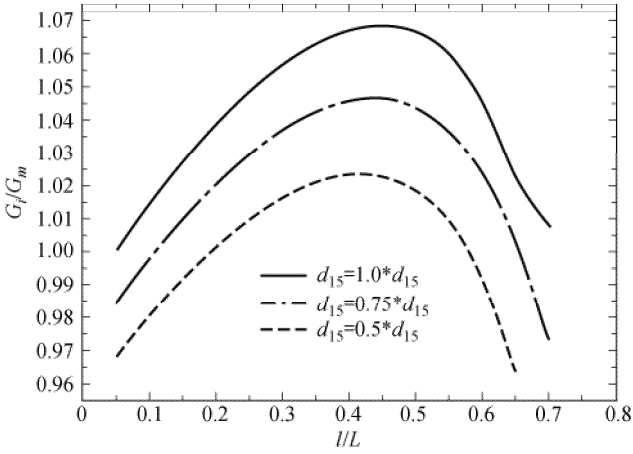

Fig. 3.15 Energy release rate G_i/G_m vs. l/L under different d_{15} for a constant mechanical loading $\sigma_a = 0.06$ GPa. G_m represents the energy release rate for $d_{15} = 1.0 * d_{15}$ and $l/L = 0.05$.

In Fig. 3.16 the energy release rate vs. electric potential loading is plotted, from which it can be seen that the energy release rate is linearly dependent on the elec-

trical loading when PFCs are subjected to a constant mechanical loading. The observation above indicates that the total energy release rate can be used as a debonding criterion for the piezoelectric fiber push-out test.

It should be mentioned that the energy release rate derived in this section is the total energy release rate. Park and Sun [44] obtained the total energy release rate and the mechanical strain rate for an electrically impermeable crack in an infinite piezoelectric medium for the three fracture modes, theoretically and experimentally. They concluded that the total energy release rate could not be used as a fracture criterion because the electrical loading always reduces the total release rate. However, it should be remembered that those results derived from the electrically impermeable condition on the crack surfaces, a condition not involved in our problem.

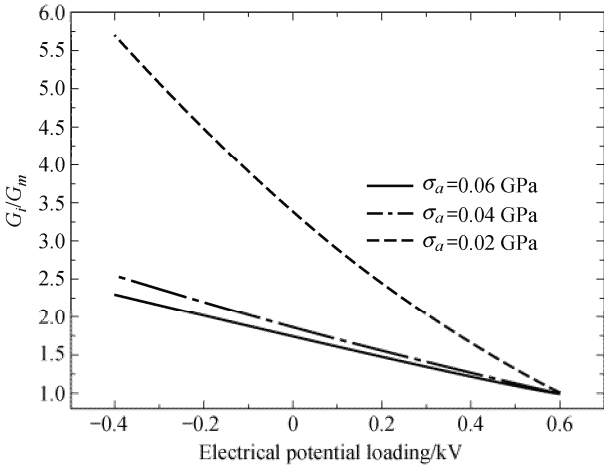

Fig. 3.16 Energy release rate vs. electrical loading under various mechanical loadings, $l/L = 0.2$. G_m represents the energy release rate for electrical loading 0.6 kV.

3.6 Micromechanics of fibrous piezoelectric composites

In the previous sections of this chapter, stress transfer and interfacial debonding criteria of fibrous piezoelectric composites were described. Determination of the effective material properties of fibrous piezoelectric composites is discussed in this section. It focuses on the developments in [25,26,34].

3.6.1 Overall elastoelectric properties of FPCs

In this subsection some exact results presented in [26,34] for effective properties of a piezoelectric composite consisting of many perfectly-bonded transversely iso-

tropic phases of cylindrical shape are briefly summarized.

Unlike the format of the constitutive relation (2.2), both Benveniste [34] and Chen [26] employed the five constants of Hill [19] (*k, l, m, n, p*) in the constitutive relation they studied. For a piezoelectric composite with a fibrous structure characterized by the fact that the phase boundaries are surfaces which can be generated by straight line parallel to the x_3-axis, the constitutive relations of a class 6*mm* of the hexagonal system for phase "*r*" are in the following form:

$$\begin{Bmatrix}\sigma_{11}\\ \sigma_{22}\\ \sigma_{33}\\ \sigma_{23}\\ \sigma_{13}\\ \sigma_{12}\end{Bmatrix}^{(r)} = \begin{bmatrix} k_r+m_r & k_r-m_r & l_r & 0 & 0 & 0\\ k_r-m_r & k_r+m_r & l_r & 0 & 0 & 0\\ l_r & l_r & n_r & 0 & 0 & 0\\ 0 & 0 & 0 & p_r & 0 & 0\\ 0 & 0 & 0 & 0 & p_r & 0\\ 0 & 0 & 0 & 0 & 0 & m_r \end{bmatrix} \begin{Bmatrix}\varepsilon_{11}\\ \varepsilon_{22}\\ \varepsilon_{33}\\ 2\varepsilon_{23}\\ 2\varepsilon_{13}\\ 2\varepsilon_{12}\end{Bmatrix}^{(r)} - \begin{bmatrix} 0 & 0 & e_{31}^{(r)}\\ 0 & 0 & e_{31}^{(r)}\\ 0 & 0 & e_{33}^{(r)}\\ 0 & e_{15}^{(r)} & 0\\ e_{15}^{(r)} & 0 & 0\\ 0 & 0 & 0 \end{bmatrix} \begin{Bmatrix}E_1\\ E_2\\ E_3\end{Bmatrix}^{(r)} \tag{3.109}$$

$$\begin{Bmatrix}D_1\\ D_2\\ D_3\end{Bmatrix}^{(r)} = \begin{bmatrix} 0 & 0 & e_{31}^{(r)}\\ 0 & 0 & e_{31}^{(r)}\\ 0 & 0 & e_{33}^{(r)}\\ 0 & e_{15}^{(r)} & 0\\ e_{15}^{(r)} & 0 & 0\\ 0 & 0 & 0 \end{bmatrix}^{\mathrm{T}} \begin{Bmatrix}\varepsilon_{11}\\ \varepsilon_{22}\\ \varepsilon_{33}\\ 2\varepsilon_{23}\\ 2\varepsilon_{13}\\ 2\varepsilon_{12}\end{Bmatrix}^{(r)} + \begin{bmatrix} \kappa_{11}^{(r)} & 0 & 0\\ 0 & \kappa_{11}^{(r)} & 0\\ 0 & 0 & \kappa_{33}^{(r)} \end{bmatrix} \begin{Bmatrix}E_1\\ E_2\\ E_3\end{Bmatrix}^{(r)} \tag{3.110}$$

where *k* represents the plane strain bulk modulus for lateral dilatation without axial extention, *l* the associated cross modulus, *m* the transverse shear modulus, *n* the modulus for longitudinal uniaxial straining, and *p* the longitudinal shear modulus. Following the procedure of Chen [26], a representative volume element *V* of the composite is chosen so that under homogeneous boundary conditions it represents the macroscopic response of the composite. The phase volume fraction c_r satisfies $c_1+c_2+\cdots+c_N=1$, where *N* is the number of phases in the composite. The volume *V* is subjected to uniform displacement and electric boundary conditions

$$u_i(S) = \varepsilon_{ij}^0 x_j, \qquad \phi(S) = -E_i^0 x_i \tag{3.111}$$

where u_i and ϕ denote the applied elastic displacement and electric potential, ε_{ij}^0 and E_i^0 are constant strain and electric field tensors. The overall material properties of the composite are then defined by

$$\bar{\boldsymbol{\sigma}} = \mathbf{L}\boldsymbol{\varepsilon}^0 - \mathbf{e}^{\mathrm{T}}\mathbf{E}^0, \qquad \bar{\mathbf{D}} = \mathbf{e}\boldsymbol{\varepsilon}^0 - \boldsymbol{\kappa}\mathbf{E}^0 \tag{3.112}$$

where $\bar{\boldsymbol{\sigma}}$ and $\bar{\mathbf{D}}$ stand for the volume average stresses and electric displacements in V. Under the boundary condition (3.111), the relationships between local and global average fields in V are given by

$$\boldsymbol{\varepsilon}^0 = \sum_{r=1}^{N} c_r \bar{\boldsymbol{\varepsilon}}_r, \qquad \mathbf{E}^0 = \sum_{r=1}^{N} c_r \bar{\mathbf{E}}_r, \qquad \bar{\boldsymbol{\sigma}} = \sum_{r=1}^{N} c_r \bar{\boldsymbol{\sigma}}_r, \qquad \bar{\mathbf{D}} = \sum_{r=1}^{N} c_r \bar{\mathbf{D}}_r \tag{3.113}$$

in which c_r is the volume fraction of material r, and

$$(\bar{\square})_r = \frac{1}{V_r}\int_{V_r} (\square)_r \mathrm{d}V \tag{3.114}$$

In deriving the following formulations for effective material properties, Benveniste [34] used two special types of loading condition (3.111):

$$\begin{Bmatrix} u_1(S) \\ u_2(S) \\ u_3(S) \end{Bmatrix} = \begin{bmatrix} \varepsilon_{11}^0 & 0 & 0 \\ 0 & \varepsilon_{22}^0 & 0 \\ 0 & 0 & \varepsilon_{33}^0 \end{bmatrix} \begin{Bmatrix} x_1 \\ x_2 \\ x_3 \end{Bmatrix}$$
$$\phi(S) = -E_3^0 x_3 \tag{3.115}$$

$$\begin{Bmatrix} u_1(S) \\ u_2(S) \\ u_3(S) \end{Bmatrix} = \begin{bmatrix} 0 & 0 & \varepsilon_{13}^0 \\ 0 & 0 & \varepsilon_{23}^0 \\ \varepsilon_{13}^0 & \varepsilon_{23}^0 & 0 \end{bmatrix} \begin{Bmatrix} x_1 \\ x_2 \\ x_3 \end{Bmatrix}$$
$$\phi(S) = -E_1^0 x_1 - E_2^0 x_2 \tag{3.116}$$

Under the loading condition (3.115), the solution can be assumed in the form

$$\begin{aligned} u_1^{(r)} &= u_1^{(r)}(x_1, x_2), \qquad u_2^{(r)} = u_2^{(r)}(x_1, x_2), \\ u_3^{(r)} &= \varepsilon_{33}^0 x_3, \qquad \phi^{(r)} = -E_3^0 x_3 \end{aligned} \tag{3.117}$$

The resulting stresses, electric displacements, equilibrium equations, and continuity conditions are

$$\begin{aligned}
\sigma_{11}^{(r)} &= (k_r + m_r)u_{1,1}^{(r)} + (k_r - m_r)u_{2,2}^{(r)} + l_r\varepsilon_{33}^0 - e_{31}^{(r)}E_3^0,\\
\sigma_{22}^{(r)} &= (k_r - m_r)u_{1,1}^{(r)} + (k_r + m_r)u_{2,2}^{(r)} + l_r\varepsilon_{33}^0 - e_{31}^{(r)}E_3^0,\\
\sigma_{33}^{(r)} &= l_r(u_{1,1}^{(r)} + u_{2,2}^{(r)}) + n_r\varepsilon_{33}^0 - e_{33}^{(r)}E_3^0,\\
\sigma_{12}^{(r)} &= m_r(u_{1,2}^{(r)} + u_{2,1}^{(r)}),\\
D_3^{(r)} &= e_{31}^{(r)}(u_{1,1}^{(r)} + u_{2,2}^{(r)}) + e_{31}^{(r)}\varepsilon_{33}^0 + \kappa_{33}^{(r)}E_3^0,\\
\sigma_{23}^{(r)} &= \sigma_{13}^{(r)} = D_1^{(r)} = D_2^{(r)} = 0
\end{aligned} \tag{3.118}$$

$$\begin{aligned}
&(k_r + m_r)u_{1,11}^{(r)} + (k_r - m_r)u_{2,21}^{(r)} + m_r(u_{1,22}^{(r)} + u_{2,12}^{(r)}) = 0,\\
&(k_r - m_r)u_{1,12}^{(r)} + (k_r + m_r)u_{2,22}^{(r)} + m_r(u_{1,21}^{(r)} + u_{2,11}^{(r)}) = 0
\end{aligned} \tag{3.119}$$

$$\begin{aligned}
&u_1^{(r)} = u_1^{(s)}, \quad u_2^{(r)} = u_2^{(s)},\\
&\sigma_{11}^{(r)}n_1 + \sigma_{12}^{(r)}n_2 = \sigma_{11}^{(s)}n_1 + \sigma_{12}^{(s)}n_2, \qquad (\text{on } \Gamma_{rs})\\
&\sigma_{21}^{(r)}n_1 + \sigma_{22}^{(r)}n_2 = \sigma_{21}^{(s)}n_1 + \sigma_{22}^{(s)}n_2
\end{aligned} \tag{3.120}$$

where $\mathbf{n} = (n_1, n_2, 0)$ denotes the normal to the interface Γ_{rs} which is the interfaces between phase r and phase s.

For the loading condition (3.116), the corresponding solutions can be assumed in the form

$$\begin{aligned}
&u_1^{(r)} = \varepsilon_{13}^0 x_3, \qquad u_2^{(r)} = \varepsilon_{23}^0 x_3,\\
&u_3^{(r)} = \psi^{(r)}(x_1, x_2) - \varepsilon_{13}^0 x_1 - \varepsilon_{23}^0 x_2, \qquad \phi^{(r)} = \phi^{(r)}(x_1, x_2)
\end{aligned} \tag{3.121}$$

The stresses and electric displacements induced by the fields (3.121) are

$$\begin{aligned}
&\sigma_{23}^{(r)} = p_r\psi_{,2}^{(r)} + e_{15}^{(r)}\phi_{,2}^{(r)}, \qquad \sigma_{13}^{(r)} = p_r\psi_{,1}^{(r)} + e_{15}^{(r)}\phi_{,1}^{(r)},\\
&D_1^{(r)} = e_{15}^{(r)}\psi_{,1}^{(r)} - \kappa_{11}^{(r)}\phi_{,1}^{(r)}, \qquad D_2^{(r)} = e_{15}^{(r)}\psi_{,2}^{(r)} - \kappa_{11}^{(r)}\phi_{,2}^{(r)}
\end{aligned} \tag{3.122}$$

whereas the equilibrium equation (3.119) becomes

$$p_r\nabla^2\psi^{(r)} + e_{15}^{(r)}\phi^{(r)} = 0, \qquad e_{15}^{(r)}\nabla^2\psi^{(r)} - \kappa_{11}^{(r)}\phi^{(r)} = 0 \tag{3.123}$$

in which the functions $\psi^{(r)}$ and $\phi^{(r)}$ can be obtained by solving (3.123) under the boundary conditions (3.116) and the following continuity conditions at the interfaces Γ_{rs}:

$$\begin{aligned}
&u_1^{(r)} = u_1^{(s)}, \quad u_2^{(r)} = u_2^{(s)},\\
&\sigma_{11}^{(r)}n_1 + \sigma_{12}^{(r)}n_2 = \sigma_{11}^{(s)}n_1 + \sigma_{12}^{(s)}n_2, \qquad (\text{on } \Gamma_{rs})\\
&\sigma_{21}^{(r)}n_1 + \sigma_{22}^{(r)}n_2 = \sigma_{21}^{(s)}n_1 + \sigma_{22}^{(s)}n_2
\end{aligned} \tag{3.124}$$

3.6.1.1 Effective properties of two-phase composites

(1) Effective constants of k, l, n, e_{31}, e_{33}, and κ_{33}.

To determine k, assume $\varepsilon_{11}^0 = \varepsilon_{22}^0$ and $\varepsilon_{33}^0 = E_3^0 = 0$ in Eq. (3.115). Then, Eqs. (3.117)-(3.120) show that this turns out to be a purely mechanical problem and k can be expressed as [34]

$$k = k_{\mathrm{m}} + \frac{c_{\mathrm{f}}}{\dfrac{1}{k_{\mathrm{f}} - k_{\mathrm{m}}} + \dfrac{c_{\mathrm{m}}}{k_{\mathrm{m}} + m_{\mathrm{m}}}} \tag{3.125}$$

where the subscripts "m" and "f " represent the related variables which are associated with matrix phase and fiber phase. The formulae for the remaining five constants can be obtained by making use of the universal connections between these moduli as recently derived by Schulgasser [22]:

$$\begin{aligned} &\frac{k_{\mathrm{f}} - k}{l_{\mathrm{f}} - l} = \frac{k_{\mathrm{m}} - k}{l_{\mathrm{m}} - l} = \frac{c_{\mathrm{m}} l_{\mathrm{m}} + c_{\mathrm{f}} l_{\mathrm{f}} - l}{c_{\mathrm{m}} n_{\mathrm{m}} + c_{\mathrm{f}} n_{\mathrm{f}} - n} = \frac{c_{\mathrm{m}} e_{31}^{(\mathrm{m})} + c_{\mathrm{f}} e_{31}^{(\mathrm{f})} - e_{31}}{c_{\mathrm{m}} e_{33}^{(\mathrm{m})} + c_{\mathrm{f}} e_{33}^{(\mathrm{f})} - e_{33}}, \\ &\frac{k_{\mathrm{f}} - k}{e_{31}^{(\mathrm{f})} - e_{31}} = \frac{k_{\mathrm{m}} - k}{e_{31}^{(\mathrm{m})} - e_{31}} = \frac{c_{\mathrm{m}} l_{\mathrm{m}} + c_{\mathrm{f}} l_{\mathrm{f}} - l}{c_{\mathrm{m}} e_{33}^{(\mathrm{m})} + c_{\mathrm{f}} e_{33}^{(\mathrm{f})} - e_{33}} = \frac{e_{31} - c_{\mathrm{m}} e_{31}^{(\mathrm{m})} - c_{\mathrm{f}} e_{31}^{(\mathrm{f})}}{c_{\mathrm{m}} \kappa_{33}^{(\mathrm{m})} + c_{\mathrm{f}} \kappa_{33}^{(\mathrm{f})} - \kappa_{33}} \end{aligned} \tag{3.126}$$

It is noted that only five of the six relations in Eq. (3.126) are independent. Once k is known from Eq. (3.125), the effective material constants l, n, e_{31}, e_{33}, and κ_{33} can be determined from Eq. (3.126).

(2) Effective constants of e_{15}, p, and κ_{11}.

The determination of these three constants involves the application of boundary condition (3.116) and the use of Eqs. (3.121)-(3.124). For simplicity, rewrite the constitutive equation (3.122) in matrix form

$$\begin{Bmatrix} \boldsymbol{\sigma} \\ \mathbf{D} \end{Bmatrix}^{(r)} = \begin{bmatrix} p_r & e_{15}^{(r)} \\ e_{15}^{(r)} & -\kappa_{11}^{(r)} \end{bmatrix} \begin{Bmatrix} \nabla\psi \\ \nabla\phi \end{Bmatrix}^{(r)} = \mathbf{L}_r \begin{Bmatrix} \nabla\psi \\ \nabla\phi \end{Bmatrix}^{(r)} \tag{3.127}$$

The real symmetric matrix $\mathbf{L}_r$ can be diagonalized by means of the transformation

$$\mathbf{L}_r^* = \mathbf{W}\mathbf{L}_r\mathbf{W}^{\mathrm{T}} \qquad (r = \mathrm{m}, \mathrm{f}) \tag{3.128}$$

where $\mathbf{W}$ may be complex, and $\mathbf{L}_r^*$ is diagonal.

Now define

$$\begin{Bmatrix} \boldsymbol{\sigma}^* \\ \mathbf{D}^* \end{Bmatrix}^{(r)} = \mathbf{W} \begin{Bmatrix} \boldsymbol{\sigma} \\ \mathbf{D} \end{Bmatrix}^{(r)}, \qquad \begin{Bmatrix} \nabla\psi^* \\ \nabla\phi^* \end{Bmatrix}^{(r)} = \left(\mathbf{W}^{\mathrm{T}}\right)^{-1} \begin{Bmatrix} \nabla\psi \\ \nabla\phi \end{Bmatrix}^{(r)} \tag{3.129}$$

so that there is

$$\begin{Bmatrix} \boldsymbol{\sigma}^* \\ \mathbf{D}^* \end{Bmatrix}^{(r)} = \mathbf{L}_r^* \begin{Bmatrix} \nabla\psi^* \\ \nabla\phi^* \end{Bmatrix}^{(r)}, \qquad \nabla\cdot\boldsymbol{\sigma}^* = 0, \qquad \nabla\cdot\mathbf{D}^* = 0 \tag{3.130}$$

Therefore, in terms of the new field quantities, the original coupled problem is reduced to two uncoupled problems. The transformed effective tensor $\mathbf{L}^*$ is also diagonal. That is,

$$\mathbf{L}^* = \mathbf{WLW}^{\mathrm{T}} \tag{3.131}$$

with

$$\mathbf{L}^* = \begin{bmatrix} p^* & 0 \\ 0 & -\kappa_{11}^* \end{bmatrix}, \qquad \mathbf{L} = \begin{bmatrix} p & e_{15} \\ e_{15} & -\kappa_{11} \end{bmatrix} \tag{3.132}$$

The above procedures imply that use can be made of known results in the uncoupled system to transform them to the coupled system. The composite cylinder results for p^* and κ_{11}^* are given by [34]

$$\begin{aligned} p^* &= p_{\mathrm{m}}^* \frac{c_{\mathrm{m}} p_{\mathrm{m}}^* + p_{\mathrm{f}}^*(1+c_{\mathrm{f}})}{p_{\mathrm{m}}^*(1+c_{\mathrm{f}}) + p_{\mathrm{f}}^* c_{\mathrm{m}}}, \\ \kappa_{11}^* &= \left(\kappa_{11}^*\right)_{\mathrm{m}} \frac{c_{\mathrm{m}}\left(\kappa_{11}^*\right)_{\mathrm{m}} + \left(\kappa_{11}^*\right)_{\mathrm{f}}(1+c_{\mathrm{f}})}{\left(\kappa_{11}^*\right)_{\mathrm{m}}(1+c_{\mathrm{f}}) + \left(\kappa_{11}^*\right)_{\mathrm{f}} c_{\mathrm{m}}} \end{aligned} \tag{3.133}$$

Equation (3.133) can be written in matrix form as

$$\begin{bmatrix} p^* & 0 \\ 0 & -\kappa_{11}^* \end{bmatrix} = \begin{bmatrix} p_{\mathrm{m}}^* & 0 \\ 0 & -\left(\kappa_{11}^*\right)_{\mathrm{m}} \end{bmatrix} \begin{bmatrix} H & 0 \\ 0 & J \end{bmatrix}^{-1} \begin{bmatrix} F & 0 \\ 0 & G \end{bmatrix} \tag{3.134}$$

where

$$\begin{aligned} H &= p_{\mathrm{m}}^*(1+c_{\mathrm{f}}) + p_{\mathrm{f}}^* c_{\mathrm{m}}, \quad J = -\left(\kappa_{11}^*\right)_{\mathrm{m}}(1+c_{\mathrm{f}}) + \left(-\kappa_{11}^*\right)_{\mathrm{f}} c_{\mathrm{m}}, \\ F &= c_{\mathrm{m}} p_{\mathrm{m}}^* + p_{\mathrm{f}}^*(1+c_{\mathrm{f}}), \quad G = c_{\mathrm{m}}\left(-\kappa_{11}^*\right)_{\mathrm{m}} + \left(-\kappa_{11}^*\right)_{\mathrm{f}}(1+c_{\mathrm{f}}) \end{aligned} \tag{3.135}$$

To transform the $\mathbf{L}^*$ into $\mathbf{L}$, multiply each side of Eq. (3.134) by W–1 and WT–1 respectively, and after some mathematical manipulation, we obtain

$$\mathbf{L} = \mathbf{L}_{\mathrm{m}}[(1+c_{\mathrm{f}})\mathbf{L}_{\mathrm{m}} + c_{\mathrm{m}}\mathbf{L}_{\mathrm{f}}]^{-1}[c_{\mathrm{m}}\mathbf{L}_{\mathrm{m}} + (1+c_{\mathrm{f}})\mathbf{L}_{\mathrm{f}}] \tag{3.136}$$

Equation (3.136) gives the effective constants p, e_{15}, κ_{11} of two-phase FPCs.

3.6.1.2 Effective properties of FPC with equal transverse shear modulus

Consider a multiphase FPC with the same transverse shear modulus for all phases and with transversely isotropic constituents described by the constitutive

laws (3.109) and (3.110). The method of derivation follows closely the analysis of Hill [19] for the uncoupled mechanical case. Let the composite be subjected to the loading condition (3.115), resulting the following fields:

$$u_1^{(r)} = \frac{\partial f^{(r)}(x_1, x_2)}{\partial x_1}, \qquad u_2^{(r)} = \frac{\partial f^{(r)}(x_1, x_2)}{\partial x_2}, \qquad u_3^{(r)} = \varepsilon_{33}^0 x_3, \qquad \phi^{(r)} = -E_3^0 x_3 \tag{3.137}$$

where f is an unknown function to be determined from the governing equation and boundary conditions. Substituting Eq. (3.137) into Eqs. (3.109) and (3.110) yields [26]

$$\begin{aligned}
\sigma_{11}^{(r)} &= (k_r + m) f_{,11}^{(r)} + (k_r - m) f_{,22}^{(r)} + l_r \varepsilon_{33}^0 - e_{31}^{(r)} E_3^0, \\
\sigma_{22}^{(r)} &= (k_r - m) f_{,11}^{(r)} + (k_r + m) f_{,22}^{(r)} + l_r \varepsilon_{33}^0 - e_{31}^{(r)} E_3^0, \\
\sigma_{33}^{(r)} &= l_r (f_{,11}^{(r)} + f_{,22}^{(r)}) + n_r \varepsilon_{33}^0 - e_{33}^{(r)} E_3^0, \\
\sigma_{12}^{(r)} &= 2m f_{,12}^{(r)}, \\
D_3^{(r)} &= e_{31}^{(r)} (f_{,11}^{(r)} + f_{,22}^{(r)}) + e_{31}^{(r)} \varepsilon_{33}^0 + \kappa_{33}^{(r)} E_3^0, \\
\sigma_{23}^{(r)} &= \sigma_{13}^{(r)} = D_1^{(r)} = D_2^{(r)} = 0
\end{aligned} \tag{3.138}$$

Benveniste [34] indicated that Eq. (3.119) are identically satisfied by requiring

$$\nabla^2 f^{(r)} = \varepsilon_{11}^{(r)} + \varepsilon_{22}^{(r)} = e_r \tag{3.139}$$

where e_r conforms with the uniform phase dilatations. It can be proved that the interface conditions of surface traction (3.124) are satisfied if [34]

$$(k_s + m) e_s + l_s \varepsilon_{33}^0 - e_{31}^{(s)} E_3^0 = (k_r + m) e_r + l_r \varepsilon_{33}^0 - e_{31}^{(r)} E_3^0 \tag{3.140}$$

For any two phases r and s, Eq. (3.140) together with the condition

$$\varepsilon_{11}^0 + \varepsilon_{22}^0 = \sum_{r=1}^{N} c_r e_r \tag{3.141}$$

enable us to determine the constants e_r. After a series of mathematical manipulations, Benveniste [34] obtained the expression for e_r as

$$e_r = \beta_r (\varepsilon_{11}^0 + \varepsilon_{22}^0) + \gamma_r \varepsilon_{33}^0 - \alpha_r E_3^0 \tag{3.142}$$

where

$$\alpha_r = \frac{1}{k_r + m} \frac{\displaystyle\sum_{s=1}^{N} \frac{c_s e_{31}^{(s)}}{k_s + m}}{\displaystyle\sum_{s=1}^{N} \frac{c_s}{k_s + m}} - \frac{c_r e_{31}^{(r)}}{k_r + m}, \qquad \beta_r = \frac{1}{k_r + m} \frac{1}{\displaystyle\sum_{s=1}^{N} \frac{c_s}{k_s + m}},$$

$$\gamma_r = \frac{1}{k_r + m} \frac{\sum_{s=1}^{N} \frac{c_s l_s}{k_s + m}}{\sum_{s=1}^{N} \frac{c_s}{k_s + m}} - \frac{c_r l_r}{k_r + m} \tag{3.143}$$

Then, the average fields used to determine the effective constants are obtained as

$$\begin{aligned} \bar{\sigma}_{11} &= (k+m)\varepsilon_{11}^0 + (k-m)\varepsilon_{22}^0 + l\varepsilon_{33}^0 - e_{31}E_3^0 \\ &= \sum_{r=1}^{N} c_r(k_r+m)\bar{\varepsilon}_{11}^{(r)} + c_r(k_r-m)\bar{\varepsilon}_{22}^{(r)} + c_r l_r \varepsilon_{33}^0 - c_r e_{31}^{(r)} E_3^0 \end{aligned} \tag{3.144}$$

$$\begin{aligned} \bar{\sigma}_{22} &= (k-m)\varepsilon_{11}^0 + (k+m)\varepsilon_{22}^0 + l\varepsilon_{33}^0 - e_{31}E_3^0 \\ &= \sum_{r=1}^{N} c_r(k_r-m)\bar{\varepsilon}_{11}^{(r)} + c_r(k_r+m)\bar{\varepsilon}_{22}^{(r)} + c_r l_r \varepsilon_{33}^0 - c_r e_{31}^{(r)} E_3^0 \end{aligned} \tag{3.145}$$

$$\begin{aligned} \bar{\sigma}_{33} &= l(\varepsilon_{11}^0 + \varepsilon_{22}^0) + n\varepsilon_{33}^0 - e_{33}E_3^0 \\ &= \sum_{r=1}^{N} c_r l_r (\bar{\varepsilon}_{11}^{(r)} + \bar{\varepsilon}_{22}^{(r)}) + c_r n_r \varepsilon_{33}^0 - c_r e_{33}^{(r)} E_3^0 \end{aligned} \tag{3.146}$$

$$\bar{\sigma}_{12} = 2m\varepsilon_{12}^0 = \sum_{r=1}^{N} c_r m \bar{\varepsilon}_{12}^{(r)} \tag{3.147}$$

$$\begin{aligned} \bar{D}_3 &= e_{31}(\varepsilon_{11}^0 + \varepsilon_{22}^0) + e_{33}\varepsilon_{33}^0 + \kappa_{33}E_3^0 \\ &= \sum_{r=1}^{N} c_r e_{33}^{(r)} (\bar{\varepsilon}_{11}^{(r)} + \bar{\varepsilon}_{22}^{(r)}) + c_r e_{33}^{(r)} \varepsilon_{33}^0 + c_r \kappa_{33}^{(r)} E_3^0 \end{aligned} \tag{3.148}$$

Making use of Eqs. (3.144)-(3.148), Benveniste [34] obtained the following formulations for predicting effective material constants k, l, n, e_{31}, e_{33}, and κ_{33}:

$$k = \frac{\sum_{r=1}^{N} \frac{c_r k_r}{k_r + m}}{\sum_{r=1}^{N} \frac{c_r}{k_r + m}}, \qquad l = \frac{\sum_{r=1}^{N} \frac{c_r l_r}{k_r + m}}{\sum_{r=1}^{N} \frac{c_r}{k_r + m}}, \qquad e_{31} = \frac{\sum_{r=1}^{N} \frac{c_r e_{31}^{(s)}}{k_r + m}}{\sum_{r=1}^{N} \frac{c_r}{k_r + m}} \tag{3.149}$$

$$n = \sum_{r=1}^{N} c_r n_r + \sum_{r=1}^{N} \frac{c_r n_r}{k_r + m} \frac{\sum_{r=1}^{N} \frac{c_r n_r}{k_r + m}}{\sum_{r=1}^{N} \frac{c_r}{k_r + m}} - \sum_{r=1}^{N} \frac{c_r n_r^2}{k_r + m} \tag{3.150}$$

$$e_{33} = \sum_{r=1}^{N} c_r e_{33}^{(r)} + \sum_{r=1}^{N} \frac{c_r e_{33}^{(r)}}{k_r + m} \frac{\sum_{r=1}^{N} \frac{c_r e_{33}^{(r)}}{k_r + m}}{\sum_{r=1}^{N} \frac{c_r}{k_r + m}} - \sum_{r=1}^{N} \frac{c_r \left(e_{33}^{(r)}\right)^2}{k_r + m} \tag{3.151}$$

$$\kappa_{33} = \sum_{r=1}^{N} c_r \kappa_{33}^{(r)} + \sum_{r=1}^{N} \frac{c_r \kappa_{33}^{(r)}}{k_r + m} \frac{\sum_{r=1}^{N} \frac{c_r \kappa_{33}^{(r)}}{k_r + m}}{\sum_{r=1}^{N} \frac{c_r}{k_r + m}} - \sum_{r=1}^{N} \frac{c_r \left(\kappa_{33}^{(r)}\right)^2}{k_r + m} \tag{3.152}$$

3.6.2 Extension to include magnetic and thermal effects

In the last subsection, a formulation for effective elastoelectric material constants of FPCs was presented. Extension of these results to include piezomagnetic and thermal effects is presented in this subsection. It is a brief review of the development in [25].

To obtain formulations for calculating effective constants of thermo-magneto-electro-elastic materials, Benveniste [25] considered a transversely isotropic, two-phase composite with a fibrous structure. The constitutive law is given by

$$\begin{aligned}
\boldsymbol{\sigma}^{(r)} &= \mathbf{c}^{(r)}\boldsymbol{\varepsilon}^{(r)} - \mathbf{e}^{\mathrm{T}(r)}\mathbf{E}^{(r)} - \tilde{\mathbf{e}}^{\mathrm{T}(r)}\mathbf{H}^{(r)} + \boldsymbol{\beta}^{(r)}\theta^{(r)}, \\
\mathbf{D}^{(r)} &= \mathbf{e}^{(r)}\boldsymbol{\varepsilon}^{(r)} + \boldsymbol{\kappa}^{(r)}\mathbf{E}^{(r)} + \boldsymbol{\alpha}^{(r)}\mathbf{H}^{(r)} + \boldsymbol{\chi}^{(r)}\theta^{(r)}, \\
\mathbf{B}^{(r)} &= \tilde{\mathbf{e}}^{(r)}\boldsymbol{\varepsilon}^{(r)} + \boldsymbol{\alpha}^{(r)}\mathbf{E}^{(r)} + \boldsymbol{\mu}^{(r)}\mathbf{H}^{(r)} + \boldsymbol{\lambda}^{(r)}\theta^{(r)}
\end{aligned} \tag{3.153}$$

where $\mathbf{B}^{(r)}$, $\mathbf{H}^{(r)}$, and $\theta^{(r)}$ denote, respectively, magnetic fluxes, magnetic field intensity, and temperature change in rth phase; Elastic properties $\mathbf{c}^{(r)}$ is a 6×6 elastic constant matrix defined in Eq. (3.109); $\mathbf{e}^{(r)}$ and $\boldsymbol{\kappa}^{(r)}$ are piezoelectric and dielectric constants defined in Eq. (3.110). $\boldsymbol{\beta}^{(r)}$, $\boldsymbol{\chi}^{(r)}$, and $\boldsymbol{\lambda}^{(r)}$ are thermal stress, pyroelectric, and pyromagnetic vectors. $\tilde{\mathbf{e}}^{(r)}$, $\boldsymbol{\alpha}^{(r)}$, and $\boldsymbol{\mu}^{(r)}$ are piezomagnetic, magnetoelectric coupling coefficient, and magnetic permeabilities matrices. These six matrices are defined by

$$\begin{aligned}
\boldsymbol{\beta}^{(r)} &= \left\{\beta_{\mathrm{T}}^{(r)} \quad \beta_{\mathrm{T}}^{(r)} \quad \beta_{\mathrm{L}}^{(r)} \quad 0 \quad 0 \quad 0\right\}^{\mathrm{T}}, \\
\boldsymbol{\chi}^{(r)} &= \left\{0 \quad 0 \quad \chi_{\mathrm{L}}^{(r)}\right\}^{\mathrm{T}}, \\
\boldsymbol{\lambda}^{(r)} &= \left\{0 \quad 0 \quad \lambda_3^{(r)}\right\}^{\mathrm{T}} \\
\tilde{\mathbf{e}}^{(r)} &= \begin{bmatrix} 0 & 0 & 0 & 0 & \tilde{e}_{15} & 0 \\ 0 & 0 & 0 & \tilde{e}_{15} & 0 & 0 \\ \tilde{e}_{31} & \tilde{e}_{31} & \tilde{e}_{33} & 0 & 0 & 0 \end{bmatrix}^{(r)},
\end{aligned} \tag{3.154}$$

$$\boldsymbol{\alpha}^{(r)} = \begin{bmatrix} \alpha_{11} & 0 & 0 \\ 0 & \alpha_{11} & 0 \\ 0 & 0 & \alpha_{33} \end{bmatrix}^{(r)}, \qquad \boldsymbol{\mu}^{(r)} = \begin{bmatrix} \mu_{11} & 0 & 0 \\ 0 & \mu_{11} & 0 \\ 0 & 0 & \mu_{33} \end{bmatrix}^{(r)} \tag{3.155}$$

where β_{T} and β_{L} are transverse and longitudinal thermal stress coefficients, χ_{L} is the longitudinal pyroelectric constant.

Benveniste [25] then considered the following two sets of loading conditions:

The first set of loading conditions consists of Eq. (3.115) and

$$\psi(S) = -H_3^0 x_3, \qquad \theta(S) = \theta_0 \tag{3.156}$$

where ψ is magnetic potential. The second set of loading conditions is defined by Eq. (3.116) and

$$\psi(S) = -H_1^0 x_1 - H_2^0 x_2 \tag{3.157}$$

together with the steady state equilibrium equations

$$\sigma_{ij,j} = 0, \qquad D_{i,i} = 0, \qquad B_{i,i} = 0 \tag{3.158}$$

Keeping this mind, he proved that there exists a specific choice of $(\boldsymbol{\varepsilon}^0, \mathbf{E}^0, \mathbf{H}^0, \theta_0)$, denoted by $(\hat{\boldsymbol{\varepsilon}}, \hat{\mathbf{E}}, \hat{\mathbf{H}}, \theta_0)$, so that the strains, electric and magnetic fields are uniform throughout the composite:

$$\overline{\boldsymbol{\varepsilon}} = \overline{\boldsymbol{\varepsilon}}^{(r)} = \hat{\boldsymbol{\varepsilon}}, \qquad \overline{\mathbf{E}} = \overline{\mathbf{E}}^{(r)} = \hat{\mathbf{E}}, \qquad \overline{\mathbf{H}} = \overline{\mathbf{H}}^{(r)} = \hat{\mathbf{H}}, \qquad \theta = \theta_0 \tag{3.159}$$

and the possible sets of $(\hat{\boldsymbol{\varepsilon}}, \hat{\mathbf{E}}, \hat{\mathbf{H}}, \theta_0)$ resulting in uniform fields are given by

$$\begin{Bmatrix} \hat{\varepsilon}_1 \\ \hat{\varepsilon}_2 \\ \hat{\varepsilon}_3 \\ \hat{E}_3 \\ \hat{H}_3 \end{Bmatrix} = \eta_1 \begin{Bmatrix} 1 \\ 1 \\ r_3 \\ 0 \\ 0 \end{Bmatrix} + \eta_2 \begin{Bmatrix} 0 \\ 0 \\ 1 \\ s_3 \\ 0 \end{Bmatrix} + \eta_3 \begin{Bmatrix} 0 \\ 0 \\ 1 \\ 0 \\ t_3 \end{Bmatrix} + \eta_4 \begin{Bmatrix} 0 \\ 0 \\ \tilde{r}_3 \\ 0 \\ 0 \end{Bmatrix} \theta_0, \tag{3.160}$$

$$\hat{\varepsilon}_4 = \hat{\varepsilon}_5 = \hat{\varepsilon}_6 = \hat{E}_1 = \hat{E}_2 = \hat{H}_1 = \hat{H}_2 = 0$$

where $\eta_i (i = 1\text{-}4)$ are arbitrary constants and

$$\begin{aligned} r_3 &= -2(k_1 - k_2)/(l_1 - l_2), \\ s_3 &= (l_1 - l_2)/(e_{31}^{(1)} - e_{31}^{(2)}), \\ t_3 &= (l_1 - l_2)/(\tilde{e}_{31}^{(1)} - \tilde{e}_{31}^{(2)}), \\ \tilde{r}_3 &= -(\beta_{\mathrm{T}}^{(1)} - \beta_{\mathrm{T}}^{(2)})/(l_1 - l_2) \end{aligned} \tag{3.161}$$

where subscripts "1" and "2" represent the variables associated with matrix and fiber materials. The uniform fields generated from Eq. (3.160) allow the derivation of exact connections between some of the effective properties. The effective con-

stants $\mathbf{c}$, $\mathbf{e}$, $\mathbf{q}$, $\boldsymbol{\beta}$, $\boldsymbol{\chi}$, $\boldsymbol{\lambda}$, $\boldsymbol{\kappa}$, $\boldsymbol{\mu}$, $\boldsymbol{\alpha}$ are defined by

$$\begin{aligned}
\overline{\boldsymbol{\sigma}} &= \mathbf{c}\overline{\boldsymbol{\varepsilon}} - \mathbf{e}^{\mathrm{T}}\overline{\mathbf{E}} - \tilde{\mathbf{e}}^{\mathrm{T}}\overline{\mathbf{H}} + \boldsymbol{\beta}\theta_0 \\
&= \sum_{r=1}^{2} c_r[\mathbf{c}^{(r)}\overline{\boldsymbol{\varepsilon}}^{(r)} - \mathbf{e}^{\mathrm{T}(r)}\overline{\mathbf{E}}^{(r)} - \tilde{\mathbf{e}}^{\mathrm{T}(r)}\overline{\mathbf{H}}^{(r)} + \boldsymbol{\beta}^{(r)}\theta_0], \\
\overline{\mathbf{D}} &= \mathbf{e}\overline{\boldsymbol{\varepsilon}} + \boldsymbol{\kappa}\overline{\mathbf{E}} + \boldsymbol{\alpha}\overline{\mathbf{H}} + \boldsymbol{\chi}\theta_0 \\
&= \sum_{r=1}^{2} c_r[\mathbf{e}^{(r)}\overline{\boldsymbol{\varepsilon}}^{(r)} + \boldsymbol{\kappa}^{(r)}\overline{\mathbf{E}}^{(r)} + \boldsymbol{\alpha}^{(r)}\overline{\mathbf{H}}^{(r)} + \boldsymbol{\chi}^{(r)}\theta_0], \\
\overline{\mathbf{B}} &= \tilde{\mathbf{e}}\overline{\boldsymbol{\varepsilon}} + \boldsymbol{\alpha}\overline{\mathbf{E}} + \boldsymbol{\mu}^{(r)}\overline{\mathbf{H}} + \boldsymbol{\lambda}^{(r)}\theta_0 \\
&= \sum_{r=1}^{2} c_r[\tilde{\mathbf{e}}^{(r)}\overline{\boldsymbol{\varepsilon}}^{(r)} + \boldsymbol{\alpha}^{(r)}\overline{\mathbf{E}}^{(r)} + \boldsymbol{\mu}^{(r)}\overline{\mathbf{H}}^{(r)} + \boldsymbol{\lambda}^{(r)}\theta_0]
\end{aligned} \tag{3.162}$$

Substituting Eqs. (3.159) and (3.160) into Eq. (3.162) and equating the coefficients $\eta_i, i = 1\text{-}4$ yield a set of exact connections between the effective properties as follows [24,25]:

$$\frac{k - \sum_{r=1}^{2} c_r k_r}{l - \sum_{r=1}^{2} c_r l_r} = \frac{l - \sum_{r=1}^{2} c_r l_r}{n - \sum_{r=1}^{2} c_r n_r} = \frac{e_{31} - \sum_{r=1}^{2} c_r e_{31}^{(r)}}{e_{33} - \sum_{r=1}^{2} c_r e_{33}^{(r)}} = \frac{k_1 - k_2}{l_1 - l_2} \tag{3.163}$$

$$\frac{e_{31} - \sum_{r=1}^{2} c_r e_{31}^{(r)}}{l - \sum_{r=1}^{2} c_r l_r} = \frac{e_{33} - \sum_{r=1}^{2} c_r e_{33}^{(r)}}{n - \sum_{r=1}^{2} c_r n_r} = \frac{\sum_{r=1}^{2} c_r \kappa_{33}^{(r)} - \kappa_{33}}{e_{33} - \sum_{r=1}^{2} c_r e_{33}^{(r)}} = \frac{e_{31}^{(1)} - e_{31}^{(2)}}{l_1 - l_2} \tag{3.164}$$

$$\frac{k - \sum_{r=1}^{2} c_r k_r}{e_{31} - \sum_{r=1}^{2} c_r e_{31}^{(r)}} = \frac{l - \sum_{r=1}^{2} c_r l_r}{e_{33} - \sum_{r=1}^{2} c_r e_{33}^{(r)}} = \frac{e_{31} - \sum_{r=1}^{2} c_r e_{31}^{(r)}}{\sum_{r=1}^{2} c_r \kappa_{33}^{(r)} - \kappa_{33}} = \frac{\kappa_1 - \kappa_2}{e_{31}^{(1)} - e_{31}^{(2)}} \tag{3.165}$$

$$\frac{\tilde{e}_{31} - \sum_{r=1}^{2} c_r \tilde{e}_{31}^{(r)}}{l - \sum_{r=1}^{2} c_r l_r} = \frac{\tilde{e}_{33} - \sum_{r=1}^{2} c_r \tilde{e}_{33}^{(r)}}{n - \sum_{r=1}^{2} c_r n_r} = \frac{\sum_{r=1}^{2} c_r \mu_{33}^{(r)} - \mu_{33}}{\tilde{e}_{33} - \sum_{r=1}^{2} c_r \tilde{e}_{33}^{(r)}} = \frac{\tilde{e}_{31}^{(1)} - \tilde{e}_{31}^{(2)}}{l_1 - l_2} \tag{3.166}$$

$$\frac{e_{33} - \sum_{r=1}^{2} c_r e_{33}^{(r)}}{\sum_{r=1}^{2} c_r \alpha_{33}^{(r)} - \alpha_{33}} = \frac{l_1 - l_2}{\tilde{e}_{31}^{(1)} - \tilde{e}_{31}^{(2)}} \tag{3.167}$$

$$\beta_1 = \beta_2 = \left(\sum_{r=1}^{2} c_r l_r - l \right) \tilde{r}_3 + \sum_{r=1}^{2} c_r \beta_{\mathrm{T}}^{(r)} \tag{3.168}$$

$$\beta_3 = \left(\sum_{r=1}^{2} c_r n_r - n \right) \tilde{r}_3 + \sum_{r=1}^{2} c_r \beta_{\mathrm{L}}^{(r)} \tag{3.169}$$

$$\chi_3 = \left(\sum_{r=1}^{2} c_r e_{33}^{(r)} - e_{33} \right) \tilde{r}_3 + \sum_{r=1}^{2} c_r \chi_{\mathrm{L}}^{(r)} \tag{3.170}$$

$$\lambda_3 = \left(\sum_{r=1}^{2} c_r \tilde{e}_{33}^{(r)} - \tilde{q}_{33} \right) \tilde{r}_3 + \sum_{r=1}^{2} c_r \lambda_3^{(r)} \tag{3.171}$$

On the whole, there are nine independent connections between the ten effective parameters k, l, n, e_{33}, e_{31}, $\tilde{e}_{31}$, $\tilde{e}_{33}$, κ_{33}, μ_{33}, α_{33}, so that knowledge of one of them allows the determination of the rest. In [25], it was proved that the parameter k can be determined by Eq. (3.125). Having obtained the value of k, the moduli l, n, e_{33}, e_{31}, $\tilde{e}_{31}$, $\tilde{e}_{33}$, κ_{33}, μ_{33}, α_{33} can thus be fully determined from Eqs. (3.163)-(3.167) above.

The remaining six effective constants (p, e_{15}, $\tilde{e}_{15}$, κ_{33}, μ_{33}, α_{33}) can be determined using the procedure described in [25]. Consider the loading type defined by Eqs. (3.116) and (3.157). The solution to this loading type can be represented by

$$\begin{aligned} &u_1^{(r)} = \varepsilon_{13}^0 x_3, \qquad u_2^{(r)} = \varepsilon_{23}^0 x_3, \qquad u_3^{(r)} = \vartheta^{(r)}(x_1, x_2) - \varepsilon_{13}^0 x_1 - \varepsilon_{23}^0 x_2, \\ &\phi^{(r)} = \phi^{(r)}(x_1, x_2), \qquad \psi^{(r)} = \psi^{(r)}(x_1, x_2) \end{aligned} \tag{3.172}$$

Benveniste [25] then cast the constitutive laws of the constituents in matrix form as

$$\begin{Bmatrix} \boldsymbol{\sigma} \\ \mathbf{D} \\ \mathbf{B} \end{Bmatrix}^{(r)} = \begin{bmatrix} p & e_{15} & \tilde{e}_{15} \\ e_{15} & -\kappa_{11} & \alpha_{11} \\ \tilde{e}_{15} & \alpha_{11} & -\mu_{11} \end{bmatrix}^{(r)} \begin{Bmatrix} \nabla \vartheta \\ \nabla \phi \\ \nabla \psi \end{Bmatrix}^{(r)} \qquad (r = 1, 2, c) \tag{3.173}$$

where the subscript "c" refers to the effective law, and the following definitions are used:

$$\begin{aligned} &\boldsymbol{\sigma} = \{\sigma_{13} \quad \sigma_{23}\}, \qquad \mathbf{D} = \{D_1 \quad D_2\}, \qquad \mathbf{B} = \{B_1 \quad B_2\}, \\ &\nabla \vartheta = \{\vartheta_{,1} \quad \vartheta_{,2}\}, \qquad \nabla \phi = \{\phi_{,1} \quad \phi_{,2}\}, \qquad \nabla \psi = \{\psi_{,1} \quad \psi_{,2}\} \end{aligned} \tag{3.174}$$

Similar to the procedure described in Subsection 3.6.1.1, define the 3×3 matrices $\mathbf{L}_r$ representing the material matrix in Eq. (3.173):

$$\mathbf{L}_r = \begin{bmatrix} p & e_{15} & \tilde{e}_{15} \\ e_{15} & -\kappa_{11} & \alpha_{11} \\ \tilde{e}_{15} & \alpha_{11} & -\mu_{11} \end{bmatrix}^{(r)} \qquad (r = 1, 2, c) \tag{3.175}$$

$\mathbf{L}_r$ can then be converted to a diagonal matrix $\mathbf{L}_r^*$ using a matrix $\mathbf{W}$:

$$\mathbf{L}_r^* = \mathbf{W}\mathbf{L}_r\mathbf{W}^{\mathrm{T}} \qquad (r = 1, 2, c) \tag{3.176}$$

The implication of this result is the existence of the following constraint relation between the components of the effective matrix $\mathbf{L}_c$:

$$\mathbf{L}_c\mathbf{L}_1^{-1}\mathbf{L}_2 = \mathbf{L}_2\mathbf{L}_1^{-1}\mathbf{L}_c \tag{3.177}$$

It can be shown that the resulting matrix on the left hand side of Eq. (3.177) is antisymmetric, so that this equation provides three connections between the six effective components to be determined. To find the remaining three connections, consider the uncoupled elastic, electric, and magnetic behavior of the composite and denote the longitudinal shear modulus, transverse dielectric, and magnetic permeability coefficients by p^*, κ_{11}^*, and μ_{11}^*. In the framework of the composite cylinder assemblage model [45], Benveniste [25] obtained the following expressions of p^*, κ_{11}^*, and μ_{11}^*:

$$f^* = f_1^* \frac{c_1 f_1^* + (1 + c_2) f_2^*}{(1 + c_2) f_1^* + c_1 f_2^*} \qquad (f = p,\ \kappa_{11},\ \mu_{11}) \tag{3.178}$$

He then defined the matrices $\mathbf{L}_r^*$:

$$\mathbf{L}_r^* = \begin{bmatrix} p_r^* & 0 & 0 \\ 0 & (-\kappa_{11}^*)_r & 0 \\ 0 & 0 & (-\mu_{11}^*)_r \end{bmatrix} \qquad (r = 1, 2, c) \tag{3.179}$$

and cast Eq. (3.178) in the form

$$\mathbf{L}_c^* = \mathbf{L}_1^*[(1 + c_2)\mathbf{L}_1^* + (1 - c_2)\mathbf{L}_2^*]^{-1}[(1 - c_2)\mathbf{L}_1^* + (1 + c_2)\mathbf{L}_2^*] \tag{3.180}$$

Making use of Eq. (3.176), it can be proved that the effective moduli of the piezomagnetoelectric composite is given by

$$\mathbf{L}_c = \mathbf{L}_1[(1 + c_2)\mathbf{L}_1 + (1 - c_2)\mathbf{L}_2]^{-1}[(1 - c_2)\mathbf{L}_1 + (1 + c_2)\mathbf{L}_2] \tag{3.181}$$

where $\mathbf{L}_1$, $\mathbf{L}_2$, and $\mathbf{L}_c$ are defined by Eq. (3.175).

3.7 Solution of composite with elliptic fiber

In this section, the thermoelectroelastic solutions presented in [35] for thermal loading applied inside and outside an elliptic piezoelectric fiber in an infinite piezoelectric matrix are presented. By combining the method of Stroh's formalism, the technique of conformal mapping, the concept of perturbation and the method of analytical continuation, a general analytical thermoelectroelastic solution is obtained for an elliptic piezoelectric cylindrical fiber embedded in an infinite piezoelectric matrix subjected to thermal loading. The loading may be a point heat source, temperature discontinuity, or a uniform remote heat flow. Special cases when the fiber becomes rigid or a hole are also investigated.

3.7.1 Conformal mapping

Consider an elliptic piezoelectric fiber embedded in an infinite matrix. The contour of their interface Γ is represented by

$$x_1 = a\cos\psi, \qquad x_2 = b\sin\psi \tag{3.182}$$

where ψ is a real parameter and $a \geqslant b > 0$ are the principal radii of the elliptic interface. It will be more convenient to transform the ellipse to a circle before solving the problem. For this, consider the mapping

$$z_k = a_{1k}\zeta_k + a_{2k}\zeta_k^{-1} \tag{3.183}$$

where

$$a_{1k} = (a - ip_k b)/2, \qquad a_{2k} = (a + ip_k b)/2 \tag{3.184}$$

Equation (3.183) will map the region outside the elliptic fiber onto the exterior of a unit circle in the ζ_k-plane. Further, the transformation (3.183) is single valued and conformal outside the ellipse, since the roots of equation

$$\mathrm{d}z_k / \mathrm{d}\zeta_k = a_{1k} - a_{2k}\zeta_k^{-2} = 0 \tag{3.185}$$

are located inside the unit circle $|\zeta_k| < 1$. In fact, the roots are $\zeta_k^0 = \pm\sqrt{a_{2k}/a_{1k}} = \pm\sqrt{m_k}\,e^{i\theta_k}$, where $(m_k)^{1/2}<1$ [46]. However, the mapping (3.183) is not single valued inside the ellipse because the roots of Eq. (3.185) are located inside the unit circle. To bypass this problem, the mapping of Ω_2 (see Fig. 3.17) is done by excluding a slit Γ_0, which represents a circle of radius $\sqrt{m_k}$ in the ζ_k-plane, from the ellipse [47]. In this case the function (3.183) will transform Γ and Γ_0 into a ring of outer and inner circles with radii $r_{\text{out}} = 1$ and $r_{\text{in}} = \sqrt{m_k}$, respectively. Moreover,

anywhere inside the ellipse and on the slit Γ_0 a function $f(\zeta_k)$ must satisfy the following condition:

$$f[\sqrt{m_k}\sigma(\theta)] = f[\sqrt{m_k}e^{2i\theta_k} / \sigma(\theta)] \tag{3.186}$$

to ensure that the field is single valued [47], where $\sigma(\theta) = e^{i\theta}$ stands for a point located on the unit circle in the ζ_k-plane, and θ is a polar angle.

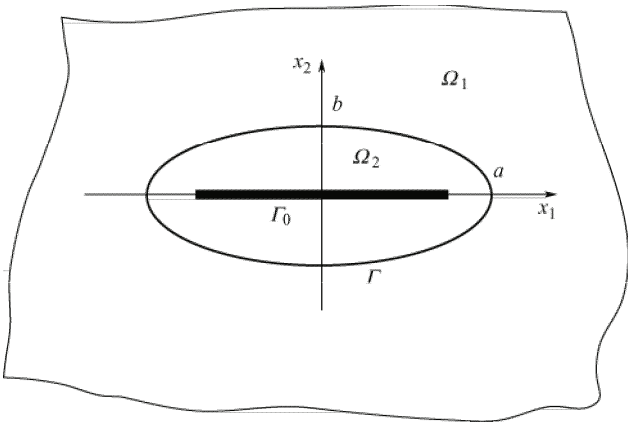

Fig. 3.17 Geometry of an elliptic fiber in a matrix.

3.7.2 Solutions for thermal loading applied outside an elliptic fiber

Consider an elliptic fiber embedded in an infinite piezoelectric matrix subjected to thermal loading located at the point (x_{10}, x_{20}) which is outside the fiber. If the fiber and matrix are assumed to be perfectly bonded along the interface, the temperature, heat flow (h_n), elastic displacements, electric potential, stress and electric displacement ($\mathbf{t}_n$) across the interface should be continuous, i.e.,

$$T_1 = T_2, \quad \vartheta_1 = \vartheta_2, \quad \mathbf{U}_1 = \mathbf{U}_2, \quad \varphi_1 = \varphi_2 \qquad \text{(along the interface)} \tag{3.187}$$

Here the following equations are used:

$$h_n = \mathfrak{F}_{,s}, \qquad \mathbf{t}_n = \boldsymbol{\varphi}_{,s} \tag{3.188}$$

where n is the normal direction of the interface, s is the arc length measured along the elliptic boundary, and $\mathbf{t}_n$ is the surface traction-charge vector. Here and in the following, the subscripts "1" and "2" (or superscripts (1) and (2)) denote the quantities associated with matrix and fiber, respectively.

3.7.2.1 General solution for thermal fields

Based on the conformal mapping described above and the concept of perturbation

given by Stagni [48], the general solution for temperature and heat-flow function can be assumed in the form

$$\begin{aligned} T_1 &= f_0(\zeta_t^{(1)}) + \overline{f_0(\zeta_t^{(1)})} + f_1(\zeta_t^{(1)}) + \overline{f_1(\zeta_t^{(1)})}, \\ \vartheta_1 &= -ik_1 f_0(\zeta_t^{(1)}) + ik_1 \overline{f_0(\zeta_t^{(1)})} - ik_1 f_1(\zeta_t^{(1)}) + ik_1 \overline{f_1(\zeta_t^{(1)})} \end{aligned} \qquad (\zeta_t^{(1)} \in \Omega_1) \quad (3.189)$$

$$\begin{aligned} T_2 &= f_2(\zeta_t^{(2)}) + \overline{f_2(\zeta_t^{(2)})}, \\ \vartheta_2 &= -ik_2 f_2(\zeta_t^{(2)}) + ik_2 \overline{f_2(\zeta_t^{(2)})} \end{aligned} \qquad (\zeta_t^{(2)} \in \Omega_2) \quad (3.190)$$

Here, f_0 can be chosen to represent the solutions associated with the unperturbed thermal field, which is holomorphic in the entire domain except for some singular points such as the point at which a point heat source is applied, and f_1 and f_2 are the functions corresponding to the perturbed field of matrix and fiber, respectively. They are holomorphic in the regions Ω_1 and Ω_2, respectively. In the ζ_t-plane, Ω_1 is the region outside the unit circle and Ω_2 is the region of the annular ring between the unit circle and the circle of radius $\sqrt{m_t}$.

For a given loading condition, the function f_0 can be obtained easily since it is related to the solution of homogeneous media. When an infinite space is subjected to a line heat source h^* and a line temperature discontinuity $\hat{T}$, both located at (x_{10}, x_{20}), the function f_0 can be chosen in the form

$$f_0(\zeta_t^{(1)}) = q_0 \ln(\zeta_t^{(1)} - \zeta_{t0}^{(1)}) \qquad (3.191)$$

where $\zeta_t^{(1)}$ and $\zeta_{t0}^{(1)}$ are related to the complex arguments $z_t^{(1)}$ and $z_{t0}^{(1)} (= x_{10} + p_1^{*(1)} x_{20})$ through the following transformation functions:

$$\zeta_t^{(1)} = \frac{z_t^{(1)} + \sqrt{z_t^{(1)2} - a^2 - p_1^{*(1)2} b^2}}{a - ip_1^{*(1)} b}, \qquad \zeta_{t0}^{(1)} = \frac{z_{t0}^{(1)} + \sqrt{z_{t0}^{(1)2} - a^2 - p_1^{*(1)2} b^2}}{a - ip_1^{*(1)} b} \qquad (3.192)$$

and q_0 is given in the form [36]

$$q_0 = \hat{T} / 4\pi i - h^* / 4\pi k \qquad (3.193)$$

When the thermal load is uniform remote heat flow $\mathbf{h}(h_{10}, h_{20})$, the function f_0 may be expressed by

$$f_0(\zeta_t^{(1)}) = q_0^* \zeta_t^{(1)} \qquad (3.194)$$

The infinite condition provides

$$q_0^* = \frac{1}{4ik_1}(a - ibp_1^{*(1)})(h_{10} / p_1^{*(1)} - h_{20}) \tag{3.195}$$

As for the function f_2, noting that it is holomorphic in the annular ring, it can be represented by Laurent's series

$$f_2(\zeta_t^{(2)}) = \sum_{j=-\infty}^{\infty} c_j \zeta_t^{(2)j} \tag{3.196}$$

whose coefficients can be related by means of Eq. (3.186) in the following manner:

$$c_{-j} = \Gamma_j^* c_j, \qquad \Gamma_j^* = \left(\frac{a + ibp_1^{*(2)}}{a - ibp_1^{*(2)}} \right)^j \tag{3.197}$$

Inserting Eqs. (3.191) and (3.196) into Eqs. (3.189) and (3.190), and later into Eqs. $(3.187)_{1,2}$, yields

$$f_1(\sigma) + \overline{f_0(\sigma)} - \sum_{j=1}^{\infty} [\overline{c}_j + \Gamma_j^* c_j]\sigma^{-j} = \sum_{j=1}^{\infty} [c_j + \overline{\Gamma}_j^* \overline{c}_j]\sigma^j - \overline{f_1(\sigma)} - f_0(\sigma) \tag{3.198}$$

$$\begin{aligned} &\overline{f_0(\sigma)} - f_1(\sigma) - \frac{k_2}{k_1} \sum_{j=1}^{\infty} [\overline{c}_j - \Gamma_j^* c_j]\sigma^{-j} \\ &= -\frac{k_2}{k_1} \sum_{j=1}^{\infty} [c_j - \overline{\Gamma}_j^* \overline{c}_j]\sigma^j + f_0(\sigma) - \overline{f_1(\sigma)} \end{aligned} \tag{3.199}$$

One of the important properties of holomorphic functions used in the method of analytic continuation is that if the function $f(\zeta)$ is holomorphic in Ω_1 (or $\Omega_0 + \Omega_2$), then $\overline{f(1/\overline{\zeta})}$ is holomorphic in $\Omega_0 + \Omega_2$ (or Ω_1), Ω_0 denoting the region inside the circle of radius $\sqrt{m_t}$. Hence, put

$$\omega(\zeta) = \begin{cases} f_1(\zeta) + \overline{f_0(1/\overline{\zeta})} - \sum_{j=1}^{\infty} [\overline{c}_j + \Gamma_j^* c_j]\zeta^{-j} & (\zeta \in \Omega_1) \\ -\overline{f_1(1/\overline{\zeta})} - f_0(\zeta) + \sum_{j=1}^{\infty} [c_j + \overline{\Gamma}_j^* \overline{c}_j]\zeta^j & (\zeta \in \Omega_0 + \Omega_2) \end{cases} \tag{3.200}$$

where the function $\omega(\zeta)$ is holomorphic and single valued in the whole plane. By Liouville's theorem, we have $\omega(\zeta)$= constant. However, constant function f does not produce stress and electric displacement (SED), which may be neglected. Thus, by letting $\omega(\zeta)$=0, we have

$$\begin{cases} \sum_{j=1}^{\infty}[\overline{c}_j + \Gamma_j^* c_j]\zeta^{-j} = f_1(\zeta) + \overline{f_0(1/\overline{\zeta})} & (\zeta \in \Omega_1) \\ \sum_{j=1}^{\infty}[c_j + \overline{\Gamma}_j^* \overline{c}_j]\zeta^{j} = \overline{f_1(1/\overline{\zeta})} + f_0(\zeta) & (\zeta \in \Omega_0 + \Omega_2) \end{cases} \tag{3.201}$$

It should be mentioned that the subscripts "1" and "2" (or superscripts (1) and (2)) are omitted in Eqs. (3.200) and (3.201). To further simplify subsequent writing, we shall omit them again in the related expressions when the distinction is unnecessary. As in Eq. (3.201), it can be determined from Eq. (3.199) that

$$\begin{cases} \frac{k_2}{k_1}\sum_{j=1}^{\infty}[\overline{c}_j - \Gamma_j^* c_j]\zeta^{-j} = -f_1(\zeta) + \overline{f_0(1/\overline{\zeta})} & (\zeta \in \Omega_1) \\ \frac{k_2}{k_1}\sum_{j=1}^{\infty}[c_j - \overline{\Gamma}_j^* \overline{c}_j]\zeta^{j} = -\overline{f_1(1/\overline{\zeta})} + f_0(\zeta) & (\zeta \in \Omega_0 + \Omega_2) \end{cases} \tag{3.202}$$

The Eqs. $(3.201)_2$ and $(3.202)_2$ provide

$$f_0(\zeta) = \frac{1}{2}\sum_{j=1}^{\infty}[(1+k_2/k_1)c_j + (1-k_2/k_1)\overline{\Gamma}_j^* \overline{c}_j]\zeta^j \tag{3.203}$$

With the use of the series representation

$$f_0(x) = \sum_{k=1}^{\infty} e_k x^k, \qquad e_k = \frac{f_0^{(k)}(0)}{k!} = \frac{1}{2\pi i}\int_C \frac{f_0(x)}{x^{k+1}}\mathrm{d}x \tag{3.204}$$

the function $f_0(\zeta)$ given in Eq. (3.191) (or (3.194)) can be expressed as

$$f_0(\zeta) = \sum_{j=1}^{\infty} e_j \zeta^j, \qquad e_j = -\frac{q_0 \zeta_{t0}^{(1)-j}}{j} \ (\text{or } e_j = \delta_{1j} q_0^*) \tag{3.205}$$

where δ_{ij}=1, when i=j; δ_{ij}=0, when $i \neq j$.

By comparing the coefficients of corresponding terms in Eqs. (3.203) and (3.205), we obtain

$$c_j = (G_0 - \overline{G}_j G_j / G_0)^{-1}(e_j - \overline{G}_j \overline{e}_j / G_0) \qquad (j = 1,\ 2, \cdots, \infty) \tag{3.206}$$

where $G_0 = (1+k_2/k_1)/2,\ G_j = (1-k_2/k_1)\Gamma_j^*/2$.

With the solution obtained for c_k, the functions f_1, g_1', and g_2' can be further written as

$$f_1(\zeta) = \sum_{j=1}^{\infty}\left(\overline{c}_j + \Gamma_j^* c_j\right)\zeta_t^{(1)-j} - \overline{q}_0 \ln\left(\zeta_t^{(1)-1} - \overline{\zeta}_{t0}^{(1)}\right) \tag{3.207}$$

$$g_1'(\zeta_t^{(1)}) = q_0 \ln(\zeta_t^{(1)} - \zeta_{t0}^{(1)}) - \overline{q}_0 \ln(\zeta_t^{(1)-1} - \overline{\zeta}_{t0}^{(1)}) + \sum_{j=1}^{\infty} \left(\overline{c}_j + \Gamma_j^* c_j\right) \zeta_t^{(1)-j} \tag{3.208}$$

$$g_2'(\zeta_t^{(2)}) = \sum_{j=1}^{\infty} c_j \left(\zeta_t^{(2)j} + \Gamma_j^* \zeta_t^{(2)-j}\right) \tag{3.209}$$

Equations (3.208) and (3.209) are the general thermal solutions for the case of line heat source and temperature discontinuity. If the load is uniform remote heat flow, the general solutions can be obtained similarly. They are

$$g_1'(\zeta_t^{(1)}) = q_0^* \zeta_t^{(1)} - \overline{q}_0^* \zeta_t^{(1)-1} + (\overline{c}_1 + \Gamma_1^* c_1) \zeta_t^{(1)-1} \tag{3.210}$$

$$g_2'(\zeta_t^{(2)}) = c_1 (\zeta_t^{(2)} + \Gamma_1^* \zeta_t^{(2)-1}) \tag{3.211}$$

3.7.2.2 General solution for electroelastic fields

The particular piezoelectric solution induced by a thermal load can be written as [35,36]

$$\mathbf{U}_{ip} = 2\,\mathrm{Re}[\mathbf{c}_i g_i(\zeta_t^{(i)})], \quad \boldsymbol{\varphi}_{ip} = 2\,\mathrm{Re}[\mathbf{d}_i g_i(\zeta_t^{(i)})] \qquad (i=1, 2) \tag{3.212}$$

where subscript "p" refers to a particular solution. The function $g(z_t)$ in Eq. (3.212) can be obtained by integrating Eqs. (3.208) and (3.209) (or (3.210) and (3.211)) with respect to z_t, which yields

$$\begin{aligned} g_1(\zeta_t^{(1)}) = {} & a_{1\tau}^{(1)} [q_0 F_1(\zeta_t^{(1)}, \zeta_{t0}^{(1)}) - \overline{q}_0 F_2(\zeta_t^{(1)-1}, \overline{\zeta}_{t0}^{(1)})] + a_{2\tau}^{(1)} [q_0 F_2(\zeta_t^{(1)}, \zeta_{t0}^{(1)}) \\ & - \overline{q}_0 F_1(\zeta_t^{(1)-1}, \overline{\zeta}_{t0}^{(1)})] + (\overline{c}_1 + \Gamma_1^* c_1) a_{1\tau}^{(1)} \ln \zeta_t^{(1)} + \sum_{j=1}^{\infty} G_{1j} \zeta_t^{(1)-j} \end{aligned} \tag{3.213}$$

$$g_2(\zeta_t^{(2)}) = \sum_{j=1}^{\infty} \left(G_{2j} \zeta_t^{(1)j} + G_{3j} \zeta_t^{(2)-j}\right) \tag{3.214}$$

for Eqs. (3.208) and (3.209), or

$$\begin{aligned} g_1(\zeta_t^{(1)}) = {} & q_0^* (a_{1\tau}^{(1)} \zeta_t^{(1)2} / 2 - a_{2\tau}^{(1)} \ln \zeta_t^{(1)}) \\ & - (\overline{q}_0^* - \overline{c}_1 - \Gamma_1^* c_1)(a_{1\tau}^{(1)} \ln \zeta_t^{(1)} + a_{2\tau}^{(1)} \zeta_t^{(1)-2} / 2) \end{aligned} \tag{3.215}$$

$$g_2(\zeta_t^{(2)}) = c_1 (a_{1\tau}^{(2)} \zeta_t^{(2)2} + a_{2\tau}^{(2)} \Gamma_1^* \zeta_t^{(2)-2}) / 2 \tag{3.216}$$

for Eqs. (3.210) and (3.211), where

$$F_1(\zeta_t, \zeta_{t0}) = (\zeta_t - \zeta_{t0})[\ln(\zeta_t - \zeta_{t0}) - 1],$$

$$F_2(\zeta_t, \zeta_{t0}) = (\zeta_t^{-1} - \zeta_{t0}^{-1}) \ln(\zeta_t - \zeta_{t0}) + \zeta_{t0}^{-1} \ln \zeta_t,$$

$$a_{1\tau}^{(k)} = (a - i p_1^{*(k)} b)/2, \qquad a_{2\tau}^{(k)} = (a + i p_1^{*(k)} b)/2, \qquad (k = 1, 2)$$

$$
\begin{aligned}
G_{1j} &= -[(\overline{c}_{j+1} + \Gamma^*_{j+1} c_{j+1}) a^{(1)}_{1\tau} - a^{(1)}_{2\tau} (\overline{c}_{j-1} + \Gamma^*_{j-1} c_{j-1}) s_{j1}] / j, \\
G_{2j} &= (a^{(2)}_{1\tau} c_{j-1} s_{j1} - a^{(2)}_{2\tau} c_{j+1}) / j, \\
G_{3j} &= -(a^{(2)}_{1\tau} \Gamma^*_{j+1} c_{j+1} - a^{(2)}_{2\tau} \Gamma^*_{j-1} c_{j-1} s_{j1}) / j
\end{aligned}
\tag{3.217}
$$

and $s_{ij} = 1$ for $i \neq j$, $s_{ij} = 0$ for $i = j$.

The particular solution (3.212) does not generally satisfy the condition $(3.187)_{3,4}$ along the interface. We therefore need to find a corrective isothermal solution for a given problem so that when it is superposed on the particular thermoelectroelastic solution the interface condition $(3.187)_{3,4}$ will be satisfied. Owing to the fact that $f(\zeta_m)$ and $g(\zeta_t)$ have the same rule affecting the SED in the general solution of a thermoelectroelastic problem [35]

$$
\begin{aligned}
& T = g'(z_t) + \overline{g'(z_t)}, \\
& \vartheta = -ikg'(z_t) + ik\overline{g'(z_t)}, \\
& h_1 = -\vartheta_{,2}, \quad h_2 = \vartheta_{,1}, \\
& \mathbf{U} = \mathbf{A}\langle f(z_\alpha)\rangle \mathbf{q} + \mathbf{c} g(z_t) + \overline{\mathbf{A}\langle f(z_\alpha)\rangle \mathbf{q}} + \overline{\mathbf{c} g(z_t)}, \\
& \boldsymbol{\varphi} = \mathbf{B}\langle f(z_\alpha)\rangle \mathbf{q} + \mathbf{d} g(z_t) + \overline{\mathbf{B}\langle f(z_\alpha)\rangle \mathbf{q}} + \overline{\mathbf{d} g(z_t)}, \\
& \boldsymbol{\Pi}_1 = -\boldsymbol{\varphi}_{,2}, \quad \boldsymbol{\Pi}_2 = \boldsymbol{\varphi}_{,1}
\end{aligned}
\tag{3.218}
$$

with

$$
z_t = x_1 + p_1^* x_2 \tag{3.219}
$$

possible function forms come from the partition of $g(\zeta_t)$. They are

$$
\begin{aligned}
f^{(j)}_{1m}(\zeta^{(j)}_m) &= a[q_0 F_1(\zeta^{(j)}_m, \zeta^{(j)}_{t0}) + q_0 F_2(\zeta^{(j)}_m, \zeta^{(j)}_{t0}) \\
&\quad - \overline{q}_0 F_1(\zeta^{(j)-1}_m, \overline{\zeta}^{(j)}_{t0}) - \overline{q}_0 F_2(\zeta^{(j)-1}_m, \overline{\zeta}^{(j)}_{t0})] / 2, \\
f^{(j)}_{2m}(\zeta^{(j)}_m) &= ip^{(j)}_m b[-q_0 F_1(\zeta^{(j)}_m, \zeta^{(j)}_{t0}) + q_0 F_2(\zeta^{(j)}_m, \zeta^{(j)}_{t0}) \\
&\quad - \overline{q}_0 F_1(\zeta^{(j)-1}_m, \overline{\zeta}^{(j)}_{t0}) + \overline{q}_0 F_2(\zeta^{(j)-1}_m, \overline{\zeta}^{(j)}_{t0})] / 2
\end{aligned}
\qquad (j=1,2) \tag{3.220}
$$

$$
f^{(j)}_{3m}(\zeta^{(j)}_m) = a^{(j)}_{1m} \ln \zeta^{(j)}_m \qquad (j=1,2) \tag{3.221}
$$

$$
\mathbf{f}^{(j)}_4(\zeta^{(j)}) = \sum_{k=1}^{\infty} \langle \zeta^{(j)k}_\alpha \rangle \mathbf{r}^{(j)}_k, \qquad \mathbf{f}^{(j)}_5(\zeta^{(j)}) = \sum_{k=1}^{\infty} \langle \zeta^{(j)-k}_\alpha \rangle \mathbf{s}^{(j)}_k \qquad (j=1,2) \tag{3.222}
$$

where $\mathbf{f}^{(j)}_k$ are four component vectors, and $\mathbf{r}^{(j)}_k$ and $\mathbf{s}^{(j)}_k$ are constant vectors with four components to be determined. It should be pointed out that the vector $\mathbf{s}^{(j)}_k$ is not the same as the symbol s_{ij} given in Eq. (3.217).

The Green's functions for the electroelastic fields can thus be chosen as

$$\mathbf{U}_j = 2\,\mathrm{Re}\left\{\sum_{k=1}^{3}\mathbf{A}_j\left\langle f_{k\alpha}^{(j)}(\zeta_\alpha^{(j)})\right\rangle\mathbf{q}_k^{(j)} + \sum_{k=4}^{5}\mathbf{A}_j\mathbf{f}_k^{(j)}(\boldsymbol{\zeta}^{(j)}) + \mathbf{c}_j g_j(\zeta_t^{(j)})\right\} \tag{3.223}$$

$$\varphi_j = 2\,\mathrm{Re}\left\{\sum_{k=1}^{3}\mathbf{B}_j\left\langle f_{k\alpha}^{(j)}(\zeta_\alpha^{(j)})\right\rangle\mathbf{q}_k^{(j)} + \sum_{k=4}^{5}\mathbf{B}_j\mathbf{f}_k^{(j)}(\boldsymbol{\zeta}^{(j)}) + \mathbf{d}_j g_j(\zeta_t^{(j)})\right\} \tag{3.224}$$

The above two expressions, together with the interface condition $(3.187)_{3,4}$, provide

$$\mathbf{q}_1^{(1)} = \mathbf{X}_1(\mathbf{A}_2^{-1}\overline{\mathbf{c}}_1 - \mathbf{B}_2^{-1}\overline{\mathbf{d}}_1) \tag{3.225}$$

$$\mathbf{q}_1^{(2)} = \mathbf{X}_2(\mathbf{B}_1^{-1}\overline{\mathbf{d}}_1 - \mathbf{A}_1^{-1}\overline{\mathbf{c}}_1) \tag{3.226}$$

$$\mathbf{q}_2^{(1)} = \overline{p}_1^{*(1)}\mathbf{P}_1^{-1}\mathbf{q}_1^{(1)} \tag{3.227}$$

$$\mathbf{q}_2^{(2)} = \overline{p}_1^{(*1)}\mathbf{P}_2^{-1}\mathbf{q}_1^{(2)} \tag{3.228}$$

$$\mathbf{q}_3^{(1)} = \left\langle a_{1\alpha}^{(1)}\right\rangle^{-1}\overline{a}_{1\tau}^{(1)}(c_1 + \overline{\Gamma}_1^{*}\overline{c}_1)\mathbf{q}_1^{(1)} \tag{3.229}$$

$$\mathbf{q}_3^{(2)} = \left\langle a_{1\alpha}^{(2)}\right\rangle^{-1}\overline{a}_{1\tau}^{(1)}(c_1 + \overline{\Gamma}_1^{*}\overline{c}_1)\mathbf{q}_1^{(2)} \tag{3.230}$$

$$\begin{aligned}&\mathbf{A}_1\mathbf{f}_5^{(1)}(\sigma) + \overline{\mathbf{A}}_1\overline{\mathbf{f}_4^{(1)}(\sigma)} - \mathbf{A}_2\mathbf{f}_5^{(2)}(\sigma) - \overline{\mathbf{A}}_2\overline{\mathbf{f}_4^{(2)}(\sigma)} + \sum_{j=1}^{\infty}(\mathbf{c}_1 G_{1j} - \overline{\mathbf{c}}_2\overline{G}_{2j} - \mathbf{c}_2 G_{3j})\sigma^{-j}\\ =&\mathbf{A}_2\mathbf{f}_4^{(2)}(\sigma) + \overline{\mathbf{A}}_2\overline{\mathbf{f}_5^{(2)}(\sigma)} - \mathbf{A}_1\mathbf{f}_4^{(1)}(\sigma) - \overline{\mathbf{A}}_1\overline{\mathbf{f}_5^{(1)}(\sigma)} - \sum_{j=1}^{\infty}(\overline{\mathbf{c}}_1\overline{G}_{1j} - \mathbf{c}_2 G_{2j} - \overline{\mathbf{c}}_2\overline{G}_{3j})\sigma^{j}\end{aligned} \tag{3.231}$$

$$\begin{aligned}&\mathbf{B}_1\mathbf{f}_5^{(1)}(\sigma) + \overline{\mathbf{B}}_1\overline{\mathbf{f}_4^{(1)}(\sigma)} - \mathbf{B}_2\mathbf{f}_5^{(2)}(\sigma) - \overline{\mathbf{B}}_2\overline{\mathbf{f}_4^{(2)}(\sigma)} + \sum_{j=1}^{\infty}(\mathbf{d}_1 G_{1j} - \overline{\mathbf{d}}_2\overline{G}_{2j} - \mathbf{d}_2 G_{3j})\sigma^{-j}\\ =&\mathbf{B}_2\mathbf{f}_4^{(2)}(\sigma) + \overline{\mathbf{B}}_2\overline{\mathbf{f}_5^{(2)}(\sigma)} - \mathbf{B}_1\mathbf{f}_4^{(1)}(\sigma) - \overline{\mathbf{B}}_1\overline{\mathbf{f}_5^{(1)}(\sigma)} - \sum_{j=1}^{\infty}(\overline{\mathbf{d}}_1\overline{G}_{1j} - \mathbf{d}_2 G_{2j} - \overline{\mathbf{d}}_2\overline{G}_{3j})\sigma^{j}\end{aligned} \tag{3.232}$$

where

$$\mathbf{X}_1 = (\mathbf{A}_2^{-1}\mathbf{A}_1 - \mathbf{B}_2^{-1}\mathbf{B}_1)^{-1}, \qquad \mathbf{X}_2 = (\mathbf{A}_1^{-1}\mathbf{A}_2 - \mathbf{B}_1^{-1}\mathbf{B}_2)^{-1} \tag{3.233}$$

Therefore, by Liouville's theorem, Eqs. (3.231) and (3.232) yield

$$\mathbf{A}_2\mathbf{f}_5^{(2)}(\sigma)+\overline{\mathbf{A}}_2\overline{\mathbf{f}_4^{(2)}(\sigma)}-\sum_{j=1}^{\infty}(\mathbf{c}_1G_{1j}-\overline{\mathbf{c}}_2\overline{G}_{2j}-\mathbf{c}_2G_{3j})\sigma^{-j}$$
$$=\mathbf{A}_1\mathbf{f}_5^{(1)}(\sigma)+\overline{\mathbf{A}}_1\overline{\mathbf{f}_4^{(1)}(\sigma)} \tag{3.234}$$

$$\mathbf{A}_2\mathbf{f}_4^{(2)}(\sigma)+\overline{\mathbf{A}}_2\overline{\mathbf{f}_5^{(2)}(\sigma)}-\sum_{j=1}^{\infty}(\overline{\mathbf{c}}_1\overline{G}_{1j}-\mathbf{c}_2G_{2j}-\overline{\mathbf{c}}_2\overline{G}_{3j})\sigma^{j}$$
$$=\mathbf{A}_1\mathbf{f}_4^{(1)}(\sigma)+\overline{\mathbf{A}}_1\overline{\mathbf{f}_5^{(1)}(\sigma)} \tag{3.235}$$

$$\mathbf{B}_2\mathbf{f}_5^{(2)}(\sigma)+\overline{\mathbf{B}}_2\overline{\mathbf{f}_4^{(2)}(\sigma)}-\sum_{j=1}^{\infty}(\mathbf{d}_1G_{1j}-\overline{\mathbf{d}}_2\overline{G}_{2j}-\mathbf{d}_2G_{3j})\sigma^{-j}$$
$$=\mathbf{B}_1\mathbf{f}_5^{(1)}(\sigma)+\overline{\mathbf{B}}_1\overline{\mathbf{f}_4^{(1)}(\sigma)} \tag{3.236}$$

$$\mathbf{B}_2\mathbf{f}_4^{(2)}(\sigma)+\overline{\mathbf{B}}_2\overline{\mathbf{f}_5^{(2)}(\sigma)}-\sum_{j=1}^{\infty}(\overline{\mathbf{d}}_1\overline{G}_{1j}-\mathbf{d}_2G_{2j}-\overline{\mathbf{d}}_2\overline{G}_{3j})\sigma^{j}$$
$$=\mathbf{B}_1\mathbf{f}_4^{(1)}(\sigma)+\overline{\mathbf{B}}_1\overline{\mathbf{f}_5^{(1)}(\sigma)} \tag{3.237}$$

The above four equations are not completely independent. For example, Eqs. (3.234) and (3.236) can be obtained from Eqs. (3.235) and (3.237). Thus only two of the equations are independent. However, there are four sets of constant vectors, i.e., $\mathbf{r}_k^{(j)}$ and $\mathbf{s}_k^{(j)}(j=1,2)$, to be determined. We need two more equations to make the solution unique. Through use of the relation (3.186) and Eqs. (3.223) and (3.224), the unknown vectors $\mathbf{r}_j^{(2)}$ and $\mathbf{s}_j^{(2)}$ appearing in $\mathbf{f}_4^{(2)}$ and $\mathbf{f}_5^{(2)}$ can be determined as follows:

$$\mathbf{r}_j^{(2)}=(\mathbf{A}_2^{-1}\left\langle\Gamma_{j\alpha}^{(2)}\right\rangle\mathbf{A}_2-\mathbf{B}_2^{-1}\left\langle\Gamma_{j\alpha}^{(2)}\right\rangle\mathbf{B}_2)^{-1}[\mathbf{A}_2^{-1}(\mathbf{c}_2G_{3j}$$
$$-\left\langle\Gamma_{j\alpha}^{(2)}\right\rangle\mathbf{c}_2G_{2j})-\mathbf{B}_2^{-1}(\mathbf{d}_2G_{3j}-\left\langle\Gamma_{j\alpha}^{(2)}\right\rangle\mathbf{d}_2G_{2j})] \qquad (j=1,\cdots,\infty) \tag{3.238}$$

$$\mathbf{s}_j^{(2)}=\mathbf{B}_2^{-1}[\left\langle\Gamma_{j\alpha}^{(2)}\right\rangle(\mathbf{B}_2\mathbf{r}_j^{(2)}+\mathbf{d}_2G_{2j})-\mathbf{d}_2G_{3j}] \qquad (j=1,\cdots,\infty) \tag{3.239}$$

where $\left\langle\Gamma_{j\alpha}^{(i)}\right\rangle=\left\langle\left(\dfrac{a+ibp_\alpha^{(i)}}{a-ibp_\alpha^{(i)}}\right)^j\right\rangle$.

Once the constant vectors $\mathbf{r}_j^{(2)}$ and $\mathbf{s}_j^{(2)}$ are obtained, the unknown vectors $\mathbf{r}_j^{(1)}$ and $\mathbf{s}_j^{(1)}$ given in $\mathbf{f}_4^{(1)}$ and $\mathbf{f}_5^{(1)}$ can be determined from Eqs. (3.234) and (3.236) (or (3.235) and (3.237)). They are

$$\mathbf{r}_j^{(1)}=i\mathbf{A}_1^{\mathrm{T}}[(\mathbf{M}_2+\overline{\mathbf{M}}_1)\mathbf{A}_2\mathbf{r}_j^{(2)}+(\overline{\mathbf{M}}_1-\overline{\mathbf{M}}_2)\overline{\mathbf{A}}_2\overline{\mathbf{s}}_j^{(2)}$$
$$-\overline{\mathbf{M}}_1(\overline{\mathbf{c}}_1\overline{G}_{1j}-\mathbf{c}_2G_{2j}-\overline{\mathbf{c}}_2\overline{G}_{3j})+i(\overline{\mathbf{d}}_1\overline{G}_{1j}-\mathbf{d}_2G_{2j}-\overline{\mathbf{d}}_2\overline{G}_{3j})] \tag{3.240}$$

$$\mathbf{s}_j^{(1)} = i\mathbf{A}_1^{\mathrm{T}}[(\mathbf{M}_2 + \overline{\mathbf{M}}_1)\mathbf{A}_2\mathbf{s}_j^{(2)} + (\overline{\mathbf{M}}_1 - \overline{\mathbf{M}}_2)\overline{\mathbf{A}}_2\overline{\mathbf{r}}_j^{(2)} - \overline{\mathbf{M}}_1(\mathbf{c}_1 G_{1j} - \overline{\mathbf{c}}_2 \overline{G}_{2j} - \mathbf{c}_2 G_{3j}) + i(\mathbf{d}_1 G_{1j} - \overline{\mathbf{d}}_2 \overline{G}_{2j} - \mathbf{d}_2 G_{3j})] \tag{3.241}$$

where

$$\begin{aligned} &\mathbf{M}_k = -i\mathbf{B}_k\mathbf{A}_k^{-1} = \mathbf{H}_k^{-1}(\mathbf{I} + i\mathbf{S}_k), \\ &\mathbf{H}_k = 2i\mathbf{A}_k\mathbf{A}_k^{\mathrm{T}}, \qquad (k=1,2) \\ &\mathbf{S}_k = i(2\mathbf{A}_k\mathbf{B}_k^{\mathrm{T}} - \mathbf{I}) \end{aligned} \tag{3.242}$$

For the case of remote heat flow, the related general solution can be obtained similarly. Set

$$\mathbf{U}_j = 2\,\mathrm{Re}\left\{\sum_{k=1}^{3}\mathbf{A}_j\mathbf{F}_k^{(j)}(\boldsymbol{\zeta}^{(j)})\mathbf{q}_k^{(j)} + \mathbf{c}_j g_j(\zeta_t^{(j)})\right\} \tag{3.243}$$

$$\boldsymbol{\varphi}_j = 2\,\mathrm{Re}\left\{\sum_{k=1}^{3}\mathbf{B}_j\mathbf{F}_k^{(j)}(\boldsymbol{\zeta}^{(j)})\mathbf{q}_k^{(j)} + \mathbf{d}_j g_j(\zeta_t^{(j)})\right\} \tag{3.244}$$

where

$$\mathbf{F}_1^{(j)}(\boldsymbol{\zeta}^{(j)}) = \left\langle \ln\zeta_m^{(j)} \right\rangle, \qquad \mathbf{F}_2^{(j)}(\boldsymbol{\zeta}^{(j)}) = \left\langle \zeta_m^{(j)2} \right\rangle, \qquad \mathbf{F}_3^{(j)}(\boldsymbol{\zeta}^{(j)}) = \left\langle \left(\zeta_m^{(j)}\right)^{-2} \right\rangle \qquad (j=1,2) \tag{3.245}$$

The interface condition $(3.187)_{3,4}$ leads to

$$\mathbf{q}_1^{(1)} = -[\overline{a}_{2\tau}^{(1)}\overline{q}_0^* + \overline{a}_{1\tau}^{(1)}(q_0^* - c_1 - \overline{\Gamma}_1^*\overline{c}_1)](\mathbf{A}_2^{-1}\mathbf{A}_1 - \mathbf{B}_2^{-1}\mathbf{B}_1)^{-1}(\mathbf{A}_2^{-1}\overline{\mathbf{c}}_1 - \mathbf{B}_2^{-1}\overline{\mathbf{d}}_1) \tag{3.246}$$

$$\mathbf{q}_1^{(2)} = -[\overline{a}_{2\tau}^{(1)}\overline{q}_0^* + \overline{a}_{1\tau}^{(1)}(q_0^* - c_1 - \overline{\Gamma}_1^*\overline{c}_1)](\mathbf{A}_1^{-1}\mathbf{A}_2 - \mathbf{B}_1^{-1}\mathbf{B}_2)^{-1}(\mathbf{B}_1^{-1}\overline{\mathbf{d}}_1 - \mathbf{A}_1^{-1}\overline{\mathbf{c}}_1) \tag{3.247}$$

$$\mathbf{q}_2^{(1)} = (\overline{\mathbf{A}}_1^{-1}\mathbf{A}_1 - \overline{\mathbf{B}}_1^{-1}\mathbf{B}_1)^{-1}[(\overline{\mathbf{A}}_1^{-1}\mathbf{A}_2 - \overline{\mathbf{B}}_1^{-1}\mathbf{B}_2)\mathbf{q}_2^{(2)} + (\overline{\mathbf{A}}_1^{-1}\overline{\mathbf{A}}_2 - \overline{\mathbf{B}}_1^{-1}\overline{\mathbf{B}}_2)\overline{\mathbf{q}}_3^{(2)} + \overline{\mathbf{A}}_1^{-1}\overline{\mathbf{g}}_1^* - \overline{\mathbf{B}}_1^{-1}\overline{\mathbf{g}}_2^*] \tag{3.248}$$

$$\mathbf{q}_2^{(2)} = \mathbf{A}_2^{-1}(\left\langle \Gamma_{2\alpha}^{(2)} \right\rangle \mathbf{A}_2\mathbf{q}_3^{(2)} - \mathbf{G}^*\mathbf{c}_2) \tag{3.249}$$

$$\mathbf{q}_3^{(1)} = (\overline{\mathbf{A}}_1^{-1}\mathbf{A}_1 - \overline{\mathbf{B}}_1^{-1}\mathbf{B}_1)^{-1}[(\overline{\mathbf{A}}_1^{-1}\mathbf{A}_2 - \overline{\mathbf{B}}_1^{-1}\mathbf{B}_2)\mathbf{q}_3^{(2)} + (\overline{\mathbf{A}}_1^{-1}\overline{\mathbf{A}}_2 - \overline{\mathbf{B}}_1^{-1}\overline{\mathbf{B}}_2)\overline{\mathbf{q}}_2^{(2)} + \overline{\mathbf{A}}_1^{-1}\mathbf{g}_1^* - \overline{\mathbf{B}}_1^{-1}\mathbf{g}_2^*] \tag{3.250}$$

$$\mathbf{q}_3^{(2)} = (\mathbf{A}_2^{-1}\left\langle \Gamma_{2m}^{(2)} \right\rangle \mathbf{A}_2 - \mathbf{B}_2^{-1}\left\langle \Gamma_{2m}^{(2)} \right\rangle \mathbf{B}_2)^{-1}(\mathbf{A}_2^{-1}\mathbf{G}^*\mathbf{c}_2 - \mathbf{B}_2^{-1}\mathbf{G}^*\mathbf{d}_2) \tag{3.251}$$

where

$$\mathbf{G}^* = c_1(a_{1\tau}^{(2)}\mathbf{I} - \left\langle \Gamma_{2m}^{(2)} \right\rangle a_{2\tau}^{(2)}) \tag{3.252}$$

$$\mathbf{g}_1^* = (\overline{c}_1\overline{a}_{1\tau}^{(2)}\overline{\mathbf{c}}_2 + c_1 a_{2\tau}^{(2)}\mathbf{c}_2)/2 - [\overline{q}_0^*\overline{a}_{1\tau}^{(1)}\overline{\mathbf{c}}_1 + a_{2\tau}^{(1)}(\overline{c}_1 + \Gamma_1^* c_1 - q_0^*)\mathbf{c}_1]/2 \tag{3.253}$$

$$\mathbf{g}_2^* = (\overline{c}_1\overline{a}_{1\tau}^{(2)}\overline{\mathbf{d}}_2 + c_1 a_{2\tau}^{(2)}\mathbf{d}_2)/2 - [\overline{q}_0^*\overline{a}_{1\tau}^{(1)}\overline{\mathbf{d}}_1 + a_{2\tau}^{(1)}(\overline{c}_1 + \Gamma_1^* c_1 - q_0^*)\mathbf{d}_1]/2 \tag{3.254}$$

3.7.3 Solutions for holes and rigid fibers

When the fiber is an insulated and traction-free hole, i.e., $\vartheta_1 = \varphi_1 = 0$ along the hole boundary, the solutions can be found in a manner similar to that described for the piezoelectric fiber. They are

$$\begin{aligned} g_1(\zeta_t^{(1)}) = a_{1\tau}^{(1)}[q_0 F_1(\zeta_t^{(1)}, \zeta_{t0}^{(1)}) + \overline{q}_0 F_2(\zeta_t^{(1)-1}, \overline{\zeta}_{t0}^{(1)})] + a_{2\tau}^{(1)}[q_0 F_2(\zeta_t^{(1)}, \zeta_{t0}^{(1)}) \\ + \overline{q}_0 F_1(\zeta_t^{(1)-1}, \overline{\zeta}_{t0}^{(1)})] \end{aligned} \tag{3.255}$$

$$\mathbf{U}_1 = -2\,\mathrm{Re}\{\mathbf{A}_1[\langle f_{1\alpha}(\zeta_\alpha^{(1)})\rangle + \langle f_{2\alpha}(\zeta_\alpha^{(1)})\rangle \mathbf{P}_1^{-1} p_1^*]\mathbf{B}_1^{-1}\mathbf{d}_1 - \mathbf{c}_1 g_1(\zeta_t^{(1)})\} \tag{3.256}$$

$$\boldsymbol{\varphi}_1 = -2\,\mathrm{Re}\{\mathbf{B}_1[\langle f_{1\alpha}(\zeta_\alpha^{(1)})\rangle + \langle f_{2\alpha}(\zeta_\alpha^{(1)})\rangle \mathbf{P}_1^{-1} p_1^*]\mathbf{B}_1^{-1}\mathbf{d}_1 - \mathbf{d}_1 g_1(\zeta_t^{(1)})\} \tag{3.257}$$

for the case of a point heat source and temperature discontinuity, and

$$g_1(\zeta_t^{(1)}) = q_0^*(a_{1\tau}^{(1)}\zeta_t^{(1)2}/2 - a_{2\tau}^{(1)}\ln\zeta_t^{(1)}) + \overline{q}_0^*(a_{1\tau}^{(1)}\ln\zeta_t^{(1)} + a_{2\tau}^{(1)}\zeta_t^{(1)-2}/2) \tag{3.258}$$

$$\mathbf{U}_1 = -2\,\mathrm{Re}\{\mathbf{A}_1[\langle f_{1\alpha}^*(\zeta_\alpha^{(1)})\rangle + \langle f_{2\alpha}^*(\zeta_\alpha^{(1)})\rangle \mathbf{P}^{-1} p_1^*]\mathbf{B}_1^{-1}\mathbf{d}_1 - \mathbf{c}_1 g_1(\zeta_t^{(1)})\} \tag{3.259}$$

$$\boldsymbol{\varphi}_1 = -2\,\mathrm{Re}\{\mathbf{B}_1[\langle f_{1\alpha}^*(\zeta_\alpha^{(1)})\rangle + \langle f_{2\alpha}^*(\zeta_\alpha^{(1)})\rangle \mathbf{P}^{-1} p_1^*]\mathbf{B}_1^{-1}\mathbf{d}_1 - \mathbf{d}_1 g_1(\zeta_t^{(1)})\} \tag{3.260}$$

for the case of remote heat flow, where $f_{1\alpha}(\zeta_\alpha^{(1)})$ and $f_{2\alpha}(\zeta_\alpha^{(1)})$ have, respectively, the same expressions as $f_{1\alpha}^{(1)}(\zeta_\alpha^{(1)})$ and $f_{2\alpha}^{(1)}(\zeta_\alpha^{(1)})$ given in Eq. (3.220), except that now $\overline{q}_0$ should be replaced by $-\overline{q}_0$, and

$$\begin{aligned} f_{1k}^*(\zeta_k^{(1)}) &= a[q_0^*(\zeta_k^{(1)2} - 2\ln\zeta_k^{(1)}) + \overline{q}_0^*(\zeta_k^{(1)-2} + 2\ln\zeta_k^{(1)})]/4, \\ f_{2k}^*(\zeta_k^{(1)}) &= ibp_k^{(1)}[\overline{q}_0^*(\zeta_k^{(1)-2} - 2\ln\zeta_k^{(1)}) - q_0^*(\zeta_k^{(1)2} + 2\ln\zeta_k^{(1)})]/4 \end{aligned} \tag{3.261}$$

Similarly, for a rigid and nonconductive fiber, the thermal boundary condition is the same as that of a hole. However, the elastic boundary condition of the fiber should be described in a manner similar to that of Hwu and Yen [47]:

$$\mathbf{u}_2 = \omega(\mathbf{u}_0\sigma + \overline{\mathbf{u}}_0\sigma^{-1})/2, \qquad \mathbf{u}_0 = \{ib,\ a,\ 0,\ 0\}^{\mathrm{T}} \qquad \text{(on the interface)} \tag{3.262}$$

where ω denotes the rigid-body rotation relative to the matrix, which can be obtained by the condition that the total moment about the origin due to the traction along the surface of the rigid fiber vanishes.

Substituting Eqs. (3.225) (or (3.258)) and (3.262) into $(3.187)_{3,4}$ provides

$$\mathbf{U}_1 = -2\,\mathrm{Re}\{\mathbf{A}_1[\langle f_{1\alpha}(\zeta_\alpha^{(1)})\rangle + \langle f_{2\alpha}(\zeta_\alpha^{(1)})\rangle \mathbf{P}_1^{-1} p_1^*]\mathbf{A}_1^{-1}\mathbf{c}_1 - \mathbf{c}_1 g_1(\zeta_t^{(1)}) - \omega\langle \zeta_\alpha^{(1)-1}\rangle \bar{\mathbf{u}}_0 / 2\} \tag{3.263}$$

$$\boldsymbol{\varphi}_1 = -2\,\mathrm{Re}\{\mathbf{B}_1[\langle f_{1\alpha}(\zeta_\alpha^{(1)})\rangle + \langle f_{2\alpha}(\zeta_\alpha^{(1)})\rangle \mathbf{P}_1^{-1} p_1^*]\mathbf{A}_1^{-1}\mathbf{c}_1 - \mathbf{d}_1 g_1(\zeta_t^{(1)}) - \omega\mathbf{B}_1\mathbf{A}_1^{-1}\langle \zeta_\alpha^{(1)-1}\rangle \bar{\mathbf{u}}_0 / 2\} \tag{3.264}$$

for the case of a point heat source and temperature discontinuity, and

$$\mathbf{U}_1 = -2\,\mathrm{Re}\{\mathbf{A}_1[\langle f_{1\alpha}^*(\zeta_\alpha^{(1)})\rangle + \langle f_{2\alpha}^*(\zeta_\alpha^{(1)})\rangle \mathbf{P}^{-1} p_1^*]\mathbf{A}_1^{-1}\mathbf{c}_1 - \mathbf{c}_1 g_1(\zeta_t^{(1)}) - \omega\langle \zeta_\alpha^{(1)-1}\rangle \bar{\mathbf{u}}_0 / 2\} \tag{3.265}$$

$$\boldsymbol{\varphi}_1 = -2\,\mathrm{Re}\{\mathbf{B}_1[\langle f_{1\alpha}^*(\zeta_\alpha^{(1)})\rangle + \langle f_{2\alpha}^*(\zeta_\alpha^{(1)})\rangle \mathbf{P}^{-1} p_1^*]\mathbf{A}_1^{-1}\mathbf{c}_1 - \mathbf{d}_1 g_1(\zeta_t^{(1)}) - \omega\mathbf{B}_1\mathbf{A}_1^{-1}\langle \zeta_\alpha^{(1)-1}\rangle \bar{\mathbf{u}}_0 / 2\} \tag{3.266}$$

for the case of a remote heat flow, where $g_1, f_{1k}, f_{2k}, f_{1k}^*, f_{2k}^*$ have the same expressions as those in Eqs. (3.255)-(3.261). Once the general solution has been obtained, ω can be determined by using the condition that the total moment about the origin due to the traction along the surface of the rigid fiber vanishes. The result is

$$\omega = -\frac{2\int_0^{2\pi} \mathbf{y}^{\mathrm{T}}\,\mathrm{Re}\{\partial \mathbf{f}_s(e^{i\psi})/\partial\psi\}\mathrm{d}\psi}{\pi\,\mathrm{Im}\{\mathbf{u}_0^{\mathrm{T}}\mathbf{B}_1\mathbf{A}_1^{-1}\bar{\mathbf{u}}_0\}} \tag{3.267}$$

where

$$\mathbf{y}^{\mathrm{T}} = \{b\sin\psi,\ -a\cos\psi,\ 0,\ 0\} \tag{3.268}$$

$$\mathbf{f}_s(\sigma) = -\mathbf{B}_1[\langle f_{1\alpha}(\sigma)\rangle + \langle f_{2m}(\sigma)\rangle \mathbf{P}_1^{-1} p_1^*]\mathbf{A}_1^{-1}\mathbf{c}_1 - \mathbf{d}_1 g_1(\sigma) \tag{3.269}$$

for the case of a point heat source and temperature discontinuity, and

$$\mathbf{f}_s(\sigma) = -\mathbf{B}_1[\langle f_{1\alpha}^*(\sigma)\rangle + \langle f_{2\alpha}^*(\sigma)\rangle \mathbf{P}^{-1} p_1^*]\mathbf{A}_1^{-1}\mathbf{c}_1 - \mathbf{d}_1 g_1(\sigma) \tag{3.270}$$

for the case of a remote heat flow.

References

[1] He LH, Lim CW: Electromechanical responses of piezoelectric fiber composites with sliding interface under anti-plane deformations. Composites Part B: Engineering **34**(4), 373-381 (2003).

[2] Smart Material Corp. http://www.smart-material.com/.
[3] Hagood NW, Kindel R, Ghandi K, Gaudenzi P: Improving transverse actuation of piezoceramics using interdigitated surface electrodes. Proc. SPIE **1917**, 341-352 (1993).
[4] Hagood N, Bent A: Composites for structural control. US Patent, 6048622 (2000).
[5] Bent AA, Hagood NW: Improved performance in piezoelectric fibre composites using interdigitated electrodes. Proc. SPIE **2441**, 196-212(1995).
[6] Wilkie WK, Bryant GR, High JW, Fox RL, Hallbaum RF, Jalink A Jr, Little BD, Mirick P H: Low-cost piezocomposite actuator for structural control applications. Proc. SPIE **3991**, 323(2000).
[7] Cannon BJ, Brei D: Feasibility study of microfabrication by coextrusion (MFCX) hollow fibers for active composites. Journal of Intelligent Material Systems and Structures **11**(9), 659-670 (2000).
[8] Liu HY, Qin QH, Mai YW: Theoretical model of piezoelectric fibre pull-out. International Journal of Solids and Structures **40**(20), 5511-5519 (2003).
[9] Gao YC, Mai YW, Cotterell B: Fracture of fiber-reinforced materials. Zeitschrift Fur Angewandte Mathematik Und Physik **39**(4), 550-572 (1988).
[10] Zhou LM, Mai YW: On the single-fiber pullout and pushout problem—effect of fiber anisotropy. Zeitschrift Fur Angewandte Mathematik Und Physik **44**(4), 769-775 (1993).
[11] Zhou LM, Kim JK, Mai YW: On the single fiber pull-out problem—effect of loading method. Composites Science and Technology **45**(2), 153-160 (1992).
[12] Zhou LM, Kim JK, Mai YW: Interfacial debonding and fiber pull-out stresses .2. A new model based on the fracture-mechanics approach. Journal of Materials Science **27**(12), 3155-3166 (1992).
[13] Zhou LM, Mai YW, Ye L: Analyses of fiber push-out test based on the fracture-mechanics approach. Composites Engineering **5**(10-11), 1199-1219 (1995).
[14] Gu B, Liu HY, Mai YW: A theoretical model on piezoelectric fibre pullout with electric input. Engineering Fracture Mechanics **73**(14), 2053-2066 (2006).
[15] Qin QH, Wang JS, Kang YL: A theoretical model for electroelastic analysis in piezoelectric fibre push-out test. Archive of Applied Mechanics **75**(8-9), 527-540 (2006).
[16] Wang JS, Qin QH: Debonding criterion for the piezoelectric fibre push-out test. Philosophical Magazine Letters **86**(2), 123-136 (2006).
[17] Wang JS, Qin QH, Kang YL: Stress and electric field transfer of piezoelectric fibre push-out under electric and mechanical loading. In: Ren WX, Gary Ong KC, Tan JSY (eds.) 9th International Conference on Inspection, Appraisal, Repairs & Maintenance of Structures, Fuzhou, China, 20-21 October, 2005, pp. 435-442. CI-Premier PTY LTD (2005).
[18] Hill R: Elastic properties of reinforced solids: Some theoretical principles. Journal of the Mechanics and Physics of Solids **11**(5), 357-372 (1963).
[19] Hill R: Theory of mechanical properties of fibre-strengthened materials.1. Elastic behaviour. Journal of the Mechanics and Physics of Solids **12**(4), 199-212 (1964).
[20] Grekov AA, Kramarov SO, Kuprienko AA: Effective properties of a transversely isotropic piezocomposite with cylindrical inclusions. Ferroelectrics **99**, 115-126 (1989).
[21] Dunn ML, Taya M: Micromechanics predictions of the effective electroelastic moduli

of piezoelectric composites. International Journal of Solids and Structures **30**(2), 161-175 (1993).

[22] Schulgasser K: Relationships between the effective properties of transversely isotropic piezoelectric composites. Journal of the Mechanics and Physics of Solids **40**(2), 473-479 (1992).

[23] Benveniste Y, Dvorak GJ: Uniform-fields and universal relations in piezoelectric composites. Journal of the Mechanics and Physics of Solids **40**(6), 1295-1312 (1992).

[24] Benveniste Y: Exact results in the micromechanics of fibrous piezoelectric composites exhibiting pyroelectricity. Proceedings of the Royal Society of London Series A: Mathematical Physical and Engineering Sciences **441**(1911), 59-81 (1993).

[25] Benveniste Y: Magnetoelectric effect in fibrous composites with piezoelectric and piezomagnetic phases. Physical Review B **51**(22), 16424-16427 (1995).

[26] Chen TY: Piezoelectric properties of multiphase fibrous composites—some theoretical results. Journal of the Mechanics and Physics of Solids **41**(11), 1781-1794 (1993).

[27] Mallik N, Ray MC: Effective coefficients of piezoelectric fiber-reinforced composites. AIAA Journal **41**(4), 704-710 (2003).

[28] Huang JH, Kuo WS: The analysis of piezoelectric/piezomagnetic composite materials containing ellipsoidal inclusions. Journal of Applied Physics **81**(3), 1378-1386 (1997).

[29] Huang JH: Analytical predictions for the magnetoelectric coupling in piezomagnetic materials reinforced by piezoelectric ellipsoidal inclusions. Physical Review B **58**(1), 12-15 (1998).

[30] Jiang CP, Tong ZH, Cheung YK: A generalized self-consistent method for piezoelectric fiber reinforced composites under antiplane shear. Mechanics of Materials **33**(5), 295-308 (2001).

[31] Jiang CP, Tong ZH, Cheung YK: A generalized self-consistent method accounting for fiber section shape. International Journal of Solids and Structures **40**(10), 2589-2609 (2003).

[32] Tong ZH, Lo SH, Jiang CP, Cheung YK: An exact solution for the three-phase thermo-electro-magneto-elastic cylinder model and its application to piezoelectric-magnetic fiber composites. International Journal of Solids and Structures **45**(20), 5205-5219 (2008).

[33] Kumar A, Chakraborty D: Effective properties of thermo-electro-mechanically coupled piezoelectric fiber reinforced composites. Materials & Design **30**(4), 1216-1222 (2009).

[34] Benveniste Y: On the micromechanics of fibrous piezoelectric composites. Mechanics of Materials **18**(3), 183-193 (1994).

[35] Qin QH: Thermoelectroelastic solution for elliptic inclusions and application to crack-inclusion problems. Applied Mathematical Modelling **25**(1), 1-23 (2000).

[36] Qin QH: Fracture Mechanics of Piezoelectric Materials. WIT Press, Southampton (2001).

[37] Zhang X, Liu HY, Mai YW, Diao XX: On steady-state fibre pull-out. Ⅰ. The stress field. Composites Science and Technology **59**(15), 2179-2189 (1999).

[38] Tiersten HF: Linear Piezoelectric Plate Vibrations. Plenum Press, New York (1969).

[39] Zhou LM: A study on the fracture mechanics of interfaces in fibre-matrix composites. PhD Thesis, University of Sydney (1994).

[40] Steinhausen R, Hauke T, Seifert W, Beige H, Watzka W, Seifert S, Sporn D, Starke S, Schonecker A: Finescaled piezoelectric 1-3 composites: Properties and modeling. Journal of the European Ceramic Society **19**(6-7), 1289-1293 (1999).

[41] Chan HLW, Li K, Choy CL: Piezoelectric ceramic fibre/epoxy 1-3 composites for high-frequency ultrasonic transducer applications. Materials Science and Engineering B: Solid State Materials for Advanced Technology **99**(1-3), 29-35 (2003).

[42] Nelson LJ: Smart piezoelectric fibre composites. Materials Science and Technology **18**(11), 1245-1256 (2002).

[43] Honda K, Kagawa Y: Debonding criterion in the pushout process of fiber-reinforced ceramics. Acta Materialia **44**(8), 3267-3277 (1996).

[44] Park SB, Sun CT: Effect of electric-field on fracture of piezoelectric ceramics. International Journal of Fracture **70**(3), 203-216 (1995).

[45] Hashin Z: Analysis of properties of fiber composites with anisotropic constituents. Journal of Applied Mechanics-Transactions of the ASME **46**(3), 543-550 (1979).

[46] Ting TCT: Green's functions for an anisotropic elliptic inclusion under generalized plane strain deformations. Quarterly Journal of Mechanics and Applied Mathematics **49**, 1-18 (1996).

[47] Hwu C, Yen WJ: On the anisotropic elastic inclusions in plane elastostatics. Journal of Applied Mechanics-Transactions of the ASME **60**(3), 626-632 (1993).

[48] Stagni L: On the elastic field perturbation by inhomogeneities in plane elasticity. Zeitschrift Fur Angewandte Mathematik Und Physik **33**(3), 315-325 (1982).

Chapter 4 Trefftz Method for Piezoelectricity

In Chapter 3, theoretical solutions for problems of PFC pull-out and push-out are presented. The solutions are, however, restricted to axi-symmetric problems. To remove this restriction, Trefftz numerical methods are presented for solving various engineering problems involved in piezoelectric materials in this chapter. Trefftz methods discussed here include the Trefftz FEM, Trefftz BEM, and the Trefftz boundary-collocation method.

4.1 Introduction

Over the past decades the Trefftz approach, introduced in 1926 [1], has been considerably improved and has now become a highly efficient computational tool for the solution of complex boundary value problems. Particularly, Trefftz FEM has been successfully applied to problems of elasticity [2], Kirchhoff plates [3], moderately thick Reissner-Mindlin plates [4], thick plates [5], general 3-D solid mechanics [6], potential problems [7], elastodynamic problems [8], transient heat conduction analysis [9], geometrically nonlinear plates [10], materially nonlinear elasticity [11], and contact problems [12]. Recently, Qin [13-16] extended this method to the case of piezoelectric materials. Wang et al. [17] analyzed singular electromechanical stress fields in piezoelectrics by combining the eigensolution approach and Trefftz FE models. As well as Trefftz FEM, Wang et al. [18] presented a Trefftz BEM for anti-plane piezoelectric problems. Sheng et al. [19] developed a Trefftz boundary collocation method for solving piezoelectric problems. The multi-region BEM [20] and the Trefftz indirect method [21] were also recently applied to electroelastic problems. This chapter, however, focuses on the results presented in [13-16,18,19,22].

4.2 Trefftz FEM for generalized plane problems

In this section, discussion is based on the formulation presented in [14]. Essentially, a family of variational formulations is presented for deriving Trefftz-FEs of generalized plane piezoelectric problems. It is based on four free energy densities, each with two kinds of independent variables as basic independent variables, i.e., $(\boldsymbol{\sigma}, \mathbf{D})$, $(\boldsymbol{\varepsilon}, \mathbf{E})$, $(\boldsymbol{\varepsilon}, \mathbf{D})$, and $(\boldsymbol{\sigma}, \mathbf{E})$.

4.2.1 Basic field equations and boundary conditions

Consider a linear piezoelectric material, in which the differential governing equa-

tions and the corresponding boundary conditions in the Cartesian coordinates x_i (i=1, 2, 3) are defined by Eqs. (1.10)-(1.12) (Chapter 1), and the relation between the strain tensor and the displacement, u_i, is governed by Eq. (1.2). For an anisotropic piezoelectric material, the constitutive relation is defined in Table 1.1 for $(\boldsymbol{\varepsilon}, \mathbf{E})$ as basic variables [14],

$$\varepsilon_{ij} = -\frac{\partial H(\boldsymbol{\sigma}, \mathbf{D})}{\partial \sigma_{ij}} = s^D_{ijkl}\sigma_{kl} + g_{kij}D_k, \qquad E_i = \frac{\partial H(\boldsymbol{\sigma}, \mathbf{D})}{\partial D_i} = -g_{ikl}\sigma_{kl} + \lambda^{\sigma}_{ik}D_k \quad (4.1)$$

for $(\boldsymbol{\sigma}, \mathbf{D})$ as basic variables,

$$\sigma_{ij} = \frac{\partial H(\boldsymbol{\varepsilon}, \mathbf{D})}{\partial \sigma_{ij}} = c^D_{ijkl}\varepsilon_{kl} + h_{kij}D_k, \qquad E_i = \frac{\partial H(\boldsymbol{\varepsilon}, \mathbf{D})}{\partial D_i} = h_{ikl}\varepsilon_{kl} + \lambda^{\varepsilon}_{ik}D_k \quad (4.2)$$

for $(\boldsymbol{\varepsilon}, \mathbf{D})$ as basic variables, and

$$\varepsilon_{ij} = -\frac{\partial H(\boldsymbol{\sigma}, \mathbf{E})}{\partial \sigma_{ij}} = s^E_{ijkl}\sigma_{kl} + d_{kij}D_k, \qquad D_i = -\frac{\partial H(\boldsymbol{\sigma}, \mathbf{E})}{\partial E_i} = d_{ikl}\sigma_{kl} + \kappa^{\sigma}_{ik}E_k \quad (4.3)$$

for $(\boldsymbol{\sigma}, \mathbf{E})$ as basic variables, and

$$H(\boldsymbol{\sigma}, \mathbf{D}) = -\frac{1}{2}s^D_{ijkl}\sigma_{ij}\sigma_{kl} + \frac{1}{2}\lambda^{\sigma}_{ij}D_iD_j - g_{kij}\sigma_{ij}D_k \quad (4.4)$$

$$H(\boldsymbol{\varepsilon}, \mathbf{D}) = \frac{1}{2}c^D_{ijkl}\varepsilon_{ij}\varepsilon_{kl} + \frac{1}{2}\lambda^{\varepsilon}_{ij}D_iD_j + h_{kij}\varepsilon_{ij}D_k \quad (4.5)$$

$$H(\boldsymbol{\sigma}, \mathbf{E}) = -\frac{1}{2}s^E_{ijkl}\sigma_{ij}\sigma_{kl} - \frac{1}{2}\kappa^{\sigma}_{ij}E_iE_j - d_{kij}\sigma_{ij}E_k \quad (4.6)$$

and $H(\boldsymbol{\varepsilon}, \mathbf{E})$ is defined in Eq. (1.1), where c^E_{ijkl}, c^D_{ijkl} and s^E_{ijkl}, s^D_{ijkl} are the stiffness and compliance coefficient tensor for $\mathbf{E}$=0 or $\mathbf{D}$=0, κ^{σ}_{ij}, $\kappa^{\varepsilon}_{ij}$ and λ^{σ}_{ij}, $\lambda^{\varepsilon}_{ij}$ are the permittivity matrix and the conversion of the permittivity constant matrix for $\boldsymbol{\sigma}$=0 or $\boldsymbol{\varepsilon}$=0.

Moreover, in the Trefftz FE form, Eqs. (4.1)-(4.6) should be completed by the following inter-element continuity requirements:

$$u_{ie} = u_{if}, \qquad \phi_e = \phi_f \qquad (\text{on } \Gamma_e \bigcap \Gamma_f, \text{ conformity}) \quad (4.7)$$

$$t_{ie} + t_{if} = 0, \quad D_{ne} + D_{nf} = 0 \qquad (\text{on } \Gamma_e \bigcap \Gamma_f, \text{ reciprocity}) \quad (4.8)$$

where "e" and "f" stand for any two neighboring elements. Eqs. (1.1), (1.2), (1.5), (1.10)-(1.12), and (4.1)-(4.8) are taken as the basis to establish the modified variational principle for Trefftz FE analysis of piezoelectric materials.

4.2.2 Assumed fields

The main objective of the Trefftz FEM is to establish an FE formulation whereby the intra-element continuity is enforced on a non-conforming internal displacement field chosen so as to *a priori* satisfy the governing differential equation of the problem under consideration [23,24]. In other words, as an obvious alternative to the Rayleigh-Ritz method as a basis for an FE formulation, the model here is based on the method of Trefftz [1]. With this method the solution domain Ω is subdivided into elements, and over each element, the assumed intra-element fields are

$$\mathbf{u}=\begin{Bmatrix} u_1 \\ u_2 \\ u_3 \\ \phi \end{Bmatrix}=\begin{Bmatrix} \breve{u}_1 \\ \breve{u}_2 \\ \breve{u}_3 \\ \breve{\phi} \end{Bmatrix}+\begin{Bmatrix} \mathbf{N}_1 \\ \mathbf{N}_2 \\ \mathbf{N}_3 \\ \mathbf{N}_4 \end{Bmatrix}\mathbf{c}=\breve{\mathbf{u}}+\sum_{j=1}\mathbf{N}_j\mathbf{c}_j=\breve{\mathbf{u}}+\mathbf{N}\mathbf{c} \tag{4.9}$$

where $\mathbf{c}_j$ stands for undetermined coefficient, and $\breve{\mathbf{u}}$ ($=\{\breve{u}_1,\breve{u}_2,\breve{u}_3,\breve{\phi}\}^{\mathrm{T}}$) and $\mathbf{N}$ are known functions. If the governing differential equation (1.10) is rewritten in a general form

$$\mathfrak{R}\mathbf{u}(\mathbf{x})+\bar{\mathbf{b}}(\mathbf{x})=0 \qquad (\mathbf{x}\in\Omega_e) \tag{4.10}$$

where $\mathfrak{R}$ stands for the differential operator matrix for Eq. (1.10), $\mathbf{x}$ the position vector, $\bar{\mathbf{b}}=\{f_1,f_2,f_3,Q\}^{\mathrm{T}}$ the known right-hand side term, the overhead bar indicates the imposed quantities and Ω_e stands for the eth element sub-domain, then $\breve{\mathbf{u}}=\breve{\mathbf{u}}(\mathbf{x})$ and $\mathbf{N}=\mathbf{N}(\mathbf{x})$ in Eq. (4.9) have to be chosen so that

$$\mathfrak{R}\breve{\mathbf{u}}+\bar{\mathbf{b}}=0 \quad \text{and} \quad \mathfrak{R}\mathbf{N}=0 \tag{4.11}$$

everywhere in Ω_e. A complete system of homogeneous solutions $\mathbf{N}_j$ can be generated by way of the solution in Stroh formalism

$$\mathbf{u}=2\,\mathrm{Re}\{\mathbf{A}\langle f(z_\alpha)\rangle\mathbf{c}\} \tag{4.12}$$

where "Re" stands for the real part of a complex number, $\mathbf{A}$ is the material eigenvector matrix which is well defined in the literature (see pp. 17-18 of [25]), $\langle f(z_\alpha)\rangle=\mathrm{diag}[f(z_1)f(z_2)f(z_3)f(z_4)]$ is a diagonal 4×4 matrix, while $f(z_i)$ is an arbitrary function with argument $z_i=x_1+p_ix_2$. p_i (i=1-4) are the material eigenvalues. Of particular interest is a complete set of polynomial solutions which may be generated by setting in Eq. (4.12) in turn

$$\begin{matrix} f(z_\alpha)=z_\alpha^k, \\ f(z_\alpha)=iz_\alpha^k \end{matrix} \qquad (k=1,2,\cdots) \tag{4.13}$$

where $i=\sqrt{-1}$. This leads, for $\mathbf{N}_j$ of Eq. (4.9), to the following sequence:

$$\mathbf{N}_{2j}=2\,\mathrm{Re}\{\mathbf{A}\left\langle z_\alpha^j\right\rangle\} \tag{4.14}$$

$$\mathbf{N}_{2j+1}=2\,\mathrm{Re}\{\mathbf{A}\left\langle iz_\alpha^j\right\rangle\} \tag{4.15}$$

The unknown coefficient **c** may be calculated from the conditions on the external boundary and/or the continuity conditions on the inter-element boundary. Thus various Trefftz element models can be obtained by using different approaches to enforce these conditions. In the majority of cases a hybrid technique is used, whereby the elements are linked through an auxiliary conforming displacement frame which has the same form as in the conventional FE method. This means that in the Trefftz FE approach, a conforming EPD field should be independently defined on the element boundary to enforce the field continuity between elements and also to link the coefficient **c**, appearing in Eq. (4.9), with nodal EPD **d** (=$\{d\}$). The frame is defined as

$$\tilde{\mathbf{u}}(\mathbf{x})=\begin{Bmatrix}\tilde{u}_1\\ \tilde{u}_2\\ \tilde{u}_3\\ \tilde{\phi}\end{Bmatrix}=\begin{bmatrix}\tilde{\mathbf{N}}_1\\ \tilde{\mathbf{N}}_2\\ \tilde{\mathbf{N}}_3\\ \tilde{\mathbf{N}}_4\end{bmatrix}\mathbf{d}=\tilde{\mathbf{N}}\mathbf{d}\qquad(\mathbf{x}\in\Gamma_e) \tag{4.16}$$

where the symbol "~" is used to specify that the field is defined on the element boundary only, **d**=**d**(**c**) stands for the vector of the nodal displacements which are the final unknowns of the problem, Γ_e represents the boundary of element *e*, and $\tilde{\mathbf{N}}$ is a matrix of the corresponding shape functions which are the same as those in conventional FE formulation. For example, along the side *A*-*O*-*B* of a particular element (see Fig. 4.1), a simple interpolation of the frame displacement and electric potential can be given in the form

$$\tilde{\mathbf{u}}(\mathbf{x})=\begin{Bmatrix}\tilde{u}_1\\ \tilde{u}_2\\ \tilde{u}_3\\ \tilde{\phi}\end{Bmatrix}=\begin{bmatrix}\mathbf{N}_A & \mathbf{N}_B\end{bmatrix}\begin{Bmatrix}\mathbf{d}_A\\ \mathbf{d}_B\end{Bmatrix}\qquad(\mathbf{x}\in\Gamma_e) \tag{4.17}$$

where

$$\mathbf{N}_A=\mathrm{diag}[N_1\ N_1\ N_1\ N_1],\qquad \mathbf{N}_B=\mathrm{diag}[N_2\ N_2\ N_2\ N_2] \tag{4.18}$$

$$\mathbf{d}_A=\{u_{1A}\ u_{2A}\ u_{3A}\ \phi_A\}^{\mathrm{T}},\qquad \mathbf{d}_B=\{u_{1B}\ u_{2B}\ u_{3B}\ \phi_B\}^{\mathrm{T}} \tag{4.19}$$

with

$$N_1 = \frac{1-\xi}{2},\ N_2 = \frac{1+\xi}{2} \tag{4.20}$$

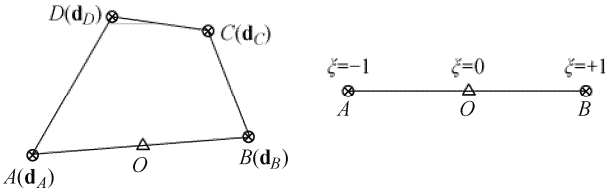

Fig. 4.1 A quadrilateral element for a generalized two-dimensional problem.

Using the above definitions the generalized boundary forces and electric displacements can be derived from Eqs. (1.11) and (4.9), and denoted by

$$\mathbf{T} = \begin{Bmatrix} t_1 \\ t_2 \\ t_3 \\ D_n \end{Bmatrix} = \begin{Bmatrix} \sigma_{1j} n_j \\ \sigma_{2j} n_j \\ \sigma_{3j} n_j \\ D_j n_j \end{Bmatrix} = \begin{Bmatrix} \breve{t}_1 \\ \breve{t}_2 \\ \breve{t}_3 \\ \breve{D}_n \end{Bmatrix} + \begin{Bmatrix} \mathbf{Q}_1 \\ \mathbf{Q}_2 \\ \mathbf{Q}_3 \\ \mathbf{Q}_4 \end{Bmatrix} \mathbf{c} = \breve{\mathbf{T}} + \mathbf{Q}\mathbf{c} \tag{4.21}$$

where $\breve{t}_i$ and $\breve{D}_n$ are derived from $\breve{\mathbf{u}}$.

4.2.3 Modified variational principle

The Trefftz FE equation for piezoelectric materials can be established by the variational approach [23]. Since the stationary conditions of the traditional potential and complementary variational functional cannot satisfy the inter-element continuity condition which is required in Trefftz FE analysis, some new variational functionals need to be developed. Following the procedure given in [24], the functional corresponding to the problem defined in Eqs. (1.1), (1.2), (1.5), (1.10)-(1.12), and (4.1)-(4.8) is constructed as

$$\Pi_m = \sum_e \Pi_{me} \tag{4.22}$$

where

$$\Pi_{me} = \Pi_e - \int_{\Gamma_e} (\phi - \tilde{\phi}) D_n \mathrm{d}s - \int_{\Gamma_e} (u_i - \tilde{u}_i) t_i \mathrm{d}s \tag{4.23}$$

with

$$\Pi_e = \iint_{\Omega_e} [H(\boldsymbol{\varepsilon}, \mathbf{E}) - \bar{b}_i u_i - \bar{q}_b \phi] \mathrm{d}\Omega - \int_{\Gamma_{te}} \bar{t}_i \tilde{u}_i \mathrm{d}s - \int_{\Gamma_{De}} \bar{D}_n \tilde{\phi} \mathrm{d}s \tag{4.24}$$

in which Eq. (1.10) is assumed to be satisfied, *a priori* and $\overline{D}_n = -\overline{q}_s$. The boundary Γ_e of a particular element consists of the following parts:

$$\Gamma_e = \Gamma_{ue} \cup \Gamma_{te} \cup \Gamma_{Ie} = \Gamma_{\phi e} \cup \Gamma_{De} \cup \Gamma_{Ie} \tag{4.25}$$

where

$$\Gamma_{ue} = \Gamma_u \cap \Gamma_e, \quad \Gamma_{te} = \Gamma_t \cap \Gamma_e, \quad \Gamma_{\phi e} = \Gamma_\phi \cap \Gamma_e, \quad \Gamma_{De} = \Gamma_D \cap \Gamma_e \tag{4.26}$$

and Γ_{Ie} is the inter-element boundary of the element "*e*".

We now show that the stationary condition of the functional (4.23) leads to Eqs. (1.11), (1.12), (4.7), (4.8), ($u_i = \tilde{u}_i$ on Γ_t) and ($\phi = \tilde{\phi}$ on Γ_D). The first-order variational of the functional (4.23) yields

$$\begin{aligned}\delta\Pi_{me} = \delta\Pi_e - \int_{\Gamma_e} [(\phi - \tilde{\phi})\delta D_n + (u_i - \tilde{u}_i)\delta t_i]\mathrm{d}s \\ + \int_{\Gamma_e} [D_n\delta(\phi - \tilde{\phi}) + t_i\delta(u_i - \tilde{u}_i)]\mathrm{d}s\end{aligned} \tag{4.27}$$

where "δ" is a variational symbol, and

$$\delta\Pi_e = \iint_{\Omega_e} [\delta H(\boldsymbol{\varepsilon}, \mathbf{E}) - \overline{b}_i\delta u_i - \overline{q}_b\delta\phi]\mathrm{d}\Omega - \int_{\Gamma_{te}} \overline{t}_i\delta\tilde{u}_i\mathrm{d}s - \int_{\Gamma_{De}} \overline{D}_n\delta\tilde{\phi}\mathrm{d}s \tag{4.28}$$

with

$$\begin{aligned}\delta\iint_{\Omega_e} H(\boldsymbol{\varepsilon}, \mathbf{E})\mathrm{d}\Omega &= \iint_{\Omega_e} (c^E_{ijkl}\varepsilon_{ij}\delta\varepsilon_{kl} - \kappa^\varepsilon_{ij}E_i\delta E_j - e_{kij}\varepsilon_{ij}\delta E_k - e_{kij}E_k\delta\varepsilon_{ij})\mathrm{d}\Omega \\ &\overset{\text{Eqs. (1.2) and (1.5)}}{=} \iint_{\Omega_e} (\sigma_{ij}\delta u_{i,j} + D_i\delta\phi_{,i})\mathrm{d}\Omega\end{aligned} \tag{4.29}$$

Integrating the domain integral term in Eq. (4.29) by parts, we can obtain

$$\begin{aligned}\iint_{\Omega_e} (\sigma_{ij}\delta u_{i,j} + D_i\delta\phi_{,i})\mathrm{d}\Omega = \int_{\Gamma_e} (t_i\delta u_i + D_n\delta\phi)\mathrm{d}s \\ - \iint_{\Omega_e} (\sigma_{ij,j}\delta u_i + D_{i,i}\delta\phi)\mathrm{d}\Omega\end{aligned} \tag{4.30}$$

Combining Eqs. (4.27), (4.28), and (4.30),

$$\begin{aligned}\delta\Pi_{me} = &-\iint_{\Omega_e} [(\sigma_{ij,j} + f_{bi})\delta u_i + (D_{i,i} + q_b)\delta\phi]\mathrm{d}\Omega + \int_{\Gamma_{\phi e}} [(\overline{\phi} - \tilde{\phi})\delta D_n \\ &+ D_n\delta(\phi - \tilde{\phi})]\mathrm{d}s + \int_{\Gamma_{ue}} [(\overline{u}_i - \tilde{u}_i)\delta t_i + t_i\delta(u_i - \tilde{u}_i)]\mathrm{d}s \\ &- \int_{\Gamma_{te}} (\overline{t}_i - t_i)\delta\tilde{u}_i\mathrm{d}s - \int_{\Gamma_{De}} (\overline{D}_n - D_n)\delta\tilde{\phi}\mathrm{d}s \\ &- \int_{\Gamma_{Ie}} [\tilde{\phi}\delta D_n + \tilde{u}_i\delta t_i + D_n\delta(\tilde{\phi} - \phi) + t_i\delta(\tilde{u}_i - u_i)]\mathrm{d}s\end{aligned} \tag{4.31}$$

Obviously, the vanishing variation of $\delta\Pi_{me}$ in Eq. (4.31) leads to $u_i = \tilde{u}_i$ on Γ_{ue}, $\phi = \tilde{\phi}$ on $\Gamma_{\phi e}$, governing differential equation (1.10) (see the first integral in Eq. (4.31)), displacement and electric potential boundary conditions (1.12) (see the second and third integrals in Eq. (4.31)), boundary conditions of traction and surface charge (1.11) (see the fourth and fifth integrals in Eq. (4.31)). The field continuity requirement Eqs. (4.7) and (4.8) can be shown in the following way. Considering that only the last integral in Eq. (4.31) can contribute to the continuity equation and when assembling elements "*e*" and "*f*", we have

$$\begin{aligned}&\int_{\Gamma_{Ie\cap If}} [\tilde{\phi}\,\delta(D_{ne} + D_{nf}) + \tilde{u}_i \delta(t_{ie} + t_{if}) + D_{ne}\delta(\tilde{\phi} - \phi_e)\\ &+ D_{nf}\delta(\tilde{\phi} - \phi_f) + t_{ie}\delta(\tilde{u}_i - u_{ie}) + t_{if}\delta(\tilde{u}_i - u_{if})]\mathrm{d}s = 0\end{aligned} \tag{4.32}$$

in which the conditions $\tilde{u}_{ie} = \tilde{u}_{if}$ and $\tilde{\phi}_{ie} = \tilde{\phi}_{if}$ are used. Equation (4.32) yields the continuity conditions (4.7) and (4.8).

4.2.4 Generation of the element stiffness equation

Noting the definition of elemental boundary (4.26), and $\bar{t}_i = \tilde{t}_i$ and $\bar{D}_n = \tilde{D}_n$ on the related boundaries, the functional (4.23) can be simplified to

$$\begin{aligned}\Pi_{me} = &\iint_{\Omega_e} [\,H(\boldsymbol{\sigma}, \mathbf{D}) - \bar{b}_i u_i - \bar{q}_b \phi]\mathrm{d}\Omega\\ &- \int_{\Gamma_e} (D_n\tilde{\phi} + t_i\tilde{u}_i)\mathrm{d}s - \int_{\Gamma_{\phi e}} D_n\bar{\phi}\,\mathrm{d}s - \int_{\Gamma_{ue}} t_i\bar{u}_i\mathrm{d}s\end{aligned} \tag{4.33}$$

Integrating the domain integral in Eq. (4.33) by parts gives

$$\begin{aligned}\iint_{\Omega_e} H(\boldsymbol{\sigma}, \mathbf{D})\mathrm{d}\Omega &= \iint_{\Omega_e} (\frac{1}{2} c^E_{ijkl}\varepsilon_{ij}\varepsilon_{kl} - \frac{1}{2}\kappa^{\varepsilon}_{ij}E_iE_j - e_{kij}\varepsilon_{ij}E_k)\mathrm{d}\Omega\\ &\overset{\text{Eq. (1.5)}}{=} \frac{1}{2}\iint_{\Omega_e} (\sigma_{ij}u_{i,j} + D_i\phi_{,i})\mathrm{d}\Omega\\ &= \frac{1}{2}\iint_{\Omega_e} [(\sigma_{ij}u_i)_{,j} + (D_i\phi)_{,i} - \sigma_{ij,j}u_i + D_{i,i}\phi]\mathrm{d}\Omega\\ &= \frac{1}{2}\int_{\Gamma_e} (t_iu_i + D_n\phi)\mathrm{d}s + \frac{1}{2}\iint_{\Omega_e} (f_{bi}u_i + q_b\phi)\mathrm{d}\Omega\end{aligned} \tag{4.34}$$

Substituting Eq. (4.34) into Eq. (4.33) yields

$$\begin{aligned}\Pi_{me} = &\frac{1}{2}\int_{\Gamma_e} (t_iu_i + D_n\phi)\mathrm{d}s - \frac{1}{2}\iint_{\Omega_e} (f_{bi}u_i + q_b\phi)\mathrm{d}\Omega\\ &- \int_{\Gamma_e} (D_n\tilde{\phi} + t_i\tilde{u}_i)\mathrm{d}s - \int_{\Gamma_{\phi e}} D_n\bar{\phi}\,\mathrm{d}s - \int_{\Gamma_{ue}} t_i\bar{u}_i\mathrm{d}s\end{aligned} \tag{4.35}$$

Making use of Eqs. (4.9), (4.16), and (4.21), Eq. (4.35) can be written as

$$\Pi_{me}^{\sigma D} = -\frac{1}{2}\mathbf{c}^{\mathrm{T}}\mathbf{H}\mathbf{c} + \mathbf{c}^{\mathrm{T}}\mathbf{S}\mathbf{d} + \mathbf{c}^{\mathrm{T}}\mathbf{r}_1 + \mathbf{d}^{\mathrm{T}}\mathbf{r}_2 + \text{terms without } \mathbf{c} \text{ or } \mathbf{d} \tag{4.36}$$

in which the matrices $\mathbf{H}$, $\mathbf{S}$ and the vectors $\mathbf{r}_1$, $\mathbf{r}_2$ are defined by

$$\mathbf{H} = -\int_{\Gamma_e} \mathbf{Q}^{\mathrm{T}}\mathbf{N}\mathrm{d}s \tag{4.37}$$

$$\mathbf{S} = -\int_{\Gamma_e} \mathbf{Q}^{\mathrm{T}}\tilde{\mathbf{N}}\mathrm{d}s \tag{4.38}$$

$$\mathbf{r}_1 = \frac{1}{2}\int_{\Gamma_e} (\mathbf{N}^{\mathrm{T}}\breve{\mathbf{T}} + \mathbf{Q}^{\mathrm{T}}\breve{\mathbf{u}})\mathrm{d}s - \frac{1}{2}\int_{\Omega_e} \mathbf{N}^{\mathrm{T}}\overline{\mathbf{b}}\,\mathrm{d}\Omega - \int_{\Gamma_{\phi e}} \mathbf{Q}_4^{\mathrm{T}}\overline{\phi}\,\mathrm{d}s - \int_{\Gamma_{ue}} \begin{bmatrix} \mathbf{Q}_1 \\ \mathbf{Q}_2 \\ \mathbf{Q}_3 \end{bmatrix}^{\mathrm{T}} \begin{Bmatrix} \overline{u}_1 \\ \overline{u}_2 \\ \overline{u}_3 \end{Bmatrix} \mathrm{d}s \tag{4.39}$$

$$\mathbf{r}_2 = -\int_{\Gamma_e} \tilde{\mathbf{N}}^{\mathrm{T}}\breve{\mathbf{T}}\mathrm{d}s \tag{4.40}$$

To enforce inter-element continuity on the common element boundary, the unknown vector $\mathbf{c}$ should be expressed in terms of nodal DOF $\mathbf{d}$. An optional relationship between $\mathbf{c}$ and $\mathbf{d}$ in the sense of variation can be obtained from

$$\frac{\partial \Pi_{me}}{\partial \mathbf{c}^{\mathrm{T}}} = -\mathbf{H}\mathbf{c} + \mathbf{S}\mathbf{d} + \mathbf{r}_1 = 0 \tag{4.41}$$

This leads to

$$\mathbf{c} = \mathbf{G}\mathbf{d} + \mathbf{g} \tag{4.42}$$

where $\mathbf{G} = \mathbf{H}^{-1}\mathbf{S}$ and $\mathbf{g} = \mathbf{H}^{-1}\mathbf{r}_1$, and then straightforwardly yields the expression of Π_{me} only in terms of $\mathbf{d}$ and other known matrices,

$$\Pi_{me} = \frac{1}{2}\mathbf{d}^{\mathrm{T}}\mathbf{G}^{\mathrm{T}}\mathbf{H}\mathbf{G}\mathbf{d} + \mathbf{d}^{\mathrm{T}}(\mathbf{G}^{\mathrm{T}}\mathbf{H}\mathbf{g} + \mathbf{r}_2) + \text{terms without } \mathbf{d} \tag{4.43}$$

Therefore, the element stiffness matrix equation can be obtained by taking the vanishing variation of the functional Π_{me} as

$$\frac{\partial \Pi_{me}}{\partial \mathbf{d}^{\mathrm{T}}} = 0 \Rightarrow \quad \mathbf{K}\mathbf{d} = \mathbf{P} \tag{4.44}$$

where $\mathbf{K}=\mathbf{G}^{\mathrm{T}}\mathbf{H}\mathbf{G}$ and $\mathbf{P}= -\mathbf{G}^{\mathrm{T}}\mathbf{H}\mathbf{g}-\mathbf{r}_2$ are, respectively, the element stiffness matrix and the equivalent nodal flow vector. The expression (4.44) is the elemental stiff-

ness-matrix equation for Trefftz FE analysis.

4.2.5 Numerical results

To illustrate the application of the element model presented above, an example of a piezoelectric prism subjected to simple tension (see Fig. 4.2) is considered. To allow comparisons with other solutions appearing in Ref. [26], the results obtained are limited to a piezoelectric prism subjected to simple tension.

This example was taken from Ding et al. [26] for a PZT-4 ceramic prism subject to a tension P=10 N/m^2 in the y-direction. The properties of the material are given as follows:

$$c_{1111} = 12.6\times10^{10}\ \text{N/m}^2,\quad c_{1122} = 7.78\times10^{10}\ \text{N/m}^2,\quad c_{1133} = 7.43\times10^{10}\ \text{N/m}^2,$$

$$c_{3333} = 11.5\times10^{10}\ \text{N/m}^2,\quad c_{3232} = 2.56\times10^{10}\ \text{N/m}^2,\quad e_{131} = 12.7\ \text{C/m}^2,$$

$$e_{311} = -5.2\ \text{C/m}^2,\quad e_{333} = 15.1\ \text{C/m}^2,\quad \kappa_{11} = 730\kappa_0,\quad \kappa_{33} = 635\kappa_0$$

where $\kappa_0 = 8.854\times10^{-12}\ \text{C}^2/(\text{N}\cdot\text{m}^2)$. The boundary conditions of the prism are

$$\sigma_{yy} = P,\quad \sigma_{xy} = D_y = 0 \qquad (\text{on edges}\quad y = \pm b)$$

$$\sigma_{xx} = \sigma_{xy} = D_x = 0 \qquad (\text{on edges}\quad x = \pm a)$$

where a=3 m, b=10 m. Owing to the symmetry of load, boundary conditions and geometry, only one quadrant of the prism is modeled by 10 (x-direction) × 20 (y-direction) elements in the Trefftz FEM analysis. Table 4.1 lists the displacements and electric potential at points A, B, C, and D using the present method and comparison is made with analytical results. It is found that the Trefftz FEM results are in good agreement with the analytical ones [26].

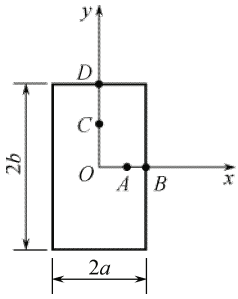

Fig. 4.2 Geometry of the piezoelectric prism in example.

Table 4.1 Trefftz FEM results and comparison with exact solution.

	Point	*A*(2,0)	*B*(3,0)	*C*(0,5)	*D*(0,10)
Trefftz	$u_1 \times 10^{10}$ /m	–0.967 4	–1.451 0	0	0
FEM	$u_2 \times 10^{9}$ /m	0	0	0.500 9	1.001 6
	ϕ/V	0	0	0.689 0	1.377 9
Exact	$u_1 \times 10^{10}$ /m	–0.967 2	–1.450 8	0	0
Ref.[27]	$u_2 \times 10^{9}$ /m	0	0	0.500 6	1.001 1
	ϕ/V	0	0	0.688 8	1.377 5

4.3 Trefftz FEM for anti-plane problems

As a special case of the problem discussed in Section 4.2, we now consider application of the Trefftz FEM to anti-plane electroelastic problems. Particularly, special trial functions which satisfy crack boundary conditions are introduced and used to develop a special purpose element with cracks.

4.3.1 Basic equations for deriving Trefftz FEM

In the case of anti-plane shear deformation involving only out-of-plane displacement u_z and in-plane electric fields, we have [13]

$$u_x = u_y = 0, \quad u_z = u_z(x, y), \quad \phi = \phi(x, y) \tag{4.45}$$

The differential governing equation (1.9) can be simplified to

$$c_{55}\nabla u_z + e_{15}\nabla\phi = 0, \quad e_{15}\nabla u_z - \kappa_{11}\nabla\phi = 0 \qquad (\text{in } \Omega) \tag{4.46}$$

with the constitutive equations (1.35) or

$$\begin{Bmatrix} \gamma_{xz} \\ \gamma_{yz} \\ E_x \\ E_y \end{Bmatrix} = \begin{bmatrix} f_{55} & 0 & g_{15} & 0 \\ 0 & f_{55} & 0 & g_{15} \\ -g_{15} & 0 & \beta_{11} & 0 \\ 0 & -g_{15} & 0 & \beta_{11} \end{bmatrix} \begin{Bmatrix} \sigma_{xz} \\ \sigma_{yz} \\ D_x \\ D_y \end{Bmatrix} \tag{4.47}$$

where $\nabla^2 = \partial^2/\partial x^2 + \partial^2/\partial y^2$ is the two-dimensional Laplace operator.

The constants f_{55}, g_{15} and β_{11} are defined by the relations

$$f_{55} = \frac{\kappa_{11}}{\Delta}, \qquad g_{15} = \frac{e_{15}}{\Delta}, \qquad \beta_{11} = \frac{c_{55}}{\Delta}, \qquad \Delta = c_{44}\kappa_{11} + e_{15}^2 \tag{4.48}$$

The boundary conditions are still defined by Eqs. (1.11) and (1.12) and the continuity conditions are given in Eqs. (4.7) and (4.8).

It is obvious from Eq. (4.46) that it is necessary for

$$c_{44}\kappa_{11} + e_{15}^2 \neq 0 \tag{4.49}$$

to have non-trivial solutions for the out-of-plane displacement and in-plane electric fields. It results in

$$\nabla u_z = 0, \qquad \nabla \phi = 0 \tag{4.50}$$

4.3.2 Trefftz functions

It is well known that solutions of the Laplace equation (4.50) may be found using the method of variable separation. By this method, the Trefftz functions are obtained as [13]

$$u_z(r,\theta) = \sum_{m=0}^{\infty} r^m (a_m \cos m\theta + b_m \sin m\theta) \tag{4.51}$$

$$\phi(r,\theta) = \sum_{m=0}^{\infty} r^m (c_m \cos m\theta + d_m \sin m\theta) \tag{4.52}$$

for a bounded region and

$$u_z(r,\theta) = a_0^* + a_0 \ln r + \sum_{m=1}^{\infty} r^{-m} (a_m \cos m\theta + b_m \sin m\theta) \tag{4.53}$$

$$\phi(r,\theta) = c_0^* + c_0 \ln r + \sum_{m=1}^{\infty} r^{-m} (c_m \cos m\theta + d_m \sin m\theta) \tag{4.54}$$

for an unbounded region, where r and θ are a pair of polar coordinates. Thus, the associated T-complete sets of Eqs. (4.51)-(4.54) can be written in the form

$$T = \{1,\ r^m \cos m\theta,\ r^m \sin m\theta\} = \{T_i\} \tag{4.55}$$

$$T = \{1,\ \ln r,\ r^{-m} \cos m\theta,\ r^{-m} \sin m\theta\} = \{T_i\} \tag{4.56}$$

4.3.3 Assumed fields

The two independent fields in the present Trefftz FEM are assumed in the following way:

(1) The non-conforming intra-element field is expressed by

$$\mathbf{u}=\begin{Bmatrix}u_z\\ \phi\end{Bmatrix}=\sum_{j=1}^{m}\begin{bmatrix}N_{1j} & 0\\ 0 & N_{2j}\end{bmatrix}\begin{Bmatrix}c_{uj}\\ c_{\phi j}\end{Bmatrix}=\begin{bmatrix}\mathbf{N}_1 & 0\\ 0 & \mathbf{N}_2\end{bmatrix}\mathbf{c}=\mathbf{N}\mathbf{c} \tag{4.57}$$

where $\mathbf{c}$ is a vector of undetermined coefficient, $\mathbf{N}_i$ are taken from the component of the series (4.55) or (4.56), and m is its number of components. The choice of m was discussed in Section 2.6 of Ref. [23]. The optimal value of m for a given type of element should be found by numerical experimentation.

(2) An auxiliary conforming field

$$\tilde{\mathbf{u}}=\begin{Bmatrix}\tilde{u}_z\\ \tilde{\phi}\end{Bmatrix}=\begin{bmatrix}\tilde{\mathbf{N}}_1 & 0\\ 0 & \tilde{\mathbf{N}}_2\end{bmatrix}\begin{Bmatrix}\mathbf{d}_u\\ \mathbf{d}_\phi\end{Bmatrix}+\begin{bmatrix}\tilde{\mathbf{N}}_{1c} & 0\\ 0 & \tilde{\mathbf{N}}_{2c}\end{bmatrix}\begin{Bmatrix}\mathbf{d}_{uc}\\ \mathbf{d}_{\phi c}\end{Bmatrix}=\tilde{\mathbf{N}}\mathbf{d}+\tilde{\mathbf{N}}_c\mathbf{d}_c \tag{4.58}$$

is independently assumed along the element boundary in terms of nodal DOF $\mathbf{d}=\{\mathbf{d}_u, \mathbf{d}_\phi\}^{\mathrm{T}}$ and $\mathbf{d}_c=\{\mathbf{d}_{uc},\mathbf{d}_{\phi c}\}^{\mathrm{T}}$, where $\tilde{\mathbf{N}}$ represents the conventional FE interpolating functions and $\tilde{\mathbf{N}}_{1c}$, $\tilde{\mathbf{N}}_{2c}$ are given in Eqs. (4.59) and (4.60) below. For example, in a simple interpolation of the frame field on the side 1-*C*-2 of a particular element (Fig. 4.3), the frame functions are defined in the following way:

$$\tilde{u}_{z12}=\tilde{N}_1u_{z1}+\tilde{N}_2u_{z2}+\sum_{J=1}^{M_u}\xi^{J-1}(1-\xi^2)u_{zCJ} \tag{4.59}$$

$$\tilde{\phi}_{12}=\tilde{N}_1\phi_1+\tilde{N}_2\phi_2+\sum_{J=1}^{M_\phi}\xi^{J-1}(1-\xi^2)\phi_{CJ} \tag{4.60}$$

where u_{zCJ} and ϕ_{CJ} are shown in Fig. 4.3, and

$$\tilde{N}_1=\frac{(1-\xi)}{2},\qquad \tilde{N}_2=\frac{(1+\xi)}{2} \tag{4.61}$$

Using the above definitions the generalized boundary forces and electric displacements can be derived from Eqs. (1.11) and (4.57), denoting

$$\mathbf{T}=\begin{Bmatrix}t_z\\ D_n\end{Bmatrix}=\begin{Bmatrix}\sigma_{3j}n_j\\ D_jn_j\end{Bmatrix}=\begin{bmatrix}\mathbf{Q}_1\\ \mathbf{Q}_2\end{bmatrix}\mathbf{c}=\mathbf{Q}\mathbf{c} \tag{4.62}$$

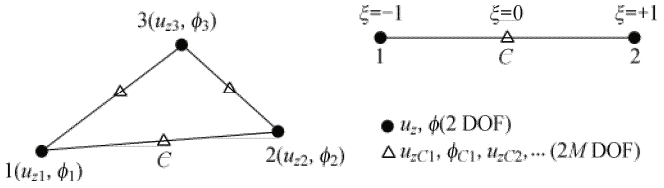

Fig. 4.3 Geometry of a triangular element.

4.3.4 Special element containing a singular corner

It is noted that singularities induced by local defects, such as angular corners, cracks, and so on, can be accurately accounted for in the conventional FE model by way of appropriate local refinement of the element mesh. However, an important feature of the Trefftz FEM is that such problems can be far more efficiently handled by the use of special purpose functions [23]. Elements containing local defects (see Fig. 4.4) are treated by simply replacing the standard regular functions **N** in Eq. (4.57) by appropriate special purpose functions. One common characteristic of such trial functions is that it is not only the governing differential equations, which are Laplace equations here, that are satisfied exactly, but also some prescribed boundary conditions at a particular portion Γ_{eS} (see Fig. 4.4) of the element boundary. This enables various singularities to be specifically taken into account without troublesome mesh refinement. Since the whole element formulation remains unchanged (except that now the frame function $\tilde{\mathbf{u}}$ in Eq. (4.58)) is defined and the boundary integration is performed only at the portion Γ_{e*} of the element boundary $\Gamma_e = \Gamma_{e*} + \Gamma_{eS}$, (see Fig. 4.4) [23], all that is needed to implement the elements containing such special trial functions is to provide the element subroutine of the standard, regular elements with a library of various optional sets of special purpose functions.

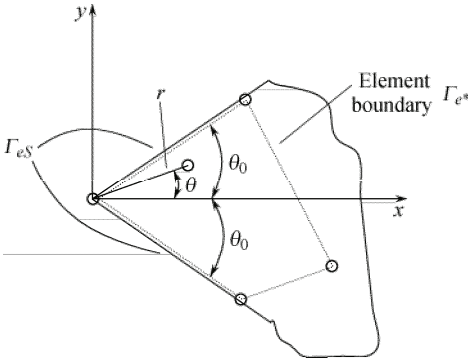

Fig. 4.4 Special element containing a singular corner.

In this section we show how special purpose functions can be constructed to satisfy both the Laplace equation (4.50) and the traction-free boundary conditions on angular corner faces (Fig. 4.4). The derivation of such functions is based on the general solution of the two-dimensional Laplace equation:

$$u_z(r,\theta) = a_0 + \sum_{n=1}^{\infty}(a_n r^{\lambda_n} + b_n r^{-\lambda_n})\cos(\lambda_n\theta) + \sum_{n=1}^{\infty}(d_n r^{\lambda_n} + e_n r^{-\lambda_n})\sin(\lambda_n\theta) \tag{4.63}$$

$$\phi(r,\theta) = e_0 + \sum_{n=1}^{\infty}(e_n r^{\lambda_n} + f_n r^{-\lambda_n})\cos(\lambda_n\theta) + \sum_{n=1}^{\infty}(g_n r^{\lambda_n} + h_n r^{-\lambda_n})\sin(\lambda_n\theta) \tag{4.64}$$

Appropriate trial functions for a singular corner element are obtained by considering an infinite wedge (Fig. 4.4) with particular boundary conditions prescribed along the sides $\theta = \pm\theta_0$ forming the angular corner. The boundary conditions on the upper and lower surfaces of the wedge are free of surface traction and surface charge:

$$\sigma_{r\theta} = c_{55}\frac{\partial u_z}{r\partial\theta} + e_{15}\frac{\partial\phi}{r\partial\theta} = 0, \qquad D_\theta = e_{15}\frac{\partial u_z}{r\partial\theta} - \kappa_{11}\frac{\partial\phi}{r\partial\theta} = 0 \tag{4.65}$$

This leads to

$$\frac{\partial u_z}{\partial\theta} = 0, \qquad \frac{\partial\phi}{\partial\theta} = 0 \qquad (\text{for } \theta = \pm\theta_0) \tag{4.66}$$

To solve this problem, we rewrite the general solution (4.63) as

$$u_z(r,\theta) = a_0 + \sum_{n=1}^{\infty}(a_n r^{\lambda_n} + b_n r^{-\lambda_n})\cos(\lambda_n\theta) + \sum_{n=1}^{\infty}(d_n r^{\beta_n} + e_n r^{-\beta_n})\sin(\beta_n\theta) \tag{4.67}$$

where λ_n and β_n are two sets of constants which are assumed to be greater than zero. Differentiating solution (4.67) and substituting it into Eq. (4.66) yield

$$\begin{aligned}\frac{\partial u_z}{\partial\theta}\Big|_{\theta=\pm\theta_0} &= -\sum_{n=1}^{\infty}\lambda_n(a_n r^{\lambda_n} + b_n r^{-\lambda_n})\sin(\pm\lambda_n\theta_0) \\ &\quad + \sum_{n=1}^{\infty}\beta_n(d_n r^{\beta_n} + e_n b^{-\beta_n})\cos(\pm\beta_n\theta_0) = 0\end{aligned} \tag{4.68}$$

Since the solution must be limited for $r = 0$, we should specify

$$b_n = e_n = 0 \tag{4.69}$$

From Eq. (4.68) it can be deduced that

$$\sin(\pm\lambda_n\theta_0) = 0, \qquad \cos(\pm\beta_n\theta_0) = 0 \tag{4.70}$$

leading to

$$\lambda_n\theta_0 = n\pi \qquad (n = 1,2,3,\cdots) \tag{4.71}$$

$$2\beta_n\theta_0 = n\pi \qquad (n = 1,3,5,\cdots) \tag{4.72}$$

Thus, for an element containing an edge crack (in this case $\theta_0 = \pi$), the solu-

tion can be written in the form

$$u_z(r,\theta) = a_0 + \sum_{n=1}^{\infty} a_n r^n \cos(n\theta) + \sum_{n=1,3,5}^{\infty} d_n r^{\frac{n}{2}} \sin(\frac{n}{2}\theta) \tag{4.73}$$

With solution (4.73), the internal function defined in Eq. (4.57) can be taken as

$$N_{2n-1} = r^n \cos(n\theta), \qquad N_{2n} = r^{\frac{(2n-1)}{2}} \sin(\frac{(2n-1)}{2}\theta) \qquad (n=1,2,3,\cdots) \tag{4.74}$$

It is obvious that the displacement function (4.73) includes the term proportional to $r^{1/2}$, whose derivative is singular at the crack tip. The solution for the second equation of (4.66) can be obtained similarly.

4.3.5 Generation of element matrix

The element matrix equation can be obtained by means of a variational approach. Following the procedure described in [24], the related variational functional used for deriving Trefftz FE formulation of the anti-plane problem may be constructed as

$$\begin{aligned} \Pi_m^{\sigma D} &= \sum_e \Pi_{me}^{\sigma D} = \sum_e \{\Pi_e^{\sigma D} - \int_{\Gamma_{De}} (\bar{D}_n - D_n)\tilde{\phi}\mathrm{d}s - \int_{\Gamma_{te}} (\bar{t} - t)\tilde{u}_z \mathrm{d}s \\ &\quad + \int_{\Gamma_{Ie}} (D_n\tilde{\phi} + t\tilde{u}_z)\mathrm{d}s\} \end{aligned} \tag{4.75}$$

$$\begin{aligned} \Pi_m^{\varepsilon E} &= \sum_e \Pi_{me}^{\varepsilon E} = \sum_e \{\Pi_e^{\varepsilon E} + \int_{\Gamma_{\phi e}} (\bar{\phi} - \phi)\tilde{D}_n \mathrm{d}s + \int_{\Gamma_{ue}} (\bar{u}_z - u_z)\tilde{t}\mathrm{d}s \\ &\quad -2\int_{\Gamma_{te}} \tilde{u}_z t\mathrm{d}s - 2\int_{\Gamma_{De}} \tilde{\phi} D_n \mathrm{d}s - \int_{\Gamma_{Ie}} (\tilde{\phi} D_n + \tilde{u}_z t)\mathrm{d}s\} \end{aligned} \tag{4.76}$$

where

$$\Pi_e^{\sigma D} = \iint_{\Omega_e} H(\sigma_{ij}, D_k)\mathrm{d}\Omega + \int_{\Gamma_{ue}} t\bar{u}_z \mathrm{d}s + \int_{\Gamma_{\phi e}} D_n \bar{\phi}\mathrm{d}s \tag{4.77}$$

$$\Pi_e^{\varepsilon E} = \iint_{\Omega_e} H(\gamma_{ij}, E_k)\mathrm{d}\Omega + \int_{\Gamma_{te}} \bar{t}\tilde{u}_z \mathrm{d}s + \int_{\Gamma_{De}} \bar{D}_n \tilde{\phi}\mathrm{d}s \tag{4.78}$$

with

$$H(\sigma_{ij}, D_k) = -\frac{1}{2} f_{55}(\sigma_{xz}^2 + \sigma_{yz}^2) - g_{15}\sigma_{xz}D_x - g_{15}\sigma_{yz}D_y + \frac{1}{2}\beta_{11}(D_x^2 + D_y^2) \tag{4.79}$$

$$H(\gamma_{ij}, E_k) = \frac{1}{2} c_{55}(\gamma_{xz}^2 + \gamma_{yz}^2) - e_{15}\gamma_{xz}E_x - e_{15}\gamma_{yz}E_y - \frac{1}{2}\kappa_{11}(E_x^2 + E_y^2) \tag{4.80}$$

in which Eq. (4.50) is assumed to be satisfied, *a priori*.

The element matrix may be then established by setting $\delta \Pi_{me}^{\sigma D} = 0$ or $\delta \Pi_{me}^{\varepsilon E} = 0$. As an illustration, we use $\delta \Pi_{me}^{\sigma D} = 0$ to derive the element stiffness matrix. To simplify the derivation, the domain integral in Eq. (4.77) is converted into a boundary integral by use of solution properties of the intra-element trial functions, for which the functional (4.75) is rewritten as

$$\Pi_{me} = \frac{1}{2}\int_{\Gamma_e} (t_z u_z + D_n \phi) \mathrm{d}s - \int_{\Gamma_e} (D_n \tilde{\phi} + t_z \tilde{u}_z) \mathrm{d}s - \int_{\Gamma_{\phi e}} D_n \overline{\phi} \mathrm{d}s - \int_{\Gamma_{ue}} t_z \overline{u}_z \mathrm{d}s \tag{4.81}$$

Substituting the expressions given in Eqs. (4.57), (4.58), and (4.62) into Eq. (4.81) produces

$$\Pi_{me}^{\sigma D} = -\frac{1}{2}\mathbf{c}^{\mathrm{T}}\mathbf{H}\mathbf{c} + \mathbf{c}^{\mathrm{T}}\mathbf{S}\mathbf{d} + \mathbf{c}^{\mathrm{T}}\mathbf{r}_1 \tag{4.82}$$

in which the matrices **H**, **S** and the vectors $\mathbf{r}_1$ are defined by

$$\begin{aligned} \mathbf{H} &= -\int_{\Gamma_e} \mathbf{Q}^{\mathrm{T}}\mathbf{N} \mathrm{d}s, \\ \mathbf{S} &= -\int_{\Gamma_e} \mathbf{Q}^{\mathrm{T}}\tilde{\mathbf{N}} \mathrm{d}s, \\ \mathbf{r}_1 &= -\int_{\Gamma_{\phi e}} \mathbf{Q}_2^{\mathrm{T}} \overline{\phi} \mathrm{d}s - \int_{\Gamma_{ue}} \mathbf{Q}_1^{\mathrm{T}} \overline{u}_z \mathrm{d}s \end{aligned} \tag{4.83}$$

The symmetry of the matrix **H** can be shown by considering the generalized energy U_e of a particular element "e":

$$\begin{aligned} 2U_e &= 2\iint_{\Omega_e} H(\sigma_{ij}, D_k) \mathrm{d}\Omega = \iint_{\Omega_e} (\sigma_{ij}\varepsilon_{ij} - D_k E_k) \mathrm{d}\Omega \\ &= \int_{\Gamma_e} (\sigma_{ij} n_j u_i + D_i n_i \phi) \mathrm{d}s = \int_{\Gamma_e} \mathbf{T}^{\mathrm{T}}\mathbf{u} \mathrm{d}s = \int_{\Gamma_e} \mathbf{u}^{\mathrm{T}}\mathbf{T} \mathrm{d}s \end{aligned} \tag{4.84}$$

where

$$\int_{\Gamma_e} \mathbf{T}^{\mathrm{T}}\mathbf{u} \mathrm{d}s = \mathbf{c}^{\mathrm{T}} \left[\int_{\Gamma_e} \mathbf{Q}^{\mathrm{T}}\mathbf{N} \mathrm{d}s \right] \mathbf{c} = \mathbf{c}^{\mathrm{T}}\mathbf{H}\mathbf{c} \tag{4.85}$$

$$\int_{\Gamma_e} \mathbf{u}^{\mathrm{T}}\mathbf{T} \mathrm{d}s = \mathbf{c}^{\mathrm{T}} \left[\int_{\Gamma_e} \mathbf{N}^{\mathrm{T}}\mathbf{Q} \mathrm{d}s \right] \mathbf{c} = \mathbf{c}^{\mathrm{T}}\mathbf{H}^{\mathrm{T}}\mathbf{c} \tag{4.86}$$

Therefore $\mathbf{H}=\mathbf{H}^{\mathrm{T}}$.

To enforce inter-element continuity on the common element boundary, the unknown vector **c** should be expressed in terms of nodal degrees of freedom **d**. An optional relationship between **c** and **d** in the sense of variation can be obtained from

$$\frac{\partial \Pi_{me}}{\partial \mathbf{c}^{\mathrm{T}}} = -\mathbf{H}\mathbf{c} + \mathbf{S}\mathbf{d} + \mathbf{r}_1 = 0 \tag{4.87}$$

This leads to

$$\mathbf{c} = \mathbf{G}\mathbf{d} + \mathbf{g} \tag{4.88}$$

where $\mathbf{G} = \mathbf{H}^{-1}\mathbf{S}$ and $\mathbf{g} = \mathbf{H}^{-1}\mathbf{r}_1$, and then straightforwardly yields the expression of Π_{me} only in terms of $\mathbf{d}$ and other known matrices:

$$\Pi_{me} = \frac{1}{2}\mathbf{d}^{\mathrm{T}}\mathbf{G}^{\mathrm{T}}\mathbf{H}\mathbf{G}\mathbf{d} + \mathbf{d}^{\mathrm{T}}\mathbf{G}^{\mathrm{T}}\mathbf{H}\mathbf{g} \tag{4.89}$$

Therefore, the element stiffness matrix equation can be obtained by taking the vanishing variation of the functional Π_{me} as

$$\frac{\partial \Pi_{me}}{\partial \mathbf{d}^{\mathrm{T}}} = 0 \quad \Rightarrow \quad \mathbf{K}\mathbf{d} = \mathbf{P} \tag{4.90}$$

where $\mathbf{K}=\mathbf{G}^{\mathrm{T}}\mathbf{H}\mathbf{G}$ and $\mathbf{P}= -\mathbf{G}^{\mathrm{T}}\mathbf{H}\mathbf{g}$ are, respectively, the element stiffness matrix and the equivalent nodal flow vector. The expression (4.90) is the elemental stiffness matrix equation for Trefftz FE analysis.

4.3.6 Numerical examples

As a numerical illustration of the formulation described above we consider an anti-plane crack of length $2c$ embedded in an infinite PZT-5H medium which is subjected to a uniform shear traction, $\sigma_{zy} = \tau_\infty$, and a uniform electric displacement, $D_y = D_\infty$ at infinity (see Fig. 4.5). The material properties of PZT-5H are as given by [13]: $c_{55} = 3.53\times10^{10}$ N/m^2, $e_{15} = 17.0$ C/m^2, $\kappa_{11} = 1.51\times10^{-8}$ C/(V·m), $J_{\mathrm{cr}} = 5.0$ N/m, where J_{cr} is the critical energy release rate. In our FE analysis, one half of the geometry configuration shown in Fig. 4.6 is used and a typical element mesh is shown in Fig. 4.7. However, due to the symmetry about the x-axis (the line AB in Fig. 4.7), only one half of the mesh in Fig. 4.7 is actually used. Since the trial functions of the crack element satisfy the crack face condition and represent the singularity at crack tip, it is unnecessary to increase the mesh density near the crack tip. In the calculation, three types of element (see Fig. 4.7) have been used.

To study the convergent performance of the proposed formulation, numerical results for different element meshes 8×8, 12×12, 16×16, 20×20, and 24×24

are presented in Table 4.2, showing that the *h*-extension performs very nicely, and Table 4.3 shows the results of J/J_{cr} versus M, where $2M$ is the number of hierarchic degrees of freedom. That also shows good convergent performance.

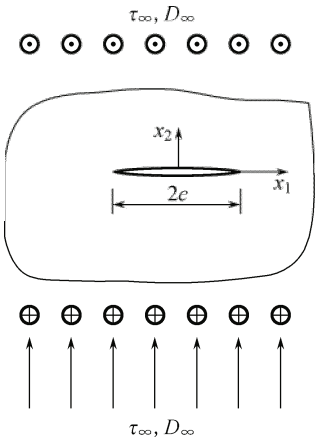

Fig. 4.5 Configuration of the cracked infinite piezoelectric medium.

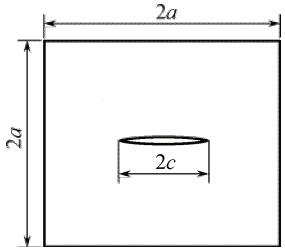

Fig. 4.6 Geometry of the cracked solid in FE analysis.

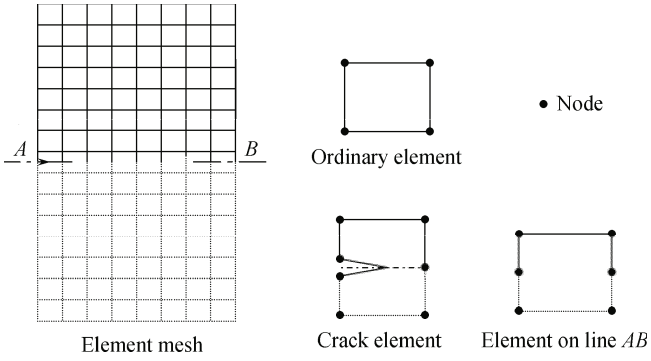

Fig. 4.7 A typical element mesh and element types.

Table 4.2 *h*-convergence study on J/J_{cr} for piezoelectric plate with a central crack (*a*/*c*=15, $D_\infty = 2\times10^{-3}$ C/m^3, and $\tau_\infty = 4.2\times10^6$ N/m^2).

Meshes	J/J_{cr}
8×8	1.595 4
12×12	1.590 8
16×16	1.589 9
20×20	1.589 5
24×24	1.589 3

Table 4.3 *p*-convergence study on J/J_{cr} for piezoelectric plate with central crack (*a*/*c*=15, 16×16, $D_\infty = 2\times10^{-3}$ C/m^3, and $\tau_\infty = 4.2\times10^6$ N/m^2).

M	J/J_{cr}
0	1.589 9
1	1.589 6
2	1.589 5
3	1.589 4

The boundary effect is investigated by using different ratios of *a*/*c* (5, 7, 10, 12, and 15). Numerical results of J/J_{cr} for different *a*/*c* are listed in Table 4.4. The accuracy of these results is adequate when *a*/*c* is greater than 10.

Table 4.4 Boundary effect study on J/J_{cr} for plate with central crack (24×24, $D_\infty = 2\times10^{-3}$ C/m^3, and $\tau_\infty = 4.2\times10^6$ N/m^2).

a/*c*	J/J_{cr}
5	1.596 8
7	1.591 7
10	1.589 8
12	1.589 4
15	1.589 3

4.4 Trefftz boundary element method for anti-plane problems

Trefftz BEM can be divided into two major categories: the direct method and the indirect method. The direct and indirect methods presented in [18] are detailed here.

4.4.1 Indirect formulation

In the indirect method, the unknown displacement u_z and electric potential ϕ are approximated by the expansions (4.57). In Eq. (4.57), N_i is taken from Eq. (4.55)

for subdomains without crack or from Eq. (4.74) for the remainder, and the generalized traction vector **T** is defined in Eq. (4.62). Then, the indirect formulation corresponding to the anti-plane problem can be expressed by

$$\int_{\Gamma_u} (\overline{u}_z - u_z) w_1 \mathrm{d}s + \int_{\Gamma_\phi} (\overline{\phi} - \phi) w_2 \mathrm{d}s + \int_{\Gamma_t} (\overline{t}_z - t_z) w_3 \mathrm{d}s + \int_{\Gamma_D} (\overline{D}_n - D_n) w_4 \mathrm{d}s = 0 \tag{4.91}$$

where w_i (i=1-4) are arbitrary weighting functions and u_z, ϕ, t, D_n have the series representations (4.57) and (4.62). If we use the Galerkin method, the weighting functions are chosen as arbitrary variations of the expressions (4.57) and (4.62), that is

$$w_1 = \mathbf{Q}_1 \delta\mathbf{c}, \quad w_2 = \mathbf{Q}_2 \delta\mathbf{c}, \quad w_3 = -\mathbf{N}_1 \delta\mathbf{c}, \quad w_4 = -\mathbf{N}_2 \delta\mathbf{c} \tag{4.92}$$

Substituting Eq. (4.92) into Eq. (4.91) yields

$$\mathbf{K}\mathbf{c} = \mathbf{f} \tag{4.93}$$

where

$$\mathbf{K} = \int_{\Gamma_u} \mathbf{Q}_1^{\mathrm{T}} \mathbf{N}_1 \mathrm{d}s - \int_{\Gamma_t} \mathbf{N}_1^{\mathrm{T}} \mathbf{Q}_1 \mathrm{d}s + \int_{\Gamma_\phi} \mathbf{Q}_2^{\mathrm{T}} \mathbf{N}_2 \mathrm{d}s - \int_{\Gamma_D} \mathbf{N}_2^{\mathrm{T}} \mathbf{Q}_2 \mathrm{d}s \tag{4.94}$$

$$\mathbf{f} = \int_{\Gamma_u} \mathbf{Q}_1^{\mathrm{T}} \overline{u}_z \mathrm{d}s - \int_{\Gamma_t} \mathbf{N}_1^{\mathrm{T}} \overline{t}_z \mathrm{d}s + \int_{\Gamma_\phi} \mathbf{Q}_2^{\mathrm{T}} \overline{\phi} \mathrm{d}s - \int_{\Gamma_D} \mathbf{N}_2^{\mathrm{T}} \overline{D}_n \mathrm{d}s \tag{4.95}$$

It should be noted that the formulation above applies only to a solution domain containing one semi-infinite crack when the particular solution (4.74) is used as the weighting function. For multi-crack problems, the domain decomposition approach is required. In this case, the solution domain is divided into several sub-domains (Fig. 4.8). For example, a domain containing two cracks can be divided into four sub-domains (Fig. 4.8), In Fig. 4.8, Ω_i (i=1-4) denote the sub-domains, Γ the outer boundary, and Γ_{lij} the inner boundaries between sub-domains. For each sub-domain, the indirect method leads to

$$\mathbf{K}_i \mathbf{c}_i = \mathbf{f}_i \qquad (i\text{=}1\text{-}4) \tag{4.96}$$

On the inner boundary $\Gamma_{\mathrm{l}ij}$, the continuity conditions provide

$$u_{zI}^i = u_{zI}^j, \quad \phi_I^i = \phi_I^j, \quad t_{zI}^i = -t_{zI}^j, \quad D_{nI}^i = -D_{nI}^j \tag{4.97}$$

where the subscript "I" stands for the inner boundary, and superscript "i" (or "j") means the ith (or jth) sub-domain. Equations (4.96) and (4.97) can be used to solve multiple crack problems.

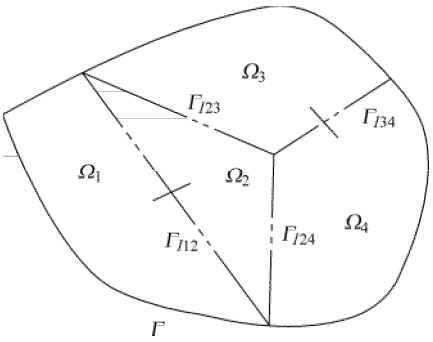

Fig. 4.8 Geometry of the four sub-domain problems.

4.4.2 The point-collocation formulations of Trefftz boundary element method

The point-collocation technique is obtained when these functions are defined by the Dirac delta function as

$$w_1 = w_2 = w_3 = w_4 = \delta(P - P_i) \tag{4.98}$$

where P_i is the collocation point.

Substituting Eqs. (4.57), (4.62), and (4.98) into Eq. (4.91) yields

$$u_z(P_i) = [\mathbf{N}_1(P_i) \quad \mathbf{0}]\mathbf{c} = \overline{w}(P_i) \qquad (\text{for } P_i \text{ on } \Gamma_w) \tag{4.99}$$

$$t_z(P_i) = \mathbf{Q}_1(P_i)\mathbf{c} = \overline{t}_z(P_i) \qquad (\text{for } P_i \text{ on } \Gamma_q) \tag{4.100}$$

$$\phi(P_i) = [\mathbf{0} \quad \mathbf{N}_2(P_i)]\mathbf{c} = \overline{\phi}(P_i) \qquad (\text{for } P_i \text{ on } \Gamma_\phi) \tag{4.101}$$

$$D_n(P_i) = \mathbf{Q}_2(P_i)\mathbf{c} = \overline{D}_n(P_i) \qquad (\text{for } P_i \text{ on } \Gamma_D) \tag{4.102}$$

The above equations may be written in index form:

$$K_{ij}c_j = f_i \tag{4.103}$$

or in matrix form which has the same form as that of Eq. (4.93), but different elements of matrix **K**. The points of collocation can be set at any location where a boundary value is known.

4.4.3 Direct formulation

The Trefftz direct formulation is obtained by considering [28]

$$\iint_{\Omega} \left(\nabla^2 u_z v_1 + \nabla^2 \phi v_2\right) \mathrm{d}\Omega = 0 \tag{4.104}$$

Performing the integration by parts and taking the right-hand side of Eq. (4.57) as weighting function, that is

$$\mathbf{v} = \begin{Bmatrix} v_1 \\ v_2 \end{Bmatrix} = \sum_{j=0}^{m} \begin{bmatrix} N_{1j} & 0 \\ 0 & N_{2j} \end{bmatrix} \begin{Bmatrix} c_{uj} \\ c_{\phi j} \end{Bmatrix} = \begin{bmatrix} \mathbf{N}_1 \\ \mathbf{N}_2 \end{bmatrix} \mathbf{c} = \mathbf{N}\mathbf{c} \tag{4.105}$$

we have

$$\mathbf{c}^{\mathrm{T}} \int_{\Gamma} (\mathbf{N}_1^{\mathrm{T}} t_z - \mathbf{Q}_1^{\mathrm{T}} u_z + \mathbf{N}_2^{\mathrm{T}} D_n - \mathbf{Q}_2^{\mathrm{T}} \phi) \mathrm{d}s = 0 \tag{4.106}$$

Since the equation is valid for arbitrary vectors **c**, we have

$$\int_{\Gamma} (\mathbf{N}_{1i}^{\mathrm{T}} t - \mathbf{Q}_{1i}^{\mathrm{T}} u_z + \mathbf{N}_{2i}^{\mathrm{T}} D_n - \mathbf{Q}_{2i}^{\mathrm{T}} \phi) \mathrm{d}s = 0 \tag{4.107}$$

The analytical results of Eq. (4.107) are, in general, impossible, and therefore a numerical procedure must be used to solve the problem. As in the conventional BEM, the boundary Γ is divided into m linear elements, for which u_z, t_z, ϕ, and D_n are approximated by

$$u_z = \sum_{i=1}^{m} u_{zi} F_i(s),\ t_z = \sum_{i=1}^{m} t_{zi} F_i(s),\ \phi = \sum_{i=1}^{m} \phi_i F_i(s),\ D_n = \sum_{i=1}^{m} D_{ni} F_i(s) \tag{4.108}$$

where u_{zi}, t_{zi}, ϕ_i and D_{ni} are, respectively, their values at node i. $s>0$ in the element located at the right of the node i, $s<0$ in the element located at the left of the node. $F_i(s)$ is a global shape function associated with the ith-node. $F_i(s)$ is zero-valued over the whole mesh except within two elements connected to the ith-node (see Fig. 4.9). Since $F_i(s)$ is assumed to be linear within each element, it has three possible forms:

$$F_i(s) = \left(\left|l_i^+\right| - s\right) / \left|l_i^+\right| \tag{4.109}$$

for a node located at the left end of a line (see Fig. 4.9(a)),

$$F_i(s) = \left(\left|l_i^-\right| + s\right) / \left|l_i^-\right| \tag{4.110}$$

for a node located at the right end of a line (see Fig. 4.9(b)), or

$$F_i(s) = \begin{cases} \left(\left|l_i^-\right| + s\right) / \left|l_i^-\right| & (\text{if } s \in l_i^-) \\ \left(\left|l_i^+\right| - s\right) / \left|l_i^+\right| & (\text{if } s \in l_i^+) \end{cases} \tag{4.111}$$

where l_i^+ and l_i^- are two elements connected to the ith node, with l_i^+ being to the

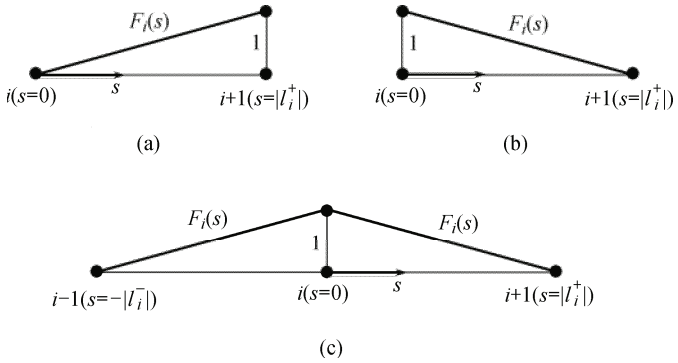

Fig. 4.9 Definitions of $F_i(s)$, $\left|l_i^+\right|$ and $\left|l_i^-\right|$.

right and l_i^- being to the left, while $\left|l_i^+\right|$ and $\left|l_i^-\right|$ denote their lengths, and

$$s=\begin{cases}0 & \text{(at node } i\text{)}\\ \left|l_i^+\right| & \text{(at node } i+1\text{)}\\ -\left|l_i^-\right| & \text{(at node } i-1\text{)}\end{cases} \tag{4.112}$$

Having performed the discretion above, we obtain

$$\mathbf{Gu}=\mathbf{Ht} \tag{4.113}$$

Applying the boundary conditions, we have

$$\begin{bmatrix}\mathbf{G}_1 & \mathbf{G}_2 & \mathbf{G}_3 & \mathbf{G}_4\end{bmatrix}\begin{Bmatrix}\overline{\mathbf{u}}_z\\ \mathbf{u}_z\\ \overline{\boldsymbol{\varphi}}\\ \boldsymbol{\varphi}\end{Bmatrix}=\begin{bmatrix}\mathbf{H}_1 & \mathbf{H}_2 & \mathbf{H}_3 & \mathbf{H}_4\end{bmatrix}\begin{Bmatrix}\overline{\mathbf{t}}\\ \mathbf{t}\\ \overline{\mathbf{D}}_n\\ \mathbf{D}_n\end{Bmatrix} \tag{4.114}$$

or simply

$$\mathbf{Kx}=\mathbf{f} \tag{4.115}$$

The direct formulation above is only suitable for single crack problems. For a multi-crack problem, as treated in Subsection 4.4.1, the domain decomposition approach is used to convert it into several single crack problems. For a particular single crack problem with sub-domain I (see Fig. 4.8), Eq. (4.115) becomes

$$\mathbf{K}_i\mathbf{x}_i=\mathbf{f}_i \qquad (\text{in } \Omega_i) \tag{4.116}$$

while on the inner boundary Γ_{Iij}, the continuity condition is again defined in Eqs. (4.7) and (4.8).

4.4.4 Numerical examples

As a numerical illustration of the proposed formulation, two simple examples are considered. To allow for comparisons with analytical results, as presented in [22,29], the results obtained are limited to a central cracked piezoelectric plate and a piezoelectric strip with two collinear cracks along its *x*-axis. In all the calculations, the PZT-5H piezoelectric ceramic material is used, the material constants of which are [25]

$$c_{44} = 3.53\times10^{10}\ \text{N/m}^2,\ e_{15} = 17.0\ \text{C/m}^2,\ \kappa_{11} = 1.51\times10^{-8}\ \text{C/(V}\cdot\text{m)},\ J_{\text{cr}} = 5.0\ \text{N/m}$$

where J_{cr} is the critical energy release rate.

Example 1

we consider again an anti-plane crack of length 2*c* embedded in an infinite PZT-5H medium which is subjected to a uniform shear traction, $\sigma_{zy} = \tau_\infty$, and a uniform electric displacement, $D_y = D_\infty$ at infinity (see Fig. 4.5). In the Trefftz boundary element calculation, only one half of the geometry configuration shown in Fig. 4.6 is used due to the symmetry of the problem. A typical boundary element mesh is shown in Fig. 4.10. The energy release rate for PZT-5H material with a crack of length 2*c*=0.02 m and *a*/*c*=14 is plotted in Fig. 4.11 as a function of electrical load, with the mechanical load fixed so that $J=J_{\text{cr}}$ at zero electric load. The results are compared with those from Qin [13] using Trefftz FEM. It is found from Fig. 4.11 that the energy release rate can be negative, which means that the crack growth may be arrested. It is also observed that there is good agreement between the two approaches although only 32 boundary elements are used in the calculation. The energy release rate appearing in Fig. 4.11 was defined in [25]

$$J = G = \lim_{\Delta x\to 0}\frac{\Delta W}{\Delta x} \tag{4.117}$$

with

$$\Delta W = 2\int_0^{\Delta x}\frac{1}{2}(\sigma_{zy}u_z + D_y\phi)\mathrm{d}x \tag{4.118}$$

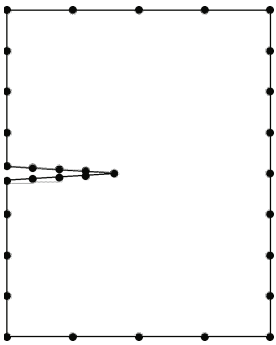

Fig. 4.10 A typical boundary mesh (32 elements).

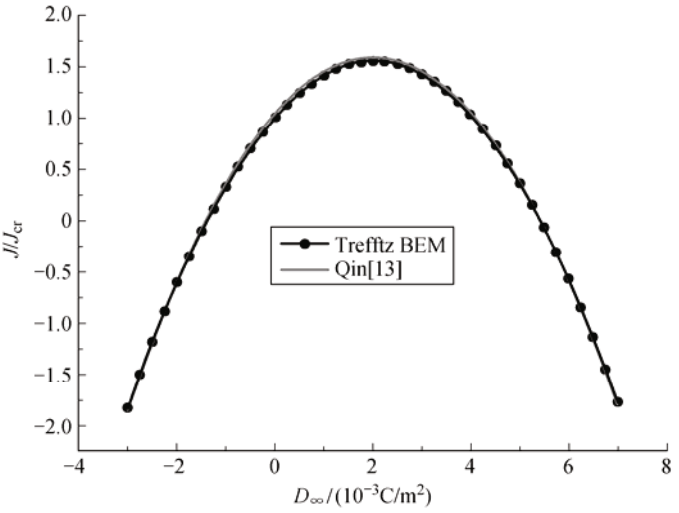

Fig. 4.11 Energy release rate in cracked PZT-5H plate (a/c=14, $\tau_\infty = 4.2\times10^6$ N/m^2, and 32 elements).

The boundary effect should be studied since we use a rectangular domain with side length 2a (see Fig. 4.6), rather than the infinite domain. The boundary effect is investigated by using different ratios of a/c (6, 10, 14, and 18). Numerical results of J/J_{cr} for different a/c are listed in Table 4.5. The accuracy of the results is adequate when a/c is greater than 14.

Table 4.5 Boundary effect study of J/J_{cr} for plate with central crack ($D_\infty = 2\times10^{-3}$ C/m^3, and $\tau_\infty = 4.2\times10^6$ N/m^2).

a/c	J/J_{cr}
6	1.598 7
10	1.592 2
14	1.589 6
18	1.589 5

To study the convergent performance of the proposed formulation, numerical results of J/J_{cr} for different element meshes 24, 32, 48, 64, and 128 boundary elements are presented in Table 4.6, which demonstrates that the h-extension performs very nicely. Table 4.7 shows the results of K_{III}/K_{IIIS} and K_D/K_{DS} for the element meshes above, also showing good convergent performance, where [25]

$$K_{IIIS} = c_{55}K_\gamma - e_{15}K_E, \qquad K_{DS} = e_{15}K_\gamma + \kappa_{11}K_E \tag{4.119}$$

with

$$K_\gamma = \frac{\kappa_{11}\tau_\infty + e_{15}D_\infty}{c_{55}\kappa_{11} + e_{15}^2}\sqrt{\pi c}, \qquad K_E = \frac{c_{55}D_\infty - e_{15}\tau_\infty}{c_{55}\kappa_{11} + e_{15}^2}\sqrt{\pi c} \tag{4.120}$$

Table 4.6 h-convergence study of J/J_{cr} for plate with central crack (a/c=14, $D_\infty = 2\times10^{-3}$ C/m^3, and $\tau_\infty = 4.2\times10^6$ N/m^2).

Elements	J/J_{cr}
24	1.596 1
32	1.591 3
48	1.590 1
64	1.589 4
128	1.589 3

Table 4.7 h-convergence study for $K_{\text{III}}/K_{\text{III}S}$ and K_D/K_{DS} for plate with central crack (a/c=14, $D_\infty = 2\times10^{-3}$C/m^3, and $\tau_\infty = 4.2\times10^6$ N/m^2).

Elements	$K_{\text{III}}/K_{\text{III}S}$	K_D/K_{DS}
24	1.254	1.195
32	1.181	1.122
48	1.112	1.089
64	1.094	1.071
128	1.092	1.070

Table 4.8 shows the results for J/J_{cr} obtained by both the indirect method and the direct method, indicating similar convergent performance. Therefore both methods are suitable for anti-plane fracture analysis, although the values of J/J_{cr} obtained from the indirect method are slightly higher than those from the direct method.

Table 4.8 J/J_{cr} for the central cracked plate from the two methods (a/c=14, $D_\infty = 2\times10^{-3}$C/m^3, and $\tau_\infty = 4.2\times10^6$ N/m^2).

Approach	Number of variables			
	48	64	96	128
Indirect method	1.598 8	1.592 4	1.590 7	1.590 1
Direct method	1.596 1	1.591 3	1.590 1	1.589 4

Example 2

Consider a piezoelectric strip of width 2h(h=2) which has an infinite extent in the y-z direction (see Fig. 4.12). The strip contains two collinear impermeable

through cracks of equal length (1−*b*) along the *x*-axis [29]. Here 2*b* is the distance between the two cracks. Both cracks are perpendicular to the edges of the strip. Assume that the strip is subjected to a constant shear stress, $\sigma_{32} = -\tau_0$, over the surface of the two cracks.

Owing to the symmetry of the problem only one half of the geometry configuration shown in Fig. 4.13 is analyzed, and each sub-domain (Ω_1 or Ω_2) is modelled by 64 boundary elements.

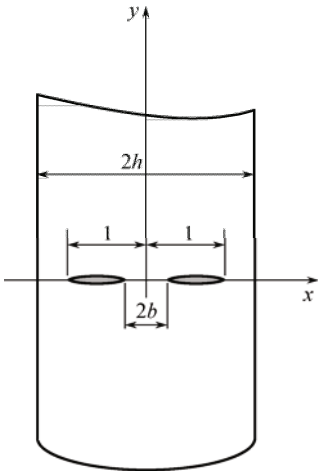

Fig. 4.12 Two cracks in a piezoelectric strip under anti-plane loading.

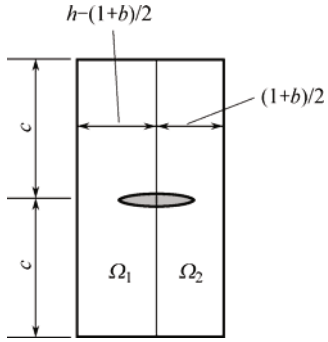

Fig. 4.13 Geometry of the two crack system in the Trefftz boundary element analysis.

Figures 4.14 and 4.15 display the variation of K_{inn}/τ_0 and K_{out}/τ_0 with the crack distance *b*, where *c*, K_{inn} and K_{out} are as defined by [29]

$$c = 12,\ K_{\text{inn}} = \lim_{x \to -b^+} \sqrt{2\pi(b+x)}\sigma_{32}(x,0),\ K_{\text{out}} = \lim_{x \to -1^-} \sqrt{-2\pi(1+x)}\sigma_{32}(x,0)$$

It can be seen from Figs. 4.14 and 4.15 that the results from the Trefftz BEM are in good agreement with analytical results [29] when the crack distance *b* is greater than 0.4. However, the discrepancy between the two methods increases along with a decrease in *b* when *b* is less than 0.4. This indicates that edge effect will become important when the ratio of crack length (1−*b*) to the distance from the crack tip to the edge of the sub-domain (*b* here) is greater than 1.5, i.e., $(1-b)/b > 1.5$. This result can help us to select an appropriate subdomian size when using the proposed formulation.

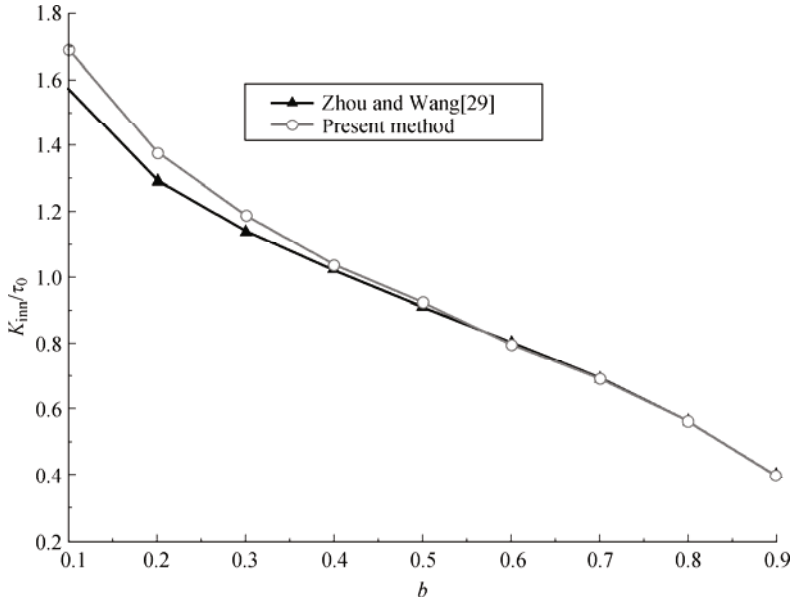

Fig. 4.14 K_{inn}/τ_0 vs crack distance b.

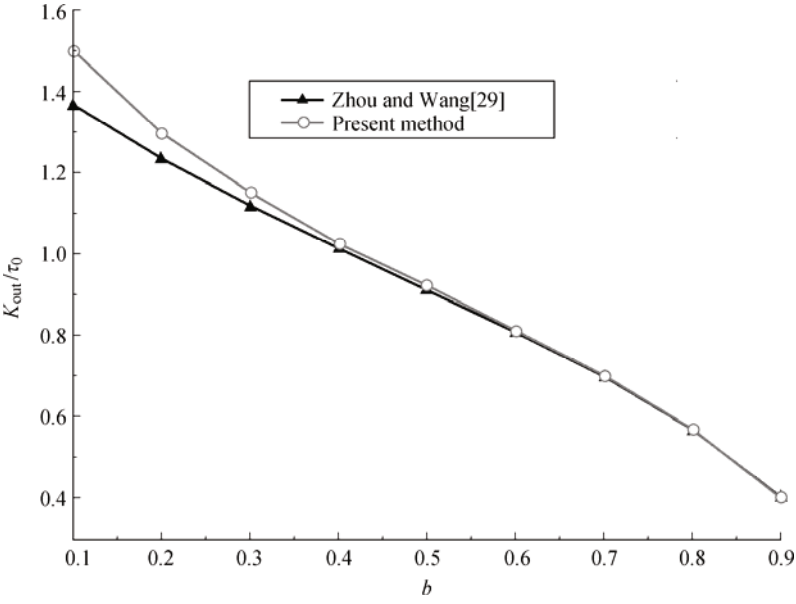

Fig. 4.15 K_{out}/τ_0 vs crack distance b.

4.5 Trefftz boundary-collocation method for plane piezoelectricity

This section presents a brief summary of the development in [19] which begins with a Trefftz solution of general plane piezoelectricity derived by Lekhnitskii's formalism. Then a boundary collocation scheme is described.

4.5.1 General Trefftz solution sets

Let (x', y') be the principal material coordinates, y' the poling direction and (x,y) the set of coordinates obtained by rotating (x', y') through an anti-clockwise rotation ξ (see Fig. 4.16). Using Lekhnitskii's formalism, a general solution of plane piezoelectricity can be written as [25]

$$\begin{Bmatrix}\sigma_{11}\\ \sigma_{22}\\ \sigma_{12}\end{Bmatrix} = 2\,\mathrm{Re}\sum_{k=1}^{3}\begin{Bmatrix}\mu_k^2\\ 1\\ -\mu_k\end{Bmatrix}\psi_k'(z_k), \qquad \begin{Bmatrix}D_1\\ D_2\end{Bmatrix} = 2\,\mathrm{Re}\sum_{k=1}^{3}\begin{Bmatrix}\varpi_k\mu_k\\ -\varpi_k\end{Bmatrix}\psi_k'(z_k) \tag{4.121}$$

$$\begin{Bmatrix}u_1\\ u_2\\ \phi\end{Bmatrix} = 2\,\mathrm{Re}\sum_{k=1}^{3}\begin{Bmatrix}p_k\\ q_k\\ s_k\end{Bmatrix}\psi_k(z_k) \tag{4.122}$$

where μ_k is the kth root of Eq. (2.8), ψ_k is an arbitrary function of the complex variable z_k, and [25]

$$\begin{aligned} &p_k = a_{11}\mu_k^2 + a_{12} - b_{21}\varpi_k, \quad q_k = a_{12}\mu_k^2 + a_{22} - b_{22}\varpi_k,\\ &s_k = -(b_{13} + \delta_{11}\varpi_k)\mu_k, \quad \varpi_k(p_k) = -\frac{(b_{21}+b_{13})\mu_k^2 + b_{22}}{\delta_{11}\mu_k^2 + \delta_{22}},\\ &z_k = x + \mu_k y = r_k(\cos\theta_k + i\sin\theta_k) \end{aligned} \tag{4.123}$$

with a_{ij}, b_{ij}, and δ_{ij} being defined by Eq. (1.25), and the polar coordinates being represented by (r_k, θ_k).

Making use of the general solutions (4.121) and (4.122), the plane piezoelectric problem is reduced to the one of solving the potential functions ψ_k. The corresponding Trefftz functions can be obtained by expressing ψ_k in terms of Taylor series [19]:

$$\psi_k(z_k) = \sum_{n=1}^{\infty}(\alpha_k^{(n)} + i\beta_k^{(n)})z_k^n \qquad (\text{for } k = 1,2,3,\cdots) \tag{4.124}$$

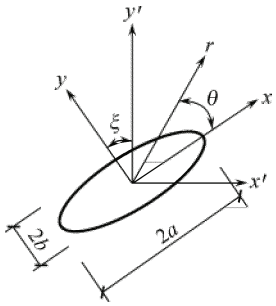

Fig. 4.16 Coordinate systems and poling direction for elliptical hole.

where α_k and β_k are real coefficients. Substituting Eq. (4.124) into the general solutions (4.121) and (4.122), the basic set of Trefftz functions can be given in the form

$$\begin{aligned}\mathbf{T}\big|_{\mathbf{u}} = 2\{&\mathrm{Re}(\mathbf{D}_1)c_1^{(n)} - \mathrm{Im}(\mathbf{D}_1)s_1^{(n)},\ -\mathrm{Re}(\mathbf{D}_1)s_1^{(n)} - \mathrm{Im}(\mathbf{D}_1)c_1^{(n)},\\ &\mathrm{Re}(\mathbf{D}_2)c_2^{(n)} - \mathrm{Im}(\mathbf{D}_2)s_2^{(n)},\ -\mathrm{Re}(\mathbf{D}_2)s_2^{(n)} - \mathrm{Im}(\mathbf{D}_2)c_2^{(n)},\\ &\mathrm{Re}(\mathbf{D}_3)c_3^{(n)} - \mathrm{Im}(\mathbf{D}_3)s_3^{(n)},\ -\mathrm{Re}(\mathbf{D}_3)s_3^{(n)} - \mathrm{Im}(\mathbf{D}_3)c_3^{(n)}\}\end{aligned}$$

$$(\text{for } n = 0,1,2,3,\cdots) \tag{4.125}$$

which corresponds to the unknown real constants $\{\alpha_1^{(n)},\ \beta_1^{(n)},\ \alpha_2^{(n)},\ \beta_2^{(n)},\ \alpha_3^{(n)},\ \beta_3^{(n)}\}$, where $c_i^{(n)} = r_i^n \cos n\theta_i$, $s_i^{(n)} = r_i^n \sin n\theta_i$, $\mathbf{D}_k = \{p_k,\ q_k,\ s_k\}^{\mathrm{T}}$, "Re" and "Im" denote, respectively, the real and imaginary parts of the subsequent expression, and the subscript "**u**" signifies that the basic solution set is for the displacement vector $\mathbf{u} = \{u_1,\ u_2,\ \phi\}^{\mathrm{T}}$.

4.5.2 Special Trefftz solution set for a problem with elliptic holes

For an arbitrarily oriented elliptic hole, Sheng et al. [19] in 2006 constructed a special set of Trefftz functions. They began with considering the following conformal mappings:

$$z_k = \frac{a - i\mu_k b}{2}\zeta_k + \frac{a + i\mu_k b}{2}\frac{1}{\zeta_k} \quad (\text{for } k = 1,2,3) \tag{4.126}$$

where a and b are the half-lengths of the hole axes (see Fig. 4.16). With the mapping, the region occupied by the piezoelectric material in the z_k-plane is mapped onto the outside of a unit circle in the ζ-plane, since it can be shown that all the roots of equation $\mathrm{d}z_k / \mathrm{d}\zeta_k = 0$ for Eq. (4.126) are located inside the unit circle $|\zeta_k| = 1$ [30]. The inverse of the mapping (4.126) provides

$$\zeta_k = \frac{z_k \pm \sqrt{z_k^2 - (a^2 + \mu_k^2 b^2)}}{a - i\mu_k b} \qquad (\text{for } k = 1,2,3) \tag{4.127}$$

in which the sign of the square root ± is chosen in such a way that $|\zeta_k| \geqslant 1$. Making use of Eq. (4.126), the elastic displacements, stresses, and electric displacements defined in Eqs. (4.121) and (4.122) can be written in the form

$$\begin{Bmatrix} \sigma_{11} \\ \sigma_{22} \\ \sigma_{12} \end{Bmatrix} = 2\,\mathrm{Re}\sum_{k=1}^{3} \begin{Bmatrix} \mu_k^2 \\ 1 \\ -\mu_k \end{Bmatrix} \frac{\psi_k'(\zeta_k)}{z_k'(\zeta_k)}, \qquad \begin{Bmatrix} D_1 \\ D_2 \end{Bmatrix} = 2\,\mathrm{Re}\sum_{k=1}^{3} \begin{Bmatrix} \varpi_k \mu_k \\ -\varpi_k \end{Bmatrix} \frac{\psi_k'(\zeta_k)}{z_k'(\zeta_k)} \tag{4.128}$$

$$\begin{Bmatrix} u_1 \\ u_2 \\ \phi \end{Bmatrix} = 2\,\mathrm{Re}\sum_{k=1}^{3} \begin{Bmatrix} p_k \\ q_k \\ s_k \end{Bmatrix} \psi_k(\zeta_k) \tag{4.129}$$

For an impermeable elliptic hole, the traction-free and charge-free conditions can be given from Eq. (4.128) as in [19]:

$$\mathrm{Re}\sum_{k=1}^{3} \psi_k(\zeta_k) = 0, \quad \mathrm{Re}\sum_{k=1}^{3} \mu_k \psi_k(\zeta_k) = 0, \quad \mathrm{Re}\sum_{k=1}^{3} \varpi_k \psi_k(\zeta_k) \qquad (\text{on } |\zeta_k| = 1) \tag{4.130}$$

Equation (4.130) can be written equivalently as

$$\begin{aligned} &\sum_{k=1}^{3} [\psi_k(\zeta_k) + \overline{\psi}_k(\zeta_k)] = 0, \quad \sum_{k=1}^{3} [\mu_k \psi_k(\zeta_k) + \overline{\mu}_k \overline{\psi}_k(\zeta_k)] = 0, \\ &\sum_{k=1}^{3} [\varpi_k \psi_k(\zeta_k) + \overline{\varpi}_k \overline{\psi}_k(\zeta_k)] = 0 \qquad (\text{on } |\zeta_k| = 1) \end{aligned} \tag{4.131}$$

or further in matrix form

$$\begin{Bmatrix} \overline{\psi}_1 \\ \overline{\psi}_2 \\ \overline{\psi}_3 \end{Bmatrix} = -\begin{bmatrix} 1 & 1 & 1 \\ \overline{\mu}_1 & \overline{\mu}_2 & \overline{\mu}_3 \\ \overline{\varpi}_1 & \overline{\varpi}_2 & \overline{\varpi}_3 \end{bmatrix}^{-1} \begin{bmatrix} 1 & 1 & 1 \\ \mu_1 & \mu_2 & \mu_3 \\ \varpi_1 & \varpi_2 & \varpi_3 \end{bmatrix} \begin{Bmatrix} \psi_1 \\ \psi_2 \\ \psi_3 \end{Bmatrix} = \begin{bmatrix} E_{11} & E_{12} & E_{13} \\ E_{21} & E_{22} & E_{23} \\ E_{31} & E_{32} & E_{33} \end{bmatrix} \begin{Bmatrix} \psi_1 \\ \psi_2 \\ \psi_3 \end{Bmatrix} \tag{4.132}$$

where E_{ij} are self-defined in Eq. (4.132).

The complex potential functions ψ_k for the hole problem can be chosen in the form of Laurent series [19]:

$$\psi_k(\zeta_k) = \sum_{n=1}^{\infty} [(\alpha_k^{(n)} + i\beta_k^{(n)})\zeta_k^n + (\alpha_k^{(-n)} + i\beta_k^{(-n)})\zeta_k^{-n}] \qquad (\text{for } k = 1,2,3,\cdots) \tag{4.133}$$

where α_k and β_k are real constants. Noting that

$$\zeta_1 = \zeta_2 = \zeta_3 = e^{i\theta} \tag{4.134}$$

at any point along the hole boundary, where θ is a polar angle, the combined use of Eqs. (4.132)-(4.134) provides six constraints on the 12 real coefficients $\alpha_k^{(n)}$, $\alpha_k^{(-n)}$, $\beta_k^{(n)}$, and $\beta_k^{(-n)}$ for a particular number n. The six constraints can be used to eliminate six real constants, say, $\alpha_k^{(-n)}$ and $\beta_k^{(-n)}$ in Eq. (4.133), which results in the following set of special Trefftz functions:

$$\mathbf{T}\big|_{\mathbf{u}}^{(\text{hole})} = \{\boldsymbol{\Phi}_{\alpha 1}^{(n)},\ \boldsymbol{\Phi}_{\beta 1}^{(n)},\ \boldsymbol{\Phi}_{\alpha 2}^{(n)},\ \boldsymbol{\Phi}_{\beta 2}^{(n)},\ \boldsymbol{\Phi}_{\alpha 3}^{(n)},\ \boldsymbol{\Phi}_{\beta 3}^{(n)}\} \qquad (\text{for } n = 0,1,2,3,\cdots) \tag{4.135}$$

where

$$\begin{aligned} \boldsymbol{\Phi}_{\alpha k}^{(n)} &= \boldsymbol{\chi}_{\alpha k}^{(n)} + \sum_{i=1}^{3} \mathrm{Re}(E_{ik})\boldsymbol{\chi}_{\alpha i}^{(-n)} - \sum_{i=1}^{3} \mathrm{Im}(E_{ik})\boldsymbol{\chi}_{\beta i}^{(-n)}, \\ \boldsymbol{\Phi}_{\beta k}^{(n)} &= \boldsymbol{\chi}_{\beta k}^{(n)} - \sum_{i=1}^{3} \mathrm{Im}(E_{ik})\boldsymbol{\chi}_{\alpha i}^{(-n)} - \sum_{i=1}^{3} \mathrm{Re}(E_{ik})\boldsymbol{\chi}_{\beta i}^{(-n)} \end{aligned} \tag{4.136}$$

with

$$\begin{aligned} \boldsymbol{\chi}_{\alpha k}^{(n)} &= 2\,\mathrm{Re}(\mathbf{D}_k)\,\mathrm{Re}(\zeta_k^n) - 2\,\mathrm{Im}(\mathbf{D}_k)\,\mathrm{Im}(\zeta_k^n), \\ \boldsymbol{\chi}_{\alpha k}^{(-n)} &= 2\,\mathrm{Re}(\mathbf{D}_k)\,\mathrm{Re}(\zeta_k^{-n}) - 2\,\mathrm{Im}(\mathbf{D}_k)\,\mathrm{Im}(\zeta_k^{-n}), \\ \boldsymbol{\chi}_{\beta k}^{(n)} &= -2\,\mathrm{Re}(\mathbf{D}_k)\,\mathrm{Im}(\zeta_k^n) - 2\,\mathrm{Im}(\mathbf{D}_k)\,\mathrm{Re}(\zeta_k^n), \\ \boldsymbol{\chi}_{\beta k}^{(-n)} &= 2\,\mathrm{Re}(\mathbf{D}_k)\,\mathrm{Im}(\zeta_k^{-n}) - 2\,\mathrm{Im}(\mathbf{D}_k)\,\mathrm{Re}(\zeta_k^{-n}) \end{aligned} \tag{4.137}$$

4.5.3 Special Trefftz solution set for impermeable crack problems

Having obtained the special Trefftz functions for elliptic hole problems, Sheng et al. [19] next derived a special set of Trefftz functions for problems containing an impermeable semi-infinite crack. In this case, the boundary conditions along the crack faces are

$$\sigma_{22} = \sigma_{12} = D_2 = 0 \qquad (\text{at crack faces } \theta = \pm\pi) \tag{4.138}$$

The potential function ψ_k in Eq. (4.124) are now in the form

$$\psi_k(z_k) = \sum_{\eta}^{\infty} (\alpha_k^{(\eta)} + i\beta_k^{(\eta)}) z_k^{\eta} = \sum_{\eta}^{\infty} (\alpha_k^{(\eta)} + i\beta_k^{(\eta)}) r_k^{\eta} (\cos\eta\theta_k + i\sin\eta\theta_k) \tag{4.139}$$

where η is no longer an integer and is to be determined by boundary conditions. To determine the unknown η substituting Eq. (4.139) into Eq. (4.121) yields

$$\phi = 2\sum_{k=1}^{3}\sum_{\eta}^{\infty} [\alpha_k^{(\eta)}(A_{sk}c_k^{(\eta)} - B_{sk}s_k^{(\eta)}) - \beta_k^{(\eta)}(A_{sk}s_k^{(\eta)} - B_{sk}c_k^{(\eta)})] \tag{4.140}$$

$$\sigma_{22} = 2\sum_{k=1}^{3}\sum_{\eta}^{\infty}\eta(\alpha_k^{(\eta)}c_k^{(\eta-1)} - \beta_k^{(\eta)}s_k^{(\eta-1)}) \tag{4.141}$$

$$\sigma_{12} = 2\sum_{k=1}^{3}\sum_{\eta}^{\infty}\eta[\alpha_k^{(\eta)}(A_{\mu k}c_k^{(\eta-1)} - B_{\mu k}s_k^{(\eta-1)}) - \beta_k^{(\eta)}(A_{\mu k}s_k^{(\eta-1)} + B_{\mu k}c_k^{(\eta-1)})] \tag{4.142}$$

$$D_2 = 2\sum_{k=1}^{3}\sum_{\eta}^{\infty}\eta[\alpha_k^{(\eta)}(A_{\varpi k}c_k^{(\eta-1)} - B_{\varpi k}s_k^{(\eta-1)}) - \beta_k^{(\eta)}(A_{\varpi k}s_k^{(\eta-1)} + B_{\varpi k}c_k^{(\eta-1)})] \tag{4.143}$$

where $c_i^{(\eta)} = r_i^{\eta}\cos\eta\theta_i$, $s_i^{(\eta)} = r_i^{\eta}\sin\eta\theta_i$, A_{sk}=Re(s_k), B_{sk}=Im(s_k), $A_{\mu k}$= –Re(μ_k), $B_{\mu k}$= –Im(μ_k), $A_{\varpi k}$= –Re(ϖ_k), and $B_{\varpi k}$= –Im(ϖ_k). Noting that $\theta_k = \pm\pi$ and r_k=r at $\theta = \pm\pi$, substituting Eqs. (4.141)-(4.143) into Eq. (4.138) provides

$$\mathbf{X}(\eta)\mathbf{G}\mathbf{q} = 0 \tag{4.144}$$

where

$$\mathbf{q} = \begin{Bmatrix} \alpha_1^{(\eta)} \\ \beta_1^{(\eta)} \\ \alpha_2^{(\eta)} \\ \beta_2^{(\eta)} \\ \alpha_3^{(\eta)} \\ \beta_3^{(\eta)} \end{Bmatrix}, \qquad \mathbf{G} = \begin{bmatrix} 1 & 0 & 1 & 0 & 1 & 0 \\ 0 & 1 & 0 & 1 & 0 & 1 \\ A_{\mu 1} & -B_{\mu 1} & A_{\mu 2} & -B_{\mu 2} & A_{\mu 3} & -B_{\mu 3} \\ B_{\mu 1} & A_{\mu 1} & B_{\mu 2} & A_{\mu 2} & B_{\mu 3} & A_{\mu 3} \\ A_{\varpi 1} & -B_{\varpi 1} & A_{\varpi 2} & -B_{\varpi 2} & A_{\varpi 3} & -B_{\varpi 3} \\ B_{\varpi 1} & A_{\varpi 1} & B_{\varpi 2} & A_{\varpi 2} & B_{\varpi 3} & A_{\varpi 3} \end{bmatrix}, \tag{4.145}$$

$$\mathbf{X}(\eta) = \text{diag}\left[\cos\eta\pi\ \sin\eta\pi\ \cos\eta\pi\ \sin\eta\pi\ \cos\eta\pi\ \sin\eta\pi\right]$$

If $\mathbf{G}$ is in full rank, the non-trivial solution of $\mathbf{q}$ can be determined by setting the determinant of $\mathbf{X}(\eta)$ at zero. The solutions to $|\boldsymbol{X}(\eta)| = 0$ yield

$$\eta = n/2 \quad (\text{ for } n = 0,1,2,3,\cdots) \tag{4.146}$$

Since Eq. (4.138) provides three constraints, only three coefficients in Eq. (4.139) are independent. Taking $\alpha_1^{(\eta)}$, $\beta_1^{(\eta)}$, and $\alpha_2^{(\eta)}$ as independent constants, the remaining three constants, $\beta_2^{(\eta)}$, $\alpha_3^{(\eta)}$, and $\beta_3^{(\eta)}$, can be found from Eq. (4.144) as

$$\begin{aligned} \beta_2^{(\eta)} &= J_1\alpha_1^{(\eta)} + J_2\beta_1^{(\eta)} + J_3\alpha_2^{(\eta)}, \\ \alpha_3^{(\eta)} &= J_4\alpha_1^{(\eta)} + J_5\beta_1^{(\eta)} + J_6\alpha_2^{(\eta)}, \\ \beta_3^{(\eta)} &= J_7\alpha_1^{(\eta)} + J_8\beta_1^{(\eta)} + J_9\alpha_2^{(\eta)} \end{aligned} \tag{4.147}$$

where

$$\begin{aligned} J_1 &= (B_{\varpi 3}B_{\mu 1} - B_{\varpi 1}B_{\mu 3})/J_0, \quad J_2 = [B_{\varpi 3}(A_{\mu 1} - A_{\mu 3}) + B_{\mu 3}(A_{\varpi 3} - A_{\varpi 1})]/J_0, \\ J_3 &= (B_{\varpi 3}B_{\mu 2} - B_{\varpi 2}B_{\mu 3})/J_0, \quad J_4 = [B_{\varpi 1}(A_{\mu 2} - A_{\mu 3}) + B_{\mu 1}(A_{\varpi 3} - A_{\varpi 2})]/J_0 \end{aligned} \tag{4.148}$$

$$\begin{aligned} J_5 &= [A_{\mu 1}(A_{\varpi 3} - A_{\varpi 2}) + A_{\mu 2}(A_{\varpi 1} - A_{\varpi 3}) + A_{\mu 3}(A_{\varpi 2} - A_{\varpi 1})]/J_0, \\ J_6 &= [B_{\varpi 2}(A_{\mu 2} - A_{\mu 3}) + B_{\mu 2}(A_{\varpi 3} - A_{\varpi 2})]/J_0, \qquad J_7 = -J_1 \end{aligned} \tag{4.149}$$

$$\begin{aligned} J_8 &= [B_{\varpi 3}(A_{\mu 1} - A_{\mu 2}) + B_{\mu 3}(A_{\varpi 2} - A_{\varpi 1})]/J_0, \quad J_9 = -J_3 \\ J_0 &= B_{\varpi 3}(A_{\mu 3} - A_{\mu 2}) + B_{\mu 3}(A_{\varpi 2} - A_{\varpi 3}) \end{aligned} \tag{4.150}$$

for odd n, i.e., $\eta = 1/2, 3/2, \cdots$, and

$$\begin{aligned} &J_1 = [B_{\varpi 3}(A_{\mu 1} - A_{\mu 3}) + B_{\mu 3}(A_{\varpi 3} - A_{\varpi 1})]/J_0, \ J_2 = [B_{\varpi 1}B_{\mu 3} - B_{\varpi 3}B_{\mu 1})/J_0, \\ &J_3 = [B_{\varpi 3}(A_{\mu 2} - A_{\mu 3}) + B_{\mu 3}(A_{\varpi 3} - A_{\varpi 2})]/J_0, \ J_4 = J_6 = -1, \quad J_5 = 0, \\ &J_7 = [B_{\varpi 2}(A_{\mu 3} - A_{\mu 1}) + B_{\mu 2}(A_{\varpi 1} - A_{\varpi 3})]/J_0, \ J_8 = [B_{\varpi 2}B_{\mu 1} - B_{\varpi 1}B_{\mu 2})/J_0, \\ &J_9 = [B_{\varpi 2}(A_{\mu 3} - A_{\mu 2}) + B_{\mu 2}(A_{\varpi 2} - A_{\varpi 3})]/J_0, \ J_0 = B_{\varpi 3}B_{\mu 2} - B_{\varpi 2}B_{\mu 3} \end{aligned} \tag{4.151}$$

for even n, i.e., $\eta = 1, 2, 3, \cdots$.

By incorporating Eqs. (4.139), (4.146), and (4.147) into the general solutions (4.121) and (4.122), a set of special Trefftz functions for a problem containing an impermeable semi-infinite crack can be obtained as

$$\begin{aligned} \mathbf{T}\big|_{\mathbf{u}}^{(\text{crack}-\text{im})} = \{&\mathbf{S}_{\alpha 1}^{(\eta)} + J_1\mathbf{S}_{\beta 2}^{(\eta)} + J_4\mathbf{S}_{\alpha 3}^{(\eta)} + J_7\mathbf{S}_{\beta 3}^{(\eta)}, \ \mathbf{S}_{\beta 1}^{(\eta)} + J_2\mathbf{S}_{\beta 2}^{(\eta)} + J_5\mathbf{S}_{\alpha 3}^{(\eta)} + J_8\mathbf{S}_{\beta 3}^{(\eta)}, \\ &\mathbf{S}_{\alpha 2}^{(\eta)} + J_3\mathbf{S}_{\beta 2}^{(\eta)} + J_6\mathbf{S}_{\alpha 3}^{(\eta)} + J_9\mathbf{S}_{\beta 3}^{(\eta)}\} \quad (\text{for } 2\eta = 0, 1, 2, \cdots) \end{aligned} \tag{4.152}$$

which corresponds to the independent constants $\{\alpha_1^{(\eta)}, \beta_1^{(\eta)}, \alpha_2^{(\eta)}\}$, and

$$\mathbf{S}_{\alpha k}^{(\eta)} = 2\,\text{Re}(\mathbf{D}_k)c_k^{(\eta)} - 2\,\text{Im}(\mathbf{D}_k)s_k^{(\eta)}, \ \mathbf{S}_{\beta k}^{(\eta)} = -2\,\text{Re}(\mathbf{D}_k)s_k^{(\eta)} - 2\,\text{Im}(\mathbf{D}_k)c_k^{(\eta)} \tag{4.153}$$

4.5.4 Special Trefftz solution set for permeable crack problems

It is noted in [19] that besides the impermeable and permeable assumptions, the upper and lower limits of the exact electric boundary conditions are to be determined. Sheng et al. then developed a set of special Trefftz functions for problems with a permeable semi-infinite crack in [19]. In this case, the boundary conditions along the crack faces (4.138) become

$$\begin{aligned} &\sigma_{22} = \sigma_{12} = 0 \qquad (\text{at crack faces } \theta = \pm\pi), \\ &\phi\big|_{\theta=\pi} = \phi\big|_{\theta=-\pi}, \quad D_2\big|_{\theta=\pi} = D_2\big|_{\theta=-\pi} \end{aligned} \tag{4.154}$$

The potential function ψ_k for this problem has the same form as that of Eq. (4.139), and in turn the expressions (4.140)-(4.143) also apply to this problem. Substituting the expressions of ϕ, σ_{12}, σ_{22} and D_2 in Eqs. (4.140)-(4.143) into Eq. (4.154), an equation analogous to Eq. (4.144) can be obtained. Then eigenvalues of η are also given by Eq. (4.146), but they have different eigenfunctions.

Noting that Eq. (4.154) provides four constraints, only two coefficients for each

η in Eq. (4.139) are independent if n is an odd integer, i.e., $\eta = 1/2, 3/2, \cdots$. When we take $\alpha_1^{(\eta)}$ and $\beta_1^{(\eta)}$ to be independent constants, the following relationships can be obtained:

$$\begin{aligned} \alpha_2^{(\eta)} &= J_{11}\alpha_1^{(\eta)} + J_{12}\beta_1^{(\eta)}, \quad & \beta_2^{(\eta)} &= J_{13}\alpha_1^{(\eta)} + J_{14}\beta_1^{(\eta)}, \\ \alpha_3^{(\eta)} &= J_{15}\alpha_1^{(\eta)} + J_{16}\beta_1^{(\eta)}, \quad & \beta_3^{(\eta)} &= J_{17}\alpha_1^{(\eta)} + J_{18}\beta_1^{(\eta)} \end{aligned} \tag{4.155}$$

in which

$$\begin{aligned} J_{11} &= [(A_{\mu 3} - A_{\mu 2})(B_{s1}B_{\varpi 3} - B_{s3}B_{\varpi 1}) + (A_{\varpi 3} - A_{\varpi 2})(B_{s3}B_{\mu 1} - B_{s1}B_{\mu 3}) \\ &\quad + (A_{s3} - A_{s2})(B_{\varpi 1}B_{\mu 3} - B_{\varpi 3}B_{\mu 1})]/J_{10}, \\ J_{12} &= [(A_{\mu 3} - A_{\mu 2})(A_{s1}B_{\varpi 3} - B_{s3}A_{\varpi 1}) + (A_{\mu 3} - A_{\mu 1})(A_{\varpi 2}B_{s3} - A_{s2}B_{\varpi 3}) \\ &\quad + (A_{\mu 2} - A_{\mu 1})(A_{s3}B_{\varpi 3} - A_{\varpi 3}B_{s3}) + (A_{s2} - A_{s1})A_{\varpi 3}B_{\mu 3} \\ &\quad + (A_{s1} - A_{s3})A_{\varpi 2}B_{\mu 3} + (A_{s3} - A_{s2})A_{\varpi 1}B_{\mu 3})]/J_{10} \end{aligned} \tag{4.156}$$

$$\begin{aligned} J_{13} &= [B_{\varpi 3}(B_{\mu 2}B_{s1} - B_{\mu 1}B_{s2}) + B_{\varpi 2}(B_{\mu 1}B_{s3} - B_{\mu 3}B_{s1}) \\ &\quad + B_{\varpi 1}(B_{\mu 3}B_{s2} - B_{\mu 2}B_{s3})]/J_{10}, \\ J_{14} &= [(A_{\mu 3} - A_{\mu 1})(B_{s2}B_{\varpi 3} - B_{s3}B_{\varpi 2}) + (A_{\varpi 3} - A_{\varpi 1})(B_{s3}B_{\mu 2} - B_{s2}B_{\mu 3}) \\ &\quad + (A_{s3} - A_{s1})(B_{\varpi 2}B_{\mu 3} - B_{\varpi 3}B_{\mu 2})]/J_{10} \end{aligned} \tag{4.157}$$

$$\begin{aligned} J_{15} &= [(A_{\mu 3} - A_{\mu 2})(B_{s2}B_{\varpi 1} - B_{s1}B_{\varpi 2}) + (A_{\varpi 3} - A_{\varpi 2})(B_{s1}B_{\mu 2} - B_{s2}B_{\mu 1}) \\ &\quad + (A_{s3} - A_{s2})(B_{\varpi 2}B_{\mu 1} - B_{\varpi 1}B_{\mu 2})]/J_{10}, \\ J_{16} &= [(A_{s2} - A_{s1})(A_{\mu 3}B_{\varpi 2} - B_{\mu 2}A_{\varpi 3}) + (A_{s3} - A_{s2})(A_{\mu 1}B_{\varpi 2} - B_{\mu 2}A_{\varpi 1}) \\ &\quad + (A_{s3} - A_{s1})(A_{\varpi 2}B_{\mu 2} - B_{\varpi 2}A_{\mu 2}) + (A_{\varpi 2} - A_{\varpi 3})A_{\mu 1}B_{s2} \\ &\quad + (A_{\varpi 3} - A_{\varpi 1})A_{\mu 2}B_{s2} + (A_{\varpi 1} - A_{\varpi 2})A_{\mu 3}B_{s2})]/J_{10}, \\ J_{17} &= -J_{13} \end{aligned} \tag{4.158}$$

$$\begin{aligned} J_{18} &= [(A_{\mu 2} - A_{\mu 1})(B_{s3}B_{\varpi 2} - B_{s2}B_{\varpi 3}) + (A_{\varpi 2} - A_{\varpi 1})(B_{s2}B_{\mu 3} - B_{s3}B_{\mu 2}) \\ &\quad + (A_{s2} - A_{s1})(B_{\varpi 3}B_{\mu 2} - B_{\varpi 2}B_{\mu 3})]/J_{10}, \\ J_{10} &= (A_{\mu 3} - A_{\mu 2})(B_{s3}B_{\varpi 2} - B_{s2}B_{\varpi 3}) + (A_{\varpi 3} - A_{\varpi 2})(B_{s2}B_{\mu 3} - B_{s3}B_{\mu 2}) \\ &\quad + (A_{s3} - A_{s2})(B_{\varpi 3}B_{\mu 2} - B_{\varpi 2}B_{\mu 3}) \end{aligned} \tag{4.159}$$

When n is an even integer, i.e., $n = 0, 2, 4, \cdots$, Sheng et al. indicated that Eq. (4.154) can provide only two independent constraints. Therefore, we have four independent coefficients in Eq. (4.139) for each n. Taking $\alpha_3^{(\eta)}$ and $\beta_3^{(\eta)}$ as dependent coefficients, we have

$$\alpha_3^{(\eta)} = -\alpha_1^{(\eta)} - \alpha_2^{(\eta)}, \quad \beta_3^{(\eta)} = J_{19}\alpha_1^{(\eta)} + J_{20}\beta_1^{(\eta)} + J_{21}\alpha_2^{(\eta)} + J_{22}\beta_2^{(\eta)} \tag{4.160}$$

where

$$\begin{aligned} J_{19} &= (A_{\mu 1} - A_{\mu 3})/B_{\mu 3}, \quad & J_{20} &= -B_{\mu 1}/B_{\mu 3}, \\ J_{21} &= (A_{\mu 2} - A_{\mu 3})/B_{\mu 3}, \quad & J_{22} &= -B_{\mu 2}/B_{\mu 3} \end{aligned} \tag{4.161}$$

Making use of Eqs. (4.121), (4.122), (4.139), (4.146), (4.155), and (4.160), a set of

special Trefftz functions for permeable semi-infinite crack problems can be found as

$$\mathbf{T}\big|_{\mathbf{u}}^{(\text{crack}-\text{p})} = \mathbf{S}_{n1}^{\mathbf{u}} \cup \mathbf{S}_{n2}^{\mathbf{u}} \tag{4.162}$$

where

$$\begin{aligned}
\mathbf{S}_{n1}^{\mathbf{u}} = \{&\mathbf{S}_{\alpha 1}^{(n1/2)} - \mathbf{S}_{\alpha 3}^{(n1/2)} + J_{19}\mathbf{S}_{\beta 3}^{(n1/2)},\ \mathbf{S}_{\beta 1}^{(n1/2)} + J_{20}\mathbf{S}_{\beta 3}^{(n1/2)},\\
&\mathbf{S}_{\alpha 2}^{(n1/2)} - \mathbf{S}_{\alpha 3}^{(n1/2)} + J_{21}\mathbf{S}_{\beta 3}^{(n1/2)},\ \mathbf{S}_{\beta 2}^{(n1/2)} + J_{22}\mathbf{S}_{\beta 3}^{(n1/2)}\} \qquad (\text{for } n1 = 0,2,\cdots),\\
\mathbf{S}_{n2}^{\mathbf{u}} = \{&\mathbf{S}_{\alpha 1}^{(n2/2)} + J_{11}\mathbf{S}_{\alpha 2}^{(n2/2)} + J_{13}\mathbf{S}_{\beta 2}^{(n2/2)} + J_{15}\mathbf{S}_{\alpha 3}^{(n2/2)} + J_{17}\mathbf{S}_{\beta 3}^{(n2/2)},\\
&\mathbf{S}_{\beta 1}^{(n2/2)} + J_{12}\mathbf{S}_{\alpha 2}^{(n2/2)} + J_{14}\mathbf{S}_{\beta 2}^{(n2/2)} + J_{16}\mathbf{S}_{\alpha 3}^{(n2/2)} + J_{17}\mathbf{S}_{\beta 3}^{(n2/2)}\} \qquad (\text{for } n2 = 1,3,\cdots)
\end{aligned} \tag{4.163}$$

with **S** being defined in Eq. (4.153).

It should be mentioned that the three electromechanical field intensity factors for plane piezoelectricity can be directly obtained from Eqs. (4.141)-(4.143) as

$$\begin{aligned}
K_{\text{I}} &= \lim_{r\to 0}\sigma_{22}\big|_{\theta=0}\sqrt{2\pi r} = \sqrt{2\pi}\sum_{i=1}^{3}\alpha_k^{(1/2)},\\
K_{\text{II}} &= \lim_{r\to 0}\sigma_{12}\big|_{\theta=0}\sqrt{2\pi r} = \sqrt{2\pi}\sum_{i=1}^{3}(\alpha_k^{(1/2)}A_{\mu k} - \beta_k^{(1/2)}B_{\mu k}),\\
K_D &= \lim_{r\to 0}D_2\big|_{\theta=0}\sqrt{2\pi r} = \sqrt{2\pi}\sum_{i=1}^{3}(\alpha_k^{(1/2)}A_{\varpi k} - \beta_k^{(1/2)}B_{\varpi k})
\end{aligned} \tag{4.164}$$

4.5.5 Boundary collocation formulation

The boundary collocation method for plane piezoelectricity is similar to that of anti-plane piezoelectricity described in Section 4.4. Essentially, the trial solution for **u** is assumed in the form

$$\tilde{\mathbf{u}} = \begin{Bmatrix}\tilde{u}_1\\ \tilde{u}_2\\ \tilde{\phi}\end{Bmatrix} = [\mathbf{N}_1,\ \mathbf{N}_2,\cdots,\mathbf{N}_m]\begin{Bmatrix}a_1\\ \vdots\\ a_m\end{Bmatrix} = \mathbf{N}\mathbf{a} \tag{4.165}$$

where $\mathbf{N}_i$ are the Trefftz functions extracted from the basic solution set Eq. (4.125), or the special solution set Eqs. (4.135), (4.152), and (4.162), a_i are the unknown real coefficients to be determined by boundary conditions. Using the expressions (4.121) and (4.122), the stresses and electric displacements induced by $\tilde{\mathbf{u}}$ can be obtained. From those, the boundary tractions $(\tilde{t}_1, \tilde{t}_2)$ and surface charge density $\tilde{\omega}$ can be derived and expressed symbolically as

$$\tilde{\mathbf{p}} = \begin{Bmatrix} \tilde{t}_1 \\ \tilde{t}_2 \\ \tilde{\omega} \end{Bmatrix} = [\mathbf{M}_1,\ \mathbf{M}_2, \cdots, \mathbf{M}_m] \begin{Bmatrix} a_1 \\ \vdots \\ a_m \end{Bmatrix} = \mathbf{Ma} \tag{4.166}$$

Since the trial functions satisfy the homogeneous form of the governing equations, only boundary conditions need to be enforced. In the boundary collocation method, the boundary conditions can be enforced by minimizing the following residuals:

$$\mathbf{R}_1 = \tilde{\mathbf{u}} - \overline{\mathbf{u}} \quad (\text{on } \Gamma_{\mathbf{u}}), \qquad \mathbf{R}_2 = \tilde{\mathbf{p}} - \overline{\mathbf{p}} \quad (\text{on } \Gamma_{\mathbf{p}}) \tag{4.167}$$

where the overbarred quantities are prescribed along the respective boundaries. In the collocation method, the residuals are coerced to be zero at selected boundary points x_i along Γ, i.e.,

$$\tilde{\mathbf{u}}(\mathbf{x}_i) - \overline{\mathbf{u}}(\mathbf{x}_i) = 0 \quad (\text{on } \Gamma_{\mathbf{u}}), \qquad \tilde{\mathbf{p}}(\mathbf{x}_i) - \overline{\mathbf{p}}(\mathbf{x}_i) = 0 \quad (\text{on } \Gamma_{\mathbf{p}}) \tag{4.168}$$

for $i = 1, 2, \cdots, n_c$, where n_c is the total number of the collocation points. The substitution of Eqs. (4.165) and (4.166) into Eq. (4.168) yields the matrix equation

$$\mathbf{Ka} = \mathbf{f} \tag{4.169}$$

where the dimension of $\mathbf{K}$ is $3n_c \times m$. Generally, the number of residuals $3n_c$ exceeds the number of unknown coefficients m. Under this circumstance, an approximate solution of the over-constrained equation system can be obtained by the least square method which pre-multiplies both sides of Eq. (4.169) with the transpose of $\mathbf{K}$.

References

[1] Trefftz TE: Ein Gegenstück zum Ritzschen Verfahren. In: Proceedings 2nd International Congress of Applied mechanics, Zurich, 131-137 (1926).

[2] Jirousek J, Venkatesh A: Hybrid Trefftz plane elasticity elements with p-method capabilities. International Journal for Numerical Methods in Engineering **35**(7), 1443-1472 (1992).

[3] Qin QH: Hybrid Trefftz finite-element approach for plate-bending on an elastic-foundation. Applied Mathematical Modelling **18**(6), 334-339 (1994).

[4] Qin QH: Hybrid-Trefftz finite-element method for Reissner plates on an elastic-foundation. Computer Methods in Applied Mechanics and Engineering **122**(3-4), 379-392 (1995).

[5] Qin QH: Nonlinear analysis of thick plates by HT FE approach. Computers & Structures **61**(2), 271-281 (1996).

[6] Stein E, Peters K: A new boundary-type finite element for 2D and 3D elastic solids. In: Onate E, Periaux J, Samuelson A (eds.) The Finite Element Method in the 1990s, A Book Dedicated to O.C. Zienkiewicz, Springer, Berlin, pp. 35-48 (1991).

[7] Wang H, Qin QH, Arounsavat D: Application of hybrid Trefftz finite element method to non-linear problems of minimal surface. International Journal for Numerical Methods in Engineering **69**(6), 1262-1277 (2007).
[8] Qin QH: Transient plate bending analysis by hybrid Trefftz element approach. Communications in Numerical Methods in Engineering **12**(10), 609-616 (1996).
[9] Jirousek J, Qin QH: Application of hybrid-Trefftz element approach to transient heat-conduction analysis. Computers & Structures **58**(1), 195-201 (1996).
[10] Qin QH, Diao S: Nonlinear analysis of thick plates on an elastic foundation by HT FE with p-extension capabilities. International Journal of Solids and Structures **33**(30), 4583-4604 (1996).
[11] Qin QH: Formulation of hybrid Trefftz finite element method for elastoplasticity. Applied Mathematical Modelling **29**(3), 235-252 (2005).
[12] Qin QH, Wang KY: Application of hybrid-Trefftz finite element method to frictional contact problems. Computer Assisted Mechanics and Engineering Sciences **15**, 319-336 (2008).
[13] Qin QH: Solving anti-plane problems of piezoelectric materials by the Trefftz finite element approach. Computational Mechanics **31**(6), 461-468 (2003).
[14] Qin QH: Variational formulations for TFEM of piezoelectricity. International Journal of Solids and Structures **40**(23), 6335-6346 (2003).
[15] Qin QH: Fracture analysis of piezoelectric materials by boundary and Trefftz finite element methods. In: Proceedings of the Sixth World Congress on Computational Mechanics in conjunction with the Second Asian-Pacific Congress on Computational Mechanics, Beijing, China, September 5-10, 2004, pp. 558-563. Tsinghua University Press, Beijing (2004).
[16] Qin QH: Trefftz plane element of piezoelectric plate with p-extension capabilities. In: Yang W (ed.) Proceedings of IUTAM Symposium "Mechanics and Reliability of Actuating Materials", Series: Solid Mechanics and Its Applications, Beijing, China, September 1-3, 2006, pp. 144-153. Springer, Dordrecht (2006).
[17] Wang HT, Sze KY, Yang XM: Analysis of electromechanical stress singularity in piezoelectrics by computed eigensolutions and hybrid-Trefftz finite element models. Computational Mechanics **38**(6), 551-564 (2006).
[18] Wang J, Cui YH, Qin QH, Jia JY: Application of Trefftz BEM to anti-plane piezoelectric problem. Acta Mechanica Solida Sinica **19**(4), 352-364 (2006).
[19] Sheng N, Sze KY, Cheung YK: Trefftz solutions for piezoelectricity by Lekhnitskii's formalism and boundary-collocation method. International Journal for Numerical Methods in Engineering **65**(13), 2113-2138 (2006).
[20] Sheng N, Sze KY: Multi-region Trefftz boundary element method for fracture analysis in plane piezoelectricity. Computational Mechanics **37**(5), 381-393 (2006).
[21] Jin WG, Sheng N, Sze KY, Li J: Trefftz indirect methods for plane piezoelectricity. International Journal for Numerical Methods in Engineering **63**(1), 139-158 (2005).
[22] Qin QH: Mode Ⅲ fracture analysis of piezoelectric materials by Trefftz BEM. Structural Engineering and Mechanics **20**(2) (2005).
[23] Qin QH: The Trefftz Finite and Boundary Element Method. WIT Press, Southampton (2000).
[24] Qin QH, Wang H: Matlab and C Programming for Trefftz Finite Element Methods.

CRC Press, Boca Raton (2009).

[25] Qin QH: Fracture Mechanics of Piezoelectric Materials. WIT Press, Southampton (2001).

[26] Ding HJ, Wang GQ, Chen WQ: A boundary integral formulation and 2D fundamental solutions for piezoelectric media. Computer Methods in Applied Mechanics and Engineering **158**(1-2), 65-80 (1998).

[27] Pak YE: Crack extension force in a piezoelectric material. Journal of Applied Mechanics-Transactions of the ASME **57**(3), 647-653 (1990).

[28] Kita E, Kamiya N, Iio T: Application of a direct Trefftz method with domain decomposition to 2D potential problems. Engineering Analysis with Boundary Elements **23**(7), 539-548 (1999).

[29] Zhou ZG, Wang B: Investigation of anti-plane shear behavior of two collinear cracks in a piezoelectric materials strip by a new method. Mechanics Research Communications **28**(3), 289-295 (2001).

[30] Ting TCT: Green's functions for an anisotropic elliptic inclusion under generalized plane strain deformations. Quarterly Journal of Mechanics and Applied Mathematics **49**, 1-18 (1996).

Chapter 5 Symplectic Solutions for Piezoelectric Materials

In Chapter 4, numerical methods including Trefftz FE and BE approaches were described. It was noted that for some singularity problems such as crack problems of piezoelectric materials, the symplectic approach is a powerful and promising tool for obtaining analytical solutions and analyzing local singularity behavior. This chapter describes symplectic solutions for piezoelectric wedges, magnetoelectroelastic strips and wedges, and three-dimensional piezoelectric materials.

5.1 Introduction

Traditionally, electroelastic coupling effects of piezoelectric materials are treated mainly using a Green's function approach [1,2], micromechanics [3,4], and the integral transform method [5-7]. These studies have been carried out in Euclidean space and they are within the framework of the semi-inverse solution method, which is similar to classical elastic mechanics. The symplectic space method in the conservative Hamiltonian system, pioneered by Zhong [8,9], is different from the traditional semi-inverse solution method. It is based on the Hamiltonian form with Legendre's transformation. The resulting Hamiltonian dual equations have derivatives with respect to the radial (or transverse) coordinate alone on one side and the angular coordinate alone on the other side. The separation of variables is employed to solve the resulting differential eigenvalue problem, and analytical solutions can be obtained by the expansion of eigenfunctions. Unlike the classical semi-inverse methods with pre-assumed trial functions, the symplectic elasticity approach is rigorously rational without any guess functions. All geometric and natural boundary conditions are imposed on the system in a natural manner. It is rational and systematic, with a clearly defined, step-by-step derivation procedure. With the symplectic model, elastic or electroelastic problems can, for example, be solved by means of analogy theory between computational structural mechanics and optimal control. Particularly, using analogy theory, the eigenfunction expansion method of the Hamiltonian operator matrix along the transverse section can be developed within the symplectic geometry space. For detailed description of this approach the reader is referred to [10,11]. For applications of the symplectic formulation to multifield materials, Gu et al. [12] and Leung et al. [13] obtained 2D solutions for transversely isotropic media using the symplectic method. Leung et al. [14] and Zhou et al. [15-17] obtained analytical stress intensity factors for finite elastic disks, edge-cracked circular piezoelectric shafts using symplectic expansion, and Mode III electromagnetic cracks. Leung et al. [18] then extended their symplectic formulation to the case of piezoelectric cantilever composite plates. Xu et al. [19] applied

the symplectic expansion method to solve three-dimensional problems for transversely isotropic piezoelectric media and introduced a 3D sub-symplectic structure for transversely isotropic piezoelectric media. Wang and Qin [20] developed a symplectic model for analyzing singularities near the apex of a multi-dissimilar piezoelectric wedge under anti-plane deformation. Zhao and Chen [21,22] presented symplectic formulations for both functionally graded piezoelectric and magneto-electroelastic materials. Recently, Li and Yao [23,24] obtained a symplectic solution for magnetoelectroelastic materials in a rectangular domain. This chapter focuses on the developments in [17,19-24].

5.2 A symplectic solution for piezoelectric wedges

A symplectic model developed in [20] for analyzing singular behavior near the apex of a multi-dissimilar piezoelectric wedge under anti-plane deformation is described in this section. Explicit solutions of elastic and electric fields are presented for the cases of composite wedges consisting of one, two and multiple piezoelectric materials.

5.2.1 Hamiltonian system by differential equation approach

Consider a 2D piezoelectric wedge of sectorial domain as shown in Fig. 5.1. The polar cylindrical coordinate (r,θ, z) is selected under the condition that the z-axis is out-of-plane, with the origin located at the central point of the cross-section. For an anti-plane electroelastic problem involving out-of-plane displacement w and in-plane electric fields only, the constitutive equations are given by Eq. (1.35) and the corresponding governing equations (1.36) and Eq. (1.2) are now rewritten in terms of polar coordinates (r,θ) as

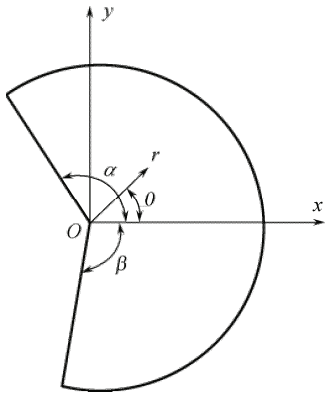

Fig. 5.1 A piezoelectric wedge.

$$\frac{\partial(r\sigma_{rz})}{\partial r}+\frac{\partial\sigma_{\theta z}}{\partial\theta}+rf_z=0,\qquad \frac{\partial(rD_r)}{\partial r}+\frac{\partial D_\theta}{\partial\theta}+rQ=0 \tag{5.1}$$

and

$$\gamma_{rz}=\frac{\partial w}{\partial r},\qquad \gamma_{\theta z}=\frac{1}{r}\frac{\partial w}{\partial\theta},\qquad E_r=-\frac{\partial\phi}{\partial r},\qquad E_\theta=-\frac{1}{r}\frac{\partial\phi}{\partial\theta} \tag{5.2}$$

where f_z and Q are body force and electric charge density. The Hamiltonian system for an anti-plane electroelastic problem can be obtained using the differential equation method. To do this, let (r,θ) represent longitudinal and transverse coordinates, respectively. Then define the dual vectors **q** and **p** as follows:

$$\mathbf{q}=\begin{Bmatrix} w\\ \phi\end{Bmatrix},\qquad \mathbf{p}=\begin{Bmatrix} S_r\\ SD_r\end{Bmatrix} \tag{5.3}$$

which are required in the Hamiltonian system, where

$$S_r=r\sigma_{rz},\qquad SD_r=rD_r \tag{5.4}$$

Further, to convert variables and equations from Euclidean space to symplectic geometry space, introduce a generalized time variable ξ such that

$$\xi=\ln(r) \tag{5.5}$$

Since ξ is now a generalized time variable, the symbol "$\cdot$" is used to represent the differentiation with respect to ξ.

Making use of Eqs. (5.1), (5.4), and (5.5), we have

$$\frac{\partial S_r}{\partial r}=\frac{1}{r}\frac{\partial S_r}{\partial\xi}=\frac{1}{r}\dot{S}_r=-\frac{\partial\sigma_{\theta z}}{\partial\theta}-rf_z=-\frac{1}{r}\left[c_{55}\frac{\partial^2 w}{\partial\theta^2}+e_{15}\frac{\partial^2\phi}{\partial\theta^2}\right]-rf_z \tag{5.6}$$

Equation (5.6) can be further written in the form

$$\dot{S}_r=-c_{55}\frac{\partial^2 w}{\partial\theta^2}-e_{15}\frac{\partial^2\phi}{\partial\theta^2}-e^{2\xi}f_z \tag{5.7}$$

Similarly, the expression of $\dot{SD}_r$ can be obtained as

$$\dot{SD}_r=-e_{15}\frac{\partial^2 w}{\partial\theta^2}+\kappa_{11}\frac{\partial^2\phi}{\partial\theta^2}-e^{2\xi}Q \tag{5.8}$$

Considering Eqs. (1.35) and (5.5), the variables S_r and SD_r can be expressed as

$$S_r=c_{55}\dot{w}+e_{15}\dot{\phi},\qquad SD_r=e_{15}\dot{w}-\kappa_{11}\dot{\phi} \tag{5.9}$$

Solving Eq. (5.9) for $\dot{w}$ and $\dot{\phi}$ yields

$$\dot{w} = f_{55}S_r + g_{15}SD_r, \quad \dot{\phi} = g_{15}S_r - \beta_{11}SD_r \tag{5.10}$$

in which

$$f_{55} = \frac{\kappa_{11}}{\Delta}, \quad g_{15} = \frac{e_{15}}{\Delta}, \quad \beta_{11} = \frac{c_{55}}{\Delta}, \quad \Delta = e_{15}^2 + c_{55}\kappa_{11} \tag{5.11}$$

The combination of Eqs. (5.7) and (5.10) provides the following matrix equation:

$$\begin{Bmatrix} \dot{w} \\ \dot{\phi} \\ \dot{S}_r \\ S\dot{D}_r \end{Bmatrix} = \begin{bmatrix} 0 & 0 & f_{55} & g_{15} \\ 0 & 0 & g_{15} & -\beta_{11} \\ -c_{55}\dfrac{\partial^2}{\partial\theta^2} & -e_{15}\dfrac{\partial^2}{\partial\theta^2} & 0 & 0 \\ -e_{15}\dfrac{\partial^2}{\partial\theta^2} & \kappa_{11}\dfrac{\partial^2}{\partial\theta^2} & 0 & 0 \end{bmatrix} \begin{Bmatrix} w \\ \phi \\ S_r \\ SD_r \end{Bmatrix} + \begin{Bmatrix} 0 \\ 0 \\ -e^{2\xi}f_z \\ -e^{2\xi}Q \end{Bmatrix} \tag{5.12}$$

Further, using the notation

$$\mathbf{v} = \begin{Bmatrix} \mathbf{q} \\ \mathbf{p} \end{Bmatrix} \tag{5.13}$$

Equation (5.12) can be written in the same form as Eq. (2.138) with

$$\mathbf{H} = \begin{bmatrix} 0 & 0 & f_{55} & g_{15} \\ 0 & 0 & g_{15} & -\beta_{11} \\ -c_{55}\dfrac{\partial^2}{\partial\theta^2} & -e_{15}\dfrac{\partial^2}{\partial\theta^2} & 0 & 0 \\ -e_{15}\dfrac{\partial^2}{\partial\theta^2} & \kappa_{11}\dfrac{\partial^2}{\partial\theta^2} & 0 & 0 \end{bmatrix} \tag{5.14}$$

$$\mathbf{h} = \left\{0\ 0\ -e^{2\xi}f_z\ -e^{2\xi}Q\right\}^{\mathrm{T}} \tag{5.15}$$

To prove that **H** is a Hamiltonian operator matrix, the rotational exchange operator matrix defined by Eq. (2.140) with n=2 is employed. With the notation **J**, Wang and Qin [20] proved that **H** satisfies the following relation:

$$\left\langle \mathbf{v}_1^{\mathrm{T}}, \mathbf{H}\mathbf{v}_2 \right\rangle = \left\langle \mathbf{v}_2^{\mathrm{T}}, \mathbf{H}\mathbf{v}_1 \right\rangle \tag{5.16}$$

where

$$\left\langle \mathbf{v}_1^{\mathrm{T}}, \mathbf{H}\mathbf{v}_2 \right\rangle = \int_{-\beta}^{\alpha} \mathbf{v}_1^{\mathrm{T}} \mathbf{J}\mathbf{H}\mathbf{v}_2 \, \mathrm{d}\theta \tag{5.17}$$

with the angles α and β being defined in Fig. 5.1. Then, according to theory of symplectic geometry [10], **H** is a Hamiltonian operator matrix.

5.2.2 Hamiltonian system by variational principle approach

In Subsection 5.2.1 we derived a Hamiltonian system using a differential equation approach. The same Hamiltonian system for the anti-plane problem of a piezoelectric wedge can also be obtained using a variational principle approach. To illustrate this approach, consider the constitutive equation (4.47) in terms of the polar coordinate system:

$$\begin{Bmatrix} \gamma_{\theta z} \\ \gamma_{rz} \\ E_r \\ E_\theta \end{Bmatrix} = \begin{bmatrix} f_{55} & 0 & 0 & g_{15} \\ 0 & f_{55} & g_{15} & 0 \\ 0 & -g_{15} & \beta_{11} & 0 \\ -g_{15} & 0 & 0 & \beta_{11} \end{bmatrix} \begin{Bmatrix} \sigma_{\theta z} \\ \sigma_{rz} \\ D_r \\ D_\theta \end{Bmatrix} \tag{5.18}$$

Based on the constitutive relation (5.18), the modified Hellinger-Reissner generalized variational principle can be stated as follows:

$$\delta \int_{r_1}^{r_2} \int_{-\beta}^{\alpha} \{\sigma_{rz} \frac{\partial w}{\partial r} + \sigma_{\theta z} \frac{1}{r} \frac{\partial w}{\partial \theta} + D_r \frac{\partial \phi}{\partial r} + D_\theta \frac{1}{r} \frac{\partial \phi}{\partial \theta} - [\frac{1}{2} f_{55}(\sigma_{\theta z}^2 + \sigma_{rz}^2) - \frac{1}{2} \beta_{11}(D_r^2 + D_\theta^2) - g_{15} D_\theta \sigma_{\theta z} - g_{15} \sigma_{rz} D_r] - wT - \phi Q\} r \mathrm{d}r \mathrm{d}\theta = 0 \tag{5.19}$$

Making use of the variable transformation (5.5), the variational equality (5.19) can be further written as

$$\delta \int_{\xi_1}^{\xi_2} \int_{-\beta}^{\alpha} \left\{ S_r \frac{\partial w}{\partial \xi} + S_\theta \frac{\partial w}{\partial \theta} + SD_r \frac{\partial \varphi}{\partial \xi} + SD_\theta \frac{\partial \varphi}{\partial \theta} - \left[\frac{1}{2} f_{55}(S_r^2 + S_\theta^2) - \frac{1}{2} \beta_{11}(SD_r^2 + SD_\theta^2) + g_{15} SD_\theta S_\theta + g_{15} SD_r S_r \right] - e^{2\xi} wT - e^{2\xi} \phi Q \right\} \mathrm{d}\xi \mathrm{d}\theta = 0 \tag{5.20}$$

where

$$\xi_1 = \ln r_1, \quad \xi_2 = \ln r_2, \quad S_\theta = r\sigma_{\theta z}, \quad SD_\theta = rD_\theta \tag{5.21}$$

Taking variation with respect to S_θ and SD_θ, Eq. (5.20) leads to

$$S_\theta = c_{55} \frac{\partial w}{\partial \theta} + e_{15} \frac{\partial \phi}{\partial \theta}, \quad SD_\theta = e_{15} \frac{\partial w}{\partial \theta} - \kappa_{11} \frac{\partial \phi}{\partial \theta} \tag{5.22}$$

Substituting Eq. (5.22) into Eq. (5.20) we can obtain the Hamiltonian mixed energy variational principle as follows:

$$\delta\int_{\xi_1}^{\xi_2}\int_{-\beta}^{\alpha}\left\{S_r\frac{\partial w}{\partial \xi}+SD_r\frac{\partial \phi}{\partial \xi}-\frac{1}{2}f_{55}S_r^2+\frac{1}{2}\beta_{11}SD_r^2-g_{15}SD_rS_r+\frac{1}{2}c_{55}\left(\frac{\partial w}{\partial \theta}\right)^2\right.$$
$$\left.-\frac{1}{2}\kappa_{11}\left(\frac{\partial \phi}{\partial \theta}\right)^2+e_{15}\frac{\partial w}{\partial \theta}\frac{\partial \phi}{\partial \theta}-e^{2\xi}wT-e^{2\xi}\phi Q\right\}\mathrm{d}\xi\mathrm{d}\theta=0 \tag{5.23}$$

Making use of Eq. (5.3), Eq. (5.23) can be further simplified to

$$\delta\int_{\xi_1}^{\xi_2}\int_{-\beta}^{\alpha}\left[\mathbf{p}^{\mathrm{T}}\dot{\mathbf{q}}-H(\mathbf{q},\mathbf{p})\right]\mathrm{d}\xi\mathrm{d}\theta=0 \tag{5.24}$$

where $H(\mathbf{q}, \mathbf{p})$ is the Hamiltonian function defined by

$$H(\mathbf{q},\mathbf{p})=-\frac{1}{2}\mathbf{q}^{\mathrm{T}}\mathbf{B}\mathbf{q}+\frac{1}{2}\mathbf{p}^{\mathrm{T}}\mathbf{D}\mathbf{p}-\mathbf{q}^{\mathrm{T}}\mathbf{h}_2 \tag{5.25}$$

in which

$$\mathbf{B}=\begin{bmatrix}-c_{55} & -e_{15}\\ -e_{15} & \kappa_{11}\end{bmatrix}\frac{\partial^2}{\partial\theta^2},\quad \mathbf{D}=\begin{bmatrix}f_{55} & g_{15}\\ g_{15} & -\beta_{11}\end{bmatrix},\quad \mathbf{h}_2=-e^{2\xi}\begin{Bmatrix}f_z\\ Q\end{Bmatrix} \tag{5.26}$$

In the derivation of Eq. (5.24), homogeneous boundary conditions were used [20].

From Eqs. (2.136) and (5.25) the following equations can be obtained:

$$\dot{\mathbf{q}}=\mathbf{D}\mathbf{p},\qquad \dot{\mathbf{p}}=\mathbf{B}\mathbf{q}+\mathbf{h}_2 \tag{5.27}$$

Using the definition of $\boldsymbol{\nu}$ defined in Eq. (5.13), Eq. (5.27) can be rewritten in the form

$$\dot{\boldsymbol{\nu}}=\mathbf{H}^{*}\boldsymbol{\nu}+\mathbf{h} \tag{5.28}$$

in which

$$\mathbf{H}^{*}=\begin{pmatrix}0 & \mathbf{D}\\ \mathbf{B} & 0\end{pmatrix} \tag{5.29}$$

where $\mathbf{H}^{*}$ is used to distinguish the matrix $\mathbf{H}$ in Eq. (5.14) and $\mathbf{h}$ is defined by Eq. (5.15). By comparing the components of $\mathbf{B}$ and $\mathbf{D}$ defined in Eq. (5.26) with those in the corresponding positions in Eq. (5.14), it is found that $\mathbf{H}^{*}$ in Eq. (5.28) is the same as $\mathbf{H}$ given in Eq. (5.14).

5.2.3 Basic eigenvalues and singularity of stress and electric fields

In Subsections 5.2.1 and 5.2.2, the dual state vector equation (5.28) was derived

using either the differential equation method or the variational principle approach. This section discusses applications of the Hamiltonian model developed to analyze the eigenvalues of the Hamiltonian operator matrix which are associated with the singularity behavior of a piezoelectric wedge.

Noting that Eq. (5.28) can be solved by the separation of the variable and the symplectic eigenfunction expansion described in Section 2.7, one can assume $\mathbf{v}$ in the form of Eq. (2.154). Substituting Eq. (2.154) into Eq. (5.28) yields the same form of solution (2.158).

Eigenfunction-vectors corresponding to the eigenvalues (2.159) and (2.160) as well as the zero eigenvalue $\mu = 0$ are denoted by $\boldsymbol{\psi}_{+i}$, $\boldsymbol{\psi}_{-i}$ and $\boldsymbol{\psi}_0$. Following the procedure in [10], Wang and Qin [20] proved that $\boldsymbol{\psi}_{+i}$ and $\boldsymbol{\psi}_{-i}$ are of adjoint symplectic orthonormalization, that is

$$\begin{aligned} &\langle \boldsymbol{\psi}_{+i}^{\mathrm{T}},\ \mathbf{J},\ \boldsymbol{\psi}_{-j} \rangle = \delta_{ij}, \qquad \langle \boldsymbol{\psi}_{-i}^{\mathrm{T}},\ \mathbf{J},\ \boldsymbol{\psi}_{+j} \rangle = -\delta_{ij}, \\ &\langle \boldsymbol{\psi}_{+i}^{\mathrm{T}},\ \mathbf{J},\ \boldsymbol{\psi}_{+j} \rangle = 0, \qquad \langle \boldsymbol{\psi}_{-i}^{\mathrm{T}},\ \mathbf{J},\ \boldsymbol{\psi}_{-j} \rangle = 0 \end{aligned} \tag{5.30}$$

in which

$$\langle \boldsymbol{\psi}_i^{\mathrm{T}},\ \mathbf{J},\ \boldsymbol{\psi}_j \rangle = \int_{-\beta}^{\alpha} \boldsymbol{\psi}_i^{\mathrm{T}} \mathbf{J} \boldsymbol{\psi}_j \mathrm{d}\theta \tag{5.31}$$

Equation (5.31) implies that $\boldsymbol{\psi}_i$ satisfies the homogeneous boundary conditions at $\theta = \alpha, -\beta$.

To prove Eq. (5.30), considering two eigenfunction-vectors, $\boldsymbol{\psi}_i$, $\boldsymbol{\psi}_j$, we have from Eq. (2.156)

$$H\boldsymbol{\psi}_i = \mu_i \boldsymbol{\psi}_i, \qquad H\boldsymbol{\psi}_j = \mu_j \boldsymbol{\psi}_j \tag{5.32}$$

in which H satisfies the following relation:

$$H^{\mathrm{T}} \cdot (\mathbf{J}\boldsymbol{\psi}_i) = -\mu_i \mathbf{J}\boldsymbol{\psi}_i \tag{5.33}$$

Multiplying $\boldsymbol{\psi}_j^{\mathrm{T}}$ on both sides of Eq. (5.33) and integrating it across the transverse section, we can obtain the following equation:

$$\langle \boldsymbol{\psi}_j^{\mathrm{T}}, H^{\mathrm{T}}, \mathbf{J}\boldsymbol{\psi}_i \rangle = -\langle \boldsymbol{\psi}_i^{\mathrm{T}}, \mathbf{J}H, \boldsymbol{\psi}_j \rangle = -\mu_i \langle \boldsymbol{\psi}_j^{\mathrm{T}}, \mathbf{J}, \boldsymbol{\psi}_i \rangle = \mu_i \langle \boldsymbol{\psi}_i^{\mathrm{T}}, \mathbf{J}, \boldsymbol{\psi}_j \rangle \tag{5.34}$$

in which Eq. (2.140) has been used. Similarly, it is easy to show that the following relation holds true:

$$\langle \boldsymbol{\psi}_i^{\mathrm{T}}, \mathbf{J}H, \boldsymbol{\psi}_j \rangle = \mu_j \langle \boldsymbol{\psi}_i^{\mathrm{T}}, \mathbf{J}, \boldsymbol{\psi}_j \rangle \tag{5.35}$$

Making use of Eqs. (5.34) and (5.35), we have

$$(\mu_i + \mu_j) \cdot \langle \boldsymbol{\psi}_i^{\mathrm{T}}, \mathbf{J}, \boldsymbol{\psi}_j \rangle = 0 \tag{5.36}$$

If $\mu_i + \mu_j \neq 0$, Eq. (5.36) is reduced to

$$\langle \boldsymbol{\psi}_i^{\mathrm{T}}, \mathbf{J}, \boldsymbol{\psi}_j \rangle = 0 \tag{5.37}$$

When $\mu_i + \mu_j = 0$, i.e., $j = -i$, $\boldsymbol{\psi}_i$ and $\boldsymbol{\psi}_{-i}$ satisfy the following relation:

$$\boldsymbol{\psi}_i^{\mathrm{T}} \mathbf{J} \boldsymbol{\psi}_{-i} \neq 0 \qquad (i = 1, 2, \cdots, n) \tag{5.38}$$

Performing the orthonormality operation, we obtain

$$\boldsymbol{\psi}_i^{\mathrm{T}} \mathbf{J} \boldsymbol{\psi}_{-i} = 1 \quad \text{and (or)} \qquad \boldsymbol{\psi}_{-i}^{\mathrm{T}} \mathbf{J} \boldsymbol{\psi}_i = -1 \qquad (i = 1, 2, \cdots, n) \tag{5.39}$$

This indicates that Eq. (5.30) holds true. The adjoint symplectic ortho-normalization relation between eigenfunctions has thus been proved.

Since $\boldsymbol{\psi}_{+i}$ and $\boldsymbol{\psi}_{-i}$ are of adjoint symplectic orthonormalization, the state vector $\boldsymbol{\psi}$ can be expressed by the linear combination of the eigenfunction-vectors as follows:

$$\boldsymbol{\psi} = \sum_{i=1}^{\infty} (a_i \boldsymbol{\psi}_i + b_i \boldsymbol{\psi}_{-i}) \tag{5.40}$$

where $\boldsymbol{\psi}_i$ and $\boldsymbol{\psi}_{-i}$ are eigenfunction-vectors corresponding to μ_i and μ_{-i}, and a_i, b_i are coefficients to be determined.

From Eqs. (5.3) and (2.158) we can obtain the following expressions:

$$\begin{Bmatrix} u \\ w \end{Bmatrix} = r^{\mu} \mathbf{q}(\theta) \tag{5.41}$$

$$\begin{Bmatrix} \sigma_{rz} \\ D_r \end{Bmatrix} = r^{\mu-1} \mathbf{p}(\theta) \tag{5.42}$$

From Eq. (5.42) it can be found that the stresses and electric displacements near the apex of a wedge are proportional to $r^{\mu-1}$; therefore the singularity order of the stresses and electric displacements is $\mathrm{Re}(\mu) - 1$.

It is obvious that the stresses and electric displacements are singular if the real part of μ is less than 1, i.e., $\mathrm{Re}(\mu) < 1$. For the potential energy to be bounded at the crack tip, it is necessary that $\mathrm{Re}(\mu) > 0$. So we focus our attention on the interval

$$0 < \mathrm{Re}(\mu) < 1 \tag{5.43}$$

Using the notation of the stress and electric field intensity factors K^{σ} and K^{D}, Eq. (5.42) can be rewritten as

$$\begin{aligned} \sigma_{rz}(r, \theta) &= K^{\sigma} r^{\lambda^* - 1} f^{\sigma}(\theta), \\ D(r, \theta) &= K^{D} r^{\lambda^* - 1} f^{D}(\theta) \end{aligned} \tag{5.44}$$

where $\lambda^* - 1$ is orders of the stress and electric field singularity, and $f^{\sigma}(\theta)$ and $f^{D}(\theta)$ are the angular functions.

From Eqs. (5.42) and (5.44) it is easy to see that

$$\boldsymbol{\psi}(\theta) = \mathbf{K}\mathbf{f}(\theta), \qquad \lambda^* = \mu \tag{5.45}$$

where

$$\mathbf{K} = \begin{bmatrix} K^{\sigma} & 0 \\ 0 & K^{D} \end{bmatrix}, \qquad \mathbf{f}(\theta) = \left\{ f^{\sigma}(\theta)\ f^{D}(\theta) \right\}^{\mathrm{T}} \tag{5.46}$$

The remaining task is to find the angular function $\mathbf{f}(\theta)$ and the generalized stress and electric displacement intensity factors $\mathbf{K}$. Therefore, we need to find eigenvalues of Eq. (2.156) which satisfy the condition (5.43). To this end, rewriting Eq. (2.156) in terms of its matrix components, we have

$$\begin{bmatrix} -\mu & 0 & f_{55} & g_{15} \\ 0 & -\mu & g_{15} & -\beta_{11} \\ -c_{55}\dfrac{\mathrm{d}^2}{\mathrm{d}\theta^2} & -e_{15}\dfrac{\mathrm{d}^2}{\mathrm{d}\theta^2} & -\mu & 0 \\ -e_{15}\dfrac{\mathrm{d}^2}{\mathrm{d}\theta^2} & \kappa_{11}\dfrac{\mathrm{d}^2}{\mathrm{d}\theta^2} & 0 & -\mu \end{bmatrix} \begin{Bmatrix} w \\ \phi \\ S_r \\ SD_r \end{Bmatrix} = 0 \tag{5.47}$$

The order of singularity in the elastic and electric fields is determined by setting the determinant of the 4×4 matrix in Eq. (5.47) to zero. This is equivalent to

$$\det \begin{bmatrix} -\mu & 0 & f_{55} & g_{15} \\ 0 & -\mu & g_{15} & -\beta_{11} \\ -c_{55}\lambda^2 & -e_{15}\lambda^2 & -\mu & 0 \\ -e_{15}\lambda^2 & \kappa_{11}\lambda^2 & 0 & -\mu \end{bmatrix} = 0 \tag{5.48}$$

where λ is the eigenvalue in the θ direction.

Equation (5.48) leads to the following equation:

$$(\lambda^2 + \mu^2)^2 = 0 \tag{5.49}$$

Thus, the solutions of λ are

$$\lambda_{1,2} = \mu i, \qquad \lambda_{3,4} = -\mu i \tag{5.50}$$

With solution (5.50), the general expressions of the elastic and electric fields can be expressed as

$$\begin{aligned} w = &\quad A_1\cos(\mu\theta) + B_1\sin(\mu\theta) + C_1\theta\cos(\mu\theta) + D_1\theta\sin(\mu\theta),\\ \phi = &\quad A_2\cos(\mu\theta) + B_2\sin(\mu\theta) + C_2\theta\cos(\mu\theta) + D_2\theta\sin(\mu\theta),\\ S_r = &\quad A_3\cos(\mu\theta) + B_3\sin(\mu\theta) + C_3\theta\cos(\mu\theta) + D_3\theta\sin(\mu\theta),\\ SD_r = &\quad A_4\cos(\mu\theta) + B_4\sin(\mu\theta) + C_4\theta\cos(\mu\theta) + D_4\theta\sin(\mu\theta) \end{aligned} \tag{5.51}$$

where $A_i,\ B_i,\ C_i,\ D_i\ \ (i = 1\text{-}4)$ are unknown constants to be determined.

Substituting Eq. (5.51) into Eq. (5.47) yields the following relationships among the four unknown constants :

$$\begin{aligned} A_3 &= \mu(c_{55}A_1 + e_{15}A_2), \qquad A_4 = \mu(e_{15}A_1 - \kappa_{11}A_2),\\ B_3 &= \mu(c_{55}B_1 + e_{15}B_2), \qquad B_4 = \mu(e_{15}B_1 - \kappa_{11}B_2),\\ D_i &= C_i = 0 \qquad (i = 1\text{-}4) \end{aligned} \tag{5.52}$$

Then Eq. (5.51) can be rewritten as

$$\begin{aligned} &\begin{Bmatrix} w \\ \phi \end{Bmatrix} = \begin{bmatrix} A_1 & B_1 \\ A_2 & B_2 \end{bmatrix} \begin{Bmatrix} \cos(\mu\theta) \\ \sin(\mu\theta) \end{Bmatrix},\\ &\begin{Bmatrix} S_r \\ SD_r \end{Bmatrix} = \mu \begin{bmatrix} c_{55} & e_{15} \\ e_{15} & -\kappa_{11} \end{bmatrix} \begin{Bmatrix} A_1 \\ A_2 \end{Bmatrix} \cos(\mu\theta) + \mu \begin{bmatrix} c_{55} & e_{15} \\ e_{15} & -\kappa_{11} \end{bmatrix} \begin{Bmatrix} B_1 \\ B_2 \end{Bmatrix} \sin(\mu\theta) \end{aligned} \tag{5.53}$$

From Eqs. (1.35) and (5.53) we have

$$\begin{Bmatrix} S_\theta \\ SD_\theta \end{Bmatrix} = \mu \begin{bmatrix} c_{55} & e_{15} \\ e_{15} & -\varepsilon_{11} \end{bmatrix} \begin{bmatrix} A_1 & B_1 \\ A_2 & B_2 \end{bmatrix} \begin{Bmatrix} -\sin(\mu\theta) \\ \cos(\mu\theta) \end{Bmatrix} \tag{5.54}$$

To obtain explicit expression of the four unknown constants, consider a piezoelectric wedge as shown in Fig. 5.1. The conditions at the boundary edges are assumed to be free of traction and electrically insulated:

$$\sigma_{\theta z}(r,\alpha) = \sigma_{\theta z}(r,-\beta) = D_\theta(r,\alpha) = D_\theta(r,-\beta) = 0 \tag{5.55}$$

Subsitituting Eqs. (5.53) and (5.54) into Eq. (5.55) yields

$$\begin{bmatrix} -c_{55}\sin(\mu\alpha) & -e_{15}\sin(\mu\alpha) & c_{55}\cos(\mu\alpha) & e_{15}\cos(\mu\alpha) \\ -e_{15}\sin(\mu\alpha) & \varepsilon_{11}\sin(\mu\alpha) & e_{15}\cos(\mu\alpha) & -\varepsilon_{11}\cos(\mu\alpha) \\ c_{55}\sin(\mu\beta) & e_{15}\sin(\mu\beta) & c_{55}\cos(\mu\beta) & e_{15}\cos(\mu\beta) \\ e_{15}\sin(\mu\beta) & -\varepsilon_{11}\sin(\mu\beta) & e_{15}\cos(\mu\beta) & -\varepsilon_{11}\cos(\mu\beta) \end{bmatrix} \begin{Bmatrix} A_1 \\ A_2 \\ B_1 \\ B_2 \end{Bmatrix} = 0 \tag{5.56}$$

The condition for the existence of non-zero solutions of $\{A_1\ A_2\ B_1\ B_2\}^{\mathrm{T}}$ is that the determinant of the coefficients matrix is zero, which leads to the following equation:

$$(c_{55}\varepsilon_{11} + e_{15}^2)^2 \sin^2\left[\mu(\alpha+\beta)\right] = 0 \tag{5.57}$$

If $\alpha = \beta = \pi$, we have $\mu = 1/2$, and the order of singularity is –1/2, which is

the classical root singularity for a semi-infinite crack. This result also verifies the validity of this method for the case of a semi-infinite crack.

Consider now a piezoelectric half-plane, i.e., $\alpha = \beta = \pi/2$. It can be easily found that no root of Eq. (5.57) can satisfy the condition $0 < \mathrm{Re}(\mu) < 1$. Therefore, there is no singularity for the piezoelectric half-plane under the homogeneous boundary condition. We also note that the singularity disappears for $\alpha + \beta \leqslant 180°$. For $180° < \alpha + \beta < 360°$, the variation of the order of singularity with $\alpha + \beta$ is plotted in Fig. 5.2. It can be seen that for a homogeneous piezoelectric wedge, the order of singularity depends on the value of $\alpha + \beta$ only.

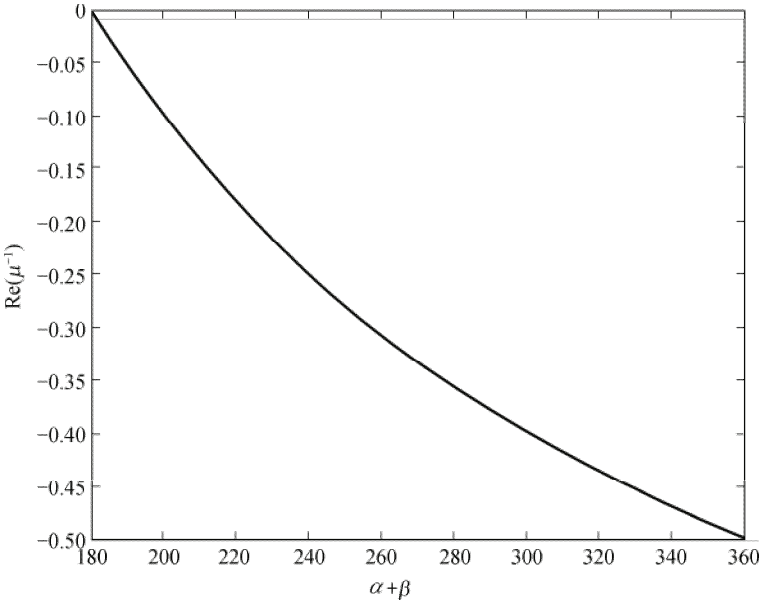

Fig. 5.2 Variation of order of singularity with $\alpha + \beta$ for a piezoelectric wedge.

It should be mentioned that for the sake of simplicity only one type of boundary condition on the edges, given as Eq. (5.55), is considered. However, for other types of boundary conditions such as clamped ($w = 0$) and electrically open ($\phi = 0$), this procedure is also applicable and the results can be obtained in a similar way.

5.2.4 Piezoelectric bimaterial wedge

For a piezoelectric bimaterial wedge as shown in Fig. 5.3, the boundary conditions are as follows:

$$\sigma_{\theta z}^{(1)}(r,\alpha)=\sigma_{\theta z}^{(2)}(r,-\beta)=D_{\theta}^{(1)}(r,\alpha)=D_{\theta}^{(2)}(r,-\beta)=0 \tag{5.58}$$

If the bimaterials are rigidly bonded at the interface, the continuity conditions on the interface are

$$\begin{aligned}&\sigma_{\theta z}^{(1)}(r,0)=\sigma_{\theta z}^{(2)}(r,0), \qquad w^{(1)}(r,0)=w^{(2)}(r,0),\\ &D_{\theta}^{(1)}(r,0)=D_{\theta}^{(2)}(r,0), \qquad E_{r}^{(1)}(r,0)=E_{r}^{(2)}(r,0)\end{aligned} \tag{5.59}$$

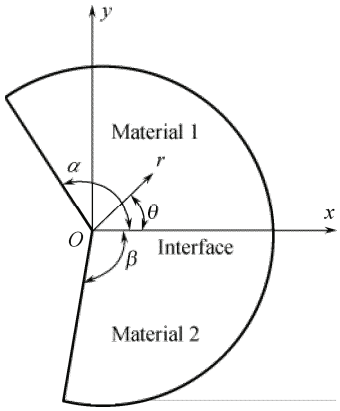

Fig. 5.3 Piezoelectric bimaterial wedge.

in which superscripts (1) and (2) denote materials 1 and 2, respectively.

As shown in Fig. 5.3, each material can be viewed as a homogeneous wedge. Using the general solution (5.53) of a homogeneous piezoelectric wedge and the continuity condition at its interface, we can easily obtain the solution for a bimaterial wedge. Keeping this in mind, substituting the solutions (5.53) and (5.54) for each material into Eq. (5.59) yields the relationship between the unknown constants:

$$\begin{bmatrix}B_1^{(2)}\\ B_2^{(2)}\end{bmatrix}=\begin{bmatrix}a_{11} & a_{12}\\ a_{21} & a_{22}\end{bmatrix}\begin{bmatrix}B_1^{(1)}\\ B_2^{(1)}\end{bmatrix} \tag{5.60}$$

in which

$$\begin{aligned}a_{11}&=\frac{1}{\Delta_2}(\kappa_{11}^{(2)}c_{55}^{(1)}+e_{15}^{(2)}e_{15}^{(1)}), \qquad a_{12}=\frac{1}{\Delta_2}(\kappa_{11}^{(2)}e_{15}^{(1)}-e_{15}^{(2)}\kappa_{11}^{(1)}),\\ a_{21}&=\frac{1}{\Delta_2}(e_{15}^{(2)}c_{55}^{(1)}-c_{55}^{(2)}e_{15}^{(1)}), \qquad a_{22}=\frac{1}{\Delta_2}(e_{15}^{(2)}e_{15}^{(1)}+c_{55}^{(2)}\kappa_{11}^{(1)})\end{aligned} \tag{5.61}$$

where

$$\Delta_2=c_{55}^{(2)}\kappa_{11}^{(2)}+(e_{15}^{(2)})^2 \tag{5.62}$$

Using the relation (5.60) and substituting the solutions (5.53) and (5.54) into Eq. (5.58) lead to

$$\begin{bmatrix} -c_{55}^{(1)}\sin(\mu\alpha) & -e_{15}^{(1)}\sin(\mu\alpha) & c_{55}^{(1)}\cos(\mu\alpha) \\ -e_{15}^{(1)}\sin(\mu\alpha) & \kappa_{11}^{(1)}\sin(\mu\alpha) & e_{15}^{(1)}\cos(\mu\alpha) \\ c_{55}^{(2)}\sin(\mu\beta) & e_{15}^{(2)}\sin(\mu\beta) & \left[c_{55}^{(2)}a_{11}+e_{15}^{(2)}a_{21}\right]\cos(\mu\beta) \\ e_{15}^{(2)}\sin(\mu\beta) & -\kappa_{11}^{(1)}\sin(\mu\beta) & \left[e_{15}^{(2)}a_{11}-\kappa_{11}^{(2)}a_{21}\right]\cos(\mu\beta) \end{bmatrix}$$

$$\begin{bmatrix} e_{15}^{(1)}\cos(\mu\alpha) \\ -\kappa_{11}^{(1)}\cos(\mu\alpha) \\ \left[c_{55}^{(2)}a_{12}+e_{15}^{(2)}a_{22}\right]\cos(\mu\beta) \\ \left[e_{15}^{(2)}a_{12}-\kappa_{11}^{(2)}a_{22}\right]\cos(\mu\beta) \end{bmatrix} \begin{Bmatrix} A_1^{(1)} \\ A_2^{(2)} \\ B_1^{(1)} \\ B_2^{(2)} \end{Bmatrix} = 0 \tag{5.63}$$

The non-zero solution of Eq. (5.63) requires that

$$\begin{aligned} &(c_{55}^{(1)}\kappa_{11}^{(1)}+e_{15}^{(1)2})\sin^2(\mu\alpha)\cos^2(\mu\beta)+(c_{55}^{(2)}\kappa_{11}^{(1)}+e_{15}^{(2)2})\sin^2(\mu\beta)\cos^2(\mu\alpha) \\ &+(c_{55}^{(1)}\kappa_{11}^{(2)}+2e_{15}^{(1)}e_{15}^{(2)}+c_{55}^{(2)}\kappa_{11}^{(1)})\sin(\mu\alpha)\sin(\mu\beta)\cos(\mu\alpha)\cos(\mu\beta)=0 \end{aligned} \tag{5.64}$$

Equation (5.64) can be further written as

$$\sin^2\left[\mu(\alpha+\beta)\right]+R_1\sin^2\left[\mu(\alpha-\beta)\right]=R_2\sin\left[\mu(\alpha+\beta)\right]\sin\left[\mu(\alpha-\beta)\right] \tag{5.65}$$

with

$$\begin{aligned} R_1&=\frac{A_{11}+A_{22}-A_{12}-A_{21}}{A_{11}+A_{22}+A_{12}+A_{21}}, & R_2&=\frac{2(A_{22}-A_{11})}{A_{11}+A_{22}+A_{12}+A_{21}}, \\ A_{11}&=e_{15}^{(1)}e_{15}^{(1)}+c_{55}^{(1)}\kappa_{11}^{(1)}, & A_{12}&=e_{15}^{(1)}e_{15}^{(2)}+\kappa_{11}^{(1)}c_{55}^{(2)}, \\ A_{21}&=e_{15}^{(2)}e_{15}^{(1)}+\kappa_{11}^{(2)}c_{55}^{(1)}, & A_{22}&=e_{15}^{(2)}e_{15}^{(2)}+c_{55}^{(2)}\kappa_{11}^{(2)} \end{aligned} \tag{5.66}$$

It is found that Eq. (5.65) is exactly the same as the equations of Chue and Chen [25]. For an interface crack, i.e., $\alpha=\beta=\pi$, we have $\mu=-1/2$, which returns to a classical –1/2 singularity. For other values of α and β, Eq. (5.65) shows that the order of singularity strongly depends on the geometry and material constants of the two piezoelectric materials. Moreover, the angular function and generalized stress and electrical intensity factors K^{σ} and K^{D} can also be obtained easily using this method. Compared to the conventional method [26], the symplectic model reviewed in this section [20] can solve singularity problems more rationally. Particularly, with an increase in the number of materials, the conventional method would induce a large number of complex equation systems which may be difficult to solve theoretically.

5.2.5 Multi-piezoelectric material wedge

In the previous two subsections the theory of Hamiltonian systems was used to develop symplectic models of a piezoelectric wedge and then to determine the orders of singularity for both a homogeneous wedge and a bimaterial wedge. Now the results obtained are extended to the case of multi-piezoelectric materials. To this end, consider a piezoelectric wedge consisting of multi-piezoelectric material elements as shown in Fig. 5.4, which is similar to the multi-elastic material wedge in [27]. Here N is the number of material elements. The polar coordinate is again selected for simplicity, and $C_0, C_1, \cdots, C_N$ are adopted to indicate the 0-N sub-polar coordinate systems. The domain Ω_i denotes the material element M_i, and α_i is the angle of M_i.

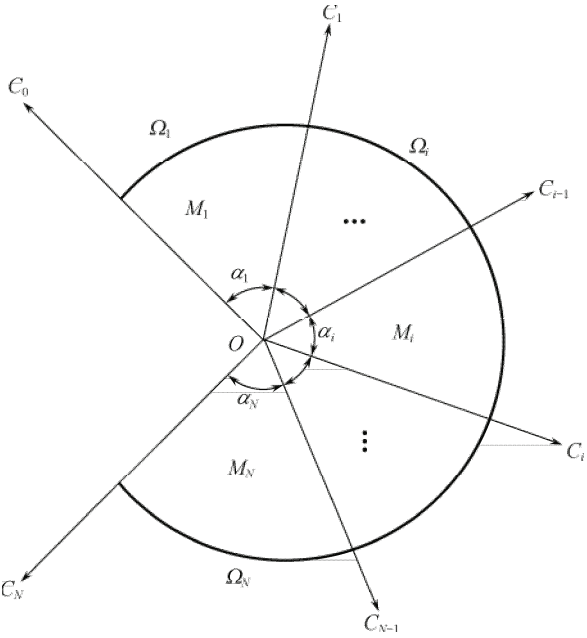

Fig. 5.4 Multi-piezoelectric material wedge.

The continuity conditions on the bonded interface region are

$$\begin{aligned} \sigma_{\theta z}^{(i)}(r,0) &= \sigma_{\theta z}^{(i+1)}(r,0), \qquad w^{(i)}(r,0) = w^{(i+1)}(r,0), \\ D_{\theta}^{(i)}(r,0) &= D_{\theta}^{(i+1)}(r,0), \qquad E_r^{(i)}(r,0) = E_r^{(i+1)}(r,0) \end{aligned} \tag{5.67}$$

in which the superscript "i" runs from 1 to N-1 which represents the associated variable which is defined in the domain Ω_i. It should be mentioned that the fields in

the two adjacent regions Ω_i and Ω_{i+1} in Eq. (5.67) are written in terms of the coordinate system C_i with both regions having $\theta = 0$ at the interface. This is for the sake of simplicity.

The boundary conditions of this problem are

$$\sigma_{\theta z}^{(1)}(r,\alpha_1) = D_{\theta}^{(1)}(r,\alpha_1) = \sigma_{\theta z}^{(N)}(r,-\alpha_N) = D_{\theta}^{(N)}(r,-\alpha_N) = 0 \tag{5.68}$$

Note that solution (5.53) also applies for each single domain Ω_i. Thus, substitution of the general solutions (5.53) for the domain Ω_i and Ω_{i+1} into Eq. (5.67) yields the relationship of the unknown constants for any two adjacent domains as follows:

$$\left\{F_i^{i+1}\right\} = \left[R(i,i+1)\right]\left\{F_i^{i}\right\} \tag{5.69}$$

where

$$\left[R(i,i+1)\right] = \begin{bmatrix} 1 & 0 & 0 & 0 \\ 0 & 1 & 0 & 0 \\ 0 & 0 & r_{11} & r_{12} \\ 0 & 0 & r_{21} & r_{22} \end{bmatrix} \tag{5.70}$$

$$\left\{F_i^{i+1}\right\} = \begin{bmatrix} A_{1i}^{i+1} & A_{2i}^{i+1} & B_{1i}^{i+1} & B_{2i}^{i+1} \end{bmatrix} \tag{5.71}$$

and

$$\begin{aligned} r_{11} &= \frac{1}{\Delta_{i+1}}(\kappa_{11}^{(i+1)}c_{55}^{(i)} + e_{15}^{(i+1)}e_{15}^{(i)}), \qquad r_{12} = \frac{1}{\Delta_{i+1}}(\kappa_{11}^{(i+1)}e_{15}^{(i)} - e_{15}^{(i+1)}\kappa_{11}^{(i)}), \\ r_{21} &= \frac{1}{\Delta_{i+1}}(e_{15}^{(i+1)}c_{55}^{(i)} - c_{55}^{(i+1)}e_{15}^{(i)}), \qquad r_{22} = \frac{1}{\Delta_{i+1}}(e_{15}^{(i+1)}e_{15}^{(i)} + c_{55}^{(i+1)}\kappa_{11}^{(i)}) \end{aligned} \tag{5.72}$$

with

$$\Delta_n = c_{55}^{(n)}\kappa_{11}^{(n)} + \left(e_{15}^{(n)}\right)^2 \tag{5.73}$$

In Eq. (5.69), the subscript "i" represents the unknown constants expressed in terms of the coordinates C_i, and the superscripts "i" and "i+1" mean the domains Ω_i, Ω_{i+1}, respectively.

In the following, the coordinate transformation is used to find the relationships between the unknown constants in general solutions of each material domain Ω_i in two coordinate systems C_i and C_{i-1}. Assuming the equality

$$\begin{Bmatrix} w_i^i \\ \phi_i^i \end{Bmatrix} = \begin{Bmatrix} w_{i-1}^i \\ \phi_{i-1}^i \end{Bmatrix} \tag{5.74}$$

and using the relationships among the trigonometric functions, we obtain

$$\left\{F_i^i\right\} = \left[T(i,i-1)\right]\left\{F_{i-1}^i\right\} \tag{5.75}$$

where

$$\left[T(i,i-1)\right] = \begin{bmatrix} \cos(\mu\alpha_i) & 0 & -\sin(\mu\alpha_i) & 0 \\ 0 & \cos(\mu\alpha_i) & 0 & -\sin(\mu\alpha_i) \\ \sin(\mu\alpha_i) & 0 & \cos(\mu\alpha_i) & 0 \\ 0 & \sin(\mu\alpha_i) & 0 & \cos(\mu\alpha_i) \end{bmatrix} \tag{5.76}$$

The combination of Eqs. (5.69) and (5.75) yields the relationship

$$\left\{F_{N-1}^N\right\} = \left[TR_N\right]\left\{F_1^1\right\} \tag{5.77}$$

where

$$\left[TR_N\right] = \prod_{i=N-1}^{2}\left\{\left[R(i,i+1)\right]\left[T(i,i-1)\right]\right\}\left[R(1,2)\right] \tag{5.78}$$

It can be seen from Eq. (5.77) that solutions in any domain can be expressed by four independent unknown constants defined in Ω_1. Considering the boundary conditions (5.68), we obtain

$$\left[M\right]\left\{F_1^1\right\} = 0 \tag{5.79}$$

where $\left[M\right]$ is a 4×4 matrix which has a similar form to that in Eq. (5.63). The existence of a nontrivial solution for $\left\{F_1^1\right\}$ requires deletion of the coefficients matrix $\left[M\right]$:

$$\det\left[M\right] = 0 \tag{5.80}$$

Then, the solution for μ can be obtained by solving Eq. (5.80), and the order of singularity is again $\mathrm{Re}(\mu)-1$ by considering the condition in Eq. (5.43).

It should be mentioned that Eq. (5.80) is highly nonlinear in terms of the variable μ and therefore an analytical solution to μ is usually impossible except for a few simple cases. In the following, our focus is on a numerical solution only. For illustration, consider a three-material wedge in which Materials 1 and 3 are assumed to be PZT-4, and Material 2 is PZT-5 (see Fig. 5.5). The material properties used are

PZT-4: $c_{55} = 25.6\times 10^9$ N/m^2, $e_{15} = 12.7$ C/N, $\kappa_{11} = 6.46\times 10^{-9}$ F/m;

PZT-5: $c_{55} = 21.1\times 10^9$ N/m^2, $e_{15} = 12.3$ C/N, $\kappa_{11} = 8.11\times 10^{-9}$ F/m.

As an example, Table 5.1 lists the orders of singularity for different values of

α_1 and $e_{15}^{(1)}$ when $\alpha_2 = \alpha_3 = \pi/3$. It can be seen from Table 5.1 that a pair of complex or two real singularity orders exist for some values of α_1 (e.g., two real singularity orders for $\alpha_1 = \pi/3$ and a pair of complex roots for $\alpha_1 = \pi$) or for some values of $e_{15}^{(1)}$. It is found from Table 5.1 that at $\alpha_1 = 2\pi/3$ the singularity order may be complex or real, depending on the values of $e_{15}^{(1)}$, which indicates that $e_{15}^{(1)}$ can affect the singularity order to some extent. Furthermore, the singularity order may become zero for some special values of α_1 and $e_{15}^{(1)}$. In conclusion, the order of singularity is a function of geometry and material constants for a multi-piezoelectric material wedge.

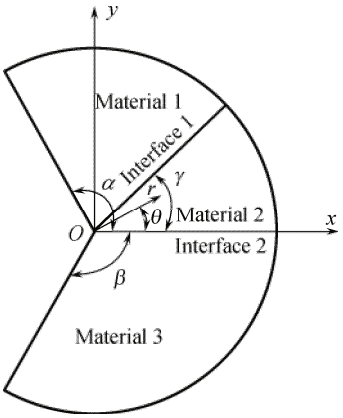

Fig. 5.5 Piezoelectric wedge of three dissimilar materials.

To prove the validity of the proposed formulation, two cases are considered as follows:

Case 1: $\alpha_1 = \alpha_2 = \pi, \quad \alpha_3 = 0$;

Case 2: $\alpha_1 = \alpha_3 = \pi, \quad \alpha_2 = 0$.

The singularity order for both cases is –1/2, which is identical with the result for an interface crack.

Table 5.1 Singularity order of a piezoelectric wedge of three dissimilar materials for different values of α_1 and $e_{15} = 12.7\ \mathrm{C/N}$ when α_2=α_3=π/3.

α_1	$e_{15}^{(1)} = 0.8e_{15}$	$e_{15}^{(1)} = 0.9e_{15}$	$e_{15}^{(1)} = e_{15}$	$e_{15}^{(1)} = 1.1e_{15}$	$e_{15}^{(1)} = 1.2e_{15}$
π/3	–0.269	–0.300	–0.324	–0.339	–0.339
2π/3	–0.783	–0.765	–0.812	0	–0.913
π	–0.959	0	0	–0.985	–0.956
4π/3	–0.079	–0.086	–0.090	–0.084	–0.095

5.3 Extension to include magnetic effect

In the last section a symplectic model for an anti-plane piezoelectric wedge was presented. Extension to anti-plane fracture problems of magnetoelectroelastic media is discussed in this section. All descriptions in this section are taken from the work of Zhou et al. [17].

5.3.1 Basic equations and their Hamiltonian system

Consider a two-dimensional magnetoelectroelastic wedge with $\beta = -\alpha$ as shown in Fig. 5.1. The constitutive equation (1.35) is extended to include the effect of the magnetic field as follows:

$$\begin{Bmatrix} \sigma_{rz} \\ \sigma_{\theta z} \\ D_r \\ D_\theta \\ B_r \\ B_\theta \end{Bmatrix} = \begin{bmatrix} c_{55} & 0 & -e_{15} & 0 & -\tilde{e}_{15} & 0 \\ 0 & c_{55} & 0 & -e_{15} & 0 & -\tilde{e}_{15} \\ e_{15} & 0 & \kappa_{11} & 0 & \alpha_{11} & 0 \\ 0 & e_{15} & 0 & \kappa_{11} & 0 & \alpha_{11} \\ \tilde{e}_{15} & 0 & \alpha_{11} & 0 & \mu_{11} & 0 \\ 0 & \tilde{e}_{15} & 0 & \alpha_{11} & 0 & \mu_{11} \end{bmatrix} \begin{Bmatrix} \gamma_{rz} \\ \gamma_{\theta z} \\ E_r \\ E_\theta \\ H_r \\ H_\theta \end{Bmatrix} \tag{5.81}$$

where $\tilde{e}_{15}$, α_{11}, and μ_{11} are, respectively, piezomagnetic, electromagnetic, and magnetic permeability coefficients. The equations of shear strain-displacement and electric field-electric potential are given by Eq. (5.2). The magnetic field-magnetic potential equation is expressed as

$$H_r = -\frac{\partial \psi}{\partial r}, \qquad H_\theta = -\frac{1}{r}\frac{\partial \psi}{\partial \theta} \tag{5.82}$$

The corresponding governing field equations are given by Eq. (5.1) and

$$\frac{\partial (rB_r)}{\partial r} + \frac{\partial B_\theta}{\partial \theta} + rI = 0 \tag{5.83}$$

where I is the body electric current. Zhou et al. [17] then presented the following potential energy density:

$$\begin{aligned} 2U = {} & c_{55}\left(\frac{\partial w}{\partial r}\right)^2 + c_{55}\left(\frac{1}{r}\frac{\partial w}{\partial \theta}\right)^2 - \kappa_{11}\left(\frac{\partial \phi}{\partial r}\right)^2 - \kappa_{11}\left(\frac{\partial \phi}{r\partial \theta}\right)^2 - \mu_{11}\left(\frac{\partial \psi}{\partial r}\right)^2 - \mu_{11}\left(\frac{\partial \psi}{r\partial \theta}\right)^2 \\ & + 2e_{15}\left(\frac{\partial w}{\partial r}\frac{\partial \phi}{\partial r} + \frac{1}{r^2}\frac{\partial w}{\partial \theta}\frac{\partial \phi}{\partial \theta}\right) + 2\tilde{e}_{15}\left(\frac{\partial w}{\partial r}\frac{\partial \psi}{\partial r} + \frac{1}{r^2}\frac{\partial w}{\partial \theta}\frac{\partial \psi}{\partial \theta}\right) \\ & - 2\alpha_{15}\left(\frac{\partial \phi}{\partial r}\frac{\partial \psi}{\partial r} - \frac{1}{r^2}\frac{\partial \phi}{\partial \theta}\frac{\partial \psi}{\partial \theta}\right) \end{aligned} \tag{5.84}$$

Then the Lagrange function L is

$$L(w,\phi,\psi) = U(w,\phi,\psi) - wf_z - \phi Q - \psi I \tag{5.85}$$

Zhou et al. then presented a new Lagrange function $\tilde{L}$ using the variable ξ defined in Eq. (5.5) as

$$\begin{aligned} 2\tilde{L}(\xi) = e^{2\xi}L(w,\phi,\psi) = c_{55}\dot{w}^2 + c_{55}\left(\frac{\partial w}{\partial\theta}\right)^2 - \kappa_{11}\dot{\phi}^2 - \kappa_{11}\left(\frac{\partial\phi}{\partial\theta}\right)^2 - \mu_{11}\dot{\psi}^2 \\ -\mu_{11}\left(\frac{\partial\psi}{\partial\theta}\right)^2 + 2e_{15}\left(\dot{w}\dot{\phi} + \frac{\partial w}{\partial\theta}\frac{\partial\phi}{\partial\theta}\right) + 2\tilde{e}_{15}\left(\dot{w}\dot{\psi} + \frac{\partial w}{\partial\theta}\frac{\partial\psi}{\partial\theta}\right) \\ -2\alpha_{15}\left(\dot{\phi}\dot{\psi} - \frac{1}{r^2}\frac{\partial\phi}{\partial\theta}\frac{\partial\psi}{\partial\theta}\right) - 2e^{2\xi}(wf_z - \phi Q - \psi I) \end{aligned} \tag{5.86}$$

Then, the Hamiltonian equation (2.138) can be obtained by defining the generalized displacement vector **q** and the dual vector **p** as

$$\mathbf{q} = \{w\ \phi\ \psi\}^{\mathrm{T}},$$

$$\mathbf{p} = \frac{\partial\tilde{L}}{\partial\dot{\mathbf{q}}} = \mathbf{c}\dot{\mathbf{q}} = \begin{bmatrix} c_{55} & e_{15} & \tilde{e}_{15} \\ e_{15} & -\kappa_{11} & -\alpha_{11} \\ \tilde{e}_{15} & -\alpha_{11} & -\mu_{11} \end{bmatrix} \begin{Bmatrix} \dot{w} \\ \dot{\phi} \\ \dot{\psi} \end{Bmatrix} = \begin{Bmatrix} S_r \\ SD_r \\ SB_r \end{Bmatrix} \tag{5.87}$$

where **c** is self-defined, S_r and SD_r are defined in Eq. (5.4), and $SB_r = rB_r$. Based on the mutual duality of the vectors **q** and **p**, the corresponding Hamiltonian function H can be expressed in the form

$$H(\mathbf{q},\mathbf{p}) = \mathbf{p}^{\mathrm{T}}\dot{\mathbf{q}} - \tilde{L}(\mathbf{q},\dot{\mathbf{q}}) \tag{5.88}$$

Substitution of Eq. (5.88) into Eq. (2.136) yields the Hamiltonian equation (2.318) with

$$\mathbf{H} = \begin{bmatrix} 0 & \mathbf{c}^{-1} \\ -\mathbf{c}\dfrac{\partial^2}{\partial\theta^2} & 0 \end{bmatrix}, \qquad \mathbf{h} = \begin{Bmatrix} 0 \\ \mathbf{h}_2 \end{Bmatrix} \tag{5.89}$$

where $\mathbf{h}_2 = -e^{2\xi}\{f_z\ Q\ I\}^{\mathrm{T}}$.

5.3.2 Eigenvalues and eigenfunctions

In the following, Zhou et al. [17] presented both zero- and nonzero-eigenvalue solutions for anti-plane crack problems of magnetoelectroelastic media. They consid-

ered only the homogeneous Eq. (2.138) with the the following traction-free, electrically and magnetically insulated natural boundary conditions:

$$\mathbf{c}\frac{\partial \mathbf{q}}{\partial \theta}\bigg|_{\theta=\pm\pi} = 0 \tag{5.90}$$

5.3.2.1 Zero-eigenvalue solutions

For analyzing the problem of zero-eigenvalue, when $\mu_j = 0$, the solutions of the equation, $\mathbf{H}\mathbf{v}_j = 0$, are required and the direct eigenfunctions and their principal vectors in Jordan form can be obtained. Zhou et al. showed that there are only six eigensolutions corresponding to zero-eigenvalue. They are divided into two groups (α and β):

$$\begin{cases} \mathbf{v}_1^{(\alpha)} = \{1\,0\,0\,0\,0\,0\}^{\mathrm{T}} \\ \mathbf{v}_2^{(\alpha)} = \{0\,1\,0\,0\,0\,0\}^{\mathrm{T}}, \\ \mathbf{v}_3^{(\alpha)} = \{0\,0\,1\,0\,0\,0\}^{\mathrm{T}} \end{cases} \quad \text{and} \quad \begin{cases} \mathbf{v}_4^{(\beta)} = \tilde{\rho}_1\{\ \xi \quad \chi_1\xi \quad \chi_2\xi - \chi/\chi_7 \quad 0 \quad 0\}^{\mathrm{T}} \\ \mathbf{v}_5^{(\beta)} = \tilde{\rho}_2\{\chi_3\xi \quad \xi \quad \chi_4\xi \quad 0 \quad -\chi/\chi_8 \quad 0\}^{\mathrm{T}} \\ \mathbf{v}_6^{(\beta)} = \tilde{\rho}_3\{\chi_5\xi\ \chi_6\xi \quad \xi \quad 0 \quad 0\ -\chi/\chi_9\}^{\mathrm{T}} \end{cases} \tag{5.91}$$

which satisfy the relationship

$$\begin{aligned} &\langle \mathbf{v}_n^{(\alpha)\mathrm{T}},\ \mathbf{J},\ \mathbf{v}_k^{(\alpha)} \rangle = \langle \mathbf{v}_n^{(\beta)\mathrm{T}},\ \mathbf{J},\ \mathbf{v}_k^{(\beta)} \rangle = 0, \\ &\langle \mathbf{v}_n^{(\alpha)\mathrm{T}},\ \mathbf{J},\ \mathbf{v}_k^{(\beta)} \rangle = \delta_{nk}, \quad \langle \mathbf{v}_n^{(\beta)\mathrm{T}},\ \mathbf{J},\ \mathbf{v}_k^{(\alpha)} \rangle = -\delta_{nk} \end{aligned} \tag{5.92}$$

In the solutions (5.91), the parameters are defined as:

$$\chi = \det|\boldsymbol{c}|,\ \chi_1{=}\chi_{10}/\chi_7,\ \chi_2{=}\chi_{11}/\chi_7,\ \chi_3{=}\chi_{10}/\chi_8,\ \chi_4{=}\chi_{12}/\chi_8,\ \chi_5{=}\chi_{11}/\chi_9,\ \chi_6{=}\chi_{12}/\chi_9,$$
$$\chi_7 = \alpha_{11}^2 - \kappa_{11}\mu_{11},\ \chi_8 = \tilde{e}_{15}^2 + c_{55}\mu_{11},\ \chi_9 = e_{15}^2 + c_{55}\kappa_{11},\ \chi_{10} = \alpha_{11}\tilde{e}_{15} - e_{15}\mu_{11},$$
$$\chi_{11} = \alpha_{11}e_{15} - \tilde{e}_{15}\kappa_{11},\quad \chi_{12} = -(c_{55}\alpha_{11} + e_{15}\tilde{e}_{15}),\quad \tilde{\rho}_1 = -\chi_7/(2\pi\chi),$$
$$\tilde{\rho}_2 = -\chi_8/(2\pi\chi),\quad \tilde{\rho}_3 = -\chi_9/(2\pi\chi)$$

5.3.2.2 Nonzero-eigenvalue solutions

To find the solution of Eq. (2.156) where $\mu \neq 0$, the characteristic determinant equation is $(\lambda^2{+}\mu^2)^3{=}0$, whose six roots are $\lambda{=}i\mu$ (triple root) and $\lambda{=}{-}i\mu$ (triple root). The general solution of Eq. (2.156) can be written as

$$\boldsymbol{\psi}_j = \begin{Bmatrix} r_{11} + r_{13}\theta + r_{15}\theta^2 \\ r_{21} + r_{23}\theta + r_{25}\theta^2 \\ r_{31} + r_{33}\theta + r_{35}\theta^2 \\ r_{41} + r_{43}\theta + r_{45}\theta^2 \\ r_{51} + r_{53}\theta + r_{55}\theta^2 \\ r_{61} + r_{63}\theta + r_{65}\theta^2 \end{Bmatrix} \cos(\mu\theta) + \begin{Bmatrix} r_{12} + r_{14}\theta + r_{16}\theta^2 \\ r_{22} + r_{24}\theta + r_{26}\theta^2 \\ r_{32} + r_{34}\theta + r_{36}\theta^2 \\ r_{42} + r_{44}\theta + r_{46}\theta^2 \\ r_{52} + r_{54}\theta + r_{56}\theta^2 \\ r_{62} + r_{64}\theta + r_{66}\theta^2 \end{Bmatrix} \sin(\mu\theta) \tag{5.93}$$

where r_{mn} (m, n=1-6) are constants to be determined from boundary conditions. Substituting the solutions into Eq. (2.156), the following relationships between the unknown constants are obtained: $\{r_{4n}\ r_{5n}\ r_{6n}\}^{\mathrm{T}} = \mu \boldsymbol{c}\{r_{1n}\ r_{2n}\ r_{3n}\}^{\mathrm{T}}$ (n=1,2); r_{mn}=0 for m=1-6 and n=3-6. As a result, the solution (5.93) can be simplified to

$$\boldsymbol{\psi}_j = \{r_{11}\ r_{21}\ r_{31}\ r_{41}\ r_{51}\ r_{61}\}^{\mathrm{T}} \cos(\mu\theta) + \{r_{12}\ r_{22}\ r_{32}\ r_{42}\ r_{52}\ r_{62}\}^{\mathrm{T}} \sin(\mu\theta) \quad (5.94)$$

Substituting the solutions (5.94) into the traction-free conditions $r\sigma_{\theta z}\big|_{\theta=\pm\alpha} = 0$, electrically and magnetically impermeable $rD_\theta\big|_{\theta=\pm\alpha} = rB_\theta\big|_{\theta=\pm\alpha} = 0$ on the lateral boundary, we have

$$\begin{bmatrix} -\sin(\mu\pi) & \cos(\mu\pi) & 0 & 0 & 0 & 0 \\ \sin(\mu\pi) & \cos(\mu\pi) & 0 & 0 & 0 & 0 \\ 0 & 0 & -\sin(\mu\pi) & \cos(\mu\pi) & 0 & 0 \\ 0 & 0 & \sin(\mu\pi) & \cos(\mu\pi) & 0 & 0 \\ 0 & 0 & 0 & 0 & -\sin(\mu\pi) & \cos(\mu\pi) \\ 0 & 0 & 0 & 0 & \sin(\mu\pi) & \cos(\mu\pi) \end{bmatrix} \begin{Bmatrix} r_{11} \\ r_{12} \\ r_{21} \\ r_{22} \\ r_{31} \\ r_{32} \end{Bmatrix} = 0 \quad (5.95)$$

The non-trivial solutions of Eq. (5.95) require that the determinant of its coefficient matrix is zero, which leads to

$$\mu_j = j/2 \qquad \left(j = \pm 1, \pm 2, \cdots (\text{triple root})\right) \quad (5.96)$$

It is obvious that μ_1=1/2 represents the order of singularity at the apex of the crack under consideration. For the crack problems, each eigenvalue is a triple root, thus there are three groups of nonzero-eigenvalue solutions. Substituting eigenvalues (5.96) into Eq. (5.95), let $r_{k1}/r_{k2} = r_k \cos(\mu\pi)/\sin(\mu\pi)$, where r_k are new constants to be determined. Then, the nonzero-eigenvalue solutions can be written as

$$\boldsymbol{\psi}_j = \{r_1\ r_2\ r_3\ \mu_j r_4\ \mu_j r_5\ \mu_j r_6\}^{\mathrm{T}} \cos[\mu_j(\theta - \pi)] \quad (5.97)$$

where $\{r_4\ r_5\ r_6\}^{\mathrm{T}} = \boldsymbol{c}\{r_1\ r_2\ r_3\}^{\mathrm{T}}$.

Zhou et al. [17] mentioned that each nonzero-eigenfunction can be represented by three nonlinear correlation eigenfunctions. Similar to the zero-eigenvalue solutions, these nonlinear correlation eigenfunctions need to be adjoint symplectic ortho-normalized and can be separated into two groups (α and β):

$$\begin{aligned} \boldsymbol{\psi}_j^{(1,\alpha)} &= \cos[\mu_j(\theta-\pi)]\{1\ 0\ 0\ \mu_j c_{55}\ \mu_j e_{15}\ \mu_j \tilde{e}_{15}\}^{\mathrm{T}}, \\ \boldsymbol{\psi}_j^{(2,\alpha)} &= \cos[\mu_j(\theta-\pi)]\{0\ 1\ 0\ \mu_j e_{15}\ -\mu_j \kappa_{11}\ -\mu_j \alpha_{11}\}^{\mathrm{T}}, \\ \boldsymbol{\psi}_j^{(3,\alpha)} &= \cos[\mu_j(\theta-\pi)]\{0\ 0\ 1\ \mu_j \tilde{e}_{15}\ -\mu_j \alpha_{11}\ -\mu_j \mu_{11}\}^{\mathrm{T}} \end{aligned} \quad (5.98)$$

and

$$\begin{aligned}
\boldsymbol{\psi}_j^{(1,\beta)} &= \rho_{1j}\cos[\mu_j(\theta-\pi)]\left\{1\ \chi_1\ \chi_2\ \mu_j\chi/\chi_7\ 0\ 0\right\}^{\mathrm{T}},\\
\boldsymbol{\psi}_j^{(2,\beta)} &= \rho_{2j}\cos[\mu_j(\theta-\pi)]\left\{\chi_3\ 1\ \chi_4\ 0\ \mu_j\chi/\chi_8\ 0\right\}^{\mathrm{T}},\\
\boldsymbol{\psi}_j^{(3,\beta)} &= \rho_{3j}\cos[\mu_j(\theta-\pi)]\left\{\chi_5\ \chi_6\ 1\ 0\ 0\ \mu_j\chi/\chi_9\right\}^{\mathrm{T}}
\end{aligned} \tag{5.99}$$

where μ_j are assumed to be positive, and $\rho_{ij} = \chi_{6+i}/(2\mu_j\pi\chi)$ (i=1-3).

Finally the solution of the problem is the linear combinations of eigenfunctions of both zero-and nonzero-eigenvalues:

$$\boldsymbol{\psi}_{\mathrm{h}} = \sum_n a_n^{(0)}\mathbf{v}_n^{(\alpha)} + \sum_n b_n^{(0)}\mathbf{v}_n^{(\beta)} + \sum_n a_n^{(i)}\boldsymbol{\psi}_n^{(i,\alpha)}e^{\mu_n\xi} + \sum_n b_n^{(i)}\boldsymbol{\psi}_n^{(i,\beta)}e^{-\mu_n\xi} \tag{5.100}$$

where the coefficients $a_n^{(0)}$, $b_n^{(0)}$, $a_n^{(i)}$, and $b_n^{(i)}$ can be determined from the boundary conditions, the subscript "h" represents the homogeneous solution.

5.3.3 Particular solutions

The general solution (5.100) applies to homogeneous equations only. A particular solution of nonhomogeneous Eqs. (5.1) and (5.83) is still needed. To this end, let the form of the special solution be

$$\boldsymbol{\psi}_{\mathrm{p}} = \sum_n E_n^{(i,\alpha)}(\xi)\boldsymbol{\psi}_n^{(i,\alpha)} + \sum_n E_n^{(i,\beta)}(\xi)\boldsymbol{\psi}_n^{(i,\beta)} \tag{5.101}$$

and the nonhomogeneous term of Eq. (2.138) (or Eq. (5.89)) is also expressed in terms of the eigenfunctions:

$$\mathbf{h} = \sum_n B_n^{(i,\alpha)}(\xi)\boldsymbol{\psi}_n^{(i,\alpha)} + \sum_n B_n^{(i,\beta)}(\xi)\boldsymbol{\psi}_n^{(i,\beta)} \tag{5.102}$$

From the adjoint symplectic orthogonality of eigenfunctions, we obtain the coefficients by the inner products as

$$B_n^{(i,\alpha)} = \left\langle \mathbf{h}^{\mathrm{T}}, \mathbf{J},\ \boldsymbol{\psi}_n^{(i,\beta)} \right\rangle, \qquad B_n^{(i,\alpha)} = -\left\langle \mathbf{h}^{\mathrm{T}}, \mathbf{J},\ \boldsymbol{\psi}_n^{(i,\alpha)} \right\rangle \tag{5.103}$$

Making use of Eqs. (2.138) and (5.101)-(5.103), we obtain

$$\dot{E}_n^{(i,\alpha)} = \mu_n E_n^{(i,\alpha)} + B_n^{(i,\alpha)}, \qquad \dot{E}_n^{(i,\beta)} = -\mu_n E_n^{(i,\beta)} + B_n^{(i,\beta)} \tag{5.104}$$

The solution of Eq. (5.104) can be expressed as

$$E_n^{(i,\alpha)} = e^{\mu_n\xi}\int_0^{\xi} B_n^{(i,\alpha)}e^{-\mu_n\eta}\,\mathrm{d}\eta, \qquad E_n^{(i,\beta)} = e^{-\mu_n\xi}\int_0^{\xi} B_n^{(i,\beta)}e^{\mu_n\eta}\,\mathrm{d}\eta \tag{5.105}$$

The particular solution $\boldsymbol{\psi}_{\mathrm{p}}$ can then be written in the form

$$\boldsymbol{\psi}_{\mathrm{p}} = \sum_n E_n^{(i,\alpha)}\boldsymbol{\psi}_n^{(i,\alpha)}e^{\mu_n\xi} + \sum_n E_n^{(i,\beta)}\boldsymbol{\psi}_n^{(i,\beta)}e^{-\mu_n\xi} \tag{5.106}$$

Therefore the solution of the problem is given as

$$\boldsymbol{\psi} = \boldsymbol{\psi}_{\mathrm{h}} + \boldsymbol{\psi}_{\mathrm{p}} \tag{5.107}$$

in which $\boldsymbol{\psi}_{\mathrm{h}}$ is defined in Eq. (5.100).

5.4 Symplectic solution for a magnetoelectroelastic strip

The symplectic duality system for a plane problem of a magnetoelectroelastic strip presented in [23,24] together with some derivations from the authors is described in this section. Methods of variable separation and symplectic eigenfunction expansion are employed to derive the symplectic formulation.

5.4.1 Basic equations

Consider a homogeneous transversely isotropic magnetoelectroelastic strip as shown in Fig. 5.6. The rectangular coordinates (x, z) are used in the analysis and the z axis is along the longitudinal direction (Fig. 5.1).

With the rectangular coordinate system shown in Fig. 5.6 and the involvement of a magnetic field, the constitutive relations (1.24) and (1.25) are extended as follows:

$$\boldsymbol{\sigma} = \begin{Bmatrix} \sigma_x \\ \sigma_z \\ \sigma_{xz} \\ D_x \\ D_z \\ B_x \\ B_z \end{Bmatrix} = \begin{bmatrix} c_{11} & c_{13} & 0 & 0 & -e_{31} & 0 & -\tilde{e}_{31} \\ c_{31} & c_{33} & 0 & 0 & -e_{33} & 0 & -\tilde{e}_{33} \\ 0 & 0 & c_{55} & -e_{15} & 0 & -\tilde{e}_{15} & 0 \\ 0 & 0 & e_{15} & \kappa_{11} & 0 & \alpha_{11} & 0 \\ e_{31} & e_{33} & 0 & 0 & \kappa_{33} & 0 & \alpha_{33} \\ 0 & 0 & \tilde{e}_{15} & \alpha_{11} & 0 & \mu_{11} & 0 \\ \tilde{e}_{31} & \tilde{e}_{33} & 0 & 0 & \alpha_{33} & 0 & \mu_{33} \end{bmatrix} \begin{Bmatrix} \varepsilon_x \\ \varepsilon_z \\ \gamma_{xz} \\ E_x \\ E_z \\ H_x \\ H_z \end{Bmatrix} = \mathbf{C}\boldsymbol{\varepsilon} \tag{5.108}$$

The inverse of Eq. (5.108) yields

$$\boldsymbol{\varepsilon} = \begin{Bmatrix} \varepsilon_x \\ \varepsilon_z \\ \gamma_{xz} \\ E_x \\ E_z \\ H_x \\ H_z \end{Bmatrix} = \begin{bmatrix} f_{11} & f_{13} & 0 & 0 & g_{31} & 0 & \tilde{g}_{31} \\ f_{13} & f_{33} & 0 & 0 & g_{33} & 0 & \tilde{g}_{33} \\ 0 & 0 & f_{55} & g_{15} & 0 & \tilde{g}_{15} & 0 \\ 0 & 0 & -g_{15} & \beta_{11} & 0 & \lambda_{11} & 0 \\ -g_{31} & -g_{33} & 0 & 0 & \beta_{33} & 0 & \lambda_{33} \\ 0 & 0 & -\tilde{g}_{15} & \lambda_{11} & 0 & \nu_{11} & 0 \\ -\tilde{g}_{31} & -\tilde{g}_{33} & 0 & 0 & \lambda_{33} & 0 & \nu_{33} \end{bmatrix} \begin{Bmatrix} \sigma_x \\ \sigma_z \\ \sigma_{xz} \\ D_x \\ D_z \\ B_x \\ B_z \end{Bmatrix} = \mathbf{C}^{-1}\boldsymbol{\sigma} \tag{5.109}$$

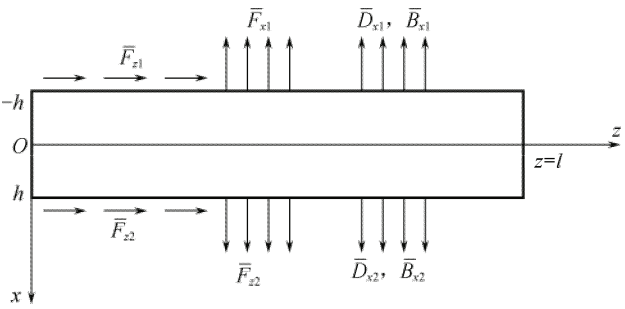

Fig. 5.6 Geometry and loading of a magnetoelectroelastic strip.

The gradient equations are defined in Eq. (1.2) and rewritten as follows:

$$\begin{Bmatrix} \varepsilon_x \\ \varepsilon_z \\ \gamma_{xz} \end{Bmatrix} = \begin{bmatrix} \dfrac{\partial}{\partial x} & 0 \\ 0 & \dfrac{\partial}{\partial z} \\ \dfrac{\partial}{\partial z} & \dfrac{\partial}{\partial x} \end{bmatrix} \begin{Bmatrix} u \\ w \end{Bmatrix}, \quad \begin{Bmatrix} E_x \\ E_z \end{Bmatrix} = -\begin{bmatrix} \dfrac{\partial \phi}{\partial x} \\ \dfrac{\partial \phi}{\partial z} \end{bmatrix}, \quad \begin{Bmatrix} H_x \\ H_z \end{Bmatrix} = -\begin{bmatrix} \dfrac{\partial \psi}{\partial x} \\ \dfrac{\partial \psi}{\partial z} \end{bmatrix} \tag{5.110}$$

The equilibrium equations of a plane magnetoelectroelastic solid are given by

$$\begin{cases} \dfrac{\partial \sigma_x}{\partial x} + \dfrac{\partial \sigma_{xz}}{\partial z} + f_x = 0 \\ \dfrac{\partial \sigma_{xz}}{\partial x} + \dfrac{\partial \sigma_z}{\partial z} + f_z = 0 \\ \dfrac{\partial D_x}{\partial x} + \dfrac{\partial D_z}{\partial z} + Q = 0 \\ \dfrac{\partial B_x}{\partial x} + \dfrac{\partial B_z}{\partial z} + M = 0 \end{cases} \tag{5.111}$$

in which f_x, f_z, Q, M are body force in x and z direction, electric charge density and electric current density, respectively.

The boundary value problem in Fig. 5.6 is completed by adding the following boundary conditions:

$$\begin{aligned} &\sigma_x = \overline{F}_{x1}(z), \quad \sigma_{xz} = \overline{F}_{z1}(z), \quad D_x = \overline{D}_{x1}, \quad B_x = \overline{B}_{x1} \quad (x = -h); \\ &\sigma_x = \overline{F}_{x2}(z), \quad \sigma_{xz} = \overline{F}_{z2}(z), \quad D_x = \overline{D}_{x2}, \quad B_x = \overline{B}_{x2} \quad (x = h) \end{aligned} \tag{5.112}$$

5.4.2 Hamiltonian principle

There are several ways to convert a Lagrange system into a Hamiltonian system,

one of which is to use the variational principle and Legendre's transformation. In the following, a description is presented of deriving system equations in symplectic space from Euclidean space. Since the energy functional plays an important role in deriving the basic equations of a coupled magnetoelectroelastic field in the Hamiltonian system, we define the energy functional, say Π , as follows:

$$\Pi = \frac{1}{2}\varepsilon_x\sigma_x + \frac{1}{2}\varepsilon_z\sigma_z + \frac{1}{2}\gamma_{xz}\sigma_{xz} - \frac{1}{2}E_xD_x - \frac{1}{2}E_zD_z - \frac{1}{2}H_xB_x - \frac{1}{2}H_zB_z \quad (5.113)$$

Using the constitutive relations, Eq. (5.113) can be further written in terms of strain, electric field, and magnetic field:

$$\begin{aligned}\Pi = {} & \frac{1}{2}c_{11}\varepsilon_x{}^2 + \frac{1}{2}c_{33}\varepsilon_z{}^2 + \frac{1}{2}c_{55}\gamma_{xz}{}^2 - \frac{1}{2}\kappa_{11}E_x{}^2 - \frac{1}{2}\kappa_{33}E_z{}^2 - \frac{1}{2}\mu_{11}H_x{}^2 \\ & - \frac{1}{2}\mu_{33}H_z{}^2 + c_{13}\varepsilon_x\varepsilon_z - e_{15}E_x\gamma_{xz} - e_{31}E_z\varepsilon_x - e_{33}E_z\varepsilon_z - \tilde{e}_{15}H_x\gamma_{xz} \\ & - \tilde{e}_{31}H_z\varepsilon_x - \tilde{e}_{33}H_z\varepsilon_z - \alpha_{11}E_xH_x - \alpha_{33}E_zH_z \end{aligned} \quad (5.114)$$

Then, based on energy functional (5.114) and following the procedure presented in [10], a variational principle corresponding to the boundary value problem (5.108)-(5.112) can be given by

$$\begin{aligned}\delta\,\Re = \delta\int_0^l\int_{-h}^{h}\left(\Pi - uX - wZ - \phi Q - \psi M\right)\mathrm{d}x\mathrm{d}z - \int_0^l\Big[(w\overline{F}_{z2} + u\overline{F}_{x2} \\ + \phi\overline{D}_{x2} + \psi\overline{B}_{x2})_{x=h} - (w\overline{F}_{z1} + u\overline{F}_{x1} + \Phi\overline{D}_{x1} + \varphi\overline{B}_{x1})_{x=-h}\Big]\mathrm{d}z = 0 \end{aligned} \quad (5.115)$$

For simplicity, introduce the following mutually work-conjugate vectors **q** and **p**:

$$\mathbf{q} = \begin{Bmatrix} w \\ u \\ \phi \\ \psi \end{Bmatrix}, \qquad \mathbf{p} = \begin{Bmatrix} \sigma \\ \tau \\ D \\ B \end{Bmatrix} = \begin{Bmatrix} \sigma_z \\ -\sigma_{xz} \\ D_z \\ B_z \end{Bmatrix} \quad (5.116)$$

where the definition of τ is different from that in [23,24], to achieve a Hamiltonian operator matrix.

To convert variables and equations from Euclidean space to symplectic geometry space, the following concepts are introduced; that is, the coordinate z is analogous to the time variable in the dynamic problem, and the dot represents the differential with respect to z , namely, $(\dot{\ }) = (\partial/\partial z)(\ )$:

$$\dot{u} = \frac{\partial u}{\partial z}, \quad \dot{w} = \frac{\partial w}{\partial z}, \quad \dot{\phi} = \frac{\partial \phi}{\partial z}, \quad \dot{\psi} = \frac{\partial \psi}{\partial z} \quad (5.117)$$

From Eq. $(5.109)_{1,4,6}$, we have

$$\begin{aligned}
\sigma_x &= \left(u_{,x} - f_{13}\sigma - g_{31}D - \tilde{g}_{31}B\right)/f_{11},\\
D_x &= \left(-C_1\tau - \nu_{11}\phi_{,x} + \lambda_{11}\psi_{,x}\right)/\Delta_*,\\
B_x &= \left(-C_2\tau + \lambda_{11}\phi_{,x} - \beta_{11}\psi_{,x}\right)/\Delta_*
\end{aligned} \tag{5.118}$$

where

$$\Delta_* = \beta_{11}\nu_{11} - \lambda_{11}^2,\ \ C_1 = \nu_{11}g_{15} - \lambda_{11}\tilde{g}_{15},\ \ C_2 = \beta_{11}\tilde{g}_{15} - \lambda_{11}g_{15} \tag{5.119}$$

Then, let $\aleph = \Pi - uX - wZ - \phi Q - \psi M$, and using Legendre's transformation, we obtain the following relationships:

$$\begin{aligned}
\sigma &= \frac{\partial \aleph}{\partial \dot{w}} = c_{13}\frac{\partial u}{\partial x} + c_{33}\dot{w} + e_{33}\dot{\phi} + \tilde{e}_{33}\dot{\psi},\\
\tau &= \frac{\partial \aleph}{\partial \dot{u}} = -c_{55}\frac{\partial w}{\partial x} - c_{55}\dot{u} - e_{15}\frac{\partial \phi}{\partial x} - \tilde{e}_{15}\frac{\partial \psi}{\partial x},\\
D &= \frac{\partial \aleph}{\partial \dot{\phi}} = e_{31}\frac{\partial u}{\partial x} + e_{33}\dot{w} - \kappa_{33}\dot{\phi} - \alpha_{33}\dot{\psi},\\
B &= \frac{\partial \aleph}{\partial \dot{\psi}} = \tilde{e}_{31}\frac{\partial u}{\partial x} + \tilde{e}_{33}\dot{w} - \alpha_{33}\dot{\phi} - \mu_{33}\dot{\psi}
\end{aligned} \tag{5.120}$$

Making use of the notation given in Eq. (5.117), we have

$$\begin{aligned}
\dot{\sigma} &= \frac{\partial \tau}{\partial x} - Z,\\
\dot{\tau} &= \frac{1}{f_{11}}\left[\frac{\partial^2 u}{\partial x^2} - f_{13}\frac{\partial \sigma}{\partial x} - g_{31}\frac{\partial D}{\partial x} - \tilde{g}_{31}\frac{\partial B}{\partial x}\right] + X,\\
\dot{D} &= \frac{1}{\Delta_*}\left[C_1\frac{\partial \tau}{\partial x} + \nu_{11}\frac{\partial^2 \phi}{\partial x^2} - \lambda_{11}\frac{\partial^2 \psi}{\partial x^2}\right] - Q,\\
\dot{B} &= \frac{1}{\Delta_*}\left[C_2\frac{\partial \tau}{\partial x} - \lambda_{11}\frac{\partial^2 \phi}{\partial x^2} + \beta_{11}\frac{\partial^2 \psi}{\partial x^2}\right] - M
\end{aligned} \tag{5.121}$$

$$\begin{aligned}
\dot{w} &= \frac{1}{f_{11}}\left[f_{13}\frac{\partial u}{\partial x} + a_1\sigma + a_2 D + a_3 B\right],\\
\dot{u} &= -\frac{\partial w}{\partial x} - \frac{C_1}{\Delta_*}\frac{\partial \phi}{\partial x} - \frac{C_2}{\Delta_*}\frac{\partial \psi}{\partial x} - a_7\tau,\\
\dot{\phi} &= \frac{1}{f_{11}}\left[g_{31}\frac{\partial u}{\partial x} + a_2\sigma + a_4 D_z + a_5 B_z\right],\\
\dot{\psi} &= \frac{1}{f_{11}}\left[\tilde{g}_{31}\frac{\partial u}{\partial x} + a_3\sigma + a_5 D_z + a_6 B_z\right]
\end{aligned} \tag{5.122}$$

in which

$$
\begin{aligned}
&a_1 = f_{11}f_{33} - f_{13}^2, \quad a_2 = f_{11}g_{33} - f_{13}g_{31}, \quad a_3 = f_{11}\tilde{g}_{33} - f_{13}\tilde{g}_{31}, \\
&a_4 = f_{11}\beta_{33} - g_{31}^2, \quad a_5 = f_{11}\lambda_{33} - g_{31}\tilde{g}_{31}, \quad a_6 = f_{11}\nu_{33} - \tilde{g}_{31}^2, \\
&a_7 = f_{55} + \frac{g_{15}C_1 + \tilde{g}_{15}C_2}{\Delta_*}
\end{aligned} \tag{5.123}
$$

Rewriting Eqs. (5.121) and (5.122) in matrix form, we obtain

$$
\begin{Bmatrix} \dot{\mathbf{q}} \\ \dot{\mathbf{p}} \end{Bmatrix} = \begin{bmatrix} \mathbf{A} & \mathbf{D} \\ \mathbf{B} & \mathbf{C} \end{bmatrix} \begin{Bmatrix} \mathbf{q} \\ \mathbf{p} \end{Bmatrix} + \mathbf{h} \tag{5.124}
$$

where matrixes **A**, **B**, **C**, and **D** are defined by

$$
\mathbf{A} = \begin{bmatrix} 0 & f_{13} & 0 & 0 \\ -f_{11} & 0 & -\dfrac{C_1 f_{11}}{\Delta_*} & -\dfrac{C_2 f_{11}}{\Delta_*} \\ 0 & g_{31} & 0 & 0 \\ 0 & \tilde{g}_{31} & 0 & 0 \end{bmatrix} \frac{\partial}{f_{11}\partial x}, \quad \mathbf{D} = \frac{1}{f_{11}} \begin{bmatrix} a_1 & 0 & a_2 & a_3 \\ 0 & a_7 f_{11} & 0 & 0 \\ a_2 & 0 & a_4 & a_5 \\ a_3 & 0 & a_5 & a_6 \end{bmatrix} \tag{5.125}
$$

$$
\mathbf{B} = \begin{bmatrix} 0 & 0 & 0 & 0 \\ 0 & \dfrac{\Delta_*}{f_{11}} & 0 & 0 \\ 0 & 0 & \nu_{11} & -\lambda_{11} \\ 0 & 0 & -\lambda_{11} & \beta_{11} \end{bmatrix} \frac{\partial^2}{\Delta_* \partial x^2}, \quad \mathbf{C} = \begin{bmatrix} 0 & f_{11} & 0 & 0 \\ -f_{13} & 0 & -g_{31} & -\tilde{g}_{31} \\ 0 & \dfrac{C_1 f_{11}}{\Delta_*} & 0 & 0 \\ 0 & \dfrac{C_2 f_{11}}{\Delta_*} & 0 & 0 \end{bmatrix} \frac{\partial}{f_{11}\partial x} \tag{5.126}
$$

and the vector **h** is

$$
\mathbf{h}^{\mathrm{T}} = (0,\ 0,\ 0,\ 0,\ -Z,\ X,\ -Q,\ -M)^{\mathrm{T}} \tag{5.127}
$$

Then, the following relationship between **A** and **C** can be obtained from Eqs. (5.125) and (5.126):

$$
\mathbf{C} = -\mathbf{A}^{\mathrm{T}} \tag{5.128}
$$

Using the definition (5.13), we can obtain Eq. (2.138) with

$$
\mathbf{H} = \begin{bmatrix} \mathbf{A} & \mathbf{D} \\ \mathbf{B} & -\mathbf{A}^{\mathrm{T}} \end{bmatrix} \tag{5.129}
$$

and **A**, **B**, **D**, **h** being defined in Eqs. (5.125)-(5.127), in which the matrices **B** and **D** are symmetric.

5.4.3 The zero-eigenvalue solutions

Due to the homogeneous boundary conditions at both sides $(x = \pm h)$, there exist

zero eigenvalues whose eigen solutions correspond to the Saint-Venant solutions when the averaged effects are included and the edge effects are also considered. To obtain the zero-eigenvalue solutions, Yao and Li [24] considered the following homogeneous boundary conditions:

$$\begin{aligned}
&\sigma_x = \left(u_{,x} - f_{13}\sigma - g_{31}D - \tilde{g}_{31}B\right)/f_{11} = 0,\\
&\tau = -c_{55}\frac{\partial w}{\partial x} - c_{55}\dot{u} - e_{15}\frac{\partial \phi}{\partial x} - \tilde{e}_{15}\frac{\partial \psi}{\partial x} = 0,\\
&D_x = (-C_1\tau - \nu_{11}\phi_{,x} + \lambda_{11}\psi_{,x})/\Delta_4 = 0,\\
&B_x = (-C_2\tau + \lambda_{11}\phi_{,x} - \beta_{11}\psi_{,x})/\Delta_4 = 0
\end{aligned} \qquad (\text{on } x = \pm h) \qquad (5.130)$$

When μ=0, Eq. (2.156) becomes

$$\mathbf{H}\boldsymbol{\psi} = 0 \qquad (5.131)$$

By solving Eq. (5.131) under the boundary conditions (5.130), Yao and Li obtained the following linear independent eigensolutions:

$$\begin{aligned}
&\mathbf{v}_1^{(0)} = \boldsymbol{\psi}_1^{(0)} = \{1\,0\,0\,0\,0\,0\,0\,0\}^{\mathrm{T}},\\
&\mathbf{v}_2^{(0)} = \boldsymbol{\psi}_2^{(0)} = \{0\,1\,0\,0\,0\,0\,0\,0\}^{\mathrm{T}},\\
&\mathbf{v}_3^{(0)} = \boldsymbol{\psi}_3^{(0)} = \{0\,0\,1\,0\,0\,0\,0\,0\}^{\mathrm{T}},\\
&\mathbf{v}_4^{(0)} = \boldsymbol{\psi}_4^{(0)} = \{0\,0\,0\,1\,0\,0\,0\,0\}^{\mathrm{T}}
\end{aligned} \qquad (5.132)$$

which represent the rigid body translation along the x- and z-directions, constant electric potential, and constant magnetic potential. Because the solutions (5.132) have symplectic orthogonality to each other, there must exist eigensolutions in Jordan form. To obtain those eigensolutions, Yao and Li considered the following equations together with the boundary conditions (5.130):

$$\mathbf{H}\boldsymbol{\psi}_j^{(i)} = \boldsymbol{\psi}_j^{(i-1)} \qquad (j = 1\text{-}4) \qquad (5.133)$$

where the subscripts "i" and "i–1" denote the Jordan normal form eigensolutions of the ith and (i−1)th order, respectively.

Substituting Eqs. (5.132) into Eq. (5.133), the first order Jordan form eigensolutions are obtained as

$$\begin{aligned}
&\boldsymbol{\psi}_1^{(1)} = \{0\ b_{1*}x\ 0\ 0\ a_{1*}\ 0\ a_{2*}\ a_{3*}\}^{\mathrm{T}},\\
&\boldsymbol{\psi}_2^{(1)} = \{-x\ 0\ 0\ 0\ 0\ 0\ 0\ 0\}^{\mathrm{T}},\\
&\boldsymbol{\psi}_3^{(1)} = \{0\ b_{2*}x\ 0\ 0\ a_{2*}\ 0\ a_{4*}\ a_{5*}\}^{\mathrm{T}},\\
&\boldsymbol{\psi}_4^{(1)} = \{0\ b_{3*}x\ 0\ 0\ a_{2*}\ 0\ a_{5*}\ a_{6*}\}^{\mathrm{T}}
\end{aligned} \qquad (5.134)$$

in which a_{i*} and b_{i*} are given by

$$\begin{bmatrix} a_{1*} & a_{2*} & a_{3*} \\ a_{2*} & a_{4*} & a_{5*} \\ a_{3*} & a_{5*} & a_{6*} \end{bmatrix} = \begin{bmatrix} f_{33} & g_{33} & \tilde{g}_{33} \\ g_{33} & -\beta_{33} & -\lambda_{33} \\ \tilde{g}_{33} & -\lambda_{33} & -\nu_{33} \end{bmatrix}^{-1},$$
$$b_{1*} = f_{13}a_{1*} + g_{31}a_{2*} + \tilde{g}_{31}a_{3*},$$
$$b_{2*} = f_{13}a_{2*} + g_{31}a_{4*} + \tilde{g}_{31}a_{5*}, \tag{5.135}$$
$$b_{3*} = f_{13}a_{3*} + g_{31}a_{5*} + \tilde{g}_{31}a_{6*}$$

It should be mentioned that the solutions (5.134) are not the direct solution of the original problem, but the solution of the original equation (2.138) with **h**=0 can be obtained by the combination of solutions (5.132) and (5.134) as

$$\mathbf{v}_i^{(1)} = \boldsymbol{\psi}_i^{(1)} + z\boldsymbol{\psi}_i^{(0)} \qquad (i = 1\text{-}4) \tag{5.136}$$

which satisfies Eq. (5.131) at the zero eigenvalue. In Eq. (5.136), $\nu_1^{(1)}$, $\nu_2^{(1)}$, $\nu_3^{(1)}$, and $\nu_4^{(1)}$ represent, respectively, uniform extension in the *z*-direction, rigid-body rotation in the *x*-*z* plane, the solution induced by the constant electric field, and the solution induced by a constant magnetic field.

Yao and Li then indicated that the solutions with subscripts 1, 3 and 4 represent the symmetric deformation in the *z*-axis, and solutions with subscripts 2 describe the behavior of the antisymmetric deformation on the *z*-axis. The eigensolutions of symmetric deformation and the eigensolutions of antisymmetric deformation are symplectic orthogonal. To obtain a set of adjoint symplectic orthonormal bases, the eigensolutions of the symmetric deformation should be orthonormalized firstly. To this end, let

$$\begin{aligned} \tilde{\boldsymbol{\psi}}_3^{(0)} &= \boldsymbol{\psi}_3^{(0)} + t_1\boldsymbol{\psi}_1^{(0)}, \quad \tilde{\boldsymbol{\psi}}_4^{(0)} = \boldsymbol{\psi}_4^{(0)} + t_2\boldsymbol{\psi}_1^{(0)} + t_3\tilde{\boldsymbol{\psi}}_3^{(0)}, \\ \tilde{\boldsymbol{\psi}}_3^{(1)} &= \boldsymbol{\psi}_3^{(1)} + t_1\boldsymbol{\psi}_1^{(1)}, \quad \tilde{\boldsymbol{\psi}}_4^{(1)} = \boldsymbol{\psi}_4^{(1)} + t_2\boldsymbol{\psi}_1^{(1)} + t_3\tilde{\boldsymbol{\psi}}_3^{(1)} \end{aligned} \tag{5.137}$$

where

$$t_1 = -a_{2*}/a_{1*}, \quad t_2 = -a_{3*}/a_{1*}, \quad t_3 = -\frac{a_{1*}a_{6*} - a_{2*}a_{3*}}{a_{1*}a_{5*} - a_{2*}^2} \tag{5.138}$$

Yao and Li then concluded that the eigensolutions of the symmetric deformation, $\boldsymbol{\psi}_1^{(0)}$, $\tilde{\boldsymbol{\psi}}_3^{(0)}$, $\tilde{\boldsymbol{\psi}}_4^{(0)}$, and $\boldsymbol{\psi}_1^{(1)}$, $\tilde{\boldsymbol{\psi}}_3^{(1)}$, $\tilde{\boldsymbol{\psi}}_4^{(1)}$, have a symplectic adjoint and orthonormal relationship. The remaining eigensolutions are symplectic orthonormal. This shows that for the eigensolutions of the symmetric deformation associated with zero eigenvalue there are six independent solutions and there is no second order Jordan form eigensolution for symmetric deformation.

For the eigensolutions associated with antisymmetric deformation, since $\boldsymbol{\psi}_2^{(0)}$ is symplectic orthonormal with $\boldsymbol{\psi}_2^{(1)}$, the second order Jordan form eigensolution is

given by

$$\boldsymbol{\psi}_2^{(2)} = \left\{0 \;\; b_{1*}x^2/2 \;\; 0 \;\; 0 \;\; -a_{1*}x \;\; 0 \;\; -a_{2*}x \;\; -a_{3*}x\right\}^{\mathrm{T}} \tag{5.139}$$

The vector $\boldsymbol{\psi}_2^{(2)}$ is not the solution of the original problem, however, from which the physical solution can be derived as follows:

$$\mathbf{v}_2^{(2)} = \boldsymbol{\psi}_2^{(2)} + z\boldsymbol{\psi}_2^{(1)} + z^2\boldsymbol{\psi}_2^{(0)}/2 \tag{5.140}$$

which represents a pure bending deformation. Because $\boldsymbol{\psi}_2^{(2)}$ is still symplectic orthonormal with $\boldsymbol{\psi}_2^{(0)}$, the third order Jordan form eigensolution $\boldsymbol{\psi}_2^{(3)}$ exists. It is

$$\boldsymbol{\psi}_2^{(3)} = \left\{a_{9*}x^3 + b_{4*}x \;\; 0 \;\; a_{7*}(x^3 - 3h^2x) \;\; a_{8*}(x^3 - 3h^2x) \right.$$
$$\left. 0 \;\; \frac{1}{2}a_{1*}(x^2 - h^2) \;\; 0 \;\; 0\right\}^{\mathrm{T}} \tag{5.141}$$

where

$$\begin{aligned}
a_{7*} &= [\beta_{11}(a_{1*}C_1 - a_{2*}\Delta_*) + \lambda_{11}(a_{1*}C_2 - a_{3*}\Delta_*)]/(6\Delta_*),\\
a_{8*} &= [\nu_{11}(a_{1*}C_2 - a_{3*}\Delta_*) + \lambda_{11}(a_{1*}C_1 - a_{2*}\Delta_*)]/(6\Delta_*),\\
a_{9*} &= -a_{7*}C_1/\Delta_4 - a_{8*}C_2/\Delta_* + (a_{1*}C + b_{1*})/6,\\
b_{4*} &= h^2(a_{1*}C/2 - 3a_{7*}C_1/\Delta_* - 3a_{8*}C_2/\Delta_*),\\
C &= f_{55} + (g_{15}C_1 + \tilde{g}_{15}C_2)/\Delta_*
\end{aligned} \tag{5.142}$$

The corresponding solution of the original equation (5.131) is as follows:

$$\mathbf{v}_2^{(3)} = \boldsymbol{\psi}_2^{(3)} + z\boldsymbol{\psi}_2^{(2)} + z^2\boldsymbol{\psi}_2^{(1)}/2 + z^3\boldsymbol{\psi}_2^{(0)}/6 \tag{5.143}$$

which represents a bending solution due to constant shear force. Because $\boldsymbol{\psi}_2^{(3)}$ is symplectic adjoint with $\boldsymbol{\psi}_2^{(0)}$, no fourth order Jordan form eigensolution for antisymmetric deformation exists.

Similarly, the orthonormalization of the eigensolutions of the antisymmetric deformation can be constructed as

$$\tilde{\boldsymbol{\psi}}_2^{(2)} = \boldsymbol{\psi}_2^{(2)} + t_4\boldsymbol{\psi}_2^{(0)}, \qquad \tilde{\boldsymbol{\psi}}_2^{(3)} = \boldsymbol{\psi}_3^{(3)} + t_4\boldsymbol{\psi}_2^{(1)} \tag{5.144}$$

where

$$t_4 = \frac{-\int_{-h}^{h}\boldsymbol{\psi}_2^{(2)\mathrm{T}}\mathbf{J}\boldsymbol{\psi}_2^{(3)}\mathrm{d}x}{\int_{-h}^{h}\boldsymbol{\psi}_2^{(1)\mathrm{T}}\mathbf{J}\boldsymbol{\psi}_2^{(2)}\mathrm{d}x} \tag{5.145}$$

Thus the set of adjoint symplectic orthonormal bases constituted by the eigen-solutions associated with zero eigenvalue is

$$\boldsymbol{\psi}_1^{(0)},\ \boldsymbol{\psi}_2^{(0)},\ \boldsymbol{\psi}_2^{(1)},\ \tilde{\boldsymbol{\psi}}_3^{(0)},\ \tilde{\boldsymbol{\psi}}_4^{(0)},\ \boldsymbol{\psi}_1^{(1)},\ \tilde{\boldsymbol{\psi}}_2^{(2)},\ \tilde{\boldsymbol{\psi}}_2^{(3)},\ \tilde{\boldsymbol{\psi}}_3^{(1)},\ \tilde{\boldsymbol{\psi}}_4^{(1)} \tag{5.146}$$

The above adjoint symplectic orthonormal bases form a complete symplectic subspace.

5.4.4 Nonzero-eigenvalue solutions

To find the solution of Eq. (2.156) where $\mu \neq 0$, the characteristic determinant equation is [23]

$$\det\begin{vmatrix}
-\mu & f_{13}\lambda/f_{11} & 0 & 0 & a_1/f_{11} & 0 & a_2/f_{11} & a_3/f_{11} \\
-\lambda & -\mu & -\dfrac{C_1\lambda}{\Delta_*} & -\dfrac{C_2\lambda}{\Delta_*} & 0 & a_7 & 0 & 0 \\
0 & g_{31}\lambda/f_{11} & -\mu & 0 & a_2/f_{11} & 0 & a_4/f_{11} & a_5/f_{11} \\
0 & \tilde{g}_{31}\lambda/f_{11} & 0 & -\mu & a_3/f_{11} & 0 & a_5/f_{11} & a_6/f_{11} \\
0 & 0 & 0 & 0 & -\mu & \lambda & 0 & 0 \\
0 & \lambda^2/f_{11} & 0 & 0 & -\lambda f_{13}/f_{11} & -\mu & -\lambda g_{31}/f_{11} & -\lambda\tilde{g}_{31}/f_{11} \\
0 & 0 & \dfrac{\nu_{11}\lambda^2}{\Delta_*} & \dfrac{-\lambda_{11}\lambda^2}{\Delta_*} & 0 & \dfrac{C_1\lambda}{\Delta_*} & -\mu & 0 \\
0 & 0 & \dfrac{-\lambda_{11}\lambda^2}{\Delta_*} & \dfrac{\beta_{11}\lambda^2}{\Delta_*} & 0 & \dfrac{C_2\lambda}{\Delta_*} & 0 & -\mu
\end{vmatrix} = 0 \tag{5.147}$$

Equation (5.147) has eight roots:

$$\lambda_i = \tilde{\lambda}_i\mu, \quad \lambda_{i+4} = -\tilde{\lambda}_i\mu \quad (i = 1\text{-}4) \tag{5.148}$$

Li and Yao [23] then obtained the general solution of Eq. (2.156) in the following form:

$$\begin{aligned}
w &= \left[\sum_{i=1}^{4} A_{1i}\cosh(\tilde{\lambda}_i\mu x) + \sum_{i=1}^{4} D_{1i}\sinh(\tilde{\lambda}_i\mu x)\right]e^{\mu z}, \\
u &= \left[\sum_{i=1}^{4} A_{2i}\sinh(\tilde{\lambda}_i\mu x) + \sum_{i=1}^{4} D_{2i}\cosh(\tilde{\lambda}_i\mu x)\right]e^{\mu z}, \\
\phi &= \left[\sum_{i=1}^{4} A_{3i}\cosh(\tilde{\lambda}_i\mu x) + \sum_{i=1}^{4} D_{3i}\sinh(\tilde{\lambda}_i\mu x)\right]e^{\mu z}, \\
\psi &= \left[\sum_{i=1}^{4} A_{4i}\cosh(\tilde{\lambda}_i\mu x) + \sum_{i=1}^{4} D_{4i}\sinh(\tilde{\lambda}_i\mu x)\right]e^{\mu z}
\end{aligned} \tag{5.149}$$

$$\begin{aligned}
\sigma &= \left[\sum_{i=1}^{4} A_{5i}\cosh(\tilde{\lambda}_i \mu x) + \sum_{i=1}^{4} D_{5i}\sinh(\tilde{\lambda}_i \mu x)\right] e^{\mu z},\\
\tau &= \left[\sum_{i=1}^{4} A_{6i}\sinh(\tilde{\lambda}_i \mu x) + \sum_{i=1}^{4} D_{6i}\cosh(\tilde{\lambda}_i \mu x)\right] e^{\mu z},\\
D &= \left[\sum_{i=1}^{4} A_{7i}\cosh(\tilde{\lambda}_i \mu x) + \sum_{i=1}^{4} D_{7i}\sinh(\tilde{\lambda}_i \mu x)\right] e^{\mu z},\\
B &= \left[\sum_{i=1}^{4} A_{8i}\cosh(\tilde{\lambda}_i \mu x) + \sum_{i=1}^{4} D_{8i}\sinh(\tilde{\lambda}_i \mu x)\right] e^{\mu z}
\end{aligned} \tag{5.150}$$

Li and Yao then divided the solution into two parts, symmetric and anti-symmetric. They considered firstly the symmetric part:

$$\begin{aligned}
w &= \sum_{i=1}^{4} A_{1i}\cosh(\tilde{\lambda}_i \mu x)e^{\mu z}, \quad u = \sum_{i=1}^{4} A_{2i}\sinh(\tilde{\lambda}_i \mu x)e^{\mu z},\\
\phi &= \sum_{i=1}^{4} A_{3i}\cosh(\tilde{\lambda}_i \mu x)e^{\mu z}, \quad \psi = \sum_{i=1}^{4} A_{4i}\cosh(\tilde{\lambda}_i \mu x)e^{\mu z},\\
\sigma &= \sum_{i=1}^{4} A_{5i}\cosh(\tilde{\lambda}_i \mu x)e^{\mu z}, \quad \tau = \sum_{i=1}^{4} A_{6i}\sinh(\tilde{\lambda}_i \mu x)e^{\mu z},\\
D &= \sum_{i=1}^{4} A_{7i}\cosh(\tilde{\lambda}_i \mu x)e^{\mu z}, \quad B = \sum_{i=1}^{4} A_{8i}\cosh(\tilde{\lambda}_i \mu x)e^{\mu z}
\end{aligned} \tag{5.151}$$

Substituting Eq. (5.151) into Eq. (2.156), A_{ji} can be related to A_{6i} as

$$A_{ji} = \frac{f_{Nj}(\tilde{\lambda}_i)}{f_{Dj}(\tilde{\lambda}_i)\mu} A_{6i} \ (j = 1\text{-}4), \qquad A_{5i} = -\tilde{\lambda}_i A_{6i}, \qquad A_{ji} = \frac{f_{Nj}(\tilde{\lambda}_i)}{f_{Dj}(\tilde{\lambda}_i)} A_{6i} \ (j = 7,8) \tag{5.152}$$

where $f_{Nj}(\tilde{\lambda}_i)$ and $f_{Dj}(\tilde{\lambda}_i)$ are the functions of $\tilde{\lambda}_i$ [23]. Then, substituting Eqs. (5.151) and (5.152) into the boundary condition (5.130) yields

$$\begin{aligned}
&\sum_{i=1}^{4}\left(\tilde{\lambda}_i \frac{f_{N2}(\tilde{\lambda}_i)}{f_{D2}(\tilde{\lambda}_i)} + f_{13}\tilde{\lambda}_i - g_{31}\frac{f_{N7}(\tilde{\lambda}_i)}{f_{D7}(\tilde{\lambda}_i)} - \tilde{g}_{31}\frac{f_{N8}(\tilde{\lambda}_i)}{f_{D8}(\tilde{\lambda}_i)}\right)\cosh(\tilde{\lambda}_i \mu h)A_{6i} = 0,\\
&\sum_{i=1}^{4}\sinh(\tilde{\lambda}_i \mu h)A_{6i} = 0,\\
&\sum_{i=1}^{4}\left(C_1 - \nu_{11}\tilde{\lambda}_i \frac{f_{N3}(\tilde{\lambda}_i)}{f_{D3}(\tilde{\lambda}_i)} + \lambda_{11}\tilde{\lambda}_i \frac{f_{N4}(\tilde{\lambda}_i)}{f_{D4}(\tilde{\lambda}_i)}\right)\sinh(\tilde{\lambda}_i \mu h)A_{6i} = 0,\\
&\sum_{i=1}^{4}\left(C_2 + \lambda_{11}\tilde{\lambda}_i \frac{f_{N3}(\tilde{\lambda}_i)}{f_{D3}(\tilde{\lambda}_i)} - \beta_{11}\tilde{\lambda}_i \frac{f_{N4}(\tilde{\lambda}_i)}{f_{D4}(\tilde{\lambda}_i)}\right)\sinh(\tilde{\lambda}_i \mu h)A_{6i} = 0
\end{aligned} \tag{5.153}$$

Equation (5.153) is further written in matrix form for simplicity:

$$[B_{ij}]\{A_{6j}\} = 0 \tag{5.154}$$

For the non-trivial solutions of Eq. (5.154), the determinant of coefficient matrix must vanish:

$$\det\left|B_{ij}\right| = 0 \tag{5.155}$$

Denote μ_n (n=1,2,⋯) as the roots of Eq. (5.155). After obtaining A_{6i} by substituting μ_n into Eq. (5.154), the solutions of Eq. (2.138) for **h**=0 and symmetric deformation are obtained as

$$\begin{aligned}
w_n &= \sum_{i=1}^{4} \frac{f_{N1}(\tilde{\lambda}_i)}{f_{D1}(\tilde{\lambda}_i)\mu_n} A_{6i} \cosh(\tilde{\lambda}_i \mu_n x) e^{\mu_n z}, \\
u_n &= \sum_{i=1}^{4} \frac{f_{N2}(\tilde{\lambda}_i)}{f_{D2}(\tilde{\lambda}_i)\mu_n} A_{6i} \sinh(\tilde{\lambda}_i \mu_n x) e^{\mu_n z}, \\
\phi_n &= \sum_{i=1}^{4} \frac{f_{N3}(\tilde{\lambda}_i)}{f_{D3}(\tilde{\lambda}_i)\mu_n} A_{6i} \cosh(\tilde{\lambda}_i \mu_n x) e^{\mu_n z}, \\
\psi_n &= \sum_{i=1}^{4} \frac{f_{N4}(\tilde{\lambda}_i)}{f_{D4}(\tilde{\lambda}_i)\mu_n} A_{6i} \cosh(\tilde{\lambda}_i \mu_n x) e^{\mu_n z}
\end{aligned} \tag{5.156}$$

$$\begin{aligned}
&\sigma_n = -\sum_{i=1}^{4} \tilde{\lambda}_i A_{6i} \cosh(\tilde{\lambda}_i \mu_n x) e^{\mu_n z}, \quad \tau_n = \sum_{i=1}^{4} A_{6i} \sinh(\tilde{\lambda}_i \mu_n x) e^{\mu_n z}, \\
&D_n = \sum_{i=1}^{4} \frac{f_{N7}(\tilde{\lambda}_i)}{f_{D7}(\tilde{\lambda}_i)\mu_n} A_{6i} \cosh(\tilde{\lambda}_i \mu_n x) e^{\mu_n z}, \\
&B_n = \sum_{i=1}^{4} \frac{f_{N8}(\tilde{\lambda}_i)}{f_{D8}(\tilde{\lambda}_i)\mu_n} A_{6i} \cosh(\tilde{\lambda}_i \mu_n x) e^{\mu_n z}
\end{aligned} \tag{5.157}$$

Similarly, the corresponding solutions of eigenvalues $\tilde{\mu}_n$ (n=1,2,⋯) for antisymmetric deformation can be obtained as

$$\begin{aligned}
&\tilde{w}_n = \sum_{i=1}^{4} D_{1i} \sinh(\tilde{\lambda}_i \tilde{\mu}_n x) e^{\tilde{\mu}_n z}, \quad \tilde{u}_n = \sum_{i=1}^{4} D_{1i} \cosh(\tilde{\lambda}_i \tilde{\mu}_n x) e^{\tilde{\mu}_n z}, \\
&\tilde{\phi}_n = \sum_{i=1}^{4} D_{3i} \sinh(\tilde{\lambda}_i \tilde{\mu}_n x) e^{\tilde{\mu}_n z}, \quad \tilde{\psi}_n = \sum_{i=1}^{4} D_{6i} \sinh(\tilde{\lambda}_i \tilde{\mu}_n x) e^{\tilde{\mu}_n z}, \\
&\tilde{\sigma}_n = \sum_{i=1}^{4} D_{5i} \sinh(\tilde{\lambda}_i \tilde{\mu}_n x) e^{\tilde{\mu}_n z}, \quad \tilde{\tau}_n = \sum_{i=1}^{4} D_{6i} \cosh(\tilde{\lambda}_i \tilde{\mu}_n x) e^{\tilde{\mu}_n z}, \\
&\tilde{D}_n = \sum_{i=1}^{4} D_{7i} \sinh(\tilde{\lambda}_i \tilde{\mu}_n x) e^{\tilde{\mu}_n z}, \quad \tilde{B}_n = \sum_{i=1}^{4} D_{8i} \sinh(\tilde{\lambda}_i \tilde{\mu}_n x) e^{\tilde{\mu}_n z}
\end{aligned} \tag{5.158}$$

Equations (5.156), (5.157), and (5.158) consist of all eigensolutions corre-

sponding to nonzero-eigenvalues. These solutions are covered in the Saint-Venant principle and decay with distance depending on the characteristics of the eigenvalues [23]. Together with the eigensolutions of zero-eigenvalue, they constitute a complete adjoint symplectic orthonormal basis.

5.5 Three-dimensional symplectic formulation for piezoelectricity

In the previous sections of this chapter, symplectic formulations for 2D piezoelectric materials were presented. The extension to 3D electroelastic problems documented in [19] is described in this section. We begin by reducing a 3D piezoelectric problem to zero-eigenvalue solutions with their Jordan chains and nonzero-eigenvalue solutions in the Hamiltonian systems. Then the solution of the problem is obtained by superimposing linearly by their symplectic eigensolutions, which form the complete space of solutions. The problem is finally reduced to finding eigenvalues and eigensolutions.

5.5.1 Basic formulations

To obtain the symplectic formulation for 3D piezoelectric materials, Xu et al. [19] considered an anisotropic piezoelectric cylinder which is transversely isotropic and anisotropic in the longitudinal direction. The corresponding relationships between stress displacement and electric displacement-electric potential are written in terms of circular cylindrical coordinate (r, θ, z) as

$$\begin{aligned}
\sigma_{rr} &= c_{11}u_{,r} + c_{12}(v_{,\theta} + u)/r + c_{13}\dot{w} + e_{31}\dot{\phi},\\
\sigma_{\theta\theta} &= c_{12}u_{,r} + c_{11}(v_{,\theta} + u)/r + c_{13}\dot{w} + e_{31}\dot{\phi},\\
\sigma_{zz} &= c_{13}u_{,r} + c_{13}(v_{,\theta} + u)/r + c_{33}\dot{w} + e_{33}\dot{\phi},\\
\sigma_{r\theta} &= c_{66}(v_{,r} - v/r + u_{,\theta}/r),\\
\sigma_{rz} &= c_{55}(w_{,r} + \dot{u}) + e_{15}\phi_{,r},\\
\sigma_{\theta z} &= c_{55}(w_{,\theta}/r + \dot{v}) + e_{15}\phi_{,\theta}/r
\end{aligned} \tag{5.159}$$

$$\begin{aligned}
D_r &= e_{15}(w_{,r} + \dot{u})/r - \kappa_{11}\phi_{,r},\\
D_\theta &= e_{15}(w_{,\theta}/r + \dot{v}) - \kappa_{11}\phi_{,\theta}/r,\\
D_z &= e_{31}u_{,r} + e_{31}(v_{,\theta} + u)/r + e_{33}\dot{w} - \kappa_{33}\dot{\phi}
\end{aligned} \tag{5.160}$$

where v is the displacement in the θ-direction and the dot above represents differential with respect to z, namely, $\dot{F} = \partial F/\partial z$. The z coordinate is considered analogously as the time coordinate. The related potential energy density is

$$
\begin{aligned}
U = r\{&c_{11}u_{,r}^2 + c_{11}(v_{,\theta}+u)^2/r^2 + c_{33}\dot{w}^2 + 2c_{12}u_{,r}(v_{,\theta}+u)/r + 2c_{13}u_{,r}\dot{w} \\
&+ 2c_{13}\dot{w}(v_{,\theta}+u)/r + c_{55}(w_{,\theta}/r+\dot{v})^2 + c_{55}(w_{,r}+\dot{u})^2 + c_{66}(v_{,r}-v/r+u_{,\theta}/r)^2 \\
&+ 2e_{31}u_{,r}\dot{\phi} + 2e_{31}\dot{\phi}(v_{,\theta}+u)/r + 2e_{33}\dot{w}\dot{\phi} + 2e_{15}(w_{,\theta}/r+\dot{v})\phi_{,\theta}/r \\
&+ 2e_{15}(w_{,r}+\dot{u})\phi_{,r} - \kappa_{11}\phi_{,r}^2 - \kappa_{11}\phi_{,\theta}^2/r^2 - \kappa_{33}\dot{\phi}^2\}/2
\end{aligned} \tag{5.161}
$$

The Lagrange function which is the potential energy U minus the work done by an external generalized force is as follows:

$$
L(\mathbf{q},\dot{\mathbf{q}}) = U(\mathbf{q},\dot{\mathbf{q}}) - uf_r - vf_\theta - wf_z - \phi Q \tag{5.162}
$$

where $\{\overline{f}_r,\overline{f}_\theta,\overline{f}_z\}^{\mathrm{T}} = \{f_r,f_\theta,f_z\}^{\mathrm{T}}/r$ represent the external body forces and $\overline{Q} = Q/r$ the density of free charges, $\mathbf{q} = \{u,v,w,\phi\}^{\mathrm{T}}$ is the primary vector in the Hamiltonian system.

5.5.2 Hamiltonian dual equations

The dual vector of $\mathbf{q}$ according to Legendre's transformation is

$$
\mathbf{p} = \frac{\partial L}{\partial \dot{\mathbf{q}}} = \begin{Bmatrix} r[c_{55}(w_{,r}+\dot{u}) + e_{15}\phi_{,r}] \\ r[c_{55}(w_{,\theta}/r+\dot{v}) + e_{15}\phi_{,\theta}/r] \\ r[c_{13}u_{,r} + c_{13}(v_{,\theta}+u)/r + c_{33}\dot{w} + e_{33}\dot{\phi}] \\ r[e_{31}u_{,r} + e_{31}(v_{,\theta}+u)/r + e_{33}\dot{w} - \kappa_{33}\dot{\phi}] \end{Bmatrix} = \begin{Bmatrix} r\sigma_{rz} \\ r\sigma_{\theta z} \\ r\sigma_z \\ rD_z \end{Bmatrix} \tag{5.163}
$$

On the basis of the mutually dual vectors $\mathbf{q}$ and $\mathbf{p}$, Xu et al. [19] then obtained the Hamiltonian function defined in Eq. (2.137). Making use of Eq. (2.136), the dual equations for the Hamiltonian system can be obtained as

$$
\begin{Bmatrix} \dot{\mathbf{p}} \\ \dot{\mathbf{q}} \end{Bmatrix} = \begin{Bmatrix} \partial H/\partial \mathbf{p} \\ -\partial H/\partial \mathbf{q} \end{Bmatrix} = \begin{bmatrix} \mathbf{A} & \mathbf{B} \\ \mathbf{C} & -\mathbf{A}^{\mathrm{T}} \end{bmatrix} \begin{Bmatrix} \mathbf{q} \\ \mathbf{p} \end{Bmatrix} + \begin{Bmatrix} \mathbf{h}_1 \\ \mathbf{h}_2 \end{Bmatrix} \tag{5.164}
$$

where [19]

$$
\mathbf{A} = \begin{bmatrix} 0 & 0 & -\partial_r & -a_1\partial_r \\ 0 & 0 & -\partial_\theta/r & -a_1\partial_\theta/r \\ -a_3(\partial_r + 1/r) & -a_3\partial_\theta/r & 0 & 0 \\ a_6(\partial_r + 1/r) & a_6\partial_\theta/r & 0 & 0 \end{bmatrix} \tag{5.165}
$$

$$
\mathbf{C} = \begin{bmatrix} -a_8 r_1^* - a_9\partial_\theta^2/r & -a_{10}\partial_r\partial_\theta - a_{11}\partial_\theta/r & 0 & 0 \\ -a_{10}\partial_r\partial_\theta - a_{11}\partial_\theta/r & -a_9 r_1^* - a_8\partial_\theta^2/r & 0 & 0 \\ 0 & 0 & 0 & 0 \\ 0 & 0 & 0 & a_{12}r_2^* \end{bmatrix} \tag{5.166}
$$

$$\mathbf{B}=\begin{bmatrix} a_2/r & 0 & 0 & 0 \\ 0 & a_2/r & 0 & 0 \\ 0 & 0 & a_4/r & a_5/r \\ 0 & 0 & a_5/r & -a_7/r \end{bmatrix} \tag{5.167}$$

$$\mathbf{h}_1=0, \qquad \mathbf{h}_2=-\{f_r \ f_\theta \ f_z \ Q\}^{\mathrm{T}} \tag{5.168}$$

with

$$\partial_r=\partial/\partial r, \quad \partial_\theta=\partial/\partial\theta, \quad r_1^*=r\partial_r^2+\partial_r-1/r, \quad r_2^*=r\partial_r^2+\partial_r+\partial_\theta^2/r \tag{5.169}$$

$$\begin{aligned} &a_1=e_{15}/c_{55}, \ a_2=1/c_{55}, \ a_3=(c_{13}\kappa_{33}+e_{31}e_{33})/(e_{33}^2+c_{33}\kappa_{33}), \\ &a_4=\kappa_{33}/(e_{33}^2+c_{33}\kappa_{33}), \ a_5=e_{33}/(e_{33}^2+c_{33}\kappa_{33}), \\ &a_6=(e_{31}c_{33}-c_{13}e_{33})/(e_{33}^2+c_{33}\kappa_{33}), \ a_7=c_{33}/(e_{33}^2+c_{33}\kappa_{33}) \end{aligned} \tag{5.170}$$

$$\begin{aligned} &a_8=c_{11}-a_3c_{13}+a_6e_{31}, \ a_9=c_{66}, \ a_{10}=a_{11}-c_{11}+c_{12}, \\ &a_{11}=a_8+c_{66}, a_{12}=\kappa_{11}+e_{15}^2/c_{55}, \ a_{13}=a_{10}-c_{66} \end{aligned} \tag{5.171}$$

The corresponding conditions of the lateral boundary can be written as [19]

$$\begin{aligned} &[a_8\partial_r u+a_{13}u/r+a_{13}\partial_\theta v/r+a_3p_3/r-a_6p_4/r]_{r=a}=\sigma_{rr}^a, \\ &a_9[\partial_\theta u/r+\partial_r v-v/r]_{r=a}=\sigma_{r\theta}^a, \\ &p_1/r\big|_{r=a}=\sigma_{rz}^a, \\ &(-a_{12}\partial_r\phi+a_1p_1/r)\big|_{r=a}=D_r^a \end{aligned} \tag{5.172}$$

5.5.3 The zero-eigenvalue solutions

For the eigenequation of the problem for zero-eigenvalue μ=0, Eq. (2.156) becomes

$$\mathbf{H}\boldsymbol{\psi}=0 \tag{5.173}$$

where traction-free natural boundary conditions are taken into consideration. Then, Xu et al. presented the direct zero-eigenvalue eigensolutions as

$$\begin{aligned} &\mathbf{v}_1^{(0)}=\boldsymbol{\psi}_1^{(0)}=\{\cos\theta \ -\sin\theta \ \ 0 \ \ 0\ 0\ 0\ 0\}^{\mathrm{T}}, \\ &\mathbf{v}_2^{(0)}=\boldsymbol{\psi}_2^{(0)}=\{\sin\theta \ \cos\theta \ \ 0 \ \ 0\ 0\ 0\ 0\}^{\mathrm{T}}, \\ &\mathbf{v}_3^{(0)}=\boldsymbol{\psi}_3^{(0)}=\{0 \ \ 0 \ \ 1 \ \ 0\ 0\ 0\ 0\}^{\mathrm{T}}, \\ &\mathbf{v}_4^{(0)}=\boldsymbol{\psi}_4^{(0)}=\{0 \ \ 0 \ \ 0 \ \ 1\ 0\ 0\ 0\}^{\mathrm{T}}, \\ &\mathbf{v}_5^{(0)}=\boldsymbol{\psi}_5^{(0)}=\{0 \ \ r \ \ 0 \ \ 0\ 0\ 0\ 0\}^{\mathrm{T}} \end{aligned} \tag{5.174}$$

The governing differential equation for Jordan form solutions then has the following relations:

$$\mathbf{H}\boldsymbol{\psi}_i^{(n+1)} = \boldsymbol{\psi}_i^{(n)} \tag{5.175}$$

The solution to the original problem can thus be expressed as

$$\mathbf{v}_i^{(n+1)} = \boldsymbol{\psi}_i^{(n+1)} + z\boldsymbol{\psi}_i^{(n)} + z^2\boldsymbol{\psi}_i^{(n-1)}/2 + z^3\boldsymbol{\psi}_i^{(n-2)}/6 + \cdots + z^{(n+1)}\boldsymbol{\psi}_i^{(0)}/(n+1)! \tag{5.176}$$

For illustration, the Jordan form of the first order is given as

$$\begin{aligned}
\boldsymbol{\psi}_1^{(1)} &= \{0 \quad 0 \quad -r\cos\theta \quad 0 \quad 0 \quad 0 \quad 0 \quad 0\}^{\mathrm{T}},\\
\boldsymbol{\psi}_2^{(1)} &= \{0 \quad 0 \quad -r\sin\theta \quad 0 \quad 0 \quad 0 \quad 0 \quad 0\}^{\mathrm{T}},\\
\boldsymbol{\psi}_3^{(1)} &= \{-a_{15}r \quad 0 \quad 0 \quad 0 \quad 0 \quad 0 \quad a_{16}r \quad a_{17}r\}^{\mathrm{T}},\\
\boldsymbol{\psi}_4^{(1)} &= \{a_{18}r \quad 0 \quad 0 \quad 0 \quad 0 \quad 0 \quad a_{19}r \quad -a_{20}r\}^{\mathrm{T}},\\
\boldsymbol{\psi}_5^{(1)} &= \{0 \quad 0 \quad 0 \quad 0 \quad 0 \quad r^2/a_2 \quad 0 \quad 0\}^{\mathrm{T}}
\end{aligned} \tag{5.177}$$

The corresponding solutions to the original problem are

$$\begin{aligned}
\mathbf{v}_1^{(1)} &= \{z\cos\theta \quad -z\sin\theta \quad -r\cos\theta \quad 0 \quad 0 \quad 0 \quad 0 \quad 0\}^{\mathrm{T}},\\
\mathbf{v}_2^{(1)} &= \{z\sin\theta \quad z\cos\theta \quad -r\sin\theta \quad 0 \quad 0 \quad 0 \quad 0 \quad 0\}^{\mathrm{T}},\\
\mathbf{v}_3^{(1)} &= \{-a_{15}r \quad 0 \quad z \quad 0 \quad 0 \quad 0 \quad a_{16}r \quad a_{17}r\}^{\mathrm{T}},\\
\mathbf{v}_4^{(1)} &= \{a_{18}r \quad 0 \quad 0 \quad z \quad 0 \quad 0 \quad a_{17}r \quad -a_{19}r\}^{\mathrm{T}},\\
\mathbf{v}_5^{(1)} &= \{0 \quad rz \quad 0 \quad 0 \quad 0 \quad r^2/a_2 \quad 0 \quad 0\}^{\mathrm{T}}
\end{aligned} \tag{5.178}$$

where

$$\begin{aligned}
&a_{14} = 2a_3^2a_7 + 2a_4a_6^2 + 4a_3a_5a_6 - (a_5^2 + a_4a_7)(a_8 + a_{13}),\\
&a_{15} = 2(a_5a_6 - a_3a_7)/a_{14}, \quad a_{16} = [a_7(a_8 + a_{13}) + a_6^2]/a_{14},\\
&a_{17} = [2a_3a_6 + a_5(a_8 + a_{13})]/a_{14}, \quad a_{18} = 2(a_3a_5 + a_4a_6)/a_{14},\\
&a_{19} = (a_4a_6 + a_3^2)/a_{14}
\end{aligned} \tag{5.179}$$

Xu et al. indicated that the physical meanings of these solutions are rigid body rotations, simple extension deformations in which the external electric displacement does not act on the ends but forces the displacement induced by a uniform electric field in which no external force exists, and torsion.

In the following, the Jordan forms of the second and third orders presented in [19] are given as

$$\begin{aligned}
\boldsymbol{\psi}_1^{(2)} &= \{(a_{15}r^2/2)\cos\theta \quad (a_{15}r^2/2)\sin\theta \quad 0\ 0\ 0\ 0 \quad -a_{16}r^2\cos\theta \quad -a_{17}r^2\cos\theta\}^{\mathrm{T}},\\
\boldsymbol{\psi}_2^{(2)} &= \{(a_{15}r^2/2)\sin\theta \quad -(a_{15}r^2/2)\cos\theta \quad 0\ 0\ 0\ 0 \quad -a_{16}r^2\sin\theta \quad -a_{17}r^2\sin\theta\}^{\mathrm{T}}
\end{aligned} \tag{5.180}$$

No solutions exist for i =3,4,5. Then the solutions to the original problem are

$$\begin{aligned}
\mathbf{v}_1^{(2)} &= \{[(a_{15}r^2 + z^2)/2]\cos\theta \quad [(a_{15}r^2 - z^2)/2]\sin\theta - zr\cos\theta \quad 0 \quad 0 \quad 0\\
&\quad -a_{16}r^2\cos\theta - a_{17}r^2\cos\theta\}^{\mathrm{T}},\\
\mathbf{v}_2^{(2)} &= \{[(a_{15}r^2 + z^2)/2]\sin\theta - [(a_{15}r^2 - z^2)/2]\cos\theta - zr\sin\theta \quad 0 \quad 0 \quad 0\\
&\quad -a_{16}r^2\sin\theta - a_{17}r^2\sin\theta\}^{\mathrm{T}}
\end{aligned} \tag{5.181}$$

The Jordan form of the third order is

$$\begin{aligned}\boldsymbol{\psi}_1^{(3)} &= \{0\ 0\ (a_{20}r^3+a_{21}ra^2)\cos\theta\,(a_{22}r^3+a_{23}ra^2)\cos\theta\\ &\quad (a_{24}r^3+a_{25}ra^2)\cos\theta\,(a_{26}r^3+a_{27}ra^2)\sin\theta\ 0\ 0\ \}^{\mathrm{T}},\\ \boldsymbol{\psi}_2^{(3)} &= \{0\ 0\ (a_{20}r^3+a_{21}ra^2)\sin\theta\,(a_{22}r^3+a_{23}ra^2)\sin\theta\\ &\quad (a_{24}r^3+a_{25}ra^2)\sin\theta-(a_{26}r^3+a_{27}ra^2)\cos\theta\ 0\ 0\}^{\mathrm{T}}\end{aligned} \tag{5.182}$$

where a is external radius of the cylinder under consideration. Again, no solutions exist for i =3,4,5. The solutions to the original problem are given by

$$\begin{aligned}\mathbf{v}_1^{(3)} &= \{(a_{15}r^2z/2+z^3/6)\cos\theta\quad (a_{15}r^2z/2-z^3/6)\sin\theta\\ &\quad (a_{20}r^3+a_{21}ra^2-rz^2/2)\cos\theta\quad (a_{22}r^3+a_{23}ra^2)\cos\theta\\ &\quad (a_{24}r^3+a_{25}ra^2)\cos\theta\,(a_{26}r^3+a_{27}ra^2)\sin\theta-a_{16}r^2z\cos\theta-a_{17}r^2z\cos\theta\}^{\mathrm{T}},\\ \mathbf{v}_2^{(3)} &= \{(a_{15}r^2z/2+z^3/6)\sin\theta\quad (a_{15}r^2z/2-z^3/6)\cos\theta\\ &\quad (a_{20}r^3+a_{21}ra^2-rz^2/2)\sin\theta\,(a_{22}r^3+a_{23}ra^2)\sin\theta\\ &\quad (a_{24}r^3+a_{25}ra^2)\sin\theta-(a_{26}r^3+a_{27}ra^2)\cos\theta-a_{16}r^2z\sin\theta-a_{17}r^2z\sin\theta\}^{\mathrm{T}}\end{aligned} \tag{5.183}$$

where

$$\begin{aligned}&a_{20}=a_2a_{16}/8-a_{15}/4-a_1a_{22},\ \ a_{21}=-3a_{20}-a_{15}/2,\quad a_{23}=-3a_{22},\\ &a_{22}=(a_1a_{16}-a_{17})/(8a_{12}),\ \ a_{24}=3a_{16}/8-a_{15}/(4a_2),\quad a_{25}=-a_{24},\\ &a_{26}=3a_{15}/(4a_2)-a_{16}/8,\quad a_{27}=a_{24}\end{aligned} \tag{5.184}$$

Based on the solutions (5.174), (5.178), (5.181), and (5.183), the adjoint symplectic orthogonality relationship of zero-eigenvalue solutions can be established in the following way. Let

$$\begin{aligned}&\mathbf{v}_1^{(\alpha)}=\mathbf{v}_1^{(0)},\ \ \mathbf{v}_2^{(\alpha)}=\mathbf{v}_2^{(0)},\ \ \mathbf{v}_3^{(\alpha)}=\mathbf{v}_3^{(0)},\ \ \mathbf{v}_4^{(\alpha)}=\mathbf{v}_4^{(0)},\ \mathbf{v}_5^{(\alpha)}=\mathbf{v}_5^{(0)},\ \ \mathbf{v}_6^{(\alpha)}=\mathbf{v}_1^{(1)},\\ &\mathbf{v}_7^{(\alpha)}=\mathbf{v}_2^{(1)},\quad \mathbf{v}_1^{(\beta)}=a_{31}(\mathbf{v}_1^{(3)}+a_{28}\mathbf{v}_1^{(1)}),\quad \mathbf{v}_2^{(\beta)}=a_{31}(\mathbf{v}_2^{(3)}+a_{28}\mathbf{v}_2^{(1)}),\\ &\mathbf{v}_3^{(\beta)}=a_{32}(\mathbf{v}_3^{(1)}+a_{29}\mathbf{v}_4^{(1)}),\ \ \mathbf{v}_4^{(\beta)}=a_{33}(\mathbf{v}_4^{(1)}+a_{30}\mathbf{v}_3^{(1)}),\quad \mathbf{v}_5^{(\beta)}=a_{34}\mathbf{v}_5^{(1)},\\ &\mathbf{v}_6^{(\beta)}=a_{35}\mathbf{v}_1^{(2)},\quad \mathbf{v}_7^{(\beta)}=a_{35}\mathbf{v}_2^{(2)}\end{aligned} \tag{5.185}$$

where

$$\begin{aligned}&a_{28}=a^2(4a_{16}a_{20}+6a_{16}a_{21}-14a_{17}a_{22}+2a_{15}a_{24}+2a_{15}a_{26})/(6a_{16}),\\ &a_{29}=a_{17}/a_{19},\ \ a_{30}=-a_{17}/a_{16},\ \ a_{31}=-a_2/[\pi a^4(a_1a_{23}+a_{21}+a_1a_{22}+a_{20})],\\ &a_{32}=-a_{19}/[\pi a^2(a_{16}a_{19}+a_{17}^2)],\quad a_{33}=a_{16}/[\pi a^2(a_{16}a_{19}+a_{17}^2)],\\ &a_{34}=-2a_2/(\pi a^4),\quad a_{35}=-4/(\pi a^4a_{16})\end{aligned} \tag{5.186}$$

The solutions of Eq. (5.185) satisfy the following relationships of the adjoint symplectic orthogonal:

$$\left\langle \mathbf{v}_i^{(\alpha)}, \mathbf{v}_j^{(\beta)} \right\rangle = -\left\langle \mathbf{v}_i^{(\beta)}, \mathbf{v}_j^{(\alpha)} \right\rangle = \delta_{ij}, \qquad \left\langle \mathbf{v}_i^{(\alpha)}, \mathbf{v}_j^{(\alpha)} \right\rangle = -\left\langle \mathbf{v}_i^{(\beta)}, \mathbf{v}_j^{(\beta)} \right\rangle = 0 \quad (5.187)$$

5.5.4 Sub-symplectic system

To obtain eigensolutions related to nonzero-eigenvalue problems

$$(\mathbf{H} - \mu\mathbf{I})\boldsymbol{\psi} = 0 \quad (5.188)$$

Xu et el. introduced a Hamiltonian system sub-symplectic structure. They proposed that the θ coordinate be taken in analogy to the time coordinate and denoted $F' = \partial F / \partial \theta$. The potential energy density (5.161) now becomes

$$\begin{aligned} L_\mu = r\{&c_{11}(\partial_r u)^2 + c_{11}(v'+u)^2/r^2 + c_{33}\mu^2 w^2 + 2c_{12}(\partial_r u)(v'+u)/r \\ &+ 2c_{13}\mu(\partial_r u)w + 2c_{13}(\mu w)(v'+u)/r + c_{55}(w'/r + \mu v)^2 + c_{55}(\partial_r w + \mu u)^2 \\ &+ c_{66}(\partial_r v - v/r + u'/r)^2 + 2e_{31}\mu(\partial_r u)\phi + 2e_{31}\mu\phi(v'+u)/r + 2e_{33}\mu^2 w\phi \\ &+ 2e_{15}(w'/r + \mu v)\phi'/r + 2e_{15}(\partial_r w + \mu u)(\partial_r \phi) - \kappa_{11}(\phi')^2/r^2 \\ &- \kappa_{11}(\partial_r \phi)^2 - \kappa_{33}\mu^2\phi^2\}/2 \end{aligned} \quad (5.189)$$

The dual vector corresponding to Eq. (5.189) is

$$\mathbf{g} = \frac{\partial L_\mu}{\partial \mathbf{q}'} = \begin{Bmatrix} c_{66}(\partial_r v - v/r + u'/r) \\ c_{11}(u+v')/r + c_{12}\partial_r u + c_3\mu w + e_{31}\mu\phi] \\ c_{55}(w'/r + \mu v) + e_{15}\phi'/r] \\ e_{15}(w'/r + \mu v) - \kappa_{11}\phi'/r] \end{Bmatrix} = \begin{Bmatrix} \sigma_{r\theta} \\ \sigma_{\theta\theta} \\ \sigma_{z\theta} \\ D_\theta \end{Bmatrix} \quad (5.190)$$

Xu et al. then mentioned that the variable $\mathbf{g}$ is dual to $\mathbf{q}$ with respect to θ and the variable $\mathbf{p}$ is dual to $\mathbf{q}$ with respect to z, of Eq. (5.163). $\mathbf{p}$ has three independent variables r, z, and θ, and $\mathbf{g}$ has two independent variables r and θ. The sub-symplectic system is then in the form

$$\begin{Bmatrix} \mathbf{q}' \\ \mathbf{g}' \end{Bmatrix} = \begin{Bmatrix} \mathbf{A}_\mu & \mathbf{B}_\mu \\ \mathbf{C}_\mu & -\mathbf{A}_\mu^{\mathrm{T}} \end{Bmatrix} \begin{Bmatrix} \mathbf{q} \\ \mathbf{g} \end{Bmatrix} \quad (5.191)$$

where

$$\mathbf{A}_\mu = \begin{bmatrix} 0 & 1 - r\partial_r & 0 & 0 \\ -1 - b_2 r\partial_r & 0 & -b_2 r\mu & -b_4 r\mu \\ 0 & -r\mu & 0 & 0 \\ 0 & 0 & 0 & 0 \end{bmatrix} \quad (5.192)$$

$$\mathbf{C}_{\mu}=\begin{bmatrix} b_9\partial_r+b_{10}r\partial_r^2-b_{11}r\mu^2 & 0 & b_{12}r\mu+b_{13}r\mu\partial_r & b^{*} \\ 0 & 0 & 0 & 0 \\ -b_{11}\mu-b_{11}r\mu^2+b_{12}r\mu\partial_r & 0 & -b_{11}\mu+b_{16}r\mu^2-b_{11}r\mu\partial_r & b^{**} \\ -b_{17}\mu+b_{19}r\mu\partial_r & 0 & -b_{17}\partial_r-b_{17}r\partial_r^2+b_{18}r\mu^2 & b^{***} \end{bmatrix} \tag{5.193}$$

$$\mathbf{B}_{\mu}=\begin{bmatrix} b_1r & 0 & 0 & 0 \\ 0 & b_5r & 0 & 0 \\ 0 & 0 & b_6r & b_7r \\ 0 & 0 & b_7r & -b_8r \end{bmatrix} \tag{5.194}$$

with

$$\begin{aligned} &b_1=1/c_{66},\ \ b_2=c_{12}/c_{11},\ \ b_3=c_{13}/c_{11},\ \ b_4=e_{31}/c_{11},\ \ b_5=1/c_{11},\\ &b_6=\kappa_{11}\Delta,\ \ b_7=e_{15}\Delta,\ \ b_8=c_{44}\Delta,\ \ b_9=c_{12}(c_{12}/c_{11}-1),\\ &b_{10}=c_{12}^2/c_{11}-c_{11},\ \ b_{11}=c_{55},\ \ b_{12}=c_{13}(c_{12}/c_{11}-1),\\ &b_{13}=b_{12}-c_{55},\ \ b_{14}=e_{31}(c_{12}/c_{11}-1),\\ &b_{15}=c_{13}c_{12}/c_{11}-e_{31}-e_{15},\ \ b_{16}=c_{13}^2/c_{11}-c_{33},\ \ b_{17}=e_{15},\ \ b_{20}=\kappa_{11},\\ &b_{18}=c_{13}e_{31}/c_{11}-e_{33},\ \ b_{19}=c_{12}e_{31}/c_{11}-e_{15}-e_{31},\ \ b_{21}=e_{31}^2/c_{11}+\kappa_{33},\\ &b^{*}=b_{14}r\mu+b_{15}r\mu\partial_r,\ \ \ b^{**}=-b_{17}\partial_r-b_{17}r\mu\partial_r+b_{18}r\mu^2,\\ &b^{***}=b_{20}\partial_r+b_{20}r\partial_r^2+b_{21}r\mu^2 \end{aligned} \tag{5.195}$$

Xu et al. assumed the eigensolutions of the sub-system (5.191) to be in the form

$$\zeta=\zeta_n(r)e^{\beta_n\theta} \tag{5.196}$$

where $\zeta=\{\mathbf{q}^{\mathrm{T}},\mathbf{g}^{\mathrm{T}}\}^{\mathrm{T}}$. In the cylindrical coordinate system, the solution ζ should satisfy the periodic condition:

$$\zeta(r,0)=\zeta(r,2\pi) \tag{5.197}$$

The axisymmetric problem can be described by zero-eigenvalue and the non-axisymmetric solutions of the problem in the form

$$\zeta=\sum C_n\zeta^{(n)}(r)e^{in\theta} \tag{5.198}$$

Substituting the eigensolution

$$\zeta=\tilde{\zeta}(r)e^{in\theta}=\begin{Bmatrix}\tilde{\mathbf{q}}(r)\\ \tilde{\mathbf{g}}(r)\end{Bmatrix}e^{in\theta} \tag{5.199}$$

into the dual equation (5.191) yields

$$\tilde{\mathbf{q}} = C_0\mu K_1^{(0)}\begin{Bmatrix} -i[J_{n-1}(r_0)+J_{n+1}(r_0)] \\ [J_{n-1}(r_0)-J_{n+1}(r_0)] \\ 0 \\ 0 \end{Bmatrix} + \sum_{j=1}^{3} C_j\mu \begin{Bmatrix} K_1^{(j)}[J_{n-1}(r_j)-J_{n+1}(r_j)] \\ iK_1^{(j)}[J_{n-1}(r_j)+J_{n+1}(r_j)] \\ K_2^{(j)}J_n(r_j) \\ K_3^{(j)}J_n(r_j) \end{Bmatrix} \tag{5.200}$$

$$\tilde{\mathbf{g}} = C_0\mu^2 \begin{Bmatrix} K_2^{(0)}(1+2n^2/r_0^2)J_n(r_0)+K_3^{(0)}J_{n-1}(r_0)/r_0+K_4^{(0)}J_{n+1}(r_0)/r_0 \\ i[K_5^{(0)}J_{n-1}(r_0)+K_6^{(0)}J_{n+1}(r_0)]/r_0 \\ K_7^{(0)}[J_{n-1}(r_0)-J_{n+1}(r_0)] \\ K_8^{(0)}[J_{n-1}(r_0)-J_{n+1}(r_0)] \end{Bmatrix}$$

$$+\sum_{j=1}^{3} C_j\mu^2 \begin{Bmatrix} i[K_4^{(j)}J_{n-1}(r_j)-K_5^{(j)}J_{n+1}(r_j)] \\ K_6^{(j)}J_{n-1}(r_j)/r_j+K_7^{(j)}J_{n+1}(r_j)/r_j+K_8^{(j)}J_n(r_j) \\ iK_9^{(j)}[J_{n-1}(r_j)+J_{n+1}(r_j)] \\ iK_{10}^{(j)}[J_{n-1}(r_j)+J_{n+1}(r_j)] \end{Bmatrix} \tag{5.201}$$

where C_j $(j=0,1,2,3)$, $\tilde{\mathbf{q}} = \{\tilde{u},\tilde{v},\tilde{w},\tilde{\phi}\}^{\mathrm{T}}$, $\tilde{\mathbf{g}} = \{\tilde{\sigma}_{r\theta},\tilde{\sigma}_{\theta\theta},\tilde{\sigma}_{z\theta},\tilde{D}_\theta\}^{\mathrm{T}}$, and

$$\begin{aligned} &K_1^{(0)} = 1/(2s_0),\ K_2^{(0)} = c_{66}/s_0^2,\ K_3^{(0)} = c_{66}(n-1)/s_0^2,\ K_4^{(0)} = c_{66}(n+1)/s_0^2, \\ &K_5^{(0)} = [c_{11}(n+1)-c_{12}(n-1)]/(2s_0^2),\ K_6^{(0)} = [c_{12}(n+1)-c_{11}(n-1)]/(2s_0^2), \\ &K_7^{(0)} = c_{55}/(2s_0),\ K_8^{(0)} = e_{15}/(2s_0) \end{aligned} \tag{5.202}$$

$$\begin{aligned} &K_1^{(j)} = 1/(2s_j),\ K_2^{(j)} = (c_{11}\kappa_{11}-m_3s_j^2+c_{55}\kappa_{33}s_j^4)/[(m_1-m_2s_j^2)s_j^2], \\ &K_3^{(j)} = (c_{11}e_{15}-m_4s_j^2+c_{55}e_{33}s_j^4)/[(m_1-m_2s_j^2)s_j^2],\ K_4^{(j)} = c_{66}(n-1)/s_j^2, \\ &K_5^{(j)} = c_{66}(n+1)/s_j^2,\ K_6^{(j)} = [(c_{12}-c_{11})(n+1)]/(2s_j^2), \\ &K_7^{(j)} = [(c_{12}-c_{11})(n-1)]/(2s_j^2),\ K_8^{(j)} = c_{13}K_2^{(j)}+e_{31}K_3^{(j)}-2c_{12}K_1^{(j)}, \\ &K_9^{(j)} = [c_{55}(1+K_2^{(j)})+e_{31}K_3^{(j)}]K_1^{(j)},\ K_{10}^{(j)} = [e_{15}(1+K_2^{(j)})-\kappa_{11}K_3^{(j)}]K_1^{(j)} \end{aligned} \tag{5.203}$$

$$\begin{aligned} &m_1 = \kappa_{11}(c_{13}+c_{55})+e_{15}(e_{15}+e_{31}),\ m_2 = \kappa_{33}(c_{13}+c_{55})+e_{33}(e_{15}+e_{31}), \\ &m_3 = c_{11}\kappa_{33}+c_{55}\kappa_{11}+(e_{15}+e_{31})^2,\ m_4 = c_{11}e_{33}+c_{55}e_{15}-(c_{13}+c_{55})(e_{15}+e_{31}) \end{aligned} \tag{5.204}$$

in which $r_j = \mu r/s_j$, $s_0^2 = c_{66}/c_{55}$, s_j^2 $(j=1,2,3)$ are the three roots of the equation

$$\gamma_3 x^3 - \gamma_2 x^2 + \gamma_1 x - \gamma_0 = 0 \tag{5.205}$$

In Eq. (5.205), the parameters γ_i (i=1=0,1,2,3) are

$$
\begin{aligned}
\gamma_0 &= c_{11}(e_{15}^2 + c_{55}\kappa_{11}),\\
\gamma_1 &= c_{55}[c_{11}\kappa_{33} + (e_{15}+e_{31})^2] + \kappa_{11}[c_{11}c_{33} + c_{55}^2 - (c_{13}+c_{55})^2]\\
&\quad + e_{15}[2c_{11}e_{33} + c_{55}e_{15} - 2(c_{13}+c_{55})(e_{15}+e_{31})],\\
\gamma_2 &= c_{33}[c_{55}\varepsilon_{11} + (e_{15}+e_{31})^2] + \kappa_{33}[c_{11}c_{33} + c_{55}^2 - (c_{13}+c_{55})^2]\\
&\quad + e_{33}[2c_{55}e_{15} + c_{11}e_{33} - 2(c_{13}+c_{55})(e_{15}+e_{31})],\\
\gamma_3 &= c_{55}(e_{33}^2 + c_{33}\kappa_{33})
\end{aligned}
\tag{5.206}
$$

5.5.5 Nonzero-eigenvalue solutions

The nonzero-eigenvalue solutions to Eq.(5.188) can be assumed in the form

$$
\boldsymbol{\psi}(r,z,\theta) = \sum c_j \boldsymbol{\psi}_j(r,\theta) e^{\mu_j z} \tag{5.207}
$$

Substituting the solutions (5.198) into Eq. (5.207) yields

$$
\boldsymbol{\psi}(r,z,\theta) = \sum C_n \boldsymbol{\psi}^{(n)}(r) e^{in\theta} e^{\mu_j z} \tag{5.208}
$$

where $\boldsymbol{\psi}^{(n)}(r) = \{\hat{\mathbf{q}}^{\mathrm{T}}, \hat{\mathbf{p}}^{\mathrm{T}}\}^{\mathrm{T}}$ is related to $\tilde{\zeta}(r) = \{\tilde{\mathbf{q}}^{\mathrm{T}}, \tilde{\mathbf{g}}^{\mathrm{T}}\}^{\mathrm{T}}$ by Eqs. (5.163), (5.164), (5.190), and (5.191), namely, $\hat{\mathbf{q}} = \tilde{\mathbf{q}}$ and

$$
\begin{aligned}
\hat{p}_1 &= -ib_{23}(\mu/n)\tilde{v} + b_{23} r\partial_r \tilde{w} + b_{23} r\partial_r \tilde{\phi} - ib_{25}(\mu/n) r^2 \tilde{g}_1,\\
\hat{p}_2 &= r\tilde{g}_3,\\
\hat{p}_3 &= b_{26}(r\partial_r + 1)\tilde{u} + i(b_{26} n + b_{27} r^2 \mu^2 / n)\tilde{v} - ib_{28}(\mu/n) r^2 \tilde{g}_3 - ib_{29}(\mu/n) r^2 \tilde{g}_4,\\
\hat{p}_4 &= b_{30}(r\partial_r + 1)\tilde{u} + i(b_{30} n + b_{27} r^2 \mu^2 / n)\tilde{v} + ib_{31}(\mu/n) r^2 \tilde{g}_3 - ib_{32}(\mu/n) r^2 \tilde{g}_4
\end{aligned}
\tag{5.209}
$$

in which

$$
\begin{aligned}
&b_{22} = 1/(a_5^2 + a_4 a_7),\ \ b_{23} = 1/a_2,\ \ b_{24} = a_1 b_{23},\ \ b_{25} = b_2 b_{23},\ \ b_{27} = a_7 b_{22},\\
&b_{26} = (a_3 a_7 - a_5 a_6) b_{22},\ \ b_{28} = (b_6 a_7 + b_7 a_5) b_{22},\ \ b_{29} = (b_7 a_7 - b_8 a_5) b_{22},\\
&b_{30} = (a_3 a_7 + a_5 a_6) b_{22},\ \ b_{31} = (b_7 a_5 - b_6 a_7) b_{22},\ \ b_{32} = (b_7 a_7 + b_8 a_5) b_{22}
\end{aligned}
\tag{5.210}
$$

From solutions (5.200), (5.201), and the relation above, we have

$$
\hat{\mathbf{p}} = C_0 \mu \begin{Bmatrix} -iK_9^{(0)} J_n(r_0) \\ r_0 K_{10}^{(0)} [J_{n-1}(r_0) - J_{n+1}(r_0)] \\ 0 \\ 0 \end{Bmatrix} + \sum_{j=1}^{3} C_j \mu \begin{Bmatrix} r_j K_{11}^{(j)} [J_{n-1}(r_j) - J_{n+1}(r_j)] \\ iK_{12}^{(j)} J_n(r_j) \\ r_j K_{13}^{(j)} J_n(r_j) \\ r_j K_{14}^{(j)} J_n(r_j) \end{Bmatrix} \tag{5.211}
$$

where

$$K_9^{(0)} = nc_{55},\ K_{10}^{(0)} = c_{55}/2,\ K_{11}^{(j)} = [c_{44}(1+K_2^{(j)}) + e_5 K_3^{(j)}]/2,\ K_{12}^{(j)} = 2nK_{11}^{(j)},$$
$$K_{13}^{(j)} = c_{33}s_j K_2^{(j)} + e_{33}s_j K_3^{(j)} - c_{13}/s_j,\ K_{14}^{(j)} = e_{33}s_j K_2^{(j)} - \kappa_{33}s_j K_3^{(j)} - e_{31}/s_j \tag{5.212}$$

The traction-free natural boundary conditions (5.172) are now transformed as follows:

$$\begin{aligned}
&[a_8 r\partial_r \hat{u} + a_{13}\hat{u} + a_{13} in\hat{v} + a_3 \hat{p}_2 - a_6 \hat{p}_3]_{r=a} = 0,\\
&[in\hat{u} + r\partial_r \hat{v} - \hat{v}]_{r=a} = 0,\\
&\hat{p}_1|_{r=a} = 0,\\
&\partial_r \hat{\phi}|_{r=a} = 0
\end{aligned} \tag{5.213}$$

where

$$\begin{bmatrix} A_{11} & A_{12} & A_{13} & A_{14} \\ A_{21} & A_{22} & A_{23} & A_{24} \\ A_{31} & A_{32} & A_{33} & A_{34} \\ A_{41} & A_{42} & A_{43} & A_{44} \end{bmatrix} \begin{Bmatrix} C_0 \\ C_1 \\ C_2 \\ C_3 \end{Bmatrix} = 0 \tag{5.214}$$

where

$$\begin{aligned}
A_{11} &= i(a_8 - a_{13})nJ_n(r_0) + (ia_{13}nr_0/2 - ia_8 nr_0/2\\
&\quad + a_3 r_0^2 s_0 r K_{10}^{(0)})[J_{n-1}(r_0) - J_{n+1}(r_0)],\\
A_{21} &= (2n^2 - r_0)J_n(r_0) - r_0[J_{n-1}(r_0) - J_{n+1}(r_0)],\\
A_{31} &= -iK_9^{(0)}J_n(r_0), \qquad A_{41} = 0
\end{aligned} \tag{5.215}$$

$$\begin{aligned}
A_{1,j} &= [a_8(n^2 - r_j^2) - a_{13}n^2 + a_3 ir_j s_j K_{12}^{(j)} - a_6 r_j^2 s_j K_{13}^{(j)}]J_n(r_j)\\
&\quad + (a_8 + a_{13})r_j[J_{n-1}(r_j) - J_{n+1}(r_j)]/2,\\
A_{2,j} &= i\{r_j[J_{n-1}(r_j) - J_{n+1}(r_j)] - J_n(r_j)\}n, \qquad (j=2,3,4)\\
A_{3,j} &= K_{11}^{(j)} r_j[J_{n-1}(r_j) - J_{n+1}(r_j)],\\
A_{4,j} &= K_2^{(j)}[J_{n-1}(r_j) - J_{n+1}(r_j)]/(2s_j)
\end{aligned} \tag{5.216}$$

in which $r_j = \mu a/s_j$ for $j = 0,1,2,3$.

The condition of the nonzero solution of Eq. (5.214) requires that

$$\det|\mathbf{A}(n,\mu)| = 0 \tag{5.217}$$

The eigenvalues obtained by Eq. (5.217) are of infinite number, denoted by μ_{nm} (m =1,2,3,⋯), and eigensolutions are given by Eqs. (5.200), (5.211), and (5.214). By using the characteristics of the Bessel function, $\mathbf{A}(-n,-\mu) = -\mathbf{A}(n,\mu)$, we obtain

$$\boldsymbol{\psi} = \sum_n \sum_m C_{nm}^{(\alpha)} \boldsymbol{\psi}_{nm}^{(\alpha)}(r) e^{\mu_{nm} z} e^{in\theta} + \sum_n \sum_m C_{nm}^{(\beta)} \boldsymbol{\psi}_{nm}^{(\beta)}(r) e^{-\mu_{nm} z} e^{-in\theta} \tag{5.218}$$

The relationships of the adjoint symplectic orthogonal are given by

$$\begin{aligned}
&\left\langle \boldsymbol{\psi}_{nm}^{(\alpha)} e^{in\theta}, \boldsymbol{\psi}_{kj}^{(\beta)}(r) e^{-ik\theta} \right\rangle = \delta_{kn}\delta_{mj}, \quad \left\langle \boldsymbol{\psi}_{nm}^{(\beta)} e^{-in\theta}, \boldsymbol{\psi}_{kj}^{(\alpha)}(r) e^{ik\theta} \right\rangle = -\delta_{kn}\delta_{mj}, \\
&\left\langle \boldsymbol{\psi}_{nm}^{(\alpha)} e^{in\theta}, \boldsymbol{\psi}_{kj}^{(\alpha)}(r) e^{ik\theta} \right\rangle = \left\langle \boldsymbol{\psi}_{nm}^{(\beta)} e^{-in\theta}, \boldsymbol{\psi}_{kj}^{(\beta)}(r) e^{ik\theta} \right\rangle = 0, \\
&\left\langle \boldsymbol{\Psi}_{nm}^{(\alpha)} e^{in\theta}, \mathbf{v}_{k}^{(\alpha)} \right\rangle = \left\langle \boldsymbol{\Psi}_{nm}^{(\beta)} e^{-in\theta}, \mathbf{v}_{k}^{(\beta)} \right\rangle = 0
\end{aligned} \tag{5.219}$$

The final solution to the problem can then be obtained as

$$\begin{aligned}
\boldsymbol{\psi} = &\sum_{m} [C_m^{(\alpha,0)} \mathbf{v}_m^{(\alpha)} + C_m^{(\beta,0)} \mathbf{v}_m^{(\beta)}] \\
&+ \sum_{n} \sum_{m} [C_{nm}^{(\alpha)} \boldsymbol{\psi}_{nm}^{(\alpha)}(r) e^{\mu_{nm} z} e^{in\theta} + C_{nm}^{(\beta)} \boldsymbol{\psi}_{nm}^{(\beta)}(r) e^{-\mu_{nm} z} e^{-in\theta}]
\end{aligned} \tag{5.220}$$

5.6 Symplectic solution for FGPMs

In previous sections of this chapter, all formulations applied to homogeneous piezoelectric materials only. A symplectic system for functionally graded piezoelectric materials is now examined. The shift-Hamiltonian matrix proposed in [21] is briefly reviewed. At the end of this section, extension to the case of functionally graded magnetoelectroelastic materials is discussed.

5.6.1 Basic formulations

In [21], Zhao and Chen considered a generalized plane strain problem of a transversely isotropic FGPM. The constitutive and governing equations are respectively defined by Eqs. (1.24) and (1.27)-(1.29). They assumed that all material properties varied exponentially with z, in the form of

$$c_{ij} = c_{ij}^0 e^{\alpha z}, \quad e_{ij} = e_{ij}^0 e^{\alpha z}, \quad \kappa_{ij} = \kappa_{ij}^0 e^{\alpha z} \tag{5.221}$$

To handle the problem induced by the continuously varying material properties, Zhao and Chen introduced new definitions of stress, electric displacement, body force, and density of free charge as

$$\begin{aligned}
&\bar{\sigma}_x = \sigma_x e^{-\alpha z}, \quad \bar{\sigma}_z = \sigma_z e^{-\alpha z}, \quad \bar{\sigma}_{xz} = \sigma_{xz} e^{-\alpha z}, \quad \bar{D}_x = D_x e^{-\alpha z}, \\
&\bar{D}_z = D_z e^{-\alpha z}, \quad \bar{f}_x = f_x e^{-\alpha z}, \quad \bar{f}_z = f_z e^{-\alpha z}, \quad \bar{Q} = Q e^{-\alpha z}
\end{aligned} \tag{5.222}$$

By way of the variables defined in Eq. (5.222), they obtained the Hamiltonian equation (2.138) in which

$$\begin{aligned}\mathbf{v} &= \left\{u \;\; w \;\; \phi \;\; \bar{\sigma}_{xz} \;\; \bar{\sigma}_z \;\; \bar{D}_z\right\}^{\mathrm{T}},\\ \mathbf{h} &= \left\{0 \;\; 0 \;\; 0 \;\; \bar{f}_x \;\; \bar{f}_z \;\; \bar{Q}\right\}^{\mathrm{T}}\end{aligned} \tag{5.223}$$

$$\mathbf{H} = \begin{bmatrix} 0 & -\dfrac{\partial}{\partial x} & -a_1\dfrac{\partial}{\partial x} & a_2 & 0 & 0 \\ -a_3\dfrac{\partial}{\partial x} & 0 & 0 & 0 & a_4 & a_5 \\ a_6\dfrac{\partial}{\partial x} & 0 & 0 & 0 & a_5 & -a_7 \\ a_8\dfrac{\partial^2}{\partial x^2} & 0 & 0 & -\alpha & -a_3\dfrac{\partial}{\partial x} & a_6\dfrac{\partial}{\partial x} \\ 0 & 0 & 0 & -\dfrac{\partial}{\partial x} & -\alpha & 0 \\ 0 & 0 & a_9\dfrac{\partial^2}{\partial x^2} & -a_1\dfrac{\partial}{\partial x} & 0 & -\alpha \end{bmatrix} \tag{5.224}$$

with

$$\begin{aligned} &a_1 = e_{15}^0/c_{55}^0,\;\; a_2 = 1/c_{55}^0,\;\; a_3 = (c_{13}^0\kappa_{33}^0 + e_{31}^0 e_{33}^0)/g,\;\; a_4 = \kappa_{33}^0/g,\\ &a_5 = e_{33}^0/g,\;\; a_6 = (e_{31}^0 c_{33}^0 - c_{13}^0 e_{33}^0)/g,\;\; a_7 = c_{33}^0/g,\\ &a_8 = -c_{11}^0 + a_3 c_{13}^0 - a_6 e_{31}^0, a_9 = \kappa_{11}^0 + (e_{15}^0)^2/c_{44},\; g = c_{33}^0\kappa_{33}^0 + (e_{33}^0)^2 \end{aligned} \tag{5.225}$$

Using Eqs. (1.24) and (5.222), $\bar{\sigma}_x$ and $\bar{D}_x$ can be expressed in terms of state variables $\mathbf{v}$ as

$$\bar{\sigma}_x = -a_8 u_{,x} + a_3\bar{\sigma}_z - a_6\bar{D}_z,\quad \bar{D}_x = -a_9\phi_{,x} + a_1\bar{\sigma}_{xz} \tag{5.226}$$

Zhao and Chen then discovered that the operator matrix $\mathbf{H}$ exhibits different characteristics from the standard Hamiltonian matrix, but it has similar properties, and they proved that the eigenvalues of $\mathbf{H}$ were symmetric with respect to $-\alpha/2$. They presented the proof as follows. It can be be proved that

$$\mathbf{J}(\mathbf{H} + \alpha\mathbf{I})\mathbf{J} = \mathbf{H}^{\mathrm{T}} \tag{5.227}$$

Supposing the polynomial of the eigenequation to be

$$f(\mu) = \left|\mu\mathbf{I} - \mathbf{H}\right| \tag{5.228}$$

we have

$$\begin{aligned} f(\mu) &= \left|\mathbf{J}(\mu\mathbf{I} - \mathbf{H})\mathbf{J}\right| = \left|\mu\mathbf{J}\mathbf{J} - \mathbf{J}\mathbf{H}\mathbf{J}\right| = \left|\mu\mathbf{J}\mathbf{J} - \mathbf{J}(\mathbf{H} + \alpha\mathbf{I})\mathbf{J} + \alpha\mathbf{J}\mathbf{J}\right| \\ &= \left|-(\alpha+\mu)\mathbf{I} - \mathbf{H}^{\mathrm{T}}\right| = \left|-(\alpha+\mu)\mathbf{I} - \mathbf{H}\right| = f(-\mu-\alpha) \end{aligned} \tag{5.229}$$

The eigenvalues of the Hamiltonian matrix **H** are symmetric with respect to $-\alpha/2$.

5.6.2 Eigenvalue properties of the Hamiltonian matrix H

To study the eigenvalue characteristics of the so-called shift-Hamiltonian matrix **H**, Zhao and Chen [21] considered the plane problem of an FGPM beam occupying the rectangular domain $\Omega:\ 0 \leqslant z \leqslant l,\ -h \leqslant x \leqslant h$, as shown in Fig. 5.6. For the homogeneous Hamiltonian equation and boundary conditions on lateral surfaces:

$$\dot{\mathbf{v}} = \mathbf{H}\mathbf{v} \tag{5.230}$$

and

$$\begin{aligned} &\bar{\sigma}_x = -a_8 u_{,x} + a_3 \bar{\sigma}_z - a_6 \bar{D}_z = 0, \\ &\bar{D}_x = -a_9 \phi_{,x} + a_1 \bar{\sigma}_{xz} = 0, \\ &\bar{\sigma}_{xz} = 0 \end{aligned} \tag{5.231}$$

the solution **v** can be assumed in the form

$$\mathbf{v}(z,x) = \xi(z)\left\{u\ w\ \phi\ \bar{\sigma}_{xz}\ \bar{\sigma}_z\ \bar{D}_x\right\}^{\mathrm{T}}(x) = \xi(z)\boldsymbol{\psi}(x) \tag{5.232}$$

Substituting Eq. (5.232) into Eq. (5.230) yields

$$\xi(z) = e^{\mu z} \tag{5.233}$$

and Eq. (2.156). Zhao and Chen then proved that the operator matrix **H** has the following properties:

If μ_i is the eigenvalue of **H**, $-\mu_i - \alpha$ is also an eigenvalue of **H**. Here μ_i and $-\mu_i - \alpha$ constitute an adjoint pair of eigenvalues (by contrast, the symplectic adjoint eigenvalue of μ_i is $-\mu_i$ for the standard Hamiltonian matrix). Similar to the treatment of the standard Hamiltonian matrix, all the eigenvalues of the shift-Hamiltonian matrix **H** can be divided into the following three groups according to the inhomogeneous parameter α:

(a) μ_i for $\mathrm{Re}(\mu_i) < -\alpha/2$ or $\mathrm{Re}(\mu_i) = -\alpha/2 \bigcap \mathrm{Im}(\mu_i) < 0$ (i=1,2,⋯, n) (5.234)

(b) $\mu_i = -\mu_i - \alpha$ (5.235)

(c) $\mu = -\alpha/2$ (5.236)

5.6.3 Eigensolutions corresponding to μ=0 and $-\alpha$

For the FGPM discussed here, the symplectic adjoint eigenvalue of zero is $-\alpha$, in-

stead of itself. When μ=0, Eq. (2.156) is reduced to Eq. (5.173). The three fundamental eigenvectors of Eq. (5.173) are given by

$$\boldsymbol{\psi}_{0,1}^{(0)} = \{1\,0\,0\,0\,0\,0\}^{\mathrm{T}},\quad \boldsymbol{\psi}_{0,2}^{(0)} = \{0\,1\,0\,0\,0\,0\}^{\mathrm{T}},\quad \boldsymbol{\psi}_{0,3}^{(0)} = \{0\,0\,1\,0\,0\,0\}^{\mathrm{T}} \tag{5.237}$$

The first-order eigenvector of Jordan normal form can be obtained from the matrix equation (5.133) as

$$\boldsymbol{\psi}_{0,1}^{(1)} = \{0\,-x\,0\,0\,0\,0\}^{\mathrm{T}} \tag{5.238}$$

The solution of the original equation (5.230) can be obtained by the combination of solutions (5.237) and (5.238) as

$$\mathbf{v}_{0,1}^{(0)} = \boldsymbol{\psi}_{0,1}^{(0)},\quad \mathbf{v}_{0,2}^{(0)} = \boldsymbol{\psi}_{0,2}^{(0)},\quad \mathbf{v}_{0,3}^{(0)} = \boldsymbol{\psi}_{0,3}^{(0)},\quad \mathbf{v}_{0,1}^{(1)} = \boldsymbol{\psi}_{0,1}^{(1)} + z\boldsymbol{\psi}_{0,1}^{(0)} \tag{5.239}$$

For the eigensolutions corresponding to the eigenvalue μ=$-\alpha$, Eq. (5.188) becomes

$$\mathbf{H}\boldsymbol{\psi}_i^{(0)} = -\alpha\boldsymbol{\psi}_i^{(0)} \tag{5.240}$$

Through a lengthy mathematical manipulation, Zhao and Chen obtained the following three fundamental eigenvectors:

$$\begin{aligned}
\boldsymbol{\psi}_{-\alpha,1}^{(0)} &= \begin{Bmatrix} a_{13}\sinh(\lambda x)/\lambda \\ a_{13}\alpha[\cosh(\lambda x)-1]/\lambda^2 \\ -1/\alpha \\ 0 \\ a_{13}a_{14}\alpha^2[1-\cosh(\lambda x)]/\lambda^2 + a_{15} \\ a_{13}a_{16}\alpha^2[1-\cosh(\lambda x)]/\lambda^2 + a_{17} \end{Bmatrix}, \\
\boldsymbol{\psi}_{-\alpha,2}^{(0)} &= \begin{Bmatrix} -a_{12}\sinh(\lambda x)/\lambda \\ -a_{12}\alpha\cosh(\lambda x)/\lambda^2 \\ 0 \\ 0 \\ a_{14}\cosh(\lambda x) \\ a_{16}\cosh(\lambda x) \end{Bmatrix}, \quad \boldsymbol{\psi}_{-\alpha,3}^{(0)} = \begin{Bmatrix} a_{12}\cosh(\lambda x)/\lambda^2 \\ a_{12}\alpha\sinh(\lambda x)/\lambda^3 \\ 0 \\ 0 \\ -a_{14}\sinh(\lambda x)/\lambda \\ -a_{16}\sinh(\lambda x)/\lambda \end{Bmatrix}
\end{aligned} \tag{5.241}$$

The corresponding first-order eigenvector of Jordan normal form can be obtained from the following matrix equation:

$$\mathbf{H}\boldsymbol{\psi}_{-\alpha,i}^{(1)} = -\alpha\boldsymbol{\psi}_{-\alpha,i}^{(1)} + \boldsymbol{\psi}_{-\alpha,i}^{(0)} \tag{5.242}$$

as

$$\boldsymbol{\psi}_{-\alpha,3}^{(1)}=\begin{Bmatrix}\dfrac{a_{20}x}{2\alpha\lambda}\sinh(\lambda x)-\dfrac{a_{22}}{\alpha\lambda^2}\cosh(\lambda h)-\dfrac{a_{20}}{\alpha\lambda^2}\cosh(\lambda x)\\ \dfrac{a_{20}}{2\lambda^2}\cosh(\lambda x)-\dfrac{a_{21}}{\lambda^2}\cosh(\lambda h)x+\left(\dfrac{6a_{19}}{\lambda^3}-\dfrac{3a_{20}}{2\lambda^3}\right)\sinh(\lambda x)\\ \dfrac{6a_{18}}{\lambda^3}\sinh(\lambda x)-\dfrac{6a_{18}}{\lambda^2}\cosh(\lambda h)x\\ \dfrac{a_{14}}{\lambda^2}[\cosh(\lambda x)-\cosh(\lambda h)]\\ \dfrac{a_{10}a_{20}x}{2\alpha}\cosh(\lambda x)+\lambda^{(1)}\sinh(\lambda x)-\dfrac{6a_{18}b_1\alpha}{\lambda^2}x\cosh(\lambda x)\\ \dfrac{a_{11}a_{20}x}{2\alpha}\cosh(\lambda x)+\lambda^{(2)}\sinh(\lambda x)-\dfrac{6a_{18}b_2\alpha}{\lambda^2}x\cosh(\lambda x)\end{Bmatrix} \tag{5.243}$$

where

$$\begin{aligned}
&a_{10}=\frac{a_6^2+a_7a_8}{a_3a_7-a_5a_6},\ a_{11}=\frac{a_3a_6+a_5a_8}{a_3a_7-a_5a_6},\ a_{12}=\frac{a_5a_6-a_3a_7}{a^*},\ a_{13}=\frac{a_3a_5+a_4a_6}{a^*},\\
&a_{14}=-a_{10}a_{12},\ \ a_{15}=\frac{a_3a_6+a_5a_8}{a^*},\ \ a_{16}=-a_{11}a_{12},\ \ a_{17}=\frac{a_3a_6+a_5a_8}{a^*},\\
&a_{18}=\frac{a_1a_{14}-a_{16}}{6a_9},\ a_{19}=\frac{a_2a_{14}-a_{12}}{6a_9}-a_1a_{18},\ a_{20}=6a_{19}-a_{12}-\frac{6a_{13}a_{18}}{a_{12}},\\
&a_{21}=6a_{13}a_{18}/a_{12},\ a_{22}=6a_{13}a_{18}/a_{12}-6a_{19}-a_{12},\ \lambda=\alpha\sqrt{a_{12}},\\
&\lambda^{(i)}=\frac{6a_{18}b_i\alpha}{\lambda^3}-\frac{a_{9+i}a_{20}}{2\alpha\lambda},\ \ a^*=a_6^2a_4+a_5^2a_8+a_4a_7a_8+2a_3a_5a_6-a_3^2a_7
\end{aligned} \tag{5.244}$$

The eigensolutions corresponding to eigenvalues $\mu=-\alpha$ can be written as

$$\begin{aligned}
&\mathbf{v}_{-\alpha,1}^{(0)}=e^{-\alpha z}\boldsymbol{\psi}_{-\alpha,1}^{(0)},\quad \mathbf{v}_{-\alpha,2}^{(0)}=e^{-\alpha z}\boldsymbol{\psi}_{-\alpha,2}^{(0)},\quad \mathbf{v}_{-\alpha,3}^{(0)}=e^{-\alpha z}\boldsymbol{\psi}_{-\alpha,3}^{(0)},\\
&\mathbf{v}_{-\alpha,3}^{(1)}=e^{-\alpha z}(\boldsymbol{\psi}_{-\alpha,3}^{(1)}+z\boldsymbol{\psi}_{-\alpha,3}^{(0)})
\end{aligned} \tag{5.245}$$

Thus the four solutions of the original boundary-value problem of a plane piezoelastic beam with free lateral boundary conditions can be constructed as

$$\mathbf{v}'=\{u\ w\ \phi\ \sigma_{xz}\ \sigma_z\ D_z\}^{\mathrm{T}}=\mathbf{M}\mathbf{v} \tag{5.246}$$

where $\mathbf{M}$=diag [1, 1, 1, $e^{\alpha z}$, $e^{\alpha z}$, $e^{\alpha z}$] is the transform matrix between the eigensolution and the original solution.

Zhao and Chen then conducted limit analysis by letting $\alpha\to 0$ and obtained the expressions of the original solutions as

$$
\begin{aligned}
\mathbf{v}'^{(0)}_{-\alpha,1} &= \left\{a_{13}\, x \;\; 0 \;\; z-1/\alpha \;\; 0 \;\; a_{15} \;\; a_{17}\right\}^{\mathrm{T}},\\
\mathbf{v}'^{(0)}_{-\alpha,2} &= \left\{-a_{12}\, x \;\; z-1/\alpha \;\; 0 \;\; 0 \;\; a_{14} \;\; a_{16}\right\}^{\mathrm{T}},\\
\mathbf{v}'^{(0)}_{-\alpha,3} &= \left\{\frac{1}{2}a_{12}\; x^2+\frac{1}{2}z^2-\frac{z}{\alpha}+\frac{1}{\alpha^2} \;\; \frac{x}{\alpha}-xz \;\; 0 \;\; 0 \;\; -a_{14}x \;\; -a_{16}x\right\}^{\mathrm{T}},\\
\mathbf{v}'^{(1)}_{-\alpha,3} &= \left\{\nu_1^* \;\; \nu_2^* \;\; a_{18}(x^3-3h^2x) \;\; \frac{a_{14}}{2}(x^2-h^2) \;\; -a_{14}xz \;\; -a_{16}xz\right\}^{\mathrm{T}}
\end{aligned}
\tag{5.247}
$$

in which

$$
\begin{aligned}
\boldsymbol{\nu}_1^* &= \frac{1}{2}a_{12}x^2z+\frac{1}{6}z^3+\frac{a_{22}h^2z}{2}-\frac{z}{\alpha^2}+\frac{2}{\alpha^3}-\frac{a_{22}}{2\alpha}h^2,\\
\boldsymbol{\nu}_2^* &= a_{19}x^3-\frac{1}{2}z^2x+a_{23}x-\frac{a_{22}h^2x}{2}+\frac{x}{\alpha^2},\quad a_{23}=-3a_{19}-\frac{a_{12}}{2}
\end{aligned}
\tag{5.248}
$$

Zhao and Chen finally indicated that by removing the constant electric potential and the rigid translations and rotations, the above degenerated results become the same as those corresponding to the zero-eigenvalue for homogeneous piezoelectric materials [13].

5.6.4 Extension to the case of magnetoelectroelastic materials

In the previous subsections a symplectic model for a plane FGPM was presented. Extension to the plane problems of magnetoelectroelastic media is discussed in this subsection.

In [22], Zhao and Chen considered the plane problem of a functionally graded magnetoelectroelastic strip occupying the rectangular domain $\Omega:\ 0\leqslant z\leqslant l$, $-h\leqslant x\leqslant h$ as shown in Fig. 5.6. With the generalized plane strain assumption, the two-dimensional constitutive and governing equations are given by Eqs. (5.108) and (5.111). All material constants are again assumed to vary exponentially along the length direction, as described by Eq. (5.222) and

$$
\tilde{e}_{ij}=\tilde{e}_{ij}^0e^{\alpha z},\quad \alpha_{ij}=\alpha_{ij}^0e^{\alpha z},\quad \mu_{ij}=\mu_{ij}^0e^{\alpha z}
\tag{5.249}
$$

In the derivation of the Hamiltonian equation, the new variables of stresses, electric displacement, and magnetic induction defined in Eq. (5.222) and

$$
\overline{B}_x=B_xe^{-\alpha z},\quad \overline{B}_z=B_ze^{-\alpha z},\quad \overline{M}=Me^{-\alpha z}
\tag{5.250}
$$

are employed.

Making use of Eqs. (5.108), (5.111), (5.222), and (5.250), the following relationships can be obtained:

$$\begin{aligned}
\overline{\sigma}_x &= -a_{34}u_{,x} + a_{25}\overline{\sigma}_z - a_{29}\overline{D}_z - a_{32}\overline{B}_z,\\
\overline{D}_x &= -a_{35}\phi_{,x} - a_{36}\psi_{,x} + a_1\overline{\sigma}_{xz},\\
\overline{B}_x &= -a_{36}\phi_{,x} - a_{37}\psi_{,x} + a_{24}\overline{\sigma}_{xz}
\end{aligned} \tag{5.251}$$

$$\begin{aligned}
\dot{u} &= -w_{,x} - a_1\phi_{,x} - a_{24}\psi_{,x} + a_2\overline{\sigma}_{xz},\\
\dot{w} &= -a_{25}u_{,x} + a_{26}\overline{\sigma}_z + a_{27}\overline{D}_z + a_{28}\overline{B}_z,\\
\dot{\phi} &= a_{29}u_{,x} + a_{27}\overline{\sigma}_z - a_{30}\overline{D}_z + a_{31}\overline{B}_z,\\
\dot{\psi} &= a_{32}u_{,x} + a_{28}\overline{\sigma}_z + a_{31}\overline{D}_z - a_{33}\overline{B}_z,\\
\dot{\overline{\sigma}}_{xz} &= a_{34}u_{,xx} - a_{25}\overline{\sigma}_{z,x} + a_{29}\overline{D}_{z,x} + a_{32}\overline{B}_{z,x} - \alpha\overline{\sigma}_{xz} - \overline{f}_x,\\
\dot{\overline{\sigma}}_z &= -\overline{\sigma}_{xz,x} - \alpha\overline{\sigma}_z - \overline{f}_z,\\
\dot{\overline{D}}_z &= a_{35}\phi_{,xx} + a_{36}\psi_{,xx} - a_1\overline{\sigma}_{xz,x} - \alpha\overline{D}_z - \overline{Q},\\
\dot{\overline{B}}_z &= a_{36}\phi_{,xx} + a_{37}\psi_{,xx} - a_{24}\overline{\sigma}_{xz,x} - \alpha\overline{B}_z - \overline{M}
\end{aligned} \tag{5.252}$$

where the dot above represents differential with respect to z, and

$$\begin{aligned}
&a_{24} = \tilde{e}^0_{15}/c^0_{55},\ a_{25} = (c^0_{13}b_1 + e^0_{31}b_2 + \tilde{e}^0_{31}b_3),\ a_{26} = (\kappa^0_{33}\mu^0_{33} - \alpha^0_{33}\alpha^0_{33})/a_0,\\
&a_{27} = (e^0_{33}\mu^0_{33} - \tilde{e}^0_{33}\alpha^0_{33})/a_0, \quad a_{28} = (\kappa^0_{33}\tilde{e}^0_{33} - e^0_{33}\alpha^0_{33})/a_0,\\
&a_{29} = (-c^0_{13}b_2 + e^0_{31}b_4 - \tilde{e}^0_{31}b_5),\ a_{30} = (c^0_{33}\mu^0_{33} - \tilde{e}^0_{33}\tilde{e}^0_{33})/a_0,\\
&a_{31} = (c^0_{33}\alpha^0_{33} - \tilde{e}^0_{33}e^0_{33})/a_0, \quad a_{32} = (-c^0_{13}b_3 + \tilde{e}^0_{31}b_6 - e^0_{31}b_5),\\
&a_{33} = (c^0_{33}\kappa^0_{33} - e^0_{33}e^0_{33})/a_0, \quad a_{34} = -c^0_{11} + c^0_{13}a_{25} - e^0_{31}a_{29},\\
&a_{35} = \kappa^0_{11} + (e^0_{15})^2/c^0_{55}, \quad a_{36} = \alpha^0_{11} + e^0_{15}\tilde{e}^0_{15}/c^0_{55},\ a_{37} = \mu^0_{11} + \tilde{e}^0_{15}\tilde{e}^0_{15}/c^0_{55},\\
&a_0 = c^0_{33}b_1 + e^0_{33}b_2 + \tilde{e}^0_{33}b_3
\end{aligned} \tag{5.253}$$

with

$$\begin{aligned}
&b_1 = \kappa^0_{33}\mu^0_{33} - \left(\alpha^0_{33}\right)^2, \quad b_2 = e^0_{33}\mu^0_{33} - \tilde{e}^0_{33}\alpha^0_{33}, \quad b_3 = \kappa^0_{33}\tilde{e}^0_{33} - e^0_{33}\alpha^0_{33},\\
&b_4 = c^0_{33}\mu^0_{33} + \left(\tilde{e}^0_{33}\right)^2, \quad b_5 = c^0_{33}\alpha^0_{33} + e^0_{33}\tilde{e}^0_{33}, \quad b_6 = c^0_{33}\kappa^0_{33} + \left(e^0_{33}\right)^2
\end{aligned} \tag{5.254}$$

Equation (5.252) is the Hamiltonian equation (2.138) in which

$$\begin{aligned}
\mathbf{v} &= \left\{u\ w\ \phi\ \psi\ \overline{\sigma}_{xz}\ \overline{\sigma}_z\ \overline{D}_z\ \overline{B}_z\right\}^{\mathrm{T}},\\
\mathbf{h} &= \left\{0\ 0\ 0\ 0\ \overline{f}_x\ \overline{f}_z\ \overline{Q}\ \overline{M}\right\}^{\mathrm{T}}
\end{aligned} \tag{5.255}$$

$$\mathbf{H} = \begin{bmatrix}
0 & -\partial_x & -a_1\partial_x & -a_{24}\partial_x & a_2 & 0 & 0 & 0\\
-a_{25}\partial_x & 0 & 0 & 0 & 0 & a_{26} & a_{27} & a_{28}\\
a_{29}\partial_x & 0 & 0 & 0 & 0 & a_{27} & -a_{30} & a_{31}\\
a_{32}\partial_x & 0 & 0 & 0 & 0 & a_{28} & a_{31} & -a_{33}\\
a_{34}\partial_x^2 & 0 & 0 & 0 & -\alpha & -a_{25}\partial_x & a_{29}\partial_x & a_{32}\partial_x\\
0 & 0 & 0 & 0 & -\partial_x & -\alpha & 0 & 0\\
0 & 0 & a_{35}\partial_x^2 & a_{36}\partial_x^2 & -a_1\partial_x & 0 & -\alpha & 0\\
0 & 0 & a_{36}\partial_x^2 & a_{37}\partial_x^2 & -a_{24}\partial_x & 0 & 0 & -\alpha
\end{bmatrix} \tag{5.256}$$

The homogeneous boundary conditions used are

$$\begin{aligned}
&\bar{\sigma}_x = -a_{34}u_{,x} + a_{25}\bar{\sigma}_z - a_{29}\bar{D}_z - a_{32}\bar{B}_z = 0, \quad \bar{\sigma}_{xz}=0,\\
&\bar{D}_x = -a_{35}\phi_{,x} - a_{36}\psi_{,x} + a_1\bar{\sigma}_{xz} = 0,\\
&\bar{B}_x = -a_{36}\phi_{,x} - a_{37}\psi_{,x} + a_{24}\bar{\sigma}_{xz} = 0
\end{aligned} \tag{5.257}$$

5.6.4.1 Eigensolutions for $\mu = 0$

There are four fundamental eigenvectors and eigensolutions for the problem defined by Eq. (5.173), which are given by Eq. (5.132). Since zero-eigenvalues are multiple, the Jordan normal form eigenvector needs to be considered. Using Eq. (5.133), the first-order Jordan form can be written as

$$\boldsymbol{\psi}_{0,1}^{(0)} = \left\{0\ -x\ 0\ 0\ 0\ 0\ 0\right\}^{\mathrm{T}} \tag{5.258}$$

The corresponding solution of the original problem is

$$\boldsymbol{\nu}_{0,1}^{(1)} = \boldsymbol{\psi}_{0,1}^{(1)} + z\boldsymbol{\psi}_{0,1}^{(0)} = \left\{z\ -x\ 0\ 0\ 0\ 0\ 0\right\}^{\mathrm{T}} \tag{5.259}$$

which represents the rigid rotation in the plane. Zhao and Chen proved that there is no other high-order Jordan form in the chain.

5.6.4.2 Eigensolutions for $\mu = -\alpha$

For the eigensolutions corresponding to the eigenvalue $\mu = -\alpha$, Eq. (5.188) is used to determine the solutions. Through a lengthy mathematical manipulation, Zhao and Chen obtained the following four fundamental eigenvectors:

$$\boldsymbol{\psi}_{-\alpha,1}^{(0)} = \begin{Bmatrix} k_2\sinh(\lambda x)/\lambda \\ k_2\alpha[\cosh(\lambda x)-1]/\lambda^2 \\ -1/\alpha \\ 0 \\ 0 \\ -k_2m_1\cosh(\lambda x)+m_4 \\ -k_2m_2\cosh(\lambda x)-m_6 \\ -k_2m_3\cosh(\lambda x)+m_8 \end{Bmatrix}, \quad \boldsymbol{\psi}_{-\alpha,2}^{(0)} = \begin{Bmatrix} k_3\sinh(\lambda x)/\lambda \\ k_3\alpha[\cosh(\lambda x)-1]/\lambda^2 \\ 0 \\ -1/\alpha \\ 0 \\ -k_3m_1\cosh(\lambda x)+m_5 \\ -k_3m_2\cosh(\lambda x)+m_7 \\ -k_3m_3\cosh(\lambda x)-m_9 \end{Bmatrix} \tag{5.260}$$

$$\boldsymbol{\psi}_{-\alpha,3}^{(0)} = \begin{Bmatrix} -k_1\sinh(\lambda x)/\lambda \\ -k_1\alpha\cosh(\lambda x)/\lambda^2 \\ 0 \\ 0 \\ 0 \\ k_1m_1\cosh(\lambda x) \\ k_1m_2\cosh(\lambda x) \\ k_1m_3\cosh(\lambda x) \end{Bmatrix}, \quad \boldsymbol{\psi}_{-\alpha,4}^{(0)} = \begin{Bmatrix} k_1\cosh(\lambda x)/\lambda^2 \\ k_1\alpha\sinh(\lambda x)/\lambda^3 \\ 0 \\ 0 \\ 0 \\ -k_1m_1\sinh(\lambda x)/\lambda \\ -k_1m_2\sinh(\lambda x)/\lambda \\ -k_1m_3\sinh(\lambda x)/\lambda \end{Bmatrix} \tag{5.261}$$

where

$$
\begin{aligned}
&m_1=[a_{29}(a_{29}a_{33}+a_{31}a_{32})+a_{32}(a_{29}a_{31}+a_{30}a_{32})-a_{34}(a_{31}^2-a_{30}a_{33})]/m_0,\\
&m_2=[a_{32}(a_{25}a_{31}+a_{27}a_{32})+a_{34}(a_{27}a_{33}+a_{28}a_{31})-a_{29}(a_{28}a_{32}-a_{25}a_{33})]/m_0,\\
&m_3=[a_{29}(a_{28}a_{29}+a_{25}a_{31})+a_{34}(a_{28}a_{30}+a_{27}a_{31})-a_{32}(a_{27}a_{29}-a_{25}a_{30})]/m_0,\\
&m_4=(a_{29}a_{33}+a_{31}a_{32})/m_0,\quad m_5=(a_{29}a_{31}+a_{30}a_{33})/m_0,\\
&m_6=(a_{28}a_{32}-a_{25}a_{33})/m_0,\quad m_7=(a_{25}a_{31}+a_{27}a_{32})/m_0,\\
&m_8=(a_{25}a_{31}+a_{28}a_{29})/m_0,\quad m_9=(a_{27}a_{29}-a_{25}a_{30})/m_0,\\
&m_0=a_{27}(a_{29}a_{33}+a_{31}a_{32})+a_{28}(a_{29}a_{31}+a_{30}a_{32})+a_{25}(a_{31}^2-a_{30}a_{33})
\end{aligned}
\tag{5.262}
$$

$$
\begin{aligned}
&k_1=1/(a_{25}+a_{26}m_1+a_{27}m_3+a_{28}m_3),\quad k_2=k_1(a_{26}m_4-a_{27}m_6+a_{28}m_8),\\
&k_3=k_1(a_{26}m_5-a_{27}m_7+a_{28}m_9),\qquad \lambda=\alpha\sqrt{k_1}
\end{aligned}
\tag{5.263}
$$

The eigensolutions corresponding to eigenvalues $\mu=-\alpha$ can be written as

$$
\tilde{\mathbf{v}}_{-\alpha,1}^{(0)}=e^{-\alpha z}\boldsymbol{\psi}_{-\alpha,1}^{(0)},\ \tilde{\mathbf{v}}_{-\alpha,2}^{(0)}=e^{-\alpha z}\boldsymbol{\psi}_{-\alpha,2}^{(0)},\ \tilde{\mathbf{v}}_{-\alpha,3}^{(0)}=e^{-\alpha z}\boldsymbol{\psi}_{-\alpha,3}^{(0)},\ \tilde{\mathbf{v}}_{-\alpha,4}^{(1)}=e^{-\alpha z}\boldsymbol{\psi}_{-\alpha,4}^{(0)} \tag{5.264}
$$

The solutions of the original problem can then be constructed as

$$
\mathbf{v}_{-\alpha,1}^{(0)}=\mathbf{M}\tilde{\mathbf{v}}_{-\alpha,1}^{(0)},\ \mathbf{v}_{-\alpha,2}^{(0)}=\mathbf{M}\tilde{\mathbf{v}}_{-\alpha,2}^{(0)},\ \mathbf{v}_{-\alpha,3}^{(0)}=\mathbf{M}\tilde{\mathbf{v}}_{-\alpha,3}^{(0)},\ \mathbf{v}_{-\alpha,4}^{(1)}=\mathbf{M}\tilde{\mathbf{v}}_{-\alpha,4}^{(0)} \tag{5.265}
$$

where $\mathbf{M}$=diag [1,1,1,1,$e^{\alpha z}$, $e^{\alpha z}$, $e^{\alpha z}$, $e^{\alpha z}$].

The corresponding first-order eigenvector of Jordan normal form can be obtained from Eq. (5.242) as

$$
\boldsymbol{\psi}_{-\alpha,4}^{(1)}=\left\{\begin{array}{c}
-\dfrac{k_6x}{2\alpha\lambda}\sinh(\lambda x)-\dfrac{k_7}{\alpha\lambda^2}\cosh(\lambda h)+\dfrac{k_6}{\alpha\lambda^2}\cosh(\lambda x)\\
-\dfrac{k_6x}{2\lambda^2}\cosh(\lambda x)-\dfrac{k_8x}{\lambda^2}\cosh(\lambda h)+\dfrac{k_9}{\lambda^3}\sinh(\lambda x)\\
\dfrac{k_4}{\lambda^2}\left[\dfrac{1}{\lambda}\sinh(\lambda x)-x\cosh(\lambda h)\right]\\
\dfrac{k_5}{\lambda^2}\left[\dfrac{1}{\lambda}\sinh(\lambda x)-x\cosh(\lambda h)\right]\\
\dfrac{k_1m_1}{\lambda^2}\left[\cosh(\lambda x)-\cosh(\lambda h)\right]\\
\dfrac{k_6m_1}{2\alpha}\left[x\cosh(\lambda x)-\dfrac{\sinh(\lambda x)}{\lambda}\right]-\dfrac{k_{10}\alpha}{\lambda^2}\left[\dfrac{\sinh(\lambda x)}{\lambda}-x\cosh(\lambda h)\right]\\
\dfrac{k_6m_2}{2\alpha}\left[x\cosh(\lambda x)-\dfrac{\sinh(\lambda x)}{\lambda}\right]-\dfrac{k_{11}\alpha}{\lambda^2}\left[\dfrac{\sinh(\lambda x)}{\lambda}-x\cosh(\lambda h)\right]\\
\dfrac{k_6m_3}{2\alpha}\left[x\cosh(\lambda x)-\dfrac{\sinh(\lambda x)}{\lambda}\right]-\dfrac{k_{12}\alpha}{\lambda^2}\left[\dfrac{\sinh(\lambda x)}{\lambda}-x\cosh(\lambda h)\right]
\end{array}\right\} \tag{5.266}
$$

where

$$
\begin{aligned}
&k_4 = k_1[a_{37}(a_1 m_1 - m_2) - a_{36}(a_{24} m_1 - m_3)]/(a_{35}a_{37} - a_{36}^2),\\
&k_5 = k_1[a_{35}(a_{24} m_1 - m_3) - a_{36}(a_1 m_1 - m_2)]/(a_{35}a_{37} - a_{36}^2),\\
&k_6 = 2k_1 + h_1 + h_2/k_1,\ \ k_7 = h_1 + h_2/k_1,\ \ k_8 = h_2/k_1,\\
&k_9 = 2k_7 + k_1/2 + k_8,\ \ k_{10} = m_4 k_4 + m_5 k_5,\ \ k_{11} = -m_6 k_4 + m_7 k_5,\\
&k_{12} = m_8 k_4 - m_9 k_5,\ \ h_1 = a_1 k_4 + a_{24} k_5 - a_2 k_1 m_1,\ \ h_2 = k_2 k_4 + k_3 k_5
\end{aligned}
\tag{5.267}
$$

The corresponding solution of the original problem is in the following form:

$$
\mathbf{v}_{-\alpha,4}^{(1)} = \mathbf{M}(e^{-\alpha z}\boldsymbol{\psi}_{-\alpha,4}^{(1)} + z\boldsymbol{\psi}_{-\alpha,4}^{(0)}) \tag{5.268}
$$

Limiting the analysis by letting $\alpha \to 0$, Zhao and Chen obtained the expressions of the original solutions as

$$
\begin{aligned}
&\mathbf{v}_{-\alpha,1}^{(0)} = \{k_2\ \ x\ \ 0\ \ z - 1/\alpha\ \ 0\ \ 0\ \ -m_1 k_2 + m_4\ \ -m_2 k_2 - m_6\ \ -m_3 k_2 + m_8\}^{\mathrm{T}},\\
&\mathbf{v}_{-\alpha,2}^{(0)} = \{k_3\ \ x\ \ 0\ \ 0\ \ z - 1/\alpha\ \ 0\ \ -m_1 k_3 + m_5\ \ -m_2 k_3 + m_7\ \ -m_3 k_3 - m_9\}^{\mathrm{T}},\\
&\mathbf{v}_{-\alpha,3}^{(0)} = \{-k_1\ \ x\ \ z - 1/\alpha\ \ 0\ \ 0\ \ 0\ \ m_1 k_1\ \ m_2 k_1\ \ m_3 k_1\}^{\mathrm{T}},\\
&\mathbf{v}_{-\alpha,4}^{(0)} = \left\{\frac{k_1 x^2 + z^2}{2} - \frac{z}{\alpha} + \frac{1}{\alpha^2}\ \ -xz + \frac{x}{\alpha}\ \ 0\ \ 0\ \ 0\ \ -m_1 k_1 x\ \ -m_2 k_1 x\ \ -m_3 k_1 x\right\}^{\mathrm{T}}
\end{aligned}
\tag{5.269}
$$

and

$$
\begin{aligned}
\mathbf{v}_{-\alpha,4}^{(1)} = \{&\frac{k_1}{2}x^2 z + \frac{z^3}{6} + \frac{k_7 h^2 z}{2} - \frac{z}{\alpha^2} + \frac{2}{\alpha^3} - \frac{k_7 h^2}{2\alpha},\ \ -\frac{1}{6}(k_1 + h_1)x^3,\\
&\frac{h_1 h^2 x}{2} - \frac{xz^2}{2} - \frac{k_7 h^2 x}{2} + \frac{x}{\alpha^2},\ \ \frac{k_5 x}{6}(x^2 - 3h^2),\ \ \frac{k_1 m_1}{2}(x^2 - h^2),\\
&-k_1 m_1 xz,\ \ -k_1 m_2 xz,\ \ -k_1 m_3 xz\}^{\mathrm{T}}
\end{aligned}
\tag{5.270}
$$

By removing the constant electric potential, the constant magnetic potential, the rigid translations and rotations, the above degenerated solutions become the same as those corresponding to the zero eigenvalue for homogeneous magnetoelectroelastic materials [24].

References

[1] Qin QH: Green's functions of magnetoelectroelastic solids with a half-plane boundary or bimaterial interface. Philosophical Magazine Letters **84**(12), 771-779 (2004).

[2] Qin QH: Green's Function and Boundary Elements in Multifield Materials. Elsevier, Oxford (2007).

[3] Li JY: Magnetoelectroelastic multi-inclusion and inhomogeneity problems and their

applications in composite materials. International Journal of Engineering Science **38**(18), 1993-2011 (2000).

[4] Qin QH, Yang QS: Macro-Micro Theory on Multifield Behaviour of Heterogeneous Materials. Higher Education Press & Springer, Beijing (2008).

[5] Yu SW, Qin QH: Damage analysis of thermopiezoelectric properties .1. Crack tip singularities. Theoretical and Applied Fracture Mechanics **25**(3), 263-277 (1996).

[6] Yu SW, Qin QH: Damage analysis of thermopiezoelectric properties .2. Effective crack model. Theoretical and Applied Fracture Mechanics **25**(3), 279-288 (1996).

[7] Chen CD: On the singularities of the thermo-electro-elastic fields near the apex of a piezoelectric bonded wedge. International Journal of Solids and Structures **43**(5), 957-981 (2006).

[8] Zhong WX: Duality System in Applied Mechanics and Optimal Control. Kluwer Academic Publishers, Boston (2004).

[9] Zhong WX, Williams FW: Physical interpretation of the symplectic orthogonality of the eigensolutions of a Hamiltonian or symplectic matrix. Computers and Structures **49**, 749-750 (1993).

[10] Yao WA, Zhong WX, Lim CW: Symplectic Elasticity. World Scientific Publishing, Singapore (2009).

[11] Lim CW, Xu XS: Symplectic elasticity: theory and applications. Applied Mechanics Reviews **63**, 050801-050810 (2010).

[12] Gu Q, Xu XS, Leung AYT: Application of Hamiltonian system for two-dimensional transversely anisotropic piezoelectric media. Journal of Zhejiang University: Science **6A**(9), 915-921 (2005).

[13] Leung AYT, Xu XS, Gu Q, Leung CTO, Zheng JJ: The boundary layer phenomena in two-dimensional transversely isotropic piezoelectric media by exact symplectic expansion. International Journal for Numerical Methods in Engineering **69**(11), 2381-2408 (2007).

[14] Leung AYT, Xu X, Zhou Z, Wu YF: Analytic stress intensity factors for finite elastic disk using symplectic expansion. Engineering Fracture Mechanics **76**(12), 1866-1882 (2009).

[15] Zhou ZH, Xu XS, Leung AYT: The mode Ⅲ stress/electric intensity factors and singularities analysis for edge-cracked circular piezoelectric shafts. International Journal of Solids and Structures **46**(20), 3577-3586 (2009).

[16] Zhou ZH, Xu XS, Leung AYT: Analytical mode Ⅲ electromagnetic permeable cracks in magnetoelectroelastic materials. Computers & Structures **89**(7-8), 631-645 (2011).

[17] Zhou ZH, Xu XS, Leung AYT: Mode Ⅲ edge-crack in magneto-electro-elastic media by symplectic expansion. Engineering Fracture Mechanics **77**(16), 3157-3173 (2010).

[18] Leung AYT, Zheng JJ, Lim CW, Zhang XC, Xu XS, Gu Q: A new symplectic approach for piezoelectric cantilever composite plates. Computers & Structures **86**(19-20), 1865-1874 (2008).

[19] Xu XS, Leung AYT, Gu Q, Yang H, Zheng JJ: 3D symplectic expansion for piezoelectric media. International Journal for Numerical Methods in Engineering **74**(12), 1848-1871 (2008).

[20] Wang JS, Qin QH: Symplectic model for piezoelectric wedges and its application in analysis of electroelastic singularities. Philosophical Magazine **87**(2), 225-251 (2007).

[21] Zhao L, Chen WQ: Symplectic analysis of plane problems of functionally graded piezoelectric materials. Mechanics of Materials **41**(12), 1330-1339 (2009).

[22] Zhao L, Chen WQ: Plane analysis for functionally graded magneto-electro-elastic materials via the symplectic framework. Composite Structures **92**(7), 1753-1761 (2010).

[23] Li XC, Yao WA: Symplectic analytical solutions for the magnetoelectroelastic solids plane problem in rectangular domain. Journal of Applied Mathematics **2011**, 165160 (2011).

[24] Yao WA, Li XC: Symplectic duality system on plane magnetoelectroelastic solids. Applied Mathematics and Mechanics-English Edition **27**(2), 195-205 (2006).

[25] Chue CH, Chen CD: Antiplane stress singularities in a bonded bimaterial piezoelectric wedge. Archive of Applied Mechanics **72**(9), 673-685 (2003).

[26] Chue CH, Chen CD: Decoupled formulation of piezoelectric elasticity under generalized plane deformation and its application to wedge problems. International Journal of Solids and Structures **39**(12), 3131-3158 (2002).

[27] Zhang HW, Zhong WX: Hamiltonian principle based stress singularity analysis near crack corners of multi-material junctions. International Journal of Solids and Structures **40**(2), 493-510 (2003).

Chapter 6 Saint-Venant Decay Problems in Piezoelectricity

As an application of the symplectic mechanics described in the previous chapter, Saint-Venant decay analysis of piezoelectric strips is presented in this chapter. Applications of state space approach to the Saint-Venant decay problem of piezoelectric laminates are also discussed. Particularly, a mixed-variable state space model for dissimilar piezoelectric laminates and multilayered graded piezoelectric materials is described. Further formulations for decay analysis of piezoelectric-piezomagnetic sandwich structures are discussed.

6.1 Introduction

Saint-Venant's principle [1], named after the French elasticity theorist Jean Claude Barré de Saint-Venant, is an old topic and has been widely studied in both elastic materials and piezoelectricity [2-5]. As stated in [6], the Saint-Venant's effect can be explained as "the strains that can be produced in a body by the application, to a small part of its surface, of a system of forces statically equivalent to zero force and zero couple, are of negligible magnitude at distances which are large compared with the linear dimensions of the part." For purely elastic materials, the problem of stress decay has been extensively investigated by many researchers [7,8]. By contrast, progress in the study of Saint-Venant decay of piezoelectric material has been much slower, due to the complex mathematical operations induced by electromechanical coupling. Batra and his co-workers [9,10] extended the energy-decay inequality techniques to the case of piezoelectric cylinders and helical piezoelectric solids. They proved that the energy stored in the piezoelectricity decreases exponentially. Fan [11] applied Stroh formalism and the eigen-expansion equation approach to an analysis of two-dimensional decay in piezoelectricity. Using the stress function approach, Ruan et al. [12] presented an approximate analysis of decay behavior for a semi-infinite piezoelectric strip. Using the state space approach as a basis, Tarn and Huang [3] studied the Saint-Venant end effects in multilayered piezoelectric laminates under generalized plane strain deformation. Borrelli et al. [13] used the energy-decay inequality technique to analyze the decay behavior of end effects in anti-plane shear deformation in piezoelectric solids and FGPMs. They subsequently extended the Airy-type stress function approach to cases of plane deformation of linear piezoelectric materials. It should be noted that the methods above often lead to a higher order of partial differential equations (PDE) which, to some extent, are difficult to solve theoretically [14]. Bisegna [15] established the Saint-Venant principle for monoclinic piezoelectric cylinders and demonstrated that the free energy

stored in the cylinder decays exponentially along the cylinder axis. Rovenski et al. [16] presented a linear analysis of homogeneous piezoelectric beams that undergo tip loading, based on the Saint-Venant's principle and semi-inverse method of solution. Vidoli et al. [17] obtained a second-order solution for the Saint-Venant problem for a straight, prismatic, homogeneous and transversely isotropic body made of a second-order piezoelectric materials. For a prismatic circular bar subjected to bending moments only at the end faces, they found that in addition to the second-order Poisson's effect proportional to the square of moment vector, there is also a torsional effect proportional to the square of the distance from the "clamped" face. Xue and Liu [4] investigated the decay of the Saint-Venant end effects for plane deformations of piezoelectric-piezomagnetic sandwich structures. He et al. [5] presented a mixed-variable state space formulation for the Saint-Venant decay analysis of FGPMs. Recently, Qin and Wang [2] developed a symplectic model for Saint-Venant analysis of a piezoelectric strip. In this chapter, the focus is on the developments in [2-5].

6.2 Saint-Venant end effects of piezoelectric strips

In this section a Hamiltonian system presented in [2] for modeling Saint-Venant decay behavior at the ends of a piezoelectric strip under plane deformation is described. The derivation is based on a differential equations approach. In the analysis, governing equations of a piezoelectric strip are first transferred into Hamiltonian form via a differential approach with multi-variables and the state space method. The approach of variable separation under the Hamiltonian system is then used to obtain the nonzero-eigenvalues and to analyze decay behavior at the ends of a piezoelectric strip.

6.2.1 Hamiltonian system for a piezoelectric strip

Consider a transversely isotropic piezoelectric strip as shown in Fig. 6.1. The polarization direction is assumed to be parallel to the z-axis. Derivation of the Hamiltonian system for the piezoelectric strip is based on the governing equation (1.10), constitutive equation (1.25), generalized strain-displacement relationship (1.2), and boundary conditions (1.11),(1.12). For the problem of a two-dimensional piezoelectric strip in the absence of body forces and electric charge density, the basic equations (5.109)-(5.111) become

$$\frac{\partial \sigma_x}{\partial x}+\frac{\partial \sigma_{xz}}{\partial z}=0, \qquad \frac{\partial \sigma_{xz}}{\partial x}+\frac{\partial \sigma_z}{\partial z}=0, \qquad \frac{\partial D_x}{\partial x}+\frac{\partial D_z}{\partial z}=0 \tag{6.1}$$

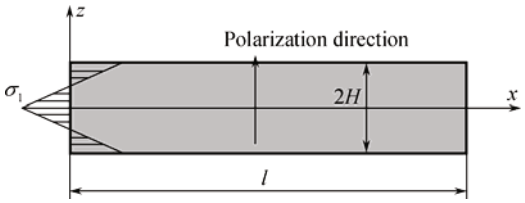

Fig. 6.1 Geometry and loading configuration of the piezoelectric strip.

$$\begin{Bmatrix}\varepsilon_x\\ \varepsilon_z\\ \gamma_{xz}\end{Bmatrix}=\begin{bmatrix}a_{11} & a_{13} & 0\\ a_{13} & a_{33} & 0\\ 0 & 0 & a_{55}\end{bmatrix}\begin{Bmatrix}\sigma_x\\ \sigma_z\\ \sigma_{xz}\end{Bmatrix}+\begin{bmatrix}0 & m_{31}\\ 0 & m_{33}\\ m_{15} & 0\end{bmatrix}\begin{Bmatrix}E_x\\ E_z\end{Bmatrix},$$
$$\begin{Bmatrix}D_x\\ D_z\end{Bmatrix}=\begin{bmatrix}0 & 0 & m_{15}\\ m_{31} & m_{33} & 0\end{bmatrix}\begin{Bmatrix}\sigma_x\\ \sigma_z\\ \sigma_{xz}\end{Bmatrix}+\begin{bmatrix}\lambda_{11} & 0\\ 0 & \lambda_{33}\end{bmatrix}\begin{Bmatrix}E_x\\ E_z\end{Bmatrix} \tag{6.2}$$

$$\varepsilon_x=\frac{\partial u}{\partial x},\quad \varepsilon_z=\frac{\partial w}{\partial z},\quad \gamma_{xz}=\frac{\partial u}{\partial z}+\frac{\partial w}{\partial x},\quad E_x=-\frac{\partial \phi}{\partial x},\quad E_z=-\frac{\partial \phi}{\partial z} \tag{6.3}$$

$$\sigma_z(\pm H)=0,\quad \sigma_{zx}(\pm H)=0,\quad D_z(\pm H)=0 \tag{6.4}$$

where a_{ij} are defined in Eq. (1.26), and

$$m_{15}=d_{15},\quad m_{31}=d_{31}-\frac{d_{31}f_{12}}{f_{11}},\quad m_{33}=d_{33}-\frac{d_{31}f_{13}}{f_{11}},$$
$$\lambda_{11}=\kappa_{11},\quad \lambda_{33}=\kappa_{33}-\frac{d_{31}^2}{f_{11}} \tag{6.5}$$

It is worth noting that at the surfaces $z=\pm H$, only homogeneous boundary conditions are considered. However, under inhomogeneous boundary conditions, i.e., where the right-hand terms of Eq. (6.4) are not equal to zero, the decay rate is the same as that for the case of homogeneous boundary conditions, although the corresponding Saint-Venant solutions without decay characteristics may be different. Moreover, the procedure here, presented initially for stress and electric displacement boundary conditions, is also valid for displacement and electric potential boundary conditions or mixed boundary conditions.

The field equations (6.1)-(6.3) can be converted into the Hamiltonian form using a differential approach. In doing so, the *x*-coordinate, defined in the longitudinal direction, is analogous to the "time coordinate" in elastic dynamics, and the *z*-coordinate is defined in the poling direction. The displacements *u*, *w* in the longitudinal and transverse directions respectively and the electric potential ϕ are chosen as state variables, and the normal stress σ_x, the shear stress τ_{xz} as well as the electric displacement D_x are defined as dual vectors to the state variables above. Denote these definitions by **q** and **p** so that

$$\mathbf{q}=\begin{Bmatrix} u \\ w \\ \phi \end{Bmatrix},\quad \mathbf{p}=\begin{Bmatrix} \sigma_x \\ \sigma_{xz} \\ D_x \end{Bmatrix} \tag{6.6}$$

where **q** and **p** are a pair of dual vectors in Hamiltonian system.

Making use of Eqs. (6.1)-(6.5), we have

$$\begin{aligned}
\dot{u} &= \left(a_{11}-\frac{a_{13}^2}{a_{33}}\right)\sigma_x+\frac{a_{13}}{a_{33}}\frac{\partial w}{\partial z}+\left(\frac{a_{13}m_{33}}{a_{33}}-m_{31}\right)\frac{\partial \phi}{\partial z},\\
\dot{w} &= -\frac{\partial u}{\partial z}+\left(a_{55}-\frac{m_{15}^2}{\lambda_{11}}\right)\sigma_{xz}+\frac{m_{15}}{\lambda_{11}}D_x,\\
\dot{\phi} &= \frac{m_{15}}{\lambda_{11}}\sigma_{xz}-\frac{1}{\lambda_{11}}D_x,\\
\dot{\sigma}_x &= -\frac{\partial \sigma_{xz}}{\partial z},\\
\dot{\sigma}_{xz} &= \frac{a_{13}}{a_{33}}\frac{\partial \sigma_x}{\partial z}-\frac{1}{a_{33}}\frac{\partial^2 w}{\partial z^2}-\frac{m_{33}}{a_{33}}\frac{\partial^2 \phi}{\partial z^2},\\
\dot{D}_x &= -\frac{m_{33}}{a_{33}}\frac{\partial^2 w}{\partial z^2}+\left(\lambda_{33}-\frac{m_{33}^2}{a_{33}}\right)\frac{\partial^2 \phi}{\partial z^2}+\left(\frac{m_{33}a_{13}}{a_{33}}-m_{31}\right)\frac{\partial \sigma_x}{\partial z}
\end{aligned} \tag{6.7}$$

where a dot "$\cdot$" over a variable or function represents differentiation with respect to x.

Further, if we define the full state vectors **v** and $\dot{\mathbf{v}}$ by

$$\dot{\mathbf{v}}=\begin{Bmatrix} \dot{\mathbf{q}} \\ \dot{\mathbf{p}} \end{Bmatrix},\quad \mathbf{v}=\begin{Bmatrix} \mathbf{q} \\ \mathbf{p} \end{Bmatrix} \tag{6.8}$$

Equation (6.7) can be rewritten as

$$\dot{\mathbf{v}}=\mathbf{H}\mathbf{v} \tag{6.9}$$

in which **H** is known as the Hamiltonian operator matrix:

$$\mathbf{H}=\begin{bmatrix}
0 & k_1\frac{\partial}{\partial z} & k_2\frac{\partial}{\partial z} & k_3 & 0 & 0 \\
-\frac{\partial}{\partial z} & 0 & 0 & 0 & k_4 & k_5 \\
0 & 0 & 0 & 0 & k_5 & k_6 \\
0 & 0 & 0 & 0 & -\frac{\partial}{\partial z} & 0 \\
0 & k_7\frac{\partial^2}{\partial z^2} & k_8\frac{\partial^2}{\partial z^2} & k_1\frac{\partial}{\partial z} & 0 & 0 \\
0 & k_8\frac{\partial^2}{\partial z^2} & k_9\frac{\partial^2}{\partial z^2} & k_2\frac{\partial}{\partial z} & 0 & 0
\end{bmatrix} \tag{6.10}$$

where

$$k_1=\frac{a_{13}}{a_{33}},\quad k_2=\frac{a_{13}m_{33}}{a_{33}}-m_{31},\quad k_3=a_{11}-\frac{a_{13}^2}{a_{33}},\quad k_4=a_{55}-\frac{m_{15}^2}{\lambda_{11}},$$
$$k_5=\frac{m_{15}}{\lambda_{11}},\quad k_6=-\frac{1}{\lambda_{11}},\quad k_7=-\frac{1}{a_{33}},\quad k_8=-\frac{m_{33}}{a_{33}},\quad k_9=\lambda_{33}-\frac{m_{33}^2}{a_{33}} \tag{6.11}$$

It should be noted that the Hamiltonian equation (6.9) is based on the constitutive equation (6.2) in which stress σ_{ij} and electric field E_i are taken as basic variables. For the constitutive equations (1.24) in which ε_{ij} and E_i are the basic variables, the corresponding symplectic form of field variables now becomes

$$\dot{u}=\frac{1}{c_{33}}\sigma_x-\frac{c_{13}}{c_{11}}\frac{\partial w}{\partial z}-\frac{e_{31}}{c_{11}}\frac{\partial \phi}{\partial z},$$

$$\dot{w}=-\frac{\partial u}{\partial z}+\frac{\kappa_{11}}{\Delta}\sigma_{xz}+\frac{e_{15}}{\Delta}D_x,$$

$$\dot{\phi}=\frac{e_{15}}{\Delta}\sigma_{xz}-\frac{c_{55}}{\Delta}D_x, \tag{6.12}$$

$$\dot{\sigma}_x=-\frac{\partial \sigma_{xz}}{\partial z},$$

$$\dot{\sigma}_{xz}=-\frac{c_{13}}{c_{11}}\frac{\partial \sigma_x}{\partial z}+\left(\frac{c_{13}^2}{c_{11}}-c_{33}\right)\frac{\partial^2 w}{\partial z^2}+\left(\frac{c_{13}e_{31}}{c_{11}}-e_{33}\right)\frac{\partial^2 \phi}{\partial z^2},$$

$$\dot{D}_x=\left(\frac{c_{13}e_{31}}{c_{11}}-e_{33}\right)\frac{\partial^2 w}{\partial z^2}+\left(\kappa_{33}+\frac{e_{31}^2}{c_{11}}\right)\frac{\partial^2 \phi}{\partial z^2}-\frac{e_{31}}{c_{11}}\frac{\partial \sigma_x}{\partial z}$$

where $\Delta=c_{55}\kappa_{11}+e_{15}^2$. The corresponding matrix of Hamiltonian operator **H** has the same form as that of Eq. (6.10), except that k_i (i = 1-9) are now defined by

$$k_1=-\frac{c_{13}}{c_{11}},\quad k_2=-\frac{e_{31}}{c_{11}},\quad k_3=\frac{1}{c_{11}},\quad k_4=\frac{\kappa_{11}}{\Delta},\quad k_5=\frac{e_{15}}{\Delta},\quad k_6=-\frac{c_{55}}{\Delta},$$
$$k_7=\frac{c_{13}^2}{c_{11}}-c_{33},\quad k_8=\frac{c_{13}e_{31}}{c_{11}}-e_{33},\quad k_9=\frac{e_{31}^2}{c_{11}}+\kappa_{33} \tag{6.13}$$

To prove that **H** is indeed a Hamiltonian operator matrix, the rotational exchange operator matrix **J** defined in Eq. (2.130) is rewritten as follows [18]:

$$\mathbf{J}=\begin{bmatrix}\mathbf{0} & \mathbf{I}_3\\ -\mathbf{I}_3 & \mathbf{0}\end{bmatrix},\quad \mathbf{J}^2=\begin{bmatrix}-\mathbf{I}_3 & 0\\ 0 & -\mathbf{I}_3\end{bmatrix},\quad \mathbf{J}^{-1}=-\mathbf{J}=\mathbf{J}^{\mathrm{T}} \tag{6.14}$$

where $\mathbf{I}_3$ is the three-order identity matrix. With the notation $\mathbf{J}$, it is easy to prove that $\mathbf{H}$ satisfies the following relation:

$$\left\langle \mathbf{v}_1^{\mathrm{T}}, \mathbf{H}\mathbf{v}_2 \right\rangle = \left\langle \mathbf{v}_2^{\mathrm{T}}, \mathbf{H}\mathbf{v}_1 \right\rangle \tag{6.15}$$

where

$$\left\langle \mathbf{v}_1^{\mathrm{T}}, \mathbf{H}\mathbf{v}_2 \right\rangle = \int_{z_1}^{z_2} \mathbf{v}_1^{\mathrm{T}} \mathbf{J}\mathbf{H}\mathbf{v}_2 \, \mathrm{d}z \tag{6.16}$$

and $\mathbf{v}_1$, $\mathbf{v}_2$ are two full state vectors satisfying the homogeneous boundary conditions (6.4) at $z = \pm H$. Therefore $\mathbf{H}$ satisfies the relation $\mathbf{JHJ}=\mathbf{H}^{\mathrm{T}}$. According to the theory of symplectic geometry [19], $\mathbf{H}$ is a Hamiltonian operator matrix.

Noting that Eq. (6.9) can be solved by the method of variable separation and the symplectic eigenfunction expansion, we assume $\mathbf{v}$ in the form

$$\mathbf{v}(x,z) = \boldsymbol{\kappa}(x)\boldsymbol{\psi}(z) \tag{6.17}$$

in which $\boldsymbol{\kappa}(x)$ is a function of x and $\boldsymbol{\psi}(z)$ depends on z only.

Substituting Eq. (6.17) into Eq. (6.9) yields the solution for $\boldsymbol{\kappa}(x)$ as

$$\boldsymbol{\kappa}(x) = e^{\mu x} \tag{6.18}$$

and the corresponding eigenvalue equation

$$\mathbf{H}\boldsymbol{\psi} = \mu\boldsymbol{\psi} \tag{6.19}$$

It should be noted that the eigenvalues of the Hamiltonian operator matrix $\mathbf{H}$ have the following property [19]: if μ_i is an eigenvalue of Eq. (6.19), then $-\mu_i$ is also an eigenvalue of Eq. (6.19). Thus all eigenvalues of $\mathbf{H}$ can be subdivided into the following three groups:

(a) μ_i, $\mathrm{Re}(\mu_i) > 0$ or $\mathrm{Im}(\mu_i) > 0$ (if $\mathrm{Re}(\mu_i) = 0$) i=1,2,⋯

(b) $\mu_{-i} = -\mu_i$ (6.20)

(c) $\mu = 0$

From Eqs. (6.9), (6.17), and (6.18), the following expression can be obtained:

$$\begin{Bmatrix} \mathbf{q} \\ \mathbf{p} \end{Bmatrix} = e^{\mu x}\boldsymbol{\psi}(z) \tag{6.21}$$

From Eq. (6.21), it is evident that all field variables including stress, electric displacements, elastic displacements, and electric potential contain the same factor $e^{\mu x}$. Therefore they will decay exponentially for a negative value of μ when x increases. The real part of eigenvalue μ with the smallest positive real part is here

known as the decay rate. The next step is to determine μ and then to analyze the end decay behavior of a piezoelectric strip using the proposed formulation.

6.2.2 Decay rate analysis

The decay parameter μ is determined by considering the equation

$$(\mathbf{H}-\mu\mathbf{I}_6)\boldsymbol{\psi}=0 \tag{6.22}$$

and setting the determinant of matrix $(\mathbf{H}-\mu\mathbf{I}_6)$ to be zero, where $\mathbf{I}_6$ is a six-order identity matrix. To this end, consider

$$\det\begin{bmatrix} -\mu & k_1\lambda & k_2\lambda & k_3 & 0 & 0 \\ -\lambda & -\mu & 0 & 0 & k_4 & k_5 \\ 0 & 0 & -\mu & 0 & k_5 & k_6 \\ 0 & 0 & 0 & -\mu & -\lambda & 0 \\ 0 & k_7\lambda^2 & k_8\lambda^2 & k_1\lambda & -\mu & 0 \\ 0 & k_8\lambda^2 & k_9\lambda^2 & k_2\lambda & 0 & -\mu \end{bmatrix}=0 \tag{6.23}$$

where $\lambda=\partial/\partial z$ and $\lambda^2=\partial^2/\partial z^2$.

The roots of Eq. (6.23) have two possible cases.

Case 1 :

$$\lambda=\pm\beta_1\mu i,\quad \lambda=(\alpha_2\pm\beta_2 i)\mu,\quad \lambda=(-\alpha_2\pm\beta_2 i)\mu \tag{6.24}$$

Case 2:

$$\lambda=\pm\beta_1\mu i,\quad \lambda=\pm\beta_2\mu i,\quad \lambda=\pm\beta_3\mu i \tag{6.25}$$

where α_2 and β_i (i =1-3) are real positive constants depending on the properties of the piezoelectric material and can be determined numerically. For piezoelectric materials PZT-5H, PZT-5, PZT-4 and Ceramic-B, the roots of Eq. (6.23) are in Case 1, which are the same as those in [14]. For certain piezoelectric materials like PZT-6B, the roots of Eq. (6.23) may be in Case 2 [2].

Thus, the general solutions for the whole state vectors can be given as follows:

$$\begin{aligned} ue^{-\mu x} &= A_1\cos(h_1)+B_1\sin(h_1)+C_1\cosh(g_2)\cos(h_2)+D_1\sinh(g_2)\cos(h_2) \\ &\quad +E_1\sinh(g_2)\sin(h_2)+F_1\cosh(g_2)\sin(h_2), \\ we^{-\mu x} &= A_2\sin(h_1)+B_2\cos(h_1)+C_2\sinh(g_2)\cos(h_2)+D_2\cosh(g_2)\cos(h_2) \\ &\quad +E_2\cosh(g_2)\sin(h_2)+F_2\sinh(g_2)\sin(h_2), \\ \phi e^{-\mu x} &= A_3\sin(h_1)+B_3\cos(h_1)+C_3\sinh(g_2)\cos(h_2)+D_3\cosh(g_2)\cos(h_2) \\ &\quad +E_3\cosh(g_2)\sin(h_2)+F_3\sinh(g_2)\sin(h_2), \end{aligned}$$

$$\begin{aligned}
\sigma_x e^{-\mu x} &= A_4\cos(h_1)+B_4\sin(h_1)+C_4\cosh(g_2)\cos(h_2)+D_4\sinh(g_2)\cos(h_2)\\
&\quad +E_4\sinh(g_2)\sin(h_2)+F_4\cosh(g_2)\sin(h_2),\\
\sigma_{xz} e^{-\mu x} &= A_5\sin(h_1)+B_5\cos(h_1)+C_5\sinh(g_2)\cos(h_2)+D_5\cosh(g_2)\cos(h_2)\\
&\quad +E_5\cosh(g_2)\sin(h_2)+F_5\sinh(g_2)\sin(h_2),\\
D_x e^{-\mu x} &= A_6\sin(h_1)+B_6\cos(h_1)+C_6\sinh(g_2)\cos(h_2)+D_6\cosh(g_2)\cos(h_2)\\
&\quad +E_6\cosh(g_2)\sin(h_2)+F_6\sinh(g_2)\sin(h_2)
\end{aligned} \tag{6.26}$$

for Case 1, and

$$\begin{aligned}
u e^{-\mu x} &= A_1\cos(h_1)+B_1\sin(h_1)+C_1\cos(h_2)+D_1\sin(h_2)+E_1\cos(h_3)+F_1\sin(h_3),\\
w e^{-\mu x} &= A_2\sin(h_1)+B_2\cos(h_1)+C_2\sin(h_2)+D_2\cos(h_2)+E_2\sin(h_3)+F_2\cos(h_3),\\
\phi e^{-\mu x} &= A_3\sin(h_1)+B_3\cos(h_1)+C_3\sin(h_2)+D_3\cos(h_2)+E_3\sin(h_3)+F_3\cos(h_3),\\
\sigma_x e^{-\mu x} &= A_4\cos(h_1)+B_4\sin(h_1)+C_4\cos(h_2)+D_4\sin(h_2)+E_4\cos(h_3)+F_4\sin(h_3),\\
\sigma_{xz} e^{-\mu x} &= A_5\sin(h_1)+B_5\cos(h_1)+C_5\sin(h_2)+D_5\cos(h_2)+E_5\sin(h_3)+F_5\cos(h_3),\\
D_x e^{-\mu x} &= A_6\sin(h_1)+B_6\cos(h_1)+C_6\sin(h_2)+D_6\cos(h_2)+E_6\sin(h_3)+F_6\cos(h_3)
\end{aligned} \tag{6.27}$$

for Case 2, where $g_j=\alpha_j\mu z$, $h_j=\beta_j\mu z$ $(j=1\text{-}3)$, and A_i, B_i, C_i, D_i, E_i, and F_i (i=1-6) are unknown coefficients.

The above general solutions can be decomposed into two separate parts: a symmetric deformation solution and an anti-symmetric deformation solution. Taking the symmetric deformation of Case 1 as an example, we have

$$\begin{aligned}
u e^{-\mu x} &= A_1\cos(h_1)+C_1\cosh(g_2)\cos(h_2)+E_1\sinh(g_2)\sin(h_2),\\
w e^{-\mu x} &= A_2\sin(h_1)+C_2\sinh(g_2)\cos(h_2)+E_2\cosh(g_2)\sin(h_2),\\
\phi e^{-\mu x} &= A_3\sin(h_1)+C_3\sinh(g_2)\cos(h_2)+E_3\cosh(g_2)\sin(h_2),\\
\sigma_x e^{-\mu x} &= A_4\cos(h_1)+C_4\cosh(g_2)\cos(h_2)+E_4\sinh(g_2)\sin(h_2),\\
\sigma_{xz} e^{-\mu x} &= A_5\sin(h_1)+C_5\sinh(g_2)\cos(h_2)+\ E_5\cosh(g_2)\sin(h_2),\\
D_x e^{-\mu x} &= A_6\sin(h_1)+C_6\sinh(g_2)\cos(h_2)+E_6\cosh(g_2)\sin(h_2)
\end{aligned} \tag{6.28}$$

Substituting Eq. (6.28) into Eq. (6.19), we can obtain relationships between A_i, C_i, and E_i as

$$A_i=\begin{cases} t_i A_1 & (i=2,3)\\ t_i\mu A_1 & (i=4\text{-}6)\end{cases},\qquad C_i=\begin{cases} r_i C_1+s_i E_1 & (i=2,3)\\ r_i\mu C_1+s_i\mu E_1 & (i=4\text{-}6)\end{cases},$$
$$E_i=\begin{cases} t_i^* C_1+w_i E_1 & (i=2,3)\\ t_i^*\mu C_1+w_i\mu E_1 & (i=4\text{-}6)\end{cases} \tag{6.29}$$

where t_i, r_i, s_i, t_i^* and w_i (i=1-6) are unknown coefficients and can be determined numerically.

From Eqs. (6.2), (6.3), and (6.11), the stress σ_z and the electric displacement

D_z can be expressed as

$$\sigma_z = -k_1\sigma_x - k_7\frac{\partial w}{\partial z} - k_8\frac{\partial \varphi}{\partial z}, \quad D_z = -k_2\sigma_x - k_8\frac{\partial w}{\partial z} - k_9\frac{\partial \varphi}{\partial z} \tag{6.30}$$

Using the boundary condition (6.4), the following equation can be obtained:

$$\begin{bmatrix} p_1C_1^* & p_2W^*C_2^* + p_3R^*S_2^* & p_4W^*\cos(h_2^*) + p_5R^*S_2^* \\ t_5S_1^* & t_5^*W^*S_2^* + r_5R^*C_2^* & w_5W^*S_2^* + s_5R^*C_2^* \\ m_1C_1^* & m_2W^*C_2^* + m_3R^*S_2^* & m_4W^*C_2^* + m_5R^*S_2^* \end{bmatrix} \begin{Bmatrix} A_1 \\ C_1 \\ E_1 \end{Bmatrix} = 0 \tag{6.31}$$

where $g_i^* = \alpha_i\mu H$, $h_i^* = \beta_i\mu H$, $W^* = \cosh(g_2^*)$, $R^* = \sinh(g_2^*)$, $C_i^* = \cos(h_i^*)$, $S_i^* = \sin(h_i^*)$, and

$$\begin{aligned}
p_1 &= -(k_7t_2 + k_8t_3)\beta_1 - k_1t_4, \\
p_2 &= -k_7(\alpha_2r_2 + \beta_2t_2^*) - k_8(\alpha_2r_3 + \beta_2t_3^*) - k_1r_4, \\
p_3 &= k_7(\beta_2r_2 - \alpha_2t_2^*) + k_8(\beta_2r_3 - \alpha_2t_3^*) - k_1t_4^*, \\
p_4 &= -k_7(\alpha_2s_2 + \beta_2w_2) - k_8(\alpha_2s_3 + \beta_2w_3) - k_1s_4, \\
p_5 &= k_7(\beta_2s_2 - \alpha_2w_2) + k_8(\beta_2s_3 - \alpha_2w_3) - k_1w_4, \\
m_1 &= -(k_8t_2 + k_9t_3)\beta_1 - k_2t_4, \\
m_2 &= -k_8(\alpha_2r_2 + \beta_2t_2^*) - k_9(\alpha_2r_3 + \beta_2t_3^*) - k_2r_4, \\
m_3 &= k_8(\beta_2r_2 - \alpha_2t_2^*) + k_9(\beta_2r_3 - \alpha_2t_3^*) - k_2t_4^*, \\
m_4 &= -k_8(\alpha_2t_2^* + \beta_2w_2) - k_9(\alpha_2t_3^* + \beta_2w_3) - k_2s_4, \\
m_5 &= k_8(\beta_2s_2 - \alpha_2w_2) + k_9(\beta_2s_3 - \alpha_2w_3) - k_2w_4
\end{aligned} \tag{6.32}$$

The condition for the existence of non-zero solutions of $\{A_1 \quad C_1 \quad E_1\}^{\mathrm{T}}$ is the determinant of the coefficients matrix being zero, which leads to the following equation:

$$\det\begin{bmatrix} p_1C_1^* & p_2W^*C_2^* + p_3R^*S_2^* & p_4W^*\cos(h_2^*) + p_5R^*S_2^* \\ t_5S_1^* & t_5^*W^*S_2^* + r_5R^*C_2^* & w_5W^*S_2^* + s_5R^*C_2^* \\ m_1C_1^* & m_2W^*C_2^* + m_3R^*S_2^* & m_4W^*C_2^* + m_5R^*S_2^* \end{bmatrix} = 0 \tag{6.33}$$

Similarly, the solution for the case of anti-symmetric deformation can be obtained as

$$\begin{aligned}
ue^{-\mu x} &= B_1\sin(h_1) + D_1\sinh(g_2)\cos(h_2) + F_1\cosh(g_2)\sin(h_2), \\
we^{-\mu x} &= B_2\cos(h_1) + D_2\cosh(g_2)\cos(h_2) + F_2\sinh(g_2)\sin(h_2), \\
\phi e^{-\mu x} &= B_3\cos(h_1) + D_3\cosh(g_2)\cos(h_2) + F_3\sinh(g_2)\sin(h_2), \\
\sigma_x e^{-\mu x} &= B_4\sin(h_1) + D_4\sinh(g_2)\cos(h_2) + F_4\cosh(g_2)\sin(h_2), \\
\sigma_{xy} e^{-\mu x} &= B_5\cos(h_1) + D_5\cosh(g_2)\cos(h_2) + F_5\sinh(g_2)\sin(h_2), \\
D_x e^{-\mu x} &= B_6\cos(h_1) + D_6\cosh(g_2)\cos(h_2) + F_6\sinh(g_2)\sin(h_2)
\end{aligned} \tag{6.34}$$

In a similar manner to that in Eq. (6.33), we have

$$\det\begin{bmatrix} p_1 S_1^* & p_2 W^* S_2^* + p_3 R^* C_2^* & p_4 W^* S_2^* + p_5 R^* C_2^* \\ a_5^* C_1^* & b_5^* R^* S_2^* + r_5^* W^* C_2^* & w_5^* R^* S_2^* + s_5^* W^* C_2^* \\ m_1 S_1^* & m_2 W^* S_2^* + m_3 R^* C_2^* & m_4 W^* S_2^* + m_5 R^* C_2^* \end{bmatrix} = 0 \tag{6.35}$$

in which

$$\begin{aligned}
p_1 &= (k_7 a_2^* + k_8 a_3^*)\beta_1 - k_1 a_4^*, \\
p_2 &= k_7(\beta_2 r_2^* - \alpha_2 b_2^*) + k_8(\beta_2 r_3^* - \alpha_2 b_3^*) - k_1 b_4^*, \\
p_3 &= -k_7(\alpha_2 r_2^* + \beta_2 b_2^*) - k_8(\alpha_2 r_3^* + \beta_2 b_3^*) - k_1 r_4^*, \\
p_4 &= k_7(\beta_2 s_2^* - \alpha_2 w_2^*) + k_8(\beta_2 s_3^* - \alpha_2 w_3^*) - k_1 w_4^*, \\
p_5 &= -k_7(\alpha_2 s_2^* + \beta_2 w_2^*) - k_8(\alpha_2 s_3^* + \beta_2 w_3^*) - k_1 s_4^*, \\
m_1 &= (k_8 a_2^* + k_9 a_3^*)\beta_1 - k_2 a_4^*, \\
m_2 &= k_8(\beta_2 r_2^* - \alpha_2 b_2^*) + k_9(\beta_2 r_3^* - \alpha_2 b_3^*) - k_2 b_4^*, \\
m_3 &= -k_8(\alpha_2 r_2^* + \beta_2 b_2^*) - k_9(\alpha_2 r_3^* + \beta_2 b_3^*) - k_2 r_4^*, \\
m_4 &= k_8(\beta_2 s_2^* - \alpha_2 w_2^*) + k_9(\beta_2 s_3^* - \alpha_2 w_3^*) - k_2 w_4^*, \\
m_5 &= -k_8(\alpha_2 s_2^* + \beta_2 w_2^*) - k_9(\alpha_2 s_3^* + \beta_2 w_3^*) - k_2 s_4^*
\end{aligned} \tag{6.36}$$

and $a_i^*, r_i^*, s_i^*, b_i^*, w_i^*$ (i = 2-6) are unknown coefficients. The equations for unknowns B_i, D_i, and F_i are as follows:

$$B_i = \begin{cases} a_i^* B_1 & (i = 2,3) \\ a_i^* \mu B_1 & (i = 4\text{-}6) \end{cases}, \qquad D_i = \begin{cases} r_i^* D_1 + s_i^* F_1 & (i = 2,3) \\ r_i^* \mu D_1 + s_i^* \mu F_1 & (i = 4\text{-}6) \end{cases},$$
$$F_i = \begin{cases} b_i^* D_1 + w_i^* F_1 & (i = 2,3) \\ b_i^* \mu D_1 + w_i^* \mu F_1 & (i = 4\text{-}6) \end{cases} \tag{6.37}$$

The solutions presented above are for piezoelectric materials whose characteristic constant of material property matrix is defined by Eq. (6.24), which is applicable to PZT-5H, PZT-5, PZT-4, and Ceramic-B under consideration. General solutions for materials with characteristic constants defined by Eq. (6.25), which are applicable to PZT-6B under consideration, can be obtained similarly and are listed below:

(1) Symmetric deformation solutions:

$$\begin{aligned}
u e^{-\mu x} &= A_1 \cos(h_1) + C_1 \cos(h_2) + E_1 \cos(h_3), \\
w e^{-\mu x} &= A_2 \sin(h_1) + C_2 \sin(h_2) + E_2 \sin(h_3), \\
\phi e^{-\mu x} &= A_3 \sin(h_1) + C_3 \sin(h_2) + E_3 \sin(h_3),
\end{aligned}$$

$$\begin{aligned}
\sigma_x e^{-\mu x} &= A_4 \cos(h_1) + C_4 \cos(h_2) + E_4 \cos(h_3), \\
\sigma_{xy} e^{-\mu x} &= A_5 \sin(h_1) + C_5 \sin(h_2) + E_5 \sin(h_3), \\
D_x e^{-\mu x} &= A_6 \sin(h_1) + C_6 \sin(h_2) + E_6 \sin(h_3)
\end{aligned} \tag{6.38}$$

The corresponding transcendental equations for nonzero eigenvectors are

$$\begin{aligned}
(p_3 m_2 - p_2 m_3) a_5 S_1^* C_2^* C_3^* + (p_2 m_1 - p_1 m_2) e_5 C_1^* C_2^* S_3^* \\
+ (p_1 m_3 - m_1 p_3) c_5 C_1^* S_2^* C_3^* = 0
\end{aligned} \tag{6.39}$$

where

$$\begin{aligned}
p_1 &= (-k_7 a_2 - k_8 a_3)\beta_1 - k_1 a_4, \quad p_2 = (-k_7 c_2 - k_8 c_3)\beta_1 - k_1 c_4, \\
p_3 &= (-k_7 e_2 - k_8 e_3)\beta_1 - k_1 e_4, \quad m_1 = (-k_8 a_2 - k_9 a_3)\beta_1 - k_2 a_4, \\
m_2 &= (-k_8 c_2 - k_9 c_3)\beta_1 - k_2 c_4, \quad m_3 = (-k_8 e_2 - k_9 e_3)\beta_1 - k_2 e_4
\end{aligned} \tag{6.40}$$

and a_i, c_i and e_i are coefficients defined by

$$A_i = \begin{cases} a_i A_1 & (i = 2,3) \\ a_i \mu A_1 & (i = 4\text{-}6) \end{cases}, \quad C_i = \begin{cases} c_i C_1 & (i = 2,3) \\ c_i \mu C_1 & (i = 4\text{-}6) \end{cases}, \quad E_i = \begin{cases} e_i E_1 & (i = 2,3) \\ e_i \mu E_1 & (i = 4\text{-}6) \end{cases} \tag{6.41}$$

which can be determined numerically.

(2) Anti-symmetric deformation solutions:

$$\begin{aligned}
u e^{-\mu x} &= B_1 \sin(h_1) + D_1 \sin(h_2) + F_1 \sin(h_3), \\
w e^{-\mu x} &= B_2 \cos(h_1) + D_2 \cos(h_2) + F_2 \cos(h_3), \\
\phi e^{-\mu x} &= B_3 \cos(h_1) + D_3 \cos(h_2) + F_3 \cos(h_3), \\
\sigma_x e^{-\mu x} &= B_4 \sin(h_1) + D_4 \sin(h_2) + F_4 \sin(h_3), \\
\sigma_{xy} e^{-\mu x} &= B_5 \cos(h_1) + D_5 \cos(h_2) + F_5 \cos(h_3), \\
D_x e^{-\mu x} &= B_6 \cos(h_1) + D_6 \cos(h_2) + F_6 \cos(h_3)
\end{aligned} \tag{6.42}$$

The corresponding transcendental equations for nonzero eigenvectors are

$$(n_3 t_2 - n_2 t_3) b_5 C_1^* S_2^* S_3^* + (n_1 t_3 - n_3 t_1) d_5 S_1^* C_2^* S h_3^* + (n_2 t_1 - n_1 t_2) f_5 S_1^* S_2^* C h_3^* = 0 \tag{6.43}$$

where

$$\begin{aligned}
n_1 &= (k_7 b_2 + k_8 b_3)\beta_1 - k_1 b_4, \quad n_2 = (k_7 d_2 + k_8 d_3)\beta_1 - k_1 d_4, \\
n_3 &= (k_7 f_2 + k_8 f_3)\beta_1 - k_1 f_4, \quad t_1 = (k_8 b_2 + k_9 b_3)\beta_1 - k_2 b_4, \\
t_2 &= (k_8 d_2 + k_9 d_3)\beta_1 - k_2 d_4, \quad t_3 = (k_8 f_2 + k_9 f_3)\beta_1 - k_2 f_4
\end{aligned} \tag{6.44}$$

and b_i, d_i and f_i are coefficients are defined by

$$B_i = \begin{cases} b_i B_1 & (i = 2,3) \\ b_i \mu B_1 & (i = 4\text{-}6) \end{cases}, \quad D_i = \begin{cases} d_i D_1 & (i = 2,3) \\ d_i \mu D_1 & (i = 4\text{-}6) \end{cases}, \quad F_i = \begin{cases} f_i F_1 & (i = 2,3) \\ f_i \mu F_1 & (i = 4\text{-}6) \end{cases} \tag{6.45}$$

The transcendental equations (6.33), (6.35), (6.39), or (6.43) can be used for

determining the eigenvalue μ for various piezoelectric strip materials. As usual, the eigenvalues are decomposed into even and odd groups. It is evident that the even decay rate, k (even), corresponds to cases of symmetric deformation solutions, whereas the odd decay rate, k (odd), corresponds to cases of anti-symmetric deformation. To characterize the end effects of piezoelectric strips, the characteristic decay length L, which is defined as the length over which the stress and the electric displacement decay to 1% of their value, has been introduced and used in the following numerical analysis: $L = \ln(100/k)$.

6.2.3 Numerical illustration

To illustrate applications of the formulation presented above in studying the Saint-Venant decay behavior of a piezoelectric strip, numerical results of decay rate and characteristic decay length for several piezoelectric strips are presented. Table 6.1 lists the material properties of PZT-5H, PZT-5, PZT-4, and Ceramic-B used in the numerical analysis, in which f_{ij} is the elastic compliance constant, d_{ij} is the piezoelectric constant, and κ_{ij}/κ_0 is relative permittivity. The corresponding values of α_2 and β_i of these materials are listed in Table 6.2. It should be mentioned that the coefficients a_i, r_i, s_i, $\cdots$ appearing in Eqs. (6.29)-(6.45) can be determined numerically using the data listed in Tables 6.1 and 6.2. The properties of PZT-6B are in a form different from that in Table 6.1 and are given separately as

Elastic constants (10^{10} N/m^2): $c_{11} = 16.8$, $c_{12} = 6.0$, $c_{33} = 16.3$, $c_{55} = 2.71$;

Piezoelectric constants (C/m^2): $e_{15} = 4.6$, $e_{31} = -0.9$, $e_{33} = 7.1$;

Dielectric permittivities (10^{-10} F/m): $\kappa_{11}/\kappa_0 = 36$, $\kappa_{33}/\kappa_0 = 34$.

Table 6.1 Piezoelectric properties.

		PZT-5H	PZT-5	PZT-4	Ceramic-B
$f_{ij}\,/\left(10^{-12}\ \mathrm{m^2/N}\right)$	f_{11}	16.5	16.4	12.4	8.6
	f_{12}	–4.78	–5.74	–3.98	–2.6
	f_{13}	–8.45	–7.22	–5.52	–2.7
	f_{33}	20.7	18.8	16.1	9.1
	f_{44}	43.5	47.5	39.1	22.2
$d_{ij}\,/\left(10^{-12}\ \mathrm{C/N}\right)$	d_{31}	–274	–172	–135	–58
	d_{33}	593	374	300	149
	d_{15}	741	584	525	242
$\kappa_{ij}/\kappa_0\ (\kappa_0 = 8.85\times10^{-12}\ \mathrm{F/m})$	κ_{11}/κ_0	1 700	1 730	1 470	1 000
	κ_{33}/κ_0	1 470	1 700	1 300	910

Table 6.2 Values of α_2 and β_i (i=1-3) for materials listed in Table 6.1.

	β_1	α_2	β_2
PZT-5H	8.210 16	0.289 22	1.010 77
PZT-5	1.077 68	0.258 98	1.076 76
PZT-4	1.187 52	0.276 48	1.085 87
Ceramic-B	1.097 21	0.227 98	1.003 05
	β_1	β_2	β_3
PZT-6B	2.101 46	1.014 33	0.517 60

To determine the complex roots of Eqs. (6.33), (6.35), (6.39), and (6.43), μ is assumed in the form: $\alpha+i\beta$. It can be determined by setting the real and imaginary parts of Eqs. (6.33), (6.35), (6.39), or (6.43) to zero to find the points of intersection of the curves defined by these four equations. Tables 6.3 and 6.4 present the results of the decay rate and the characteristic decay length. Comparison with the results from other techniques is also made. It can be seen from Tables 6.3 and 6.4 that the proposed symplectic method provides reasonably accurate estimates for decay rate and characteristic decay length. It is also found that for all the piezoelectric materials considered in this chapter except PZT-5H, L (even) >L (odd), which coincides with the findings in [20]. Moreover, PZT-5H has the largest decay length L (odd) and the smallest decay rate k (odd), which may be caused by the fact that the value of β_1 for PZT-5H is the largest in Table 6.2. For PZT-6B, it is also the case that L (even) > L (odd).

Table 6.3 Decay rate of several piezoelectric strips.

	Decay rate k (even)			Decay rate k (odd)		
	[14][a]	[14][b]	Present	[14][a]	[14][b]	Present
PZT-5H	1.104/H	1.864/H	1.157/H	0.436/H	0.428/H	0.572/H
PZT-5	1.092/H	1.230/H	1.244/H	2.811/H	2.610/H	2.918/H
PZT-4	1.337/H	1.210/H	1.226/H	2.125/H	2.571/H	2.748/H
Ceramic-B	1.016/H	1.330/H	1.309/H	2.638/H	2.571/H	2.963/H
PZT-6B			1.352/H			2.129/H

[a]Exact results taken from [14]; [b]Asymptotic results taken from [14].

Table 6.4 Characteristic decay length of several piezoelectric strips.

	Decay length L (even)			Decay length L (odd)		
	[14][a]	[14][b]	Present	[14][a]	[14][b]	Present
PZT-5H	2.083×2H	1.234×2H	1.990×2H	5.275×2H	5.373×2H	4.025×2H
PZT-5	2.016×2H	1.870×2H	1.851×2H	0.818×2H	0.881×2H	0.789×2H
PZT-4	2.172×2H	1.900×2H	1.878×2H	1.082×2H	0.895×2H	0.838×2H
Ceramic-B	2.263×2H	1.730×2H	1.759×2H	0.872×2H	0.816×2H	0.777×2H
PZT-6B			1.702×2H			1.082×2H

[a]Exact results taken from [14]; [b]Asymptotic results taken from [14].

6.3 Saint-Venant decay in anti-plane dissimilar laminates

In this section, the mixed-variable state space formulation developed in [5] for FGPM strips and laminates is briefly described. For dissimilar homogeneous piezoelectric laminates, the state space formulation is degenerated to a Hamiltonian system. Using the formulation presented in [5], results for the Saint-Venant end effects in a single FGPM strip and an FGPM laminate are presented. The decay rates for multi-layered FGPM laminates are also discussed.

6.3.1 Basic equations for anti-plane piezoelectric problem

Consider a single FGPM strip which is transversely isotropic and with the poling direction in the z-axis but graded in the y axis (Fig. 6.2). It is assumed to be graded in the transverse direction (y-axis) only. The constitutive equations for the FGPM under anti-plane deformation are defined by Eq. (1.35) and are rewritten in terms of elastic displacement and electric potential as follows:

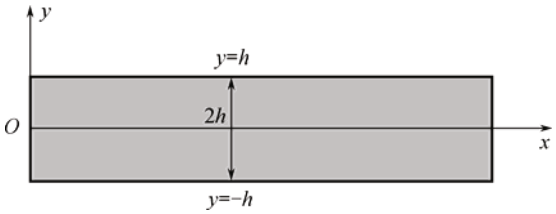

Fig. 6.2 Schematic diagram of a single FGPM strip.

$$\begin{aligned} \sigma_{xz} &= c_{55}(y)w_{,x} + e_{15}(y)\phi_{,x}, \quad \sigma_{yz} = c_{55}(y)w_{,y} + e_{15}(y)\phi_{,y}, \\ D_x &= e_{15}(y)w_{,x} - \kappa_{11}(y)\phi_{,x}, \quad D_y = e_{15}(y)w_{,y} - \kappa_{11}(y)\phi_{,y} \end{aligned} \tag{6.46}$$

where the material constants $c_{55}(y)$, $e_{15}(y)$, and $\kappa_{11}(y)$ are here assumed to vary in the following exponential form:

$$c_{55}(y) = c_{55}^0 e^{\beta y}, \quad e_{15}(y) = e_{15}^0 e^{\beta y}, \quad \kappa_{11}(y) = \kappa_{11}^0 e^{\beta y} \tag{6.47}$$

where β is the inhomogeneous parameter characterizing the degree of the material gradient in the y-direction and c_{55}^0, e_{15}^0, and κ_{11}^0 are the reference material parameters. The equilibrium equation and Maxwell's equation (1.10) now become

$$\frac{\partial \sigma_{xz}}{\partial x}+\frac{\partial \sigma_{yz}}{\partial y}=0, \qquad \frac{\partial D_x}{\partial x}+\frac{\partial D_y}{\partial y}=0 \tag{6.48}$$

in which the body force $\mathbf{f}_b$ and the electric charge density q_b are assumed to be zero for simplicity. The boundary conditions are considered to be self-equilibrated at the end $x = 0$, and the stress and electric displacement are supposed to vanish on the surfaces $y = \pm h$.

6.3.2 Mixed-variable state space formulation

Following the description in Section 6.2, the field equations (6.46)-(6.48) can also be converted into the Hamiltonian form using the mixed-variable state space method. To obtain the mixed-variable state space formulation, the x axis is assumed to be analogous to the time coordinate in elastic dynamics, and the y axis is taken to be in the transverse direction. Then, the dual state vectors **q** and **p** are introduced as

$$\mathbf{p}=\begin{Bmatrix} w \\ \phi \end{Bmatrix}, \qquad \mathbf{q}=\begin{Bmatrix} \sigma_0 \\ D_0 \end{Bmatrix} \tag{6.49}$$

where

$$\sigma_0 = e^{-\beta y}\sigma_{xz}, \quad D_0 = e^{-\beta y}D_x \tag{6.50}$$

Denoting the differential with respect to x by the symbol "$\cdot$", Eq. $(6.46)_{1,3}$ can be rewritten as

$$\sigma_{xz} = c_{55}^0 e^{\beta y}\dot{w} + e_{15}^0 e^{\beta y}\dot{\phi}, \quad D_x = e_{15}^0 e^{\beta y}\dot{w} - \kappa_{11}^0 e^{\beta y}\dot{\phi} \tag{6.51}$$

Solving Eq. (6.51) for $\dot{w}$ and $\dot{\phi}$, we obtain the following expressions:

$$\dot{w} = \frac{\kappa_{11}^0}{\Delta_0}\tau_0 + \frac{e_{15}^0}{\Delta_0}D_0, \quad \dot{\phi} = \frac{e_{15}^0}{\Delta_0}\tau_0 - \frac{c_{55}^0}{\Delta_0}D_0 \tag{6.52}$$

where $\Delta_0 = c_{55}^0\kappa_{11}^0 + (e_{15}^0)^2$.

The expressions of $\dot{\tau}_0$ and $\dot{D}_0$ can be obtained by considering Eqs. $(6.46)_{2,4}$, (6.47), (6.48), and (6.50) as

$$\begin{aligned} \dot{\sigma}_0 &= -c_{55}^0(w_{,yy} + \beta w_{,y}) - e_{15}^0(\phi_{,yy} + \beta\phi_{,y}), \\ \dot{D}_0 &= -e_{15}^0(w_{,yy} + \beta w_{,y}) + \kappa_{11}^0(\phi_{,yy} + \beta\phi_{,y}) \end{aligned} \tag{6.53}$$

Equations (6.52) and (6.53) can be written again as Eq. (6.9), where **v** is given in (6.8), but **q** and **p** are now defined by Eq. (6.49), and the operator matrix **H** is in the form

$$\mathbf{H}=\begin{bmatrix} 0 & 0 & \dfrac{\kappa_{11}^0}{\Delta_0} & \dfrac{e_{15}^0}{\Delta_0} \\ 0 & 0 & \dfrac{e_{15}^0}{\Delta_0} & -\dfrac{c_{55}^0}{\Delta_0} \\ -c_{55}^0\left(\dfrac{\partial^2}{\partial y^2}+\beta\dfrac{\partial}{\partial y}\right) & -e_{15}^0\left(\dfrac{\partial^2}{\partial y^2}+\beta\dfrac{\partial}{\partial y}\right) & 0 & 0 \\ -e_{15}^0\left(\dfrac{\partial^2}{\partial y^2}+\beta\dfrac{\partial}{\partial y}\right) & \kappa_{11}^0\left(\dfrac{\partial^2}{\partial y^2}+\beta\dfrac{\partial}{\partial y}\right) & 0 & 0 \end{bmatrix} \tag{6.54}$$

It should be mentioned that for the case of homogeneous piezoelectric material ($\beta=0$) the operator matrix $\mathbf{H}$ is a Hamiltonian operator matrix and Eq. (6.9) is a Hamiltonian equation [21], whereas for the FGPM case ($\beta\neq 0$), $\mathbf{H}$ is not a Hamiltonian operator matrix due to the material inhomogeneity, and thus the governing equation cannot be directed into the Hamiltonian system, and it is difficult to find the adjoint symplectic orthonormalization eigenvector $\boldsymbol{\psi}$ to obtain the electroelastic fields using a procedure similar to that in [21]. However, the decay rate still corresponds to the nonzero-eigenvalue of the operator matrix.

To prove that $\mathbf{H}$ is a Hamiltonian operator matrix for the case of homogeneous piezoelectric materials, the rotational exchange operator matrix $\mathbf{J}$ given in Eq. (6.14) now becomes

$$\mathbf{J}=\begin{bmatrix} \mathbf{0} & \mathbf{I}_2 \\ -\mathbf{I}_2 & \mathbf{0} \end{bmatrix},\quad \mathbf{J}^2=\begin{bmatrix} -\mathbf{I}_2 & 0 \\ 0 & -\mathbf{I}_2 \end{bmatrix},\quad \mathbf{J}^{-1}=-\mathbf{J}=\mathbf{J}^{\mathrm{T}} \tag{6.55}$$

where $\mathbf{I}_2$ is a two-order identity matrix. With the notation $\mathbf{J}$, it is easy to prove that $\mathbf{H}$ satisfies the following relation by performing a procedure similar to that in [21] and

$$\left\langle \mathbf{v}_1^{\mathrm{T}}, \mathbf{H}\mathbf{v}_2 \right\rangle = \left\langle \mathbf{v}_2^{\mathrm{T}}, \mathbf{H}\mathbf{v}_1 \right\rangle \tag{6.56}$$

where

$$\left\langle \mathbf{v}_1^{\mathrm{T}}, \mathbf{H}\mathbf{v}_2 \right\rangle = \int_{y_1}^{y_2} \mathbf{v}_1^{\mathrm{T}}\mathbf{J}\mathbf{H}\mathbf{v}_2 \mathrm{d}y \tag{6.57}$$

The proof of Eq. (6.56) can be found in [5]. Then, according to theory of symplectic geometry [19], $\mathbf{H}$ is proved to be a Hamiltonian operator matrix.

6.3.3 Decay rate of FGPM strip

In this subsection the separable variation method is used to solve the state space equation (6.5). With the method of variable separation, the dual vector $\mathbf{v}$ can be

assumed in the form of Eq. (6.17). Then Eqs. (6.18)-(6.21) also apply here, except that the eigenvector $\boldsymbol{\psi}$ is now defined by

$$\boldsymbol{\psi}(y)=\begin{Bmatrix}\mathbf{q}(y)\\ \mathbf{p}(y)\end{Bmatrix} \tag{6.58}$$

Then, we have

$$\begin{Bmatrix}\mathbf{q}\\ \mathbf{p}\end{Bmatrix}=e^{\mu x}\boldsymbol{\psi}(y) \tag{6.59}$$

For the case of dissimilar homogeneous piezoelectric materials, since the eigenvalues of the Hamiltonian operator matrix have the property described in Eq. (6.20), their corresponding eigenfunction-vectors are written as $\boldsymbol{\psi}_{+i}$, $\boldsymbol{\psi}_{-i}$, and $\boldsymbol{\psi}_0$. Following the procedure presented in [19], it is easy to prove that $\boldsymbol{\psi}_{+i}$ and $\boldsymbol{\psi}_{-i}$ are of adjoint symplectic orthonormalization, that is,

$$\begin{aligned}&\langle\boldsymbol{\psi}_{+i}^{\mathrm{T}},\ \mathbf{J},\ \boldsymbol{\psi}_{-j}\rangle=\delta_{ij},\quad \langle\boldsymbol{\psi}_{-i}^{\mathrm{T}},\ \mathbf{J},\ \boldsymbol{\psi}_{+j}\rangle=-\delta_{ij},\\ &\langle\boldsymbol{\psi}_{+i}^{\mathrm{T}},\ \mathbf{J},\ \boldsymbol{\psi}_{+j}\rangle=0,\qquad \langle\boldsymbol{\psi}_{-i}^{\mathrm{T}},\ \mathbf{J},\ \boldsymbol{\psi}_{-j}\rangle=0\end{aligned} \tag{6.60}$$

in which

$$\langle\boldsymbol{\psi}_i^{\mathrm{T}},\ \mathbf{J},\ \boldsymbol{\psi}_j\rangle=\int_{y_1}^{y_2}\boldsymbol{\psi}_i^{\mathrm{T}}\mathbf{J}\boldsymbol{\psi}_j\mathrm{d}y \tag{6.61}$$

Equation (6.61) implies that $\boldsymbol{\psi}_i$ satisfies the homogeneous boundary conditions at $y=y_1$ and y_2.

It should be mentioned that the eigenvalues μ might be real, complex, and only the real part is related to the decay behavior. From Eqs. (6.49) and (6.59) we can obtain the following expressions:

$$\begin{Bmatrix}w\\ \phi\end{Bmatrix}=e^{\mu x}\begin{Bmatrix}w_1(y)\\ \phi_1(y)\end{Bmatrix},\qquad \begin{Bmatrix}\sigma_{xz}\\ D_x\end{Bmatrix}=e^{\mu x}e^{\beta y}\begin{Bmatrix}\sigma_1(y)\\ D_1(y)\end{Bmatrix} \tag{6.62}$$

where w_1, ϕ_1, σ_1, D_1 are the functions of y. It is obvious from Eq. (6.62) that both the shear stress and the electric displacement contain the factor $e^{\mu x}$. Thus, it can be easily found that both shear stress and electric displacement decay exponentially for an eigenvalue of μ with a negative real part when x increases. In fact, μ has four types of solutions which include $\mu=a\pm bi$, $\mu=-a\pm bi$ $(a>0,b>0)$. The real part of μ with the smallest positive value, say a, is here taken as the decay rate k, i.e.,

$$k=a \tag{6.63}$$

To determine μ and to analyze the Saint-Venant decay behavior for FGPM strips, Eq. (6.19) can be rewritten as

$$\begin{bmatrix} -\mu & 0 & \frac{\kappa_{11}^0}{\Delta_0} & \frac{e_{15}^0}{\Delta_0} \\ 0 & -\mu & \frac{e_{15}^0}{\Delta_0} & -\frac{c_{55}^0}{\Delta_0} \\ -c_{55}^0\left(\frac{\partial^2}{\partial y^2}+\beta\frac{\partial}{\partial y}\right) & -e_{15}^0\left(\frac{\partial^2}{\partial y^2}+\beta\frac{\partial}{\partial y}\right) & -\mu & 0 \\ -e_{15}^0\left(\frac{\partial^2}{\partial y^2}+\beta\frac{\partial}{\partial y}\right) & \kappa_{11}^0\left(\frac{\partial^2}{\partial y^2}+\beta\frac{\partial}{\partial y}\right) & 0 & -\mu \end{bmatrix} \begin{Bmatrix} w \\ \phi \\ \sigma_0 \\ D_0 \end{Bmatrix} = 0 \tag{6.64}$$

Letting the determinant of the coefficient matrix of Eq. (6.64) be equal to zero, and noting that $\partial/\partial y$ is replaced by λ and $\partial^2/\partial y^2$ is replaced by λ^2, we have

$$\det\begin{bmatrix} 0 & 0 & \frac{\kappa_{11}^0}{\Delta_0} & \frac{e_{15}^0}{\Delta_0} \\ 0 & 0 & \frac{e_{15}^0}{\Delta_0} & -\frac{c_{55}^0}{\Delta_0} \\ -c_{55}^0(\lambda^2+\beta\lambda) & -e_{15}^0(\lambda^2+\beta\lambda) & 0 & 0 \\ -e_{15}^0(\lambda^2+\beta\lambda) & \kappa_{11}^0(\lambda^2+\beta\lambda) & 0 & 0 \end{bmatrix} = 0 \tag{6.65}$$

Equation (6.65) can be written as

$$(\lambda^2+\beta\lambda+\mu^2)^2 = 0 \tag{6.66}$$

Then, the solution of λ is in the form

$$\lambda_{1,2} = -\frac{\beta}{2}+\frac{1}{2}\sqrt{\beta^2-4\mu^2}, \quad \lambda_{3,4} = -\frac{\beta}{2}-\frac{1}{2}\sqrt{\beta^2-4\mu^2} \tag{6.67}$$

Thus, the general solutions of the elastic and electric fields to Eq. (6.64) can be given as the following two cases:

Case 1: $\beta^2-4\mu^2 \leqslant 0$

In the case of $\beta^2-4\mu^2 \leqslant 0$, we can easily arrive at

$$\begin{aligned} we^{\frac{\beta}{2}y} &= A_1\cos\left(\frac{m}{2}y\right)+B_1\sin\left(\frac{m}{2}y\right)+C_1y\cos\left(\frac{m}{2}y\right)+D_1y\sin\left(\frac{m}{2}y\right), \\ \phi e^{\frac{\beta}{2}y} &= A_2\cos\left(\frac{m}{2}y\right)+B_2\sin\left(\frac{m}{2}y\right)+C_2y\cos\left(\frac{m}{2}y\right)+D_2y\sin\left(\frac{m}{2}y\right), \\ \sigma e^{\frac{\beta}{2}y} &= A_3\cos\left(\frac{m}{2}y\right)+B_3\sin\left(\frac{m}{2}y\right)+C_3y\cos\left(\frac{m}{2}y\right)+D_3y\sin\left(\frac{m}{2}y\right), \\ De^{\frac{\beta}{2}y} &= A_4\cos\left(\frac{m}{2}y\right)+B_4\sin\left(\frac{m}{2}y\right)+C_4y\cos\left(\frac{m}{2}y\right)+D_4y\sin\left(\frac{m}{2}y\right) \end{aligned} \tag{6.68}$$

in which A_i, B_i, C_i, and D_i ($i = 1\text{-}4$) are unknown constants to be determined and

$$m = \sqrt{4\mu^2 - \beta^2} \tag{6.69}$$

Substituting Eq. (6.68) into Eq. (6.64) can lead to the following relationships between the unknown constants:

$$\begin{aligned} &A_3 = \mu(c_{44}A_1 + e_{15}A_2), \quad A_4 = \mu(e_{15}A_1 - \kappa_{11}A_2), \\ &B_3 = \mu(c_{44}B_1 + e_{15}B_2), \quad B_4 = \mu(e_{15}B_1 - \kappa_{11}B_2), \\ &D_i = C_i = 0 \quad (i = 1\text{-}4) \end{aligned} \tag{6.70}$$

Making use of Eq. (6.70), Eq. (6.68) can be rewritten as

$$\begin{aligned} we^{\frac{\beta}{2}y} &= A_1\cos\left(\frac{m}{2}y\right) + B_1\sin\left(\frac{m}{2}y\right), \\ \phi e^{\frac{\beta}{2}y} &= A_2\cos\left(\frac{m}{2}y\right) + B_2\sin\left(\frac{m}{2}y\right), \\ \sigma e^{\frac{\beta}{2}y} &= \mu\left[c_{55}^0\cos\left(\frac{m}{2}y\right)A_1 + e_{15}^0\cos\left(\frac{m}{2}y\right)A_2 + c_{55}^0\sin\left(\frac{m}{2}y\right)B_1 + e_{15}^0\sin\left(\frac{m}{2}y\right)B_1\right], \\ De^{\frac{\beta}{2}y} &= \mu\left[e_{15}^0\cos\left(\frac{m}{2}y\right)A_1 - \kappa_{11}^0\cos\left(\frac{m}{2}y\right)A_2 + e_{15}^0\sin\left(\frac{m}{2}y\right)B_1 - \kappa_{11}^0\sin\left(\frac{m}{2}y\right)B_2\right] \end{aligned} \tag{6.71}$$

From Eqs. $(6.46)_{2,4}$ and (6.71), we have

$$\begin{aligned} \sigma_{yz} &= c_{55}^0 P(y)A_1 + e_{15}^0 P(y)A_2 - c_{55}^0 N(y)B_1 - e_{15}^0 N(y)B_2, \\ D_y &= e_{15}^0 P(y)A_1 - \kappa_{11}^0 P(y)A_2 - e_{15}^0 N(y)B_1 + \kappa_{11}^0 N(y)B_2 \end{aligned} \tag{6.72}$$

in which

$$\begin{aligned} P(y) &= -\frac{1}{2}e^{-\frac{\beta}{2}y}\left[m\sin\left(\frac{m}{2}y\right) + \beta\cos\left(\frac{m}{2}y\right)\right], \\ N(y) &= -\frac{1}{2}e^{-\frac{\beta}{2}y}\left[m\cos\left(\frac{m}{2}y\right) - \beta\sin\left(\frac{m}{2}y\right)\right] \end{aligned} \tag{6.73}$$

Considering now the FGPM strip shown in Fig. 6.2, assume that the boundary conditions are self-equilibrated at the end $x = 0$, and the stress and electric displacement are supposed to vanish on the surfaces $y = \pm h$, i.e.,

$$\sigma_{yz}(x, \pm h) = 0, \quad D_y(x, \pm h) = 0 \tag{6.74}$$

Substituting Eq. (6.72) into Eq. (6.74), the following equation can be obtained:

$$\begin{bmatrix} c_{55}^0 P(h) & e_{15}^0 P(h) & -c_{55}^0 N(h) & -e_{15}^0 N(h) \\ e_{15}^0 P(h) & -\kappa_{11}^0 P(h) & -e_{15}^0 N(h) & \kappa_{11}^0 N(h) \\ c_{55}^0 P(-h) & e_{15}^0 P(-h) & -c_{55}^0 N(-h) & -e_{15}^0 N(-h) \\ e_{15}^0 P(-h) & -\kappa_{11}^0 P(-h) & -e_{15}^0 N(-h) & \kappa_{11}^0 N(-h) \end{bmatrix} \begin{Bmatrix} A_1 \\ A_2 \\ B_1 \\ B_2 \end{Bmatrix} = 0 \tag{6.75}$$

The existence of nonzero solutions $\{A_1 \quad A_2 \quad B_1 \quad B_2\}^{\mathrm{T}}$ requires the determinant of the coefficient matrix to be zero, which can lead to the equation

$$16\mu^2 \Delta_0^2 \sin^2(mh) = 0 \tag{6.76}$$

Thus, we can obtain

$$m = \frac{n\pi}{h} \qquad (n = 0, \pm 1, \pm 2, \cdots) \tag{6.77}$$

Substituting Eq. (6.77) into Eq. (6.69), we can obtain the eigenvalue as follows:

$$\mu = \frac{\pm\sqrt{\beta^2 + n^2\pi^2 / h^2}}{2} \tag{6.78}$$

Note that the solutions w and ϕ decay exponentially with $e^{\mu x}$ with distance from the end $x = 0$ for negative values of μ. The real part of the eigenvalue μ with smallest positive real part is here known as the decay rate k, which is obtained as

$$k = \frac{\sqrt{\beta^2 + \pi^2 / h^2}}{2} \tag{6.79}$$

It can be easily found that the decay rate heavily depends on the value of the material inhomogeneous parameter β of an FGPM strip. It should be mentioned that the case of $k = \beta/2$ for $n = 0$ should be removed and Eq. (6.79) should be adopted when choosing the value of the decay rate k using Eq. (6.78), due to the fact that the decay rate k depends on the value of the thickness h of the FGPM strip, and that if $\beta = 0$, the decay rate will be equal to zero for homogeneous piezoelectric materials. Thus, in the following numerical examples for two-layered and multi-layered FGPMs, the roots of $\mu = \beta/2$ should also be removed. Note that the FGPM strip is a homogeneous piezoelectric material strip when $\beta = 0$, and Eq. (6.79) is reduced to

$$k = \frac{\pi}{2h} \tag{6.80}$$

This result is the same as that of Borrelli et al. [20].

In Fig. 6.3, the decay rate of single FGPM strips with various thicknesses h for different values of β has been plotted to show the effect of the inhomogeneous parameter on the decay rate. It can be seen that the decay rate increases with the increase of β, which agrees well with the results of Borrelli et al. [13]. This indicates that material inhomogeneity has a significant influence on the decay of end effects.

Case 2: $\beta^2 - 4\mu^2 > 0$

In the case of $\beta^2 - 4\mu^2 > 0$, the solution to Eq. (6.65) is obtained as

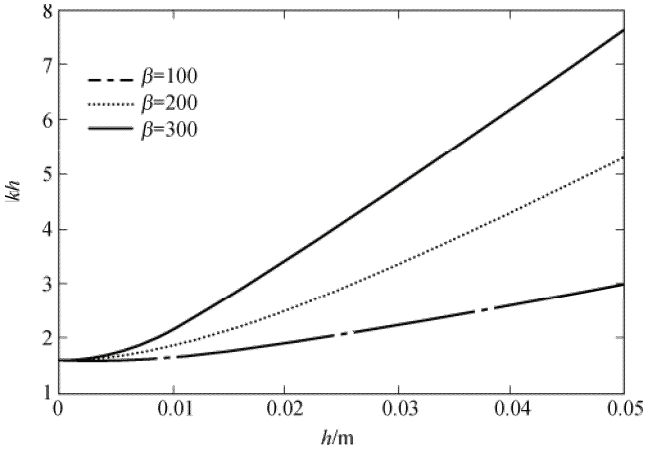

Fig. 6.3 Variation of the decay rate k with various h for different material inhomogeneous parameters β.

$$\begin{aligned}
w &= A_1 e^{\frac{1}{2}(m-\beta)y} + B_1 e^{-\frac{1}{2}(m+\beta)y} + C_1 y e^{\frac{1}{2}(m-\beta)y} + D_1 e^{-\frac{1}{2}(m+\beta)y},\\
\phi &= A_2 e^{\frac{1}{2}(m-\beta)y} + B_2 e^{-\frac{1}{2}(m+\beta)y} + C_2 y e^{\frac{1}{2}(m-\beta)y} + D_2 e^{-\frac{1}{2}(m+\beta)y},\\
\sigma &= A_3 e^{\frac{1}{2}(m-\beta)y} + B_3 e^{-\frac{1}{2}(m+\beta)y} + C_3 y e^{\frac{1}{2}(m-\beta)y} + D_3 e^{-\frac{1}{2}(m+\beta)y},\\
D &= A_4 e^{\frac{1}{2}(m-\beta)y} + B_4 e^{-\frac{1}{2}(m+\beta)y} + C_4 y e^{\frac{1}{2}(m-\beta)y} + D_4 e^{-\frac{1}{2}(m+\beta)y}
\end{aligned} \tag{6.81}$$

in which

$$m = \sqrt{\beta^2 - 4\mu^2} \tag{6.82}$$

Using Eq. (6.64), we can obtain the same relationships between A_i, B_i, C_i, D_i as shown in Eq. (6.70). Then the shear stress and electric displacement σ_{yz} and D_y in the transverse direction can be expressed as

$$\begin{aligned}
\sigma_{yz} &= -\frac{1}{2} e^{-\frac{\beta}{2}y}\Big[c_{55}^0(\beta - m)e^{\frac{m}{2}y}A_1 + e_{15}^0(\beta - m)e^{\frac{m}{2}y}A_2\\
&\quad + c_{55}^0(\beta + m)e^{-\frac{m}{2}y}B_1 + e_{15}^0(\beta + m)e^{-\frac{m}{2}y}B_2\Big],\\
D_y &= -\frac{1}{2} e^{-\frac{\beta}{2}y}\Big[e_{15}^0(\beta - m)e^{\frac{m}{2}y}A_1 - \kappa_{11}^0(\beta - m)e^{\frac{m}{2}y}A_2\\
&\quad + e_{15}^0(\beta + m)e^{-\frac{m}{2}y}B_1 - \kappa_{11}^0(\beta + m)e^{-\frac{m}{2}y}B_2\Big]
\end{aligned} \tag{6.83}$$

Thus, following a similar procedure to that in Case 1, we can obtain the following equations:

$$m = \sqrt{\beta^2 - 4\mu^2} = 0 \tag{6.84}$$

which violates the assumption of $m>0$, and therefore it is impossible for $\beta^2-4\mu^2>0$ to appear.

Now, let us solve the decay rate k for two-layered and multi-layered FGPM laminates and dissimilar piezoelectric material laminates using the coordinate transformation technique and the interface continuity conditions.

6.3.4 Two-layered FGPM laminates and dissimilar piezoelectric laminates

For two-layered FGPM laminates as shown in Fig. 6.4, the boundary conditions are as follows:

$$\sigma_{yz}^{(1)}(x,h_1)=\sigma_{yz}^{(2)}(x,-h_2)=D_y^{(1)}(x,h_1)=D_y^{(2)}(x,-h_2)=0 \tag{6.85}$$

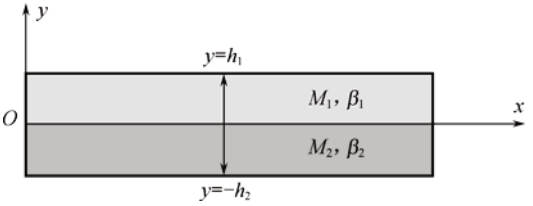

Fig. 6.4 Schematic diagram of a two-layered FGPM laminate.

and the interface continuity conditions for two-layered fully bonded FGPM laminates are

$$\begin{aligned}&\sigma_{yz}^{(1)}(x,0)=\sigma_{yz}^{(2)}(x,0),\ \ w^{(1)}(x,0)=w^{(2)}(x,0),\\&D_y^{(1)}(x,0)=D_y^{(2)}(x,0),\ \ \phi^{(1)}(x,0)=\phi^{(2)}(x,0)\end{aligned} \tag{6.86}$$

in which the superscripts "(1)" and "(2)" denote material 1 (M_1) and material 2 (M_2), respectively. It should be mentioned that here we are considering the more general and complex case of dissimilar materials. In the special case of $\beta_1=\beta_2=0$, the laminates degenerate to dissimilar homogeneous piezoelectric material laminates. However, in the case of $\beta_1\neq 0$ or $\beta_2\neq 0$, the laminate is reduced to an FGPM laminate, and this case is considered for the analysis of multi-dissimilar materials. Substituting the solutions of Eqs. (6.71) and (6.72) for M_1 and M_2 into Eq. (6.86), we obtain the following relationship between the coefficients:

$$\begin{Bmatrix}A_1^{(2)}\\A_2^{(2)}\\B_1^{(2)}\\B_2^{(2)}\end{Bmatrix}=\begin{bmatrix}1&0&0&0\\0&1&0&0\\a_{11}&a_{12}&a_{13}&a_{14}\\a_{21}&a_{22}&a_{23}&a_{24}\end{bmatrix}\begin{Bmatrix}A_1^{(1)}\\A_2^{(1)}\\B_1^{(1)}\\B_2^{(1)}\end{Bmatrix} \tag{6.87}$$

in which

$$
\begin{aligned}
a_{11} &= \frac{1}{\Delta_a}\left[\beta^{(1)}(e_{15}^{(1)}e_{15}^{(2)} + c_{55}^{(1)}\kappa_{11}^{(2)}) - \beta^{(2)}(e_{15}^{(2)2} + c_{55}^{(2)}k_{11}^{(2)})\right],\\
a_{12} &= \frac{1}{\Delta_a}\left[\beta^{(1)}(e_{15}^{(1)}\kappa_{11}^{(2)} - e_{15}^{(2)}\kappa_{11}^{(1)})\right],\\
a_{13} &= \frac{1}{\Delta_a}\left[m^{(1)}(-e_{15}^{(1)}e_{15}^{(2)} - c_{55}^{(1)}\kappa_{11}^{(2)})\right],\\
a_{14} &= \frac{1}{\Delta_a}\left[m^{(1)}(e_{15}^{(2)}\kappa_{11}^{(1)} - e_{15}^{(1)}\kappa_{11}^{(2)})\right]
\end{aligned}
\tag{6.88}
$$

$$
\begin{aligned}
a_{21} &= \frac{1}{\Delta_a}\left[\beta^{(1)}(-e_{15}^{(1)}c_{55}^{(2)} + e_{15}^{(2)}c_{55}^{(1)})\right],\\
a_{22} &= \frac{1}{\Delta_a}\left[\beta^{(1)}(e_{15}^{(1)}e_{15}^{(2)} + c_{55}^{(2)}\kappa_{11}^{(1)}) - \beta^{(2)}(e_{15}^{(2)2} + c_{55}^{(2)}\kappa_{11}^{(2)})\right],\\
a_{23} &= \frac{1}{\Delta_a}\left[m^{(1)}(e_{15}^{(1)}c_{55}^{(2)} - e_{15}^{(2)}c_{55}^{(1)})\right],\\
a_{24} &= \frac{1}{\Delta_a}\left[m^{(1)}(-c_{55}^{(2)}\kappa_{11}^{(1)} - e_{15}^{(2)}e_{15}^{(1)})\right]
\end{aligned}
\tag{6.89}
$$

with

$$
\Delta_a = -m^{(2)}(e_{15}^{(2)2} + c_{55}^{(2)}\kappa_{11}^{(2)}) \tag{6.90}
$$

Combining Eqs. (6.72), (6.85), and (6.87) yields

$$
\mathbf{M}\mathbf{F}^{(1)} = 0 \tag{6.91}
$$

in which

$$
\mathbf{M} = \begin{bmatrix}
c_{55}^{(1)}P^{(1)}(h_1) & e_{15}^{(1)}P^{(1)}(h_1) & -c_{55}^{(1)}N^{(1)}(h_1) & -e_{15}^{(1)}N^{(1)}(h_1)\\
e_{15}^{(1)}P^{(1)}(h_1) & -\kappa_{11}^{(1)}P^{(1)}(h_1) & -e_{15}^{(1)}N^{(1)}(h_1) & \kappa_{11}^{(1)}N^{(1)}(h_1)\\
a_{31} & a_{32} & a_{33} & a_{34}\\
a_{41} & a_{42} & a_{43} & a_{44}
\end{bmatrix} \tag{6.92}
$$

Where

$$
\begin{aligned}
a_{31} &= c_{55}^{(2)}P^{(2)}(-h_2) - N^{(2)}(-h_2)(c_{55}^{(2)}a_{11} + e_{15}^{(2)}a_{21}),\\
a_{32} &= e_{15}^{(2)}P^{(2)}(-h_2) - N^{(2)}(-h_2)(c_{55}^{(2)}a_{12} + e_{15}^{(2)}a_{22}),\\
a_{33} &= -N^{(2)}(-h_2)(c_{55}^{(2)}a_{13} + e_{15}^{(2)}a_{23}),\\
a_{34} &= -N^{(2)}(-h_2)(c_{55}^{(2)}a_{14} + e_{15}^{(2)}a_{24})
\end{aligned}
\tag{6.93}
$$

$$
\begin{aligned}
a_{41} &= e_{15}^{(2)}P^{(2)}(-h_2) - N^{(2)}(-h_2)(e_{15}^{(2)}a_{11} - \kappa_{11}^{(2)}a_{21}),\\
a_{42} &= -\kappa_{11}^{(2)}P^{(2)}(-h_2) - N^{(2)}(-h_2)(e_{15}^{(2)}a_{12} - \kappa_{11}^{(2)}a_{22}),\\
a_{43} &= -N^{(2)}(-h_2)(e_{15}^{(2)}a_{13} - \kappa_{11}^{(2)}a_{23}),\\
a_{44} &= -N^{(2)}(-h_2)(e_{15}^{(2)}a_{14} - \kappa_{11}^{(2)})
\end{aligned}
\tag{6.94}
$$

and

$$\mathbf{F}^{(1)} = \left\{ A_1^{(1)} \quad A_2^{(1)} \quad B_1^{(1)} \quad B_2^{(1)} \right\}^{\mathrm{T}} \tag{6.95}$$

The non-zero solution $\mathbf{F}^{(1)}$requires the determinant of the coefficients matrix $\mathbf{M}$ to be zero:

$$\det \mathbf{M} = 0 \tag{6.96}$$

Thus, the solution for μ can be obtained by solving Eq. (6.96) and then the decay rate can also be obtained by choosing the appropriate value of μ.

6.3.4.1 Two-layered FGPM laminates

Here PZT-4 is taken as an example for illustration. Its properties are $c_{44} = 25.6\times10^9$ Pa , $e_{15} = 12.7$ C/N, and $k_{11} = 6.46\times10^{-9}$ F/m .

To show the effect of material inhomogeneity on the end effect, the decay rates of the two-layered FGPM laminate with h_2 = 0.03 m and various h_1 are calculated from Eq. (6.96) and plotted in Fig. 6.5 for different values of β_2 and β_1=100. For the case of $\beta_1 = \beta_2$=100, the two-layered FGPM laminate is reduced to a single layer FGPM strip, and the decay rate can be obtained from Eq (6.79). The results obtained from Eq. (6.79) and their counterparts obtained from Eq. (6.96) by numerical methods are also plotted in Fig. 6.5. It is observed that the results obtained from Eq. (6.96) agree well with those obtained from Eq. (6.79) in the case of $\beta_1 = \beta_2$. Also, it can be seen that the decay rate varies with the inhomogeneous parameters β_1 and β_2. It can be found that the decay rate of the end effects increases with the increase of β_2. Furthermore, the decay rate decreases with an increase of the value of h_1.

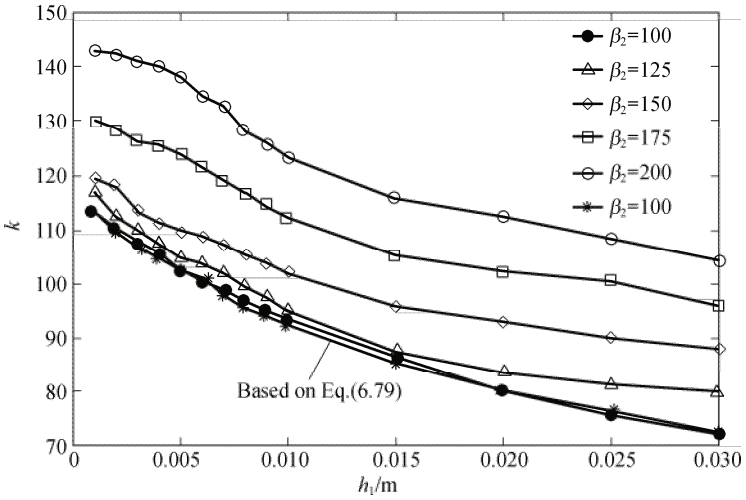

Fig. 6.5 Variation of the decay rate k with various h_1 for different values of β_2 and β_1=100, h_2=0.03 m.

To illustrate the effect of material inhomogeneity on the end effects of FGPM laminates, the variation of the decay rate k with the values of β_2 is plotted in Fig. 6.6 for a two-layered FGPM with a fixed thickness $h_1 = h_2 = 0.02$ m. It can again be observed that the decay rate increases with the increase of β_2. From Figs. 6.5 and 6.6, we can see that material inhomogeneity has a significant influence on the decay behavior for both the two-layered case and the single strip case.

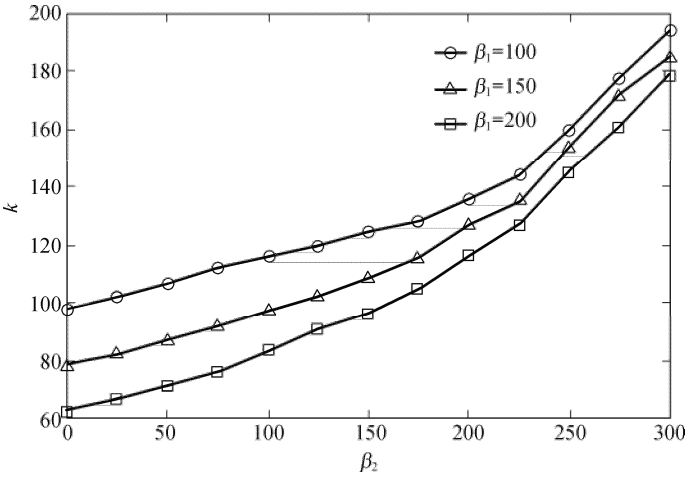

Fig. 6.6 The dependency of the decay rate k on β_2 for different β_1 and fixed thickness $h_1 = h_2 = 0.02$ m.

6.3.4.2 Two-layered dissimilar piezoelectric material laminates

Now we consider two-layered dissimilar piezoelectric material laminates composed of a first layer of PZT-4 and a second layer of PZT-5. The properties of PZT-4 are $c_{55}^{(1)} = 25.6\times10^9$ Pa, $e_{15}^{(1)} = 12.7$ C/N, and $k_{11}^{(1)} = 6.46\times10^{-9}$ F/m, and the properties of PZT-5 are $c_{55}^{(2)} = 21.1\times10^9$ Pa, $e_{15}^{(2)} = 12.3$ C/N, and $k_{11}^{(2)} = 8.11\times10^{-9}$ F/m. Using the boundary conditions and the solutions for each layer, Eq. (6.96) can be simplified as follows:

$$\begin{aligned}&(c_{55}^{(1)}\kappa_{11}^{(1)} + e_{15}^{(1)2})\sin^2(\mu h_1)\cos^2(\mu h_2) + (c_{55}^{(2)}\kappa_{11}^{(1)} + e_{15}^{(2)2})\sin^2(\mu h_2)\cos^2(\mu h_1)\\ &+(c_{55}^{(1)}\kappa_{11}^{(2)} + 2e_{15}^{(1)}e_{15}^{(2)} + c_{55}^{(2)}\kappa_{11}^{(1)})\sin(\mu h_1)\sin(\mu h_2)\cos(\mu h_1)\cos(\mu h_2) = 0\end{aligned} \tag{6.97}$$

or written as

$$\sin^2[\mu(h_1+h_2)] + R_1\sin^2[\mu(h_1-h_2)] = R_2\sin[\mu(h_1+h_2)]\sin[\mu(h_1-h_2)] \tag{6.98}$$

with

$$
\begin{aligned}
R_1 &= \frac{A_{11}+A_{22}-A_{12}-A_{21}}{A_{11}+A_{22}+A_{12}+A_{21}}, \qquad R_2 = \frac{2(A_{22}-A_{11})}{A_{11}+A_{22}+A_{12}+A_{21}}, \\
A_{11} &= e_{15}^{(1)}e_{15}^{(1)} + c_{55}^{(1)}\kappa_{11}^{(1)}, \qquad A_{12} = e_{15}^{(1)}e_{15}^{(2)} + \kappa_{11}^{(1)}c_{55}^{(2)}, \\
A_{21} &= e_{15}^{(2)}e_{15}^{(1)} + \kappa_{11}^{(2)}c_{55}^{(1)}, \qquad A_{22} = e_{15}^{(2)}e_{15}^{(2)} + c_{55}^{(2)}\kappa_{11}^{(2)}
\end{aligned} \tag{6.99}
$$

In the case of $h_1 = h_2$, it can be seen from Eq. (6.98) that the roots of μ do not depend on the piezoelectric properties, and the solution to Eq. (6.98) is

$$\mu = \frac{n\pi}{2h} \tag{6.100}$$

and the decay rate is

$$k = \frac{\pi}{2h} \tag{6.101}$$

In the case of $h_1 \neq h_2$, Eq. (6.98) can be solved numerically. The decay rates of two-layered dissimilar piezoelectric material laminates are plotted in Fig. 6.7 for different h_1 and h_2. It is observed that the decay rate decreases with increases of h_1 and h_2. When h_1 is small, the difference between the decay rates for different thicknesses of h_2 is large, which implies that the magnitude of the thickness h_2 significantly affects the decay rate provided h_1 is small. As h_1 increases, the effect of thickness h_2 on the decay rate decreases, and it can be negligible when h_1 is sufficiently large. Further, the decay rate drops quickly with the increase of h_1 when both h_1 and h_2 are small, say, when h_1 is less than 0.02 m and h_2 is less than 0.01 m, as shown in Fig. 6.7. However, the decay rate varies slowly when h_1 or h_2 is very large and approaches a constant when h_1 or h_2 is sufficiently large, indicating again that the effect of the thicknesses h_1 and h_2 on the decay rate can be ignored when either h_1 or h_2 is sufficiently large.

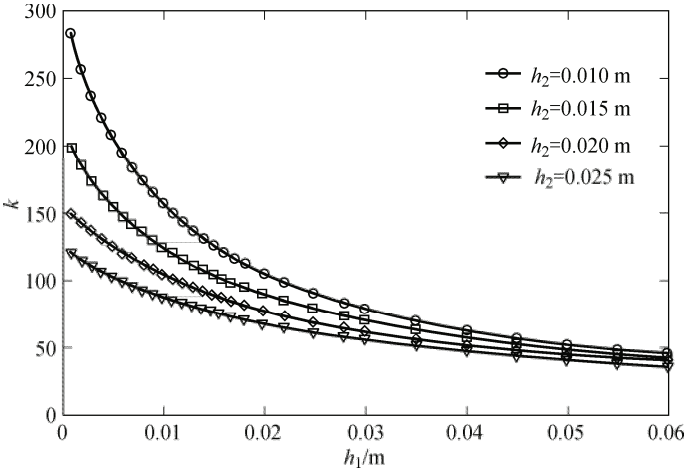

Fig. 6.7 Variation of the decay rate k with various h_2 for two-layered dissimilar piezoelectric laminates.

6.4 Saint-Venant decay in multilayered piezoelectric laminates

This section presents a summary of the development in [3]. In that work, Tarn and Huang developed a state space approach in the context of generalized plane strain for studying the Saint-Venant end effects on multilayered laminates of piezoelectric materials. They showed that the electromechanical interaction has significant effects on the internal field in a self-equilibrated strip or laminate. The Saint-Venant end effects are more pronounced and the decay length is more extensive in homogeneous strips or composite laminates with stiff piezoelectric layers than in those with soft piezoelectric layers.

6.4.1 State space formulation

For a piezoelectric laminate composed of n layers in a self-equilibrated state as shown in Fig. 6.8, Tarn and Huang developed the following state space formulation for a monoclinic system of class 2*mm* with the x_3-axis being the polarization direction. They begin by considering the constitutive equation (1.6), but in the special form for a multilayered structure, as

$$\begin{bmatrix} \boldsymbol{\varepsilon} \\ \mathbf{D} \end{bmatrix}_k = \begin{bmatrix} \mathbf{f} & \mathbf{d} \\ \mathbf{d}^{\mathrm{T}} & \boldsymbol{\kappa} \end{bmatrix}_k \begin{bmatrix} \boldsymbol{\sigma} \\ \mathbf{E} \end{bmatrix}_k \tag{6.102}$$

where $\boldsymbol{\varepsilon}$, $\boldsymbol{\sigma}$, $\mathbf{D}$, and $\mathbf{E}$ are defined in Eqs. (2.3) and (2.4), and $\mathbf{f}$, $\mathbf{d}$, $\boldsymbol{\kappa}$ used in [3] are given as

$$\mathbf{f} = \begin{bmatrix} f_{11} & f_{12} & f_{13} & 0 & 0 & f_{16} \\ f_{12} & f_{22} & f_{23} & 0 & 0 & f_{26} \\ f_{13} & f_{23} & f_{33} & 0 & 0 & f_{36} \\ 0 & 0 & 0 & f_{44} & f_{45} & 0 \\ 0 & 0 & 0 & f_{45} & f_{55} & 0 \\ f_{16} & f_{26} & f_{36} & 0 & 0 & f_{66} \end{bmatrix}, \quad \mathbf{d} = \begin{bmatrix} 0 & 0 & d_{31} \\ 0 & 0 & d_{32} \\ 0 & 0 & d_{33} \\ d_{14} & d_{24} & 0 \\ d_{15} & d_{25} & 0 \\ 0 & 0 & d_{36} \end{bmatrix}, \quad \boldsymbol{\kappa} = \begin{bmatrix} \kappa_{11} & \kappa_{12} & 0 \\ \kappa_{12} & \kappa_{22} & 0 \\ 0 & 0 & \kappa_{33} \end{bmatrix} \tag{6.103}$$

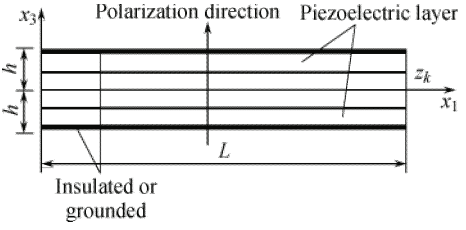

Fig. 6.8 Configuration of a piezoelectric laminate.

In the problem they studied the laminate was subjected to self-equilibrated loads at $x_1 = 0$ and L (Fig. 6.8). The boundary conditions on the top and bottom surfaces are free from traction and electric voltage or surface charge so that

$$\sigma_{13} = \sigma_{23} = \sigma_{33} = 0, \quad \phi = 0 \text{ or } D_3 = 0 \quad (\text{on } x_3 = \pm h) \tag{6.104}$$

The continuity conditions on the interface $x_3 = z_k$ ($k = 1, 2, \cdots, n$) require

$$\begin{aligned} &[u_1 \quad u_2 \quad u_3 \quad \phi]_k = [u_1 \quad u_2 \quad u_3 \quad \phi]_{k+1}, \\ &[\sigma_{13} \quad \sigma_{23} \quad \sigma_{33} \quad D_3]_k = [\sigma_{13} \quad \sigma_{23} \quad \sigma_{33} \quad D_3]_{k+1} \end{aligned} \tag{6.105}$$

To simplify the following derivation they separated the field variables into transverse components and those in the x_1-x_2 plane (denoted by a subscript p), and rewrote Eq. (6.102) as (the subscript k here has been dropped for conciseness)

$$\begin{aligned} &\boldsymbol{\varepsilon}_p = \mathbf{f}_{pp}\boldsymbol{\sigma}_p + \mathbf{f}_{p3}\sigma_{33} - \mathbf{d}_p\phi_{,3}, \\ &\varepsilon_{33} = \mathbf{S}_{p3}^{\mathrm{T}}\sigma_p + f_{33}\sigma_{33} - d_{33}\phi_{,3}, \\ &\boldsymbol{\varepsilon}_s = \mathbf{f}_{ss}\boldsymbol{\sigma}_s - \mathbf{d}_s\mathbf{L}\phi, \\ &\mathbf{D}_p = \mathbf{d}_s^{\mathrm{T}}\sigma_s - \boldsymbol{\kappa}\mathbf{L}\phi, \\ &D_3 = \mathbf{d}_p^{\mathrm{T}}\boldsymbol{\sigma}_p + d_{33}\sigma_{33} - \kappa_{33}\phi_{,3} \end{aligned} \tag{6.106}$$

where

$$\begin{aligned} &\boldsymbol{\varepsilon}_p = \{\varepsilon_{11} \quad \varepsilon_{22} \quad 2\varepsilon_{12}\}^{\mathrm{T}}, \quad \boldsymbol{\sigma}_p = \{\sigma_{11} \quad \sigma_{22} \quad \sigma_{12}\}^{\mathrm{T}}, \quad \mathbf{D}_p = \{D_1 \quad D_2\}^{\mathrm{T}}, \\ &\boldsymbol{\varepsilon}_s = \{2\varepsilon_{13} \quad 2\varepsilon_{23}\}^{\mathrm{T}}, \qquad \boldsymbol{\sigma}_s = \{\sigma_{13} \quad \sigma_{23}\}^{\mathrm{T}} \end{aligned} \tag{6.107}$$

$$\begin{aligned} &\mathbf{f}_{pp} = \begin{bmatrix} s_{11} & s_{12} & s_{16} \\ s_{12} & s_{22} & s_{26} \\ s_{16} & s_{26} & s_{66} \end{bmatrix}, \quad \mathbf{f}_{p3} = \begin{bmatrix} s_{13} \\ s_{23} \\ s_{36} \end{bmatrix}, \quad \mathbf{d}_p = \begin{bmatrix} d_{31} \\ d_{32} \\ d_{36} \end{bmatrix}, \quad \mathbf{f}_{ss} = \begin{bmatrix} s_{55} & s_{45} \\ s_{45} & s_{44} \end{bmatrix}, \\ &\mathbf{d}_s = \begin{bmatrix} d_{15} & d_{25} \\ d_{14} & d_{24} \end{bmatrix}, \qquad \boldsymbol{\kappa} = \begin{bmatrix} \kappa_{11} & \kappa_{12} \\ \kappa_{12} & \kappa_{22} \end{bmatrix}, \qquad \mathbf{L} = \begin{bmatrix} \partial/\partial x_1 \\ \partial/\partial x_2 \end{bmatrix} \end{aligned} \tag{6.108}$$

In the derivation of the state space formulation for decay analysis, Tarn and Huang [3] took u_1, u_2, u_3, ϕ, $\boldsymbol{\sigma}_s$, σ_{33}, and D_3 as the primary variables and then arranged the basic equations in the form

$$\begin{aligned} &\mathbf{u}_{,3} = -\mathbf{L}u_3 - \mathbf{d}_s\mathbf{L}\phi + \mathbf{S}_{ss}\boldsymbol{\sigma}_s, \\ &u_{3,3} = \tilde{\mathbf{S}}_{p3}^{\mathrm{T}}\mathbf{S}_{pp}^{-1}\mathbf{L}_p\mathbf{u} + (\tilde{s}_{33} - \mathbf{S}_{p3}^{\mathrm{T}}\mathbf{S}_{pp}^{-1}\tilde{\mathbf{S}}_{p3})\sigma_{33} - \tilde{d}_{33}D_3, \\ &\phi_{,3} = \tilde{\kappa}_{33}^{-1}\mathbf{d}_p^{\mathrm{T}}\mathbf{S}_{pp}^{-1}\mathbf{L}_p\mathbf{u} + \tilde{d}_{33}\sigma_{33} - \tilde{\kappa}_{33}^{-1}D_3 \end{aligned} \tag{6.109}$$

$$\begin{aligned} &\sigma_{s,3} = -\mathbf{L}_p^{\mathrm{T}}[\mathbf{S}_{pp}^{-1}(\mathbf{G}\mathbf{L}_p\mathbf{u} - \tilde{\mathbf{S}}_{p3}\sigma_{33} - \tilde{\kappa}_{33}^{-1}\mathbf{d}_p D_3)], \\ &\sigma_{33,3} = -\mathbf{L}^{\mathrm{T}}\boldsymbol{\sigma}_s, \\ &D_{3,3} = \mathbf{L}^{\mathrm{T}}(\boldsymbol{\kappa}\mathbf{L}\phi - \mathbf{d}_s^{\mathrm{T}}\boldsymbol{\sigma}_s) \end{aligned} \tag{6.110}$$

$$\begin{aligned}\boldsymbol{\sigma}_p &= \mathbf{S}_{pp}^{-1}(\mathbf{G}\mathbf{L}_p\mathbf{u} - \tilde{\mathbf{S}}_{p3}\sigma_{33} - \tilde{\kappa}_{33}^{-1}\mathbf{d}_p D_3),\\ \mathbf{D}_p &= -\boldsymbol{\kappa}\mathbf{L}\phi + \mathbf{d}_s^{\mathrm{T}}\boldsymbol{\sigma}_s\end{aligned} \tag{6.111}$$

where

$$\begin{aligned}&\tilde{\mathbf{S}}_{p3} = \mathbf{S}_{p3} - \tilde{d}_{33}\mathbf{d}_p, \quad \tilde{s}_{33} = s_{33} - \tilde{d}_{33}d_{33}, \quad \mathbf{G} = \mathbf{I} + \tilde{\kappa}_{33}^{-1}\mathbf{d}_p\mathbf{d}_p^{\mathrm{T}}\mathbf{S}_{pp}^{-1},\\ &\tilde{\kappa}_{33} = \kappa_{33} - \mathbf{d}_p^{\mathrm{T}}\mathbf{S}_{pp}^{-1}\mathbf{d}_p, \quad \tilde{d}_{33} = \tilde{\kappa}_{33}^{-1}(d_{33} - \mathbf{d}_p^{\mathrm{T}}\mathbf{S}_{pp}^{-1}\mathbf{S}_{p3})\end{aligned} \tag{6.112}$$

$$\mathbf{u} = \begin{bmatrix} u_1 \\ u_2 \end{bmatrix}, \quad \mathbf{L}_p^{\mathrm{T}} = \begin{bmatrix} \partial/\partial x_1 & 0 & \partial/\partial x_2 \\ 0 & \partial/\partial x_2 & \partial/\partial x_1 \end{bmatrix} \tag{6.113}$$

The state space equations (6.109) and (6.110) of a linear piezoelectric material can be rewritten in matrix form as

$$\frac{\partial}{\partial x_3}\begin{bmatrix} u_1 \\ u_2 \\ u_3 \\ \phi \\ \sigma_{13} \\ \sigma_{23} \\ \sigma_{33} \\ D_3 \end{bmatrix} = \begin{bmatrix} 0 & 0 & -\partial_1 & l_{14} & s_{44} & s_{45} & 0 & 0 \\ 0 & 0 & 0 & l_{15} & s_{45} & s_{55} & 0 & 0 \\ l_{31} & l_{32} & 0 & 0 & 0 & 0 & a_{37} & \tilde{d}_{33} \\ l_{41} & l_{42} & 0 & 0 & 0 & 0 & \tilde{d}_{33} & -\tilde{\kappa}_{33}^{-1} \\ l_{51} & l_{52} & 0 & 0 & 0 & 0 & l_{31} & l_{41} \\ l_{52} & l_{62} & 0 & 0 & 0 & 0 & l_{32} & l_{42} \\ 0 & 0 & 0 & 0 & -\partial_1 & 0 & 0 & 0 \\ 0 & 0 & 0 & l_{84} & l_{14} & l_{15} & 0 & 0 \end{bmatrix}\begin{bmatrix} u_1 \\ u_2 \\ u_3 \\ \phi \\ \sigma_{13} \\ \sigma_{23} \\ \sigma_{33} \\ D_3 \end{bmatrix} \tag{6.114}$$

where the field variables are independent of x_2 for a problem of generalized plane strain, and

$$\begin{aligned}&l_{14} = -d_{14}\partial_1, \quad l_{15} = -d_{15}\partial_1, \quad l_{31} = a_{31}\partial_1, \quad l_{32} = a_{32}\partial_1,\\ &l_{41} = a_{41}\partial_1, \quad l_{42} = a_{42}\partial_1, \quad l_{51} = a_{51}\partial_{11}, \quad l_{52} = a_{52}\partial_{11},\\ &l_{62} = a_{62}\partial_{11}, \quad l_{84} = \kappa_{11}\partial_{11}\end{aligned} \tag{6.115}$$

$$\begin{aligned}&\begin{bmatrix} a_{31} & a_{32} \end{bmatrix} = \tilde{\mathbf{S}}_{p3}^{\mathrm{T}}\mathbf{S}_{pp}^{-1}\mathbf{H}^{\mathrm{T}}, \quad a_{37} = \tilde{s}_{33} - \tilde{\mathbf{S}}_{p3}^{\mathrm{T}}\mathbf{S}_{pp}^{-1}\tilde{\mathbf{S}}_{p3},\\ &\begin{bmatrix} a_{41} \\ a_{42} \end{bmatrix} = \tilde{\kappa}_{33}^{-1}\mathbf{H}\mathbf{S}_{pp}^{-1}\mathbf{d}_p, \quad \begin{bmatrix} a_{51} & a_{52} \\ a_{52} & a_{62} \end{bmatrix} = -\mathbf{H}\mathbf{S}_{pp}^{-1}\mathbf{G}\mathbf{H}^{\mathrm{T}}, \quad \mathbf{H} = \begin{bmatrix} 1 & 0 & 0 \\ 0 & 0 & 1 \end{bmatrix}\end{aligned} \tag{6.116}$$

Equation (6.111) can be further written as

$$\begin{bmatrix} \sigma_{11} \\ \sigma_{22} \\ \sigma_{12} \end{bmatrix} = \begin{bmatrix} b_{11} & b_{12} \\ b_{21} & b_{22} \\ b_{31} & b_{32} \end{bmatrix}\frac{\partial}{\partial x_1}\begin{bmatrix} u_1 \\ u_2 \end{bmatrix} + \begin{bmatrix} b_{17} \\ b_{27} \\ b_{37} \end{bmatrix}\sigma_{33} + \begin{bmatrix} b_{18} \\ b_{28} \\ b_{38} \end{bmatrix}D_3 \tag{6.117}$$

$$\begin{bmatrix} D_1 \\ D_2 \end{bmatrix} = \begin{bmatrix} \kappa_{11} \\ \kappa_{12} \end{bmatrix}\phi_{,1} + \begin{bmatrix} d_{14} & d_{15} \\ d_{24} & d_{25} \end{bmatrix}\begin{bmatrix} \sigma_{13} \\ \sigma_{23} \end{bmatrix} \tag{6.118}$$

where

$$\begin{bmatrix} b_{11} & b_{12} \\ b_{21} & b_{22} \\ b_{31} & b_{32} \end{bmatrix} = \mathbf{S}_{pp}^{-1}\mathbf{G}\mathbf{H}^{\mathrm{T}}, \quad \begin{bmatrix} b_{17} \\ b_{27} \\ b_{37} \end{bmatrix} = -\mathbf{S}_{pp}^{-1}\tilde{\mathbf{S}}_{p3}, \quad \begin{bmatrix} b_{18} \\ b_{28} \\ b_{38} \end{bmatrix} = -\tilde{\kappa}_{33}^{-1}\mathbf{S}_{pp}^{-1}\mathbf{d}_p \tag{6.119}$$

Equations (6.114), (6.117), and (6.118) constitute all the state field formulations needed in the decay analysis.

6.4.2 Eigensolution and decay rate equation

To obtain the decay solutions to the space state differential equations (6.114) above, suppose that the solution has the following form:

$$\begin{aligned} \{u_1, u_2, u_3, \phi, \sigma_{13}, \sigma_{23}, \sigma_{33}, D_3\}_k = {} & e^{-\lambda x_1}\begin{bmatrix} u & v & w & \varphi & \tau_{13} & \tau_{23} & \tau_{33} & \Lambda_3 \end{bmatrix}_k \\ & + e^{\gamma(x_1-a)}\begin{bmatrix} \tilde{u} & \tilde{v} & \tilde{w} & \tilde{\varphi} & \tilde{\tau}_{13} & \tilde{\tau}_{23} & \tilde{\tau}_{33} & \tilde{\Lambda}_3 \end{bmatrix}_k \end{aligned} \tag{6.120}$$

where λ and γ are the decay factors to be determined; u, v, w,$\cdots$ and $\tilde{u}$, $\tilde{v}$, $\tilde{w}$,$\cdots$ are unknown functions of x_3. Tarn and Huang [3] indicated that the first exponential function depicts the decay from the end x_1=0 with a decay rate λ; the second one depicts the decay from the end x_1=L with a decay rate γ. As x_1 increases, the influence of the first term decreases whereas the influence of the second term increases. For a semi-infinite strip, $L\to\infty$, the second term vanishes, and only the decay from x_1=0 needs to be considered.

Substitution of Eq. (6.120) into Eq. (6.114) yields two sets of equations as follows:

$$\frac{\mathrm{d}}{\mathrm{d}x_3}\mathbf{X}_k = \lambda\mathbf{A}_k\mathbf{X}_k, \quad \frac{\mathrm{d}}{\mathrm{d}x_3}\tilde{\mathbf{X}}_k = -\gamma\mathbf{A}_k\tilde{\mathbf{X}}_k \tag{6.121}$$

where

$$\mathbf{A}_k = \begin{bmatrix} 0 & 0 & 1 & d_{14} & f_{44} & f_{45} & 0 & 0 \\ 0 & 0 & 0 & d_{15} & f_{45} & f_{55} & 0 & 0 \\ -a_{31} & -a_{32} & 0 & 0 & 0 & 0 & a_{37} & \tilde{d}_{33} \\ -a_{41} & -a_{42} & 0 & 0 & 0 & 0 & \tilde{d}_{33} & -\tilde{\kappa}_{11}^{-1} \\ a_{51} & a_{52} & 0 & 0 & 0 & 0 & -a_{31} & -a_{41} \\ a_{52} & a_{62} & 0 & 0 & 0 & 0 & -a_{32} & -a_{42} \\ 0 & 0 & 0 & 0 & 1 & 0 & 0 & 0 \\ 0 & 0 & 0 & \kappa_{11} & d_{14} & d_{15} & 0 & 0 \end{bmatrix}_k \tag{6.122}$$

$$\begin{aligned}\mathbf{X}_k &= \left[\lambda u \quad \lambda v \quad \lambda w \quad \lambda\varphi \quad \tau_{13} \quad \tau_{23} \quad \tau_{33} \quad \Lambda_3\right]_k^{\mathrm{T}},\\ \tilde{\mathbf{X}}_k &= \left[-\gamma\tilde{u} \quad -\gamma\tilde{v} \quad -\gamma\tilde{w} \quad -\gamma\tilde{\varphi} \quad \tilde{\tau}_{13} \quad \tilde{\tau}_{23} \quad \tilde{\tau}_{33} \quad \tilde{\Lambda}_3\right]_k^{\mathrm{T}}\end{aligned} \tag{6.123}$$

It is noted that Eq. $(6.121)_1$ is mathematically the same as Eq. $(6.121)_2$ if $\lambda = -\gamma$. This indicates that the decay rates from both ends are the same and both equations result in the same through-thickness variation of the field variables. Consequently, Tarn and Huang treated Eq. $(6.121)_1$ as the first part and Eq. $(6.121)_2$ as the second part.

The solution of Eq. $(6.121)_1$ is

$$\mathbf{X}_k(x_3) = \mathbf{P}_k(x_3 - z_{k-1})\mathbf{X}_k(z_{k-1}) \tag{6.124}$$

where the transfer matrix $\mathbf{P}_k$ is given by

$$\mathbf{P}_k(x_3 - z_{k-1}) = e^{\lambda A_k (x_3 - z_{k-1})} \tag{6.125}$$

Using the continuity condition (6.105) and Eq. (6.124), we have

$$\mathbf{X}_{k+1}(z_k) = \mathbf{P}_k(z_k - z_{k-1})\mathbf{X}_k(z_{k-1}) \qquad (k = 1, 2, \cdots, n-i) \tag{6.126}$$

Applying Eq. (6.126) recursively yields

$$\mathbf{X}(x_3) = \mathbf{T}_k(x_3)\mathbf{X}_k(h) \qquad (z_{k-1} \leqslant x_3 \leqslant z_k) \tag{6.127}$$

where

$$\mathbf{T}_k(x_3) = \begin{cases} \mathbf{P}_1(x_3 - h) & (k = 1) \\ \mathbf{P}_k(x_3 - x_{k-1})\mathbf{T}_{k-1}(z_{k-1}) & (k = 2, 3, \cdots, n) \end{cases} \tag{6.128}$$

Letting $x_3 = -h$, Eq. (6.127) becomes

$$\mathbf{X}(-h) = \mathbf{T}_n(-h)\mathbf{X}(h) \tag{6.129}$$

Denoting

$$\begin{aligned}&\mathbf{U} = \lambda\left\{u \quad v \quad w \quad \phi\right\}^{\mathrm{T}}, \quad \mathbf{S} = \left\{\tau_{13} \quad \tau_{23} \quad \tau_{33} \quad \Lambda_3\right\}^{\mathrm{T}},\\ &\begin{Bmatrix}\mathbf{U}(-h)\\ \mathbf{S}(-h)\end{Bmatrix} = \begin{bmatrix}\mathbf{T}_{uu}(-h) & \mathbf{T}_{us}(-h)\\ \mathbf{T}_{su}(-h) & \mathbf{T}_{ss}(-h)\end{bmatrix}\begin{Bmatrix}\mathbf{U}(h)\\ \mathbf{S}(h)\end{Bmatrix}\end{aligned} \tag{6.130}$$

and considering $\mathbf{S}(h)=\mathbf{S}(-h)=0$, we have

$$\mathbf{T}_{su}(-h)\mathbf{U}(h) = 0 \tag{6.131}$$

to which the non-trivial solution $\mathbf{U}(h)$ exists if the determinant of the coefficient matrix vanishes,

$$\det\left|\mathbf{T}_{su}(-h)\right| = 0 \tag{6.132}$$

Then, the decay factor λ, subsequently $\mathbf{U}(h)$, can be determined from Eq. (6.132).

The primary state variables are determined from

$$\mathbf{U}(x_3)=\mathbf{T}_{uu}(x_3)\mathbf{U}(h),\qquad \mathbf{S}(x_3)=\mathbf{T}_{su}(x_3)\mathbf{U}(h) \tag{6.133}$$

When both the top and bottom surfaces are grounded, i.e, ϕ=0, Eq. (6.130) becomes

$$\begin{gathered}\hat{\mathbf{U}}=\begin{Bmatrix}\lambda u & \lambda v & \lambda w & \Lambda_3\end{Bmatrix}^{\mathrm{T}},\quad \hat{\mathbf{S}}=\begin{Bmatrix}\tau_{13} & \tau_{23} & \tau_{33} & \lambda\phi\end{Bmatrix}^{\mathrm{T}},\\ \begin{bmatrix}\hat{\mathbf{U}}(-h)\\ \hat{\mathbf{S}}(-h)\end{bmatrix}=\begin{bmatrix}\hat{\mathbf{T}}_{uu}(-h) & \hat{\mathbf{T}}_{us}(-h)\\ \hat{\mathbf{T}}_{su}(-h) & \hat{\mathbf{T}}_{ss}(-h)\end{bmatrix}\begin{bmatrix}\hat{\mathbf{U}}(h)\\ \hat{\mathbf{S}}(h)\end{bmatrix}\end{gathered} \tag{6.134}$$

Again, with the boundary conditions $\hat{\mathbf{S}}(h)=\hat{\mathbf{S}}(-h)=0$, the decay rate is determined from

$$\det\left|\hat{\mathbf{T}}_{su}(-h)\right|=0 \tag{6.135}$$

Once the primary state variables have been determined, the other stress and electric displacement components are determined from Eqs. (6.117) and (6.118) as follows:

$$\begin{bmatrix}\sigma_{11}\\ \sigma_{22}\\ \sigma_{12}\end{bmatrix}_k=e^{-\lambda x_1}\left(-\begin{bmatrix}b_{11} & b_{12}\\ b_{21} & b_{22}\\ b_{31} & b_{32}\end{bmatrix}\begin{bmatrix}\lambda u\\ \lambda v\end{bmatrix}+\begin{bmatrix}b_{17}\\ b_{27}\\ b_{37}\end{bmatrix}\tau_{33}+\begin{bmatrix}b_{18}\\ b_{28}\\ b_{38}\end{bmatrix}\Lambda_3\right)_k \tag{6.136}$$

$$\begin{bmatrix}D_1\\ D_2\end{bmatrix}_k=e^{-\lambda x_1}\left(\begin{bmatrix}\kappa_{11}\\ \kappa_{12}\end{bmatrix}\lambda\phi+\begin{bmatrix}d_{14} & d_{15}\\ d_{24} & d_{25}\end{bmatrix}\begin{bmatrix}\tau_{13}\\ \tau_{23}\end{bmatrix}\right)_k \tag{6.137}$$

As a special case of multilayered structures, Tarn and Huang considered a monoclinic piezoelectric strip and developed the corresponding formulations in [3]. For piezoelectric materials of the orthorhombic system of class 2*mm*, Eq. $(6.121)_1$ reduces to

$$\frac{\mathrm{d}}{\mathrm{d}x_3}\begin{bmatrix}\lambda u\\ \lambda w\\ \lambda\varphi\\ \tau_{13}\\ \tau_{33}\\ \Lambda_3\end{bmatrix}=\lambda\left(\begin{bmatrix}0 & 1 & 0 & s_{44} & 0 & 0\\ -a_{31} & 0 & 0 & 0 & a_{37} & \tilde{d}_{33}\\ -a_{41} & 0 & 0 & 0 & \tilde{d}_{33} & -\tilde{\kappa}_{33}^{-1}\\ a_{51} & 0 & 0 & 0 & -a_{31} & -a_{41}\\ 0 & 0 & 0 & 1 & 0 & 0\\ 0 & 0 & \kappa_{11} & 0 & 0 & 0\end{bmatrix}\begin{bmatrix}\lambda u\\ \lambda w\\ \lambda\varphi\\ \tau_{13}\\ \tau_{33}\\ \Lambda_3\end{bmatrix}+\begin{bmatrix}0\\ 0\\ 0\\ 0\\ 0\\ d_{15}\end{bmatrix}\tau_{23}\right) \tag{6.138}$$

$$\frac{\mathrm{d}}{\mathrm{d}x_3}\begin{bmatrix}\lambda v\\ \tau_{23}\end{bmatrix}=\lambda\left(\begin{bmatrix}0 & s_{55}\\ 1/s_{66} & 0\end{bmatrix}\begin{bmatrix}\lambda v\\ \tau_{23}\end{bmatrix}+\begin{bmatrix}d_{15}\\ 0\end{bmatrix}\lambda\varphi\right) \tag{6.139}$$

Equations (6.136) and (6.137) also reduce to

$$\begin{bmatrix}\sigma_{11}\\ \sigma_{22}\end{bmatrix}=\frac{e^{-\lambda x_1}}{\aleph}\left(-\begin{bmatrix}b_{11}\\ b_{21}\end{bmatrix}\lambda\mu+\begin{bmatrix}b_{17}\\ b_{27}\end{bmatrix}\tau_{33}+\begin{bmatrix}b_{18}\\ b_{28}\end{bmatrix}\Delta_3\right),\quad \sigma_{12}=-\frac{e^{-\lambda x_1}}{s_{66}}\lambda v \tag{6.140}$$

$$D_1=e^{-\lambda x_1}(\kappa_{11}\lambda\varphi+d_{15}\tau_{23}),\quad D_2=e^{-\lambda x_1}d_{24}\tau_{13} \tag{6.141}$$

where

$$\begin{aligned}&a_{31}=(\tilde{s}_{13}s_{22}-\tilde{s}_{23}s_{12})/\aleph,\quad a_{41}=\tilde{\kappa}_{33}^{-1}(d_{31}s_{22}-d_{32}s_{12})/\aleph,\\ &a_{37}=\tilde{s}_{33}+[s_{23}(\tilde{s}_{13}s_{12}-\tilde{s}_{23}s_{11})-s_{13}(\tilde{s}_{13}s_{22}-\tilde{s}_{23}s_{12})]/\aleph,\\ &a_{51}=\tilde{\kappa}_{33}^{-1}(d_{32}^2s_{12}^2-d_{31}^2s_{22}^2)/\aleph-s_{22}/\aleph,\quad \aleph=s_{11}s_{22}-s_{12}^2\end{aligned} \tag{6.142}$$

$$\begin{bmatrix}b_{11}\\ b_{21}\end{bmatrix}=\begin{bmatrix}s_{22}+\tilde{\kappa}_{33}^{-1}[s_{22}(d_{31}^2s_{22}-d_{31}d_{32}s_{12})+s_{12}(d_{32}^2s_{12}-d_{31}d_{32}s_{22})]/\aleph\\ -s_{12}-\tilde{\kappa}_{33}^{-1}[s_{11}(d_{32}^2s_{12}-d_{31}d_{32}s_{22})+s_{12}(d_{31}^2s_{22}-d_{31}d_{32}s_{12})]/\aleph\end{bmatrix} \tag{6.143}$$

$$\begin{bmatrix}b_{17}\\ b_{27}\end{bmatrix}=\begin{bmatrix}\tilde{s}_{23}s_{12}-\tilde{s}_{13}s_{22}\\ \tilde{s}_{13}s_{12}-\tilde{s}_{23}s_{11}\end{bmatrix},\quad \begin{bmatrix}b_{18}\\ b_{28}\end{bmatrix}=\tilde{\kappa}_{33}^{-1}\begin{bmatrix}d_{32}s_{12}-d_{31}s_{22}\\ d_{31}s_{12}-d_{32}s_{11}\end{bmatrix} \tag{6.144}$$

Tarn and Huang found from Eqs. (6.138) and (6.139) that the field variables in the x_1-x_3 plane are associated with the antiplane shear σ_{23}, and the antiplane deformation and shear stress are associated with the electromechanical field in the x_1-x_3 plane through ϕ. The in-plane and antiplane field variables are coupled unless d_{15}=0. Only in orthorhombic piezoelectric materials with d_{15}=0 does a 2-D loading give rise to plane deformation, and the antiplane shears σ_{12}, σ_{23} and displacement u_2 are independent of the electric field. From the material properties of various piezoelectric materials listed in Table 1 of [12], all have non-zero d_{15}. This suggests that the applicability of a 2-D formulation for piezoelectric strips without accounting for the antiplane field variables is very limited. The plane strain or plane stress assumption is invalid for electroelastic analysis in general.

6.5 Decay rate of piezoelectric-piezomagnetic sandwich structures

In this section the decay of Saint-Venant end effects for plane deformations of piezoelectric (PE)-piezomagnetic (PM) sandwich structures presented in [4] is described. The structures studied are subjected to a self-equilibrated magneto-electro-elastic load. The upper and lower surfaces of the sandwich structure are mechanically free, electrically open or shorted as well as magnetically open or shorted.

6.5.1 Basic equations and notations in multilayered structures

In [4], Xue and Liu considered a sandwich structure as shown in Fig. 6.9. The PE layers and PM layers are assumed to possess transversely isotropic properties. The x_3-axis is the polarization direction of both two materials. The thickness of the sandwich plate is $2h$ and the thickness of the mid-layer is $2f$. The constitutive equations of the PE and PM media in the context of plane strain are, respectively, given by

$$\boldsymbol{\sigma}^e = \mathbf{c}^e\boldsymbol{\varepsilon}^e + (\mathbf{e}^e)^{\mathrm{T}}\boldsymbol{\Phi}^e, \quad \mathbf{D}^e = \mathbf{e}^e\boldsymbol{\varepsilon}^e - \boldsymbol{\kappa}^e\boldsymbol{\Phi}^e, \quad \mathbf{B}^e = -\boldsymbol{\mu}^e\boldsymbol{\Psi}^e \tag{6.145}$$

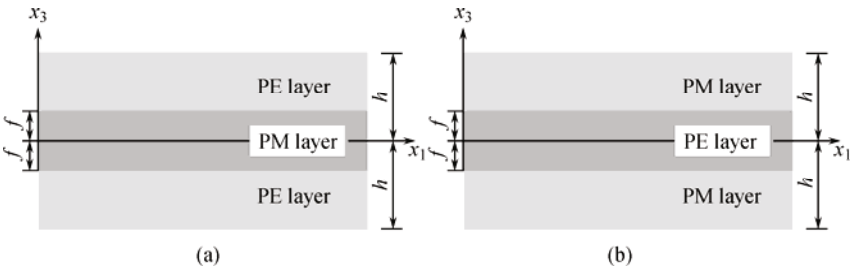

Fig. 6.9 Piezoelectric-piezomagnetic sandwich plate. (a) PE-PM-PE structures; (b) PM-PE-PM structures.

and

$$\boldsymbol{\sigma}^m = \mathbf{c}^m\boldsymbol{\varepsilon}^m + (\mathbf{h}^m)^{\mathrm{T}}\boldsymbol{\Psi}^m, \quad \mathbf{D}^m = -\boldsymbol{\kappa}^m\boldsymbol{\Phi}^m, \quad \mathbf{B}^m = \mathbf{h}^m\boldsymbol{\varepsilon}^m - \boldsymbol{\mu}^m\boldsymbol{\Psi}^m \tag{6.146}$$

where the superscripts "e"and "m"denote the quantities to be associated with PE and PM materials respectively, and

$$\begin{aligned}
&\boldsymbol{\sigma}^n = \left\{\sigma_{11}^n \quad \sigma_{33}^n \quad \sigma_{13}^n\right\}^{\mathrm{T}}, \quad \mathbf{D}^n = \left\{D_1^n \quad D_3^n\right\}^{\mathrm{T}}, \quad \mathbf{B}^n = \left\{B_1^n \quad B_3^n\right\}^{\mathrm{T}},\\
&\boldsymbol{\varepsilon}^n = \left\{\varepsilon_{11}^n \quad \varepsilon_{33}^n \quad \varepsilon_{13}^n\right\}^{\mathrm{T}}, \quad \boldsymbol{\Phi}^n = \left\{\phi_{,1}^n \quad \phi_{,3}^n\right\}^{\mathrm{T}}, \quad \boldsymbol{\Psi}^n = \left\{\psi_{,1}^n \quad \psi_{,3}^n\right\}^{\mathrm{T}},\\
&\mathbf{c}^n = \begin{bmatrix} c_{11}^n & c_{13}^n & 0 \\ c_{13}^n & c_{33}^n & 0 \\ 0 & 0 & c_{44}^n \end{bmatrix}, \quad \mathbf{e}^n = \begin{bmatrix} 0 & 0 & e_{15}^n \\ e_{31}^n & e_{33}^n & 0 \end{bmatrix}, \quad \mathbf{h}^n = \begin{bmatrix} 0 & 0 & h_{15}^n \\ h_{31}^n & h_{33}^n & 0 \end{bmatrix}, \quad (n = e, m)\\
&\boldsymbol{\kappa}^n = \begin{bmatrix} \kappa_{11}^n & 0 \\ 0 & \kappa_{33}^n \end{bmatrix}, \qquad \boldsymbol{\mu}^n = \begin{bmatrix} \mu_{11}^n & 0 \\ 0 & \mu_{33}^n \end{bmatrix}
\end{aligned} \tag{6.147}$$

The strain-displacement relations (1.2) and governing equations (1.10) are now in the form

$$\begin{aligned} &\varepsilon_{ij}^n = \frac{u_{i,j}^n + u_{j,i}^n}{2}, \\ &\sigma_{ij,j}^n = 0, \quad D_{i,i}^n = 0, \quad B_{i,i}^n = 0 \end{aligned} \tag{6.148}$$

For the boundary conditions of the problem Xue and Liu studied, the structures are considered to be subjected to self-equilibrated magneto-electro-elastic loads at $x_1 = 0$. The upper and lower surfaces of the structures are mechanically free, and electrically shorted (S) or open (O) and magnetically open or shorted, i.e.,

$$\begin{aligned} &\sigma_{13}^n = \sigma_{33}^n = 0, \\ &\phi^n = 0 \text{ (S)} \quad \text{or} \quad D_3^n = 0 \text{ (O)}, \qquad (\text{on } x_3 = \pm h) \\ &\psi^n = 0 \text{ (O)} \quad \text{or} \quad B_3^n = 0 \text{ (S)} \end{aligned} \tag{6.149}$$

The continuity conditions on the interface $x_3 = \pm f$ require

$$\begin{aligned} &\left\{ u_1^e \quad u_3^e \quad \phi^e \quad \psi^e \right\}^{\mathrm{T}} = \left\{ u_1^m \quad u_3^m \quad \phi^m \quad \psi^m \right\}^{\mathrm{T}}, \\ &\left\{ \sigma_{13}^e \quad \sigma_{33}^e \quad D_3^e \quad B_3^e \right\}^{\mathrm{T}} = \left\{ \sigma_{13}^m \quad \sigma_{33}^m \quad D_3^m \quad B_3^m \right\}^{\mathrm{T}} \end{aligned} \tag{6.150}$$

Xue and Liu also employed the dimensionless variable approach, which is useful for simple deduction and calculation. In setting forth the normalization formulation, four key properties are selected as the reference values: (a) half of the sandwich thickness h; (b) an elastic modulus c^0; (c) a piezoelectric constant e^0; and (d) a piezomagnetic constant h^0. The geometry, mechanical displacements, electrical potential, magnetic potential and the material constants can then be normalized as

$$\begin{aligned} &\bar{x}_1 = \frac{x_1}{h}, \ \bar{x}_3 = \frac{x_3}{h}, \ \bar{u}_1 = \frac{u_1}{h}, \ \bar{u}_3 = \frac{u_3}{h}, \ \bar{\phi} = \frac{\phi}{E^0 h}, \ \bar{\psi} = \frac{\psi}{H^0 h}, \\ &\bar{\boldsymbol{\sigma}}^n = \frac{\boldsymbol{\sigma}^n}{c^0}, \ \bar{\boldsymbol{\varepsilon}}^n = \boldsymbol{\varepsilon}^n, \ \bar{\boldsymbol{\Phi}}^n = \frac{\boldsymbol{\Phi}^n}{E^0}, \ \bar{\boldsymbol{\Psi}}^n = \frac{\boldsymbol{\Psi}^n}{H^0}, \ \bar{\mathbf{e}}^n = \frac{\mathbf{e}^n}{e^0}, \ \bar{\mathbf{h}}^n = \frac{\mathbf{h}^n}{h^0}, \\ &\bar{\mathbf{c}}^n = \frac{\mathbf{c}^n}{c^0}, \quad \bar{\mathbf{D}}^n = \frac{\mathbf{D}^n}{e^0}, \quad \bar{\mathbf{B}}^n = \frac{\mathbf{B}^n}{h^0}, \quad \bar{\boldsymbol{\kappa}}^n = \frac{\boldsymbol{\kappa}^n}{\kappa^0}, \quad \bar{\boldsymbol{\mu}}^n = \frac{\boldsymbol{\mu}^n}{\mu^0} \end{aligned} \tag{6.151}$$

where $E^0 = c^0 / e^0$, $H^0 = c^0 / h^0$, $\kappa^0 = (e^0)^2 / c^0$, and $\mu^0 = (h^0)^2 / c^0$.

6.5.2 Space state differential equations for analyzing decay rate

Making use of Eqs. (6.145), (6.146), and (6.151), a set of normalized form of constitutive equations for both PE and PM materials is obtained as

$$\overline{\boldsymbol{\varepsilon}}^e = \overline{\mathbf{S}}^e\overline{\boldsymbol{\sigma}}^e - (\overline{\mathbf{d}}^e)^{\mathrm{T}}\overline{\boldsymbol{\Phi}}^e, \quad \overline{\mathbf{D}}^e = \overline{\mathbf{d}}^e\overline{\boldsymbol{\sigma}}^e - \overline{\boldsymbol{\kappa}}^{e0}\overline{\boldsymbol{\Phi}}^e, \quad \overline{\mathbf{B}}^e = -\overline{\boldsymbol{\mu}}^e\overline{\boldsymbol{\Psi}}^e \tag{6.152}$$

and

$$\overline{\boldsymbol{\varepsilon}}^m = \overline{\mathbf{S}}^m\overline{\boldsymbol{\sigma}}^m - (\overline{\mathbf{g}}^m)^{\mathrm{T}}\overline{\boldsymbol{\Psi}}^m, \quad \overline{\mathbf{D}}^m = -\overline{\boldsymbol{\kappa}}^m\overline{\boldsymbol{\Phi}}^m, \quad \overline{\mathbf{B}}^m = \overline{\mathbf{g}}^m\overline{\boldsymbol{\sigma}}^m - \overline{\boldsymbol{\mu}}^{m0}\overline{\boldsymbol{\Psi}}^m \tag{6.153}$$

where

$$\begin{aligned} &\overline{\mathbf{S}}^e = (\overline{\mathbf{c}}^e)^{-1}, \quad \overline{\mathbf{d}}^e = \overline{\mathbf{S}}^e(\overline{\mathbf{e}}^e)^{\mathrm{T}}, \quad \overline{\boldsymbol{\kappa}}^{e0} = \overline{\mathbf{e}}^e\overline{\mathbf{S}}^e(\overline{\mathbf{e}}^e)^{\mathrm{T}} + \overline{\boldsymbol{\kappa}}^e, \\ &\overline{\mathbf{S}}^m = (\overline{\mathbf{c}}^m)^{-1}, \quad \overline{\mathbf{g}}^m = \overline{\mathbf{S}}^m(\overline{\mathbf{h}}^m)^{\mathrm{T}}, \quad \overline{\boldsymbol{\mu}}^{m0} = \overline{\mathbf{h}}^m\overline{\mathbf{S}}^m(\overline{\mathbf{h}}^m)^{\mathrm{T}} + \overline{\boldsymbol{\mu}}^m \end{aligned} \tag{6.154}$$

and the remaining variables are defined in the same way as those of Eq. (6.147). For convenience, Eq. (6.152) is rewritten in the following form:

$$\overline{\varepsilon}_{11}^e = \overline{s}_{11}^e\overline{\sigma}_{11}^e + \overline{s}_{13}^e\overline{\sigma}_{33}^e - \overline{d}_{31}^e\overline{\phi}_{,3}^e \tag{6.155}$$

$$\overline{\varepsilon}_{33}^e = \overline{s}_{13}^e\overline{\sigma}_{11}^e + \overline{s}_{33}^e\overline{\sigma}_{33}^e - \overline{d}_{33}^e\overline{\phi}_{,3}^e \tag{6.156}$$

$$2\overline{\varepsilon}_{13}^e = \overline{s}_{44}^e\overline{\sigma}_{13}^e - \overline{d}_{15}^e\overline{\phi}_{,1}^e \tag{6.157}$$

$$\overline{D}_1^e = \overline{d}_{15}^e\overline{\sigma}_{13}^e - \overline{\kappa}_{11}^e\overline{\phi}_{,1}^e \tag{6.158}$$

$$\overline{D}_3^e = \overline{d}_{31}^e\overline{\sigma}_{11}^e + \overline{d}_{33}^e\overline{\sigma}_{33}^e - \overline{\kappa}_{33}^e\overline{\phi}_{,3}^e \tag{6.159}$$

$$\overline{B}_1^e = -\overline{\mu}_{11}^e\overline{\psi}_{,1}^e \tag{6.160}$$

$$\overline{B}_3^e = -\overline{\mu}_{33}^e\overline{\psi}_{,3}^e \tag{6.161}$$

From Eqs. (6.155), (6.159), and (6.161), we have

$$\overline{\sigma}_{11}^e = f_{11}^e\overline{\varepsilon}_{11}^e - (f_{11}^e\overline{s}_{13}^e + f_{12}^e\overline{d}_{33}^e)\overline{\sigma}_{33}^e + f_{12}^e\overline{D}_3^e \tag{6.162}$$

$$\overline{\phi}_{,3}^e = f_{21}^e\overline{\varepsilon}_{11}^e - (f_{21}^e\overline{s}_{13}^e + f_{22}^e\overline{d}_{33}^e)\overline{\sigma}_{33}^e + f_{22}^e\overline{D}_3^e \tag{6.163}$$

$$\overline{\psi}_{,3}^e = f_{33}^e\overline{B}_3^e \tag{6.164}$$

where

$$\begin{aligned} &f_{11}^e = \frac{\overline{\kappa}_{33}^e}{\overline{s}_{11}^e\overline{\kappa}_{33}^e - \overline{d}_{31}^e\overline{d}_{31}^e}, \quad f_{12}^e = \frac{-\overline{d}_{31}^e}{\overline{s}_{11}^e\overline{\kappa}_{33}^e - \overline{d}_{31}^e\overline{d}_{31}^e}, \quad f_{21}^e = f_{12}^e, \\ &f_{22}^e = \frac{-\overline{s}_{11}^e}{\overline{s}_{11}^e\overline{\kappa}_{33}^e - \overline{d}_{31}^e\overline{d}_{31}^e}, \quad f_{33}^e = -\frac{1}{\overline{\mu}_{33}^e} \end{aligned} \tag{6.165}$$

Equations (6.148), (6.156), and (6.162)-(6.164) lead to

$$\overline{u}_{3,3}^e = n_{11}^e\overline{\varepsilon}_{11}^e + n_{33}^e\overline{\sigma}_{33}^e + n_{13}^e\overline{D}_3^e \tag{6.166}$$

where

$$\begin{aligned} n_{11}^e &= \overline{s}_{13}^e f_{11}^e + \overline{d}_{33}^e f_{12}^e, \\ n_{33}^e &= \overline{s}_{33}^e - \overline{s}_{13}^e \overline{s}_{13}^e f_{11}^e - 2\overline{s}_{13}^e \overline{d}_{33}^e f_{12}^e + \overline{d}_{33}^e \overline{d}_{33}^e f_{22}^e, \\ n_{13}^e &= \overline{s}_{13}^e f_{12}^e - \overline{d}_{33}^e f_{22}^e \end{aligned} \tag{6.167}$$

Finally, making use of Eqs. (6.148), (6.157), (6.158), (6.160), and (6.162), we obtain

$$\begin{gathered} \overline{D}_{3,3}^e = -(\overline{d}_{15}^e \overline{\sigma}_{13}^e + \overline{\kappa}_{11}^e \overline{\phi}_{,1}^e)_{,1}, \quad \overline{B}_{3,3}^e = (\overline{\mu}_{11}^e \overline{\psi}_{,1}^e)_{,1}, \quad \overline{\sigma}_{33,3}^e = \overline{\sigma}_{13,1}^e, \\ \overline{\sigma}_{13,3}^e = -[f_{11}^e \overline{\varepsilon}_{11}^e - (f_{11}^e \overline{s}_{13}^e + f_{12}^e \overline{d}_{33}^e)\overline{\sigma}_{33}^e + f_{12}^e \overline{D}_3^e]_{,1}, \quad \overline{u}_{1,3}^e = -\overline{u}_{3,1}^e + \overline{s}_{44}^e \overline{\sigma}_{13}^e - \overline{d}_{15}^e \overline{\phi}_{,1}^e \end{gathered} \tag{6.168}$$

Equations (6.163), (6.164), (6.166), and (6.168) consist of the differential equations of PE materials for decay analysis. Similarly the differential equations for PM materials can be obtained as follows:

$$\begin{gathered} \overline{u}_{1,3}^m = -\overline{u}_{3,1}^m + \overline{s}_{44}^m \overline{\sigma}_{13}^m - \overline{g}_{15}^m \overline{\psi}_{,1}^m, \quad \overline{D}_{3,3}^m = \overline{\kappa}_{11}^m \overline{\phi}_{,11}^m, \quad \overline{B}_{3,3}^m = \overline{\mu}_{11}^m \overline{\psi}_{,11}^m - \overline{g}_{15}^m \overline{\sigma}_{13,1}^m, \\ \overline{\sigma}_{33,3}^m = \overline{\sigma}_{13,1}^m, \quad \overline{\sigma}_{13,3}^m = -[f_{11}^m \overline{\varepsilon}_{11}^m - (f_{11}^m \overline{s}_{13}^m + f_{13}^m \overline{g}_{33}^m)\overline{\sigma}_{33}^m + f_{13}^m \overline{B}_3^m]_{,1}, \\ \overline{\phi}_{,3}^m = f_{22}^m \overline{D}_3^m, \quad \overline{\psi}_{,3}^m = f_{31}^m \overline{\varepsilon}_{11}^m - (f_{31}^m \overline{s}_{13}^m + f_{33}^m \overline{g}_{33}^m)\overline{\sigma}_{33}^m + f_{33}^m \overline{B}_3^m, \\ \overline{u}_{3,3}^m = n_{11}^m \overline{\varepsilon}_{11}^m + n_{33}^m \overline{\sigma}_{33}^m + n_{13}^m \overline{B}_3^m \end{gathered} \tag{6.169}$$

where

$$\begin{gathered} f_{11}^m = \frac{\overline{\mu}_{33}^m}{\overline{s}_{11}^m \overline{\mu}_{33}^m - \overline{g}_{31}^m \overline{g}_{31}^m}, \quad f_{13}^m = \frac{-\overline{g}_{31}^m}{\overline{s}_{11}^m \overline{\mu}_{33}^m - \overline{g}_{31}^m \overline{g}_{31}^m}, \quad f_{31}^m = f_{13}^m, \\ f_{22}^m = \frac{-1}{\overline{\kappa}_{33}^m}, \quad f_{33}^m = \frac{-\overline{s}_{11}^m}{\overline{s}_{11}^m \overline{\mu}_{33}^m - \overline{g}_{31}^m \overline{g}_{31}^m}, \quad n_{11}^m = \overline{s}_{13}^m f_{11}^m - \overline{g}_{33}^m f_{13}^m, \\ n_{33}^m = \overline{s}_{33}^m - \overline{s}_{13}^m \overline{s}_{13}^m f_{11}^m - 2\overline{s}_{13}^m \overline{g}_{33}^m f_{13}^m + \overline{g}_{33}^m \overline{g}_{33}^m f_{33}^m, \quad n_{13}^m = \overline{s}_{13}^m f_{13}^m - \overline{g}_{33}^m f_{33}^m \end{gathered} \tag{6.170}$$

6.5.3 Solutions to the space state differential equations

To obtain the decay solutions to the space state differential equations described in Subsection 6.5.2, denote $\mathbf{K}^n = \{\overline{u}_1^n, \overline{u}_3^n, \overline{\phi}^n, \overline{\psi}^n, \overline{\sigma}_{13}^n, \overline{\sigma}_{33}^n, \overline{D}_3^n, \overline{B}_3^n\}$. As $\overline{x}_1$ increases, the influence of $\mathbf{K}^n$ which determines the self-equilibrated state at the end decreases. Then the solutions to be found can be expressed in the form

$$\mathbf{K}^n = e^{-\lambda^n \overline{x}_1} \begin{Bmatrix} \tilde{u}^n & \tilde{w}^n & \tilde{\phi}^n & \tilde{\psi}^n & \tilde{\sigma}_{13}^n & \tilde{\sigma}_{33}^n & \tilde{D}_3^n & \tilde{B}_3^n \end{Bmatrix} \tag{6.171}$$

Noting that $\overline{u}_1^e = \overline{u}_1^m$ on the interface, we can conclude that $\lambda^e = \lambda^m = \lambda$. Sub-

stitution of Eq. (6.171) into Eqs. (6.163), (6.164), (6.166), (6.168), and (6.169) yields

$$\frac{\mathrm{d}}{\mathrm{d}\bar{x}_3}\mathbf{X}^n = \lambda \mathbf{A}^n \mathbf{X}^n \qquad (n = e, m) \tag{6.172}$$

where

$$\mathbf{X}^n = e^{-\lambda^n \bar{x}_1}\left\{\lambda\tilde{u}^n \quad \lambda\tilde{w}^n \quad \lambda\tilde{\phi}^n \quad \lambda\tilde{\psi}^n \quad \tilde{\sigma}_{13}^n \quad \tilde{\sigma}_{33}^n \quad \tilde{D}_3^n \quad \tilde{B}_3^n\right\} \tag{6.173}$$

$$\mathbf{A}^e = \begin{bmatrix} 0 & 1 & \bar{d}_{15}^e & 0 & \bar{s}_{44}^e & 0 & 0 & 0 \\ -n_{11}^e & 0 & 0 & 0 & 0 & n_{33}^e & n_{13}^e & 0 \\ -f_{21}^e & 0 & 0 & 0 & 0 & -f_{21}^e\bar{s}_{13}^e - f_{22}^e\bar{d}_{33}^e & f_{22}^e & 0 \\ 0 & 0 & 0 & 0 & 0 & 0 & 0 & f_{33}^e \\ -f_{11}^e & 0 & 0 & 0 & 0 & -f_{11}^e\bar{s}_{13}^e - f_{12}^e\bar{d}_{33}^e & f_{12}^e & 0 \\ 0 & 0 & 0 & 0 & 1 & 0 & 0 & 0 \\ 0 & 0 & \bar{\kappa}_{11}^e & 0 & \bar{d}_{15}^e & 0 & 0 & 0 \\ 0 & 0 & 0 & \bar{\mu}_{11}^e & 0 & 0 & 0 & 0 \end{bmatrix} \tag{6.174}$$

$$\mathbf{A}^m = \begin{bmatrix} 0 & 1 & 0 & \bar{g}_{15}^m & \bar{s}_{44}^m & 0 & 0 & 0 \\ -n_{11}^m & 0 & 0 & 0 & 0 & n_{33}^m & 0 & n_{13}^m \\ 0 & 0 & 0 & 0 & 0 & 0 & f_{22}^m & 0 \\ -f_{31}^m & 0 & 0 & 0 & 0 & -f_{31}^m\bar{s}_{13}^m - f_{33}^m\bar{g}_{33}^m & 0 & f_{33}^m \\ -f_{11}^m & 0 & 0 & 0 & 0 & -f_{11}^m\bar{s}_{13}^m - f_{13}^m\bar{g}_{33}^m & 0 & f_{13}^m \\ 0 & 0 & 0 & 0 & 1 & 0 & 0 & 0 \\ 0 & 0 & \bar{\kappa}_{11}^m & 0 & 0 & 0 & 0 & 0 \\ 0 & 0 & 0 & \bar{\mu}_{11}^m & \bar{g}_{15}^m & 0 & 0 & 0 \end{bmatrix} \tag{6.175}$$

Then the solution to Eq. (6.172) is

$$\mathbf{X}^n(\bar{x}_3) = \mathbf{P}^n(\bar{x}_3 - z_i)\mathbf{X}^n(z_i) \qquad (n = e,\ m;\ i = 1,2) \tag{6.176}$$

where

$$\mathbf{P}^n(\bar{x}_3 - z_i) = e^{\lambda \mathbf{A}^n(\bar{x}_3 - z_i)} \qquad (z_1 = f,\ z_2 = -f) \tag{6.177}$$

Using the solution (6.176), Xue and Liu derived characteristic equations for decay analysis by considering four types of boundary conditions of PE-PM-PE sandwich structures.

Case 1: Electrically open and magnetically shorted:

$$\sigma_{13}^e = \sigma_{33}^e = 0, \quad D_3^e = 0, \quad B_3^n = 0 \qquad (\text{on } x_3 = \pm h) \tag{6.178}$$

The solution for the boundary condition (6.178) is

$$\mathbf{X}^n(\bar{x}_3) = \begin{cases} \mathbf{P}^e(\bar{x}_3 - h)\mathbf{X}^e(h) & (n = e;\ f < \bar{x}_3 < h) \\ \mathbf{P}^m(\bar{x}_3 - f)\mathbf{X}^m(f) & (n = m;\ -f < \bar{x}_3 < f) \\ \mathbf{P}^e(\bar{x}_3 + f)\mathbf{X}^e(-f) & (n = e;\ -h < \bar{x}_3 < -f) \end{cases} \tag{6.179}$$

Using continuity conditions (6.150) and Eq. (6.179), we have

$$\mathbf{X}^e(\bar{x}_3) = \mathbf{P}^e(\bar{x}_3 + f)\mathbf{P}^m(-2f)\mathbf{P}^e(f - h)\mathbf{X}^e(h) \tag{6.180}$$

When $\bar{x}_3 = -h$, Eq. (6.180) becomes

$$\mathbf{X}(-h) = T(-h)\mathbf{X}(h) \tag{6.181}$$

where

$$T(-h) = \mathbf{P}^e(f - h)\mathbf{P}^m(-2f)\mathbf{P}^e(f - h)\mathbf{X}(h) \tag{6.182}$$

Denote

$$\begin{gathered} \mathbf{U} = \lambda\left\{\tilde{u} \quad \tilde{w} \quad \tilde{\phi} \quad \tilde{\psi}\right\}^{\mathrm{T}}, \qquad \mathbf{S} = \left\{\tilde{\sigma}_{13} \quad \tilde{\sigma}_{33} \quad \tilde{D}_3 \quad \tilde{B}_3\right\}^{\mathrm{T}}, \\ \begin{Bmatrix} \mathbf{U}(-h) \\ \mathbf{S}(-h) \end{Bmatrix} = \begin{bmatrix} \mathbf{T}_{uu}(-h) & \mathbf{T}_{us}(-h) \\ \mathbf{T}_{su}(-h) & \mathbf{T}_{ss}(-h) \end{bmatrix} \begin{Bmatrix} \mathbf{U}(h) \\ \mathbf{S}(h) \end{Bmatrix} \end{gathered} \tag{6.183}$$

and considering $\mathbf{S}(h)$=$\mathbf{S}(-h)$=0, we have

$$\mathbf{T}_{su}(-h)\mathbf{U}(h) = 0 \tag{6.184}$$

If there is a nonzero solution $\mathbf{U}(h)$ to Eq. (6.184), it must be

$$\det\left|\mathbf{T}_{su}(-h)\right| = 0 \tag{6.185}$$

Thus, the decay factor λ can be determined from Eq. (6.185), which is the characteristic equation for Case 1.

Case 2: Electrically open and magnetically open:

$$\sigma_{13}^e = \sigma_{33}^e = 0, \quad D_3^e = 0, \quad \psi^e = 0 \qquad (\text{on } x_3 = \pm h) \tag{6.186}$$

In this case, the state space variable defined in Eq. (6.183) and the corresponding efficient matrices $\mathbf{A}^e$ and $\mathbf{A}^m$ become

$$\mathbf{U} = \left\{\lambda\tilde{u} \quad \lambda\tilde{w} \quad \lambda\tilde{\phi} \quad \tilde{B}_3\right\}^{\mathrm{T}}, \qquad \mathbf{S} = \left\{\tilde{\sigma}_{13} \quad \tilde{\sigma}_{33} \quad \tilde{D}_3 \quad \lambda\tilde{\psi}\right\}^{\mathrm{T}} \tag{6.187}$$

$$\mathbf{A}^e = \begin{bmatrix} 0 & 1 & \overline{d}_{15}^e & 0 & \overline{s}_{44}^e & 0 & 0 & 0 \\ -n_{11}^e & 0 & 0 & 0 & 0 & n_{33}^e & n_{13}^e & 0 \\ -f_{21}^e & 0 & 0 & 0 & 0 & -f_{21}^e\overline{s}_{13}^e - f_{22}^e\overline{d}_{33}^e & f_{22}^e & 0 \\ 0 & 0 & 0 & 0 & 0 & 0 & 0 & \overline{\mu}_{11}^e \\ -f_{11}^e & 0 & 0 & 0 & 0 & -f_{11}^e\overline{s}_{13}^e - f_{12}^e\overline{d}_{33}^e & f_{12}^e & 0 \\ 0 & 0 & 0 & 0 & 1 & 0 & 0 & 0 \\ 0 & 0 & \overline{\kappa}_{11}^e & 0 & \overline{d}_{15}^e & 0 & 0 & 0 \\ 0 & 0 & 0 & f_{33}^e & 0 & 0 & 0 & 0 \end{bmatrix} \tag{6.188}$$

$$\mathbf{A}^m = \begin{bmatrix} 0 & 1 & 0 & 0 & \overline{s}_{44}^m & 0 & 0 & \overline{g}_{15}^m \\ -n_{11}^m & 0 & 0 & n_{13}^m & 0 & n_{33}^m & 0 & 0 \\ 0 & 0 & 0 & 0 & 0 & 0 & f_{22}^m & 0 \\ 0 & 0 & 0 & 0 & \overline{g}_{15}^m & 0 & 0 & \overline{\mu}_{11}^m \\ -f_{11}^m & 0 & 0 & f_{13}^m & 0 & -f_{11}^m\overline{s}_{13}^m - f_{13}^m\overline{g}_{33}^m & 0 & 0 \\ 0 & 0 & 0 & 0 & 1 & 0 & 0 & 0 \\ 0 & 0 & \overline{\kappa}_{11}^m & 0 & 0 & 0 & 0 & 0 \\ -f_{31}^m & 0 & 0 & f_{33}^m & \overline{g}_{15}^m & -f_{31}^m\overline{s}_{13}^m - f_{33}^m\overline{g}_{33}^m & 0 & 0 \end{bmatrix} \tag{6.189}$$

Then, the corresponding characteristic equation can be obtained in the same way as in Case 1.

Case 3: Electrically shorted and magnetically shorted:

$$\sigma_{13}^e = \sigma_{33}^e = 0, \quad \phi^e = 0, \quad B_3^e = 0 \qquad (\text{on } x_3 = \pm h) \tag{6.190}$$

In this case, the state space variable defined in Eq. (6.183) and the corresponding efficient matrices $\mathbf{A}^e$ and $\mathbf{A}^m$ become

$$\mathbf{U} = \left\{ \lambda\tilde{u} \quad \lambda\tilde{w} \quad \tilde{D}_3 \quad \lambda\tilde{\psi} \right\}^{\mathrm{T}}, \qquad \mathbf{S} = \left\{ \tilde{\sigma}_{13} \quad \tilde{\sigma}_{33} \quad \lambda\tilde{\phi} \quad \tilde{B}_3 \right\}^{\mathrm{T}} \tag{6.191}$$

$$\mathbf{A}^e = \begin{bmatrix} 0 & 1 & 0 & 0 & \overline{s}_{44}^e & 0 & \overline{d}_{15}^e & 0 \\ -n_{11}^e & 0 & n_{13}^e & 0 & 0 & n_{33}^e & 0 & 0 \\ 0 & 0 & 0 & 0 & \overline{d}_{15}^e & 0 & \overline{\kappa}_{11}^e & 0 \\ 0 & 0 & 0 & 0 & 0 & 0 & 0 & f_{33}^e \\ -f_{11}^e & 0 & f_{12}^e & 0 & 0 & -f_{11}^e\overline{s}_{13}^e - f_{12}^e\overline{d}_{33}^e & 0 & 0 \\ 0 & 0 & 0 & 0 & 1 & 0 & 0 & 0 \\ -f_{21}^e & 0 & f_{22}^e & 0 & 0 & -f_{21}^e\overline{s}_{13}^e - f_{22}^e\overline{d}_{33}^e & 0 & 0 \\ 0 & 0 & 0 & \overline{\mu}_{11}^e & 0 & 0 & 0 & 0 \end{bmatrix} \tag{6.192}$$

$$\mathbf{A}^m = \begin{bmatrix} 0 & 1 & 0 & \overline{g}_{15}^m & \overline{s}_{44}^m & 0 & 0 & 0 \\ -n_{11}^m & 0 & 0 & 0 & 0 & n_{33}^m & 0 & n_{13}^m \\ 0 & 0 & 0 & 0 & 0 & 0 & \overline{\kappa}_{11}^m & 0 \\ -f_{31}^m & 0 & 0 & 0 & 0 & -f_{31}^m\overline{s}_{13}^m - f_{33}^m\overline{g}_{33}^m & 0 & f_{33}^m \\ -f_{11}^m & 0 & 0 & 0 & 0 & -f_{11}^m\overline{s}_{13}^m - f_{13}^m\overline{g}_{33}^m & 0 & f_{13}^m \\ 0 & 0 & 0 & 0 & 1 & 0 & 0 & 0 \\ 0 & 0 & f_{22}^m & 0 & 0 & 0 & 0 & 0 \\ 0 & 0 & 0 & \overline{\mu}_{11}^m & \overline{g}_{15}^m & 0 & 0 & 0 \end{bmatrix} \tag{6.193}$$

Case 4: Electrically shorted and magnetically open:

$$\sigma_{13}^e = \sigma_{33}^e = 0, \quad \phi^e = 0, \quad \psi^e = 0 \qquad (\text{on } x_3 = \pm h) \tag{6.194}$$

In this case, the state space variable defined in Eq. (6.183) and the corresponding efficient matrices $\mathbf{A}^e$ and $\mathbf{A}^m$ become

$$\mathbf{U} = \left\{ \lambda\tilde{u} \quad \lambda\tilde{w} \quad \tilde{D}_3 \quad \tilde{B}_3 \right\}^{\mathrm{T}}, \qquad \mathbf{S} = \left\{ \tilde{\sigma}_{13} \quad \tilde{\sigma}_{33} \quad \lambda\tilde{\phi} \quad \lambda\tilde{\psi} \right\}^{\mathrm{T}} \tag{6.195}$$

$$\mathbf{A}^e = \begin{bmatrix} 0 & 1 & 0 & 0 & \overline{s}_{44}^e & 0 & \overline{d}_{15}^e & 0 \\ -n_{11}^e & 0 & n_{13}^e & 0 & 0 & n_{33}^e & 0 & 0 \\ & 0 & 0 & 0 & \overline{d}_{15}^e & 0 & \overline{\kappa}_{11}^e & 0 \\ 0 & 0 & 0 & 0 & 0 & 0 & 0 & \overline{\mu}_{11}^e \\ -f_{11}^e & 0 & f_{12}^e & 0 & 0 & -f_{11}^e\overline{s}_{13}^e - f_{12}^e\overline{d}_{33}^e & 0 & 0 \\ 0 & 0 & 0 & 0 & 1 & 0 & 0 & 0 \\ -f_{21}^e & 0 & f_{22}^e & 0 & 0 & -f_{21}^e\overline{s}_{13}^e - f_{22}^e\overline{d}_{33}^e & 0 & 0 \\ 0 & 0 & 0 & f_{33}^e & 0 & 0 & 0 & 0 \end{bmatrix} \tag{6.196}$$

$$\mathbf{A}^m = \begin{bmatrix} 0 & 1 & 0 & 0 & \overline{s}_{44}^m & 0 & 0 & \overline{g}_{15}^m \\ -n_{11}^m & 0 & 0 & n_{13}^m & 0 & n_{33}^m & 0 & 0 \\ 0 & 0 & 0 & 0 & 0 & 0 & \overline{\kappa}_{11}^m & 0 \\ 0 & 0 & 0 & 0 & \overline{g}_{15}^m & 0 & 0 & \overline{\mu}_{11}^m \\ -f_{11}^m & 0 & 0 & f_{13}^m & 0 & -f_{11}^m\overline{s}_{13}^m - f_{13}^m\overline{g}_{33}^m & 0 & 0 \\ 0 & 0 & 0 & 0 & 1 & 0 & 0 & 0 \\ 0 & 0 & f_{22}^m & 0 & 0 & 0 & 0 & 0 \\ -f_{31}^m & 0 & 0 & f_{33}^m & 0 & -f_{31}^m\overline{s}_{13}^m - f_{33}^m\overline{g}_{33}^m & 0 & 0 \end{bmatrix} \tag{6.197}$$

For the PM-PE-PM sandwich structures, the relevant characteristic equations

can be obtained similarly.

References

[1] Saint-Venant AJCB: Memoire sur la Torsion des Prismes. Mem. Divers Savants **14**, 233-560 (1855).

[2] Qin QH, Wang JS: Hamiltonian system for analyzing Saint-Venant end effects of piezoelectric strips. Journal of Mechanics and MEMS **1**(1), 59-71 (2009).

[3] Tarn JQ, Huang LJ: Saint-Venant end effects in multilayered piezoelectric laminates. International Journal of Solids and Structures **39**(19), 4979-4998 (2002).

[4] Xue Y, Liu J: Decay rate of Saint-Venant end effects for plane deformations of piezoelectric-piezomagnetic sandwich structures. Acta Mechanica Solida Sinica **23**(5), 407-419 (2010).

[5] He XQ, Wang JS, Qin QH: Saint-Venant decay analysis of FGPM laminates and dissimilar piezoelectric laminates. Mechanics of Materials **39**(12), 1053-1065 (2007).

[6] Love AEH: A Treatise on the Mathematical Theory of Elasticity. Cambridge University Press, Cambridge (1927).

[7] Horgan CO: Recent developments concerning Saint-Venant's principle: an update. Applied Mechanics Reviews **42**, 295-303 (1989).

[8] Horgan CO: Recent developments concerning Saint-Venant's principle: a second update. Applied Mechanics Reviews **49**, s101-s111 (1996).

[9] Batra RC, Yang JS: Saint-Venants principle in linear piezoelectricity. Journal of Elasticity **38**(2), 209-218 (1995).

[10] Batra RC, Zhong X: Saint-Venant's principle for a helical piezoelectric body. Journal of Elasticity **43**(1), 69-79 (1996).

[11] Fan H: Decay-rates in a piezoelectric strip. International Journal of Engineering Science **33**(8), 1095-1103 (1995).

[12] Ruan XP, Danforth SC, Safari A, Chou TW: Saint-Venant end effects in piezoceramic materials. International Journal of Solids and Structures **37**(19), 2625-2637 (2000).

[13] Borrelli A, Horgan CO, Patria MC: Exponential decay of end effects in anti-plane shear for functionally graded piezoelectric materials. Proceedings of the Royal Society of London Series A-Mathematical Physical and Engineering Sciences **460**(2044), 1193-1212 (2004).

[14] Borrelli A, Horgan CO, Patria MC: Saint-Venant end effects for plane deformations of linear piezoelectric solids. International Journal of Solids and Structures **43**(5), 943-956 (2006).

[15] Bisegna P: The Saint-Venant problem for monoclinic piezoelectric cylinders. Zeitschrift Fur Angewandte Mathematik Und Mechanik **78**(3), 147-165 (1998).

[16] Rovenski V, Harash E, Abramovich H: Saint-Venant's problem for homogeneous piezoelectric beams. Journal of Applied Mechanics-Transactions of the ASME **74**(6),

1095-1103 (2007).

[17] Vidoli S, Batra RC, dell'Isola F: Saint-Venant's problem for a second-order piezoelectric prismatic bar. International Journal of Engineering Science **38**(1), 21-45 (2000).

[18] Zhong WX, Williams FW: Physical interpretation of the symplectic orthogonality of the eigensolutions of a Hamiltonian or symplectic matrix. Computers and Structures **49**, 749-750 (1993).

[19] Yao WA, Zhong WX, Lim CW: Symplectic Elasticity. World Scientific Publishing, Singapore (2009).

[20] Borrelli A, Horgan CO, Patria MC: Saint-Venant principle for anti-plane shear deformations of linear piezoelectric materials. SIAM Journal on Applied Mathematics **62**, 2027-2044 (2003).

[21] Wang JS, Qin QH: Symplectic model for piezoelectric wedges and its application in analysis of electroelastic singularities. Philosophical Magazine **87**(2), 225-251 (2007).

Chapter 7 Penny-Shaped Cracks

This chapter applies the formulation presented in the first two chapters to a range of piezoelectric problems containing penny-shaped cracks. It includes a penny-shaped crack in an infinite piezoelectric plate, a piezoelectric strip, a fiber embedded in a matrix, a piezoelectric cylinder with elastic coating, and the fundamental solution for penny-shaped crack problems.

7.1 Introduction

Over recent years, significant efforts have been made to study fracture behavior of piezoelectric materials in the presence of cracks [1-3]. Among various crack problems, a penny-shaped crack in a piezoelectric cylinder is most popular and is the subject of many reports in the literature [4-10]. Using the Fourier and Hankel transforms, Narita et al. [4] obtained the stress intensity factor, the total energy release rate, and the mechanical strain energy release rate for a penny-shaped crack in a piezoceramic cylinder under mode Ⅰ loading. Yang and Lee [5], using the potential function approach and Hankel transform, and Lin et al. [6], using Fourier and Hankel transforms, investigated a piezoelectric cylinder with a penny-shaped crack embedded in an infinite matrix. The field intensity factors (FIFs) for different loading cases were respectively analyzed in [7-10], and the energy release rate (ERR) was derived by Eriksson [11]. Yang and Lee [12] investigated the problems of a penny-shaped crack in a piezoelectric cylinder and in a piezoelectric cylinder surrounded by an elastic medium. Wang et al. [13] analyzed the problem of a penny-shaped crack in a piezoelectric medium of finite thickness. Li and Lee [14] investigated the effects of electrical load on crack growth of penny-shaped dielectric cracks in a piezoelectric layer. Feng et al. [15] considered the dynamic fracture behavior of a penny-shaped crack in a piezoelectric layer.

The penny-shaped crack problem can be treated as a limiting case of a spheroidal crack, or directly as a crack with flat surfaces. The spheroidal problem is a piezoelectric analog of Eshelby's elastic problem [16]. That approach was taken by Wang [17], Kogan et al. [7], Huang [18], and Chiang and Weng [19]. The electroelastic analysis of a penny-shaped crack in a piezoelectric material is of practical importance, since it represents an idealization of internal flaws that are inherent in many piezoelectric materials [20]. The fracture behavior of a penny-shaped crack embedded in an infinite piezoelectric material was first studied by Kudryavtsev et al. [21], who gave a special solution of the stresses and displacement fields. Wang [17], using the Fourier transform method, presented the expressions of the crack opening displacement, interaction and the stress intensity factors. Chen et al. [22] presented a three-dimensional (3-D) closed-form solution for a penny-shaped crack in 3-D piezoelectric ceramic subjected to normal mechanical loading and electrical charges

on crack faces. Chen and Shioya [9] performed an exact analysis of a penny-shaped crack in a 3-D piezoelectric ceramic under shear loading over the crack faces. Huang [18], utilizing the eigenstrain formulation and Cauchy's residue theorem, presented a unified explicit expression for the electroelastic fields inside a flat ellipsoidal crack. Wang et al. [13] developed a model to treat a penny-shaped crack in a finite piezoelectric layer subjected to axially symmetric loading. Kogan et al. [7] derived explicit expressions for the stress intensity factors of a penny-shaped crack in a piezoelectric material under various remote loading conditions. However, most of the work has not considered the contribution of electrostatic energy to the crack driving force, and none of the work has provided complete solutions to the fracture mechanics of a penny-shaped crack in an infinite piezoelectric material when subjected to axisymmetric loading. Lin et al. [20] extended the same approach to analyze the electroelastic interaction of a penny-shaped crack in a piezoelectric ceramic under mode Ⅰ loading, but they did not explicitly give a closed-form solution of the crack driving force as a function of the electrostatic energy. Qin et al. [23] presented a solution for a penny-shaped crack in a piezoelectric cylinder with elastic coating. In this chapter we focus on the development presented in [6,13,20,23-25].

7.2 An infinite piezoelectric material with a penny-shaped crack

All formulations in this section are taken from the work of Lin et al. [20]. In their paper, they consider an infinite piezoelectric ceramic containing a penny-shaped crack of radius a under axisymmetric electromechanical loads (Fig. 7.1). For convenience, a cylindrical coordinate system (r,θ,z) originating at the center of the crack is used, with the *z*-axis perpendicular to the crack plane. The piezoelectric material is assumed to be transversely isotropic with the poling direction parallel to the *z*-axis and hexagonal symmetry. It is subjected to the far-field of a normal stress, $\sigma_z = \sigma_\infty$ and a uniform electric displacement $D_z = D_\infty$.

The constitutive equations for piezoelectric materials which are transversely isotropic and poled along the *z*-axis can be written as [26]

$$\sigma_{\theta\theta} = c_{12}u_{r,r} + c_{11}\frac{u_r}{r} + c_{13}u_{z,z} + e_{31}\phi_{,z} \tag{7.1}$$

$$\sigma_{zz} = c_{13}u_{r,r} + c_{13}\frac{u_r}{r} + c_{33}u_{z,z} + e_{33}\phi_{,z} \tag{7.2}$$

$$\sigma_{rr} = c_{11}u_{r,r} + c_{12}\frac{u_r}{r} + c_{13}u_{z,z} + e_{31}\phi_{,z} \tag{7.3}$$

$$\sigma_{rz} = c_{55}(u_{z,r} + u_{r,z}) + e_{15}\phi_{,r} \tag{7.4}$$

$$D_r = e_{15}(u_{z,r} + u_{r,z}) - \kappa_{11}\phi_{,r} \tag{7.5}$$

$$D_z = e_{31}\left(u_{r,r} + \frac{u_r}{r}\right) + e_{33}u_{z,z} - \kappa_{33}\phi_{,z} \tag{7.6}$$

The governing equations can then be expressed in terms of displacements and electric potential as

$$c_{11}\left(u_{r,rr} + \frac{u_{r,r}}{r} - \frac{u_r}{r^2}\right) + c_{55}u_{r,zz} + (c_{13} + c_{44})u_{z,rz} + (e_{31} + e_{15})\phi_{,rz} = 0 \tag{7.7}$$

$$(c_{13} + c_{55})\left(u_{r,rz} + \frac{u_{r,z}}{r}\right) + c_{33}u_{z,zz} + c_{55}\left(u_{z,rr} + \frac{u_{z,r}}{r}\right) + e_{15}\left(\phi_{,rr} + \frac{\phi_{,r}}{r}\right) + e_{33}\phi_{,zz} = 0 \tag{7.8}$$

$$(e_{31} + e_{15})\left(u_{r,rz} + \frac{u_{r,z}}{r}\right) + e_{15}\left(u_{z,rr} + \frac{u_{z,r}}{r}\right) + e_{33}u_{z,zz} - \kappa_{11}\left(\phi_{,rr} + \frac{\phi_{,r}}{r}\right) - \kappa_{33}\phi_{,zz} = 0 \tag{7.9}$$

The electric field components may be written in terms of an electric potential $\phi(r,z)$ as

$$E_r = -\phi_{,r}, \quad E_z = -\phi_{,z} \tag{7.10}$$

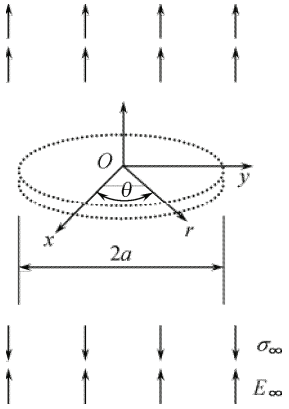

Fig. 7.1 A penny-shaped crack embedded in an infinite piezoelectric material.

In a vacuum, the constitutive equations (7.5) and (7.6) and the governing equation (7.9) become

$$D_r = \kappa_0 E_r, \quad D_z = \kappa_0 E_z \tag{7.11}$$

$$\phi_{,rr} + \frac{\phi_{,r}}{r} + \phi_{,zz} = 0 \tag{7.12}$$

The problem of determining the distribution of stress and electric displacement in the vicinity of the crack is then equivalent to that of finding the distribution of stress and electric displacement in the semi-infinite piezoelectric material $z \geqslant 0$, $0 \leqslant r \leqslant \infty$, subjected to the following boundary conditions:

$$\begin{aligned} &\sigma_{zr}(r,0) = 0 \quad (0 \leqslant r < \infty), \qquad \sigma_{zz}(r,0) = 0 \quad (0 \leqslant r < a), \\ &u_z(r,0) = 0 \quad (a \leqslant r < \infty) \end{aligned} \tag{7.13}$$

$$\begin{aligned} &E_r(r,0) = E_r^c(r,0), \quad D_z(r,0) = D_z^c(r,0) \qquad (0 \leqslant r < a), \\ &\phi(r,0) = 0 \quad (a \leqslant r < \infty) \end{aligned} \tag{7.14}$$

$$\sigma_{zz}(r,z) = \sigma_\infty, \quad E_z(r,z) = E_\infty \qquad (z \to \infty) \tag{7.15}$$

where E_r^c and D_z^c are respectively the electric field and electric displacement in the void inside the crack. The far-field normal stress can be expressed in terms of E_∞ as

$$\sigma_\infty = \sigma_0 - \frac{(c_{11}+c_{12})e_{33} - 2c_{13}e_{31}}{c_{11}+c_{12}} E_\infty \tag{7.16}$$

where σ_0 is a uniform normal stress for a closed-circuit condition with the potential forced to remain zero.

The solution to the boundary value problem stated above is as follows [20]:

Assume that the solutions u_r, u_z and ϕ are of the form

$$u_r(r,z) = \frac{2}{\pi}\sum_{j=1}^{3}\int_0^\infty a_j A_j(\alpha)\exp(-\mu_j \alpha z) J_1(\alpha r)\mathrm{d}\alpha + a_\infty r \tag{7.17}$$

$$u_z(r,z) = \frac{2}{\pi}\sum_{j=1}^{3}\int_0^\infty \frac{1}{\mu_j} A_j(\alpha)\exp(-\mu_j \alpha z) J_0(\alpha r)\mathrm{d}\alpha + b_\infty z \tag{7.18}$$

$$\phi(r,z) = -\frac{2}{\pi}\sum_{j=1}^{3}\int_0^\infty \frac{b_j}{\mu_j} A_j(\alpha)\exp(-\mu_j \alpha z) J_0(\alpha r)\mathrm{d}\alpha - c_\infty z \tag{7.19}$$

where $A_j(\alpha)$ $(j=1,2,3)$ are the unknowns to be solved, μ_j $(j=1,2,3)$ are the roots of the characteristic equation (2.8), and $J_0(\ )$ and $J_1(\ )$ are the zero and first order Bessel functions of the first kind, respectively. The real constants a_∞, b_∞, and c_∞ can be obtained by applying far-field loading conditions as

$$\begin{aligned} a_\infty &= \frac{c_{13}\sigma_\infty + (c_{13}e_{33} - c_{33}e_{31})E_\infty}{2c_{13}^2 - c_{33}(c_{11}+c_{12})}, \\ b_\infty &= \frac{-(c_{11}+c_{12})\sigma_\infty + [2c_{13}e_{31} - (c_{11}+c_{12})e_{33}]E_\infty}{2c_{13}^2 - c_{33}(c_{11}+c_{12})}, \\ c_\infty &= E_\infty \end{aligned} \tag{7.20}$$

The constants a_j and b_j are

$$\begin{aligned} a_j &= \frac{(e_{31}+e_{15})(c_{33}\mu_j^2-c_{55})-(c_{13}+c_{55})(e_{33}\mu_j^2-e_{15})}{(c_{55}\mu_j^2-c_{11})(e_{33}\mu_j^2-e_{15})+(c_{13}+c_{55})(e_{31}+e_{15})\mu_j^2}, \\ b_j &= \frac{(c_{55}\mu_j^2-c_{11})a_j+(c_{13}+c_{55})}{e_{31}+e_{15}} \end{aligned} \tag{7.21}$$

To determine the coefficients A_j, applying the Fourier transform to Eq. (7.12), we have

$$\phi^c = \frac{2}{\pi}\int_0^\infty C(\alpha)\sinh(\alpha z)J_0(\alpha r)\mathrm{d}\alpha \qquad (0 \leqslant r < a) \tag{7.22}$$

where the superscript "c"stands for the variable associated with the void inside the crack, and $C(\alpha)$ is unknown. Thus, the boundary conditions $(7.13)_1$ and (7.14) yield the following relations between unknown functions:

$$\begin{aligned} &\frac{f_1}{\mu_1}A_1(\alpha)+\frac{f_2}{\mu_2}A_2(\alpha)+\frac{f_3}{\mu_3}A_3(\alpha)=0, \\ &\frac{b_1}{\mu_1}A_1(\alpha)+\frac{b_2}{\mu_2}A_2(\alpha)+\frac{b_3}{\mu_3}A_3(\alpha)=0 \end{aligned} \tag{7.23}$$

where

$$f_j = c_{55}(a_j\mu_j^2+1)-e_{15}b_j \qquad (j=1,2,3) \tag{7.24}$$

Making use of the mixed boundary conditions $(7.13)_{2,3}$, we have

$$\begin{aligned} &\int_0^\infty \alpha F D(\alpha)J_0(\alpha r)\mathrm{d}\alpha = -\frac{\pi}{2}\sigma_\infty \qquad (0 \leqslant r < a), \\ &\int_0^\infty D(\alpha)J_0(\alpha r)\mathrm{d}\alpha = 0 \qquad\qquad\quad (a \leqslant r < \infty) \end{aligned} \tag{7.25}$$

where

$$\begin{aligned} &D(\alpha)=\frac{A_1(\alpha)}{d_1}=\frac{A_2(\alpha)}{d_2}=\frac{A_3(\alpha)}{d_3}, \quad F=\sum_{j=1}^{3}g_j d_j, \\ &d_1=\mu_1(b_2f_3-b_3f_2), \quad d_2=\mu_2(b_3f_1-b_1f_3), \quad d_3=\mu_3(b_1f_2-b_2f_1), \\ &g_j=c_{13}a_j-c_{33}+e_{33}b_j \qquad (j=1,2,3) \end{aligned} \tag{7.26}$$

It is noted from Eq. (7.26) that $D(\alpha)$ is the only unknown in Eq. (7.25). The set of dual integral (7.25) may be obtained by using a new function $\Psi(\xi)$ defined by

$$D(\alpha) = -\frac{a^2\sigma_\infty}{F}\int_0^1 \Psi(\xi)\sin(a\alpha\xi)\mathrm{d}\xi \tag{7.27}$$

Having satisfied Eq. (7.25) for $a \leqslant r < \infty$, the remaining condition for $0 \leqslant r < a$ leads to an Able integral equation for $\Psi(\xi)$. The solution for $\Psi(\xi)$ is expressed by

$$\Psi(\xi) = \xi \tag{7.28}$$

The displacements and electric potential near the crack border are then obtained as

$$\begin{aligned}
u_r &= \frac{K_{\mathrm{I}}\sqrt{r_1}}{F}\sum_{j=1}^{3} a_j d_j \left\{\left(\cos^2\theta_1 + \mu_j^2 \sin^2\theta_1\right)^{1/2} + \cos\theta_1\right\}^{1/2}, \\
u_z &= -\frac{K_{\mathrm{I}}\sqrt{r_1}}{F}\sum_{j=1}^{3} \frac{d_j}{\mu_j} \left\{\left(\cos^2\theta_1 + \mu_j^2 \sin^2\theta_1\right)^{1/2} - \cos\theta_1\right\}^{1/2}, \\
\phi &= \frac{K_{\mathrm{I}}\sqrt{r_1}}{F}\sum_{j=1}^{3} \frac{b_j d_j}{\mu_j} \left\{\left(\cos^2\theta_1 + \mu_j^2 \sin^2\theta_1\right)^{1/2} - \cos\theta_1\right\}^{1/2}
\end{aligned} \tag{7.29}$$

where the polar coordinates r_1 and θ_1 are defined as

$$r_1 = \left\{(r-a)^2 + z^2\right\}^{1/2}, \quad \theta_1 = \tan^{-1}\left(\frac{z}{r-a}\right) \tag{7.30}$$

Substituting Eq. (7.29) into the constitutive equations (7.1)-(7.6), we obtain the singular parts of the stress and electric displacements in the neighborhood of the crack border as

$$\begin{aligned}
&\sigma_{rr} = \frac{K_{\mathrm{I}}}{2F\sqrt{r_1}}\sum_{j=1}^{3} m_j d_j R_j^c(\theta_1), \quad \sigma_{zz} = \frac{K_{\mathrm{I}}}{2F\sqrt{r_1}}\sum_{j=1}^{3} g_j d_j R_j^c(\theta_1), \\
&\sigma_{zr} = -\frac{K_{\mathrm{I}}}{2F\sqrt{r_1}}\sum_{j=1}^{3} \frac{f_j d_j}{\mu_j} R_j^s(\theta_1)
\end{aligned} \tag{7.31}$$

$$D_r = -\frac{K_{\mathrm{I}}}{2F\sqrt{r_1}}\sum_{j=1}^{3} \frac{n_j d_j}{\mu_j} R_j^s(\theta_1), \quad D_z = \frac{K_{\mathrm{I}}}{2F\sqrt{r_1}}\sum_{j=1}^{3} h_j d_j R_j^c(\theta_1) \tag{7.32}$$

where

$$\begin{aligned}
h_j &= e_{31}a_j + e_{33} - \kappa_{33}b_j, \\
m_j &= c_{11}a_j - c_{13} + e_{31}b_j, \qquad (j = 1,2,3) \\
n_j &= e_{15}(\mu_j^2 a_j + 1) + \kappa_{11}b_j
\end{aligned} \tag{7.33}$$

The stress intensity factor K_{I} for the crack model is obtained as

$$K_{\mathrm{I}} = \lim_{r \to a^+} \sigma_{zz}(r,0)\sqrt{2(r-a)} = \frac{2}{\pi}\sigma_\infty \sqrt{a} \tag{7.34}$$

The electric displacement intensity factor K_D is given by

$$K_D = \lim_{r\to a^+} D_z(r,0)\sqrt{2(r-a)} = \left(\frac{1}{F}\sum_{j=1}^{3} h_j d_j\right) K_{\mathrm{I}} \tag{7.35}$$

7.3 A penny-shaped crack in a piezoelectric strip

In this section we present a brief review of the results given in [13]. Consider a piezoelectric layer with a penny-shaped crack of radius a as shown in Fig. 7.2.

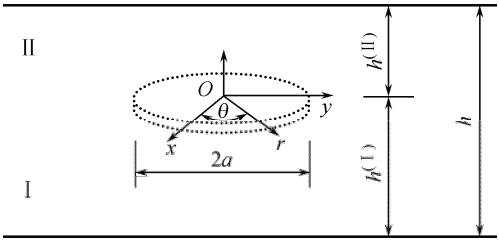

Fig. 7.2 A piezoelectric strip with a penny-shaped crack.

For the sake of convenience, Eqs. (7.17)-(7.19) are rewritten in the form

$$\mathbf{U} = \int_0^\infty F(\alpha)((A_1 J_1(\alpha r),\ A_3 J_0(\alpha r), A_4 J_0(\alpha r)) e^{\mu\alpha z}\mathrm{d}\alpha \tag{7.36}$$

where $\mathbf{U}=\{u_r,\ u_z,\ \phi\}^{\mathrm{T}}$, $F(\alpha)$ is an unknown function to be determined, μ and A_j are eigenvalue and eigenvector respectively of Eq. (2.6) which is rewritten as follows:

$$\begin{bmatrix} c_{11}-c_{55}\mu^2 & (c_{13}+c_{55})\mu & (e_{31}+e_{15})\mu \\ (c_{13}+c_{55})\mu & c_{33}\mu^2-c_{55} & e_{33}\mu^2-e_{15} \\ (e_{31}+e_{15})\mu & e_{33}\mu^2-e_{15} & \kappa_{11}-\kappa_{33}\mu^2 \end{bmatrix} \begin{Bmatrix} A_1 \\ A_3 \\ A_4 \end{Bmatrix} = 0 \tag{7.37}$$

In terms of these eigenvalues and eigenvectors, a general expression for the displacements and electric potential can be written as

$$\mathbf{U} = \int_0^\infty [G(\alpha r)][A(z)]\{F\}\mathrm{d}\alpha \tag{7.38}$$

where

$$[G(\alpha r)] = \mathrm{diag}[J_1(\alpha r),\ J_1(\alpha r),\ J_1(\alpha r)], \quad [A(z)] = \begin{bmatrix} A_{k\beta} e^{\alpha\mu_\beta z} \\ A_{4\beta} e^{\alpha\mu_\beta z} \end{bmatrix}, \tag{7.39}$$
$$[F] = \{F_\beta\}^{\mathrm{T}} \qquad (k=1,3; \qquad \beta = 1,2,3,4,5,6)$$

Substituting Eq. (7.38) into the constitutive equations (7.2), (7.4), and (7.6) yields

$$\{T(r,z)\}=\begin{Bmatrix}\sigma_{rz}\\ \sigma_{zz}\\ D_z\end{Bmatrix}=\int_0^\infty \alpha[G(\alpha r)][B]\{F\}\mathrm{d}\alpha \tag{7.40}$$

where

$$\begin{aligned}
B_{1\beta}(z)&=(c_{55}\mu_\beta A_{1\beta}-c_{55}A_{3\beta}-e_{15}A_{4\beta})e^{\alpha\mu_\beta z},\\
B_{2\beta}(z)&=(c_{13}A_{1\beta}+c_{33}\mu_\beta A_{3\beta}+e_{33}\mu_\beta A_{4\beta})e^{\alpha\mu_\beta z},\\
B_{3\beta}(z)&=(e_{31}A_{1\beta}+e_{33}\mu_\beta A_{3\beta}-\kappa_{33}\mu_\beta A_{4\beta})e^{\alpha\mu_\beta z}
\end{aligned} \tag{7.41}$$

Noting that superscripts "(Ⅰ)"and "(Ⅱ)"represent the related variables associated with the materials occupying the lower and upper parts (see Fig. 7.2) and assuming that $\{t^{(0)}(r)\}$ represents $\{T^{(\mathrm{I})}(r,z^{(\mathrm{I})}=0)\}$ or $\{T^{(\mathrm{II})}(r,z^{(\mathrm{II})}=0)\}$, the boundary conditions can be rewritten as

$$\begin{aligned}
\{T^{(\mathrm{I})}(r,z=-h^{(\mathrm{I})})\}&=\{t^{(\mathrm{I})}(r)\},\\
\{T^{(\mathrm{II})}(r,z=h^{(\mathrm{II})})\}&=\{t^{(\mathrm{II})}(r)\}
\end{aligned} \tag{7.42}$$

The mixed boundary conditions along the crack line are

$$\begin{aligned}
&\{t(r)\}=\{t^{(0)}(r)\}\qquad (r<a),\\
&\{U^{(\mathrm{I})}(r,z=0)\}=\{U^{(\mathrm{II})}(r,z=0)\}\qquad (r\geqslant a)
\end{aligned} \tag{7.43}$$

The unknown vector $\{F\}$ can be expressed in terms of $\{t^{(i)}(r)\}$, (i=0, Ⅰ, Ⅱ) by utilizing the inverse Hankel transform to Eq. (7.40) as

$$\{F^{(\mathrm{I})}\}=\left[C^{(\mathrm{I})}\right]\begin{Bmatrix}\Gamma^{(0)}(\alpha)\\ \Gamma^{(\mathrm{I})}(\alpha)\end{Bmatrix},\qquad \{F^{(\mathrm{II})}\}=\left[C^{(\mathrm{II})}\right]\begin{Bmatrix}\Gamma^{(\mathrm{II})}(\alpha)\\ \Gamma^{(0)}(\alpha)\end{Bmatrix} \tag{7.44}$$

where $\Gamma^{(i)}(\alpha)$, $(i=0,\mathrm{I},\mathrm{II})$ is the Hankel transform of $\{t^{(i)}(r)\}$, and

$$\{C^{(\mathrm{I})}\}=\begin{bmatrix}B(0)\\ B(-h^{(\mathrm{I})})\end{bmatrix}^{-1},\qquad \{C^{(\mathrm{II})}\}=\begin{bmatrix}B(h^{(\mathrm{II})})\\ B(0)\end{bmatrix}^{-1} \tag{7.45}$$

Substituting Eq. (7.44) into Eq. (7.38), we obtain

$$\begin{aligned}
\{U^{(\mathrm{I})}\}&=\int_0^\infty [G(\alpha r)[D_1^{(\mathrm{I})}\ D_2^{(\mathrm{I})}]\begin{Bmatrix}\Gamma^{(0)}(\alpha)\\ \Gamma^{(\mathrm{I})}(\alpha)\end{Bmatrix}\mathrm{d}\alpha,\\
\{U^{(\mathrm{II})}\}&=\int_0^\infty [G(\alpha r)[D_1^{(\mathrm{II})}\ D_2^{(\mathrm{II})}]\begin{Bmatrix}\Gamma^{(\mathrm{II})}(\alpha)\\ \Gamma^{(0)}(\alpha)\end{Bmatrix}\mathrm{d}\alpha
\end{aligned} \tag{7.46}$$

where

$$[D_1^{(\mathrm{I})}\ D_2^{(\mathrm{I})}]=[A^{(\mathrm{I})}(y)][C^{(\mathrm{I})}],\qquad [D_1^{(\mathrm{II})}\ D_2^{(\mathrm{II})}]=[A^{(\mathrm{II})}(y)][C^{(\mathrm{II})}] \tag{7.47}$$

are two 4×4 matrices.

Making use of the continuity condition (7.43), we have

$$\int_0^\infty [G(\alpha r)]([L]\{\Gamma^{(\mathrm{I})}\}+[M]\{\Gamma^{(0)}\}+[N]\{\Gamma^{(\mathrm{II})}\})\mathrm{d}\alpha=0 \qquad (r\geqslant a) \tag{7.48}$$

where

$$[L(\alpha)]=[D_2^{(\mathrm{I})}(0)],\ \ [M(\alpha)]=[D_1^{(\mathrm{I})}(0)]-[D_2^{(\mathrm{II})}(0)],\ \ [N(\alpha)]=-[D_1^{(\mathrm{II})}(0)] \tag{7.49}$$

From Eq. (7.47), the solution of $\Gamma(\alpha)$ can be expressed in terms of an unknown vector $\{d(r)\}=\{d_{u_r}(r),d_{u_z}(r),d_\phi(r)\}^{\mathrm{T}}$ as

$$[M]\{\Gamma^{(0)}\}=-[L]\{\Gamma^{(\mathrm{I})}\}-[N]\{\Gamma^{(\mathrm{II})}\}+\alpha^{1/2}\int_0^a\begin{Bmatrix}d_{u_r}J_{3/2}(\alpha r)\\ d_{u_z}J_{1/2}(\alpha r)\\ d_\phi J_{1/2}(\alpha r)\end{Bmatrix}\mathrm{d}r \tag{7.50}$$

Define $[K(\alpha)]=[M(\alpha)]^{-1}-[M(\infty)]^{-1}$, then it follows from Eq. (7.50) that

$$\{\Gamma^{(0)}\}=-\{\Gamma_b(\alpha)\}+([M(\infty)]^{-1}+[K(\alpha)])\alpha^{1/2}\int_0^a\begin{Bmatrix}d_{u_r}(x)J_{3/2}(\alpha x)\\ d_{u_z}(x)J_{1/2}(\alpha x)\\ d_\phi(x)J_{1/2}(\alpha x)\end{Bmatrix}\mathrm{d}x \tag{7.51}$$

where

$$[\Gamma_b(\alpha)]=[M(\alpha)]^{-1}[L]\{\Gamma^{(\mathrm{I})}(\alpha)\}+[M(\infty)]^{-1}[N]\{\Gamma^{(\mathrm{II})}(\alpha)\} \tag{7.52}$$

The solution of $\{d(r)\}$ can be obtained by substituting the crack surface condition (7.43) into Eq. (7.51):

$$[M(\infty)]^{-1}\int_0^\infty\left(\alpha^{3/2}[G(\alpha r)]\quad\int_0^a\begin{Bmatrix}d_{u_r}(x)J_{3/2}(\alpha x)\\ d_{u_z}(x)J_{1/2}(\alpha x)\\ d_\phi(x)J_{1/2}(\alpha x)\end{Bmatrix}\mathrm{d}x\right)\mathrm{d}\alpha$$

$$+\int_0^\infty\left(\alpha^{3/2}[G(\alpha r)][K(\alpha)]\int_0^a\begin{Bmatrix}d_{u_r}(x)J_{3/2}(\alpha x)\\ d_{u_z}(x)J_{1/2}(\alpha x)\\ d_\phi(x)J_{1/2}(\alpha x)\end{Bmatrix}\mathrm{d}x\right)\mathrm{d}\alpha=\sigma_b(r)\qquad (r<a) \tag{7.53}$$

where

$$\sigma_b(r) = \{t^{(0)}(r)\} + \int_0^\infty \alpha[G(\alpha r)]\{\Gamma_b(\alpha)\}\mathrm{d}\alpha \tag{7.54}$$

Equation (7.53) can be used for solving $\{d(r)\}$ numerically. Once $\{d\}$ is solved from Eq. (7.53), the stress and electric displacement intensity factors can be calculated using the following equation:

$$\{K\} = \sqrt{2(r-a)}\{t(r)\}_{r\to a^+} = -\sqrt{\frac{2a}{\pi}}[M(\infty)]^{-1}\{d(a)\} \tag{7.55}$$

The displacement and electric potential jumps between the upper and lower faces of the crack can be calculated from (7.46) and (7.50) as

$$\Delta\{U\} = \{U^{(\mathrm{II})}(r,0)\} - \{U^{(\mathrm{I})}(r,0)\} = -\int_0^a \int_0^\infty \alpha^{1/2}[G(\alpha r)]\begin{Bmatrix} d_{u_r} J_{3/2}(\alpha r) \\ d_{u_z} J_{1/2}(\alpha r) \\ d_\phi J_{1/2}(\alpha r) \end{Bmatrix} \mathrm{d}r\mathrm{d}\alpha \tag{7.56}$$

Integration of Eq. (7.56) with respect to α yields

$$\Delta\{U\} = -\sqrt{\frac{2}{\pi}}\int_r^a \begin{Bmatrix} d_{u_r}(x)\sqrt{r}/x \\ d_{u_z}(x)/\sqrt{x} \\ d_\phi(x)/\sqrt{x} \end{Bmatrix} \frac{1}{\sqrt{x^2 - r^2}}\mathrm{d}x \tag{7.57}$$

7.4 A fiber with a penny-shaped crack embedded in a matrix

This section focuses on problems of a piezoelectric cylindrical fiber with a penny-shaped crack embedded in a matrix. It is a brief summary of the development presented in [6]. Consider a piezoelectric fiber of infinite length with radius b, embedded in an elastic matrix having Young's modulus E and Poisson's ratio υ (see Fig. 7.3). The fiber contains a penny-shaped crack whose center is located at the origin of the fiber (Fig. 7.3), and is subjected to the normal stress, $\sigma_{zz} = \sigma_\infty$, and electric field, $E_z = E_\infty$ at infinity.

The constitutive and governing equations for both piezoelectric fiber and void inside the crack are given by Eqs. (7.1)-(7.12). The related field equations for an elastic matrix are

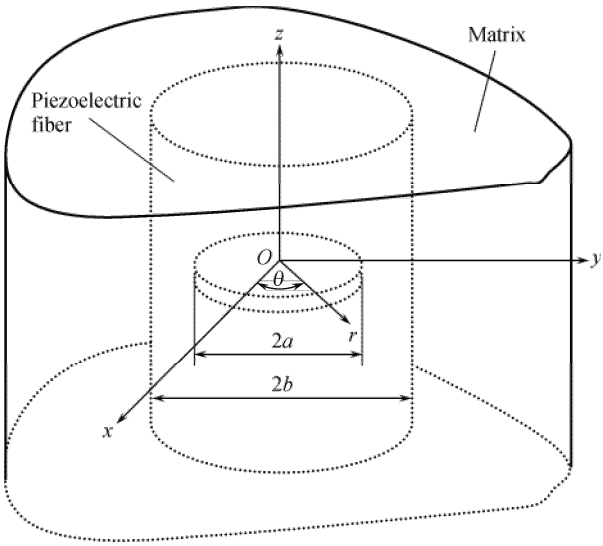

Fig. 7.3 A piezoelectric cylindrical fiber with a penny-shaped crack embedded in a matrix.

$$\sigma_{rr}^E=(2G+\lambda)u_{r,r}^E+\lambda\left(\frac{u_r^E}{r}+u_{z,z}^E\right),\quad \sigma_{\theta\theta}^E=\lambda u_{r,r}^E+(2G+\lambda)\frac{u_r^E}{r}+\lambda u_{z,z}^E,$$
$$\sigma_{zz}^E=\lambda\left(\frac{u_r^E}{r}+u_{r,r}^E\right)+(2G+\lambda)u_{z,z}^E,\quad \sigma_{rz}^E=G\left(u_{r,z}^E+u_{z,r}^E\right) \tag{7.58}$$

$$(2G+\lambda)\left(u_{r,rr}^E+\frac{u_{r,r}^E}{r}-\frac{u_r^E}{r^2}\right)+Gu_{r,zz}^E+(G+\lambda)u_{z,rz}^E=0,$$
$$(G+\lambda)\left(u_{r,rz}^E+\frac{u_{r,z}^E}{r}\right)+(2G+\lambda)u_{z,zz}^E+G\left(u_{z,rr}^E+\frac{u_{z,r}^E}{r}\right)=0 \tag{7.59}$$

where the superscript "E "represents the corresponding variable associated with the elastic matrix, the constant $2G=E/(1+\upsilon)$ is the modulus of rigidity, and $\lambda=2G\upsilon/(1-2\upsilon)$.

Due to the symmetry of the problem about the plane of z=0, we consider the semi-infinite region $z\geqslant 0,\ 0\leqslant r<\infty,\ 0\leqslant\theta\leqslant 2\pi$. The related boundary conditions can be expressed in the form

$$\begin{aligned}&\sigma_{zr}(r,0)=0\ \ (0\leqslant r<b),\quad \sigma_{zr}^E(r,0)=0\ \ (b\leqslant r<\infty),\\&\sigma_{zz}(r,0)=0\ \ (0\leqslant r<a),\ \ u_z(r,0)=0\ \ (a\leqslant r\leqslant b),\\&u_z^E(r,0)=0\ \ (b\leqslant r<\infty)\end{aligned} \tag{7.60}$$

$$\begin{aligned}&E_r(r,0)=E_r^c(r,0),\ \ D_z(r,0)=D_z^c(r,0)\qquad (0\leqslant r<a),\\&\phi(r,0)=0\ \ (a\leqslant r\leqslant b)\end{aligned} \tag{7.61}$$

$$\begin{aligned} &u_r(b,z)=u_r^E(b,z), \quad u_z(b,z)=u_z^E(b,z),\\ &\sigma_{rr}(b,z)=\sigma_{rr}^E(b,z), \quad \sigma_{rz}(b,z)=\sigma_{rz}^E(b,z),\\ &D_r(b,z)=0 \end{aligned} \tag{7.62}$$

$$\begin{aligned} &\sigma_{zz}(r,z)=\sigma_\infty, \quad E_z(r,z)=E_\infty \quad (0\leqslant r\leqslant b,\ z\to\infty),\\ &\sigma_{zz}^E(r,z)=\sigma_\infty^E \quad (b\leqslant r<\infty,\ z\to\infty) \end{aligned} \tag{7.63}$$

where

$$\begin{aligned} &\sigma_\infty=\sigma_0-e_2E_\infty, \quad \sigma_\infty^E=c_1\sigma_\infty+(c_1e_1-e_2)E_\infty,\\ &c_1=\frac{(2G+\lambda)[2(G+\lambda)-c_{11}-c_{12}]-2\lambda(\lambda-c_{13})}{c_{33}[2(G+\lambda)-c_{11}-c_{12}]-2c_{13}(\lambda-c_{13})},\\ &e_1=e_{33}+\frac{2c_{13}e_{31}}{2(G+\lambda)-c_{11}-c_{12}}, \quad e_2=\frac{2\lambda e_{31}}{2(G+\lambda)-c_{11}-c_{12}} \end{aligned} \tag{7.64}$$

Following the procedure described in Section 7.2, the solutions of u_r, u_z, ϕ, u_r^E, and u_z^E can be assumed in the form

$$\begin{aligned} u_r(r,z)=\frac{2}{\pi}\sum_{j=1}^{3}\int_0^\infty &[a_jA_j(\alpha)\exp(-\mu_j\alpha z)J_1(\alpha r)\\ &+a_j'B_j(\alpha)I_1(\mu_j'\alpha r)\cos(\alpha z)]\mathrm{d}\alpha+a_\infty r \end{aligned} \tag{7.65}$$

$$\begin{aligned} u_z(r,z)=\frac{2}{\pi}\sum_{j=1}^{3}\int_0^\infty &[\frac{1}{\mu_j}A_j(\alpha)\exp(-\mu_j\alpha z)J_0(\alpha r)\\ &+\frac{1}{\mu_j'}B_j(\alpha)I_0(\mu_j'\alpha r)\sin(\alpha z)]\mathrm{d}\alpha+b_\infty z \end{aligned} \tag{7.66}$$

$$\begin{aligned} \phi(r,z)=\frac{2}{\pi}\sum_{j=1}^{3}\int_0^\infty &[-\frac{b_j}{\mu_j}A_j(\alpha)\exp(-\mu_j\alpha z)J_0(\alpha r)\\ &+\frac{b_j'}{\mu_j'}B_j(\alpha)I_0(\mu_j'\alpha r)\sin(\alpha z)]\mathrm{d}\alpha-c_\infty z \end{aligned} \tag{7.67}$$

$$\begin{aligned} u_r^E(r,z)=\frac{2}{\pi}\int_0^\infty &\{-K_1(\alpha r)B_4(\alpha)+[4(1-\upsilon)K_2(\alpha r)\\ &+\alpha rK_0(\alpha r)]B_5(\alpha)\}\cos(\alpha z)\mathrm{d}\alpha+a_\infty b+d_\infty(r-b) \end{aligned} \tag{7.68}$$

$$u_z^E(r,z)=\frac{2}{\pi}\int_0^\infty[-K_0(\alpha r)B_4(\alpha)+\alpha rK_1(\alpha r)B_5(\alpha)]\sin(\alpha z)\mathrm{d}\alpha+e_\infty z \tag{7.69}$$

where A_j and B_j are the unknowns to be solved, $I_0(\ )$ and $I_1(\ )$ are the zero and first order modified Bessel functions of the first kind, and $K_0(\ )$, $K_1(\ )$, and $K_2(\ )$ are the zero, first and second order modified Bessel functions of the second kind, respec-

tively. The real constants $a_\infty, b_\infty, c_\infty, d_\infty$, and e_∞ are determined from far-field loading conditions. In the present problem, these constants are obtained as

$$\begin{aligned} a_\infty &= d_\infty = \frac{(c_{13}-\lambda)\sigma_\infty[(c_{13}-\lambda)e_{33}-c_{33}e_{31}]E_\infty}{2c_{13}(c_{13}-\lambda)-c_{33}(c_{11}+c_{12}-2\lambda-2G)}, \\ b_\infty &= e_\infty = \frac{-(c_{11}+c_{12}-2\lambda-2G)(\sigma_\infty+e_{33}E_\infty)+2c_{13}e_{31}E_\infty}{2c_{13}(c_{13}-\lambda)-c_{33}(c_{11}+c_{12}-2\lambda-2G)}, \\ c_\infty &= E_\infty \end{aligned} \tag{7.70}$$

The constants μ_j, a_j, and b_j are defined in Section 7.2, and $\mu_j'^2 = 1/\mu_j^2$, $b_j' = -b_j$, and $a_j' = -a_j\mu_j^2$. The boundary conditions (7.60) and (7.61) lead again to Eq. (7.23).

Application of the mixed boundary conditions in Eq. (7.60) gives rise to a pair of dual integral equations:

$$\begin{aligned} &\int_0^\infty \alpha F D(\alpha) J_0(\alpha r)\mathrm{d}\alpha - \sum_{j=1}^{3}\int_0^\infty \alpha g_j\mu_j B_j(\alpha) I_0(\mu_j'\alpha r)\mathrm{d}\alpha = -\frac{\pi}{2}\sigma_\infty \quad (0 \leqslant r < a), \\ &\int_0^\infty D(\alpha) J_0(\alpha r)\mathrm{d}\alpha = 0 \qquad (a \leqslant r \leqslant b) \end{aligned} \tag{7.71}$$

where $D(\alpha)$ and g_j are defined in Eq. (7.26). The solution of integral equation (7.71) may be obtained by using a new function $\Psi(\xi)$, defined by

$$D(\alpha) = -\frac{\sigma_\infty}{F}a^2\int_0^1 \Psi(\xi)\sin(a\alpha\xi)\mathrm{d}\xi \tag{7.72}$$

The function $\Psi(\xi)$ is governed by the following Fredholm integral equation of the second kind:

$$\Psi(\xi) + \int_0^1 \Psi(\eta)K(\xi,\eta)\mathrm{d}\eta = \xi \tag{7.73}$$

The kernel function $K(\xi,\eta)$ is

$$K(\xi,\eta) = \frac{4}{\pi^2 F}\sum_{j=1}^{3} g_j\mu_j^2\int_0^\infty E_j(\alpha,\eta)\sinh(\mu_j'\,\alpha\xi)\mathrm{d}\alpha \tag{7.74}$$

where the functions $E_j(\alpha,\eta)$ $(j=1,2,3)$ are given by

$$E_j(\alpha,\eta) = \sum_{i=1}^{5}\frac{D_i(\alpha,\eta)Q_{i,j}(\alpha)}{|C|} \qquad (j=1,2,3) \tag{7.75}$$

with

$$C=\begin{bmatrix} c_{1,1}(\alpha) & c_{1,2}(\alpha) & c_{1,3}(\alpha) & c_{1,4}(\alpha) & c_{1,5}(\alpha) \\ c_{2,1}(\alpha) & c_{2,2}(\alpha) & c_{2,3}(\alpha) & c_{2,4}(\alpha) & c_{2,5}(\alpha) \\ c_{3,1}(\alpha) & c_{3,2}(\alpha) & c_{3,3}(\alpha) & c_{3,4}(\alpha) & c_{3,5}(\alpha) \\ c_{4,1}(\alpha) & c_{4,2}(\alpha) & c_{4,3}(\alpha) & c_{4,4}(\alpha) & c_{4,5}(\alpha) \\ c_{5,1}(\alpha) & c_{5,2}(\alpha) & c_{5,3}(\alpha) & c_{5,4}(\alpha) & c_{5,5}(\alpha) \end{bmatrix} \tag{7.76}$$

$$\begin{aligned} &c_{1,j}(\alpha)=a'_jI_1(\mu'_j\alpha b/a),\quad c_{2,j}(\alpha)=\mu_jI_0(\mu'_j\alpha b/a),\\ &c_{3,j}(\alpha)=-m_j\mu_j\alpha I_0(\mu'_j\alpha b/a)+\frac{b}{a}(c_{12}-c_{11})I_1(\mu'_j\alpha b/a),\quad (j=1,2,3)\\ &c_{4,j}(\alpha)=-f_jI_1(\mu'_j\alpha b/a),\quad c_{5,j}(\alpha)=-n_jI_1(\mu'_j\alpha b/a) \end{aligned} \tag{7.77}$$

$$\begin{aligned} &c_{1,4}(\alpha)=K_1(\alpha b/a),\qquad c_{2,4}(\alpha)=K_0(\alpha b/a),\\ &c_{3,4}(\alpha)=-2G[\alpha K_0(\alpha b/a)]+\frac{b}{a}K_1(\alpha b/a),\\ &c_{4,4}(\alpha)=2GK_1(\alpha b/a),\quad c_{5,4}(\alpha)=0 \end{aligned} \tag{7.78}$$

$$\begin{aligned} c_{1,5}(\alpha)&=-4(1-\upsilon)\left[K_0(\alpha b/a)+\frac{2a}{\alpha b}K_1(\alpha b/a)\right]+\frac{\alpha b}{a}K_1(\alpha b/a),\\ c_{2,5}(\alpha)&=-\frac{\alpha b}{a}K_0(\alpha b/a),\quad c_{5,5}(\alpha)=0,\\ c_{3,5}(\alpha)&=\frac{2Gb}{a}\left[\left(4-4\upsilon+\frac{\alpha^2b^2}{a^2}\right)K_0(\alpha b/a)+(3-2\upsilon)\frac{\alpha b}{a}K_1(\alpha b/a)\right],\\ c_{4,5}(\alpha)&=2G\left[\frac{\alpha b}{a}K_0(\alpha b/a)+(2-2\upsilon)K_1(\alpha b/a)\right] \end{aligned} \tag{7.79}$$

$$\begin{aligned} D_1(\alpha,\eta)&=\sum_{j=1}^{3}\frac{a_jd_j}{\mu_j}K_1(\mu'_j\alpha b/a)\sinh(\mu'_j\alpha\eta),\\ D_2(\alpha,\eta)&=\sum_{j=1}^{3}\frac{d_j}{\mu_j^2}\left[(c_{12}-c_{11})\frac{a_ja}{b}-\frac{m_j\alpha}{\mu_j}\right]K_0(\mu'_j\alpha b/a)\sinh(\mu'_j\alpha\eta),\\ D_3(\alpha,\eta)&=\sum_{j=1}^{3}\frac{d_j}{\mu_j}K_0(\mu'_j\alpha b/a)\sinh(\mu'_j\alpha\eta) \end{aligned} \tag{7.80}$$

$$\begin{aligned} D_4(\alpha,\eta)&=\sum_{j=1}^{3}\frac{f_jd_j}{\mu_j^3}K_1(\mu'_j\alpha b/a)\sinh(\mu'_j\alpha\eta),\\ D_5(\alpha,\eta)&=\sum_{j=1}^{3}\frac{n_jd_j}{\mu_j}K_1(\mu'_j\alpha b/a)\sinh(\mu'_j\alpha\eta) \end{aligned} \tag{7.81}$$

$$\begin{aligned} m_j &= c_{11}a_j - c_{13} + e_{31}b_j, \\ n_j &= e_{15}(a_j\mu_j^2 + 1) + \kappa_{11}b_j \end{aligned} \tag{7.82}$$

$|C|$ is the determinant of the square matrix C and $Q_{i,j}(\alpha)$ are the co-factors of the elements $c_{i,j}(\alpha)$. Once the solution $\Psi(\xi)$ is obtained, the stress intensity factor K_{I} for the exact crack model can be calculated by

$$K_{\mathrm{I}} = \lim_{r\to a^+}\{2(r-a)\}^{1/2}\sigma_{zz}(r,0) = \frac{2}{\pi}\sigma_\infty\sqrt{a}\Psi(1) \tag{7.83}$$

The electric displacement intensity factor K_D can also be calculated by

$$K_D = \lim_{r\to a^+}\{2(r-a)\}^{1/2}D_z(r,0) = \left(\frac{1}{F}\sum_{j=1}^{3}h_j d_j\right)K_{\mathrm{I}} \tag{7.84}$$

where $h_j = e_{31}a_j + e_{33} - \kappa_{33}b_j$.

7.5 Fundamental solution for penny-shaped crack problem

The fundamental solution presented in [24] for a penny-shaped crack subjected to a point load is reviewed in this section.

7.5.1 Potential approach

Consider a transversely isotropic piezoelectric material weakened by a penny-shaped crack subjected to a pair of point forces P and a pair of point surface charge Q as shown in Fig. 7.4. The linear constitutive relations used in this problem are defined as

$$\begin{aligned} &\sigma_{xx} = c_{11}u_{,x} + c_{12}v_{,y} + c_{13}w_{,z} + e_{31}\phi_{,z}, \quad \sigma_{yy} = c_{12}u_{,x} + c_{11}v_{,y} + c_{13}w_{,z} + e_{31}\phi_{,z}, \\ &\sigma_{zz} = c_{13}u_{,x} + c_{13}v_{,y} + c_{33}w_{,z} + e_{33}\phi_{,z}, \quad \sigma_{xz} = c_{55}(u_{,z} + w_{,x}) + e_{15}\phi_{,x}, \\ &\sigma_{yz} = c_{55}(v_{,z} + w_{,y}) + e_{15}\phi_{,y}, \qquad\qquad \sigma_{xy} = c_{66}(u_{,y} + v_{,x}) \end{aligned} \tag{7.85}$$

$$\begin{aligned} &D_x = e_{15}(u_{,z} + w_{,x}) - \kappa_{11}\phi_{,x}, \quad D_y = e_{15}(v_{,z} + w_{,y}) - \kappa_{11}\phi_{,y}, \\ &D_z = e_{31}(u_{,x} + v_{,y}) + e_{33}w_{,z} - \kappa_{33}\phi_{,z} \end{aligned} \tag{7.86}$$

Introducing a new function $U=u+iv$, the governing equation (1.10) can be re-written as

$$\frac{1}{2}(c_{11} + c_{66})\nabla U + c_{55}U_{,zz} + \frac{1}{2}(c_{11} - c_{66})\Lambda^2\overline{U} + (c_{13} + c_{55})\Lambda w_{,z} + (e_{15} + e_{31})\phi_{,z} = 0 \tag{7.87}$$

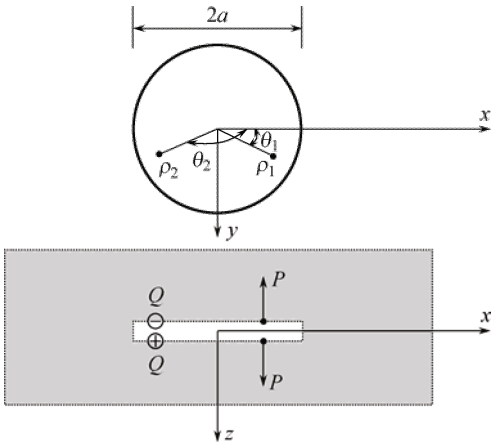

Fig. 7.4 A penny-shaped crack subjected to point loads.

$$\frac{1}{2}(c_{13}+c_{55})(\bar{\Lambda}U+\Lambda\bar{U})_{,z}+c_{55}\nabla w+c_{33}w_{,zz}+e_{15}\nabla\phi+e_{33}\phi_{,zz}=0 \tag{7.88}$$

$$\frac{1}{2}(e_{15}+e_{31})(\bar{\Lambda}U+\Lambda\bar{U})_{,z}+e_{15}\nabla w+e_{33}w_{,zz}-\kappa_{11}\nabla\phi-\kappa_{33}\phi_{,zz}=0 \tag{7.89}$$

where $\nabla=\partial^2/\partial x^2+\partial^2/\partial y^2$, $\Lambda=\partial/\partial x+i\partial/\partial y$ and an overbar indicates the complex conjugate value. The general solution to Eqs. (7.87)-(7.89) can be written in the following form:

$$U=\Lambda\left(\sum_{j=1}^{3}F_j+iF_4\right),\quad w=\sum_{j=1}^{3}\alpha_{j1}\frac{\partial F_j}{\partial z_j},\quad \phi=\sum_{j=1}^{3}\alpha_{j2}\frac{\partial F_j}{\partial z_j} \tag{7.90}$$

where

$$\begin{aligned}
&\alpha_{j1}=\frac{c_{11}\kappa_{11}-m_3\mu_j^2+c_{55}\kappa_{33}\mu_j^4}{(m_1-m_2\mu_j^2)\mu_j},\qquad \alpha_{j2}=\frac{c_{11}e_{15}-m_4\mu_j^2+c_{55}e_{33}\mu_j^4}{(m_1-m_2\mu_j^2)\mu_j},\\
&m_1=\kappa_{11}(c_{13}+c_{55})+e_{15}(e_{15}+e_{31}),\quad m_2=\kappa_{33}(c_{13}+c_{55})+e_{33}(e_{15}+e_{31}),\\
&m_3=c_{11}\kappa_{33}+c_{55}\kappa_{11}+(e_{15}+e_{31})^2,\quad m_4=c_{11}e_{33}+c_{55}e_{15}-(e_{15}+e_{31})(c_{13}+c_{55})
\end{aligned} \tag{7.91}$$

and $z_i=\mu_i z$, $\mu_4^2=c_{66}/c_{44}$, and μ_i^2 $(i=1,2,3)$ are the roots of Eq. (2.8).

Substitution of Eq. (7.90) into Eqs. (7.85) and (7.86) yields the following expressions for stresses and electric displacements:

$$\begin{aligned}
&\sigma_1=2\sum_{i=1}^{3}[c_{66}-c_{11}+c_{13}\mu_i\alpha_{i1}+e_{31}\mu_i\alpha_{i2}]\frac{\partial^2 F_i}{\partial z_i^2},\\
&\sigma_2=2c_{66}\Lambda^2(F_1+F_2+F_3+iF_4),\qquad \sigma_{zz}=\sum_{i=1}^{3}\gamma_{1i}\frac{\partial^2 F_i}{\partial z_i^2}
\end{aligned} \tag{7.92}$$

$$\begin{aligned}
\tau_z &= \Lambda\left\{\sum_{i=1}^{3}[c_{55}(\mu_i+\alpha_{i1})+e_{15}\alpha_{i2}]\frac{\partial F_i}{\partial z_i}+i\mu_4 c_{55}\frac{\partial F_4}{\partial z_4}\right\},\\
D &= \Lambda\left\{\sum_{i=1}^{3}[e_{15}(\mu_i+\alpha_{i1})-\kappa_{11}\alpha_{i2}]\frac{\partial F_i}{\partial z_i}+i\mu_4 e_{15}\frac{\partial F_4}{\partial z_4}\right\},\\
D_z &= \sum_{i=1}^{3}\gamma_{2i}\frac{\partial^2 F_i}{\partial z_i^2}
\end{aligned} \tag{7.93}$$

where $\sigma_1=\sigma_{xx}+\sigma_{yy}, \sigma_2=\sigma_{xx}-\sigma_{yy}+2i\sigma_{xy}, \tau_z=\sigma_{xz}+i\sigma_{yz}$ and $D=D_x+iD_y$ and $\gamma_{1i}=-c_{13}+c_{33}\mu_i\alpha_{i1}+e_{33}\mu_i\alpha_{i2}$, $\gamma_{2i}=-e_{31}+e_{33}\mu_i\alpha_{i1}-\kappa_{33}\mu_i\alpha_{i2}$.

7.5.2 Solution for crack problem

Having obtained general expression of stresses and electric displacements in the potential theory, we consider now a flat crack S in a piezoelectric material, with arbitrary pressure p and surface charge q applied symmetrically to the upper and lower crack faces. The boundary conditions are

$$\begin{aligned}
&\sigma_{zz}=-p(x,y), \quad D_z=q(x,y), \quad w=\phi=0 \quad ((x,y,0)\notin S),\\
&\tau_z=0 \qquad (-\infty<(x,y)<\infty)
\end{aligned} \tag{7.94}$$

The condition can be satisfied by expressing F_i in terms of the following two harmonic functions G and H:

$$F_i(z)=c_iG(z_i)+d_iH(z_i) \quad (i=1,2,3), \qquad F_4(z)=0 \tag{7.95}$$

To satisfy the third condition in Eq. (7.94),

$$\sum_{i=1}^{3}c_i[c_{44}(\mu_i+\alpha_{i1})+e_{15}\alpha_{i2}]=0, \quad \sum_{i=1}^{3}d_i[c_{44}(\mu_i+\alpha_{i1})+e_{15}\alpha_{i2}]=0 \tag{7.96}$$

The two functions G and H are defined as

$$G(\rho,\varphi,z)=\iint_S\frac{\omega(N)}{R(M,N)}\mathrm{d}S, \qquad H(\rho,\varphi,z)=\iint_S\frac{\Phi(N)}{R(M,N)}\mathrm{d}S \tag{7.97}$$

where $\omega(N)$ and $\Phi(N)$ represent the crack face displacement w and electric potential ϕ at point $N(r,\varphi,0)$, respectively. $R(M,N)$ is the distance between the points $M(\rho,\theta,z)$ and $N(r,\varphi,0)$. Making use of the property of the potential of a simple layer, the condition $w=\phi=0,\ (x,y,0)\notin S$ is already identically satisfied. Moreover, the following relations hold true inside the crack:

$$\left.\frac{\partial G}{\partial z}\right|_{z=0}=-2\pi\omega=-2\pi w(x,y,0), \quad \left.\frac{\partial H}{\partial z}\right|_{z=0}=-2\pi\Phi=-2\pi\phi(x,y,0) \tag{7.98}$$

Making use of Eqs. (7.90), (7.95), and (7.98), we obtain the following relations:

$$\sum_{i=1}^{3} c_i\alpha_{i1} = -\frac{1}{2\pi},\ \sum_{i=1}^{3} d_i\alpha_{i1} = 0,\ \sum_{i=1}^{3} c_i\alpha_{i2} = 0,\ \sum_{i=1}^{3} d_i\alpha_{i2} = -\frac{1}{2\pi} \tag{7.99}$$

c_i and d_i are then solved from Eqs. (7.96) and (7.99) as follows:

$$\begin{Bmatrix} c_1 \\ c_2 \\ c_3 \end{Bmatrix} = [A]\begin{Bmatrix} 1 \\ -1 \\ 0 \end{Bmatrix},\ \begin{Bmatrix} d_1 \\ d_2 \\ d_3 \end{Bmatrix} = [A]\begin{Bmatrix} e_{15}/c_{44} \\ 0 \\ -1 \end{Bmatrix},\ [A] = \frac{1}{2\pi}\begin{bmatrix} \mu_1 & \mu_2 & \mu_3 \\ \alpha_{11} & \alpha_{21} & \alpha_{31} \\ \alpha_{12} & \alpha_{22} & \alpha_{32} \end{bmatrix}^{-1} \tag{7.100}$$

Taking consideration of the first condition in Eq. (7.94), the following integro-differential equations are obtained:

$$\begin{aligned} p(N_0) &= -g_1\Delta\iint_S \frac{\omega(N)}{R(N_0,N)}\mathrm{d}S - g_2\Delta\iint_S \frac{\Phi(N)}{R(N_0,N)}\mathrm{d}S, \\ q(N_0) &= -g_3\Delta\iint_S \frac{\omega(N)}{R(N_0,N)}\mathrm{d}S - g_4\Delta\iint_S \frac{\Phi(N)}{R(N_0,N)}\mathrm{d}S \end{aligned} \qquad (N_0 \in S) \tag{7.101}$$

where

$$g_1 = -\sum_{i=1}^{3} c_i\gamma_{1i},\ g_2 = -\sum_{i=1}^{3} d_i\gamma_{1i},\ g_3 = \sum_{i=1}^{3} c_i\gamma_{2i},\ g_4 = \sum_{i=1}^{3} d_i\gamma_{2i} \tag{7.102}$$

Equation (7.101) can be rewritten as

$$\begin{aligned} g_4p(N_0) - g_2q(N_0) &= -\frac{1}{4\pi^2 A}\Delta\iint_S \frac{\omega(N)}{R(N_0,N)}\,\mathrm{d}S, \\ g_1p(N_0) - g_3q(N_0) &= -\frac{1}{4\pi^2 A}\Delta\iint_S \frac{\Phi(N)}{R(N_0,N)}\,\mathrm{d}S \end{aligned} \qquad (N_0 \in S) \tag{7.103}$$

where $A = 1/[4\pi^2(g_1g_4 - g_2g_3)]$.

7.5.3 Fundamental solution for penny-shaped crack problem

For the case of a penny-shaped crack, the solutions to Eq. (7.103) are obtained as

$$\begin{aligned} \omega(\rho,\theta) &= \frac{2A}{\pi}\int_0^{2\pi}\int_0^a \frac{1}{R}\tan^{-1}\left(\frac{\eta}{R}\right)[g_4p(\rho_0,\theta_0) - g_2q(\rho_0,\theta_0)]\rho_0\mathrm{d}\rho_0\mathrm{d}\theta_0, \\ \Phi(\rho,\theta) &= \frac{2A}{\pi}\int_0^{2\pi}\int_0^a \frac{1}{R}\tan^{-1}\left(\frac{\eta}{R}\right)[g_1p(\rho_0,\theta_0) - g_3q(\rho_0,\theta_0)]\rho_0\mathrm{d}\rho_0\mathrm{d}\theta_0 \end{aligned} \tag{7.104}$$

where a is the radius of the crack and

$$R=[\rho^2+\rho_0^2-2\rho\rho_0\cos(\theta-\theta_0)]^{1/2},\quad \eta=[(a^2-\rho^2)(a^2-\rho_0^2)]^{1/2}/a \tag{7.105}$$

To obtain the whole elastoelectric field, substitution of Eq. (7.104) into (7.97) gives

$$\begin{aligned} G(\rho,\theta,z)&=\frac{2A}{\pi}\int_0^{2\pi}\int_0^a K(\rho,\theta,z,\rho_0,\theta_0)[g_4p(\rho_0,\theta_0)-g_2q(\rho_0,\theta_0)]\rho_0\mathrm{d}\rho_0\mathrm{d}\theta_0,\\ H(\rho,\theta,z)&=\frac{2A}{\pi}\int_0^{2\pi}\int_0^a K(\rho,\theta,z,\rho_0,\theta_0)[g_1p(\rho_0,\theta_0)-g_3q(\rho_0,\theta_0)]\rho_0\mathrm{d}\rho_0\mathrm{d}\theta_0 \end{aligned} \tag{7.106}$$

where the Green's function K reads

$$K(M,N_0)=\int_0^{2\pi}\int_0^a\frac{1}{R(N,N_0)}\tan^{-1}\left[\frac{(a^2-r^2)^{1/2}(a^2-\rho_0^2)^{1/2}}{aR(N,N_0)}\right]\frac{r\mathrm{d}r\mathrm{d}\psi}{R(M,N)} \tag{7.107}$$

where $M=M(\rho,\theta,z),\ N=N(r,\psi,0),\ N_0=N_0(\rho_0,\theta_0,0).$

If the penny-shaped crack is subjected to a pair of normal point forces P in opposite directions at the points $(\rho_1,\theta_1,0^{\pm})$, $\rho_1<a$ and a pair of point charges Q acting at the points $(\rho_2,\theta_2,0^{\pm})$, $\rho_2<a$ as shown in Fig. 7.4. Making use of the property of the δ-function, the fundamental solution for the elastoelectric field is obtained as

$$\begin{aligned} U&=4A\sum_{i=1}^{3}[\beta_{i1}f_{11}(z_i)P+\beta_{i2}f_{12}(z_i)Q],\\ w&=-4A\sum_{i=1}^{3}\alpha_{i1}[\beta_{i1}f_{21}(z_i)P+\beta_{i2}f_{22}(z_i)Q],\\ \phi&=-4A\sum_{i=1}^{3}\alpha_{i2}[\beta_{i1}f_{21}(z_i)P+\beta_{i2}f_{22}(z_i)Q] \end{aligned} \tag{7.108}$$

$$\begin{aligned} \sigma_1&=8A\sum_{i=1}^{3}[(c_{66}-c_{11})+c_{13}\mu_i\alpha_{i1}+e_{31}\mu_i\alpha_{i2}][\beta_{i1}f_{31}(z_i)P+\beta_{i2}f_{32}(z_i)Q],\\ \sigma_2&=8Ac_{66}\sum_{i=1}^{3}[\beta_{i1}f_{41}(z_i)P+\beta_{i2}f_{42}(z_i)Q] \end{aligned} \tag{7.109}$$

$$\begin{aligned} \sigma_{zz}&=4A\sum_{i=1}^{3}\gamma_{1i}[\beta_{i1}f_{31}(z_i)P+\beta_{i2}f_{32}(z_i)Q],\\ \tau_z&=4A\sum_{i=1}^{3}[c_{44}(\mu_i+\alpha_{i1})+e_{15}\alpha_{i2}][\beta_{i1}f_{51}(z_i)P+\beta_{i2}f_{52}(z_i)Q] \end{aligned} \tag{7.110}$$

$$D = 4A\sum_{i=1}^{3}[e_{15}(\mu_i + \alpha_{i1}) - \kappa_{11}\alpha_{i2}][\beta_{i1}f_{51}(z_i)P + \beta_{i2}f_{52}(z_i)Q],$$
$$D_z = 4A\sum_{i=1}^{3}\gamma_{2i}[\beta_{i1}f_{31}(z_i)P + \beta_{i2}f_{32}(z_i)Q] \tag{7.111}$$

where

$$f_{1i}(z) = \frac{1}{\overline{t}_i}\left\{\frac{z}{R_i}\tan^{-1}\left(\frac{h_i}{R_i}\right)\right\} - B\tan^{-1}\left(\frac{\overline{s}_i}{(l_2^2 - a^2)^{1/2}}\right),$$
$$f_{2i}(z) = \frac{1}{R_i}\tan^{-1}\left(\frac{h_i}{R_i}\right), \tag{7.112}$$
$$f_{3i}(z) = \frac{z}{R_i^3}\tan^{-1}\left(\frac{h_i}{R_i}\right) - \frac{h_i}{z(R_i^2 + h_i^2)}\left[\frac{\rho^2 - l_1^2}{l_2^2 - l_1^2} - \frac{z^2}{R_i^2}\right]$$

$$f_{4i}(z) = \frac{B}{\overline{t}_i}\left(\frac{2}{\overline{t}_i} - \frac{\rho_i e^{i\theta_i}}{\overline{s}_i^2}\right)\tan^{-1}\left[\frac{\overline{s}_i}{(l_2^2 - a^2)^{1/2}}\right] - \frac{z(3R_i^2 - z^2)}{\overline{t}_i^2 R_i^3}\tan^{-1}\left(\frac{h_i}{R_i}\right)$$
$$+ \frac{B(l_2^2 - a^2)^{1/2}\rho_i e^{i\theta_i}}{\overline{t}_i\overline{s}_i[l_2^2 - \rho\rho_i e^{-i(\theta-\theta_i)}]} - \frac{zh_i}{R_i^2 + h_i^2}\left[\frac{t_i}{\overline{t}_i R_i^2} - \frac{\rho^2 e^{2i\theta}}{(l_2^2 - l_1^2)(l_2^2 - \rho^2)}\right], \tag{7.113}$$
$$f_{5i}(z) = \frac{t_i}{R_i^3}\tan^{-1}\left(\frac{h_i}{R_i}\right) + \frac{h_i}{R_i^2 + h_i^2}\left[\frac{\rho e^{i\theta}}{l_2^2 - l_1^2} + \frac{t_i}{R_i^2}\right]$$

$$\beta_{i1} = c_i g_4 - d_i g_3, \qquad \beta_{i2} = d_i g_1 - c_i g_2, \qquad t_i = \rho e^{i\theta} - \rho_i e^{i\theta_i},$$
$$\overline{s}_i = (a^2 - \rho\rho_i e^{-i(\theta-\theta_i)})^{1/2}, \qquad h_i = (a^2 - l_1^2)^{1/2}(a^2 - \rho_i^2)^{1/2}/a,$$
$$R_i = [\rho^2 + \rho_i^2 - 2\rho\rho_i\cos(\theta - \theta_i) + z^2]^{1/2}, \qquad B = \frac{(a^2 - \rho_i^2)^{1/2}}{\overline{s}_i}, \tag{7.114}$$
$$l_1^2 = \frac{1}{2}\{[(\rho + a)^2 + z^2]^{1/2} - [(\rho - a)^2 + z^2]^{1/2}\},$$
$$l_2^2 = \frac{1}{2}\{[(\rho + a)^2 + z^2]^{1/2} + [(\rho - a)^2 + z^2]^{1/2}\}$$

7.6 A penny-shaped crack in a piezoelectric cylinder

In this section, the developments in [25] for the response of elastic stress and electric displacement in a long piezoelectric cylinder with a centered pennyshaped crack are presented. The long piezoelectric cylinder is subjected to two types of boundary conditions: (a) the piezoelectric cylinder is inserted in a smooth rigid bore of radius *b*; (b) the surface of the piezoelectric cylinder is stress and electric charge free.

Based on the potential function approach and Hankel transform, a system of dual integral equations is obtained, and then reduced to a Fredholm integral equation of the second kind. Numerical results of various field intensity factors for PZT-6B cylinder are obtained to show the effect of the ratio a/b on the fracture behavior of the cracked piezoelectric cylinder (a is the radius of the crack and b is the radius of the PZT-6B cylinder).

7.6.1 Problem statement and basic equation

Consider a piezoelectric cylinder of radius b containing a centered penny-shaped crack of radius a under axisymmetric electromechanical loads (Fig. 7.5). For convenience, a cylindrical coordinate system (r,θ,z) originating at the center of the crack is used, with the z-axis along the axis of symmetry of the cylinder. The cylinder is assumed to be a transversely isotropic piezoelectric material with the poling direction parallel to the z-axis. It is subjected to the far-field of a normal stress, $\sigma_z = \bar{\sigma}(r)$ and a normal electric displacement, $D_z = \bar{D}(r)$.

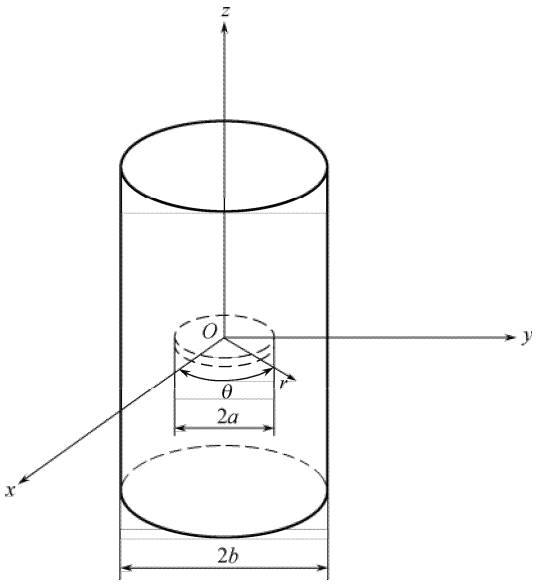

Fig. 7.5 Penny-shaped crack in a piezoelectric cylinder.

The constitutive equations are defined in Eqs. (7.1)-(7.6). The equilibrium equation and the equation of electrostatics for this problem are given as

$$\begin{aligned}
&\sigma_{rr,r}+\sigma_{rz,z}+\frac{\sigma_{rr}-\sigma_{\theta\theta}}{r}=0,\\
&\sigma_{rz,r}+\sigma_{zz,z}+\frac{\sigma_{rz}}{r}=0,\\
&D_{r,r}+D_{z,z}+\frac{D_r}{r}=0
\end{aligned} \tag{7.115}$$

In the derivation of the analytic solution, the following potential functions are introduced [5,27]:

$$u_r=\frac{\partial \Phi}{\partial r},\quad u_z=k_1\frac{\partial \Phi}{\partial z},\quad \phi=-k_2\frac{\partial \Phi}{\partial z} \tag{7.116}$$

where $\Phi(r,z)$ is the potential function, and k_1 and k_2 are unknown constants to be determined.

Substituting Eq. (7.116) into Eqs. (7.1)-(7.6), and then into Eq. (7.115), we have

$$\Phi_{,rr}+\frac{1}{r}\Phi_{,r}+n\Phi_{,zz}=0 \tag{7.117}$$

where

$$\begin{aligned}
n&=\frac{c_{44}+(c_{13}+c_{44})k_1-(e_{31}+e_{15})k_2}{c_{11}}\\
&=\frac{c_{33}k_1-e_{33}k_2}{c_{44}k_1+c_{13}+c_{44}-e_{15}k_2}=\frac{e_{33}k_1+\kappa_{33}k_2}{e_{15}k_1+e_{15}+e_{31}+\kappa_{11}k_2}
\end{aligned} \tag{7.118}$$

Obviously, Eq. (7.118) leads to Eq. (2.8). According to Eq. (2.8) and the principle of superposition, the governing equation (7.117) becomes

$$\sum_{i=1}^{3}\left[\Phi_{i,rr}+\frac{1}{r}\Phi_{i,rr}+\Phi_{i,z_iz_i}\right]=0$$

or

$$\begin{aligned}
&c_{11}\sum_{i=1}^{3}\left(\frac{\partial \Phi_i}{\partial r^2}+\frac{1}{r}\frac{\partial \Phi_i}{\partial r}\right)+\sum_{i=1}^{3}\left\{\left[c_{55}+k_{1i}(c_{13}+c_{55})+k_{2i}(e_{31}+e_{15})\right]\frac{\partial \Phi_i}{\partial z^2}\right\}=0,\\
&\sum_{i=1}^{3}\left\{\left[c_{44}k_{1i}+c_{13}+c_{55}+e_{15}k_{2i}\right]\left(\frac{\partial \Phi_i}{\partial r^2}+\frac{1}{r}\frac{\partial \Phi_i}{\partial r}\right)+\left[c_{33}k_{1i}+e_{33}k_{2i}\right]\frac{\partial \Phi_i}{\partial z^2}\right\}=0,\\
&\sum_{i=1}^{3}\left\{\left[e_{15}k_{1i}+e_{31}+e_{15}-d_{11}k_{2i}\right]\left(\frac{\partial \Phi_i}{\partial r^2}+\frac{1}{r}\frac{\partial \Phi_i}{\partial r}\right)+\left[e_{33}k_{1i}-d_{33}k_{2i}\right]\frac{\partial \Phi_i}{\partial z^2}\right\}=0
\end{aligned} \tag{7.119}$$

where $z_i=z/\sqrt{n_i}=\mu_i z$, μ_i are the roots of Eq. (2.8) and $\Phi_i(r,z)$ $(i=1,2,3)$ are the corresponding potential functions. The displacement and electric potential equations are then in the form

$$u_r = \sum_{i=1}^{3} \frac{\partial \Phi_i}{\partial r}, \quad u_z = \sum_{i=1}^{3} k_{1i} \frac{\partial \Phi_i}{\partial z}, \quad \phi = -\sum_{i=1}^{3} k_{2i} \frac{\partial \Phi_i}{\partial z} \tag{7.120}$$

where k_{1i} and k_{2i} ($i = 1,2,3$) are determined from Eq. (7.118).

Following the procedure presented in [27], we take the solution of Eq. (7.119) in the form

$$\Phi_i(r,z) = \int_0^\infty \frac{1}{\xi} \left[A_i(\xi) I_0\left(\frac{\xi r}{\mu_i}\right) \cos(\xi z) + B_i(\xi) \exp(-\xi \mu_i z) J_0(\xi r) \right] \mathrm{d}\xi \tag{7.121}$$

where $A_i(\xi),\ B_i(\xi),\ (i = 1,2,3)$ are the unknown functions to be determined.

Then we have expressions of the components of displacement, stress and electric displacement in the following form:

$$\begin{aligned} u_z(r,z) = &-\sum_{i=1}^{3} k_{1i} \int_0^\infty A_i(\xi) I_0\left(\frac{\xi r}{\mu_i}\right) \sin(\xi z) \mathrm{d}\xi \\ &- \sum_{i=1}^{3} k_{1i} s_i \int_0^\infty B_i(\xi) J_0(\xi r) e^{-\xi \mu_i z} \mathrm{d}\xi + \overline{a}(r) z \end{aligned} \tag{7.122}$$

$$u_r(r,z) = \sum_{i=1}^{3} \frac{1}{\mu_i} \int_0^\infty A_i(\xi) I_1\left(\frac{\xi r}{\mu_i}\right) \cos(\xi z) \mathrm{d}\xi - \sum_{i=1}^{3} \int_0^\infty B_i(\xi) J_1(\xi r) e^{-\xi \mu_i z} \mathrm{d}\xi \tag{7.123}$$

$$\begin{aligned} \phi(r,z) = &\sum_{i=1}^{3} k_{2i} \int_0^\infty A_i(\xi) I_1\left(\frac{\xi r}{\mu_i}\right) \sin(\xi z) \mathrm{d}\xi \\ &+ \sum_{i=1}^{3} k_{2i} s_i \int_0^\infty B_i(\xi) J_0(\xi r) e^{-\xi \mu_i z} \mathrm{d}\xi - \overline{b}(r) z \end{aligned} \tag{7.124}$$

$$\begin{aligned} \sigma_z = &-\sum_{i=1}^{3} \frac{F_{1i}}{\mu_i^2} \int_0^\infty \xi A_i(\xi) I_0\left(\frac{\xi r}{\mu_i}\right) \cos(\xi z) \mathrm{d}\xi \\ &+ \sum_{i=1}^{3} F_{1i} \int_0^\infty \xi B_i(\xi) J_0(\xi r) e^{-\xi \mu_i z} \mathrm{d}\xi + \overline{c}(r) \end{aligned} \tag{7.125}$$

$$\begin{aligned} \sigma_r = &-\sum_{i=1}^{3} \frac{F_{5i}}{\mu_i^2} \int_0^\infty \xi A_i(\xi) I_0\left(\frac{\xi r}{\mu_i}\right) \cos(\xi z) \mathrm{d}\xi \\ &+ \frac{c_{11} - c_{12}}{2} \sum_{i=1}^{3} \frac{1}{\mu_i^2} \int_0^\infty \xi A_i(\xi) I_2\left(\frac{\xi r}{\mu_i}\right) \cos(\xi z) \mathrm{d}\xi \\ &+ \sum_{i=1}^{3} F_{5i} \int_0^\infty \xi B_i(\xi) J_0(\xi r) e^{-\xi \mu_i z} \mathrm{d}\xi \\ &+ \frac{c_{11} - c_{12}}{2} \sum_{i=1}^{3} \int_0^\infty \xi B_i(\xi) J_2(\xi r) e^{-\xi \mu_i z} \mathrm{d}\xi \end{aligned} \tag{7.126}$$

$$\sigma_{zr} = -\sum_{i=1}^{3} \frac{F_{3i}}{\mu_i^2} \int_0^{\infty} \xi A_i(\xi) I_1\left(\frac{\xi r}{\mu_i}\right) \sin(\xi z) \mathrm{d}\xi + \sum_{i=1}^{3} F_{3i} \int_0^{\infty} \xi B_i(\xi) J_1(\xi r) e^{-\xi \mu_i z} \mathrm{d}\xi \tag{7.127}$$

$$D_z = -\sum_{i=1}^{3} \frac{F_{2i}}{\mu_i^2} \int_0^{\infty} \xi A_i(\xi) I_0\left(\frac{\xi r}{\mu_i}\right) \cos(\xi z) \mathrm{d}\xi + \sum_{i=1}^{3} F_{2i} \int_0^{\infty} \xi B_i(\xi) J_0(\xi r) e^{-\xi \mu_i z} \mathrm{d}\xi + \overline{\mathrm{d}}(r) \tag{7.128}$$

$$D_r = -\sum_{i=1}^{3} \frac{F_{4i}}{\mu_i^2} \int_0^{\infty} \xi A_i(\xi) I_1\left(\frac{\xi r}{\mu_i}\right) \sin(\xi z) \mathrm{d}\xi + \sum_{i=1}^{3} F_{4i} \int_0^{\infty} \xi B_i(\xi) J_1(\xi r) e^{-\xi \mu_i z} \mathrm{d}\xi \tag{7.129}$$

where

$$\begin{aligned} &F_{1i} = (c_{33}k_{1i} - e_{33}k_{2i})\mu_i^2 - c_{13}, \quad F_{2i} = (e_{33}k_{1i} + d_{33}k_{2i})\mu_i^2 - e_{31}, \\ &F_{3i} = \left[c_{44}(1+k_{1i}) - e_{15}k_{2i}\right]\mu_i, \quad F_{4i} = \left[e_{15}(1+k_{1i}) + d_{11}k_{2i}\right]\mu_i, \\ &F_{5i} = (c_{13}k_{1i} - e_{31}k_{2i})\mu_i^2 - \frac{c_{11}+c_{12}}{2} \end{aligned} \tag{7.130}$$

$$\overline{a}(r) = \frac{d_{33}\overline{\sigma}(r) + \overline{e}_{33}\overline{D}(r)}{c_{33}d_{33} + e_{33}^2}, \quad \overline{b}(r) = \frac{c_{33}\overline{D}(r) - e_{33}\overline{\sigma}(r)}{c_{33}d_{33} + e_{33}^2}, \tag{7.131}$$

$$\overline{c}(r) = \overline{\sigma}(r), \quad \overline{d}(r) = \overline{D}(r)$$

7.6.2 Derivation of integral equations and their solution

In the derivation, we consider separately two sets of boundary conditions.

Case 1: In the first case it is assumed that the piezoelectric cylindrical surface is free from shear and is supported in such a way that the radial component of the displacement vector vanishes on the surface. Such a situation would arise physically if the piezoelectric cylinder was embedded in a rigid cylindrical hollow (of exactly the same radius) and was then deformed by the application of a known stress and an electric displacement at the end of the piezoelectric cylinder. The problem of determining the distribution of stress and electric displacement in the vicinity of the crack is equivalent to that of finding the distribution of stress and electric displacement in the semi-infinite cylinder $z \geqslant 0$, $0 \leqslant r \leqslant a$, when its plane boundary $z = 0$ is subjected to the condition:

$$\begin{aligned} &\sigma_z(r,0) = 0, \quad D_z(r,0^+) = D_z(r,0^-), \quad E_r(r,0^+) = E_r(r,0^+) \quad (0 \leqslant r < a), \\ &u_z(r,0) = 0, \quad \phi(r,0) = 0 \qquad (a < r < b), \\ &\sigma_{rz}(r,0) = 0 \quad (0 \leqslant r < b) \end{aligned} \tag{7.132}$$

and its curved boundary $r = b$ is subjected to the conditions:

$$u_r(b,z)=0,\quad \sigma_{rz}(b,z)=0,\quad D_r(b,z)=0 \tag{7.133}$$

From the boundary conditions (7.132) and (7.133), and making use of the Fourier inversion theorem and the Hankel inversion theorem, we find that

$$\begin{aligned} &A_1(\xi)=\frac{1}{\Delta(\xi)}\sum_{i=1}^{3}N_{1i}(\xi)f_{1i}(\xi),\quad A_2(\xi)=\frac{1}{\Delta(\xi)}\sum_{i=1}^{3}N_{2i}(\xi)f_{2i}(\xi),\\ &A_3(\xi)=\frac{1}{\Delta(\xi)}\sum_{i=1}^{3}N_{3i}(\xi)f_{3i}(\xi) \end{aligned} \tag{7.134}$$

$$B_1(\xi)=M_1B_1(\xi),\quad B_2(\xi)=M_2B_1(\xi),\quad B_3(\xi)=M_3B_1(\xi) \tag{7.135}$$

in which

$$M_1=1,\quad M_2=\frac{F_{31}k_{23}\mu_3-F_{33}k_{21}\mu_1}{F_{33}k_{22}\mu_2-F_{32}k_{23}\mu_3},\quad M_3=\frac{F_{32}k_{21}\mu_1-F_{31}k_{22}\mu_2}{F_{33}k_{22}\mu_2-F_{32}k_{23}\mu_3} \tag{7.136}$$

$$\begin{aligned} &f_{1i}(\xi)=\frac{2}{\pi}\int_0^{\infty}\frac{\eta B_1(\eta)J_1(\eta b)}{\eta^2\mu_i^2+\xi^2}\mathrm{d}\eta,\quad f_{2i}(\xi)=\frac{2}{\pi}\int_0^{\infty}\frac{\eta^2 B_1(\eta)J_0(\eta b)}{\eta^2\mu_i^2+\xi^2}\mathrm{d}\eta,\\ &f_{3i}(\xi)=\frac{2}{\pi}\int_0^{\infty}\frac{\eta^2 B_1(\eta)J_2(\eta b)}{\eta^2\mu_i^2+\xi^2}\mathrm{d}\eta \end{aligned} \tag{7.137}$$

$$\begin{aligned} \Delta(\xi)=&\left[h_{12}(\xi)h_{33}(\xi)-h_{32}(\xi)h_{13}(\xi)\right]h_{21}(\xi)+\left[h_{31}(\xi)h_{13}(\xi)-h_{11}(\xi)h_{33}(\xi)\right]h_{22}(\xi)\\ &+\left[h_{11}(\xi)h_{32}(\xi)-h_{31}(\xi)h_{12}(\xi)\right]h_{23}(\xi) \end{aligned} \tag{7.138}$$

$$\begin{aligned} N_{1i}(\xi)=&\left[h_{13}(\xi)h_{22}(\xi)-h_{12}(\xi)h_{23}(\xi)\right]g_{3i}+\left[h_{12}(\xi)h_{33}(\xi)-h_{13}(\xi)h_{32}(\xi)\right]g_{2i}\\ &+\left[h_{23}(\xi)h_{32}(\xi)-h_{22}(\xi)h_{33}(\xi)\right]g_{1i} \end{aligned} \tag{7.139}$$

$$\begin{aligned} N_{2i}(\xi)=&\left[h_{11}(\xi)h_{23}(\xi)-h_{21}(\xi)h_{13}(\xi)\right]g_{3i}+\left[h_{13}(\xi)h_{31}(\xi)-h_{11}(\xi)h_{33}(\xi)\right]g_{2i}\\ &+\left[h_{21}(\xi)h_{33}(\xi)-h_{31}(\xi)h_{23}(\xi)\right]g_{1i} \end{aligned} \tag{7.140}$$

$$\begin{aligned} N_{3i}(\xi)=&\left[h_{12}(\xi)h_{21}(\xi)-h_{11}(\xi)h_{22}(\xi)\right]g_{3i}+\left[h_{11}(\xi)h_{32}(\xi)-h_{31}(\xi)h_{12}(\xi)\right]g_{2i}\\ &+\left[h_{22}(\xi)h_{31}(\xi)-h_{21}(\xi)h_{32}(\xi)\right]g_{1i} \end{aligned} \tag{7.141}$$

with

$$h_{1i}(\xi)=\frac{F_{4i}}{\mu_i^2}I_1\left(\frac{\xi b}{\mu_i}\right),\quad g_{1i}=F_{4i}M_i,\quad h_{2i}(\xi)=\frac{F_{3i}}{\mu_i^2}I_1\left(\frac{\xi b}{\mu_i}\right),$$
$$g_{2i}=F_{3i}M_i\mu_i,\quad h_{3i}(\xi)=\frac{1}{\mu_i}I_1\left(\frac{\xi b}{\mu_i}\right),\quad g_{3i}=M_i\mu_i \tag{7.142}$$

From Eqs. $(7.132)_{1,4}$, we can obtain a system of dual integral equations:

$$-\int_0^\infty \xi\left[\frac{F_{11}}{\mu_1^2}I_0\left(\frac{\xi r}{\mu_1}\right)A_1(\xi)+\frac{F_{12}}{\mu_2^2}I_0\left(\frac{\xi r}{\mu_2}\right)A_2(\xi)+\frac{F_{13}}{\mu_3^2}I_0\left(\frac{\xi r}{\mu_3}\right)A_3(\xi)\right]\mathrm{d}\xi$$
$$+\int_0^\infty \xi\left[M_1F_{11}+M_2F_{12}+M_3F_{13}\right]B_1(\xi)J_0(\xi r)\mathrm{d}\xi=-\overline{c}(r)\quad(0\leqslant r<a) \tag{7.143}$$

$$\int_0^\infty\left[M_1k_{11}s_1+M_2k_{12}s_2+M_3k_{13}s_3\right]B_1(\xi)J_0(\xi r)\mathrm{d}\xi=0\quad(a<r<b) \tag{7.144}$$

Thess equations can be solved by using the function $\psi(\alpha)$, defined by

$$B_1(\xi)=\int_0^a\psi(\alpha)\sin(\xi\alpha)\mathrm{d}\alpha \tag{7.145}$$

where $\psi(0)=0$.

Using solutions of the following integrals:

$$\int_0^\infty \sin(sz)e^{-uz}\mathrm{d}z=\frac{s}{s^2+u^2},\quad \int_0^\infty \cos(sz)e^{-uz}\mathrm{d}z=\frac{u}{s^2+u^2},$$

$$\int_0^t\frac{rI_0(\xi r)}{\sqrt{t^2-r^2}}\mathrm{d}r=\frac{\sinh(\xi t)}{\xi},\quad \int_0^\infty\frac{J_0(ru)\sin(ut)}{s^2+u^2}\mathrm{d}u=\frac{\sinh(st)K_0(rs)}{s}\quad(t<r)$$

$$\int_0^\infty\frac{J_0(ru)\sin(ut)}{s^2+u^2}\mathrm{d}u=\frac{\sinh(st)K_0(rs)}{s}\quad(t<r)$$

$$\int_0^\infty\frac{uJ_1(ru)\sin(ut)}{s^2+u^2}\mathrm{d}u=\sinh(st)K_1(rs)\quad(t<r)$$

$$\int_0^\infty\frac{u^2J_0(ru)\sin(ut)}{s^2+u^2}\mathrm{d}u=-s\cdot\sinh(st)K_0(rs)\quad(t<r)$$

$$\int_0^\infty\frac{u^2J_2(ru)\sin(ut)}{s^2+u^2}\mathrm{d}u=s\cdot\sinh(st)K_2(rs)\quad(t<r)$$

as well as the solution

$$f(t)=\frac{2\sin\pi\alpha}{\pi}\frac{\mathrm{d}}{\mathrm{d}t}\int_0^t\frac{ug(u)}{(t^2-u^2)^{1-\alpha}}\mathrm{d}u\quad(a<t<b)$$

of the integral equation

$$\int_0^{\infty} \frac{f(t)}{(x^2-t^2)^{\alpha}} \mathrm{d}t = g(x) \quad (0<\alpha<1, \quad a<x<b)$$

we can obtain a Fredholm integral equation of the second kind in the form

$$\psi(\alpha) + \int_0^a \psi(\beta) L(\alpha,\beta) \mathrm{d}\beta = \frac{2}{\pi m_0} \int_0^{\alpha} \frac{r\overline{c}(r)}{\sqrt{\alpha^2-r^2}} \mathrm{d}r \tag{7.146}$$

where

$$L(\alpha,\beta) = \frac{4}{\pi^2 m_0} \sum_{j=1}^{3} \frac{F_{1j}}{\mu_j} \int_0^{\infty} \frac{1}{\Delta(\xi)} \sinh\left(\frac{\xi\alpha}{\mu_j}\right) \sum_{i=1}^{3} \frac{1}{\mu_i^2} N_{ji}(\xi) \sinh\left(\frac{\xi\beta}{\mu_i}\right) K_1\left(\frac{\xi b}{\mu_i}\right) \mathrm{d}\xi \tag{7.147}$$

Case 2: In the second case we assume that the piezoelectric cylindrical surface is stress free. The conditions (7.132) remain the same, and the boundary conditions (7.133) are replaced by the following conditions:

$$\sigma_{rr}(b,z) = 0, \quad \sigma_{rz}(b,z) = 0, \quad D_r(b,z) = 0 \quad (z \geqslant 0) \tag{7.148}$$

Performing a procedure similar to that in Case 1, we have

$$\begin{aligned} A_1(\xi) &= \frac{1}{\Delta(\xi)} \sum_{i=1}^{3} \left[N_{1i}(\xi) f_{1i}(\xi) + P_{1i}(\xi) f_{2i}(\xi) + W_{1i}(\xi) f_{3i}(\xi) \right], \\ A_2(\xi) &= \frac{1}{\Delta(\xi)} \sum_{i=1}^{3} \left[N_{2i}(\xi) f_{1i}(\xi) + P_{2i}(\xi) f_{2i}(\xi) + W_{2i}(\xi) f_{3i}(\xi) \right], \\ A_3(\xi) &= \frac{1}{\Delta(\xi)} \sum_{i=1}^{3} \left[N_{3i}(\xi) f_{1i}(\xi) + P_{3i}(\xi) f_{2i}(\xi) + W_{3i}(\xi) f_{3i}(\xi) \right] \end{aligned} \tag{7.149}$$

in which

$$\begin{aligned} N_{1i}(\xi) &= \left[h_{52}(\xi) - h_{42}(\xi) \right] \left[h_{33}(\xi) g_{2i} - h_{23}(\xi) g_{3i} \right] \\ &\quad + \left[h_{53}(\xi) - h_{43}(\xi) \right] \left[h_{22}(\xi) g_{3i} - h_{32}(\xi) g_{2i} \right], \\ P_{1i}(\xi) &= \frac{1}{\xi} \left[h_{23}(\xi) h_{32}(\xi) - h_{22}(\xi) h_{33}(\xi) \right] g_{5i}, \\ W_{1i}(\xi) &= \frac{1}{\xi} \left[h_{23}(\xi) h_{32}(\xi) - h_{22}(\xi) h_{33}(\xi) \right] g_{4i} \end{aligned} \tag{7.150}$$

$$
\begin{aligned}
N_{2i}(\xi) &= \left[h_{53}(\xi) - h_{43}(\xi)\right]\left[h_{31}(\xi)g_{2i} - h_{21}(\xi)g_{3i}\right] \\
&\quad + \left[h_{51}(\xi) - h_{41}(\xi)\right]\left[h_{23}(\xi)g_{3i} - h_{33}(\xi)g_{2i}\right], \\
P_{2i}(\xi) &= \frac{1}{\xi}\left[h_{21}(\xi)h_{33}(\xi) - h_{23}(\xi)h_{31}(\xi)\right]g_{5i}, \\
W_{2i}(\xi) &= \frac{1}{\xi}\left[h_{21}(\xi)h_{33}(\xi) - h_{23}(\xi)h_{31}(\xi)\right]g_{4i}
\end{aligned}
\tag{7.151}
$$

$$
\begin{aligned}
N_{3i}(\xi) &= \left[h_{51}(\xi) - h_{41}(\xi)\right]\left[h_{32}(\xi)g_{2i} - h_{22}(\xi)g_{3i}\right] \\
&\quad + \left[h_{52}(\xi) - h_{42}(\xi)\right]\left[h_{21}(\xi)g_{3i} - h_{31}(\xi)g_{2i}\right], \\
P_{3i}(\xi) &= \frac{1}{\xi}\left[h_{22}(\xi)h_{31}(\xi) - h_{21}(\xi)h_{32}(\xi)\right]g_{5i}, \\
W_{3i}(\xi) &= \frac{1}{\xi}\left[h_{22}(\xi)h_{31}(\xi) - h_{21}(\xi)h_{32}(\xi)\right]g_{4i}
\end{aligned}
\tag{7.152}
$$

$$
\begin{aligned}
\Delta(\xi) &= \left\{\left[-h_{53}(\xi) + h_{43}(\xi)\right]h_{32}(\xi) + \left[h_{52}(\xi) - h_{42}(\xi)\right]h_{33}(\xi)\right\}h_{21}(\xi) \\
&\quad + \left\{\left[h_{53}(\xi) - h_{43}(\xi)\right]h_{31}(\xi) + \left[-h_{51}(\xi) + h_{41}(\xi)\right]h_{33}(\xi)\right\}h_{22}(\xi) \\
&\quad + \left\{\left[h_{51}(\xi) - h_{41}(\xi)\right]h_{32}(\xi) + \left[-h_{52}(\xi) + h_{42}(\xi)\right]h_{31}(\xi)\right\}h_{23}(\xi)
\end{aligned}
\tag{7.153}
$$

with

$$
h_{4i}(\xi) = \frac{c_{11} - c_{12}}{2}\frac{1}{\mu_i^2}I_2\left(\frac{\xi b}{\mu_i}\right), \quad g_{4i} = \frac{c_{11} - c_{12}}{2}M_i\mu_i \tag{7.154}
$$

$$
h_{5i}(\xi) = \frac{F_{5i}}{\mu_i^2}I_0\left(\frac{\xi b}{\mu_i}\right), \quad g_{5i} = F_{5i}M_i\mu_i \tag{7.155}
$$

and the remaining steps are the same as those in Case 1.

Then we can obtain a Fredholm integral equation of the second kind which is exactly the same as that given in Eqs. (7.143) and (7.144), except that the kernel $L(\alpha, \beta)$ takes the form

$$
\begin{aligned}
L(\alpha,\beta) &= \frac{4}{\pi^2 m_0}\sum_{j=1}^{3}\frac{F_{1j}}{\mu_j}\int_0^{\infty}\frac{1}{\Delta(\xi)}\sinh\left(\frac{\xi\alpha}{\mu_j}\right)\sum_{i=1}^{3}\frac{1}{\mu_i^2}\sinh\left(\frac{\xi\beta}{\mu_i}\right) \\
&\quad \times\left\{N_{ji}(\xi)K_1\left(\frac{\xi b}{\mu_i}\right) - \frac{\xi}{\mu_i}P_{ji}(\xi)K_0\left(\frac{\xi b}{\mu_i}\right) + \frac{\xi}{\mu_i}W_{ji}(\xi)K_2\left(\frac{\xi b}{\mu_i}\right)\right\}\mathrm{d}\xi
\end{aligned}
\tag{7.156}
$$

The field intensity factors are then expressed in the form

$$
\begin{aligned}
K_{\mathrm{I}} &= \lim_{r\to a^+}\sqrt{2\pi(r-a)}\sigma_{zz}(r,0) = \sqrt{\frac{\pi}{a}}m_0\psi(a),\\
K_D &= \lim_{r\to a^+}\sqrt{2\pi(r-a)}D_z(r,0) = \sqrt{\frac{\pi}{a}}m_1\psi(a),\\
K_\varepsilon &= \lim_{r\to a^+}\sqrt{2\pi(r-a)}\varepsilon_{zz}(r,0) = \sqrt{\frac{\pi}{a}}m_2\psi(a),\\
K_E &= \lim_{r\to a^+}\sqrt{2\pi(r-a)}E_z(r,0) = \sqrt{\frac{\pi}{a}}m_3\psi(a)
\end{aligned}
\tag{7.157}
$$

in which

$$
\begin{aligned}
m_0 &= -(M_1F_{11} + M_2F_{12} + M_3F_{13}),\\
m_1 &= -(F_{21}M_1 + F_{22}M_2 + F_{23}M_3),\\
m_2 &= -(k_{11}\mu_1^2M_1 + k_{12}\mu_1^2M_2 + k_{13}\mu_1^3M_3),\\
m_3 &= -(k_{21}\mu_1^2M_1 + k_{22}\mu_2^2M_2 + k_{23}\mu_3^2M_3)
\end{aligned}
\tag{7.158}
$$

and K_{I}, K_D, K_ε, and K_E are the stress intensity factor, electric displacement intensity factor, strain intensity factor and electric field intensity factor, respectively.

7.6.3 Numerical results and discussion

The material used in the numerical analysis is PZT-6B ceramic and its material properties are as follows:

Elastic constants (10^{10} N/m^2) : $c_{11} = 16.8,\ c_{12} = 6.0,\ c_{33} = 16.3,\ c_{55} = 2.71$;

Piezoelectric constants(C/m^2): $e_{15} = 4.6,\ e_{31} = -0.9,\ e_{33} = 7.1$;

Dielectric permittivities (10^{-10} F/m): $\kappa_{11} = 36,\ \kappa_{33} = 34$, $d_{33} = 34$.

From Eqs. (7.122)-(7.129), it is clear that once the functions $A_i(\xi)$, $B_i(\xi)$ are known, the stress and electric displacement inside the piezoelectric cylinder can be obtained. Determination of the stress intensity factor requires solution of the function $\psi(\xi)$. The Fredholm integral equation of the second kind (7.146) can be solved numerically using a Gaussian quadrature formula. Then we can estimate all intensity factors using Eq. (7.157).

It can be found easily that the stress intensity factor is not dependent on the mechanical loading unless the piezoelectric cylinder is under the far-field stress and electric displacement in these two loading cases. This observation confirms the results presented in [4,5]. The variation of the normalized stress intensity factor, electric displacement intensity factor and strain intensity factor with the ratio of crack radius to PZT-6B cylinder radius is shown in Fig. 7.6. It can be seen that all the

intensity factors have a similar distribution along the dimensionless crack radius. When the value of a/b increases from 0.0 to 0.65 the normalized intensity factors remain constant, but when the value exceeds 0.65, all intensity factors increase rapidly. However, the intensity factors increase more rapidly in Case 2 than in Case 1, which may be caused by the different loading conditions on the surface of the piezoelectric cylinder in radial direction.

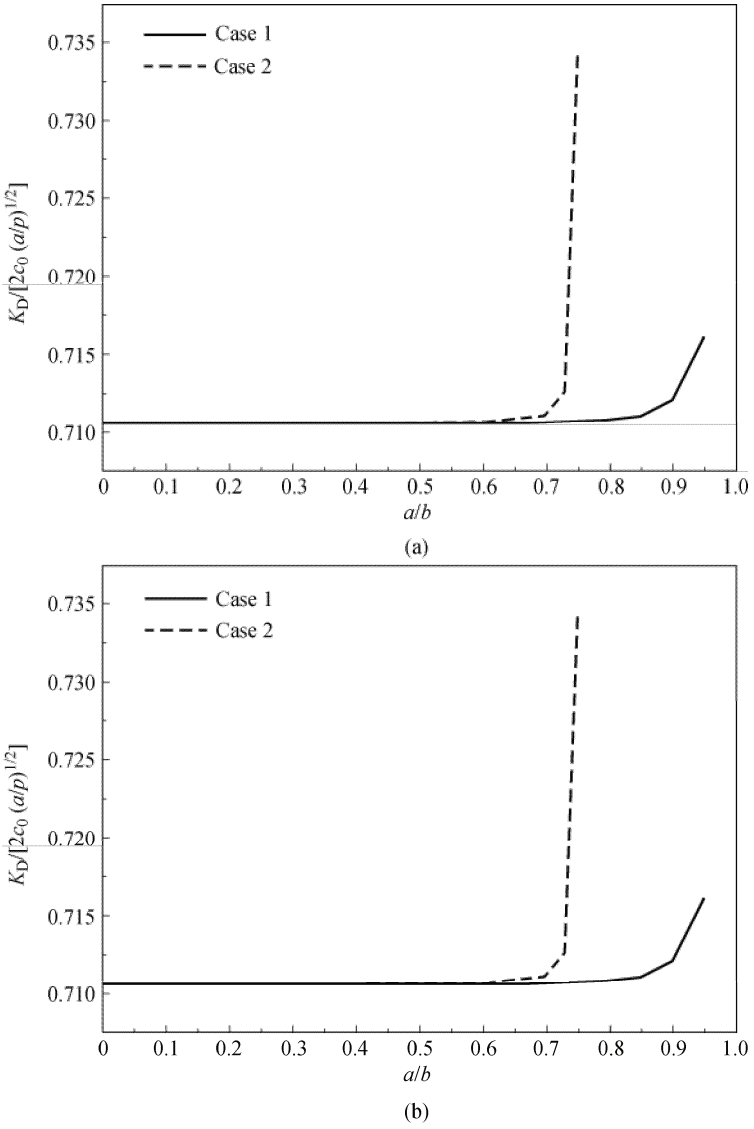

Fig. 7.6 (a) Normalized stress intensity factor against the ratio *a*/*b*; (b) Normalized electric displacement intensity factor against the ratio *a*/*b*; (c) Normalized strain intensity factor against the ratio *a*/*b*.

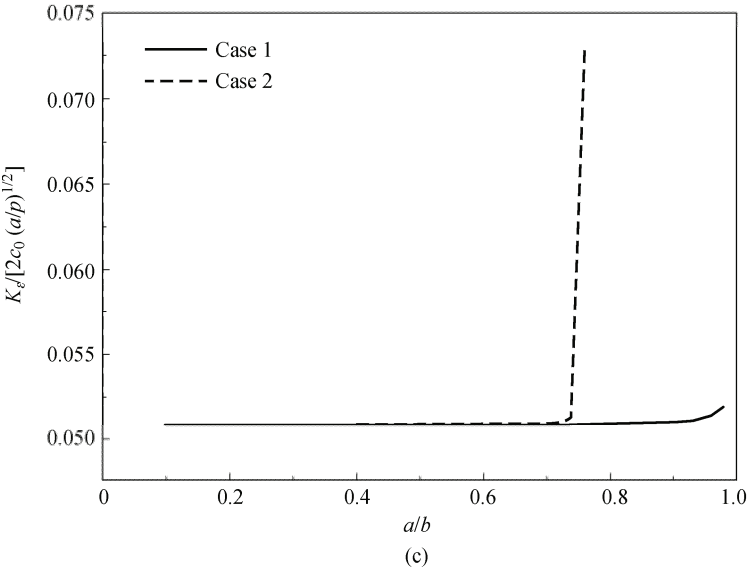

Fig. 7.6 Continued.

7.7 A fiber with a penny-shaped crack and an elastic coating

In the previous section we presented a solution to the problem of a penny-shaped crack in a piezoelectric cylinder. The problem of a penny-shaped crack in a piezoelectric fiber with an elastic coating is described in this section. By using the potential function method and Hankel transform, this problem is formulated as the solution of a system of dual integral equations which are reduced to a Fredholm integral equation of the second kind. Numerical analysis is conducted to investigate the effect of the thickness and the elastic material properties of the coating on the fracture behavior of piezoelectric fiber composites.

7.7.1 Formulation of the problem

Consider a piezoelectric fiber with a finite elastic coating and containing a centered penny-shaped crack of radius a under axisymmetric electromechanical loading (Fig. 7.7). For convenience, a cylindrical coordinate system (r,θ,z) originating at the center of the crack is used, with the z-axis along the axis of symmetry of the cylinder. The fiber is assumed to be a transversely isotropic piezoelectric material with

the poling direction parallel to the z-axis, and the elastic coating is also transversely isotropic. They are subjected to the far-field of a normal strain, $\varepsilon_z = \overline{\varepsilon}(r)$ and a normal electric loading, $E_z = \overline{E}(r)$.

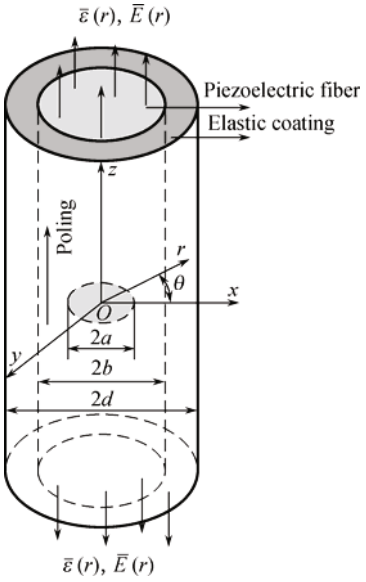

Fig. 7.7 Piezoelectric fiber with a finite elastic coating and containing a pennyshaped crack under mechanical and electrical loading.

The constitutive equations for piezoelectric materials which are transversely isotropic and poled along the z-axis are defined in Eqs. (7.1)-(7.6) and the governing equations used are Eqs. (7.115). As in the previous section, the potential functions (7.120) are employed and rewritten as follows:

$$u_r = \sum_{i=1}^{3} \Phi_{i,r}, \quad u_z = \sum_{i=1}^{3} k_{1i} \Phi_{i,z}, \quad \phi = -\sum_{i=1}^{3} k_{2i} \Phi_{i,z} \tag{7.159}$$

Substituting Eq. (7.159) into the field equations (7.115), we again obtain Eq. (7.119).

It is obvious from Fig. 7.7 that the problem is subject to the following boundary conditions:

$$\begin{aligned} &\sigma_{zz}(r,0) = 0 \quad (0 \leqslant r < a), \\ &u_z(r,0) = 0 \quad (a < r < b), \\ &\phi(r,0) = 0 \quad (a < r < b), \\ &\sigma_{rz}(r,0) = 0 \quad (0 \leqslant r < b) \end{aligned} \tag{7.160}$$

$$\begin{aligned} &D_z(r,0^+) = D_z(r,0^-) \quad (0 \leqslant r < a),\\ &E_r(r,0^+) = E_r(r,0^-) \quad (0 \leqslant r < a),\\ &D_r(b,z) = 0 \qquad\qquad (0 < z < \infty) \end{aligned} \tag{7.161}$$

In this section, the following continuity and loading conditions are used:

(1) The continuity conditions for elastic displacements and tractions at the interface between the fiber and elastic coating $(0 < z < \infty)$ are given by

$$\begin{aligned} &u_z(b,z) = u_z^c(b,z), \quad u_r(b,z) = u_r^c(b,z),\\ &\sigma_r(b,z) = \sigma_r^c(b,z), \quad \sigma_{rz}(b,z) = \sigma_{rz}^c(b,z) \end{aligned} \tag{7.162}$$

(2) Loading conditions at infinity are

$$\varepsilon_z(r,\infty) = \overline{\varepsilon}(r), \qquad E_z(r,\infty) = \overline{E}(r), \qquad \varepsilon_z^c(r,\infty) = \overline{\varepsilon}(r) \tag{7.163}$$

(3) Loading conditions over the surface of the coating are

$$u_r^c(d,z) = 0, \quad \sigma_{rz}^c(d,z) = 0 \qquad (0 < z < \infty) \tag{7.164}$$

where the superscript "c" represents the related variable associated with the coating material.

Following the procedure discussed in Section 7.6, the electric and elastic fields for the piezoelectric fiber have the same form as those of Eqs. (7.121)-(7.131).

For the elastic coating, the corresponding potential functions can be assumed in the form

$$u_z^c = \sum_{i=1}^{2} k_i^c \frac{\partial \Phi_i^c}{\partial z}, \quad u_r^c = \sum_{i=1}^{2} \frac{\partial \Phi_i^c}{\partial r} \tag{7.165}$$

In a manner similar to that discussed in Section 7.6, the potential functions for the elastic coating layer can be assumed in the form

$$\Phi_i^c(r,z) = \int_0^\infty \frac{1}{\xi}\left[C_i(\xi) I_0\left(\frac{\xi r}{\mu_i^c}\right) + D_i(\xi) K_0\left(\frac{\xi r}{\mu_i^c}\right)\right] \cos(\xi z)\mathrm{d}\xi \tag{7.166}$$

Making use of Eq. (7.166), the elastic displacements and stresses in the elastic coating can be given in the form

$$u_z^c(r,z) = -\sum_{i=1}^{2} k_i^c \int_0^\infty \left[C_i(\xi) I_0\left(\frac{\xi r}{\mu_i^c}\right) + D_i(\xi) K_0\left(\frac{\xi r}{\mu_i^c}\right)\right] \sin(\xi z)\mathrm{d}\xi + \overline{a}(r) z \tag{7.167}$$

$$u_r^c(r,z) = \sum_{i=1}^{2} \frac{1}{\mu_i^c} \int_0^\infty \left[C_i(\xi) I_1\left(\frac{\xi r}{\mu_i^c}\right) - D_i(\xi) K_1\left(\frac{\xi r}{\mu_i^c}\right)\right] \cos(\xi z)\mathrm{d}\xi \tag{7.168}$$

$$\sigma_r^c(r,z)=-\sum_{i=1}^{2}\frac{F_{3i}^c}{s_i^{c2}}\int_0^\infty \xi\left[C_i(\xi)I_0\left(\frac{\xi r}{\mu_i^c}\right)+D_i(\xi)K_0\left(\frac{\xi r}{\mu_i^c}\right)\right]\cos(\xi z)\mathrm{d}\xi$$
$$+\frac{c_{11}^c-c_{12}^c}{2}\sum_{i=1}^{2}\frac{1}{(\mu_i^c)^2}\int_0^\infty \xi\left[C_i(\xi)I_2\left(\frac{\xi r}{\mu_i^c}\right)+D_i(\xi)K_2\left(\frac{\xi r}{\mu_i^c}\right)\right]\cos(\xi z)\mathrm{d}\xi \tag{7.169}$$

$$\sigma_{rz}^c(r,z)=-\sum_{i=1}^{2}\frac{F_{2i}^c}{\mu_i^{c2}}\int_0^\infty \xi\left[C_i(\xi)I_1\left(\frac{\xi r}{\mu_i^c}\right)-D_i(\xi)K_1\left(\frac{\xi r}{\mu_i^c}\right)\right]\sin(\xi z)\mathrm{d}\xi \tag{7.170}$$

in which

$$F_{2i}^c=c_{44}^c(1+k_i^c)\mu_i^c,\quad F_{3i}^c=c_{13}^c k_i^c(\mu_i^c)^2-\frac{c_{11}^c+c_{12}^c}{2} \tag{7.171}$$

Using the boundary conditions (7.160)-(7.164), the Fourier inversion theorem and the Hankel inversion theorem, we obtain

$$A_1(\xi)=\frac{1}{\Delta(\xi)}\sum_{i=1}^{3}\left[N_{1i}(\xi)f_{1i}(\xi)+P_{1i}(\xi)f_{2i}(\xi)+W_{1i}(\xi)f_{3i}(\xi)+Y_{1i}(\xi)f_{4i}(\xi)\right] \tag{7.172}$$

$$A_2(\xi)=\frac{1}{\Delta(\xi)}\sum_{i=1}^{3}\left[N_{2i}(\xi)f_{1i}(\xi)+P_{2i}(\xi)f_{2i}(\xi)+W_{2i}(\xi)f_{3i}(\xi)+Y_{2i}(\xi)f_{4i}(\xi)\right] \tag{7.173}$$

$$A_3(\xi)=\frac{1}{\Delta(\xi)}\sum_{i=1}^{3}\left[N_{3i}(\xi)f_{1i}(\xi)+P_{3i}(\xi)f_{2i}(\xi)+W_{3i}(\xi)f_{3i}(\xi)+Y_{3i}(\xi)f_{4i}(\xi)\right] \tag{7.174}$$

$$C_1(\xi)=\sum_{i=1}^{3}\left[M_{3i}A_i(\xi)+M_{4i}(\xi)f_{2i}(\xi)\right] \tag{7.175}$$

$$C_2(\xi)=\sum_{i=1}^{3}\left[M_{5i}A_i(\xi)+M_{6i}(\xi)f_{2i}(\xi)\right] \tag{7.176}$$

$$D_1(\xi)=\sum_{i=1}^{2}M_{1i}C_i(\xi) \tag{7.177}$$

$$D_2(\xi)=\sum_{i=1}^{2}M_{2i}C_i(\xi) \tag{7.178}$$

in which

$$N_{1i}(\xi)=\left[H_{13}(\xi)H_{32}(\xi)-H_{12}(\xi)H_{33}(\xi)\right]g_{1i}(\xi)+\left[h_{13}(\xi)H_{32}(\xi)-H_{12}(\xi)H_{33}(\xi)\right]h_{5i}(\xi),$$
$$N_{2i}(\xi)=\left[H_{11}(\xi)H_{33}(\xi)-H_{31}(\xi)H_{13}(\xi)\right]g_{1i}(\xi)+\left[h_{11}(\xi)H_{33}(\xi)-H_{13}(\xi)H_{31}(\xi)\right]h_{5i}(\xi),$$
$$N_{3i}(\xi)=\left[H_{12}(\xi)H_{31}(\xi)-H_{11}(\xi)H_{32}(\xi)\right]g_{1i}(\xi)+\left[h_{12}(\xi)H_{31}(\xi)-H_{11}(\xi)H_{32}(\xi)\right]h_{5i}(\xi)$$

$$P_{1i}(\xi)=\left[h_{13}(\xi)H_{32}(\xi)-h_{12}(\xi)H_{33}(\xi)\right]H_{2i}(\xi)+\left[h_{12}(\xi)H_{13}(\xi)-h_{13}(\xi)H_{12}(\xi)\right]H_{4i}(\xi),$$

$$P_{2i}(\xi)=\left[h_{11}(\xi)H_{33}(\xi)-h_{13}(\xi)H_{31}(\xi)\right]H_{2i}(\xi)+\left[h_{13}(\xi)H_{11}(\xi)-h_{11}(\xi)H_{13}(\xi)\right]H_{4i}(\xi),$$

$$P_{3i}(\xi)=\left[h_{12}(\xi)H_{31}(\xi)-h_{11}(\xi)H_{32}(\xi)\right]H_{2i}(\xi)+\left[h_{11}(\xi)H_{12}(\xi)-h_{12}(\xi)H_{11}(\xi)\right]H_{4i}(\xi)$$

$$W_{1i}(\xi)=\left[h_{13}(\xi)H_{12}(\xi)-h_{12}(\xi)H_{13}(\xi)\right]h_{8i}(\xi),$$

$$W_{2i}(\xi)=\left[h_{11}(\xi)H_{13}(\xi)-h_{13}(\xi)H_{11}(\xi)\right]h_{8i}(\xi),$$

$$W_{3i}(\xi)=\left[h_{12}(\xi)H_{11}(\xi)-h_{11}(\xi)H_{12}(\xi)\right]h_{8i}(\xi),$$

$$Y_{1i}(\xi)=\left[h_{13}(\xi)H_{12}(\xi)-h_{12}(\xi)H_{13}(\xi)\right]h_{9i}(\xi),$$

$$Y_{2i}(\xi)=\left[h_{11}(\xi)H_{13}(\xi)-h_{13}(\xi)H_{11}(\xi)\right]h_{9i}(\xi),$$

$$Y_{3i}(\xi)=\left[h_{12}(\xi)H_{11}(\xi)-h_{11}(\xi)H_{12}(\xi)\right]h_{9i}(\xi),$$

$$\begin{aligned}\Delta(\xi)=&\,h_{11}(\xi)\left[H_{13}(\xi)H_{32}(\xi)-H_{12}(\xi)H_{33}(\xi)\right]\\&+h_{12}(\xi)\left[H_{11}(\xi)H_{33}(\xi)-H_{31}(\xi)H_{13}(\xi)\right]\\&+h_{13}(\xi)\left[H_{12}(\xi)H_{31}(\xi)-H_{11}(\xi)H_{32}(\xi)\right]\end{aligned}$$

$$f_{1i}(\xi)=\frac{2}{\pi}\int_0^\infty\frac{\eta B_1(\eta)J_1(\eta b)}{\eta^2\mu_i^2+\xi^2}\mathrm{d}\eta,\quad f_{2i}(\xi)=\frac{2}{\pi}\int_0^\infty\frac{B_1(\eta)J_0(\eta b)}{\eta^2\mu_i^2+\xi^2}\mathrm{d}\eta\ ,$$

$$f_{3i}(\xi)=\frac{2}{\pi}\int_0^\infty\frac{\eta^2 B_1(\eta)J_0(\eta b)}{\eta^2\mu_i^2+\xi^2}\mathrm{d}\eta,\quad f_{4i}(\xi)=\frac{2}{\pi}\int_0^\infty\frac{\eta^2 B_1(\eta)J_2(\eta b)}{\eta^2\mu_i^2+\xi^2}\mathrm{d}\eta$$

where $B_i(\xi)$ and the related coefficients M_i are defined by Eqs. (7.135) and (7.136), respectively, and $h_{ji}(\xi)$, $M_{ij}(\xi)$, and $H_{ji}(\xi)$ are defined as

$$h_{1i}(\xi)=\frac{F_{4i}}{\mu_i^{\,2}}I_1\left(\frac{\xi b}{\mu_i}\right),\quad h_{2i}(\xi)=k_{1i}I_0\left(\frac{\xi b}{s_i}\right),\quad h_{3i}=k_{1i}M_i\mu_i\ ,$$

$$h_{4i}=\frac{1}{\mu_i}I_1\left(\frac{\xi b}{\mu_i}\right),\quad h_{5i}=M_i\mu_i,\quad h_{6i}=\frac{F_{5i}}{\mu_i^{\,2}}I_0\left(\frac{\xi b}{\mu_i}\right),$$

$$h_{7i}=\frac{c_{11}-c_{12}}{2}\frac{1}{\mu_i^{\,2}}I_2\left(\frac{\xi b}{\mu_i}\right),\quad h_{8i}=F_{5i}M_i\mu_i,\quad h_{9i}=\frac{c_{11}-c_{12}}{2}M_i\mu_i,$$

$$h_{10i}=\frac{F_{3i}}{\mu_i^{\,2}}I_1\left(\frac{\xi b}{\mu_i}\right),\quad h_{11i}=F_{3i}M_i$$

$$M_{1i}(\xi)=\frac{g_{13,2}(\xi)g_{14,i}(\xi)-g_{15,2}(\xi)g_{12,i}(\xi)}{g_{13,2}(\xi)g_{15,1}(\xi)-g_{15,2}(\xi)g_{13,1}(\xi)},$$

$$M_{2i}(\xi)=\frac{g_{13,1}(\xi)g_{14,i}(\xi)-g_{15,1}(\xi)g_{12,i}(\xi)}{g_{13,1}(\xi)g_{15,2}(\xi)-g_{15,1}(\xi)g_{13,2}(\xi)},$$

$$M_{3i}(\xi)=\frac{G_{22}(\xi)h_{2i}(\xi)-G_{12}(\xi)h_{10i}(\xi)}{G_{22}(\xi)G_{11}(\xi)-G_{12}(\xi)G_{21}},$$

$$M_{4i}(\xi)=\frac{G_{22}(\xi)h_{3i}(\xi)+G_{12}(\xi)h_{11i}(\xi)}{G_{22}(\xi)G_{11}(\xi)-G_{12}(\xi)G_{21}},$$

$$M_{5i}(\xi)=\frac{G_{21}(\xi)h_{2i}(\xi)-G_{11}(\xi)h_{10i}(\xi)}{G_{21}(\xi)G_{12}(\xi)-G_{11}(\xi)G_{22}},$$

$$M_{6i}(\xi)=\frac{G_{21}(\xi)h_{3i}(\xi)+G_{11}(\xi)h_{11i}(\xi)}{G_{21}(\xi)G_{12}(\xi)-G_{11}(\xi)G_{22}}$$

$$H_{1i}(\xi)=t_i(\xi)M_{3i}(\xi)+t_2(\xi)M_{5i}(\xi)-h_{4i}(\xi),$$

$$H_{2i}(\xi)=t_1(\xi)M_{4i}(\xi)+t_2(\xi)M_{6i}(\xi),$$

$$H_{3i}(\xi)=r_1(\xi)M_{3i}(\xi)+r_2(\xi)M_{5i}(\xi)-\left[h_{7i}(\xi)-h_{6i}(\xi)\right]\xi,$$

$$H_{4i}(\xi)=r_1(\xi)M_{4i}(\xi)+r_2(\xi)M_{6i}(\xi)$$

$$G_{1i}(\xi)=g_{2i}(\xi)+g_{31}(\xi)M_{1i}(\xi)+g_{32}(\xi)M_{2i}(\xi),$$

$$G_{2i}(\xi)=g_{10,i}(\xi)-g_{11,1}(\xi)M_{1i}(\xi)-g_{11,2}(\xi)M_{2i}(\xi)$$

$$t_i(\xi)=g_{4i}(\xi)-g_{51}(\xi)M_{1i}(\xi)-g_{52}(\xi)M_{2i}(\xi)$$

$$r_i(\xi)=\left[g_{7i}(\xi)-g_{6i}(\xi)\right]\xi+\left[g_{91}(\xi)-g_{81}(\xi)\right]\xi M_{1i}(\xi)+\left[g_{92}(\xi)-g_{82}(\xi)\right]\xi M_{2i}(\xi)$$

$$g_{1i}(\xi)=F_{4i}M_i(\xi),\quad g_{2i}=k_i^cI_0\left(\frac{\xi b}{\mu_i^c}\right),\quad g_{3i}=k_i^cK_0\left(\frac{\xi b}{\mu_i^c}\right),$$

$$g_{4i}=\frac{1}{\mu_i^c}\left(\frac{\xi b}{\mu_i^c}\right),\quad g_{5i}=\frac{1}{\mu_i^c}K_1\left(\frac{\xi b}{\mu_i^c}\right),\quad g_{6i}=\frac{F_{3i}^c}{(\mu_i^c)^2}I_0\left(\frac{\xi b}{\mu_i^c}\right),$$

$$g_{7i}=\frac{c_{11}^c-c_{12}^c}{2}\frac{1}{(\mu_i^c)^2}I_2\left(\frac{\xi b}{\mu_i^c}\right),\quad g_{8i}=\frac{F_{3i}^c}{\mu_i^c}K_0\left(\frac{\xi b}{\mu_i^c}\right),\quad g_{9i}=\frac{c_{11}^c-c_{12}^c}{2}\frac{1}{(\mu_i^c)^2}K_2\left(\frac{\xi b}{\mu_i^c}\right),$$

$$g_{10i}=\frac{F_{2i}^c}{(\mu_i^c)^2}I_1\left(\frac{\xi b}{\mu_i^c}\right),\quad g_{11i}=\frac{F_{2i}^c}{(\mu_i^c)^2}K_1\left(\frac{\xi b}{\mu_i^c}\right),\quad g_{12i}=\frac{1}{\mu_i^c}I_1\left(\frac{\xi \mathrm{d}}{\mu_i^c}\right),$$

$$g_{13i}=\frac{1}{\mu_i^c}K_1\left(\frac{\xi d}{\mu_i^c}\right),\quad g_{14i}=\frac{F_{2i}^c}{(\mu_i^c)^2}I_1\left(\frac{\xi d}{\mu_i^c}\right),\quad g_{15i}=\frac{F_{2i}^c}{(\mu_i^c)^2}K_1\left(\frac{\xi d}{\mu_i^c}\right)$$

7.7.2 Fredholm integral equation of the problem

Making use of Eqs. $(7.160)_{1,2}$ and (7.172)-(7.178), the following system of dual integral equations can be deduced:

$$-\int_0^\infty \xi\left[\frac{F_{11}}{\mu_1^2}I_0\left(\frac{\xi r}{\mu_1}\right)A_1(\xi)+\frac{F_{12}}{\mu_2^2}I_0\left(\frac{\xi r}{\mu_2}\right)A_2(\xi)+\frac{F_{13}}{\mu_3^2}I_0\left(\frac{\xi r}{\mu_3}\right)A_3(\xi)\right]\mathrm{d}\xi$$
$$+\int_0^\infty \xi\left[M_1F_{11}+M_2F_{12}+M_3F_{13}\right]B_1(\xi)J_0(\xi r)\mathrm{d}\xi=-\overline{c}(r)\qquad(0\leqslant r<a)\tag{7.179}$$

$$\int_0^\infty\left[M_1k_{11}\mu_1+M_2k_{12}\mu_2+M_3k_{13}\mu_3\right]B_1(\xi)J_0(\xi r)\mathrm{d}\xi=0\quad(a<r<b)\tag{7.180}$$

These equations can be solved using the function $\psi(\alpha)$ defined by

$$B_1(\xi)=\int_0^a\psi(\alpha)\sin(\xi\alpha)\mathrm{d}\alpha\tag{7.181}$$

where $\psi(0)=0$.

Using the solutions of integral equations defined in Section 7.6.2, we can obtain a Fredholm integral equation of the second kind in the form

$$\psi(\alpha)+\int_0^a\psi(\beta)L(\alpha,\beta)\mathrm{d}\beta=\frac{2}{\pi m_0}\int_0^a\frac{r\overline{c}(r)}{\sqrt{\alpha^2-r^2}}\mathrm{d}r\tag{7.182}$$

in which

$$L(\alpha,\beta)=\frac{4}{\pi^2m_0}\sum_{j=1}^3\frac{F_{1j}}{\mu_j}\int_0^\infty\frac{1}{\Delta(\xi)}\sinh\left(\frac{\xi\alpha}{\mu_j}\right)\sum_{i=1}^3\frac{1}{\mu_i^2}\sinh\left(\frac{\xi\beta}{\mu_i}\right)\left[N_{ji}(\xi)K_1\left(\frac{\xi b}{\mu_i}\right)\right.$$
$$\left.+\frac{\mu_i}{\xi}P_{ji}(\xi)K_0\left(\frac{\xi b}{\mu_i}\right)-\frac{\xi}{\mu_i}W_{ji}(\xi)K_0\left(\frac{\xi b}{\mu_i}\right)+\frac{\xi}{\mu_i}Y_{ji}(\xi)K_2\left(\frac{\xi b}{\mu_i}\right)\right]\mathrm{d}\xi\tag{7.183}$$

The stress intensity can thus be expressed in terms of function $\psi(\xi)$, as in [5]:

$$K_{\mathrm{I}}=\lim_{r\to a^+}\sqrt{2\pi(r-a)}\sigma_{zz}(r,0)=\sqrt{\frac{\pi}{a}}m_0\psi(a)\tag{7.184}$$

in which

$$m_0 = -(M_1 F_{11} + M_2 F_{12} + M_3 F_{13}) \tag{7.185}$$

7.7.3 Numerical results and discussion

To investigate the effect of elastic coating on the fracture behavior of piezoelectric fiber composites, numerical studies are conducted based on the analytic solutions obtained above. Material properties used in this study are:

(1) Piezoelectric fiber:

Elastic constants (10^{10} N/m^2) : $c_{11} = 16.8,\ c_{12} = 6.0,\ c_{33} = 16.3,\ c_{44} = 2.71$;

Piezoelectric constants (C/m^2): $e_{15} = 4.6,\ e_{31} = -0.9,\ e_{33} = 7.1$;

Dielectric permittivities (10^{-10} F/m) : $\kappa_{11} = 36,\ \kappa_{33} = 34$.

(2) Elastic coating:

Elastic constants (10^{10} N/m^2) :

$$c_{11} = 0.83,\ c_{12} = 0.28,\ c_{13} = 0.03,\ c_{33} = 8.68,\ c_{55} = 0.42.$$

It can be seen from Eq. (7.184) that determination of the stress intensity factor requires solution of the function $\psi(\xi)$. The Fredholm integral equation of the second kind (7.182) can be solved numerically using a Gaussian quadrature formula. In the calculation, $b = 40$ mm, $\bar{\varepsilon}(r) = 1.0 \times 10^{-5}$, $\bar{\bar{E}}(r) = 10 \times 10^5\ \mathrm{V \cdot m}$, are used.

The variations of the normalized stress intensity factor with the ratio of crack radius to fiber radius a/b under different thickness and elastic constants of the coating are shown in Figs. 7.8 and 7.9. It can be seen from Fig. 7.8 that the stress intensity factor decreases with increase of the ratio a/b, which is different from the results in [28]. It is also evident that thickness of the elastic coating has an important effect on the stress intensity factor, and greater thickness will lead to a higher decay rate and a smaller value of the stress intensity factor. This means that thicker coating layers can slow crack propagation.

The variation of the stress intensity factor with the ratio a/b under different elastic constants c_{33} of the coating layer is plotted in Fig. 7.9. It can be seen from the figure that the stress intensity factor may increase or decrease with the ratio a/b depending on the value of c_{33} of the coating. When c_{33} of the coating is greater than that of the piezoelectric fiber, the stress intensity factor will increase along with an increase in the a/b. Obviously, the decay rate of the stress intensity factor depends strongly on the value of c_{33} when it is smaller than that of the piezoelectric fiber.

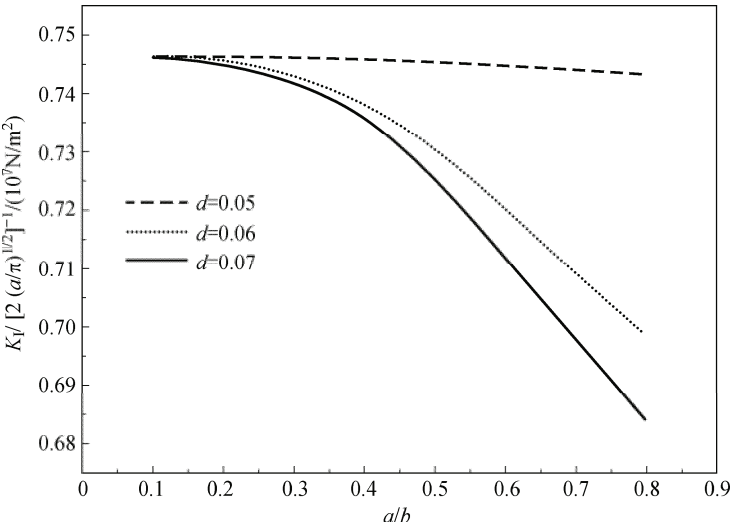

Fig.7.8 Variation of the stress intensity factor with the ratio a/b under different thicknesses of the coating.

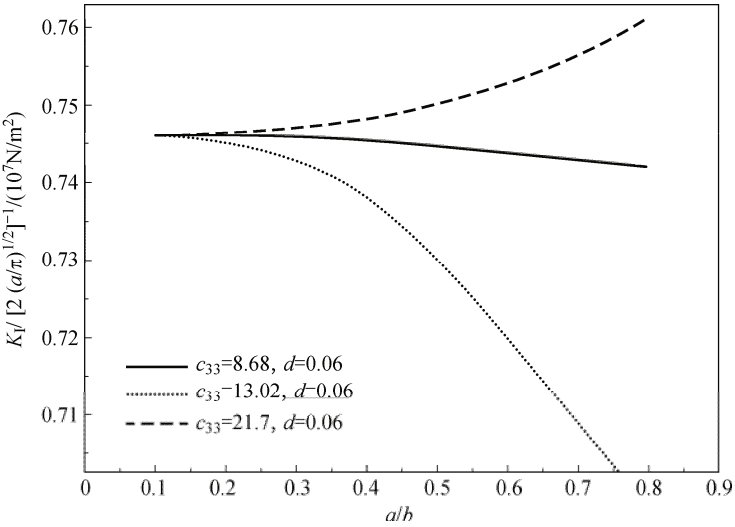

Fig.7.9 Variation of the stress intensity factor with the ratio a/b under different elastic constants c_{33} of the coating.

References

[1] Yu SW, Qin QH: Damage analysis of thermopiezoelectric properties .2. Effective

crack model. Theoretical and Applied Fracture Mechanics **25**(3), 279-288 (1996).

[2] Qin QH, Yu SW: An arbitrarily-oriented plane crack terminating at the interface between dissimilar piezoelectric materials. International Journal of Solids and Structures **34**(5), 581-590 (1997).

[3] Qin QH, Mai YW: A closed crack tip model for interface cracks in thermopiezoelectric materials. International Journal of Solids and Structures **36**(16), 2463-2479 (1999).

[4] Narita F, Lin S, Shindo Y: Penny-shaped crack in a piezoceramic cylinder under mode Ⅰ loading. Archives of Mechanics **55**(3), 275-304 (2003).

[5] Yang JH, Lee KY: Penny shaped crack in a piezoelectric cylinder surrounded by an elastic medium subjected to combined in-plane mechanical and electrical loads. International Journal of Solids and Structures **40**(3), 573-590 (2003).

[6] Lin S, Narita F, Shindo Y: Electroelastic analysis of a piezoelectric cylindrical fiber with a penny-shaped crack embedded in a matrix. International Journal of Solids and Structures **40**(19), 5157-5174 (2003).

[7] Kogan L, Hui CY, Molkov V: Stress and induction field of a spheroidal inclusion or a penny-shaped crack in a transversely isotropic piezoelectric material. International Journal of Solids and Structures **33**(19), 2719-2737 (1996).

[8] Karapetian E, Sevostianov I, Kachanov M: Penny-shaped and half-plane cracks in a transversely isotropic piezoelectric solid under arbitrary loading. Archive of Applied Mechanics **70**(1-3), 201-229 (2000).

[9] Chen WQ, Shioya T: Complete and exact solutions of a penny-shaped crack in a piezoelectric solid: antisymmetric shear loadings. International Journal of Solids and Structures **37**(18), 2603-2619 (2000).

[10] Yang FQ: General solutions of a penny-shaped crack in a piezoelectric material under opening mode-Ⅰ loading. Quarterly Journal of Mechanics and Applied Mathematics **57**(4), 529-550 (2004).

[11] Eriksson K: Energy release rates for the penny-shaped crack in a linear piezoelectric solid. International Journal of Fracture **116**(2), L23-L28 (2002).

[12] Yang JH, Lee KY: Penny-shaped crack in a piezoelectric cylinder under electromechanical loads. Archive of Applied Mechanics **73**, 323-336 (2003).

[13] Wang BL, Noda N, Han JC, Du SY: A penny-shaped crack in a transversely isotropic piezoelectric layer. European Journal of Mechanics A:Solids **20**(6), 997-1005 (2001).

[14] Li XF, Lee KY: Effects of electric field on crack growth for a penny-shaped dielectric crack in a piezoelectric layer. Journal of the Mechanics and Physics of Solids **52**(9), 2079-2100 (2004).

[15] Feng WJ, Li YS, Ren DL: Transient response of a piezoelectric layer with a penny-shaped crack under electromechanical impacts. Structural Engineering and Mechanics **23**(2), 163-175 (2006).

[16] Eshelby JD: The determination of the elastic field of an ellipsoidal inclusion, and related problems. Proceedings of the Royal Society of London Series A:Mathematical

and Physical Sciences **241**(1226), 376-396 (1957).

[17] Wang B: 3-dimensional analysis of a flat elliptic crack in a piezoelectric material. International Journal of Engineering Science **30**(6), 781-791 (1992).

[18] Huang JH: A fracture criterion of a penny-shaped crack in transversely isotropic piezoelectric media. International Journal of Solids and Structures **34**(20), 2631-2644 (1997).

[19] Chiang CR, Weng GJ: The nature of stress and electric-displacement concentrations around a strongly oblate cavity in a transversely isotropic piezoelectric material. International Journal of Fracture **134**(3-4), 319-337 (2005).

[20] Lin S, Narita F, Shindo Y: Electroelastic analysis of a penny-shaped crack in a piezoelectric ceramic under mode Ⅰ loading. Mechanics Research Communications **30**(4), 371-386 (2003).

[21] Kudryavtsev BA, Parton VZ, Rakitin VI: Breakdown mechanics of piezoelectric materials:axisymmeric crack on boundary with conductor. Prikladnaya Matematika I Mekhanika **39**(2), 352-362 (1975).

[22] Chen WQ, Shioya T, Ding HJ: Integral equations for mixed boundary value problem of a piezoelectric half-space and the applications. Mechanics Research Communications **26**(5), 583-590 (1999).

[23] Qin QH, Wang JS, Li XL: Effect of elastic coating on fracture behaviour of piezoelectric fibre with a penny-shaped crack. Composite Structures **75**(1-4), 465-471 (2006).

[24] Chen WQ, Shioya T: Fundamental solution for a penny-shaped crack in a piezoelectric medium. Journal of the Mechanics and Physics of Solids **47**(7), 1459-1475 (1999).

[25] Wang JS, Qin QH: Penny-shaped crack in a solid piezoelectric cylinder with two typical boundary conditions. Journal of Beijing University of Technology **32**(SUPPL), 29-34 (2006).

[26] Qin QH: Fracture Mechanics of Piezoelectric Materials. WIT Press, Southampton (2001).

[27] Yang JH, Lee KY: Penny shaped crack in a three-dimensional piezoelectric strip under in-plane normal loadings. Acta Mechanica **148**(1-4), 187-197 (2001).

[28] He LH, Lim CW: Electromechanical responses of piezoelectric fiber composites with sliding interface under anti-plane deformations. Composites Part B:Engineering **34**(4), 373-381 (2003).

Chapter 8 Solution Methods for Functionally Graded Piezoelectric Materials

In the previous two chapters Saint-Venant decay and penny-shaped crack problems were discussed. The material properties of the piezoelectric materials considered there were homogeneous or piecewise homogeneous. This chapter presents solution methods for piezoelectric materials with continuously varying properties. It focuses on problems of an angularly graded piezoelectric wedge, solutions for FGPM beams, problems of parallel cracks in an FGPM strip, and mode Ⅲ cracks in a two-bonded FGPM.

8.1 Introduction

FGMs are composite materials formed of two or more constituent phases with a continuously variable composition. During design, the requirements of structural strength, reliability and lifetime of piezoelectric structures/components call for enhanced mechanical performance, including stress and deformation distribution under multifield loading. In recent years, the emergence of FGMs has demonstrated that they have the potential to reduce stress concentration and to provide improved residual stress distribution, enhanced thermal properties, and higher fracture toughness. Consequently, a new kind of material, FGPM, has been developed to improve the reliability of piezoelectric structures by extending the concept of the well-known FGM to piezoelectric materials [1]. At present, FGPMs are usually associated with particulate composites where the volume fraction of particles varies in one or several directions. One of the advantages of a monotonous variation of volume fraction of constituent phases is elimination of the stress discontinuities that are often encountered in laminated composites and accordingly, avoidance of delamination-related problems. How all these aspects can be improved and what the mechanisms might be are popular topics which have received much attention from researchers. Wang and Noda [2] investigated the thermally induced fracture of a functionally graded piezoelectric layer bonded to a metal. Ueda studied the fracture of an FGPM strip with a normal crack [3,4], of a symmetrical FGPM strip with a center crack [5] due to a thermal load, mixed-mode thermoelectromechanical fracture problems for an FGPM strip with a two-dimensional crack [6,7], and a penny-shaped crack [8,9]. Li and Weng [10] solved the problem of an FGPM strip containing a finite crack normal to boundary surfaces. Hu et al. [11] studied the problem of a crack located in a functionally graded piezoelectric interlayer between two dissimilar homogeneous piezoelectric half-planes. Rao and Kuna [12] presented an interaction integral method for computing stress intensity factors (SIFs)

and electric displacement intensity factor (EDIF) for cracks in FGPMs under thermoelectromechanical loading. Borrelli et al. [13] used the energy-decay inequality technique to analyze the decay behavior of end effects in anti-plane shear deformation in piezoelectric solids and FGPMs. Zhong and Shang [14] developed an exact solution for a functionally graded piezothermoelectric rectangular plate. Dai et al. [15] conducted a theoretical study of electromagnetoelastic behavior for an FGPM cylinder and sphere. They then extended their solutions to include thermal effects [16]. Zhong and Yu [17] presented a general solution for an FGPM beam with arbitrarily graded material properties along the beam thickness direction. Based on the layerwise finite element model, Shakeri and Mirzaeifar [18] performed a static and dynamic analysis of a thick FGM plate with piezoelectric layers. Wang et al. [19] analytically investigated the axisymmetric bending of circular plates whose material properties vary along the thickness. Using the Fourier transform technique, Chue and Yeh [20] developed a system of singular integral equations for angle cracks in two bonded FGPMs under anti-plane shear. Chue and Ou [21] presented a solution for Mode Ⅲ crack in two bonded FGPMs. More recently, Li and Ding [22] presented a solution to the problem of a periodic array of parallel cracks in an FGPM strip bonded to an FGP substrate. Chen and Bian [23] studied wave propagation characteristics of an axially polarized, functionally graded, piezoceramic cylindrical transducer submerged in an infinite fluid medium. Ueda [24] addressed the problem of two coplanar cracks in an FGPM strip under transient thermal loading. Salah et al. [25] examined the propagation of ultrasonic guided waves in FGPMs. Wang et al. [26] studied the singularity behavior of electroelastic fields in a wedge with angularly graded piezoelectric material(AGPM) under anti-plane deformation. Chue and Yeh [27] extended the results of [21] to the case of two arbitrarily oriented cracks in two bonded FGM strips. This chapter focuses on the developments in [17,21,22,26].

8.2 Singularity analysis of angularly graded piezoelectric wedge

Analytical solutions of AGPM presented in [26] are described in this section. The mixed variable state space formulation for an AGPM wedge under anti-plane deformation is used to investigate the singular behavior of stresses and electric fields at the apex of AGPM wedges under anti-plane deformation.

8.2.1 Basic formulations and the state space equation

In [26], Wang et al. considered an AGPM wedge with angularly graded material properties such as shear modulus, piezoelectric constant and dielectric constant, as shown in Fig. 8.1, under anti-plane deformation. The poling direction is along the

z-axis perpendicular to the r-θ plane, where r and θ are polar coordinates. The constitutive relation equations are defined by Eq. (1.35), where the material constants c_{44}, e_{15}, and κ_{11} are assumed to vary in the following exponential form:

$$c_{44}(\theta) = c_{44}^0 e^{\eta\theta}, \quad e_{15}(\theta) = e_{15}^0 e^{\eta\theta}, \quad \varepsilon_{11}(\theta) = \kappa_{11}^0 e^{\eta\theta} \tag{8.1}$$

and the subscripts "1", "2", "4", and "5" in Eq. (1.35) are now replaced by "θz", "rz", "r" and "θ", respectively.

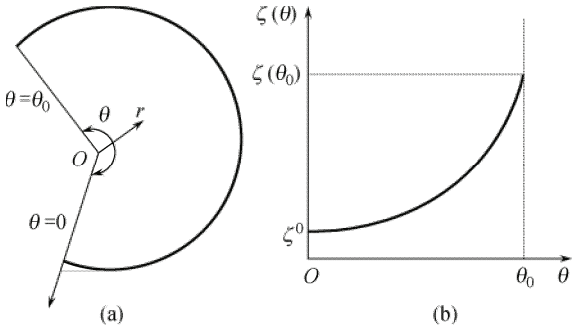

Fig. 8.1 (a) Diagram of an AGPM wedge; (b) Variation of material properties.

In Eq. (8.1), η represents the inhomogeneity degree of the material gradient along the angular direction. Using Eq. (8.1), η can be written as

$$\eta = \frac{1}{\theta}\ln\frac{\zeta(\theta)}{\zeta^0} \qquad (\zeta = c_{44},\ e_{15},\ \text{or}\ \kappa_{11}) \tag{8.2}$$

where ζ^0 represents c_{44}^0, e_{15}^0, or κ_{11}^0, which is the associated material property at $\theta = 0$ and is known as the reference material parameter.

The governing, the shear strain-displacement, and the electric field-electric potential equations are defined by Eqs. (5.1) and (5.2) with $T = Q = 0$.

To simplify the derivation and transform the differential equations (5.1) and (5.2) into a state space equation, define the following state variables:

$$\begin{aligned} S_\theta &= e^{-\eta\theta} r\tau_{\theta z}, \qquad SD_\theta = e^{-\eta\theta} rD_\theta, \\ S_r &= e^{-\eta\theta} r\tau_{rz}, \qquad SD_r = e^{-\eta\theta} rD_r \end{aligned} \tag{8.3}$$

From Eqs. (1.35), (5.1), and (5.2), we have

$$\begin{aligned} \frac{\partial(r\tau_{rz})}{\partial r} &= \frac{1}{r}\frac{\partial(r\tau_{rz})}{\partial\xi} = -\frac{\partial\tau_{\theta z}}{\partial\theta} = -\frac{1}{r}c_{44}^0 e^{\eta\theta}\left(\frac{\partial^2 w}{\partial\theta^2} + \eta\frac{\partial w}{\partial\theta}\right) - \frac{1}{r}e_{15}^0 e^{\eta\theta}\left(\frac{\partial^2\phi}{\partial\theta^2} + \eta\frac{\partial\phi}{\partial\theta}\right), \\ \frac{\partial(rD_r)}{\partial r} &= \frac{1}{r}\frac{\partial(rD_r)}{\partial\xi} = -\frac{\partial D_\theta}{\partial\theta} = -\frac{1}{r}e_{15}^0 e^{\eta\theta}\left(\frac{\partial^2 w}{\partial\theta^2} + \eta\frac{\partial w}{\partial\theta}\right) + \frac{1}{r}\kappa_{11}^0 e^{\eta\theta}\left(\frac{\partial^2\phi}{\partial\theta^2} + \eta\frac{\partial\phi}{\partial\theta}\right) \end{aligned} \tag{8.4}$$

and then the following equations can be obtained:

$$\begin{aligned}\dot{S}_r &= -c_{44}^0\left(\frac{\partial^2 w}{\partial\theta^2}+\eta\frac{\partial w}{\partial\theta}\right)-e_{15}^0\left(\frac{\partial^2\phi}{\partial\theta^2}+\eta\frac{\partial\phi}{\partial\theta}\right),\\ S\dot{D}_r &= -e_{15}^0\left(\frac{\partial^2 w}{\partial\theta^2}+\eta\frac{\partial w}{\partial\theta}\right)+\kappa_{11}^0\left(\frac{\partial^2\phi}{\partial\theta^2}+\eta\frac{\partial\phi}{\partial\theta}\right)\end{aligned} \tag{8.5}$$

where "$\cdot$" denotes the differential with respect to ξ which is defined in Eq. (5.5).

The combination of Eqs. (1.35) and (5.2) leads to the following equation:

$$\dot{S}_r = c_{44}^0\dot{w}+e_{15}^0\dot{\phi}, \quad S\dot{D}_r = e_{15}^0\dot{w}-\kappa_{11}^0\dot{\phi} \tag{8.6}$$

Then we obtain

$$\dot{w} = \frac{\kappa_{11}^0}{\Delta}S_r+\frac{e_{15}^0}{\Delta}SD_r, \quad \dot{\phi} = \frac{e_{15}^0}{\Delta}S_r-\frac{c_{44}^0}{\Delta}SD_r \tag{8.7}$$

in which

$$\Delta = (e_{15}^0)^2+c_{44}^0\kappa_{11}^0 \tag{8.8}$$

Equations (8.5) and (8.7) can be rewritten into the following matrix form:

$$\left\{\dot{\mathbf{p}}^{\mathrm{T}},\dot{\mathbf{q}}^{\mathrm{T}}\right\}^{\mathrm{T}} = \mathbf{H}\left\{\mathbf{p}^{\mathrm{T}},\mathbf{q}^{\mathrm{T}}\right\}^{\mathrm{T}} \tag{8.9}$$

in which

$$\mathbf{p} = \left\{w,\phi\right\}^{\mathrm{T}}, \quad \mathbf{q} = \left\{S_r,SD_r\right\}^{\mathrm{T}} \tag{8.10}$$

$$\mathbf{H} = \begin{bmatrix} 0 & 0 & \frac{\kappa_{11}^0}{\Delta} & \frac{e_{15}^0}{\Delta} \\ 0 & 0 & \frac{e_{15}^0}{\Delta} & -\frac{c_{44}^0}{\Delta} \\ -c_{44}^0\left(\frac{\partial^2}{\partial\theta^2}+\eta\frac{\partial}{\partial\theta}\right) & -e_{15}^0\left(\frac{\partial^2}{\partial\theta^2}+\eta\frac{\partial}{\partial\theta}\right) & 0 & 0 \\ -e_{15}^0\left(\frac{\partial^2}{\partial\theta^2}+\eta\frac{\partial}{\partial\theta}\right) & \kappa_{11}^0\left(\frac{\partial^2}{\partial\theta^2}+\eta\frac{\partial}{\partial\theta}\right) & 0 & 0 \end{bmatrix} \tag{8.11}$$

Then Eq. (8.9) can be simplified into the state space equation (2.136), where

$$\mathbf{v} = \left\{\mathbf{p}^{\mathrm{T}},\mathbf{q}^{\mathrm{T}}\right\}^{\mathrm{T}} \tag{8.12}$$

We can then assume

$$\mathbf{v}(\xi,\theta) = \boldsymbol{\kappa}(\xi)\boldsymbol{\psi}(\theta) \tag{8.13}$$

in which

$$\boldsymbol{\psi}(\theta)=\left\{\mathbf{q}^{\mathrm{T}}(\theta),\ \mathbf{p}^{\mathrm{T}}(\theta)\right\}^{\mathrm{T}} \tag{8.14}$$

Using the separate variables method, we have

$$\boldsymbol{\kappa}(\xi)=e^{\mu\,\xi}=r^{\mu} \tag{8.15}$$

$$\mathbf{H}\boldsymbol{\psi}=\mu\boldsymbol{\psi} \tag{8.16}$$

Thus, the following equations can be obtained:

$$\left\{w,\ \ \phi\right\}^{\mathrm{T}}=r^{\mu}\left\{w(\theta),\phi(\theta)\right\}^{\mathrm{T}},\quad \left\{\tau_{rz},D_r\right\}^{\mathrm{T}}=r^{\mu-1}e^{\eta\theta}\left\{\tau_{rz}(\theta),D_r(\theta)\right\}^{\mathrm{T}} \tag{8.17}$$

It can be seen from Eq. (8.17) that the stress and electric field have the $\mathrm{Re}(\mu-1)$ singularity at the apex of the AGPM wedge when $r\to 0$.

It should be mentioned that in the case of homogeneous piezoelectric material ($\eta=0$) the operator matrix $\mathbf{H}$ is a Hamiltonian operator matrix and Eq. (8.9) is a Hamiltonian equation [28], whereas in the case of inhomogeneous piezoelectric material ($\eta\neq 0$), $\mathbf{H}$ is not a Hamiltonian operator matrix, because of the material inhomogeneity, and thus the governing equation cannot be directed into the Hamiltonian system, and it is difficult to find the adjoint symplectic orthonormalization eigenvector $\boldsymbol{\Psi}$ to obtain the electroelastic fields using a procedure similar to that in [28]. However, the singular order can still be obtained, which also corresponds to the nonzero eigenvalue of the operator matrix. The singular order k is given as

$$k=\mathrm{Re}(\mu-1) \tag{8.18}$$

and μ must satisfy the condition $0<\mathrm{Re}(\mu)<1$.

To find the nonzero-eigenvalue μ, we have from Eq. (8.16):

$$\left|\mathbf{H}-\mu\mathbf{I}\right|=0 \tag{8.19}$$

in which $\mathrm{d}/\mathrm{d}\theta$ is replaced by λ and $\mathrm{d}^2/\mathrm{d}\theta^2$ is replaced by λ^2, and $\mathbf{I}$ is the four-order identity matrix. Eq. (8.19) can be simplified to

$$(\lambda^2+\eta\lambda+\mu^2)^2=0 \tag{8.20}$$

Then we can obtain the solution of λ as

$$\lambda_{1,2}=-\frac{\eta}{2}+\frac{1}{2}\sqrt{\eta^2-4\mu^2},\qquad \lambda_{3,4}=-\frac{\eta}{2}-\frac{1}{2}\sqrt{\eta^2-4\mu^2} \tag{8.21}$$

In the case of $\eta^2-4\mu^2\leqslant 0$, we can easily reach

$$
\begin{aligned}
\tilde{w} &= e^{-\frac{\eta}{2}\theta}\left[A_1\cos\left(\frac{m}{2}\theta\right)+B_1\sin\left(\frac{m}{2}\theta\right)+C_1\theta\cos\left(\frac{m}{2}\theta\right)+D_1\theta\sin\left(\frac{m}{2}\theta\right)\right],\\
\tilde{\phi} &= e^{-\frac{\eta}{2}\theta}\left[A_2\cos\left(\frac{m}{2}\theta\right)+B_2\sin\left(\frac{m}{2}\theta\right)+C_2\theta\cos\left(\frac{m}{2}\theta\right)+D_2\theta\sin\left(\frac{m}{2}\theta\right)\right],\\
\tilde{S}_r &= e^{-\frac{\eta}{2}\theta}\left[A_3\cos\left(\frac{m}{2}\theta\right)+B_3\sin\left(\frac{m}{2}\theta\right)+C_3\theta\cos\left(\frac{m}{2}\theta\right)+D_3\theta\sin\left(\frac{m}{2}\theta\right)\right],\\
S\tilde{D}_r &= e^{-\frac{\eta}{2}\theta}\left[A_4\cos\left(\frac{m}{2}\theta\right)+B_4\sin\left(\frac{m}{2}\theta\right)+C_4\theta\cos\left(\frac{m}{2}\theta\right)+D_4\theta\sin\left(\frac{m}{2}\theta\right)\right]
\end{aligned}
\tag{8.22}
$$

in which $\left\{\tilde{w}\quad\tilde{\phi}\quad\tilde{S}_r\quad S\tilde{D}_r\right\}=e^{-\mu\xi}\left\{w\quad\phi\quad S_r\quad SD_r\right\}$, A_i, B_i, C_i, D_i (i=1-4) are unknown constants to be determined, and

$$
m=\sqrt{4\mu^2-\eta^2} \tag{8.23}
$$

Substituting Eq. (8.22) into Eq. (8.16) leads to the following relationships between the unknown constants:

$$
\begin{aligned}
&A_3=\mu(c_{44}^0A_1+e_{15}^0A_2), \qquad A_4=\mu(e_{15}^0A_1-\kappa_{11}^0A_2),\\
&B_3=\mu(c_{44}^0B_1+e_{15}^0B_2), \qquad B_4=\mu(e_{15}^0B_1-\kappa_{11}^0B_2),\\
&C_i=D_i=0 \qquad (i=1\text{-}4)
\end{aligned}
\tag{8.24}
$$

By using Eq. (8.24), Eq. (8.22) can be rewritten as

$$
\begin{aligned}
\tilde{w} &= e^{-\frac{\eta}{2}\theta}\left[A_1\cos\left(\frac{m}{2}\theta\right)+B_1\sin\left(\frac{m}{2}\theta\right)\right],\\
\tilde{\phi} &= e^{-\frac{\eta}{2}\theta}\left[A_2\cos\left(\frac{m}{2}\theta\right)+B_2\sin\left(\frac{m}{2}\theta\right)\right],\\
\tilde{S}_r &= e^{-\frac{\eta}{2}\theta}\left[\mu c_{44}^0\cos\left(\frac{m}{2}\theta\right)A_1+\mu e_{15}^0\cos\left(\frac{m}{2}\theta\right)A_2+\mu c_{44}^0\sin\left(\frac{m}{2}\theta\right)B_1\right.\\
&\quad\left.+\mu e_{15}^0\sin\left(\frac{m}{2}\theta\right)B_2\right],\\
S\tilde{D}_r &= e^{-\frac{\eta}{2}\theta}\left[\mu e_{15}^0\cos\left(\frac{m}{2}\theta\right)A_1-\mu\kappa_{11}^0\cos\left(\frac{m}{2}\theta\right)A_2+\mu e_{15}^0\sin\left(\frac{m}{2}\theta\right)B_1\right.\\
&\quad\left.-\mu\kappa_{11}^0\sin\left(\frac{m}{2}\theta\right)B_2\right]
\end{aligned}
\tag{8.25}
$$

From Eqs. (1.35) and (8.25), we have

$$
\begin{aligned}
S_\theta^{(\theta)} &= c_{44}^0P(\theta)A_1+e_{15}^0P(\theta)A_2-c_{44}^0N(\theta)B_1-e_{15}^0N(\theta)B_2,\\
SD_\theta^{(\theta)} &= e_{15}^0P(\theta)A_1-\kappa_{11}^0P(\theta)A_2-e_{15}^0N(\theta)B_1+\kappa_{11}^0N(\theta)B_2
\end{aligned}
\tag{8.26}
$$

where

$$\begin{aligned} P(\theta) &= -\frac{1}{2}e^{-\frac{\eta}{2}\theta}\left[m\sin\left(\frac{m}{2}\theta\right)+\eta\cos\left(\frac{m}{2}\theta\right)\right], \\ N(\theta) &= -\frac{1}{2}e^{-\frac{\eta}{2}\theta}\left[m\cos\left(\frac{m}{2}\theta\right)-\eta\sin\left(\frac{m}{2}\theta\right)\right] \end{aligned} \tag{8.27}$$

Considering the AGPM wedge shown in Fig. 8.1, the conditions at the edges are assumed to be free of traction and electrically insulated:

$$\tau_{\theta z}(r,0) = \tau_{\theta z}(r,\theta_0) = D_\theta(r,0) = D_\theta(r,\theta_0) = 0 \tag{8.28}$$

Substituting Eq. (8.26) into Eq. (8.28), the following equation can be obtained:

$$\begin{bmatrix} c_{44}^0 P(\theta_0) & e_{15}^0 P(\theta_0) & -c_{44}^0 N(\theta_0) & -e_{15}^0 N(\theta_0) \\ e_{15}^0 P(\theta_0) & -\kappa_{11}^0 P(\theta_0) & -e_{15}^0 N(\theta_0) & \kappa_{11}^0 N(\theta_0) \\ c_{44}^0 P(0) & e_{15}^0 P(0) & -c_{44}^0 N(0) & -e_{15}^0 N(0) \\ e_{15}^0 P(0) & -\kappa_{11}^0 P(0) & -e_{15}^0 N(0) & \kappa_{11}^0 N(0) \end{bmatrix} \begin{Bmatrix} A_1 \\ A_2 \\ B_1 \\ B_2 \end{Bmatrix} = 0 \tag{8.29}$$

The existence of nonzero solutions $\{A_1 \quad A_2 \quad B_1 \quad B_2\}^{\mathrm{T}}$ requires the determinant of the coefficients matrix to be zero, which can lead to the equation

$$16\Delta^2\mu^2\sin^2\left(\frac{m}{2}\theta_0\right) = 0 \tag{8.30}$$

Thus, we obtain

$$m = \frac{2n\pi}{\theta_0} \qquad (n=1,2,\cdots) \tag{8.31}$$

Using Eq. (8.23) the eigenvalue can be obtained as follows:

$$\mu = \sqrt{\frac{\eta^2}{4}+\frac{\pi^2}{\theta_0^2}} \tag{8.32}$$

Using the condition: $0 < \mu < 1$, it can be determined that the wedge angle θ_0 must satisfy the following condition if there are singular electroelastic fields at the apex of the single AGPM wedge:

$$\sqrt{\pi^2+\frac{1}{4}\ln^2\left(\frac{c_{44}(\theta_0)}{c_{44}^0}\right)} < \theta_0 \leqslant 2\pi \tag{8.33}$$

In the case of $\eta^2 - 4\mu^2 < 0$, using a procedure similar to that from Eq. (8.22) to Eq. (8.31) we can easily prove that this is an impossible occurrence.

8.2.2 Two AGPM wedges

For a bi-material wedge system consisting of two AGPMs as shown in Fig. 8.2, considered traction free and electrically insulated, the boundary conditions are as follows:

$$\tau_{\theta z}^{(1)}(r,\alpha) = \tau_{\theta z}^{(2)}(r,-\beta) = D_{\theta}^{(1)}(r,\alpha) = D_{\theta}^{(2)}(r,-\beta) = 0 \tag{8.34}$$

in which the superscripts "(1)" and "(2)" denote AGPM1 and AGPM2, respectively, and $\alpha = \theta_2 - \theta_1$, $\beta = \theta_1 - \theta_0$. If the two AGPMs are fully bonded at the interface, the continuity conditions on the interface are

$$\begin{aligned} &\tau_{\theta z}^{(1)}(r,0) = \tau_{\theta z}^{(2)}(r,0), \qquad w^{(1)}(r,0) = w^{(2)}(r,0), \\ &D_{\theta}^{(1)}(r,0) = D_{\theta}^{(2)}(r,0), \qquad E_r^{(1)}(r,0) = E_r^{(2)}(r,0) \end{aligned} \tag{8.35}$$

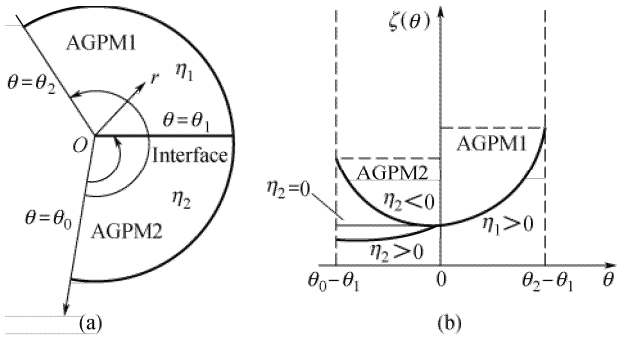

Fig. 8.2 Diagram of a bi-AGPM wedge system and the variation of the materials' inhomogeneity. (a) Geometry configuration of the AGPM1-AGPM2 wedge system; (b) Variation of material properties with the angle variable θ.

Using Eqs. (8.26) and (8.35), we can obtain

$$\begin{Bmatrix} A_1^{(2)} \\ A_2^{(2)} \\ B_1^{(2)} \\ B_2^{(2)} \end{Bmatrix} = \begin{bmatrix} 1 & 0 & 0 & 0 \\ 0 & 1 & 0 & 0 \\ a_{11} & a_{12} & a_{13} & a_{14} \\ a_{21} & a_{22} & a_{23} & a_{24} \end{bmatrix} \begin{Bmatrix} A_1^{(1)} \\ A_2^{(1)} \\ B_1^{(1)} \\ B_2^{(1)} \end{Bmatrix} \tag{8.36}$$

where a_{1i} and a_{2i} (i = 1-4) are given as

$$
\begin{aligned}
a_{11} &= \frac{1}{\Delta_0}\left[\eta^{(1)}(e_{15}^{(1)}e_{15}^{(2)} + c_{44}^{(1)}\kappa_{11}^{(2)}) - \eta^{(2)}(e_{15}^{(2)^2} + c_{44}^{(2)}\kappa_{11}^{(2)})\right], \\
a_{12} &= \frac{1}{\Delta_0}\left[\eta^{(1)}(e_{15}^{(1)}\kappa_{11}^{(2)} - e_{15}^{(2)}\kappa_{11}^{(1)})\right], \quad a_{13} = \frac{1}{\Delta_0}\left[m^{(1)}(-e_{15}^{(1)}e_{15}^{(2)} - c_{44}^{(1)}\kappa_{11}^{(2)})\right], \\
a_{14} &= \frac{1}{\Delta_0}\left[m^{(1)}(e_{15}^{(2)}\kappa_{11}^{(1)} - e_{15}^{(1)}\kappa_{11}^{(2)})\right], \quad a_{21} = \frac{1}{\Delta_0}\left[\eta^{(1)}(-e_{15}^{(1)}c_{44}^{(2)} + e_{15}^{(2)}c_{44}^{(1)})\right], \\
a_{22} &= \frac{1}{\Delta_0}\left[\eta^{(1)}(e_{15}^{(1)}e_{15}^{(2)} + c_{44}^{(2)}\kappa_{11}^{(1)}) - \eta^{(2)}(e_{15}^{(2)^2} + c_{44}^{(2)}\kappa_{11}^{(2)})\right], \\
a_{23} &= \frac{1}{\Delta_0}\left[m^{(1)}(e_{15}^{(1)}c_{44}^{(2)} - e_{15}^{(2)}c_{44}^{(1)})\right], \quad a_{24} = \frac{1}{\Delta_0}\left[m^{(1)}(-c_{44}^{(2)}\kappa_{11}^{(1)} - e_{15}^{(2)}e_{15}^{(1)})\right]
\end{aligned}
\tag{8.37}
$$

with

$$
\Delta_0 = -m^{(2)}(e_{15}^{(2)^2} + c_{44}^{(2)}\kappa_{11}^{(2)}), \quad m^{(i)} = \sqrt{4\mu - \left(\eta^{(i)}\right)^2}
\tag{8.38}
$$

Combination of Eqs. (8.26), (8.34), and (8.35) leads to the equation

$$
\left[\mathbf{M}\right]\left\{\mathbf{F}^{(1)}\right\} = 0
\tag{8.39}
$$

where

$$
\mathbf{F}^{(1)} = \left\{A_1^{(1)} \quad A_2^{(1)} \quad B_1^{(1)} \quad B_2^{(1)}\right\}^{\mathrm{T}}
\tag{8.40}
$$

$$
\left[\mathbf{M}\right] = \begin{bmatrix}
c_{44}^{(1)}P^{(1)}(\alpha) & e_{15}^{(1)}P^{(1)}(\alpha) & -c_{44}^{(1)}N^{(1)}(\alpha) & -e_{15}^{(1)}N^{(1)}(\alpha) \\
e_{15}^{(1)}P^{(1)}(\alpha) & -\kappa_{11}^{(1)}P^{(1)}(\alpha) & -e_{15}^{(1)}N^{(1)}(\alpha) & \kappa_{11}^{(1)}N^{(1)}(\alpha) \\
b_{11} & b_{12} & b_{13} & b_{14} \\
b_{21} & b_{22} & b_{23} & b_{24}
\end{bmatrix}
\tag{8.41}
$$

with b_{1i} and b_{2i} (i = 1-4) being given as

$$
\begin{aligned}
b_{11} &= c_{44}^{(2)}P^{(2)}(-\beta) - N^{(2)}(-\beta)(a_{11}c_{44}^{(2)} + a_{21}e_{15}^{(2)}), \\
b_{12} &= e_{15}^{(2)}P^{(2)}(-\beta) - N^{(2)}(-\beta)(a_{12}c_{44}^{(2)} + a_{22}e_{15}^{(2)}), \\
b_{13} &= -N^{(2)}(-\beta)(a_{13}c_{44}^{(2)} + a_{23}e_{15}^{(2)}), \\
b_{14} &= -N^{(2)}(-\beta)(a_{14}c_{44}^{(2)} + a_{24}e_{15}^{(2)}), \\
b_{21} &= e_{15}^{(2)}P^{(2)}(-\beta) - N^{(2)}(-\beta)(a_{11}e_{15}^{(2)} - a_{21}\kappa_{11}^{(2)}), \\
b_{22} &= -\kappa_{11}^{(2)}P^{(2)}(-\beta) - N^{(2)}(-\beta)(a_{12}e_{15}^{(2)} - a_{22}\kappa_{11}^{(2)}), \\
b_{23} &= -N^{(2)}(-\beta)(a_{13}e_{15}^{(2)} - a_{23}\kappa_{11}^{(2)}), \\
b_{24} &= -N^{(2)}(-\beta)(a_{14}e_{15}^{(2)} - a_{24}\kappa_{11}^{(2)})
\end{aligned}
\tag{8.42}
$$

In the following, the case of an AGPM-AGM wedge system is taken as a special case for an AGPM-AGPM wedge. In Fig. 8.2, AGPM1 is replaced by AGM1. The boundary conditions for the AGPM-AGM wedge now become

$$\tau_{\theta z}^{(1)}(r,\alpha)=\tau_{\theta z}^{(2)}(r,-\beta)=D_{\theta}^{(1)}(r,\alpha)=0 \tag{8.43}$$

and the continuity conditions at the interface are

$$\tau_{\theta z}^{(1)}(r,0)=\tau_{\theta z}^{(2)}(r,0),\quad w^{(1)}(r,0)=w^{(2)}(r,0),\quad D_{\theta}^{(1)}(r,0)=0 \tag{8.44}$$

Then, following a procedure similar to that for Eq. (8.36), we can arrive at

$$\begin{aligned}
&A_2^{(1)}=\frac{e_{15}^{(1)}}{\kappa_{11}^{(1)}}A_1^{(1)}-\frac{e_{15}^{(1)}}{\kappa_{11}^{(1)}}\frac{m^{(1)}}{\eta^{(1)}}B_1^{(1)}+\frac{m^{(1)}}{\eta^{(1)}}B_2^{(1)},\quad A_1^{(2)}=A_1^{(1)},\\
&B_1^{(2)}=\frac{c_{44}^{(2)}\eta^{(2)}-\delta^{(1)}\eta^{(1)}}{c_{44}^{(2)}}\frac{1}{m^{(2)}}A_1^{(1)}+\frac{\delta^{(1)}}{c_{44}^{(2)}}\frac{m^{(1)}}{m^{(2)}}B_1^{(1)}
\end{aligned} \tag{8.45}$$

in which

$$\delta^{(1)}=c_{44}^{(1)}+\frac{e_{15}^{(1)2}}{\kappa_{11}^{(1)}} \tag{8.46}$$

Using the boundary conditions Eqs. (8.43) and (8.45), the following equation can be obtained:

$$\begin{bmatrix}
\delta^{(1)}P^{(1)}(\alpha) & -\dfrac{e_{15}^{(1)2}}{\kappa_{11}^{(1)}}\dfrac{m^{(1)}}{\eta^{(1)}}P^{(1)}(\alpha)-c_{44}^{(1)}N^{(1)}(\alpha) & e_{15}^{(1)}\left[\dfrac{m^{(1)}}{\eta^{(1)}}P^{(1)}(\alpha)-N^{(1)}(\alpha)\right]\\
0 & e_{15}^{(1)}\left[\dfrac{m^{(1)}}{\eta^{(1)}}P^{(1)}(\alpha)-N^{(1)}(\alpha)\right] & \kappa_{11}^{(1)}\left[N^{(1)}(\alpha)-\dfrac{m^{(1)}}{\eta^{(1)}}P^{(1)}(\alpha)\right]\\
a^{*} & -\delta^{(1)}\dfrac{m^{(1)}}{m^{(2)}}N^{(2)}(-\beta) & 0
\end{bmatrix}
\begin{Bmatrix}A_1^{(1)}\\B_1^{(1)}\\B_2^{(1)}\end{Bmatrix}=0 \tag{8.47}$$

where

$$a^{*}=c_{44}^{(2)}P^{(2)}(-\beta)+\left[\delta^{(1)}\eta^{(1)}-c_{44}^{(2)}\eta^{(2)}\right]\frac{1}{m^{(2)}}N^{(2)}(-\beta) \tag{8.48}$$

If AGM1 is a conductor such as aluminum or nickel, the continuity conditions are the same as in Eq. (8.44) except that $D_{\theta}^{(1)}(r,0)=0$ is replaced by $\phi^{(1)}(r,0)=$

0 . The boundary conditions are the same as those given in Eq. (8.43).

The relations between the coefficients of AGM1 and AGPM2 are

$$\begin{aligned} A_1^{(1)} &= A_1^{(2)}, \qquad A_2^{(1)} = 0, \\ B_1^{(2)} &= \frac{c_{44}^{(2)}\eta^{(2)} - c_{44}^{(1)}\eta^{(1)}}{c_{44}^{(2)}m^{(2)}} A_1^{(1)} + \frac{c_{44}^{(1)}}{c_{44}^{(2)}}\frac{m^{(1)}}{m^{(2)}} B_1^{(1)} + \frac{e_{15}^{(1)}}{c_{44}^{(2)}}\frac{m^{(1)}}{m^{(2)}} B_2^{(1)} \end{aligned} \tag{8.49}$$

and the characteristic equation is

$$\begin{bmatrix} c_{44}^{(1)}P^{(1)}(\alpha) & -c_{44}^{(1)}N^{(1)}(\alpha) & -e_{15}^{(1)}N^{(1)}(\alpha) \\ e_{15}^{(1)}P^{(1)}(\alpha) & -e_{15}^{(1)}N^{(1)}(\alpha) & \kappa_{11}^{(1)}N^{(1)}(\alpha) \\ b^* & -c_{44}^{(1)}\dfrac{m^{(1)}}{m^{(2)}}N^{(2)}(-\beta) & -e_{15}^{(1)}\dfrac{m^{(1)}}{m^{(2)}}N^{(2)}(-\beta) \end{bmatrix} \begin{Bmatrix} A_1^{(1)} \\ B_1^{(1)} \\ B_2^{(1)} \end{Bmatrix} = 0 \tag{8.50}$$

in which

$$b^* = c_{44}^{(2)}P^{(2)}(-\beta) - \frac{c_{44}^{(2)}\eta^{(2)} - c_{44}^{(1)}\eta^{(1)}}{m^{(2)}} N^{(2)}(-\beta) \tag{8.51}$$

8.2.3 AGPM-EM-AGPM wedge system

In the following, the wedge consisting of AGPM1, an elastic material (EM) conductor, and AGPM2, as shown in Fig. 8.3, is considered. Ω_1, Ω_2, and Ω_3 denote AGPM1, EM, and AGPM2, respectively. The polar coordinate systems are again selected for simplicity, and c_1 and c_2 are adopted to indicate the sub-polar coordinate systems. The interface conditions are:

On interface 1:

$$\tau_{\theta z}^{(1)}(r,0) = \tau_{\theta z}^{(2)}(r,0), \quad w^{(1)}(r,0) = w^{(2)}(r,0), \quad \phi^{(1)}(r,0) = 0 \tag{8.52}$$

On interface 2:

$$\tau_{\theta z}^{(3)}(r,0) = \tau_{\theta z}^{(2)}(r,0), \quad w^{(3)}(r,0) = w^{(2)}(r,0), \quad \phi^{(3)}(r,0) = 0 \tag{8.53}$$

The relationship of the unknown constants for two adjacent domains can be obtained from Eqs. (8.52) and (8.53) as

$$A_{21}^{(1)} = 0, \quad A_{22}^{(3)} = 0 \tag{8.54}$$

$$\begin{Bmatrix} A_{11}^{(2)} \\ B_{11}^{(2)} \end{Bmatrix} = \begin{bmatrix} 1 & 0 & 0 \\ -\dfrac{\eta^{(1)}}{\mu} & \dfrac{m^{(1)}}{\mu} & \dfrac{e_{15}^0}{c_{44}^0}\dfrac{m^{(1)}}{\mu} \end{bmatrix} \begin{Bmatrix} A_{11}^{(1)} \\ B_{11}^{(1)} \\ B_{21}^{(1)} \end{Bmatrix}, \quad \begin{Bmatrix} A_{12}^{(2)} \\ B_{12}^{(2)} \end{Bmatrix} = \begin{bmatrix} \cos(\mu\gamma) & -\sin(\mu\gamma) \\ \sin(\mu\gamma) & \cos(\mu\gamma) \end{bmatrix} \begin{Bmatrix} A_{11}^{(2)} \\ B_{11}^{(2)} \end{Bmatrix} \tag{8.55}$$

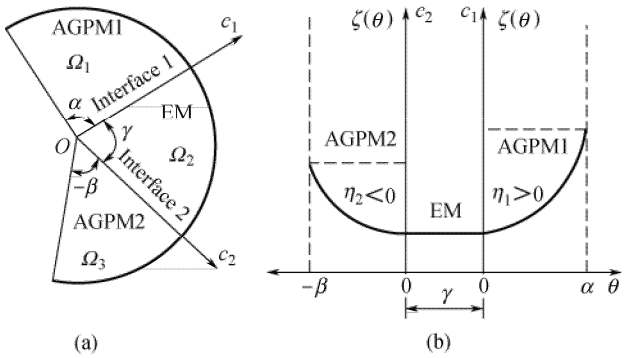

Fig. 8.3 Diagram of AGPM1-EM-AGPM2 wedge system. (a) Geometry configuration of the AGPM1-EM-AGPM2 wedge system; (b) Variation of material properties with the angle variable θ.

$$\begin{Bmatrix} A_{21}^{(2)} \\ B_{21}^{(2)} \end{Bmatrix} = \begin{bmatrix} 1 & 0 & 0 \\ -\dfrac{\eta^{(3)}}{\mu} & \dfrac{m^{(3)}}{\mu} & \dfrac{e_{15}^{*}}{c_{44}^{*}}\dfrac{m^{(3)}}{\mu} \end{bmatrix} \begin{Bmatrix} A_{12}^{(3)} \\ B_{12}^{(3)} \\ B_{22}^{(3)} \end{Bmatrix} \tag{8.56}$$

where the second subscript denotes the coordinate system.

The coordinate transformation [29] is used to find the relationships between the unknown constants in general solutions of each material domain, yielding the following equations:

$$A_{12}^{(3)} = s_{11}A_{11}^{(1)} + s_{12}B_{11}^{(1)} + s_{13}B_{21}^{(1)}, \quad B_{12}^{(3)} = s_{21}A_{11}^{(1)} + s_{22}B_{11}^{(1)} + s_{23}B_{21}^{(1)} + s_{24}B_{22}^{(3)} \tag{8.57}$$

where s_{1i} $(i = 1\text{-}3)$ and s_{2i} $(i = 1\text{-}4)$ are given by

$$\begin{aligned} s_{11} &= \cos(\mu\gamma) - \frac{\eta^{(1)}}{\mu}\sin(\mu\gamma), \quad s_{12} = -\frac{m^{(1)}}{\mu}\sin(\mu\gamma), \quad s_{13} = \frac{e_{15}^{0}}{c_{44}^{0}}d_{12}, \\ s_{21} &= \frac{1}{m^{(3)}}\left[\mu\sin(\mu\gamma) + (\eta^{(3)} - \eta^{(1)})\cos(\mu\gamma) - \frac{\eta^{(1)}\eta^{(3)}}{\mu}\sin(\mu\gamma)\right], \\ s_{22} &= \frac{m^{(1)}}{m^{(3)}}\left[\cos(\mu\gamma) - \frac{\eta^{(3)}}{\mu}\sin(\mu\gamma)\right], \quad s_{23} = \frac{e_{15}^{0}}{c_{44}^{0}}d_{22}, \quad s_{24} = -\frac{e_{15}^{0}}{c_{44}^{0}} \end{aligned} \tag{8.58}$$

According to the traction free and electrically insulated boundary conditions, we can obtain

$$\begin{bmatrix} c_{44}P^{(1)}(\alpha) & -c_{44}N^{(1)}(\alpha) & -e_{15}N^{(1)}(\alpha) & 0 \\ e_{15}P^{(1)}(\alpha) & -e_{15}N^{(1)}(\alpha) & \kappa_{11}N^{(1)}(\alpha) & 0 \\ t_{11} & t_{12} & t_{13} & 0 \\ t_{21} & t_{22} & t_{23} & t_{24} \end{bmatrix} \begin{Bmatrix} A_{11}^{(1)} \\ B_{11}^{(1)} \\ B_{21}^{(1)} \\ B_{22}^{(3)} \end{Bmatrix} = 0 \tag{8.59}$$

in which t_{1i} $(i=1-3)$ and t_{2i} $(i=1-4)$ are given by

$$\begin{aligned} &t_{11} = c_{44}^0\left[s_{11}P^{(3)}(-\beta) - s_{21}N^{(3)}(-\beta)\right],\ t_{12} = c_{44}^0\left[s_{12}P^{(3)}(-\beta) - s_{22}N^{(3)}(-\beta)\right], \\ &t_{13} = c_{44}^0\left[s_{13}P^{(3)}(-\beta) - s_{23}N^{(3)}(-\beta)\right],\ t_{21} = e_{15}^0\left[s_{11}P^{(3)}(-\beta) - s_{21}N^{(3)}(-\beta)\right], \\ &t_{22} = e_{15}^0\left[s_{12}P^{(3)}(-\beta) - s_{22}N^{(3)}(-\beta)\right],\ t_{23} = e_{15}^0\left[s_{13}P^{(3)}(-\beta) - s_{23}N^{(3)}(-\beta)\right], \\ &t_{24} = \left[-s_{24}e_{15}^0 + \kappa_{11}^0\right]N^{(3)}(-\beta) \end{aligned} \tag{8.60}$$

Equations (8.39), (8.50), and (8.59) are transcendental and have numerous roots which may be real or a complex quantity. They can be solved using the numerical method and then the admissible values of μ can be obtained. In the following, the effects of angular inhomogeneity on the singularity of electro-elastic fields of wedge system are investigated via numerical results.

8.2.4 Numerical results and discussion

In the following numerical studies, the material properties of PZT-4 are taken as the reference material properties as follows: $c_{44}^0 = 25.6\times10^9$ N/m^2, $e_{15}^0 = 12.7$ C/N and $\kappa_{11}^0 = 6.46\times10^{-9}$ F/m.

8.2.4.1 A single AGPM wedge

In Fig. 8.4, the variation of the singular order for single AGPM wedge with the wedge angle from 180° to 360° is plotted to show the effect of material angular inhomogeneity on the singularity of electro-elastic fields, in which the angular inhomogeneity parameter ρ is defined as

$$\rho = \frac{c_{44}(\theta_0)}{c_{44}^0} = \frac{e_{15}(\theta_0)}{e_{15}^0} = \frac{\kappa_{11}(\theta_0)}{\kappa_{11}^0} \tag{8.61}$$

It can be seen from Fig. 8. 4 that $\rho = 1.0$ ($\eta = 0$) for a homogeneous piezoelectric wedge and thus there is no singularity for the piezoelectric half plane ($\theta_0 = 180°$). Hence, the classic root exists for the singularity of a semi-infinite crack ($\theta_0 = 360°$). Moreover, the singularity disappears when $\theta_0 \leqslant 180°$. These results are consistent with those of [29,30]. The range of wedge angle in which singularity exists is given in Eq. (8.33) for inhomogeneous piezoelectric materials, but

the singular order for the semi-infinite crack ($\theta_0 = 360°$) is not equal to the classic root (–0.5). The angular material inhomogeneity leads to a smaller singular order than that of homogeneous material, and a larger inhomogeneity parameter η can produce a smaller singularity. For a single AGPM wedge, the singular order relates only to the value of η, the wedge angle and the boundary conditions.

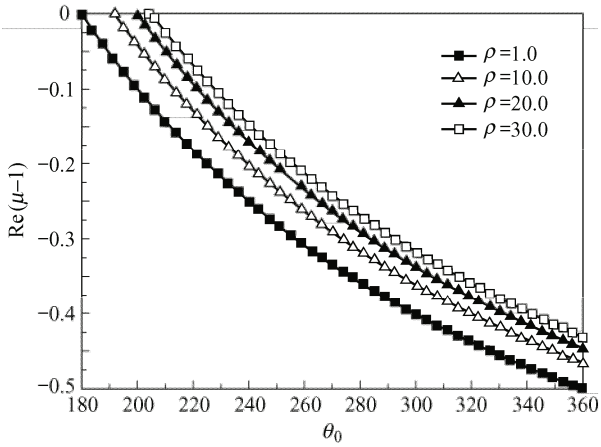

Fig. 8.4 Variation of the singular order with the wedge angle for different angular inhomogeneities.

8.2.4.2 AGPM-AGPM wedge system

Consider an AGPM-AGPM wedge system as shown in Fig. 8.2(a), in which the AGPM1 and AGPM2 have different inhomogeneity degrees η_1 and η_2, as shown in Fig. 8.2(b). The material properties of PZT-4 are again taken as the reference material properties for AGPM1 and AGPM2, and $\alpha = 180°$ and $\beta = 180°$, and in this case the wedge can denote a semi-infinite crack. The variation of the singular order with η_1 for different η_2 is given in Fig. 8.5. It should be mentioned that according to Eq. (8.2), we have

$$\eta_1 = \frac{1}{\theta_2 - \theta_1} \ln \frac{c_{44}(\theta_2)}{c_{44}(\theta_1)}, \quad \eta_2 = \frac{1}{\theta_1 - \theta_0} \ln \frac{c_{44}(\theta_1)}{c_{44}(\theta_0)} \tag{8.62}$$

in which $\eta_1 < 0$ implies that $c_{44}(\theta_2) < c_{44}(\theta_1)$, and $\eta_1 > 0$ implies that $c_{44}(\theta_2) > c_{44}(\theta_1)$. Meanwhile $\eta_2 < 0$ implies that $c_{44}(\theta_1) < c_{44}(\theta_0)$, and $\eta_2 > 0$ implies that $c_{44}(\theta_1) > c_{44}(\theta_0)$. For a fixed value of η_2, we can see that the singularity becomes more severe when η_1 varies from a negative to a positive value. However, a larger value of η_2 can lead to a less severe singularity. This behavior demonstrates that the angular material inhomogeneity can be used to control the singularity of the electro-elastic fields for a bi-AGPM wedge.

The variation of the singular order with α and the value of η_2 is plotted in Fig. 8.6 for a bi-AGPM wedge system in which $\beta = 180°$, $\eta_1 = 1.2$. It is observed that the degree of singularity increases with the increase of the value α from $0°$ to $180°$. When $\alpha = 0°$, the bi-AGPM wedge degenerates to a single wedge with wedge angle $\beta = 180°$, and in this case the wedge becomes a half plane, and there is no singularity when η_2 equals –0.6, 0, and 0.6. When $\alpha = 180°$, the wedge system can be a bi-AGPM semi-infinite crack, and the singularity may not be the classical root singularity when AGPM2 is the homogeneous piezoelectric material ($\eta_2 = 0$). When $\eta_2 > 0$ there is a less severe singularity, whereas when $\eta_2 < 0$ the singularity becomes more severe.

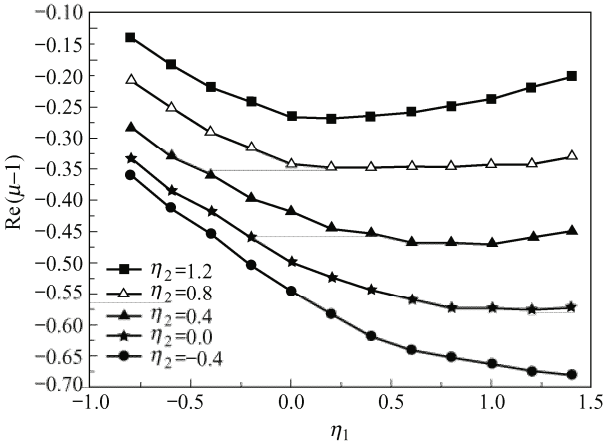

Fig. 8.5 Variation of the singular order with angular material inhomogeneity for an AGPM1-AGPM2 wedge system ($\alpha = 180°$, $\beta = 180°$).

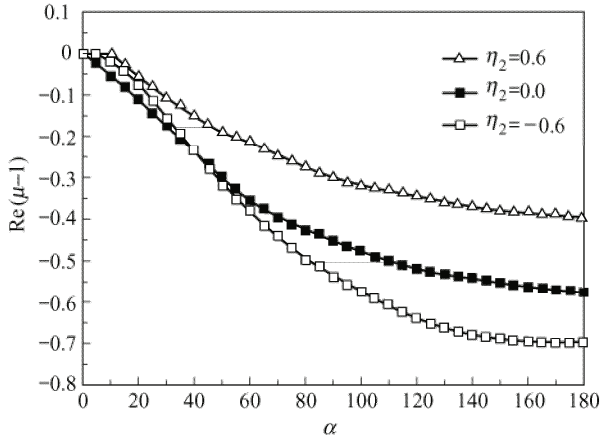

Fig. 8.6 Variation of the singular order with α for different values of η_2 ($\beta = 180°$, $\eta_1 = 1.2$).

Figure 8.7 shows the variation of singularity for an AGPM2-AGM1 wedge system with $\beta = 180°$ and $\eta_1 = 1.0$ for various wedge angles α. When $\eta_2 = 0$, the AGM becomes a homogeneous elastic material (EM). It can be observed that the singularity behavior is similar to that of the bi-AGPM wedge, as shown in Fig. 8.6. A positive value of η_2 leads to a small value of the singular order whereas a negative value of η_2 can produce a larger singular order compared to the case of the AGPM-EM wedge.

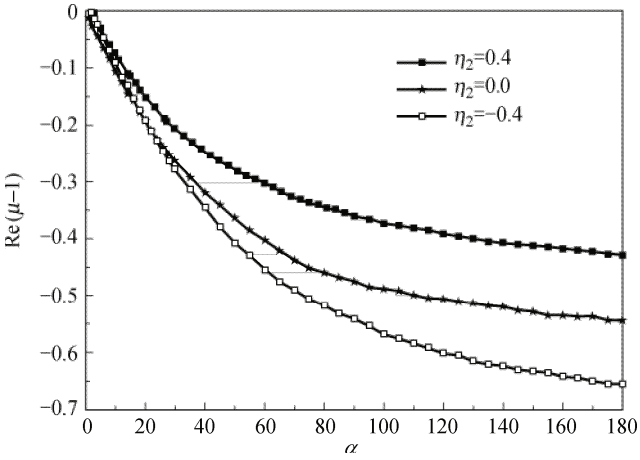

Fig. 8.7 Singularity for AGPM-AGM wedge system ($\beta = 180°$ and $\eta_1 = 1.0$).

The singularity behavior of an AGPM-AGM conductor wedge system is presented in Fig. 8.8, with $\beta = 270°$ and $\eta_2 = -0.8$. With the increase of the wedge angle α, the singularity increases for all the values of η_2. For a small value α of the AGM, the singularity depends mainly on the AGPM, and η_1 has little effect on the singularity behavior of the AGPM-AGM wedge. With an increase in the value of α, the material inhomogeneity degree η_1 of the AGM conductor has more effect on the singularity of electro-elastic fields, but a small value of η_1 will cause a weak singularity.

8.2.4.3 AGPM-EM conductor-AGPM wedge system

Finally, the singularity of an AGPM-EM conductor-AGPM wedge system is shown in Fig. 8.9, with $\alpha = \beta = 90°$, $\gamma = 180°$, $\eta_2 = 0$, $\eta_3 = -1.2$. The material properties of PZT-4 are again taken as the reference material properties, and the reference elastic constant c_{44} of the EM conductor is the same as that of the AGPM. The material inhomogeneity takes a "U" form, as shown in Fig. 8.3(b). This three-material wedge denotes an interface crack between AGPM1 and AGPM2. The numerical results in Fig. 8.9 show the singularity of the three-material wedge system, which is more complex than that of a two-materials wedge system. Multi-root singularity exists, such as two-roots singularity and three-roots singularity. The

variation from one to three roots depends on the value of η_1, and some values around $\eta_1 = -0.1$ and $\eta_1 = 0.3$ can lead to very strong singularities which are larger than –0.9. It is noted that two real roots singularity can exist with the value of η_1 varying in the ranges of [–1.80, –0.15] and [1.90, 4.60], in which the singularity degree decreases when η_1 increases from –1.8 to –0.15. After that, the singularity tends to increase until η_1=2. Thus, for the multi-material wedge system the degree of singularity can also be made as weak as the two-material wedge system by choosing an appropriate degree of angular inhomogeneity. It should be mentioned that only the three-material wedge system is considered here as an example of a multi-material wedge for the model described in this section. Four-material wedges and wedges containing even more materials can be solved using a similar procedure.

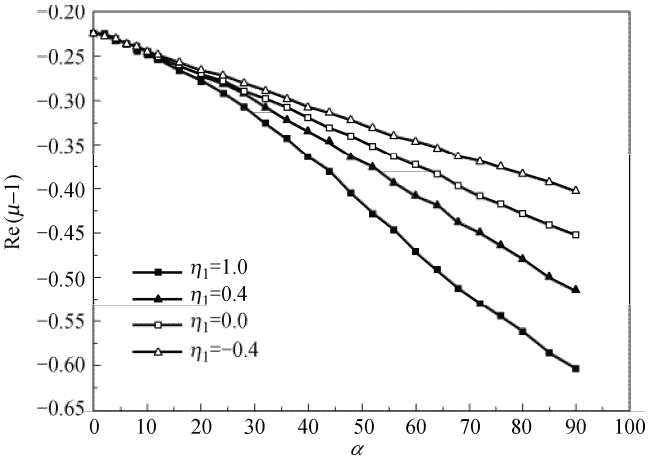

Fig. 8.8 Singularity behavior of an AGPM-AGM conductor wedge system with $\beta = 270°$, $\alpha = 90°$ and $\eta_2 = -0.8$.

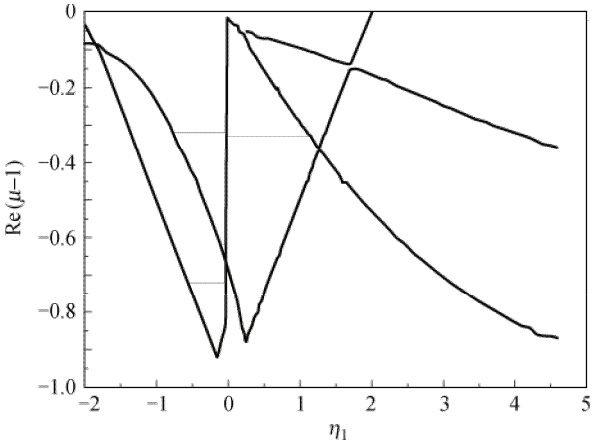

Fig. 8.9 Singularity behavior of AGPM-EM conductor-AGPM wedge system with $\alpha = \beta = 90°$, $\gamma = 180°$, $\eta_2 = 0$, and $\eta_3 = -1.2$.

8.3 Solution to FGPM beams

A general solution presented in [17] for FGPM beams with arbitrary graded material properties along the beam thickness direction is described in this section. The beam under consideration may be subjected to normal and shear tractions of polynomial form on the upper and lower surfaces, while the end boundary conditions can be cantilever, simply supported or rigidly clamped.

8.3.1 Basic formulation

Consider an FGPM beam with an arbitrary composition gradient through the thickness. In the absence of body forces and free electric charges, the mechanical and electric equilibrium equations are defined by Eq. (2.163), and the strain-displacement and electric field-electric potential relations are given by Eq. (1.2). When σ_{ij} and E_i are chosen as independent variables, the constitutive equation (1.24) becomes

$$\begin{Bmatrix} \varepsilon_x \\ \varepsilon_z \\ \gamma_{xz} \\ D_x \\ D_z \end{Bmatrix} = \begin{bmatrix} a_{11} & a_{13} & 0 & 0 & d_{31} \\ a_{13} & a_{33} & 0 & 0 & d_{33} \\ 0 & 0 & a_{55} & d_{15} & 0 \\ 0 & 0 & d_{15} & \kappa_{11} & 0 \\ d_{31} & d_{33} & 0 & 0 & \kappa_{33} \end{bmatrix} \begin{Bmatrix} \sigma_x \\ \sigma_z \\ \sigma_{xz} \\ E_x \\ E_z \end{Bmatrix} \tag{8.63}$$

Substituting Eqs. (1.2), (1.31), and (8.63) into Eqs. (1.30) and (2.163), Eqs. (1.32) and (1.33) now become differential equations for Airy stress function U and electric potential ϕ, as

$$\left(d_{31}U_{,33}\right)_{,3} + \left(d_{33}U_{,11}\right)_{,3} - d_{15}U_{,113} = \left(\kappa_{33}\phi_{,3}\right)_{,3} + \kappa_{11}\phi_{,11} \tag{8.64}$$

$$\begin{aligned} &\left(a_{11}U_{,33} + a_{13}U_{,11}\right)_{,33} + \left(a_{55}U_{,113}\right)_{,3} + a_{13}U_{,1133} + a_{33}U_{,1111} \\ &\qquad = \left(d_{13}\phi_{,3}\right)_{,33} + d_{33}\phi_{,113} - \left(d_{15}\phi_{,11}\right)_{,3} \end{aligned} \tag{8.65}$$

8.3.2 Solution procedure

To obtain the solution to Eqs. (8.64) and (8.65), Zhong and Yu [17] introduced the following form of Airy stress and electric potential functions:

$$U = \sum_{i=0}^{n} x^i f_i(z), \quad \phi = \sum_{i=0}^{n} x^i g_i(z) \tag{8.66}$$

Substituting Eq. (8.66) into Eqs. (1.2) and (1.31) yields

$$\begin{Bmatrix}\sigma_x\\ \sigma_y\\ \sigma_{xy}\end{Bmatrix}=\begin{Bmatrix}\sum\limits_{k=0}^{n}x^k\dfrac{\mathrm{d}^2 f_k(z)}{\mathrm{d}z^2}\\ \sum\limits_{k=2}^{n}k(k-1)x^{k-2}f_k(z)\\ -\sum\limits_{k=1}^{n}kx^{k-1}\dfrac{\mathrm{d}f_k(z)}{\mathrm{d}z}\end{Bmatrix} \tag{8.67}$$

$$\begin{Bmatrix}E_x\\ E_y\end{Bmatrix}=-\begin{Bmatrix}\sum\limits_{k=1}^{n}kx^{k-1}g_k(z)\\ \sum\limits_{k=0}^{n}x^k\dfrac{\mathrm{d}g_k(z)}{\mathrm{d}z}\end{Bmatrix} \tag{8.68}$$

Then, by substituting Eq. (8.66) into Eqs. (8.64) and (8.65), we obtain the governing equations for $f_i(z)$ and $g_i(z)$ as

$$\begin{aligned}&\frac{\mathrm{d}}{\mathrm{d}z}\left(d_{31}\frac{\mathrm{d}^2 f_k(z)}{\mathrm{d}z^2}-\kappa_{33}\frac{\mathrm{d}g_k(z)}{\mathrm{d}z}\right)=G_k^0(z),\\ &\frac{\mathrm{d}^2}{\mathrm{d}z^2}\left(a_{11}\frac{\mathrm{d}^2 f_k(z)}{\mathrm{d}z^2}-d_{31}\frac{\mathrm{d}g_k(z)}{\mathrm{d}z}\right)=F_k^0(z)\qquad(k=0,1,\cdots,n)\end{aligned} \tag{8.69}$$

where

$$G_k^0(z)=\begin{cases}0 & (k=n-1,n)\\ L_1\left[\dfrac{\mathrm{d}X_{k+2}^{33}}{\mathrm{d}z}-Y_{i+2}^{15}-Z_{i+2}^{11}\right] & (\text{others})\end{cases} \tag{8.70}$$

$$F_k^0(z)=\begin{cases}0 & (k=n-1,n)\\ L_1\left[\dfrac{\mathrm{d}^2 R_{k+2}^{13}}{\mathrm{d}z^2}+\dfrac{\mathrm{d}S_{k+2}^{55}}{\mathrm{d}z}+\dfrac{\mathrm{d}V_{k+2}^{15}}{\mathrm{d}z}+T_{i+2}^{13}-W_{i+2}^{33}\right] & (k=n-3,n-2)\\ L_1\left[\dfrac{\mathrm{d}^2 R_{k+2}^{13}}{\mathrm{d}z^2}+\dfrac{\mathrm{d}S_{k+2}^{55}}{\mathrm{d}z}+\dfrac{\mathrm{d}V_{k+2}^{15}}{\mathrm{d}z}+T_{i+2}^{13}-W_{i+2}^{33}+L_2R_{k+4}^{33}\right] & (\text{others})\end{cases} \tag{8.71}$$

with the following notations being defined as:

$$
\begin{aligned}
&L_1 = -(k+1)(k+2),\ \ L_2 = (k+3)(k+4),\quad R_k^{ij} = a_{ij}(z) f_k(z),\\
&S_k^{ij} = a_{ij}(z)\frac{\mathrm{d}f_k(z)}{\mathrm{d}z},\quad T_k^{ij} = a_{ij}(z)\frac{\mathrm{d}^2 f_k(z)}{\mathrm{d}z^2},\quad V_k^{ij} = d_{ij}(z) g_k(z),\\
&W_k^{ij} = d_{ij}(z)\frac{\mathrm{d}g_k(z)}{\mathrm{d}z},\ \ X_k^{ij} = d_{ij}(z) f_k(z),\qquad Y_k^{ij} = d_{ij}(z)\frac{\mathrm{d}f_k(z)}{\mathrm{d}z},\\
&Z_k^{ij} = \kappa_{ij}(z) g_k(z)
\end{aligned}
\tag{8.72}
$$

Equation (8.69) gives a recurrence relation for $f_i(z)$ and $g_i(z)$. Zhong and Yu obtained the general solution for $f_n(z)$, $g_n(z)$, $f_{n-1}(z)$, and $g_{n-1}(z)$ using the condition $F_n^0(z) = G_n^0(z) = F_{n-1}^0(z) = G_{n-1}^0(z)$. Then, $f_i(z)$, $g_i(z)$ (i = n–2, ⋯, 1, 0) can be solved one by one using the solution obtained for $f_n(z)$, $g_n(z)$, $f_{n-1}(z)$, and $g_{n-1}(z)$. Hence, the solutions of $f_i(z)$ and $g_i(z)$ can be written in general form as

$$
\begin{aligned}
&f_k(z) = F_k^4(z) + \overline{A}_k \hat{H}_1(z) + \overline{B}_k \hat{H}_0(z) - \overline{E}_k \hat{J}_0(z) + \overline{C}_k z + \overline{D}_k,\\
&g_k(z) = G_k^3(z) + \overline{A}_k \hat{J}_1(z) + \overline{B}_i \hat{J}_0(z) - \overline{E}_i \hat{I}_0(z) + \overline{K}_k
\end{aligned}
\tag{8.73}
$$

where $\overline{A}_k$, $\overline{B}_k$, $\overline{C}_k$, $\overline{D}_k$, $\overline{E}_k$, and $\overline{K}_k$ are unknown constants, and

$$
\begin{aligned}
&F_k^4(z) = \int_0^z F_k^3(z)\mathrm{d}z,\ \ F_k^3(z) = \int_0^z \frac{\kappa_{33}(z)F_k^2(z) - d_{31}(z)G_k^1(z)}{\Delta(z)}\mathrm{d}z,\\
&F_k^2(z) = \int_0^z F_k^1(z)\mathrm{d}z,\ \ F_k^1(z) = \int_0^z F_k^0(z)\mathrm{d}z,\ \ G_k^1(z) = \int_0^z G_k^0(z)\mathrm{d}z,\\
&G_k^3(z) = \int_0^z \frac{d_{31}(z)F_k^2(z) - a_{11}(z)G_k^1(z)}{\Delta(z)}\mathrm{d}z,\ \ F_{n-1}^1 = F_n^1 = F_{n-1}^2 = F_n^2 = 0,\\
&G_{n-1}^1 = G_n^1 = F_{n-1}^3 = F_n^3 = F_{n-1}^4 = F_n^4 = 0,\quad \Delta(z) = (a_{11}\kappa_{33} - d_{31}^2)(z)
\end{aligned}
\tag{8.74}
$$

$$
\begin{aligned}
&\hat{H}_k(z) = \int_0^z H_k(z)\mathrm{d}z,\quad \hat{I}_k(z) = \int_0^z I_k(z)\mathrm{d}z,\quad \hat{J}_k(z) = \int_0^z J_k(z)\mathrm{d}z,\\
&H_k(z) = \int_0^z \frac{\kappa_{33}(z)z^k}{\Delta(z)}\mathrm{d}z,\ \ I_k(z) = \int_0^z \frac{a_{11}(z)z^k}{\Delta(z)}\mathrm{d}z,\ \ J_k(z) = \int_0^z \frac{d_{31}(z)z^k}{\Delta(z)}\mathrm{d}z
\end{aligned}
\tag{8.75}
$$

Making use of Eqs. (1.2), (8.63), (8.67), (8.68), and (8.73), the expressions for elastic displacements and electric displacements can be obtained as

$$
\begin{aligned}
u = &\sum_{k=0}^{n}\frac{x^{k+1}}{k+1}\left(T_k^{11} - W_k^{31}\right) + \sum_{k=2}^{n} k x^{k-1} R_k^{13}\\
&- \overline{T}_1^{13} + \overline{W}_1^{13} - 6\overline{R}_3^{33} - \hat{S}_1^{55} - \hat{V}_1^{15} - \overline{a}z + \overline{c},\\
w = &\sum_{k=0}^{n} x^k\left(\hat{T}_k^{13} - \hat{W}_k^{13} - \frac{x^2\overline{A}_k}{-L_1}\right) + \sum_{k=2}^{n} k(k-1)x^{k-2}\hat{R}_k^{33} + \overline{a}x + \overline{d}
\end{aligned}
\tag{8.76}
$$

$$
\begin{aligned}
D_x &= \sum_{k=0}^{n-1}(k+1)x^k\left(Y_{k+1}^{15}-Z_{k+1}^{11}\right),\\
D_z &= \sum_{k=0}^{n-2}x^k\left(G_k^1+\overline{E}_k-L_1X_{k+2}^{33}\right)+x^{n-1}\overline{E}_{n-1}+x^n\overline{E}_n
\end{aligned}
\tag{8.77}
$$

where $\overline{a}$, $\overline{c}$, and $\overline{d}$ are integral constants related to the rigid motions of the beam, and

$$
\begin{aligned}
&\hat{R}_i^{kl}=\int_0^z R_i^{kl}\mathrm{d}z, \quad \hat{S}_i^{kl}=\int_0^z S_i^{kl}\mathrm{d}z, \quad \hat{T}_i^{kl}=\int_0^z T_i^{kl}\mathrm{d}z, \quad \hat{W}_i^{kl}=\int_0^z W_i^{kl}\mathrm{d}z,\\
&\hat{V}_i^{kl}=\int_0^z V_i^{kl}\mathrm{d}z, \quad \overline{W}_i^{kl}=\int_0^z \hat{W}_i^{kl}\mathrm{d}z, \quad \overline{R}_i^{kl}=\int_0^z \hat{R}_i^{kl}\mathrm{d}z, \quad \overline{S}_i^{kl}=\int_0^z \hat{S}_i^{kl}\mathrm{d}z,\\
&\overline{T}_i^{kl}=\int_0^z \hat{T}_i^{kl}\mathrm{d}z
\end{aligned}
\tag{8.78}
$$

As can be seen from the solution presented above, there exist 6(n+1) unknown constants, $\overline{a},\overline{c},\overline{d},\overline{A}_0,\overline{B}_0,\overline{E}_0,\overline{K}_0,\overline{A}_1,\overline{B}_1,\overline{C}_1,\overline{K}_1$ and $\overline{A}_i,\overline{B}_i,\overline{C}_i,\overline{D}_i,\overline{E}_i,\overline{K}_i$ (i=2, 3, ⋯, n), which are to be determined from the boundary conditions.

To determine these constants, Zhong and Yu evaluated the concentrated normal force N_0, the concentrated shear force P_0, the concentrated moment M_0 and the concentrated electric load Θ_0 at the left end (x = 0) of the beam under consideration, by means of the following formulations:

$$
\begin{aligned}
N_0 &= b\int_{-h/2}^{h/2}\sigma_x\big|_{x=0}\mathrm{d}z, \qquad M_0 = b\int_{-h/2}^{h/2}\sigma_x\big|_{x=0}z\mathrm{d}z,\\
P_0 &= b\int_{-h/2}^{h/2}\sigma_{xz}\big|_{x=0}\mathrm{d}z, \qquad \Theta_0 = b\int_{-h/2}^{h/2}D_x\big|_{x=0}\mathrm{d}z
\end{aligned}
\tag{8.79}
$$

Their counterparts at the right end (x = l), N_l, P_l, M_l, and Θ_l, are given by

$$
\begin{aligned}
N_l &= b\int_{-h/2}^{h/2}\sigma_x\big|_{x=l}\mathrm{d}z, \qquad M_l = b\int_{-h/2}^{h/2}\sigma_x\big|_{x=l}z\mathrm{d}z,\\
P_l &= b\int_{-h/2}^{h/2}\sigma_{xz}\big|_{x=l}\mathrm{d}z, \qquad \Theta_l = b\int_{-h/2}^{h/2}D_x\big|_{x=l}\mathrm{d}z
\end{aligned}
\tag{8.80}
$$

in which b, h, and l are, respectively, the width, thickness, and length of the beam.

They proved then that the following equilibrium equations are automatically satisfied

$$
\begin{aligned}
N_l &= N_0 + b\int_0^l(\sigma_{xz}\big|_{z=-h/2}-\sigma_{xz}\big|_{z=h/2})\mathrm{d}z,\\
M_l &= M_0 + P_0l - b\int_0^l(\sigma_z\big|_{z=h/2}-\sigma_z\big|_{z=-h/2})(l-x)\mathrm{d}z\\
&\quad -\frac{bh}{2}\int_0^l(\sigma_{zx}\big|_{z=h/2}+\sigma_{zx}\big|_{z=-h/2})\mathrm{d}z,\\
P_l &= P_0 + b\int_0^l(\sigma_z\big|_{z=-h/2}-\sigma_z\big|_{z=h/2})\mathrm{d}z, \qquad \Theta_l = \Theta_0
\end{aligned}
\tag{8.81}
$$

if the upper and lower surfaces of the beam are subjected to normal and shear tractions of polynomial form as follows:

$$\begin{aligned} \sigma_z\big|_{z=h/2} &= \sum_{k=0}^{n-2} \overline{\gamma}_k x^k, \qquad \sigma_{xz}\big|_{z=h/2} = \sum_{k=0}^{n-1} \overline{\beta}_k x^k, \\ \sigma_z\big|_{z=-h/2} &= \sum_{k=0}^{n-2} \hat{\gamma}_k x^k, \qquad \sigma_{xz}\big|_{z=-h/2} = \sum_{k=0}^{n-1} \hat{\beta}_k x^k \end{aligned} \tag{8.82}$$

where $\overline{\gamma}$, $\hat{\gamma}$, $\overline{\beta}$, and $\hat{\beta}$ are known constants.

Making use of Eqs. (1.2), (8.63), and (8.76), we have

$$\begin{aligned} &f_k\left(\frac{h}{2}\right) = \frac{\overline{\gamma}_{k-2}}{k(k-1)}, \quad f_k\left(-\frac{h}{2}\right) = \frac{\hat{\gamma}_{k-2}}{k(k-1)} \qquad (k = 2,3,\cdots,n), \\ &\left.\frac{\mathrm{d}f_k}{\mathrm{d}z}\right|_{z=h/2} = -\frac{\overline{\beta}_{k-1}}{k}, \quad \left.\frac{\mathrm{d}f_k}{\mathrm{d}z}\right|_{z=h/2} = -\frac{\hat{\beta}_{k-1}}{k} \qquad (k = 1,2,\cdots,n) \end{aligned} \tag{8.83}$$

Considering further the electric boundary conditions on the upper and lower surfaces of the beam,

$$D_z\big|_{z=h/2} = D_z\big|_{z=-h/2} = 0 \tag{8.84}$$

we can obtain from Eqs. (8.77) and (8.84)

$$\begin{aligned} &G_k^1\left(\frac{h}{2}\right) + \overline{E}_k - L_1 X_{k+2}^{33}\left(\frac{h}{2}\right) = 0, \\ &G_k^1\left(-\frac{h}{2}\right) + \overline{E}_k - L_1 X_{k+2}^{33}\left(-\frac{h}{2}\right) = 0 \qquad (k = 0,1,\cdots,n-2) \end{aligned} \tag{8.85}$$

$$\overline{E}_n = \overline{E}_{n-1} = 0 \tag{8.86}$$

Noting that Eqs. (8.83) and (8.85) constitute $6n$–2 independent linear algebraic equations for the $6(n+1)$ unknowns mentioned above, eight more equations are needed. Zhong and Yu obtained these equations by considering the end boundary conditions of a beam. For example, for a cantilever FGPM beam clamped at one end ($x = l$) and subjected to a concentrated normal force N_*, a concentrated shear force P_* and a concentrated moment M_* at the other end ($x = 0$), the end boundary conditions are given as

$$\begin{aligned} &N_0 = N_*, \ P_0 = P_*, \ M_0 = M_*, \ \Theta_0 = 0 \qquad (\text{at } x = 0), \\ &u = w = \phi = 0, \quad w_{,x} = 0 \ (\text{or } u_{,x} = 0) \qquad (\text{at } x = 0, \ z = 0) \end{aligned} \tag{8.87}$$

8.4 Parallel cracks in an FGPM strip

This section describes the solution presented in [22] for the problem of a periodic

array of cracks in an FGPM strip bonded to a different FGPM. The corresponding singular integral equation is derived using the Fourier integral transform approach and can be solved numerically using the Lobatto-Chebyshev integration technique.

8.4.1 Basic formulation

In [22], Li and Ding considered an FGPM strip perfectly bonded to another FGPM in the y direction, as shown in Fig. 8.10. The FGPM1 (see Fig. 8.10) is considered to contain periodic cracks perpendicular to the interface. The length of each crack is $2a_0$ along the x direction. The centre of each crack is located at $x = d$. The distance between two nearest parallel cracks is $2c$ (see Fig. 8.10). If the poling direction of the two FGPMs is assumed to be along the z-axis, the constitutive equation (1.35) now becomes

$$\begin{aligned}
\tau_{xz}^{(k)} &= c_{55}^{(k)}(x)\frac{\partial w^{(k)}}{\partial x} + e_{15}^{(k)}(x)\frac{\partial \phi^{(k)}}{\partial x}, \quad \tau_{yz}^{(k)} = c_{55}^{(k)}(x)\frac{\partial w^{(k)}}{\partial y} + e_{15}^{(k)}(x)\frac{\partial \phi^{(k)}}{\partial y}, \\
D_x^{(k)} &= e_{15}^{(k)}(x)\frac{\partial w^{(k)}}{\partial x} - \kappa_{11}^{(k)}(x)\frac{\partial \phi^{(k)}}{\partial x}, \quad D_y^{(k)} = e_{15}^{(k)}(x)\frac{\partial w^{(k)}}{\partial y} - \kappa_{11}^{(k)}(x)\frac{\partial \phi^{(k)}}{\partial y}
\end{aligned} \tag{8.88}$$

where the superscript "(k)" represents the variable associated with material k, and all material constants are assumed to vary in the following form:

$$\begin{aligned}
&c_{55}^{(1)}(x) = c_{55}^{0}e^{\beta x}, \quad e_{15}^{(1)}(x) = e_{15}^{0}e^{\beta x}, \quad \kappa_{11}^{(1)}(x) = \kappa_{11}^{0}e^{\beta x} \quad (0 < x < h), \\
&c_{55}^{(2)}(x) = c_{55}^{0}e^{\gamma x}, \quad e_{15}^{(2)}(x) = e_{15}^{0}e^{\gamma x}, \quad \kappa_{11}^{(2)}(x) = \kappa_{11}^{0}e^{\gamma x} \quad (x < 0)
\end{aligned} \tag{8.89}$$

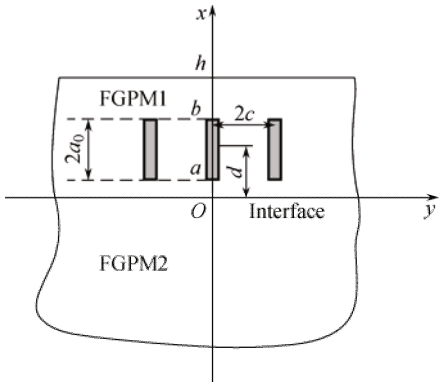

Fig. 8.10 Configuration of a periodically cracked FGPM1 strip bonded to FGPM2.

In Eq. (8.89), the subscript "0" stands for material properties at the interface or reference value of material constants. For the two-material system shown in Fig.

8.10, the governing equations (1.10) are now written in the form

$$\frac{\partial \tau_{xz}^{(k)}}{\partial x}+\frac{\partial \tau_{yz}^{(k)}}{\partial y}=0, \quad \frac{\partial D_x^{(k)}}{\partial x}+\frac{\partial D_y^{(k)}}{\partial y}=0 \quad (k=1,2) \tag{8.90}$$

Substituting Eq. (8.88) into Eq. (8.90) and making use of the relation (8.89) yield

$$\begin{aligned} &\nabla^2 w^{(1)}+\beta\frac{\partial w^{(1)}}{\partial x}=0, \quad \nabla^2 \vartheta^{(1)}+\beta\frac{\partial \vartheta^{(1)}}{\partial x}=0, \\ &\phi^{(1)}(x,y)=\frac{e_{15}^0}{\kappa_{11}^0}w^{(1)}(x,y)+\vartheta^{(1)}(x,y) \end{aligned} \tag{8.91}$$

for FGPM1, and

$$\begin{aligned} &\nabla^2 w^{(2)}+\gamma\frac{\partial w^{(2)}}{\partial x}=0, \quad \nabla^2 \vartheta^{(2)}+\gamma\frac{\partial \vartheta^{(2)}}{\partial x}=0, \\ &\phi^{(2)}(x,y)=\frac{e_{15}^0}{\kappa_{11}^0}w^{(2)}(x,y)+\vartheta^{(2)}(x,y) \end{aligned} \tag{8.92}$$

where $\nabla^2=\partial^2/\partial x^2+\partial^2/\partial y^2$ is the two-dimensional Laplace operator.

Due to the periodicity and symmetry of the problem, Li and Ding [22] considered the solution domain for $0<y<c$ only. The continuity condition at the interface is

$$\begin{aligned} &w^{(1)}(0,y)=w^{(2)}(0,y), \quad \phi^{(1)}(0,y)=\phi^{(2)}(0,y), \\ &\sigma_{xz}^{(1)}(0,y)=\sigma_{xz}^{(2)}(0,y), \quad D_x^{(1)}(0,y)=D_x^{(2)}(0,y) \end{aligned} \tag{8.93}$$

and the outer surface boundary conditions of the problem shown in Fig. 8.10 are defined by

$$\begin{aligned} &\sigma_{xz}^{(1)}(h,y)=0, \quad D_x^{(1)}(h,y)=0, \\ &w^{(2)}(x,0)=0, \quad \phi^{(2)}(x,0)=0 \quad (-\infty\leqslant x<0), \\ &w^{(1)}(x,c)=0, \quad \phi^{(1)}(x,c)=0 \quad (0<x<h), \\ &w^{(2)}(x,c)=0, \quad \phi^{(2)}(x,c)=0 \quad (-\infty\leqslant x<0) \end{aligned} \tag{8.94}$$

At each crack face, the boundary conditions are given by

$$\begin{aligned} &w^{(1)}(x,0)=0, \quad \phi^{(1)}(x,0)=0 \quad (0<x<a,\ b<x<h), \\ &\sigma_{yz}^{(1)}(x,0)=-\sigma(x), \quad D_y^{(1)}(x,0)=-D(x) \quad (a<x<b) \end{aligned} \tag{8.95}$$

for impermeable cracks, and

$$\begin{aligned} &w^{(1)}(x,0)=0 \quad (0<x<a,\ b<x<h), \\ &\phi^{(1)}(x,0)=0 \quad (0<x<h), \\ &\sigma_{yz}^{(1)}(x,0)=-\sigma(x), \quad D_y^{(1)}(x,0)=-D_c(x)=-D(x) \ \ (a<x<b) \end{aligned} \tag{8.96}$$

for permeable cracks, where $D_c(x, 0)$ denotes the electric displacement within the

crack void itself.

8.4.2 Singular integral equations and field intensity factors

$$\begin{aligned}
w^{(1)}(x,y) &= \frac{1}{2\pi}\int_{-\infty}^{\infty}[A_1(\alpha)\exp(m_1 y)+A_2(\alpha)\exp(m_1 y)]e^{i\alpha x}\mathrm{d}\alpha \\
&\quad+\sum_{k=1}^{\infty}[C_{1k}(\gamma_k)\exp(p_{1k}x)+C_{2k}(\gamma_k)\exp(p_{2k}x)]\sin(\gamma_k y), \\
\phi^{(1)}(x,y) &= \frac{1}{2\pi}\int_{-\infty}^{\infty}[B_1(\alpha)\exp(m_1 y)+B_2(\alpha)\exp(m_1 y)]e^{i\alpha x}\mathrm{d}\alpha \\
&\quad+\sum_{k=1}^{\infty}[D_{1k}(\gamma_k)\exp(p_{1k}x)+D_{2k}(\gamma_k)\exp(p_{2k}x)]\sin(\gamma_k y)
\end{aligned} \tag{8.97}$$

$$\begin{aligned}
w^{(2)}(x,y) &= \sum_{k=1}^{\infty}E_{2k}(\gamma_k)\exp(q_k x)\sin(\gamma_k y), \\
\phi^{(2)}(x,y) &= \sum_{k=1}^{\infty}F_{2k}(\gamma_k)\exp(q_k x)\sin(\gamma_k y)
\end{aligned} \tag{8.98}$$

where A_1, A_2, B_1, B_2, C_{1k}, C_{2k}, D_{1k}, D_{2k}, E_{2k}, and F_{2k} are unknown constants to be determined, and

$$\begin{aligned}
&m_1 = -m_2 = \sqrt{\alpha^2 + i\beta\alpha}, \quad p_{1k} = -\frac{\beta}{2} - \lambda_k, \quad p_{2k} = -\frac{\beta}{2} + \lambda_k, \\
&\lambda_k = \sqrt{\frac{\beta^2}{4} + \gamma_k^2}, \quad q_k = -\frac{\gamma}{2} + \lambda_k', \quad \lambda_k' = \sqrt{\frac{\gamma^2}{4} + \gamma_k^2}, \quad \gamma_k = \frac{k\pi}{c}
\end{aligned} \tag{8.99}$$

To determine the unknown constants above, Li and Ding defined the following two dislocation functions:

$$g_1(x) = \begin{cases} \dfrac{\partial w^{(1)}(x,0)}{\partial x} & (a < x < b) \\ 0 & (x < a,\ x > b), \end{cases} \qquad g_2(x) = \begin{cases} \dfrac{\partial \phi^{(1)}(x,0)}{\partial x} & (a < x < b) \\ 0 & (x < a,\ x > b) \end{cases} \tag{8.100}$$

Substituting Eq. (8.97) into Eq. (8.100) and making use of the continuity condition (8.93) and boundary conditions (8.94) and (8.95), we obtain

$$\begin{aligned}
A_1(\alpha) &= -\frac{i}{\alpha}\frac{e^{m_2 c}}{e^{m_1 c} - e^{m_2 c}}\int_a^b g_1(u)e^{i\alpha u}\mathrm{d}u, \\
A_2(\alpha) &= \frac{i}{\alpha}\frac{e^{m_1 c}}{e^{m_1 c} - e^{m_2 c}}\int_a^b g_1(u)e^{i\alpha u}\mathrm{d}u, \\
B_1(\alpha) &= -\frac{i}{\alpha}\frac{e^{m_2 c}}{e^{m_1 c} - e^{m_2 c}}\int_a^b [g_2(u) - \frac{e_{15}^0}{\kappa_{11}^0}g_1(u)]e^{i\alpha u}\mathrm{d}u, \\
B_2(\alpha) &= \frac{i}{\alpha}\frac{e^{m_1 c}}{e^{m_1 c} - e^{m_2 c}}\int_a^b [g_2(u) - \frac{e_{15}^0}{\kappa_{11}^0}g_1(u)]e^{i\alpha u}\mathrm{d}u
\end{aligned} \tag{8.101}$$

$$
\begin{aligned}
C_{1j} &= \frac{-\gamma_j(p_{2j}-q_j)}{c\Delta_3\lambda_j}\int_a^b g_1(u)[e^{-p_{1j}(u-h)}+e^{-p_{2j}(u-h)}]\mathrm{d}u,\\
C_{2j} &= \frac{\gamma_j e^{p_{1j}h}}{c\Delta_3 p_{2j}\lambda_j}\int_a^b g_1(u)[p_{2j}(p_{1j}-q_j)e^{p_{1j}u}+p_{1j}(q_j-p_{2j})e^{-p_{2j}u}]\mathrm{d}u
\end{aligned}
\tag{8.102}
$$

$$
\begin{aligned}
D_{1j} &= \frac{-\gamma_j(p_{2j}-q_j)}{c\Delta_3\lambda_j}\int_a^b g_1(u)[e^{-p_{1j}(u-h)}+e^{-p_{2j}(u-h)}]\mathrm{d}u,\\
D_{2j} &= \frac{\gamma_j e^{p_{1j}h}}{c\Delta_3 p_{2j}\lambda_j}\int_a^b\left[g_2(u)-\frac{e_{15}^0}{\kappa_{11}^0}g_1(u)\right][p_{2j}(p_{1j}-q_j)e^{p_{1j}u}\\
&\quad + p_{1j}(q_j-p_{2j})e^{-p_{2j}u}]\mathrm{d}u
\end{aligned}
\tag{8.103}
$$

$$
\begin{aligned}
E_{2j} &= \frac{\gamma_j p_{2j}(p_{1j}-p_{2j})}{c\Delta_3\lambda_j p_{2j}}\int_a^b g_1(u)[e^{-p_{1j}(u-h)}+e^{-p_{2j}(u-h)}]\mathrm{d}u,\\
F_{2j} &= \frac{\gamma_j p_{2j}(p_{1j}-p_{2j})}{c\Delta_3\lambda_j p_{2j}}\int_a^b\left[g_2(u)-\frac{e_{15}^0}{\kappa_{11}^0}g_1(u)\right][e^{-p_{1j}(u-h)}-e^{-p_{2j}(u-h)}]\mathrm{d}u
\end{aligned}
\tag{8.104}
$$

with

$$
\Delta_3 = p_{1j}(\gamma_j+p_{2j})e^{p_{2j}} - p_{2j}(\gamma_j+p_{1j})e^{p_{1j}} \tag{8.105}
$$

Substituting Eqs. (8.100)-(8.104) into Eq. (8.95) yields

$$
\begin{aligned}
\sigma(x) &= e^{\beta x}\frac{1}{\pi}\int_a^b[c_{55}^0 g_1(u)+e_{15}^0 g_2(u)]\left[\frac{1}{u-x}+K(u,x)\right]\mathrm{d}u,\\
D(x) &= e^{\beta x}\frac{1}{\pi}\int_a^b[e_{15}^0 g_1(u)-\kappa_{11}^0 g_2(u)]\left[\frac{1}{u-x}+K(u,x)\right]\mathrm{d}u
\end{aligned}
\tag{8.106}
$$

in which the kernel function $K(u,x)$ is given by

$$
K(u,x) = F_1(u,x)+F_2(u,x)+F_3(u,x) \tag{8.107}
$$

where

$$
\begin{aligned}
F_1(u,x) &= \frac{1}{2}\int_{-\infty}^{\infty}\frac{i}{\alpha}\left[\frac{m_2 e^{m_1 c}-m_1 e^{m_2 c}}{e^{m_1 c}-e^{m_2 c}}+|\alpha|\right]e^{i\alpha(u-x)}\mathrm{d}\alpha,\\
F_2(u,x) &= \frac{\pi}{c}\sum_{j=1}^{\infty}\left[F_{2j}+e^{-\gamma_j(2h-u-x)}\right],\quad F_3(u,x) = -\frac{\pi}{c(e^{\pi(2h-u-x)/c}-1)},\\
F_{2j}(u,x) &= \frac{-e^{p_{1j}x}\gamma_j^2}{\lambda_j p_{2j}\Delta_3}\left[p_{2j}(p_{2j}-q_j)e^{-p_{1j}(u-h)}-e^{-p_{2j}(u-h)}\right]\\
&\quad + \frac{e^{p_{2j}x}e^{p_{1j}h}\gamma_j^2}{\lambda_j p_{2j}\Delta_3}\left[p_{2j}(p_{1j}-q_j)e^{-p_{1j}u}+p_{1j}(q_j-p_{2j})e^{p_{2j}u}\right]
\end{aligned}
\tag{8.108}
$$

To solve the singular integral equations (8.106), Li and Ding introduced the following normalized quantities and related functions:

$$\begin{aligned} &\tilde{x} = (x-d)/a_0, \quad \tilde{u} = (u-d)/a_0, \quad f_1(\tilde{u}) = g_1(u), \\ &f_2(\tilde{u}) = g_2(u), \quad \sigma(\tilde{x}) = \sigma(x)e^{-\beta x}, \quad D(\tilde{x}) = D(x)e^{-\beta x} \end{aligned} \tag{8.109}$$

Using the definition (8.109), Eq. (8.106) can be rewritten as

$$\begin{aligned} \sigma(\tilde{x}) &= \frac{1}{\pi}\int_{-1}^{1}[c_{55}^0 f_1(\tilde{u}) + e_{15}^0 f_2(\tilde{u})]\left[\frac{1}{\tilde{u}-\tilde{x}} + K(a_0\tilde{u}+d, a_0\tilde{x}+d)\right]\mathrm{d}\tilde{u}, \\ D(\tilde{x}) &= \frac{1}{\pi}\int_{-1}^{1}[e_{15}^0 f_1(\tilde{u}) - \kappa_{11}^0 f_2(\tilde{u})]\left[\frac{1}{\tilde{u}-\tilde{x}} + K(a_0\tilde{u}+d, a_0\tilde{x}+d)\right]\mathrm{d}\tilde{u} \end{aligned} \tag{8.110}$$

They then mentioned that for an internal crack, functions $f_1(\tilde{u})$ and $f_2(\tilde{u})$ must fulfill the condition of single-valuedness as

$$\int_{-1}^{1} f_1(\tilde{u})\mathrm{d}\tilde{u} = \int_{-1}^{1} f_2(\tilde{u})\mathrm{d}\tilde{u} = 0 \tag{8.111}$$

It is obvious that Eq. (8.110) is a singular integral equation of the first kind. It can be solved numerically by the Lobatto-Chebyshev integration approach. Thus the relationship between functions $f_1(\tilde{u})$ and $f_2(\tilde{u})$ and weighting function $F_i(\tilde{u})$, which can be used to evaluate intensity factors, is given by

$$f_1(\tilde{u}) = \frac{F_1(\tilde{u})}{\sqrt{(1+\tilde{u})(1-\tilde{u})}}, \quad f_2(\tilde{u}) = \frac{F_2(\tilde{u})}{\sqrt{(1+\tilde{u})(1-\tilde{u})}} \tag{8.112}$$

Making use of Eq. (8.112), the field intensity factors can be calculated by [22]

$$\begin{aligned} K_3(b) &= -c_{55}^0 e^{\beta b}\sqrt{a_0}F_1(1) - e_{15}^0 e^{\beta b}\sqrt{a_0}F_2(1), \\ K_3(a) &= c_{55}^0 e^{\beta a}\sqrt{a_0}F_1(-1) + e_{15}^0 e^{\beta a}\sqrt{a_0}F_2(-1), \\ K_3^D(b) &= -e_{15}^0 e^{\beta b}\sqrt{a_0}F_1(1) + \kappa_{11}^0 e^{\beta b}\sqrt{a_0}F_2(1), \\ K_3^D(a) &= e_{15}^0 e^{\beta a}\sqrt{a_0}F_1(-1) - \kappa_{11}^0 e^{\beta a}\sqrt{a_0}F_2(-1) \end{aligned} \tag{8.113}$$

For the electrically permeable case, the corresponding stress and electric displacement can be similarly obtained as

$$\begin{aligned} \sigma(x) &= e^{\beta x}\frac{1}{\pi}\int_a^b c_{55}^0\left[\frac{1}{u-x} + K(u,x)\right]g_1(u)\mathrm{d}u, \\ D(x) &= e^{\beta x}\frac{1}{\pi}\int_a^b e_{15}^0\left[\frac{1}{u-x} + K(u,x)\right]g_1(u)\mathrm{d}u \end{aligned} \tag{8.114}$$

and the corresponding field intensity factors are defined in the form

$$\begin{aligned} &K_3(b) = -c_{55}^0 e^{\beta b}\sqrt{a_0}F_1(1), \quad K_3(a) = c_{55}^0 e^{\beta a}\sqrt{a_0}F_1(-1), \\ &K_3^D(b) = -e_{15}^0 e^{\beta b}\sqrt{a_0}F_1(1), \quad K_3^D(a) = e_{15}^0 e^{\beta a}\sqrt{a_0}F_1(-1) \end{aligned} \tag{8.115}$$

Making use of Eqs. (8.113) and (8.115), Li and Ding finally presented, respectively, the energy release rate G_3 and the energy density factors S_3, as

$$\begin{aligned} G_3(a) &= \frac{1}{2e^{\beta a}}\left[\frac{\kappa_{11}^0 K_3^2(a) + 2e_{15}^0 K_3(a) K_3^D(a) - c_{55}^0 (K_3^D(a))^2}{c_{55}^0 \kappa_{11}^0 + \left(e_{15}^0\right)^2}\right], \\ G_3(b) &= \frac{1}{2e^{\beta b}}\left[\frac{\kappa_{11}^0 K_3^2(b) + 2e_{15}^0 K_3(b) K_3^D(b) - c_{55}^0 (K_3^D(b))^2}{c_{55}^0 \kappa_{11}^0 + \left(e_{15}^0\right)^2}\right] \end{aligned} \tag{8.116}$$

$$\begin{aligned} S_3(a) &= \frac{1}{8e^{\beta a}}\left[\frac{\kappa_{11}^0 K_3^2(a) - e_{15}^0 K_3(a) K_3^D(a) + 2c_{55}^0 (K_3^D(a))^2}{c_{55}^0 \kappa_{11}^0 + \left(e_{15}^0\right)^2}\right], \\ S_3(b) &= \frac{1}{8e^{\beta b}}\left[\frac{\kappa_{11}^0 K_3^2(b) - e_{15}^0 K_3(b) K_3^D(b) + 2c_{55}^0 (K_3^D(b))^2}{c_{55}^0 \kappa_{11}^0 + \left(e_{15}^0\right)^2}\right] \end{aligned} \tag{8.117}$$

for an impermeable crack, and

$$G_3(a) = 4S_3(a) = \frac{K_3^2(a)}{2c_{55}^0 e^{\beta a}}, \quad G_3(b) = 4S_3(b) = \frac{K_3^2(b)}{2c_{55}^0 e^{\beta b}} \tag{8.118}$$

for a permeable crack.

8.5 Mode Ⅲ cracks in two bonded FGPMs

The fracture behavior of a crack perpendicular to the interface of two bonded FGPMs is described in this section. Under antiplane shear and in-plane electric displacement, Chue and Ou [21] reduced the problem to a set of singular integral equations and solved them numerically using the Gauss-Chebyshev integration technique.

8.5.1 Basic formulation of the problem

The development presented in [21] is considered there. In [21], Chue and Ou considered a system of two FGPMs perfectly bonded together along the *y*-axis in which a crack of length $2a_0$ is located at $y = 0$ and in $a \leqslant x \leqslant b$ (see Fig. 8.11). The poling directions of the two FGPMs are oriented along the *z*-axis. For the problem of antiplane deformation, the constitutive relations and the governing equations are, respectively, defined by Eqs. (8.88) and (8.90). The variations of material properties are assumed in the exponential forms defined by Eq. (8.89), except that the domain

($0< x < h$) in Eq. $(8.89)_1$ is replaced by ($x >0$).

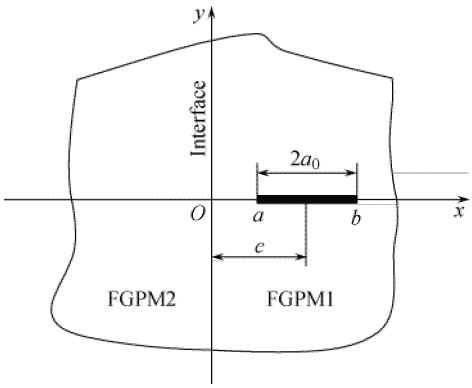

Fig. 8.11 Geometry of two bonded FGPMs containing a crack.

Substituting Eq. (8.88) into Eq. (8.90) and using the relation (8.89) provide the following equations for FGPM1 and FGPM2, respectively:

$$\begin{aligned} &c_{55}^0\left(\frac{\partial^2 w^{(1)}}{\partial x^2}+\frac{\partial^2 w^{(1)}}{\partial y^2}\right)+e_{15}^0\left(\frac{\partial^2 \phi_1}{\partial x^2}+\frac{\partial^2 \phi^{(1)}}{\partial y^2}\right)+\beta\left(c_{55}^0\frac{\partial w^{(1)}}{\partial x}+e_{15}^0\frac{\partial \phi^{(1)}}{\partial x}\right)=0,\\ &e_{15}^0\left(\frac{\partial^2 w^{(1)}}{\partial x^2}+\frac{\partial^2 w^{(1)}}{\partial y^2}\right)-\kappa_{11}^0\left(\frac{\partial^2 \phi^{(1)}}{\partial x^2}+\frac{\partial^2 \phi^{(1)}}{\partial y^2}\right)+\beta\left(e_{15}^0\frac{\partial w^{(1)}}{\partial x}-\kappa_{11}^0\frac{\partial \phi^{(1)}}{\partial x}\right)=0 \end{aligned} \tag{8.119}$$

$$\begin{aligned} &c_{55}^0\left(\frac{\partial^2 w^{(2)}}{\partial x^2}+\frac{\partial^2 w^{(2)}}{\partial y^2}\right)+e_{15}^0\left(\frac{\partial^2 \phi^{(2)}}{\partial x^2}+\frac{\partial^2 \phi^{(2)}}{\partial y^2}\right)+\gamma\left(c_{55}^0\frac{\partial w^{(2)}}{\partial x}+e_{15}^0\frac{\partial \phi^{(2)}}{\partial x}\right)=0,\\ &e_{15}^0\left(\frac{\partial^2 w^{(2)}}{\partial x^2}+\frac{\partial^2 w^{(2)}}{\partial y^2}\right)-\kappa_{11}^0\left(\frac{\partial^2 \phi^{(2)}}{\partial x^2}+\frac{\partial^2 \phi^{(2)}}{\partial y^2}\right)+\gamma\left(e_{15}^0\frac{\partial w^{(2)}}{\partial x}-\kappa_{11}^0\frac{\partial \phi^{(2)}}{\partial x}\right)=0 \end{aligned} \tag{8.120}$$

Using the Fourier integral transform, Chue and Ou then wrote the solutions of Eqs. (8.119) and (8.120) in the following form:

$$\begin{aligned} w^{(1)}(x,y)&=\frac{1}{2\pi}\int_{-\infty}^{\infty} f_{11}(\alpha,y)e^{-i\alpha x}\mathrm{d}\alpha+\frac{2}{\pi}\int_0^{\infty} g_{11}(x,\alpha)\sin(\alpha y)\mathrm{d}\alpha,\\ \phi^{(1)}(x,y)&=\frac{1}{2\pi}\int_{-\infty}^{\infty} f_{21}(\alpha,y)e^{-i\alpha x}\mathrm{d}\alpha+\frac{2}{\pi}\int_0^{\infty} g_{21}(x,\alpha)\sin(\alpha y)\mathrm{d}\alpha \end{aligned} \tag{8.121}$$

$$\begin{aligned} w^{(2)}(x,y)&=\frac{2}{\pi}\int_0^{\infty} g_{12}(x,\alpha)\sin(\alpha y)\mathrm{d}\alpha,\\ \phi^{(2)}(x,y)&=\frac{2}{\pi}\int_0^{\infty} g_{22}(x,\alpha)\sin(\alpha y)\mathrm{d}\alpha \end{aligned} \tag{8.122}$$

in which

$$
\begin{aligned}
f_{11}(\alpha, y) &= A_1(\alpha)\exp\left(-y\sqrt{\alpha^2 + i\alpha\beta}\right),\\
f_{21}(\alpha, y) &= B_1(\alpha)\exp\left(-y\sqrt{\alpha^2 + i\alpha\beta}\right),\\
g_{11}(x, \alpha) &= C_1(\alpha)\exp\left(\left[-\beta - \sqrt{\beta^2 + 4\alpha^2}\right]x/2\right),\\
g_{21}(x, \alpha) &= D_1(\alpha)\exp\left(\left[-\beta - \sqrt{\beta^2 + 4\alpha^2}\right]x/2\right),\\
g_{12}(x, \alpha) &= E_2(\alpha)\exp\left(\left[-\gamma + \sqrt{\gamma^2 + 4\alpha^2}\right]x/2\right),\\
g_{22}(x, \alpha) &= F_2(\alpha)\exp\left(\left[-\gamma + \sqrt{\gamma^2 + 4\alpha^2}\right]x/2\right)
\end{aligned}
\tag{8.123}
$$

where $A_1(\alpha)$, $B_1(\alpha)$, $C_1(\alpha)$, $D_1(\alpha)$, $E_2(\alpha)$, and $F_2(\alpha)$ are unknown functions to be determined from boundary conditions. In the following, Chue and Ou considered both permeable and impermeable crack surface conditions.

8.5.2 Impermeable crack problem

For an impermeable crack embedded in a two-FGPMs system as shown in Fig. 8.11, we have the following continuity conditions along the interface $x = 0$, symmetric conditions with respect to the x-axis, and the crack face conditions:

(1) Continuity conditions along the interface $x = 0$.

$$
\begin{aligned}
&w^{(1)}(0, y) = w^{(2)}(0, y), \quad \phi^{(1)}(0, y) = \phi^{(2)}(0, y),\\
&\sigma_{xz}^{(1)}(0, y) = \tau_{xz}^{(2)}(0, y), \quad D_x^{(1)}(0, y) = D_x^{(2)}(0, y)
\end{aligned}
\tag{8.124}
$$

(2) Symmetric conditions.

If all external loads are symmetric with respect to the x-axis, it is sufficient to consider the upper surface for $y \geqslant 0$ and to assume

$$
w^{(1)}(x, 0) = 0, \quad \phi^{(1)}(x, 0) = 0 \qquad (\text{for } 0 \leqslant x < a \text{ and } b < x < \infty) \tag{8.125}
$$

$$
w^{(2)}(x, 0) = 0, \quad \phi^{(2)}(x, 0) = 0 \qquad (\text{for } -\infty \leqslant x < 0) \tag{8.126}
$$

(3) Conditions on the crack surfaces.

The crack surface is assumed to be impermeable and simultaneously subjected to electrical displacement $D(x)$ and shear traction $\sigma(x)$:

$$
\sigma_{yz}^{(1)}(x, 0) = \sigma(x), \quad D_y^{(1)}(x, 0) = D(x) \qquad (\text{for } a < x < b) \tag{8.127}
$$

Chue and Ou [21] then noted that $D(x)$ and $\sigma(x)$ in Eq. (8.127) can be obtained from the remote electrical and mechanical loads using the superposition method.

After applying the continuity conditions Eq. (8.124) and taking the Fourier inverse transform, the four unknown functions $C_1(\alpha)$, $D_1(\alpha)$, $E_2(\alpha)$, and $F_2(\alpha)$ can be

expressed by the rest of the two functions $A_1(\alpha)$ and $B_1(\alpha)$ as

$$\begin{aligned}
&E_2(\alpha)-C_1(\alpha)=\frac{1}{2\pi}\int_{-\infty}^{\infty}\left(\frac{\alpha}{\alpha^2+\rho^2+i\beta\rho}\right)A_1(\rho)\mathrm{d}\rho,\\
&F_2(\alpha)-D_1(\alpha)=\frac{1}{2\pi}\int_{-\infty}^{\infty}\left(\frac{\alpha}{\alpha^2+\rho^2+i\beta\rho}\right)B_1(\rho)\mathrm{d}\rho,\\
&c_{55}^0sE_2(\alpha)+e_{15}^0sF_2(\alpha)-c_{55}^0pC_1(\alpha)-e_{15}^0pD_1(\alpha)\\
&\qquad=-\frac{1}{2\pi}\int_{-\infty}^{\infty}\left(\frac{i\rho\alpha}{\alpha^2+\rho^2+i\beta\rho}\right)\left[c_{55}^0A_1(\rho)+e_{15}^0B_1(\rho)\right]\mathrm{d}\rho,\\
&e_{15}^0sE_2(\alpha)-\kappa_{11}^0sF_2(\alpha)-e_{15}^0pC_1(\alpha)+\kappa_{11}^0pD_1(\alpha)\\
&\qquad=\frac{1}{2\pi}\int_{-\infty}^{\infty}\left(\frac{i\rho\alpha}{\alpha^2+\rho^2+i\beta\rho}\right)\left[-e_{15}^0A_1(\rho)+\kappa_{11}^0B_1(\rho)\right]\mathrm{d}\rho
\end{aligned}\tag{8.128}$$

where

$$p=\frac{-\beta-\sqrt{\beta^2+4\alpha^2}}{2},\quad s=\frac{-\gamma+\sqrt{\gamma^2+4\alpha^2}}{2}\tag{8.129}$$

As in Section 8.4, introduce two dislocation functions defined by Eq. (8.100). Then, substituting Eq. (8.123) into Eq. (8.121), later into Eq. (8.100), and applying the conditions (8.125), Chue and Ou indicated that $g_1(x)$ and $g_2(x)$ must satisfy the following equations:

$$\int_a^b g_1(t)\mathrm{d}t=\int_a^b g_2(t)\mathrm{d}t=0\tag{8.130}$$

The two remaining unknown functions can then be obtained as

$$A_1(\alpha)=\frac{i}{a}\int_a^b g_1(t)e^{i\alpha t}\mathrm{d}t,\quad B_1(\alpha)=\frac{i}{a}\int_a^b g_2(t)e^{i\alpha t}\mathrm{d}t\tag{8.131}$$

By using the residue theorem, they obtained the four unknown functions $C_1(\alpha)$, $D_1(\alpha)$, $E_2(\alpha)$, and $F_2(\alpha)$ as

$$\begin{aligned}
&C_1(\alpha)=\frac{(s-n_1)\alpha}{2n_1(p-s)\alpha_1}\int_a^b g_1(t)e^{-n_1t}\mathrm{d}t,\quad D_1(\alpha)=\frac{(s-n_1)\alpha}{2n_1(p-s)\alpha_1}\int_a^b g_2(t)e^{-n_1t}\mathrm{d}t,\\
&E_2(\alpha)=\frac{(p-n_1)\alpha}{2n_1(p-s)\alpha_1}\int_a^b g_1(t)e^{-n_1t}\mathrm{d}t,\quad F_2(\alpha)=\frac{(p-n_1)\alpha}{2n_1(p-s)\alpha_1}\int_a^b g_2(t)e^{-n_1t}\mathrm{d}t
\end{aligned}\tag{8.132}$$

where $n_1=\alpha_1-\beta/2$ and $\alpha_1=\sqrt{\alpha^2+\beta^2/4^2}$.

Making use of Eqs. (8.121), (8.123), (8.131), and (8.132), the condition (8.127) yields

$$\begin{aligned}\sigma_{yz}^{(1)}(x,0)=\sigma(x)&=e^{\beta x}\frac{1}{\pi}\int_a^b[c_{55}^0 g_1(t)+e_{15}^0 g_2(t)][k_1(x,t)+k_2(x,t)]\mathrm{d}t,\\ D_y^{(1)}(x,0)=D(x)&=e^{\beta x}\frac{1}{\pi}\int_a^b[e_{15}^0 g_1(t)-\kappa_{11}^0 g_2(t)][k_1(x,t)+k_2(x,t)]\mathrm{d}t\end{aligned}\tag{8.133}$$

where

$$k_1(x,t)=\frac{i}{2}\int_{-\infty}^{\infty}\left(\frac{-\sqrt{\alpha^2+i\beta\alpha}}{\alpha}\right)e^{i\alpha(t-x)}\mathrm{d}\alpha \tag{8.134}$$

$$k_2(x,t)=e^{\frac{\beta(t-x)}{2}}\int_0^{\infty}\left[\frac{\alpha^2(s-n_1)}{(p-s)n_1\sqrt{\alpha^2+\beta^2/4}}\right]e^{-(i+x)\sqrt{\alpha^2+\beta^2/4}}\mathrm{d}\alpha \tag{8.135}$$

To solve the singular integral equation (8.133), define a function $K_2(\alpha)$ as the factor in the integrand of Eq. (8.135) as

$$K_2(\alpha)=\frac{\alpha^2(s-n_1)}{(p-s)n_1\sqrt{\alpha^2+\beta^2/4}}=\frac{\alpha^2\left(\alpha_1-\alpha_2+\dfrac{\gamma-\beta}{2}\right)}{\alpha_1\left(\alpha_1+\alpha_2+\dfrac{\beta-\gamma}{2}\right)\left(\alpha_1-\dfrac{\beta}{2}\right)} \tag{8.136}$$

where $\alpha_2=\sqrt{\alpha^2+\gamma^2/4}$.

By separating the singular term of the kernels $k_1(x, t)$, Eq. (8.133) can be rewritten as

$$\begin{aligned}\sigma(x)&=e^{\beta x}\frac{1}{\pi}\int_a^b[c_{55}^0 g_1(t)+e_{15}^0 g_2(t)]\left[\frac{1}{t-x}+h_1(x,t)+k_2(x,t)\right]\mathrm{d}t,\\ D(x)&=e^{\beta x}\frac{1}{\pi}\int_a^b[e_{15}^0 g_1(t)-\kappa_{11}^0 g_2(t)]\left[\frac{1}{t-x}+h_1(x,t)+k_2(x,t)\right]\mathrm{d}t\end{aligned}\tag{8.137}$$

where

$$\begin{aligned}h_1(x,t)=&\int_0^{\infty}\left[\left(1+\frac{\beta^2}{\alpha^2}\right)^{0.25}\cos\left(\frac{\theta}{2}\right)-1\right]\sin\alpha(t-x)\mathrm{d}\alpha\\ &+\int_0^{A}\left(1+\frac{\beta^2}{\alpha^2}\right)^{0.25}\sin\left(\frac{\theta}{2}\right)\cos\alpha(t-x)\mathrm{d}\alpha\\ &+\int_A^{\infty}\left[\left(1+\frac{\beta^2}{\alpha^2}\right)^{0.25}\sin\left(\frac{\theta}{2}\right)-\frac{\beta}{2\alpha}\right]\cos\alpha(t-x)\mathrm{d}\alpha+\frac{\beta}{2}\int_A^{\infty}\frac{\cos\alpha(t-x)}{\alpha}\mathrm{d}\alpha\end{aligned}\tag{8.138}$$

with $\tan\theta=\beta/\alpha$ and A as an arbitrary positive constant.

The solutions of the singular integral equation with the Cauchy type kernel have the form

$$g_i(t)=\frac{G_i(t)}{\sqrt{(t-a)(b-t)}} \qquad (i=1,2) \tag{8.139}$$

where $G_i(t)$ are bounded functions. Chue and Ou then obtained the stress intensity factors and electric displacement intensity factors as

$$\begin{aligned}
k_3(b)&=\lim_{x\to b^+}\sqrt{2(x-b)}\sigma_{yz}^{(1)}(x,0)=-\frac{e^{\beta b}}{\sqrt{(b-a)/2}}[c_{55}^0G_1(b)+e_{15}^0G_2(b)],\\
k_3(a)&=\lim_{x\to a^-}\sqrt{2(a-x)}\sigma_{yz}^{(1)}(x,0)=\frac{e^{\beta a}}{\sqrt{(b-a)/2}}[c_{55}^0G_1(a)-e_{15}^0G_2(a)],\\
k_3^D(b)&=\lim_{x\to b^+}\sqrt{2(x-b)}D_y^{(1)}(x,0)=-\frac{e^{\beta b}}{\sqrt{(b-a)/2}}[e_{15}^0G_1(b)-\kappa_{11}^0G_2(b)],\\
k_3^D(a)&=\lim_{x\to a^-}\sqrt{2(a-x)}D_y^{(1)}(x,0)=\frac{e^{\beta a}}{\sqrt{(b-a)/2}}[e_{15}^0G_1(a)-\kappa_{11}^0G_2(a)]
\end{aligned} \tag{8.140}$$

To obtain the numerical solution of $G_i(a)$ and $G_i(b)$ (i = 1, 2), they normalized Eqs. (8.137) and conditions (8.130) into the following form:

$$\begin{aligned}
\sigma(x)&=e^{\beta x^*}\int_{-1}^{1}[c_{55}^0f_1(\bar{t})+e_{15}^0f_2(\bar{t})]\left[\frac{1}{(\bar{t}-\bar{x})\pi}+h_1(x^*,t^*)+k_2(x^*,t^*)\right]\mathrm{d}\bar{t},\\
D(x)&=e^{\beta x^*}\int_{-1}^{1}[e_{15}^0f_1(\bar{t})-\kappa_{11}^0f_2(\bar{t})]\left[\frac{1}{(\bar{t}-\bar{x})\pi}+h_1(x^*,t^*)+k_2(x^*,t^*)\right]\mathrm{d}\bar{t}
\end{aligned} \tag{8.141}$$

$$\int_{-1}^{1}f_1(\bar{t})\mathrm{d}\bar{t}=\int_{-1}^{1}f_2(\bar{t})\mathrm{d}\bar{t}=0 \tag{8.142}$$

where

$$\begin{aligned}
&\bar{x}=(x-c)/a_0,\quad \bar{t}=(t-c)/a_0,\quad x^*=a_0\bar{x}+c,\quad t^*=a_0\bar{t}+c,\\
&f_1(\bar{t})=g_1(t),\quad f_2(\bar{t})=g_2(t)
\end{aligned} \tag{8.143}$$

Equation (8.141) is similar to Eq. (8.110) and again the singular integral equation of the first kind. Following the same manner of treatment as Eq. (8.112), we can obtain the relationship between function $f_i(\bar{t})$ and the weighting function $F_i(\bar{t})$ as

$$f_1(\bar{t})=\frac{F_1(\bar{t})}{\sqrt{(1+\bar{t})(1-\bar{t})}},\quad f_2(\bar{t})=\frac{F_2(\bar{t})}{\sqrt{(1+\bar{t})(1-\bar{t})}} \tag{8.144}$$

Thus, Eqs. (8.141) and (8.142) can be solved by using the definition (8.144) and reducing these two equations into the following Chebyshev polynomial:

$$\begin{aligned}
\sigma(x_r) &= \frac{e^{\beta x^{**}}}{n}\sum_{k=1}^{n}[c_{55}^0 F_1(t_k) + e_{15}^0 F_2(t_k)] \\
&\quad \times\left[\frac{1}{t_k - x_r} + \pi\{h_1(x^{**}, t^{(k)}) + k_2(x^{**}, t^{(k)})\}\right], \\
D(x_r) &= \frac{e^{\beta x^{**}}}{n}\sum_{k=1}^{n}[e_{15}^0 F_1(t_k) - \kappa_{11}^0 F_2(t_k)] \\
&\quad \times\left[\frac{1}{t_k - x_r} + \pi\{h_1(x^{**}, t^{(k)}) + k_2(x^{**}, t^{(k)})\}\right], \\
&\frac{\pi}{n}\sum_{k=1}^{n} F_1(t_k) = 0, \qquad \frac{\pi}{n}\sum_{k=1}^{n} F_2(t_k) = 0
\end{aligned} \tag{8.145}$$

where

$$\begin{aligned}
&x^{**} = a_0 x_r + c, \qquad t^{(k)} = a_0 t_k + c, \\
&t_k = \cos\frac{(2k-1)\pi}{2n}, \qquad x_r = \cos\frac{r\pi}{n} \qquad (k = 1, \cdots, n;\ r = 1, \cdots, n-1)
\end{aligned} \tag{8.146}$$

Making use of the relationships between Eqs. (8.139), (8.143), and (8.144), the field intensity factors (8.140) can be rewritten as

$$\begin{aligned}
k_3(b) &= -e^{\beta b}\sqrt{a_0}[c_{55}^0 F_1(1) + e_{15}^0 F_2(1)], \\
k_3(a) &= e^{\beta a}\sqrt{a_0}[c_{55}^0 F_1(-1) + e_{15}^0 F_2(-1)], \\
k_3^D(b) &= -e^{\beta b}\sqrt{a_0}[e_{15}^0 F_1(1) - \kappa_{11}^0 F_2(1)], \\
k_3^D(a) &= e^{\beta a}\sqrt{a_0}[e_{15}^0 F_1(-1) - \kappa_{11}^0 F_2(-1)]
\end{aligned} \tag{8.147}$$

where the unknown values of $F_i(-1)$ and $F_i(1)$ can be obtained from the quadratic extrapolation from $F_i(t_n-1)$, $F_i(t_n-2)$, $F_i(t_n-3)$ and $F_i(t_2)$, $F_i(t_3)$, $F_i(t_4)$, respectively.

8.5.3 Permeable crack problem

In [21], Chue and Ou also considered the case of a permeable crack face. In this case, the symmetric condition $(8.125)_2$ and crack face condition $(8.127)_2$ are modified to be

$$\phi^{(1)}(x, 0) = 0 \qquad (\text{for } 0 \leqslant x < \infty) \tag{8.148}$$

$$D_y^{(1)}(x, 0) = D_c(x) \qquad (\text{for } a < x < b) \tag{8.149}$$

where D_c is defined in Eq. (8.96).

To satisfy the conditions of the permeable crack problem, Chue and Ou indi-

cated that they need one dislocation function $g_1(x)$ only. Similar to the procedure in Subsection 8.5.2, the corresponding stress and electric displacement can be written as

$$\begin{aligned}\sigma(x) &= c_{55}^0 e^{\beta x}\frac{1}{\pi}\int_a^b[\frac{1}{t-x}+h_1(x,t)+k_2(x,t)]g_1(t)\mathrm{d}t,\\ D_c(x) &= e_{15}^0 e^{\beta x}\frac{1}{\pi}\int_a^b[\frac{1}{t-x}+h_1(x,t)+k_2(x,t)]g_1(t)\mathrm{d}t\end{aligned} \tag{8.150}$$

The corresponding stress intensity factor k_3 and the electric displacement intensity factor k_3^D are given by

$$\begin{aligned}k_3(b) &= -e^{\beta b}c_{55}^0\sqrt{a_0}F_1(1), \quad k_3(a) = e^{\beta a}c_{55}^0\sqrt{a_0}F_1(-1),\\ k_3^D(b) &= -e^{\beta b}e_{15}^0\sqrt{a_0}F_1(1), \quad k_3^D(a) = e^{\beta a}e_{15}^0\sqrt{a_0}F_1(-1)\end{aligned} \tag{8.151}$$

Chue and Ou finally noted that since the crack is assumed to be electrically permeable, the condition (8.148) results in the electrical field E_y being continuous across the crack surfaces and remaining at a finite value at the crack tips. However, from the constitutive equations of piezoelectric material, the electrical displacement D_y is related to the shear strain γ_{yz} and the piezoelectric constant e_{15}. Therefore, D_y must be singular at the crack tips, due to the discontinuous displacement of the crack surface. The corresponding electrical displacement intensity factors k_3^D thus depend only on the material constant e_{15}^0 but not on the applied electric load.

References

[1] Zhu XH, Wang Q, Meng ZY: A functionally gradient piezoelectric actuator prepared by powder metallurgical process in pnn-pz-pt system. Journal of Materials Science Letters **14**(7), 516-518 (1995).

[2] Wang BL, Noda N: Thermally induced fracture of a smart functionally graded composite structure. Theoretical and Applied Fracture Mechanics **35**(2), 93-109 (2001).

[3] Ueda S: Thermally induced fracture of a functionally graded piezoelectric layer. Journal of Thermal Stresses **27**(4), 291-309 (2004).

[4] Ueda S: A cracked functionally graded piezoelectric material strip under transient thermal loading. Acta Mechanica **199**(1-4), 53-70 (2008).

[5] Ueda S: Thermoelectromechanical response of a center crack in a symmetrical functionally graded piezoelectric strip. Journal of Thermal Stresses **30**(2), 125-143 (2007).

[6] Ueda S: Thermal intensity factors for a parallel crack in a functionally graded

piezoelectric strip. Journal of Thermal Stresses **30**(4), 321-342 (2007).

[7] Ueda S: Effects of crack surface conductance on intensity factors for a functionally graded piezoelectric material under thermal load. Journal of Thermal Stresses **30**(7), 731-752 (2007).

[8] Ueda S: A penny-shaped crack in a functionally graded piezoelectric strip under thermal loading. Engineering Fracture Mechanics **74**(8), 1255-1273 (2007).

[9] Ueda S: Transient thermoelectroelastic response of a functionally graded piezoelectric strip with a penny-shaped crack. Engineering Fracture Mechanics **75**(5), 1204-1222 (2008).

[10] Li C, Weng GJ: Antiplane crack problem in functionally graded piezoelectric materials. Journal of Applied Mechanics-Transactions of the ASME **69**(4), 481-488 (2002).

[11] Hu KQ, Zhong Z, Jin B: Anti-plane shear crack in a functionally gradient piezoelectric layer bonded to dissimilar half spaces. International Journal of Mechanical Sciences **47**(1), 82-93 (2005).

[12] Rao BN, Kuna M: Interaction integrals for thermal fracture of functionally graded piezoelectric materials. Engineering Fracture Mechanics **77**(1), 37-50 (2010).

[13] Borrelli A, Horgan CO, Patria MC: Exponential decay of end effects in anti-plane shear for functionally graded piezoelectric materials. Proceedings of the Royal Society of London Series A: Mathematical Physical and Engineering Sciences **460**(2044), 1193-1212 (2004).

[14] Zhong Z, Shang ET: Exact analysis of simply supported functionally graded piezothermoelectric plates. Journal of Intelligent Material Systems and Structures **16**(7-8), 643-651 (2005).

[15] Dai HL, Fu YM, Yang JH: Electromagnetoelastic behaviors of functionally graded piezoelectric solid cylinder and sphere. Acta Mechanica Sinica **23**(1), 55-63 (2007).

[16] Dai HL, Hong L, Fu YM, Xiao X: Analytical solution for electromagneto-thermoelastic behaviors of a functionally graded piezoelectric hollow cylinder. Applied Mathematical Modelling **34**(2), 343-357 (2010).

[17] Zhong Z, Yu T: Electroelastic analysis of functionally graded piezoelectric material beams. Journal of Intelligent Material Systems and Structures **19**(6), 707-713 (2008).

[18] Shakeri M, Mirzaeifar R: Static and dynamic analysis of thick functionally graded plates with piezoelectric layers using layerwise finite element model. Mechanics of Advanced Materials and Structures **16**(8), 561-575 (2009).

[19] Wang Y, Xu RQ, Ding HJ: Analytical solutions of functionally graded piezoelectric circular plates subjected to axisymmetric loads. Acta Mechanica **215**(1-4), 287-305 (2010).

[20] Chue CH, Yeh CN: Angle cracks in two bonded functionally graded piezoelectric material under anti-plane shear. Theoretical and Applied Fracture Mechanics **53**(3), 233-250 (2010).

[21] Chue CH, Ou YL: Mode Ⅲ crack problems for two bonded functionally graded

piezoelectric materials. International Journal of Solids and Structures **42**(11-12), 3321-3337 (2005).

[22] Li X, Ding SH: Periodically distributed parallel cracks in a functionally graded piezoelectric (FGP) strip bonded to an FGP substrate under static electromechanical load. Computational Materials Science **50**(4), 1477-1484 (2011).

[23] Chen WQ, Bian ZG: Wave propagation in submerged functionally graded piezoelectric cylindrical transducers with axial polarization. Mechanics of Advanced Materials and Structures **18**(1), 85-93 (2011).

[24] Ueda S: Normal cracks in a functionally graded piezoelectric material strip under transient thermal loading. Journal of Thermal Stresses **34**(5-6), 431-457 (2011).

[25] Salah IB, Wali Y, Ghozlen MHB: Love waves in functionally graded piezoelectric materials by stiffness matrix method. Ultrasonics **51**(3), 310-316 (2011).

[26] Wang JS, He XQ, Qin QH: Singularity analysis of electro-mechanical fields in angularly inhomogeneous piezoelectric composites wedges. In: Kuna M, Ricoeur A (eds.). Proceedings of the IUTAM Symposium on Multiscale Modelling of Fatigue, Damage and Fracture in Smart Materials. IUTAM Bookseries, Vol. 24, pp. 153-162. Springer, Dordrecht(2011).

[27] Chue CH, Yeh CN: Mode Ⅲ fracture problem of two arbitrarily oriented cracks located within two bonded functionally graded material strips. Meccanica **46**(2), 447-469 (2011).

[28] Yao WA, Zhong WX, Lim CW: Symplectic Elasticity. World Scientific Publishing, Singapore (2009).

[29] Wang JS, Qin QH: Symplectic model for piezoelectric wedges and its application in analysis of electroelastic singularities. Philosophical Magazine **87**(2), 225-251 (2007).

[30] Chue CH, Chen CD: Antiplane stress singularities in a bonded bimaterial piezoelectric wedge. Archive of Applied Mechanics **72**(9), 673-685 (2003).

Index

O

P

Q

R

S

T

U

V